

Springer Proceedings in Energy

Jonathan D. Nixon  
Amin Al-Habaibeh  
Vladimir Vukovic  
Abhishek Asthana *Editors*

# Energy and Sustainable Futures: Proceedings of the 3rd ICESF, 2022

OPEN ACCESS

 Springer

# **Springer Proceedings in Energy**

## **Series Editors**

Muhammad H. Rashid, Department of Electrical and Computer Engineering,  
Florida Polytechnic University, Lakeland, FL, USA

Mohan Lal Kolhe, Faculty of Engineering and Science, University of Agder,  
Kristiansand, Norway

The series Springer Proceedings in Energy covers a broad range of multidisciplinary subjects in those research fields closely related to present and future forms of energy as a resource for human societies. Typically based on material presented at conferences, workshops and similar scientific meetings, volumes published in this series will constitute comprehensive state-of-the-art references on energy-related science and technology studies. The subjects of these conferences will fall typically within these broad categories:

- Energy Efficiency
- Fossil Fuels
- Nuclear Energy
- Policy, Economics, Management & Transport
- Renewable and Green Energy
- Systems, Storage and Harvesting
- Materials for Energy

eBook Volumes in the Springer Proceedings in Energy will be available online in the world's most extensive eBook collection, as part of the Springer Energy eBook Collection. To submit a proposal or for further inquiries, please contact the Springer Editor in your region:

Kamiya Khatter (India)

Email: [kamiya.khatter@springer.com](mailto:kamiya.khatter@springer.com)

Loyola D'Silva (All other countries)

Email: [loyola.dsilva@springer.com](mailto:loyola.dsilva@springer.com)

Jonathan D. Nixon · Amin Al-Habaibeh ·  
Vladimir Vukovic · Abhishek Asthana  
Editors


# Energy and Sustainable Futures: Proceedings of the 3rd ICESF, 2022

 Springer

### *Editors*

Jonathan D. Nixon  
Research Centre for Computational Science  
and Mathematical Modelling  
Coventry University  
Coventry, UK

Amin Al-Habaibeh  
School of Architecture Design and the Built  
Environment  
Nottingham Trent University  
Nottingham, UK

Vladimir Vukovic   
School of Computing, Engineering  
and Digital Technologies  
Teesside University  
Middlesbrough, UK

Abhishek Asthana  
Department of Engineering  
and Mathematics  
Sheffield Hallam University  
Sheffield, UK



ISSN 2352-2534

ISSN 2352-2542 (electronic)

Springer Proceedings in Energy

ISBN 978-3-031-30959-5

ISBN 978-3-031-30960-1 (eBook)

<https://doi.org/10.1007/978-3-031-30960-1>

© The Editor(s) (if applicable) and The Author(s) 2023. This book is an open access publication.

**Open Access** This book is licensed under the terms of the Creative Commons Attribution 4.0 International License (<http://creativecommons.org/licenses/by/4.0/>), which permits use, sharing, adaptation, distribution and reproduction in any medium or format, as long as you give appropriate credit to the original author(s) and the source, provide a link to the Creative Commons license and indicate if changes were made.

The images or other third party material in this book are included in the book's Creative Commons license, unless indicated otherwise in a credit line to the material. If material is not included in the book's Creative Commons license and your intended use is not permitted by statutory regulation or exceeds the permitted use, you will need to obtain permission directly from the copyright holder.

The use of general descriptive names, registered names, trademarks, service marks, etc. in this publication does not imply, even in the absence of a specific statement, that such names are exempt from the relevant protective laws and regulations and therefore free for general use.

The publisher, the authors, and the editors are safe to assume that the advice and information in this book are believed to be true and accurate at the date of publication. Neither the publisher nor the authors or the editors give a warranty, expressed or implied, with respect to the material contained herein or for any errors or omissions that may have been made. The publisher remains neutral with regard to jurisdictional claims in published maps and institutional affiliations.

This Springer imprint is published by the registered company Springer Nature Switzerland AG  
The registered company address is: Gewerbestrasse 11, 6330 Cham, Switzerland

# Preface

The world needs to act now to save our planet and mitigate the impact of climate change and loss of biodiversity. The recent increase in energy prices after the COVID-19 global pandemic further highlights the pressing challenges regarding widespread energy poverty and the lack of energy security. Everyone now has a role to play in ensuring the security and sustainability of our energy supplies for future generations.

This book contains research papers presented at the 3rd International Conference on Energy and Sustainable Futures (ICESF), which took place at Coventry University, UK, in 2022. The ICESF is an annual conference organised by the UK-based Doctorial Training Alliance (DTA) programme. It is a multi-disciplinary conference focused on addressing the future challenges and opportunities for meeting global energy targets and sustainable development goals. The conference brought together academia researchers, industry experts and research students to showcase the latest innovations and research on a wide range of topics in the areas of energy and sustainability, including renewable energy, ICT, control, computational fluid dynamics, optimisation, energy governance, materials in energy research and energy storage. A total of 33 papers were selected by a technical programme committee for presentation at the conference and for inclusion in this book.

Coventry, UK  
Nottingham, UK  
Middlesbrough, UK  
Sheffield, UK

Jonathan D. Nixon  
Amin Al-Habaibeh  
Vladimir Vukovic  
Abhishek Asthana

**Acknowledgements** The editors would like to acknowledge the Doctorial Training Alliance and Coventry University for organising and supporting the publication of this proceedings from the 3rd International Conference on Energy and Sustainable Futures (ICESF).

# Contents

<b>1</b>	<b>Investigating Energy Cost Impact on Private Residential Buildings in the West Midlands Region of the UK</b> .....	<b>1</b>
	Ali Abdi, Abdullahi Ahmed, Rachitra Gunatilake, and Ishmael Onungwe	
<b>2</b>	<b>Towards an Effective Artificial Intelligence Systems for Condition Monitoring of Off-Shore Wind Turbines: The Application of Sensor Fusion</b> .....	<b>11</b>
	Amin Al-Habaibeh, Bubaker Shakmak, Ampea Boateng, and Hyunjoo Lee	
<b>3</b>	<b>CFD Based Aerodynamics Conjugate Heat Transfer and Airgap Fluid Flow Thermal Analysis to a Wheel Hub Motor for Electric Scooters</b> .....	<b>21</b>
	A. M. Divakaran, E. Abo-Serie, E. I. Gkanas, J. Jewkes, and S. Shepherd	
<b>4</b>	<b>Learning from the Past for a Sustainable Future: Environmental Monitoring and 3D Modelling to Assess the Thermal Performance of Heritage Buildings</b> .....	<b>31</b>
	D. Antón, Amin Al-Habaibeh, and T. Queiroz	
<b>5</b>	<b>Oil and Gas Supply Chain: Analysing Stakeholder Sustainability Risk Perception</b> .....	<b>41</b>
	Ashem Egila, Muhammad Mustafa Kamal, and Benny Tjahjono	
<b>6</b>	<b>Using Machine Learning to Predict Synthetic Fuel Spray Penetration from Limited Experimental Data Without Computational Fluid Dynamics</b> .....	<b>51</b>
	Bryn Richards and Nwabueze Emekwuru	
<b>7</b>	<b>Computational Analysis of Hydro-powered Bunyip Pump</b> .....	<b>61</b>
	Scott Daniel Beard, Mansour Al Qubeissi, and Bidur Khanal	

<b>8</b>	<b>Simulating the Effects of Inertia and Frequency Response Services on Transient Propagation in a Networked Grid</b> .....	73
	A. Christian Cooke and B. Benjamin Mestel	
<b>9</b>	<b>Multi-objective Energy Management Model for Stand-Alone Photovoltaic-Battery Systems: Application to Refugee Camps</b> .....	81
	Daniel Bammeke, Jonathan D. Nixon, James Brusey, and Elena Gaura	
<b>10</b>	<b>Flow Simulation of a New Horizontal Axis Wind Turbine with Multiple Blades for Low Wind Speed</b> .....	93
	Essam Abo-Serie and Elif Oran	
<b>11</b>	<b>Indoor Thermal Comfort Controller Integrating Human Interaction in the Control-Loop as a Live Component</b> .....	107
	Edgar Segovia, Paul van Schaik, and Vladimir Vukovic	
<b>12</b>	<b>Investigating the Utilisation of Waste Sand from Sand Casting Processes for Concrete Products for Environmental Sustainability</b> .....	117
	Sirwan Faraj and Amin Al-Habaibeh	
<b>13</b>	<b>Application of Observational Weather Data in Evaluating Resilience of Power Systems and Adaptation to Extreme Wind Events</b> .....	127
	Francis Mujjuni, Tom Betts, and Richard E. Blanchard	
<b>14</b>	<b>The ‘Mousetrap’: Challenges of the Fluctuating Demand on the Electricity Grid in the UK</b> .....	137
	George Milev and Amin Al-Habaibeh	
<b>15</b>	<b>Assessment of Effectiveness of Hollow Fins for Performance Enhancement of Solar Still Device Using Simulation Approach</b> .....	145
	Hafiz Khadim Ullah, Sikiru Oluwarotimi Ismail, and Kumar Shantanu Prasad	
<b>16</b>	<b>Development of a CFD Model for the Estimation of Windage Losses Inside the Narrow Air Gap of an Enclosed High-Speed Flywheel</b> .....	157
	Mahmoud Eltaweel, Christos Kalyvas, Yong Chen, and Mohammad Reza Herfatmanesh	
<b>17</b>	<b>The Analysis of Sensory Data from Smart Office Environment Towards the Development of an Intelligent System</b> .....	169
	Jack Hall, Bubaker Shakmak, Amin Al-Habaibeh, and Eiman Kanjo	
<b>18</b>	<b>Investigation of Working Fluid Performance in a Refrigeration Cycle</b> .....	179
	J. Radulovic, J. Bull, and J. M. Buick	



<b>19</b>	<b>Energy Policy as a Tool for Promoting Power System Resilience: Malawi's Challenges and Potential Solutions</b> .....	187
	Joyce Nyuma Chivunga, Zhengyu Lin, and Richard Blanchard	
<b>20</b>	<b>Quantitative Assessment of Damage in Composites by Implementing Acousto-ultrasonics Technique</b> .....	209
	Kumar Shantanu Prasad, Gbanaibolou Jombo, Sikiru O. Ismail, Yong K. Chen, and Hom N. Dhakal	
<b>21</b>	<b>Multiple-Criteria Optimization of Residential Buildings Envelope Toward nZEBs: Simplified Approach for Damascus Post-war</b> .....	219
	Lina A. Khaddour and Siegfried K. Yeboah	
<b>22</b>	<b>Design and Prototype an Educational Proton-Exchange Membrane Fuel Cell Model</b> .....	235
	M. R. Rahman, F. S. Hosseini, P. Taleghani, M. Ghassemi, and M. Chizari	
<b>23</b>	<b>The Impact of Strategic Environmental Management Capabilities on the Competitiveness of an Oil and Gas Industry's Supply Chain: An Empirical Evaluation of the Natural Resource-Based View of Firms</b> .....	245
	Olatunde Olajide, Muhammad Mustafa Kamal, Dong-Wook Kwak, Qile He, and Ming Lim	
<b>24</b>	<b>Towards the Tees Valley Energy Transition—Residential Decarbonisation and Skills Analysis</b> .....	257
	Paul van Schaik, Matthew Cotton, Huda Dawood, Nashwan Dawood, Elena Imani, Michael Knowles, Charlotte Leighton, Susan Lorrimer, Andrea Mountain, Edgar Segovia, Rosemary Stubbs, and Natasha Vall	
<b>25</b>	<b>Multi-objective Optimisation of a Wastewater Anaerobic Digestion System</b> .....	265
	R. J. Ashraf, Jonathan D. Nixon, and J. Brusey	
<b>26</b>	<b>Energy Demand Reduction in Data Centres Using Computational Fluid Dynamics</b> .....	275
	R. Sethuramalingam, Abhishek Asthana, S. Xyggaki, K. Liu, J. Eduardo, S. Wilson, and C. Bater	
<b>27</b>	<b>Short Review of Biodiesel Production by the Esterification/ Transesterification of Wastewater Containing Fats Oils and Grease (FOGs)</b> .....	285
	Rawaz A. Ahmed and Katherine Huddersman	

<b>28</b>	<b>The Use of Photovoltaic Solar Panels to Reduce Temperature-Induced Bridge Deformations</b> .....	<b>301</b>
	Sushmita Borah and Amin Al-Habaibeh	
<b>29</b>	<b>Exploring Windows Opening Behaviour of Occupants of Residential Buildings Using Artificial Intelligence</b> .....	<b>311</b>
	Sherna Salim and Amin Al-Habaibeh	
<b>30</b>	<b>Performance of Different Optimization Solvers for Designing Solar Linear Fresnel Reflector Power Generation Systems</b> .....	<b>323</b>
	M. P. G. Sirimanna, Jonathan D. Nixon, and M. S. Innocente	
<b>31</b>	<b>Thermal Optimisation Model for Cooling Channel Design Using the Adjoint Method in 3D Printed Aluminium Die-Casting Tools</b> .....	<b>333</b>
	Tongyan Zeng, Essam F. Abo-Serie, Manus Henry, and James Jewkes	
<b>32</b>	<b>The Effect of Vane Number in Casing Treatment of an Axial-Flow Compressor</b> .....	<b>341</b>
	Sara Soodani, SeyedVahid Hosseini, Mohammad Hakimi, and Mohammad Akhlaghi	
<b>33</b>	<b>Development of an Affordable MGT-CHP for Domestic Applications</b> .....	<b>351</b>
	Seyedvahid Hosseini, Seyed Hossein Madani, Sara Hatami, Ali Izadi, Mohamad Ali Sarkandi, Ali Norouzi, and Mahmoud Chizari	

# About the Editors

**Dr. Jonathan D. Nixon** is Associate Director at Coventry University’s Research Centre for Computational Science and Mathematical Modelling. Dr. Nixon has carried out a wide range of research projects on solar, wind and bio-energy technologies, with a particular focus on improving their performance and reliability for disadvantaged communities. His research has involved deploying smart solar energy interventions in refugee camps in Africa, designing hybrid solar-biomass systems in rural India and improving the performance of wind turbine in cold climates. He is currently leading the Innovate UK Energy Catalyst project Solar Energy Transitions (SET): Inclusive e-cooking in sub-Saharan Africa. He was Conference Chair for the 3rd International Conference on Energy and Sustainable Futures held at Coventry University in 2022.

**Prof. Amin Al-Habaibeh** is Professor of Intelligent Engineering Systems within the product design team at Nottingham Trent University. Amin’s research helps reshaping futures by creating a positive impact on individuals and society. He is Director of the national DTA Energy (Doctoral Training Alliance) and also Director of Product Innovation Centre. His research and teaching activities focus on several multi-disciplinary topics in the broad area of product design and innovation, automation, energy, condition monitoring and artificial intelligence. Amin is currently leading the Innovative and Sustainable Built Environment Technologies research group (iSBET) and co-founder of the Advance Design and Manufacturing Engineering Centre (ADMEC). Amin has over 180 international publications and patents, and his research work has been highlighted by major TV channels and newspapers such as the CNN, the BBC, The Daily Telegraph, The Guardian, The Sun and The Daily Mail.

**Dr. Vladimir Vukovic** works as Senior Research Lecturer in BIM and Energy Reduction in Built Environment at Teesside University. Dr. Vukovic’s research interests include sustainable (energy efficient, socially acceptable, environmentally

friendly) building design and operation—whole life cycle approach—and in particular: building information modelling (BIM) and digital construction twins, cyber-physical system simulation and optimization, predictive controls, indoor environmental quality, energy efficiency implications on occupants' well-being and productivity, energy-aware social networking enabled through smart metering, energy blockchain and augmented reality applications in the built environment. Dr. Vukovic currently serves as Deputy Director of Doctoral Training Alliance (DTA) in Energy.

**Dr. Abhishek Asthana** (CEng FEI FIET FHEA Ph.D. MEng MRes BEng) is Director of Hallam Energy and Reader in Energy Engineering at Sheffield Hallam University and Deputy Director of the Doctoral Training Alliance in Energy (DTA Energy). Abhishek is Reviewer for the International Energy Agency's (IEA) Renewable Energy Division in Paris, Research Committee Member for the UK Energy Research Centre (UKERC) and Member of the Parliamentary Group for Energy Studies (PGES). He has led 65 industrial energy efficiency and decarbonisation projects in the last 14 years. He has co-authored more than 60 papers, five books, numerous book chapters, invented four patents and eight commercial software packages in energy engineering.

# Chapter 1

## Investigating Energy Cost Impact on Private Residential Buildings in the West Midlands Region of the UK



Ali Abdi, Abdullahi Ahmed, Rachitra Gunatilake, and Ishmael Onungwe

**Abstract** With the housing sector accounting for a huge share of the overall energy consumption rate globally, it is imperative to ascertain the energy efficiency of residential buildings and its cost implication on dwellers. This paper focuses on investigating the types of residential buildings available in the West Midlands region of United Kingdom, the level of comfort derived by dwellers from energy provisions on their buildings during different times of the year and the impact of energy cost on dwellers. The paper also explores factors influencing energy consumption patterns in residential buildings within the study area. The methodology adopted in this paper are secondary and primary data sources. The secondary data is based on updated literature from existing scholarly publications, while the primary data is based on semi-structured interview conducted with residents or dwellers of private residential buildings within the West Midlands region of United Kingdom. Qualitative analytical approach was used to synthesize the data obtained. Findings reveal that the energy efficiency or the sustainable rating of a building is a major determinant of a residential building energy consumption. Other findings are housing technical, socioeconomic status of dwellers, demography, dwellers preference and behaviour, climatic condition, and geographic factor. Further on, the outcome of the interviews reveals an upward increase in the cost of energy with its effect impacting residents negatively because of living wage in the presence of inflation and global economic meltdown.

**Keywords** Efficiency · Dwellers · Energy · Sustainability · Consumption

---

A. Abdi (✉)

Faculty of Engineering, Environment and Computing Priory Street, Coventry University,  
Coventry CV1 5FB, England  
e-mail: [abdia7@uni.coventry.ac.uk](mailto:abdia7@uni.coventry.ac.uk)

A. Ahmed

Faculty of Engineering and Built Environment, Canterbury Christ Church, Canterbury, Kent CT1  
1QU, England

R. Gunatilake · I. Onungwe

Global Banking School, Department of Construction Management, Birmingham B5 5SE, England

© The Author(s) 2023

J. D. Nixon et al. (eds.), *Energy and Sustainable Futures: Proceedings of the 3rd ICESF*,  
2022, Springer Proceedings in Energy, [https://doi.org/10.1007/978-3-031-30960-1\\_1](https://doi.org/10.1007/978-3-031-30960-1_1)

## 1.1 Introduction

The extent to which a building is sustainably designed, the climatic condition of the geographical location of a building and the age of building are influencing factors of the energy system and its efficiency. Hence, the consumption of energy in a building is basically characterized by the extent to which energy is lost through the building envelope which can be said to be the physical structural form of the building, and the extent at which energy usage is required by dwellers for their overall physical comfort [1, 2]. Basically, buildings are responsible for about 40% energy usage, 25% water usage and 40% absorption of global natural resources which in turn emits about one-third of Green-House Gas (GHG), [1, 3]. For sustainability to be achieved within the built environment, there must be a balance between energy consumption which translates into cost implication on dwellers and its ecological effect [4].

On the premise that the housing sector is one significant energy user, it is imperative to understand the rate of energy consumption and its requirements on each building to enhance energy efficiency, cost minimisation and environmental sustainability. With the United Kingdom having one of the oldest existing buildings in the European Union (EU), wherein many of such buildings were constructed in Victorian times [5]; this research was necessitated to investigate the rate at which energy is consumed, the level of physical comfort derived by dwellers at different times of the year owing to climatic condition with regards to energy consumption, the cost of energy and its impact on dwellers.

Though, several research have discussed factors or drivers influencing dwellers' energy consumption rate in several parts of the world [6, 7]; it is important to note that the study on the cost impact of energy consumption and the drivers of the rate of energy consumption as it relates to dwellers' physical comfort in private residential buildings in the West Midlands region of United Kingdom is lacking. Hence, the reason for this research in the face of increasing energy cost which can be seen as presented in Fig. 1.1.

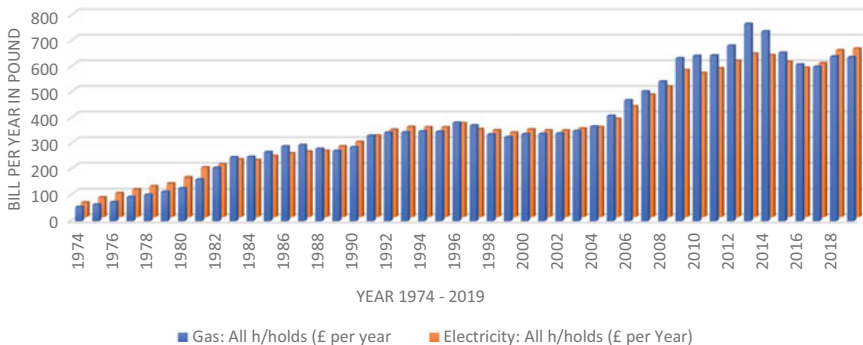


**Fig. 1.1** Increase in energy cost from 1974–2019

**Table 1.1** Energy performance certificates (EPCs) classification

S. No	Categories	Ratings	Description
1	A	100–92	Most efficient
2	B	91–81	
3	C	68–55	
4	D	54–39	
5	E	38–21	
6	F	20–1	Least efficient

*Source* Review of the energy performance of buildings; Economidou [9]

In the UK, Energy Performance Certificates (EPCs), is a pointer to the energy cost expectation of buildings with respect to physical comfort attainment by dwellers. This is because a top-rated categorized building is indicative of a sustainable dwelling, thereby requiring minimum energy consumption which will lead to minimal cost impact. EPC rating ranges from 0 to 100, with residential buildings categorized from A to G [8]. Table 1.1 shows the range and categories for ratings based on EPC classification.

Undoubtedly, the quest toward energy efficiency goes beyond cost maximisation and enhances residents' healthy living and well-being. An inefficient energy residence is a breeding ground for respiratory infections, cardiovascular, hypothermia, heart attacks and mental problems. An energy-inefficient building is prone to cold, leading to condensation and moulds and can contribute to the wheezing of older people and young children [10]. Subsequently, energy consumption in residential buildings is not solely attributed to the age of the building but also factors such as the attainment of the functional requirement of the building, technical characterisation and residents' socioeconomic attributes relating to lifestyle are also indicators [11]. Dwellers' living pattern and behaviour contributes significantly to the extent of energy consumption with an estimate accounting for 30% heating energy consumption, and 50% cooling energy consumption specifically in low-income residents [12].

Considering the high cost of procuring energy, the time is now to improve the functional requirement of buildings globally in relation to thermal performance to enhance dwellers' comfort and healthy living with economic energy consumption. Nowadays, design and construction of new buildings are currently focusing on high energy performance with minimum dependence on consumption. Thus, buildings should be designed based on microclimate considerations [13]. These echoes widespread calls for a 'green economic stimulus' within which the home energy efficiency programme plays a significant part [9]. Such schemes would have substantial health benefits and address the UK's long-term problem of excess winter deaths exacerbated by cold homes. Figure 1.2 shows a breakdown of energy consumption of various sectors, with keen interest in the building sector which comprises of residential and commercial, with the micro distribution of energy utilization well-presented [14].

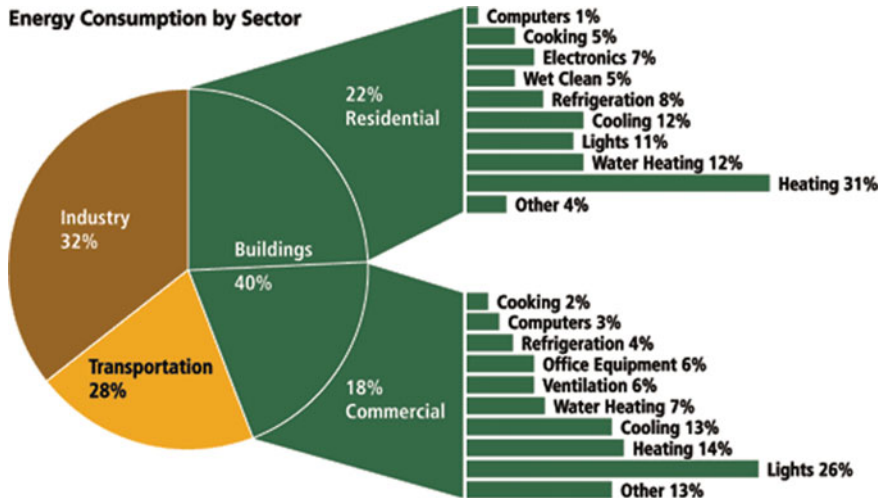


Fig. 1.2 Breakdown of energy consumption by sectors. *Source* De Simone [14]

## 1.2 Methodology

The methodology adopted in this research presentation on ascertaining the impact of cost based on energy consumption by residential dwellers are drawn from secondary and primary data sources. The secondary data is based on updated published scholarly literature, and the primary data is based on interviews conducted with residents or dwellers of private residential buildings in the West Midlands region of United Kingdom. The outcome of the interviews was synthesize using qualitative analytical approach. The interview applied a purposive technique targeted at obtaining detailed experiences from residents or dwellers of the selected buildings. Summarily, 20 private residential buildings were selected based on several characteristics or elements that distinguished them based on energy consumption drivers, dwellers' physical comfort and building functionality. Also, cost implication was put into consideration.

Going forward, the interview data were synthesized using content analysis in consonance with [14]; wherein the analytical processes allow for identifying, organising, describing, and coding textual materials. Content analysis also provides flexibility and a more accessible form of research. The data were analysed to investigate the energy cost impact of the private residential buildings selected. Subsequently, all audio recording was transcribed verbatim, and lines of text were numbered. Once transcribed, the data was coded and inputted into NVivo computer software. The codes were developed by selecting themes directly related to the study's aim and objectives. Below are some of the probing questions and themes generated for the study interviews.



### 1.3 Results and Discussion

#### Research questions:

**Questions 1a: Is the house you live in warm enough to make you feel comfortable during winter?**

#### Response from Interviewees.

*“— My house does not warm up properly, you have to keep heating and it is costing a lot in energy bills....” -Terrace Tennant 1, Birmingham.*

In follow-up and probing further.

**Questions 1a: What could be the contributing factors for your house not being warm enough?** *“— first of all, our property is not a recent day design; it was built in the 1920s, it has an EPC rating of E, and it does not have good insulation. These I believe could be one main contributing factor to the circulatory heating duration leading to high energy consumption and huge cost demand...” Terrace Tennant 1, Birmingham.*

**Questions 1b: How much does your average yearly bill for energy cost?**

*“— It costs us £2200 for electricity and gas per year. The prices have doubled over a period.*

**Questions 2a: What is the frequency or duration within which the heating system of your house gets warm enough to your desired expectation and living comfort?**

*“My experience with respect to the optimal heating duration of my house depends on factors that I cannot really explain. This is because in most cases it takes much longer for the heating impact to be felt. Sometimes it takes up to an hour for the house to get warm to the temperature that residents will feel it” Three-bedroom Flat owner 2, Coventry.*

**Questions 2b: Are you invariably saying that your house heating system does not pick and heat up the house within a specific duration?**

*“I would not be wrong if I say so, as the minimum time the heating system has been felt is mostly after an hour or more. Even at that, not every section of the house gets the warm temperature as expected” Detached house tenant 1, Wolverhampton.*

**Questions 3a: How would you describe the consistency of your bill for each month?**

*“Hmmm! The bill from E.ON Next does not come uniformly, but some level of variation is usually noticed. This variation is always on the increasing side”. Terrace Tennant 1, Birmingham.*

**Questions 3b: Would you rather say your billing cost is because of the EPC rating and category of your building?**

*“Ehhh, rating is a technical word, and since I am not a professional or knowledgeable in that trade, I can say the condition of the building could be responsible for the billing cost. However, I cannot conclude about the views that bills are tempered with”* **Semi-detached house owner 1, Birmingham.**

**Questions 4a: How would you describe the impact of your energy billing cost on your income?**

*“It will be pitiable to explain the impact of the cost of my energy bills. This is because I spend a huge percentage of my income on energy bill deductions.”* **Terrace Tenant 2, Coventry.**

**Questions 4b: Could your energy cost be linked to the age of your residence, considering the cost impact as presented above?**

*“Oh yes, it would not be out of place to say that the age of the building is another major factor for the cost of my energy bill. But I would appreciate any means by which this cost impact can be reduced”.* **Three-bedroom Flat owner 2, Coventry.**

## 1.4 Discussion

Despite the lack of literature directly related to private tenants and owners' responses to high energy cost experiences, the interview results show that the type of residential buildings lived by the tenants are responsible for increased energy costs to a great extent. Amongst the answers given by the respondents or interviewees, high energy cost contributes to them falling into fuel poverty as they spend a higher proportion of their income on utility bills. Of course, the building type lived by the dwellers contributes to the situation; however, efforts should be made to prioritise energy standards in private houses. Renovation, refurbishment and retrofitting of older buildings present the opportunity to improve its energy efficiency hence reducing energy cost and carbon footprint. This idea is in consonance with [13]; where buildings are focusing on sustainable design and construction to reduce over dependence on high energy consumption since the age of the building which can be linked to building functionality are contributing factors to the usage or consumption of energy.

On top of all the payment issues, energy prices have risen since Brexit, starting from October 2021, the energy price cap set by Ofgem no longer applied, leaving energy companies to set up their prices. The respondents interviewed have also stated that their cost of living increased since the price hike, leading them to adapt coping strategies. Table 1.2 below illustrates key themes featuring the interview participant's experience. In view of the increasing price of energy, Fig. 1.1; is a true representation of this experience.

**Table 1.2** Key themes from the interview

Content	Frequency
High energy bills	12
Cold housing	11
Insulation	15
Energy efficiency	13
Inadequate heating	16
Fuel poverty	15
Comfort	10
Temperature	14

Findings from the secondary source of data extracted from scholarly published literature reveal that housing technical, socioeconomic status of dwellers, demography, dwellers' preference and behaviour, climatic condition, and geographic factor are residence energy consumption determinants. In essence, these factors and more were also observed from the interview as pointed out by the interviewees expressing the cost impact of energy consumption as residents or dwellers.

## 1.5 Conclusion

In general, the building sector is a major consumer of energy with complex drivers and influencing factors leading to this consumption of energy with huge cost impact on dwellers. Also, owning and renting private homes, especially the ones built in Victoria times, contributes to financial impact due to high energy costs with associated problem of 'heat and eat' dilemma. The interview result clearly shows the detrimental effect of living in private homes that are prohibitively expensive to heat because of high energy costs pointing to inefficient homes. According to the participants, living in inadequate homes with poor insulation is depressing, stressful and damaging to their mental and physical health. Hence, spending more of their budget on energy than on households with better-insulated homes means that any increase in energy bills by the suppliers will have a profound effect. In essence, the government must step in toward allocating funding for private homes to improve their energy efficiency and EPC rating in attaining sustainable state and achieving functional buildings. Similarly, to help tenants, private landlords should register their properties with the local government to ensure they have an EPC rating of C and above.

## References

1. E. Dean, Energy efficiency for buildings, United Nations environment programme (UNEP) division of technology, industry, and economics France. Available from <http://www.unep.org/energy>.
2. B. Fateh, B.Y. Adel, O. Nessrine, Investigating the factors shaping residential energy consumption patterns in France: evidence from quantile regression. *European J. Comp. Econ.* **17**(1), 127–151 ISSN 1824-2979. (2020) Available from <https://doi.org/10.25428/1824-2979/202001-127-151>
3. P. Cerin, L.G. Hassel, N. Semenova, Energy performance and housing prices. *Sustain. Dev.* **22**(6), 404–419 (2014)
4. G. Trotta, J. Spangenberg, S. Lorek, Energy efficiency in the residential sector: identification of promising policy instruments and private initiatives among selected European countries. *Energy. Eff.* **11**(8), 2111–2135 (2018)
5. M.A.P.S. Ferreira, M. Almeida, A.C.R.A. Rodrigues, Cost-optimal energy efficiency levels are the first step in achieving cost effective renovation in residential buildings with a nearly-zero energy target. *Energy Build.* **133**, 724–737 (2016)
6. D. Brounen, N. Kok, J.M. Quigley, Residential energy use and conservation: economics and demographics. *Eur. Econ. Rev.* **56**(5), 931–945 (2012)
7. H. Estiri, A structural equation model of energy consumption in the United States: untangling the complexity of per-capita residential energy use. *Energy Res. Soc. Sci.* **6**, 109–120 (2015)
8. A. Bennadji, M. Seddiki, J. Alabid, R. Laing, D. Gray, Predicting energy savings of the UK housing stock under a step-by-step energy retrofit scenario towards net-zero. *Energies* **2022**(15), 3082 (2022)
9. M. Economidou, B. Atanasiu, C. Despret, J. Maio, I. Nolte, O. Rapf, S. Zinetti, Europe's buildings under the microscope. A country-by-country review of the energy performance of buildings (2011)
10. V. Ballesteros-Arjona, L. Oliveras, J.B. Munoz, A.O. de Labry Lima, J. Carrere, E.M. Ruiz, A. Peralta, A.C. León, I.M. Rodríguez, A. Daponte-Codina, M. Mari-Dell'Olmo, What are the effects of energy poverty and interventions to ameliorate it on people's health and well-being? A scoping review with an equity lens. *Energy Res. Soc. Sci.* **87**, 102456 (2022)
11. M.J. Lőrincz, J.L. Ramírez-Mendiola, J. Torriti, Impact of time-use behaviour on residential energy consumption in the United Kingdom. *Energies* **14**(19), 6286 (2021)
12. B. Dong, Z. Li, G. Mcfadden, An investigation on energy-related occupancy behaviour for low-income residential buildings. *Sci. Technol. Built Environ.* **21**(6), 892–901 (2015)
13. O.K. Akande, O. Fabiyi, I.C. Mark, Sustainable approach to developing energy efficient buildings for resilient future of the built environment in Nigeria. *American J. Civil Eng. Architect.* **3**(4), 144–152 (2015)
14. M. De Simone, G. Fajilla, Occupant behaviour: a key factor in energy performance of buildings. Methods for its detection in houses and in offices. *J. World Architect.* **2**(2) (2018)

**Open Access** This chapter is licensed under the terms of the Creative Commons Attribution 4.0 International License (<http://creativecommons.org/licenses/by/4.0/>), which permits use, sharing, adaptation, distribution and reproduction in any medium or format, as long as you give appropriate credit to the original author(s) and the source, provide a link to the Creative Commons license and indicate if changes were made.

The images or other third party material in this chapter are included in the chapter's Creative Commons license, unless indicated otherwise in a credit line to the material. If material is not included in the chapter's Creative Commons license and your intended use is not permitted by statutory regulation or exceeds the permitted use, you will need to obtain permission directly from the copyright holder.



# Chapter 2

## Towards an Effective Artificial Intelligence Systems for Condition Monitoring of Off-Shore Wind Turbines: The Application of Sensor Fusion



Amin Al-Habaibeh, Bubaker Shakmak, Ampea Boateng, and Hyunjoo Lee

**Abstract** In the face of increasing energy demand and the upsurge in the recent energy prices post Covid-19 pandemic, scientists and technologists around the world are working to develop more efficient renewable energy alternatives. Among such technologies, wind turbines play an important role as a very mature clean energy technology. But minimising maintenance costs and downtime is critical for off-shore wind turbines; and researchers around the world are trying to develop comprehensive online and real time monitoring systems to monitor the health of wind turbines to advance condition-based maintenance (CBM) strategies in order to reduce cost and enhance availability. There is a need to use sensor fusion since a single type of sensor is not expected to capture the needed information regarding the health of the wind turbine due to the complexity of the operational conditions such as wind speed, wind direction, power output, environmental temperatures; in addition to many other factors. Industrial case study will be presented in this paper to explore the sensor fusion option and discuss how to select the most suitable sensors to detect a specific fault, or group of faults, among hundreds of sensors. This is considered a critical step for the development of an artificial intelligence CBM system. The paper presents the use of the ASPS approach (Automated Sensor and Signal Processing Selection). The results show that the suggested methodology could easily identify the sensors and signal processing methods that are sensitive to fault conditions for future diagnostics and prognostics.

**Keywords** Wind turbine · Data fusion technology · Condition monitoring · AI

---

A. Al-Habaibeh (✉) · B. Shakmak  
Product Innovation Centre, Nottingham Trent University, Nottingham, UK  
e-mail: [Amin.Al-Habaibeh@ntu.ac.uk](mailto:Amin.Al-Habaibeh@ntu.ac.uk)

A. Boateng · H. Lee  
Off-Shore Renewable Energy Catapult, Blyth, UK

## 2.1 Introduction

Wind turbines are complex systems that include mechanical, electrical, hydraulic and instrumentation sub-systems. Off-shore wind turbines include further complexities due to their distance from the shore and the cost of access and maintenance. Hence there is a need to develop Condition-Based Maintenance strategy in order to plan the required maintenance without reduction in the availability of the wind turbine. Corrective maintenance (operate to failure) is not an option as it could be costly process and given the sea and weather conditions, timely access for maintenance might not be possible. Particularly that off-shore wind turbines need specialised equipment and training. Preventive or scheduled maintenance means to schedule maintenance regardless of the conditions of the wind turbine; in most cases this will include significant additional costs and possibly unnecessary maintenance procedures and spare parts. For further generic descriptions of the three maintenance strategies, please refer to Graisa and Al-Habaibeh [1]. Therefore, The use of Condition-Based Maintenance is critical for the effective and commercially viable operation of wind turbines. When considering the key components and sub-systems of an off-shore wind turbine, see Fig. 2.1, it becomes apparent the complexity of the wind turbine and the need for condition-based maintenance to enhance productivity and reduce cost.

Numerous research work has been done to present sensor fusion for off-shore wind turbines. For example [2] has presented data fusion-based damage identification for offshore wind turbines; where a damage sensitivity index is suggested that is a function of the energy ratio between the acceleration and angular velocity. However, the proposed work had some limitations in the validation process and the limited number of signals. In reference [3] a fault diagnosis method for wind turbine gearbox bearings with fusion of vibration and current signals is presented. The results show that the proposed method can learn enhanced fault-related features particularly on compound faults. Reference [4] presents the use of ASPS approach for condition monitoring of helical gears using automated selection of features and sensors. The results show that the methodology can help sensor fusion by selecting the most sensitive sensors and signal processing methods to the detection of faults. A comprehensive literature review [5] has presented the challenges and opportunities for using artificial intelligence in the offshore wind sector. The survey concludes that the identification of technological priorities for the integration in off-shore wind turbines is still needed in order to deliver a better offshore wind farm lifecycle management. Based on the above, there is still a limitation of how to develop a suitable sensor fusion system for off-shore wind turbines due to the complex nature of the signals and the variability of operational parameters.

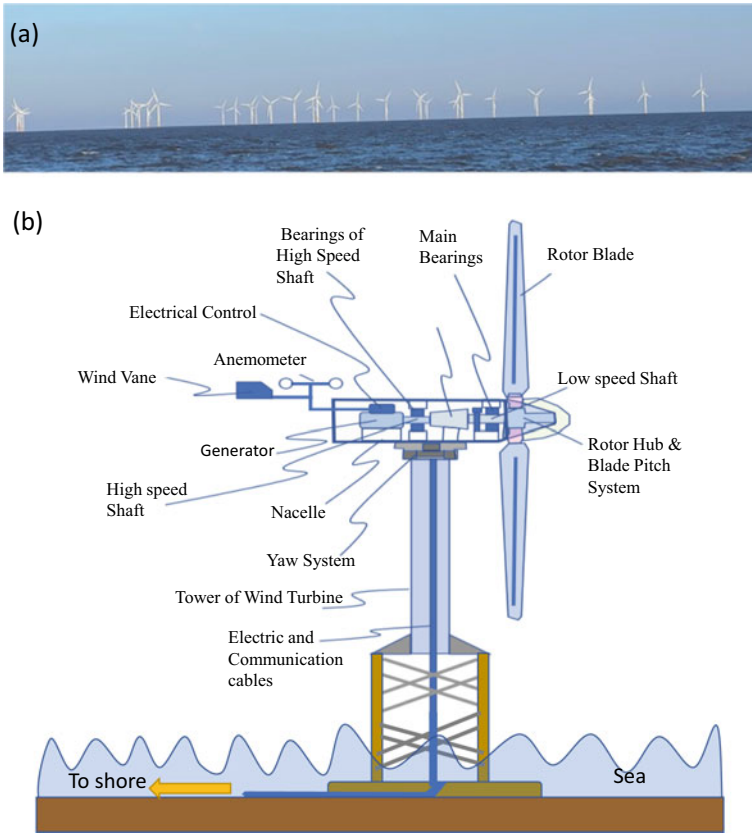


**Fig. 2.1** a Off-shore wind turbines, and b a simplified structure and key components of off-shore wind turbine

## 2.2 The Wind Turbine Under Consideration

The data considered for this paper is captured from the operation of a 7 MW wind turbine with a standard hub height of about 110 m above mean sea level and rotor diameter of about 171 m. It has a minimum rotor speed of 5.9 rpm and rated average rotor speed of about 10.6 rpm. The minimum wind speed of operation is 3.5 m/s and the maximum wind speed of operation is 25 m/s; with rated average wind speed of 13 m/s. The data provided by the SCADA system for this paper includes a wide range of sensory data, with a sampling rate of 1 sample per 10 min. Figure 2.2 presents the complexity of the of the sensory data captured from the SCADA system of the off-shore wind turbine between May 2017 and October 2018. The data includes 287 alarm signals, 388 electrical signals, 105 control signals, 321 temperature signals and 143 pressure signals. This is in addition to other signals. As presented in Fig. 2.2, mainly 6 groups of signals are captured via the SCADA system as shown in Fig. 2.2.



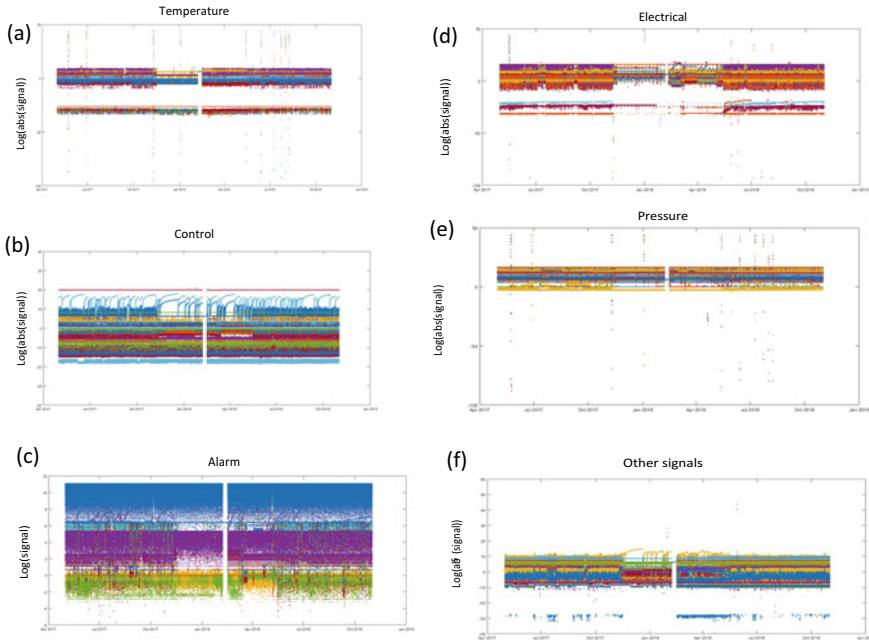


**Fig. 2.2** Examples of the sensory data captured from the SCADA system of the off-shore wind turbine between May 2017 and October 2018

The data in Fig. 2.2 is grouped as temperature (a), control (b), alarm (c), electrical (d), pressure (e) and other signals (f). Due to the variation in the data type and values, Eq. (2.1) is used to present the data as a normalised way to compare between the signals.

$$S = \log|x| \quad (2.1)$$

where  $S$  is the processed signal and  $x$  is the raw signal from the SCADA system.

Due to the complexity of the data, it is difficult to implement an artificial intelligence system without the use of a simplified methodology to detect the most suitable signals that have high sensitivity to a fault or group of faults. The ASPS approach suggested in [4] is implemented with some suitable modification. The implemented signal processing methods are: maximum, minimum, mean, standard deviation (std), Root mean square (RMS), maximum of absolute value max(abs), coefficient of variation, Skewness, Kurtosis, Crest, Clearance, RSS, Covariance, Interquartile, Range. For further details, see [6].

As presented in Fig. 2.3, the signal data is divided as ‘before’ and ‘after fault’, where after fault is a period after removing or dealing with an existing fault. A wide range of normalised features are extracted from the signals (before and after the fault) and the difference is compared to create a  $\Delta$  variable which is then used to populate

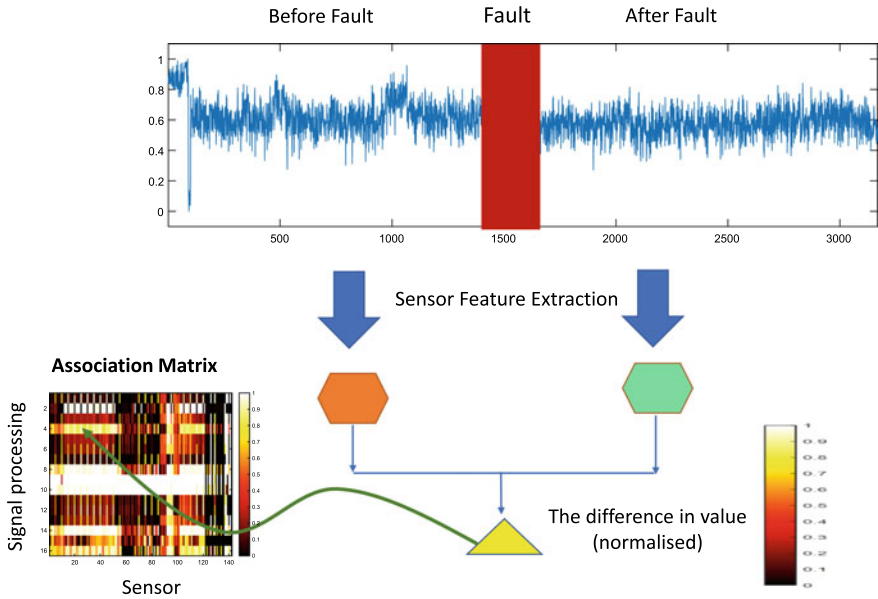


**Fig. 2.3** The adaptation of the ASPS approach to detect the difference in feature values due to a fault, or group of faults

an association matrix to present the change in a sensory characteristic feature ( $\Delta$  of a given sensor and signal processing method). In this case, the method attempts to recognise the most sensitive features to detect a fault uses a ‘black-box’ concept, which is based on the relationship between the inputs and outputs, without the need to fully analyse each signal or feature in relation to the fault.

### 2.3 Results and Discussion

In this case study of the off-shore wind turbine, some maintenance and faults were detected between the 6th of November and the 9th of November, therefore, we have selected two periods before and after the faults to see which signals have changed before and after those faults. This paper presents the concept and methodology in detail; and future work will include its relationship to the success of the artificial intelligent CBM system. Figure 2.4 presents the association matrix for the main 5 sensors categories. Each pixel in the association matrix presents the  $\Delta$  value of the sensitivity to a sensory signal and signal processing method (sensory characteristic feature) to the fault under consideration (before and after the faults). The data is normalised so that the maximum sensitivity is 1 and the minimum sensitivity is 0; with a colour map to reflect the values as suitable.

### Association Matrix of Sensitivity

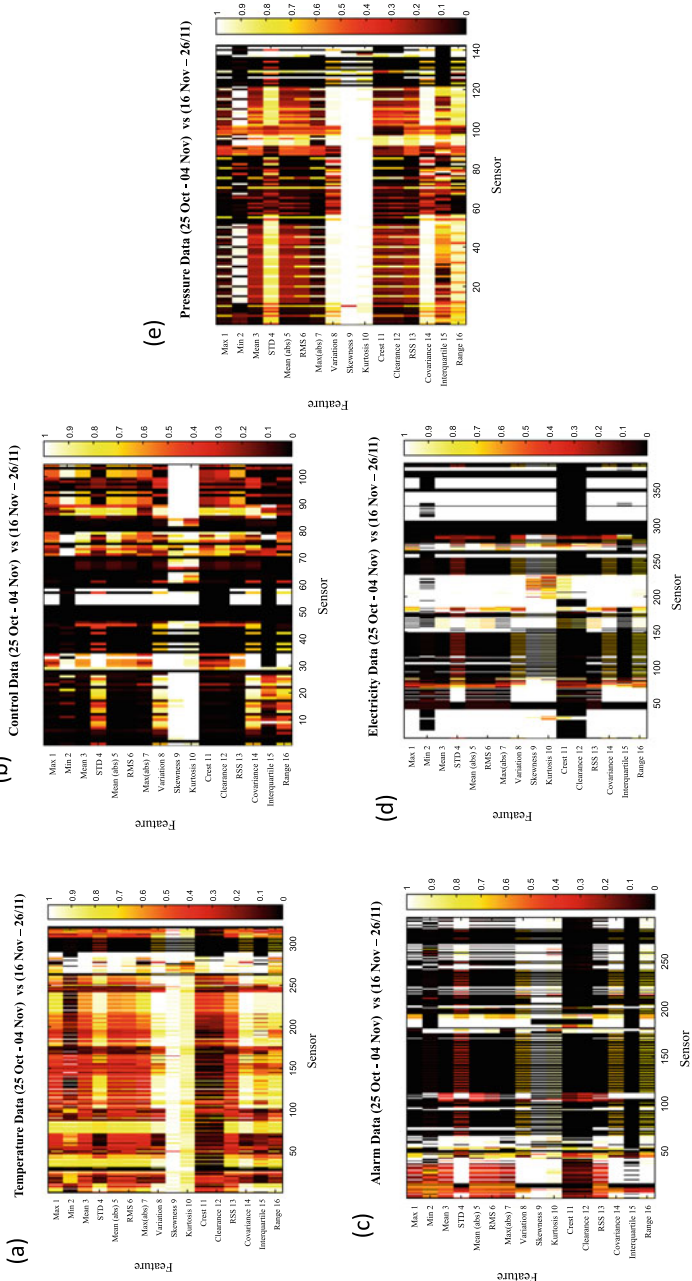
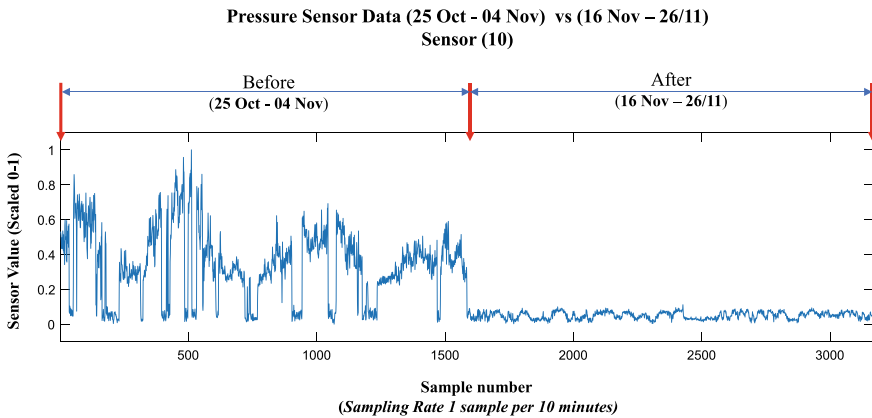


Fig. 2.4 The association matrix for the main 5 groups of sensory signals

When considering examples of the signals that have been identified to have the most sensitivity, Fig. 2.5 presents a pressure sensor which clearly shows a different behaviour or levels before and after the fault period. Similarly, Fig. 2.6 presents an example of one of temperature sensors which is found to be sensitive to the change in the conditions.

When the data in Fig. 2.6 is processed by the 16 signal processing methods presented above, Fig. 2.7 presents the comparison between ‘before’ and ‘after’ values and how the sensitivity of the sensory characteristic features is the calculated and normalised to create the association matrix.



**Fig. 2.5** One of the pressure sensors that was detected to have high sensitivity and its values before and after the fault generation

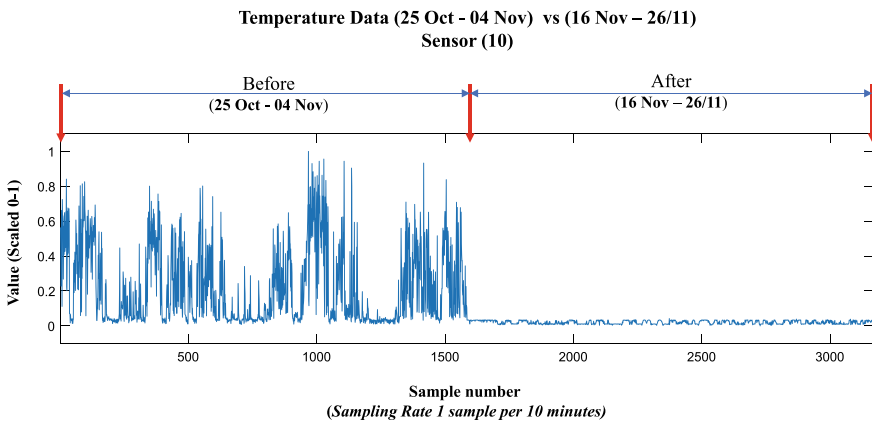


**Fig. 2.6** A Temperature sensor which has been found to have high sensitivity and its values before and after the fault generation

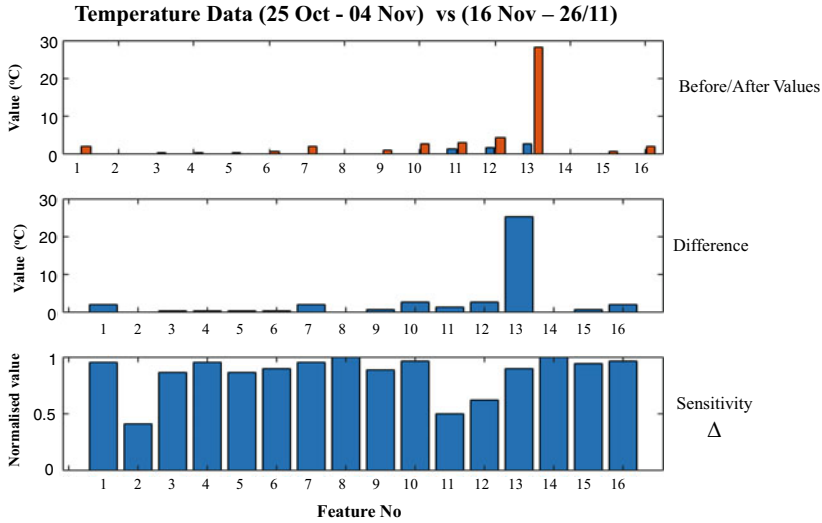


**Fig. 2.7** The way the sensitivity of the sensory characteristic features are calculated and introduced to the association matrix

## 2.4 Conclusion and Future Work

When an off-shore wind turbine presents over 1254 sensory signals, it is become difficult to select the most sensitive ones for a specific fault or group of faults, particularly with the complex operational conditions of wind turbines. Hence, the implementation of artificial intelligence system becomes a challenging task. To enhance the design and reliability of artificial intelligence system, the selection of the most sensitive sensory signals and signal processing methods is needed. In this paper, the authors use a modified ASPS approach [4] for the selectin of the most sensitive sensory characteristic features before and after a fault, or group of faults. The results show that the suggested methodology is able to detect the sensitive sensors to enable in the future the design and implementation of a reliable Condition-Based Maintenance strategy using artificial intelligence.

**Acknowledgements** The authors would like to thank Innovate UK and EPSRC for funding this research work; grant Reference EP/S515711/1.

## References

1. M. Graisa, A. Al-Habaibeh, An investigation into current production challenges facing the Libyan cement industry and the need for innovative Total Productive Maintenance (TPM) strategy. *J. Manuf. Technol. Manage.* **22**(4), 541–558. ISSN 1741–038X

2. S. Jeong, E.J. Kim, D.H. Shin, J.W. Park, S.H. Sim, Data fusion-based damage identification for a monopile offshore wind turbine structure using wireless smart sensors. *Ocean Eng.* **195**, 2020, 106728, ISSN 0029-8018, <https://doi.org/10.1016/j.oceaneng.2019.106728>
3. J. Guoqian, J. Chenling, N. Shiqiang, W. Xin, H. Qun, X. Ping, Multiview enhanced fault diagnosis for wind turbine gearbox bearings with fusion of vibration and current signals. *Measurement* **196**, 2022, 111159, ISSN 0263-2241,
4. H. Alkhadafe, A. Al-Habaibeh, A. Lotfi, Condition monitoring of helical gears using automated selection of features and sensors. *Measurement*, **93**, 164–177, ISSN 0263-2241, <https://doi.org/10.1016/j.measurement.2016.07.011>
5. D. Mitchell, J. Blanche, S. Harper, T. Lim, R. Gupta, O. Zaki, W. Tang, V. Robu, S. Watson, D. Flynn, A review: challenges and opportunities for artificial intelligence and robotics in the offshore wind sector. *Energy AI* **8**, 100146, ISSN 2666-5468
6. M. Vetterli, J. Kovačević, V.K. Goyal, *Foundations of Signal Processing*, Cambridge University Press, 3rd edn. 9/4/2014, EAN 9781107038608, ISBN10: 110703860

**Open Access** This chapter is licensed under the terms of the Creative Commons Attribution 4.0 International License (<http://creativecommons.org/licenses/by/4.0/>), which permits use, sharing, adaptation, distribution and reproduction in any medium or format, as long as you give appropriate credit to the original author(s) and the source, provide a link to the Creative Commons license and indicate if changes were made.

The images or other third party material in this chapter are included in the chapter's Creative Commons license, unless indicated otherwise in a credit line to the material. If material is not included in the chapter's Creative Commons license and your intended use is not permitted by statutory regulation or exceeds the permitted use, you will need to obtain permission directly from the copyright holder.



# Chapter 3

## CFD Based Aerodynamics Conjugate Heat Transfer and Airgap Fluid Flow Thermal Analysis to a Wheel Hub Motor for Electric Scooters



A. M. Divakaran, E. Abo-Serie, E. I. Gkanas, J. Jewkes, and S. Shepherd

**Abstract** The geometry of commercially available wheel hub motors inherently restricts packaging space and may prevent the introduction of more sophisticated, efficient, and expensive cooling systems. Due to the limited available space in the wheels, commercial hub motors often rely on aerodynamic passive cooling. The small air-gap (0.5–1 mm) between the coils and the magnets results in heat transfer to the magnets and consequently increases their temperature. As a result, the performance of the permanent magnets (PMs) will be limited and also will heavily affect their lifetime; thus, advanced cooling strategies must be introduced. In the current study, a three-dimensional (3D) thermal model was developed for a commercially available 500 W scooter hub motor under a constant heat load of 180 W using Computational Fluid Dynamics (CFD) (= 64%). The spatial distribution of the temperature for the motor parts are evaluated considering both the internal and external fluid flow dynamics. Further, analysis of airflow in the the gap is performed and the results from the CFD is compared with the published correlations. The flow in such small motor was found to be laminar with Taylor number below 40. Results also showed that enhancement of the cooling is necessary to avoid damage of the winding vernish and to reduce the magnets temperature particularly when the motor works at high torque with low efficiency.

**Keywords** Thermal management · Computational fluid dynamics · Taylor's correlations · Outer-rotor machines

---

A. M. Divakaran (✉) · E. I. Gkanas · S. Shepherd  
Institute of Future Transport and Cities, Centre for Advanced Low Carbon Propulsion System,  
Coventry University, Coventry, UK  
e-mail: [mambazhasa@uni.coventry.ac.uk](mailto:mambazhasa@uni.coventry.ac.uk)

E. Abo-Serie · J. Jewkes  
School of Engineering, The University of Leicester, Leicester, UK

### 3.1 Introduction

An effective thermal management system can improve the efficiency, stability, and lifespan of the traction motors used in electric vehicles. So, it is essential to study and evaluate the cooling performance of such machines at different operating conditions. PM based brushless DC wheel hub motors have many advantages such as higher efficiency and power density, simplified transmission link, better power output control, and more space in the vehicles. Nevertheless having effective cooling is one of the major challenges [1]. A significant number of publications are available on the various cooling techniques used in electrical machines but very few on cooling wheel hub motors [2–4]. The techniques focus on ensuring adequate heat dissipation from the electric coils as a source of heat to the surrounding air by creating low thermal resistance path that should be away from the magnets locations for the heat to be dissipated. Effective cooling helps to achieve the cooling system goal of lowering the temperature of the sensitive components such as the windings and PMs, and also the bearings [5]. The hub motor heat transmission was successfully modeled by Fasil et al. [6] using computational fluid dynamics (CFD), finite element (FE), and lumped parameter (LP) models investigated the heat dissipation in wheel hub motor. They used LP model to calculate the temperature of the components in the motor and validated it with the FE method and CFD for investigating the internal and external flow analysis and convective heat transfer for the wheel motor. The electrical machines can be broadly classified into two major types, totally enclosed and ventilated and the cooling need to be adjust for each type. Air-gap is a very important parameter for motor performance and it is not possible to change for cooling purposes. However, the characteristics of the flow and heat flux distribution is very crucial as it can affect the performance of the magnets. Depending on the motor size and operating conditions, the size of the air-gap between the stator and the rotor varies for different types of machines. Small or light duty machines have a small airgap (0.5–1 mm) to reduce electromagnetic losses, while heavy duty machines have a large air gap to lessen drag due to the high magnetic field [7]. It is difficult to capture the physics of fluid flow in an airgap, however there have been efforts towards the development of empirical correlations for both the spinning inner cylinder and stationary outer cylinder [8, 9]. Effective thermal management, or how well the temperature is kept below the thermal limit of the PMs (150 °C), determines the machine's lifespan and performance [8].

The flow characteristics in the air gap region of cylindrical machines can be determined with the non-dimensional Taylor number ( $Ta$ ). The Taylor number provides a relative effect of inertial and viscous force for annulus fluid flow between rotating cylindrical surfaces. When the fluid flow dynamics is laminar, conduction is only the mode of heat transfer in the air gap for low-speed operation ranges below 1000 RPM. The creation of vortices and turbulent flow, which appear at 1300 RPM and 4600 RPM, results in an increase in heat transfer (for a 1 mm air gap). When the  $Ta$



is less than 41, the flow is laminar, and the “Nu” is 2, indicating that heat transfer is only with conduction and when the  $Ta$  is between 41 and 100, when the flow changes to a vortex, and when the  $Ta$  is greater than 100, the flow becomes turbulent [9].

Howey and Holmes [8] reviewed the nondimensional parameters for both the cylindrical and disc-type machines with worked-out examples. The main outcome of this study was that for accurate thermal modelling of the electrical machines the knowledge of surface or air gap convective heat transfer is essential. On another study the authors reviewed many non-dimensional parameters and most commonly used heat transfer correlations for various gap sizes [9]. They also highlighted the effect of slots on the cylindrical surface to the non-dimensional numbers in comparison with a smooth cylinder of the same size. Considering this, Hosain et al. [10] investigated the effect of Taylor vortices on the heat transfer in the air gap region for a cylindrical inner rotor machine. They validated the numerical simulation results with the empirical correlation results and pinpointed the periodic temperature and heat transfer pattern. The air gap in axial flux motors represents heat transfer between two concentric cylinders, many published literature can be found representing the inner cylinder rotating and stationary outer cylinder [11]. But in hub motors, the outer cylinder is rotating and the inner cylinder is stationary. In [8], the authors reviewed the correlations for dimensionless quantities, cylindrical machines and disc-type machines. However, the application of these correlation to estimate the non dimensional quantities in the air-gap for a wheel hub brushless dc machine has not been investigated.

In this paper, a wheel hub motor commonly used in electric scooters has been investigated for conjugate heat transfer for a steady state heat loss of 180 W in the windings. The continuous power rating and electrical specification of the motor is 500 W, 3-phase 48 V. The topology of the hub motor is outer rotor axial flux PM brushless DC machine, Figs. 3.1a and 3.2a. The stator core consist of windings and the shaft and the rotor comprises of permanent magnets, sleeve and rotor body. An air-gap of 0.5 mm exists between the rotor and and stator. A computational fluid dynamics (CFD) based study has been carried out to assess the heat transfer from the winding (source) to the ambient air and to investigate the small air-gap fluid flow. Nusselt number (Nu) and heat transfer coefficient at the air gap has determined numerically with CFD analysis, and compared, validated with the correlations in the published literature.

## 3.2 Methodology

The design geometry used in the current study is for conjugate heat transfer assessment and verification, which resembles a small wheel hub motor used in electric scooters. The purpose of using the complete design geometry of the motor is to investigate the heat transfer mechanism in the wheel hub motor and to determine the heat transfer coefficient on the rotor surface. The components of the motor geometry considered for the setting up the thermal model has all the components as shown in Fig. 3.1. Conformal meshing is achieved with a polyhedral prism layer mesh, the

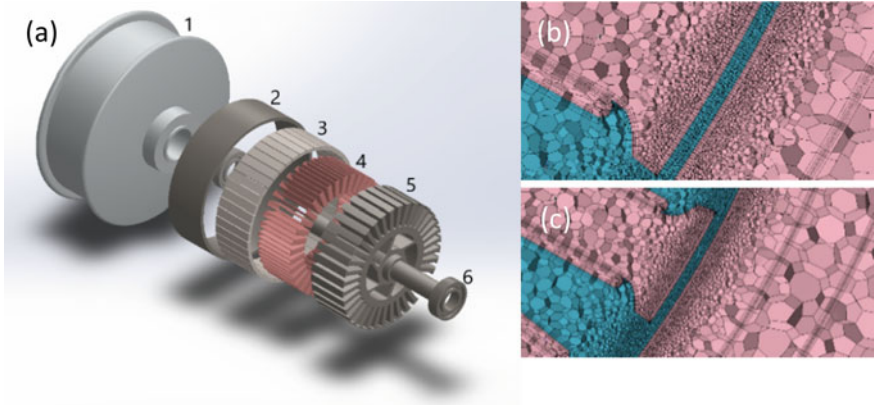


**Fig. 3.1** Shows the geometry of the motor considered for the simulation **a** 3D CAD exploded view 1. Rotor 2. Rotor sleeve or rotor core 3. PMs 4. Windings 5. Stator and shaft 6. Bearings, **b, c** Small section of meshing the fluid and solid domain with air gap refinement (33 million cells)

mesh domain contains 33 million cells with very fine prism layers at the solid–fluid interface and the air-gap region, Fig. 3.1b, c. The computational domain includes the external fluid domain, rotating region, internal fluid and solid domain, and the components of the motor are shown in 3.2b. The motor stator consists of the motor windings, stator and shaft and the rotor consist of a permanent magnet, sleeve, rotor and bearings. A rotating region is created around the rotor that rotates at a speed of 482 rpm with no-slip boundary conditions at the solid–fluid interfaces.

The rotational reference frame is set at the appropriate solid–fluid interface with no-slip boundary conditions to generate the velocity gradient. Both internal and external fluid flow are considered in the simulation to make the conjugate heat transfer simulation analysis more realistic. Outer walls of the ambient fluid domain are set at a velocity inlet (0.5 m/s), pressure outlet, and convection boundary conditions (20 °C, 20 W/m<sup>2</sup>K). A constant heat generation of 180W is assigned to the copper winding as one block which is calculated based on total heat loss in the motor (assuming  $\eta=64\%$ ). This is considered as a worst case scenario. Steady-state Realizable k-epsilon turbulence model with coupled solid energy physics was used to model the turbulence together with enhanced wall treatment. A mesh independent study was performed at an early stage of this study.

To compare CFD results in the air-gap the following dimensionless parameters have been used [5]

$$Nu = \frac{hD_h}{k} \quad (3.1)$$

$$T_{am} = \frac{\omega_a R_m^{0.5} (b-a)^{1.5}}{v} \quad (3.2)$$

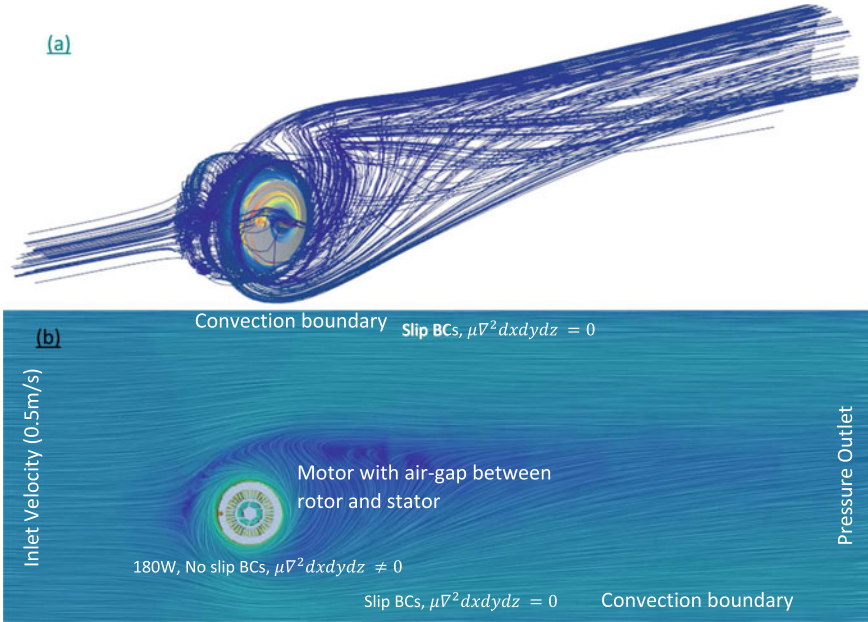


**Fig. 3.2** Shows the simulation domain and fluid flow. **a** Streamlines on the external motor surface **b** Shows the simulation domain with boundary conditions (whole domain resulted in 33 Million cells)

$$F_g = \frac{\pi^2}{41.19\sqrt{S}} \left( 1 - \frac{(b-a)}{2R_m} \right) \tag{3.3}$$

$$S = 0.0571 \left( 1 - 0.652 \frac{\frac{(b-a)}{R_m}}{1 - \frac{(b-a)}{2R_m}} \right) + 0.00056 \left( 1 - 0.652 \frac{\frac{(b-a)}{R_m}}{1 - \frac{(b-a)}{2R_m}} \right)^{-1} \tag{3.4}$$

$$\frac{T_{am}^2}{F_g^2} < 1700; \text{ the flow is laminar} \tag{3.5}$$

$$1700 < \frac{T_{am}^2}{F_g^2} < 10^4; \text{ the flow is laminar with vortices} \tag{3.6}$$

where,  $T_{am}$  is the Taylor number,  $Nu$ —Nusselt number,  $h$ —heat transfer coefficient ( $W/m^2K$ ),  $D_h$ —hydraulic diameter (m),  $\omega_a$ —angular speed in rad/sec,  $k$ —thermal conductivity ( $W/mK$ ),  $R_m$ —mean radius ( $(a + b)/2$ ),  $b$ —outer cylinder radius (m),  $a$ —inner cylinder radius (m),  $F_g$ —geometric factor.

### 3.3 Results and Discussion

When the heat loss in the winding is 180 W ( $\eta = 64\%$ ) at 482 RPM, the maximum temperature in the winding was 325 °C. The temperature drops to 266 °C when the speed of the motor doubled (964 rpm) as shown in Fig. 3.3a, b . The maximum temperature in the winding is beyond the thermal limit of all the classes of insulation materials available in the market (maximum hotpoint temperature 240 °C). The temperature rise beyond the thermal limit damages the insulation and also results in demagnetization of the PMs [12]. Clearly this mode of motor operation at low rpm and low efficiency require an efficient thermal management system. The heat transfer coefficient ( $h$ ) for the rotor surface is found to vary between 0-175 W/m<sup>2</sup>K at 482 rpm and 0-330 W/m<sup>2</sup>K at 964 rpm. However, the average surface ' $h$ ' on the rotor is 16.2 W/m<sup>2</sup>K and 24.7 W/m<sup>2</sup>K at 482 rpm and 964 rpm respectively, Fig. 3.4a, b. A wide range in ' $h$ ' value is observed on the rotor surface, which is due to the presence of one fin and one air-vent on the rotor surface, which has been introduced for design manager study which is not within the scope of this study.

The Nusselt number and heat transfer coefficient in the air gap is determined using heat flux and the temperature difference between the air gap fluid volume and rotor surface. The calculated Taylor number ( $Ta$ ) for the two simulation conditions is 6.7 and 13.4 which is less than 41. Therefore no vortices are expected to be formed inside the airgap and the flow is laminar.

The Nusselt number for this type of flow is approximately 2 and the heat transfer in the gap can be considered as conduction. With further increase in the angular speed of the motor, the ' $Ta$ ' will also increase and can exceed the critical value at an extremely higher speed of 4500 rpm or more which is higher than the operating range of this machine., shows the simulation values for the ' $Nu$ ' and ' $h$ ' which are

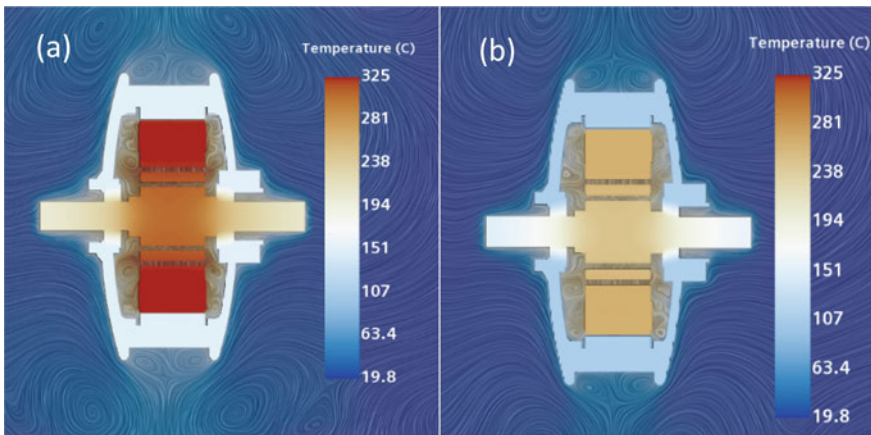


**Fig. 3.3** Shows the temperature distribution on a section plane at 180 W heat load in the hub motor **a** the temperature profile for 482 rpm **b** the temperature profile at 964 rpm

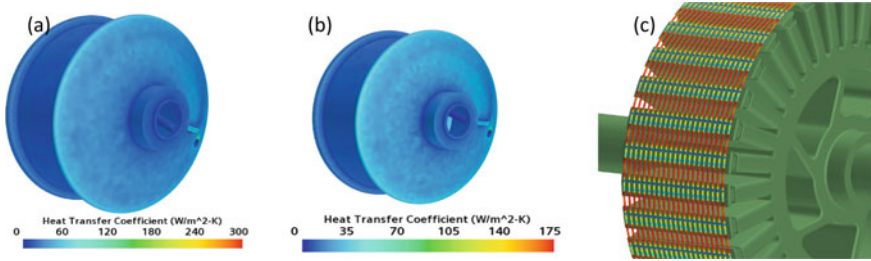


**Fig. 3.4** Shows the heat transfer coefficient on the surface of the rotor and air gap fluid flow, **a, b** the rotor surface heat transfer coefficient at 482 rpm and 964 rpm respectively **c** shows the streamline of the fluid particle in the air-gap at 482 rpm

**Table 3.1** Shows the  $Nu$ ,  $h$  and  $h_{avg}$  calculated numerically and with the correlations

Quantities	482 rpm		964 rpm	
	Simulation	Correlation	Simulation	Correlation
$Nu$ (air gap)	1.77	2.0088	1.93	2.009
$h$ (air-gap, $W/m^2K$ )	46.3	50.23	50.3	50.23
$h_{avg}$ (rotor surface, $W/m^2K$ )	16.2	–	24.7	–

numerically determined and compared with the correlations values. The correlations in both cases show a variation of 8.5% because the correlation for Nusselt number in laminar flow only depends on the rotor and stator radius. In fact the Nusselt number depends on the angular velocity of the fluid flow which resulted in slight variation in the values calculated numerically with that of correlations. These values shows an overall good agreement (Table 3.1).

### 3.4 Conclusion

In the current work, the conjugate heat transfer across the motor from the winding to the ambient temperature was studied, providing detailed insight into the heat transfer and fluid flow inside the air-gap. The model and assessment predict overall heat transfer and Nusselt number in the air gap with good agreement to the correlation values. The simulation results also point out the rotor surface heat transfer coefficient which will be taken into consideration as boundary conditions for the further studies. This validation study gives an insight and understanding of the heat transfer and fluid dynamics which serves as a baseline results for further development of advanced aerodynamic cooling for the wheel hub motors. The baseline design shows that the motor may fail if it works at low rpm with high torque due to the high temperature of the coils. Next stage of the research study will be mainly focussing on the experimental validation of the simulation model for a constant power loss

and also investigate the effect of design modifications with the fins and air-vents on the surface of the rotor. Additionally, the optimization of the air-vents for maximum heat transfer from the windings to the ambient air could significantly bring down the temperature hike in the windings.

## References

1. B. Gombert, R. Fischer, W. Heinrich, Wheel-hub motors. Criteria of construction and vehicle integration; Elektrische Radnabenmotoren. Konstruktionskriterien und Fahrzeugintegration' (2010)
2. J. Huang et al., A hybrid electric vehicle motor cooling system—Design, model, and control. *IEEE Trans. Veh. Technol.* **68**(5), 4467–4478 (2019)
3. Z. Huang, F. Marquez, M. Alakula, J. Yuan, Characterization and application of forced cooling channels for traction motors in HEVs, in *2012 XXth International Conference on Electrical Machines* (2012), pp 1212–1218
4. L. Wang, W. Haifeng, Steady-state thermal simulation of the stator coil of the evaporative inner cooling system in wind turbines, in *2012 IEEE 6th International Conference on Information and Automation for Sustainability*, 2012, pp. 248–251
5. S. Nategh et al., A review on different aspects of traction motor design for railway applications. *IEEE Trans. Ind. Appl.* **56**(3), 2148–2157 (2020)
6. M. Fasil, D. Plesner, J.H. Walther, N. Mijatovic, J. Holbøll, B.B. Jensen, Numerical and experimental investigation of heat flow in permanent magnet brushless DC hub motor. *SAE Int. J. Altern. Powertrains* **4**(1), 46–57 (2015)
7. T. Jokinen, V. Hrabovcova, J. Pyrhonen, *Design of Rotating Electrical Machines*. John Wiley & Sons, 2013.
8. D.A. Howey, P.R. Childs, A.S. Holmes, Air-gap convection in rotating electrical machines. *IEEE Trans. Ind. Electron.* **59**(3), 1367–1375 (2010)
9. R. Wrobel, P.H. Mellor, N. McNeill, D.A. Staton, Thermal performance of an open-slot modular-wound machine with external rotor. *IEEE Trans. Energy Convers.* **25**(2), 403–411 (2010)
10. M.L. Hosain, R.B. Fdhila, K. Rönnerberg, Air-gap flow and thermal analysis of rotating machines using CFD. *Energy Procedia* **105**, 5153–5159 (2017)
11. G.I. Taylor, Distribution of velocity and temperature between concentric rotating cylinders. *Proc. R. Soc. Lond. Ser. Math. Phys. Sci.* **151**(874), 494–512 (1935)
12. Y. Yang et al., Thermal management of electric machines. *IET Electr. Syst. Transp.* **7**(2), 104–116 (2017)

**Open Access** This chapter is licensed under the terms of the Creative Commons Attribution 4.0 International License (<http://creativecommons.org/licenses/by/4.0/>), which permits use, sharing, adaptation, distribution and reproduction in any medium or format, as long as you give appropriate credit to the original author(s) and the source, provide a link to the Creative Commons license and indicate if changes were made.

The images or other third party material in this chapter are included in the chapter's Creative Commons license, unless indicated otherwise in a credit line to the material. If material is not included in the chapter's Creative Commons license and your intended use is not permitted by statutory regulation or exceeds the permitted use, you will need to obtain permission directly from the copyright holder.



# Chapter 4

## Learning from the Past for a Sustainable Future: Environmental Monitoring and 3D Modelling to Assess the Thermal Performance of Heritage Buildings



D. Antón, Amin Al-Habaibeh, and T. Queiroz

**Abstract** There are numerous lessons to be learned from historic buildings, such as the rich diversity of their traditional architecture, the use of natural and local materials, their durability and resilience, or because they allow for thermal comfort in severe climatic and weather conditions. Today, many of these heritage buildings are still standing and in use, but their shape may have changed significantly from when they were built. In this sense, to accurately analyse historic buildings, 3D models that approximate their geometry (as-is/as-built models) must be produced. Based on terrestrial laser scanning 3D point clouds, as-is 3D modelling can represent the geometrical alterations of the assets to enable diverse analyses and simulations. This work addresses Ye Olde Trip to Jerusalem building, claimed to be the oldest inn in England, UK (1189 AD). Hence, this historic building presents numerous deformations such as warped and tilted walls, recess in walls, non-planar ceilings, and an irregular arrangement of bent ceiling beams. This Grade II listed building is located near Nottingham Castle, beneath Castle Rock, the natural promontory on which the castle is situated. A part of the inn is inside rock-hewn caves under Castle Rock, making it a unique landmark with special indoor thermal conditions.

---

D. Antón (✉) · A. Al-Habaibeh

Product Innovation Centre, Department of Product Design, School of Architecture, Design and the Built Environment, Nottingham Trent University, 50 Shakespeare Street, Nottingham NG1 4FQ, UK

e-mail: [daniel.antongarcia@ntu.ac.uk](mailto:daniel.antongarcia@ntu.ac.uk); [danton@us.es](mailto:danton@us.es)

A. Al-Habaibeh

e-mail: [Amin.Al-Habaibeh@ntu.ac.uk](mailto:Amin.Al-Habaibeh@ntu.ac.uk)

*Present Address:*

D. Antón

Departamento de Expresión Gráfica e Ingeniería en la Edificación, Escuela Técnica Superior de Ingeniería de Edificación, Universidad de Sevilla, 4A Reina Mercedes Avenue, 41012 Seville, Spain

T. Queiroz

4D Virtual Lab Ltd. Unit 24 Wilford Business Park, Ruddington Lane, Nottingham NG11 7EP, UK



Due to the complex geometry of the building, laser scanning-based 3D modelling is found essential to communicate the building's features to help understand its thermal behaviour. This paper aims to investigate how Ye Olde Trip to Jerusalem building is capable of regulating indoor temperature and humidity in different locations, for which the as-is 3D modelling and environmental monitoring of this historic building are discussed. Based on the findings, the lessons learnt from studying old buildings could be utilised to enhance the sustainability of modern buildings.

**Keywords** 3D scanning · Geometrical alterations · Sustainability · Thermal comfort · Historic buildings

## 4.1 Introduction

There are numerous lessons to be learned from historic buildings, such as the rich diversity of their traditional architecture, the use of natural and local materials, their durability and resilience, or because they allow for thermal comfort in severe climatic and/or weather conditions [1–3]. Today, many of these heritage buildings are still standing and in use, but their shape may have changed significantly from when they were built. In this sense, to accurately analyse these assets, 3D models that approximate the geometry of historic buildings—so-called as-is or as-built models [4]—must be produced. Based on terrestrial laser scanning 3D point clouds, as-is 3D modelling can represent the geometrical alterations of the assets. This enables diverse analyses and simulations.

However, current modelling and analysis of historic buildings are usually based on ideal or excessively simplified geometries [5]. This includes non-deformed 3D models generated from traditional measurement methods data; also, those models developed using Terrestrial Laser Scanning (TLS) point clouds as a reference to create the 3D objects defining the buildings instead of implementing some degree of automation to use those spatial data to represent the geometrical alterations of the buildings. Antón et al. [6] described that the 3D models produced may not represent the real condition of these assets, their features, and/or singularities. Furthermore, the analysis outcomes may not fully represent the actual performance of these heritage assets if those geometrical alterations are not modelled.

This work addresses the case study of the Ye Olde Trip to Jerusalem building, claimed to be the oldest inn in England (UK), dating back to 1189 AD. Therefore, this historic pub presents numerous and significant deformations such as warped and tilted walls, recess in walls, non-planar ceilings, and an irregular arrangement of bent ceiling beams. This Grade II listed building [7] is located near Nottingham Castle, beneath Castle Rock, the natural sandstone promontory on which the castle is situated. A part of the inn is inside rock-hewn caves under Castle Rock, making it a unique landmark with special indoor thermal conditions.

Research has been found that there are many lessons to be learnt from heritage buildings towards future sustainability in modern buildings [8, 9]. This paper aims to assess the thermal regulations of different sections of the building and the way they can regulate indoor temperature and relative humidity with particular interest to the cave section, for which the as-is 3D modelling and environmental monitoring of this historic building are discussed.

The rest of this paper is organised as follows: the methodology is described in Sect. 4.2, comprising the approach, equipment, and statistical analysis for the thermal performance assessment; the as-is 3D modelling approach is also explained. Next, Sect. 4.3 presents and discusses the modelling results and the temperature (T) and relative humidity (RH) data from the sensors installed. The conclusions of this research are drawn in Sect. 4.4.

## 4.2 Methodology

With a view to assess the thermal performance of Ye Olde Trip to Jerusalem building, ambient temperature and humidity sensors were used, see Fig. 4.1. This environmental monitoring characterises the indoor and outdoor hygrothermal conditions of this singular heritage building, thus revealing users' comfort inside. To do this, three OMEGA temperature and humidity data loggers (OM-CP-RHTEMP101A) were used. As shown in Fig. 4.1c, two were installed inside the building: the first (ID 1\_Cave) was attached to the cave wall in the top-floor room; the second sensor (ID 2\_ColdRoom), was in the downstairs room (with three walls facing the exterior) of the highest body of the building. The rooms monitored were not cooled nor heated. Finally, the third sensor (ID 3\_Exterior) was installed outside, under the roof eaves, and protected from direct sunlight, wind, and rain. The thermal monitoring details were as follows:

- Start date and time: 24/06/2022; 10:30 am.- Duration: 14 days
- End date and time: 08/07/2022; 10:30 am. - Reading interval: 15 min.

Next, in order to compare the data from the three sensors, and thus characterise the rooms against each other and the exterior, statistical data were calculated from the temperature and humidity values. This included the maximum, minimum, and average values; the distribution analysis through the standard deviation and the coefficient of variation (standard deviation divided by the mean); and the covariance, and correlation coefficient to evaluate the relationship between the two variables (temperature and relative humidity).

In relation to the as-is 3D modelling of Ye Olde Trip to Jerusalem building, TLS technology was first used to record the geometry of this case study. The 3D survey

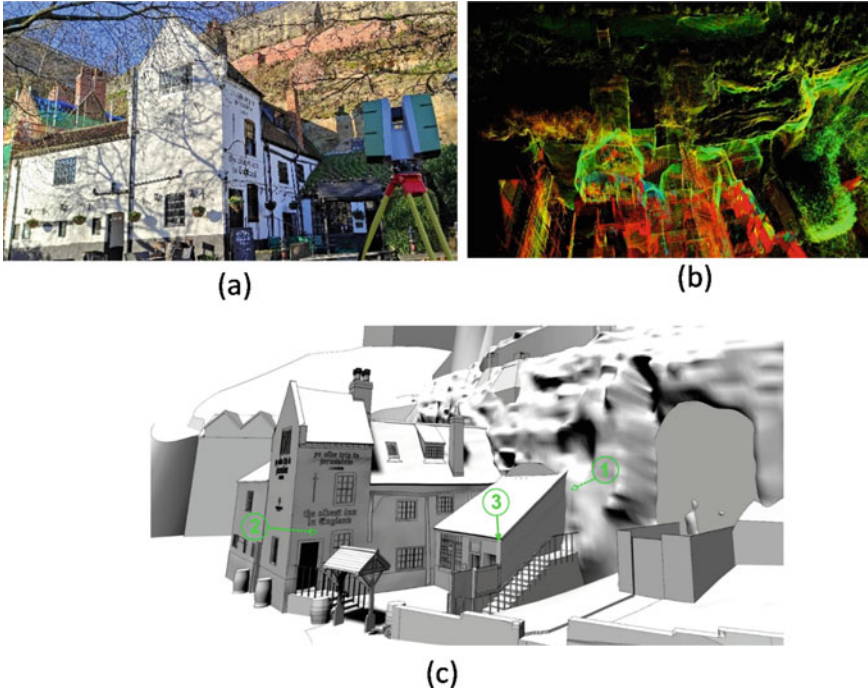


**Fig. 4.1** a Photograph of Ye Olde Trip to Jerusalem and TLS device; b 3D point cloud data with intensities; c As-Is 3D model with installed sensors

consisted of 31 stations (or scan positions) throughout the building and its surroundings, strategically set to avoid laser beam occlusions. The scanning resolution was set to 6 mm at 10 m. Following the recording, the 31 individual clouds were (1) automatically registered, i.e., aligned and merged in the same global coordinate system through cloud constraints set in Leica Cyclone software, (2) segmented to remove noise and undesired elements, and (3) subsampled to 20 mm to ease data processing. Later, GPS data were collected to geo-reference the global 3D point cloud.

Once the data were obtained, the as-is 3D modelling took place. To do this, manual and semi-automatic processes were implemented to create its building components. This was achieved by using the point clouds in CloudCompare software to produce 3D polygon meshes defining the cave surface. To build warped walls and other large, deformed components, Rhinoceros software was used to (1) create non-planar surfaces automatically fitting the building's wall faces point clouds, (2) ensure a close volume defining the wall shape, and (3) producing a solid object from it. Finally, extruding planar surfaces from contours also produced solid objects.

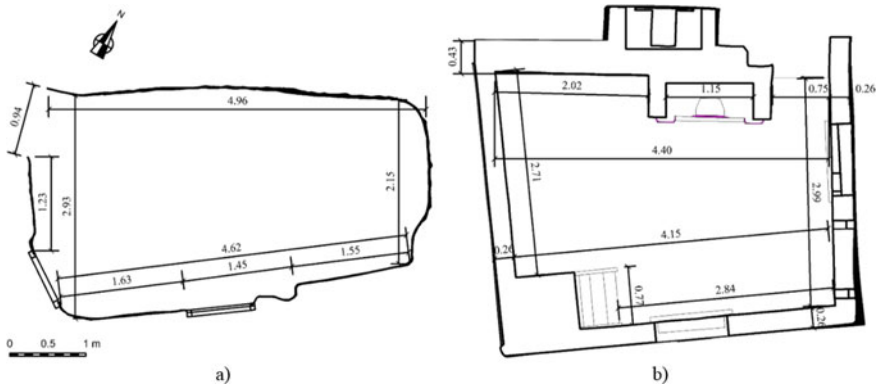


**Fig. 4.2** Floorplans: **a** cave room upstairs (sensor 1); **b** cold room downstairs (sensor 2)

## 4.3 Results and Discussion

### 4.3.1 As-Is 3D Modelling

Focusing on the digital reconstitution of the case study, Fig. 4.1 shows the combination of the manual and semi-automatic approaches to produce its as-is 3D model. The location of each sensor is also indicated in the image above. The level of detail of the surroundings is lower than that of the inn so that the computational resources in 3D visualisation are reduced. After all, the building's geometry was given greater importance.

Despite a thoroughly planned 3D survey, furniture, and decorative elements inside and outside the building implied laser beam occlusions. As a result, the 3D point cloud presented certain gaps (lack of points) that did not allow for 3D meshing all wall faces and ceilings. Consequently, the creation of best-fit non-planar surfaces led to represent the geometrical alterations of this heritage building. The as-built 3D modelling enabled accurate measurements of each room. Figure 4.2 displays the floorplan of each room monitored as indicated in Fig. 4.1. The volume of the rooms is  $31.79 \text{ m}^3$  and  $29.30 \pm 1.1 \cdot 10^{-5} \text{ m}^3$ , respectively.

### 4.3.2 Environmental Monitoring

The three OMEGA sensors collected 1345 temperature and relative humidity (two channels) recordings each in the time interval set (14 days). Graphs displaying the data from sensors 1, 2, and 3 are given below (see Figs. 4.3, 4.4, and 4.5).

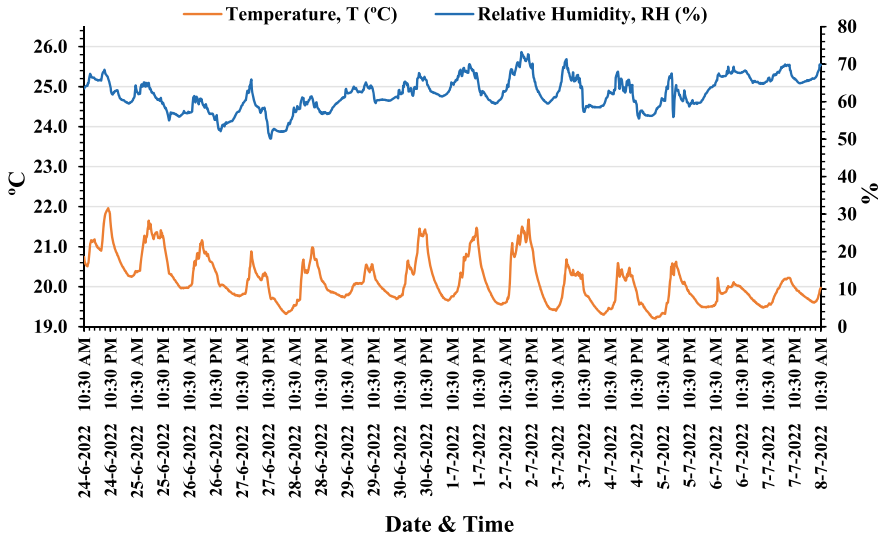


Fig. 4.3 Temperature and relative humidity from sensor 1 (The cave section)

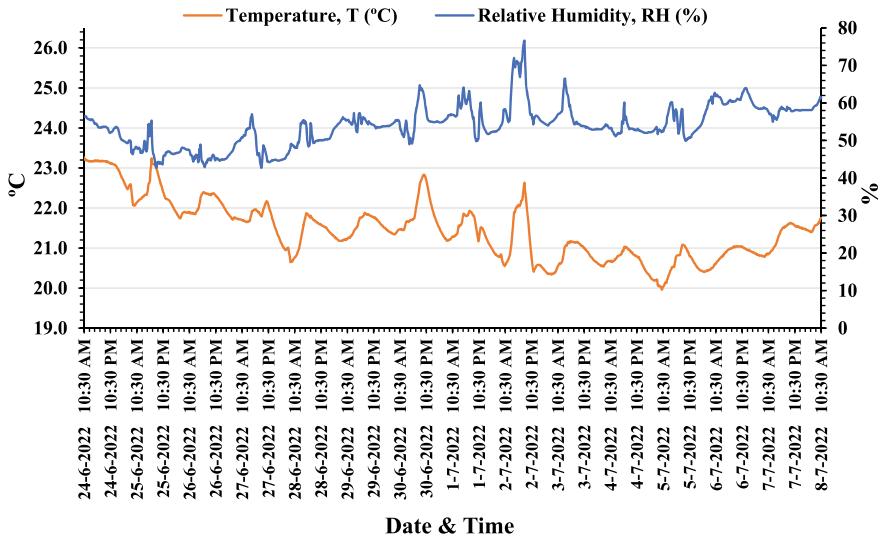


Fig. 4.4 Temperature and relative humidity from sensor 2 (The cold-room)

It is worth noting that building occupation was not considered, although the inn's opening and closing time was from 11am to 11 pm from Monday to Sunday, which may have an impact on the data. The statistical data from the sensors' recordings are presented in Table 4.1, where the highest values appear in bold for clarity.

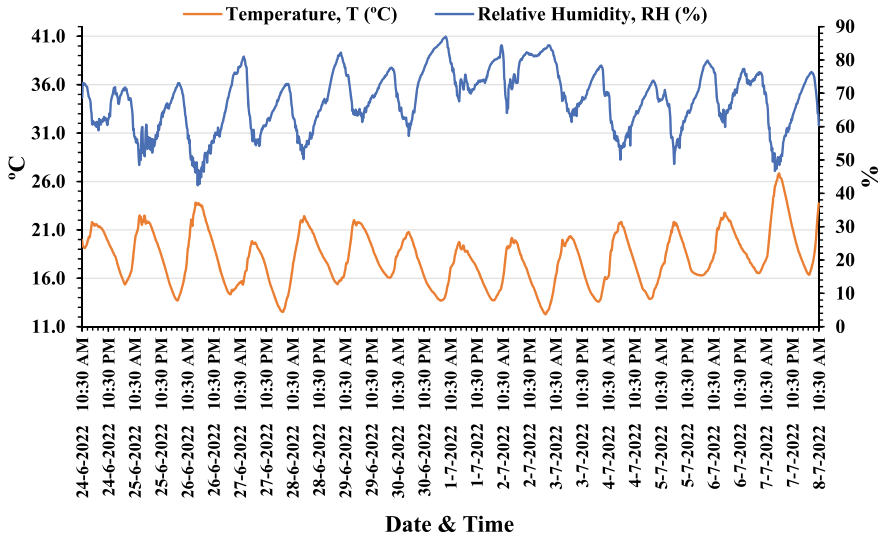


Fig. 4.5 Temperature and relative humidity from sensor 3 (exterior)

Table 4.1 Sensors 1 (the cave), 2 (the cold-room), and 3 (the exterior) temperature and relative humidity statistics

	Maximum	Minimum	Average	Standard deviation	Coefficient of variation	Covariance	Correlation coefficient
<i>Sensor 1</i>							
T (°C)	21.96	19.20	20.14	0.5693	0.0283	<b>0.9156</b>	<b>0.3708</b>
RH (%)	73.20	<b>50.10</b>	62.08	4.3376	0.0699		
<i>Sensor 2</i>							
T (°C)	23.26	<b>19.96</b>	<b>21.45</b>	0.7369	0.0344	- 0.8925	- 0.2247
RH (%)	76.60	42.70	53.87	5.3902	0.1001		
<i>Sensor 3</i>							
T (°C)	<b>26.82</b>	12.29	18.07	<b>2.8218</b>	<b>0.1561</b>	- 19.0773	- 0.7542
RH (%)	<b>87.00</b>	42.40	<b>68.11</b>	<b>8.9641</b>	<b>0.1316</b>		

The graphs show a more uniform behaviour of *sensor 1* against *sensor 2* during the temperature and humidity monitoring. The former sensor detected a lower temperature curve than the latter, but a higher relative humidity. *Sensor 3* also provides uniform data, and a higher amplitude (minimum–maximum values) of each 24-h cycle (day and night) since the device recorded (more extreme) outdoor conditions.

The hygrothermal performance of the selected rooms of Ye Olde Trip to Jerusalem can also be quantified. Firstly, mentioned should be made to absolute and relative minimum and maximum values during the monitoring period. *Sensor 1*, always below 22 °C, exceeds 21.5 °C on three days (21.43%), whereas *sensor 2* is over that temperature 71.43% of the cycles (10 days). Focusing on minimum values, *sensor 1* is below 20°C for 92.86% cycles (13 days), but *sensor 2* reaches that point only on 5–7–22 (10 am). The average T of *sensor 2* is 6.5% higher than that of *sensor 1*, whereas the mean RH of the latter is 15.24% higher. *Sensor 1* exceeds 60% RH (relative maximum values, cycles) during the monitoring period in 921 recordings (68.48% of the total). In contrast, *sensor 2* reaches that point in 158 recordings (11.75%).

Secondly, the distribution of the sensor data is worth examining. Both the standard deviation and the coefficient of variation indicate a lower dispersion of the data from *sensor 1*, which makes the cave area of Ye Olde Trip to Jerusalem present lower variable indoor temperature and relative humidity values against the other (more exposed) room and the exterior (the latter being in bold).

Finally, the relationship between the temperature and relative humidity should be evaluated. The cave's (Table 4.1) positive values (in bold) of the covariance and correlation coefficient clearly show that both variables jointly increase and decrease (direct relationship) during the monitoring, according to the graph in Fig. 4.3. In Fig. 4.4 and Table 4.1 (*Sensor 2*), this is not that constant since the behaviour is more variable and represents an overall negative relationship. The values in Fig. 4.5 and Table 4.1 (*sensor 3*) indicate a strong, inverse relationship between the two variables; when the temperature increases, the relative humidity decreases.

## 4.4 Conclusion

This paper proves that modelling of complex geometrical features of heritage buildings allows for accurate representation, which has an impact on the accuracy of measurements if the as-is condition is achieved. It also supports understanding of the building structure and its influence in the hygrothermal behaviour. 3D laser scanning and modelling of physical structures will support the creation of Digital Twins (DTs) to accurately preserve the heritage building in a digital format and allow for integrating simulation data in the virtual model.

In this work, the calculation of selected room volumes of Ye Olde Trip to Jerusalem was conducted to provide the environmental monitoring geometrical conditions. Given the irregular shape of the cave surface and warped walls, these measurements would be less accurate if following a non-as-is 3D modelling approach.

Regarding the hygrothermal performance assessment of those selected rooms, statistical data demonstrated that the cave area can regulate indoor temperature and relative humidity against the downstairs room (building) in response to exterior change in environmental conditions.

Further work will address the integration of sensor data into as-is models. Thus, benefiting from a more accurate geometry, heat flow, surface pressure, and humidity simulations, among others, can be carried out to precisely evaluate the behaviour of heritage buildings.

**Acknowledgements** This work has been funded by the England European Regional Development Fund (ERDF) (reference 08R20S04177) as part of the European Structural and Investment Funds Growth Programme 2014-2020, the University of Nottingham and Nottingham Trent University through the Live Experiential and Digital Diversification - Nottingham (LEADD:NG) project. Special thanks to Karl Gibson for granting access to Ye Olde Trip to Jerusalem and easing the surveys; also, to Sherna Salim for supporting sensor settings. This work has also been supported by funding for a post-doctoral researcher contract from the VI Plan Propio de Investigación y Transferencia of Universidad de Sevilla (reference VIPPIT-2020-II.5), Spain.

## References

1. H.E. Huerto-Cardenas, F. Leonforte, N. Aste, C. Del Pero, G. Evola, V. Costanzo, E. Lucchi, Validation of dynamic hygrothermal simulation models for historical buildings: State of the art, research challenges and recommendations. *Build. Environ.* **180**, 107081 (2020). <https://doi.org/10.1016/j.buildenv.2020.107081>
2. A. Yüksel, M. Arıcı, M. Krajčák, M. Civan, H. Karabay, A review on thermal comfort, indoor air quality and energy consumption in temples. *J. Build. Eng.* **35**, 102013 (2021). <https://doi.org/10.1016/j.job.2020.102013>
3. M. Hosseini, K. Javanroodi, V.M. Nik, High-resolution impact assessment of climate change on building energy performance considering extreme weather events and microclimate—Investigating variations in indoor thermal comfort and degree-days. *Sustain. Cities Soc.* **78**, 103634 (2022). <https://doi.org/10.1016/J.SCS.2021.103634>
4. Y. Alshwabkeh, A. Baik, A. Fallatah, (2021). As-textured as-built bim using sensor fusion, zee ain historical village as a case study. *Remote Sensing* **13**, 5135, 13, 24:5135. <https://doi.org/10.3390/RS13245135>
5. D. Antón, B. Medjdoub, R. Shrahily, J. Moyano, Accuracy evaluation of the semi-automatic 3D modeling for historical building information models. *Int. J. Architect. Heritage* **12**(5), 790–805 (2018). <https://doi.org/10.1080/15583058.2017.1415391>
6. D. Antón, P. Pineda, B. Medjdoub, A. Iranzo, As-built 3D heritage city modelling to support numerical structural analysis: application to the assessment of an archaeological remain. *Remote Sensing* **11**(11), 1276 (2019). <https://doi.org/10.3390/rs11111276>
7. Historic England, Trip to Jerusalem Public House, Non Civil Parish - 1271192, Listing. (1952). Retrieved June 2, 2022 from <https://historicengland.org.uk/listing/the-list/list-entry/1271192?section=official-list-entry>
8. A. Al-Habaibeh, Architectural lessons for the future, via the past. *The UNESCO Courier* (2019-4), pp. 28–33. ISSN 2220-2269, Available on line at: <https://en.unesco.org/courier/2019-4/architectural-lessons-future-past>
9. A. Al-Habaibeh, Could traditional architecture offer relief from soaring temperatures in the Gulf? *The Conversation.* (2015), Available on line at: <https://theconversation.com/could-traditional-architecture-offer-relief-from-soaring-temperatures-in-the-gulf-49760>



**Open Access** This chapter is licensed under the terms of the Creative Commons Attribution 4.0 International License (<http://creativecommons.org/licenses/by/4.0/>), which permits use, sharing, adaptation, distribution and reproduction in any medium or format, as long as you give appropriate credit to the original author(s) and the source, provide a link to the Creative Commons license and indicate if changes were made.

The images or other third party material in this chapter are included in the chapter's Creative Commons license, unless indicated otherwise in a credit line to the material. If material is not included in the chapter's Creative Commons license and your intended use is not permitted by statutory regulation or exceeds the permitted use, you will need to obtain permission directly from the copyright holder.



# Chapter 5

## Oil and Gas Supply Chain: Analysing Stakeholder Sustainability Risk Perception



Ashem Egila, Muhammad Mustafa Kamal, and Benny Tjahjono

**Abstract** Recent developments on a worldwide scale have highlighted the continued importance of the oil and gas supply chain, despite the growing demand for a more diverse energy portfolio, especially in many developing countries. This study investigates the sustainability risks present within the oil and gas supply chain by analysing the subjective risk perceptions of internal stakeholders. In the context of this study, sustainability risk factors are identified across the three pillars of sustainability (environmental, social, and economic). A quantitative research survey design of oil and gas industry stakeholders was undertaken, specifically identifying top management, middle management, supervisors, and operations to assess any variation in sustainability-related risk perception. Failure mode and effect analysis (FMEA) and partial least squares structural equation modelling (PLS-SEM) were used to determine the relative importance of the selected risks. The results indicate that stakeholder risk perception significantly impacted sustainability risk management within the oil and gas sectors. It also shows that socioeconomic risk variables were considered more severe and frequent than environmental risk factors as the most significant for internal stakeholders in the oil and gas industries within the study context.

**Keywords** Risk perception · Sustainability risk · Oil and gas · Stakeholder theory

---

A. Egila (✉) · M. M. Kamal · B. Tjahjono  
Centre for Business in Society, Coventry University, Coventry, UK  
e-mail: [egilaa@coventry.ac.uk](mailto:egilaa@coventry.ac.uk)

M. M. Kamal  
e-mail: [ad2802@coventry.ac.uk](mailto:ad2802@coventry.ac.uk)

B. Tjahjono  
e-mail: [ac8300@coventry.ac.uk](mailto:ac8300@coventry.ac.uk)

## 5.1 Introduction

Many industrial sectors are increasingly concerned about supply chain sustainability-related risk factors. However, there are limited quantitative methods for evaluating sustainability risk using a triple bottom line (economic, social and environmental) [1]. Evidence of sustainable risk management is sparse in many emerging and developing nations, and most developing countries experience more challenges in adopting the sustainability risk framework due to complex supply chains [2, 3]. Sustainability risk management must be understood to ensure global supply chains are more equitable, as low-income countries suffer more from sustainability than high-income countries do [4]. Sustainable risk perception is ambiguous and varies among industrial sectors, as does stakeholder involvement [5–8]. Many industry stakeholders worry about supply chain sustainability hazards (e.g. [2, 9, 10]).

The oil and gas business has a limited quantitative approach to analysing supply chain sustainability risk using the triple bottom line (economic, social, and environmental). Despite calls to improve energy transition and switch to more sustainable ways, it is evident, especially for low-income developing nations, that the SDG ambition will be a problem [4]. Mismanaging sustainability risks can damage a company's brand and operations when stakeholders anticipate social, ecological, and economic sustainability [1, 11]. Economic development and social activities that rely on the oil and gas industry require sustainable risk management. Developing countries with weak laws and a lack of political will need to balance economic growth with environmental sustainability. Thus, sustainability initiatives can be side-lined for short-term productivity and job advantages (Omanga et al. 2014). Previous studies on sustainability risk perception have generated varied results, [2] confirmed that endogenous environmental threats are regarded as the most relevant across industries, and the interconnectedness between numerous sustainability-related risks is relatively high. In other studies, technological and institutional risks were biggest sustainability threats for telecom corporations [12]. Corruption, inflation, and supply-and-demand volatility are agro-food supply chain concerns [10]. However, some studies have not investigated the technological and institutional issues affecting agro-food sustainability [13]. Given the segment's role in economic development, what are the oil and gas industry's most significant sustainability risks in the oil and gas industries. Researchers have stressed on supplier and logistics management for healthy O&G supply chains [14]. Others say that MNCs have established sustainability plans for their operations, but few have involved (tier-one) suppliers. MNCs rarely engage their suppliers, despite the higher occurrence of environmental and social breaches that can jeopardise their operations and reputation [15]. Hence understanding the risk perception of decision-making is crucial. Subjective judgments regarding risky events are essential to risk perception. This affects the risks people care about and how they tackle them. Risk perception is vital to how many stakeholders know and

comprehend dangers and how they feel about them [16]. Discordant risk perceptions among stakeholders [17]. This study quantified the risk perception of oil and gas stakeholder risk perceptions. Based on literature and interviews, a questionnaire was devised to assess stakeholders' perceptions of each risk by evaluating their risk anxiety to drive successful proactive risk mitigation measures. This evaluates stakeholder risk perception and reveals differences.

## 5.2 Literature and Theory Development

Sustainability risk management (SRM) is an extension of enterprise risk management that aims to maximise environmental, social, and economic performance for a company's survival [18]. Therefore, it involves controlling the identification, assessment, and response strategies accessed by different industries [10, 12, 19]. However, few studies have examined this from the context of an oil and gas. For instance [20] discussed SRM within the oil and gas sector and discovered that the three most common hurdles in sustainability risk identification and prioritisation include its inherent difficulty to quantify and frequent subjectivity based on stakeholder perceptions—rather than the result of objective criteria such as regulatory requirements, cost or revenue potential and timescale of impacts. As Sustainability impacts are also inherently longer-term focused, researchers have highlighted the importance of risk culture in driving effective SRM practices [21]. Building on this mechanism and drawing on stakeholder theory, the previous researchers have developed a conceptualisation of sustainability risks, laying the basis for future investigations in this respective field [3]. As a result, we integrated sustainability risk management by identifying the effects of sustainability issues on stakeholders, actively including sustainability in objectives across the levels of the organisational hierarchy, and developing concrete support to identifying, assess, and manage sustainability risks. Companies can enhance their competitiveness while providing leadership during the sustainability transition [4]. Risk perception studies examine people's judgments when asked to characterise and evaluate hazardous activities and technologies. Previous scholars have acknowledged that risk perception can aid risk analysis and policy-making by providing a basis for understanding and anticipating public responses to hazards, thereby improving the communication of risk information among lay people, technical experts, and decision-makers [22]. Therefore, comparing different stakeholders' perceptions of each risk by measuring the levels of their concern about risks can be used to make the critical hypothesis for this research as shown in Fig. 5.1.

***H1 stakeholder risk perception positively impacts sustainability risk management in the oil and gas supply chain.***

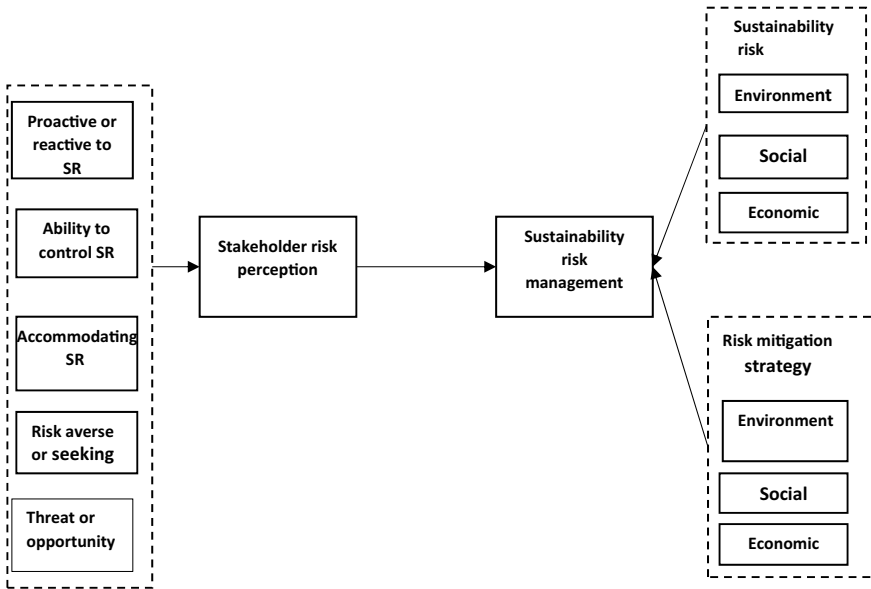


Fig. 5.1 Conceptualising stakeholder risk perception in oil and gas supply chains

### 5.2.1 The conceptual model

See (Fig. 5.1).

## 5.3 Methodology

The questionnaire was developed from a literature review and pilot survey from academics and experts from the oil and gas supply chain. These questions used closed-end Likert scales to measure stakeholder risk perception for each criterion. A survey of 265 stakeholders working within different oil and gas companies in Nigeria was conducted; subsequently, analyses were conducted between top management (30), middle management (86), supervisors (72), operations (67), and others (10) to assess and analyse several dimensions of sustainability-related risk. The questionnaire was sent to targeted stakeholders using an exponential non-discriminate snowballing technique over a 3 month period. The initial process involved determining the severity, frequency, and ease of detection for each internal stakeholder category used to develop the latent model variables that connected all lower-order constructs. However, given that the model was a reflective formative higher-order model, six of the latent lower-order constructs were formatted as higher-order constructs. A hierarchical component model was established for each sustainability risk factor and mitigation strategy category. However, some measurement items did not reach the

threshold and were subsequently deleted or retained because of their relevance to theory in the lower-order format. Using redundancy analysis, the test for collinearity, VIF, and convergent validity was approximately 0.7 for most variables. Cronbach Alpha, composite reliability, and AVE were all suitable except for environmental risk factors highlighted below in Table 5.2. Subsequently, the path model is analysed and discussed.

### 5.4 Result and Discussion

Initially failure mode effect analysis (FMEA) was used to measure the severity and frequency (SRM), which was compared among stakeholders to determine any significant differences in patterns. These categories are shown the Table 5.1. The result shows that the top three sustainability-related risk factors revealed by the survey are unfair wages, excess working hours, working life (SRM6), man-made disasters (SRM1), and unhealthy and unsafe work (SRM5) for the overall internal stakeholders.

However, for different stakeholder groups, top management perceives that economic risk factors, including Unfair wages, excessive working hours, Work-life balance, industrial actions, strikes and boycotts (SRM6, SRM9), were the primary concerns based on the response. In contrast, middle management and supervisors focus predominately on the social risk factors: unfair wages, excessive working hours, Work-life balance, and unhealthy and unsafe working environments (SRM6, SRM5). However, operator staff members were more concerned about man-made disasters (SRM6). The analysis used FMEA to identify the severity, frequency, and mitigation

**Table 5.1** Sustainability risk factors

		1	2	3	4	5	6
Man-made disaster	SRM1	11.43	10.85	10.31	12.82	13.8	11.38
Natural disasters	SRM2	9.57	8.28	7.17	8.34	9.4	8.18
Waste management, energy consumption	SRM3	11.37	9.49	8.83	10.27	11.1	9.78
Discrimination and unethical activities	SRM4	9.77	7.9	8.51	8.87	9	8.56
Unhealthy and unsafe work	SRM5	11.4	11.41	10.56	11.6	12.3	11.26
Unfair wages, excessive working hours, Work-life balance	SRM6	12.33	11.9	12.13	11.58	13.4	11.98
volatility of product prices, exchange rates, inflation, subsidies, and taxes	SRM7	11.6	10.53	9.78	11.39	12.7	10.75
Bribery, false claims, corruption	SRM8	11.03	10.85	9.76	10.34	13.3	10.54
Industrial action, strikes, boycotts	SRM9	11.73	9.34	8.71	10.15	12.7	9.77

Note 1 = Top management, 2 = Middle management, 3 = supervisors, 4 = operator, 5 = others, All = 6

**Table 5.2** Construct validity and reliability

	Items		Cronbach's alpha	Composite reliability	AVE
Stakeholder risk perception	SRP_1	0.794	0.643	0.804	0.580
	SRP_4	0.819			
	SRP_5	0.662			
Environment risk	SRM1	0.875	0.776	0.868	0.687
	SRM2	0.840			
	SRM3	0.768			
Social risk	SRM4	0.664	0.817	0.891	0.731
	SRM5	0.881			
	SRM6	0.832			
Economic risk	SRM7	0.820	0.817	0.891	0.731
	SRM8	0.887			
	SRM9	0.857			
Environment risk mitigation strategy	RSM_1	- 0.324 <sup>a</sup>	0.568	0.009 <sup>a</sup>	0.226 <sup>a</sup>
	RSM_2	0.717			
	RSM_3	- 0.245 <sup>a</sup>			
Social risk mitigation strategy	RSM_4	0.711	0.661	0.809	0.588
	RSM_5	0.727			
	RSM_6	0.854			
Economic risk mitigation strategy	RSM_7	0.069 <sup>a</sup>	0.673	0.849	0.739
	RSM_8	0.744			
	RSM_9	0.924			

Note values with "a" indicates not acceptable and would be considered for elimination

strategies. At the same time, top management considers Industrial action, strikes, boycotts (SRM9), and the role of Bribery, false claims, and corruption (SRM8) as significant risk factors that should be prioritised. Middle management and supervisors were more concerned about unfair wages, excessive working hours, no work-life balance (SRM6) and an unhealthy and unsafe working environment (SRM5). However, given the high correlation between the risk factors, any attempt to address the critical risk priority would have a ripple effect on other risk factors that are ultimately correlated.

The results revealed that socioeconomic factors are perceived as more significant risk factors by stakeholders contributing to the sustainability of the oil and gas supply chain than environmental risks. This can be attributed environment's significant behaviour when the impact is influenced by the availability of resources or energy from the environment or alters ecosystems (Stern 2000). As a result, perceptions are influenced by the by-products of human needs for physical comfort, mobility, labour, enjoyment, power, and personal security, and humanity has developed to

satisfy these desires and will have a more significant impact on human decision-making in developing nations where there is often a scarcity. The study also identified the proposed response strategies as the most important factors to consider when addressing the various risks associated with the supply chain. The high interconnectedness of various sustainability-related risks has revealed the need for effective risk management strategies. It also calls for integrated risk management frameworks to help companies develop sustainable strategies. This preliminary study provides academics and practitioners with an exemplar of sustainability risk management from a developing country’s oil and gas perspective. The result of this study is beneficial for practitioners, mainly does who can use this study as guidance on how to identify and select the critical sustainability risks and plan mitigating strategies accordingly as well as decision-makers to reassess stakeholders’ varying judgments when considering sustainability risk assessment.

The relationships between the path constructs were tested, as shown in Fig. 5.2. The estimation results are shown in Tables 5.2 and 5.3. Following parameter estimation, bootstrapping was performed to confirm the robustness of the findings. Thus 5000 bootstrap samples were built by re-sampling with replacements from the original sample. The summary results for bootstrapping are provided in Table 5.2. After verifying the hypotheses, we ran a confirmatory factor analysis to determine convergent and discriminant validity [23]. Table 5.2 provides standardisation coefficients for factor loadings, scale composite reliability, and overall variance average (AVE), which were significantly higher than the lower value specified (ideally be above  $\alpha = 0.7$ ,  $SCR = 0.7$ , and  $AVE = 0.5$ ) except for environmental risk mitigation strategy where the item loading composite reliability and AVE were below. However, given its theoretical relevance, it was not eliminated because stakeholders often perceive their inability to respond to environmental factors, which may explain the outlier compared to other sustainability variables. The theoretical constructs framework has convergent validity for the higher order construction used to formulate the sustainability risk management properties, and the independent variable stakeholder risk perception was accepted.

We can therefore conclude that constructs of our theoretical framework possess convergent validity higher-order latent variables to determine the discriminant validity of the model, as shown in Table 5.3.

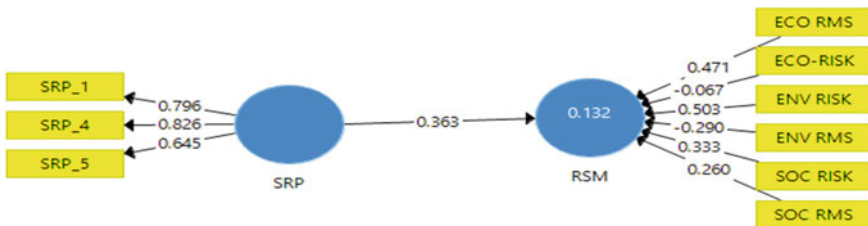


Fig. 5.2 PLS model



**Table 5.3** Discriminant validity

Construct reliability and validity					Discriminant validity		
	Cronbach's Alpha	rho_A	C.R	(AVE)		RSM	SRP
RSM		1			RSM		
SRP	0.64	0.68	0.8	0.57	SRP	0.363	0.76

**Table 5.4** Model fit

	$\beta$	(M)	SD	T Statistics	P Value	
SRP -> RSM	0.3633	0.3919	0.0518	7.0136	0.000	Supported
R <sup>2</sup>	F <sup>2</sup>	Model fit				
0.132	0.152	0.056				

The model result is shown in Table 5.4, which analysed the loading of the key hypotheses that stakeholder risk perception positively impacts sustainability risk management ( $p > 0.001$ ). Standard root means squared residual (SRMR) was used to access the model fit (SRMR = 0.056); a value below 0.08 is considered a good fit in the covariance-based structural equation. The path was positively between the latent variables SRP and RSM, and the R<sup>2</sup> value was 13 per cent (R<sup>2</sup> = 0.13) in RSM was accounted for by this model.

Consequently, it can be concluded that stakeholder risk perception would significantly impact sustainability risk management which implies that SRP contributes uniquely to the decision of how different categories of stakeholders prioritise response to sustainability events.

## 5.5 Conclusion

The purpose of this research was to provide a means to investigate the measurement of latent variables to evaluate the theoretical relationship underlying the diverse perceptions and prioritisation of sustainability risk factors in Nigeria's oil and gas supply chain. In the model, stakeholder risk perception highly predicts sustainability risk management. Consequently, the more significant the risk perception, the greater the impact on SRM. However, some of the evaluation items did not adequately address the requirements. These included environmental risk mitigation strategy which did not accurately represent the item due to the alleged inability of stakeholders to respond effectively to natural and man-made disasters.

In addition, the dependent variable could only be explained at a rate of 13%, indicating that additional antecedent factors are needed to investigate the model. The result highlighted the similarity between the top and middle management, supervisors, and operation staff's perceived sustainability risk factors. It further indicated more significant concern for unfair wages, excessive working hours, working life, illness, and a safe working environment.

A major drawback of this study is the absence of crucial antecedent variables that influence sustainability risk management. The survey results show that more predictive variables are required to account for the variance in RSM. In addition, the study's design did not account for the importance of external stakeholders in collaborative decision-making. In addition, despite their unique cultural influence, this was universally relevant within the setting of developing countries, which may limit the generalisability of the study. In the subsequent phase, we plan to investigate additional variables that may influence the risk perceptions of oil and gas supply chain stakeholders.

## References

1. M. Xu, Y. Cui, M. Hu, X. Xu, Z. Zhang, S. Liang, S. Qu, Supply chain sustainability risk and assessment. *J. Cleaner Prod.* **225**, 857–867 (2019). Scopus. <https://doi.org/10.1016/j.jclepro.2019.03.307>
2. M. Giannakis, T. Papadopoulos, Supply chain sustainability: a risk management approach. *Int. J. Prod. Econ.* **171**, 455–470 (2016). <https://doi.org/10.1016/j.ijpe.2015.06.032>
3. H. Hofmann, C. Busse, C. Bode, M. Henke, Sustainability-related supply chain risks: conceptualization and management. *Bus. Strategy Environ.* **23**(3), 160–172. Scopus
4. J. Schulte, S. Hallstedt, Company risk management considering the sustainability transition. *Sustainability* **10**(11), 4137 (2018). <https://doi.org/10.3390/su10114137>
5. C. Busse, Doing well by doing good? The self-interest of buying firms and sustainable supply chain management. *J. Supply Chain Manage.* **52**(2), 28–47 (2016). Scopus. <https://doi.org/10.1111/jscm.12096>
6. S. Hajmohammad, A. Shevchenko, Mitigating sustainability risk in supplier populations: An agent-based simulation study. *Int. J. Oper. Prod. Manage.* **40**(7–8), 897–920 (2020). Scopus
7. J. Meinschmidt, M.C. Schleper, K. Foerstl, Tackling the sustainability iceberg: a transaction cost economics approach to lower tier sustainability management. *Int. J. Oper. Prod. Manage.* **38**(10), 1888–1914 (2018). Scopus. <https://doi.org/10.1108/IJOPM-03-2017-0141>
8. C. Wijethilake, T. Lama, Sustainability core values and sustainability risk management: moderating effects of top management commitment and stakeholder pressure. *Bus. Strateg. Environ.* **28**(1), 143–154 (2019). <https://doi.org/10.1002/bse.2245>
9. M. Abdel-Basset, R. Mohamed, A novel plithogenic TOPSIS- CRITIC model for sustainable supply chain risk management. *J. Cleaner Prod.* **247**. Scopus. (2020) <https://doi.org/10.1016/j.jclepro.2019.119586>
10. C. Benabdallah, A. El-Amraoui, F. Delmotte, A. Frikha, *An integrated rough-DEMATEL method for sustainability risk assessment in agro-food supply chain*, ed. by M. F.-Z.Y. Benadada. Proceedings—2020 5th International Conference on Logistics Operations Management, GOL 2020. Institute of Electrical and Electronics Engineers Inc. <https://doi.org/10.1109/GOL49479.2020.9314712>
11. U. Juettner, K. Windler, A. Podleisek, M. Gander, S. Meldau, Implementing supplier management strategies for supply chain sustainability risks in multinational companies. *TQM J.* **32**(5), 923–938 (2020). <https://doi.org/10.1108/TQM-05-2019-0136>

12. F. Valinejad, D. Rahmani, Sustainability risk management in the supply chain of telecommunication companies: a case study. *J. Cleaner Prod.* **203**, 53–67 (2018). Scopus. <https://doi.org/10.1016/j.jclepro.2018.08.174>
13. A. Choirun, I. Santoso, R. Astuti, Sustainability risk management in the agri-food supply chain: literature review, in *IOP Conference Series: Earth and Environmental Science*, vol. 475, ed. by F.D. Effendi, S. Suhartini, W.B. Sunarharum, H.Y. Setiawan, N.M. Sabrina, P. Setiani, M. Nur, N.L. Rahmah, C.G. Perdani, N. Istianah, R. Septifani, N. Lusiana, A.W. Putranto, Z. Iqbal, D.Y. Ali, T. Hasna (Institute of Physics Publishing, 2020). <https://doi.org/10.1088/1755-1315/475/1/012050>
14. W.N.K. Wan Ahmad, J. Rezaei, M.P. de Brito, L.A. Tavasszy, The influence of external factors on supply chain sustainability goals of the oil and gas industry. *Resour. Policy* **49**, 302–314 (2016). <https://doi.org/10.1016/j.resourpol.2016.06.006>
15. V.H. Villena, D.A. Gioia, On the riskiness of lower-tier suppliers: managing sustainability in supply networks. *J. Oper. Manage.* **64**, 65–87 (2018). <https://doi.org/10.1016/j.jom.2018.09.004>
16. H.-J. Paek, T. Hove, Risk perceptions and risk characteristics, 15 (2021)
17. D. Zhao, A.P. McCoy, B.M. Kleiner, T.H. Mills, H. Lingard, Stakeholder perceptions of risk in construction. *Saf. Sci.* **82**, 111–119 (2016). <https://doi.org/10.1016/j.ssci.2015.09.002>
18. N.A. Manab, N.A.A. Aziz, Integrating knowledge management in sustainability risk management practices for company survival. *Manage. Sci. Lett.* **9**(4), 585–594 (2019). Scopus
19. W. Liu, W. Wei, X. Yan, D. Dong, Z. Chen, Sustainability risk management in a smart logistics ecological chain: an evaluation framework based on social network analysis. *J. Cleaner Prod.* 276 (2020). Scopus. <https://doi.org/10.1016/j.jclepro.2020.124189>
20. T. Cort, S. Gudernatch, Are enterprise risk management frameworks effective for prioritizing sustainability risks in the oil and gas sector? in *Society of Petroleum Engineers - SPE International Conference on Health, Safety and Environment 2014: The Journey Continues*, 2, 936–941. Scopus. <https://www.scopus.com/inward/record.uri?eid=2-s2.0-84905818096&doi=10.2118%2f168432-ms&partnerID=40&md5=2a205019bf548e13d20262134f2ee067>
21. N.A.A. Aziz, N.A. Manab, Does risk culture matter for sustaining the business? Evidence from Malaysian environmentally sensitive listed companies. *Int. J. Manage. Sustain.* **9**(2), 91–100 (2020). Scopus
22. P. Slovic, Perception of risk. *Science* **236**(4799), 280–285 (1987). Scopus. <https://doi.org/10.1126/science.3563507>
23. C. Fornell, D.F. Larcker, Evaluating structural equation models with unobservable variables and measurement error. *J. Mark. Res.* **18**(1), 39–50 (1981). <https://doi.org/10.2307/3151312>

**Open Access** This chapter is licensed under the terms of the Creative Commons Attribution 4.0 International License (<http://creativecommons.org/licenses/by/4.0/>), which permits use, sharing, adaptation, distribution and reproduction in any medium or format, as long as you give appropriate credit to the original author(s) and the source, provide a link to the Creative Commons license and indicate if changes were made.

The images or other third party material in this chapter are included in the chapter's Creative Commons license, unless indicated otherwise in a credit line to the material. If material is not included in the chapter's Creative Commons license and your intended use is not permitted by statutory regulation or exceeds the permitted use, you will need to obtain permission directly from the copyright holder.



# Chapter 6

## Using Machine Learning to Predict Synthetic Fuel Spray Penetration from Limited Experimental Data Without Computational Fluid Dynamics



Bryn Richards and Nwabueze Emekwuru

**Abstract** Machine Learning (ML) is increasingly used to predict fuel spray characteristics, but ML conventionally requires large datasets for training. There is a problem of limited training data in the field of synthetic fuel sprays. One solution is to reproduce experimental results using Computational Fluid Dynamics (CFD) and then to augment or replace experimental data with more abundant CFD output data. However, this approach can obscure the relationship of the neural network to the training data by introducing new factors, such as CFD grid design, turbulence model, near-wall treatment, and the particle tracking approach. This paper argues that CFD can be eliminated as a data augmentation tool in favour of a systematic treatment of the uncertainty in the neural network training. Confidence intervals are calculated for neural network outputs, and these encompass both (1) uncertainty due to errors in experimental measurements of the neural networks' training data and (2) uncertainty due to under-training the neural networks with limited experimental data. This approach potentially improves the usefulness of artificial neural networks for predicting the behaviour of sprays in engineering applications. Confidence intervals represent a more rigorous and trustworthy measure of the reliability of a neural network's predictions than a conventional validation exercise. Furthermore, when data are limited, the best use of all available data is to improve the training of a neural network and our confidence in that training, rather than to reserve data for ad-hoc testing, which exercise can only at best approximate a confidence interval.

**Keywords** Artificial neural networks · Confidence intervals · Uncertainty · Machine learning · Fuel spray penetration · Synthetic fuel · Polyoxymethylene dimethyl ethers (OME) · Diesel

---

B. Richards (✉) · N. Emekwuru  
Faculty of Engineering, Environment and Computing, Coventry University, Priory Street,  
Coventry, UK  
e-mail: [richa377@uni.coventry.ac.uk](mailto:richa377@uni.coventry.ac.uk)

## 6.1 Introduction

Machine learning is increasingly used to predict fuel spray characteristics, such as spray penetration [1, 2]. However, the cost of fuel spray experiments limits the available training data. When a neural network is trained on limited data, there is a trade-off between over-fitting the data and over-simplifying the neural network (providing too few nodes or layers within the network). A nonlinear phenomenon, such as spray breakup, requires a degree of neural network complexity that cannot be trained reliably with the quantity of experimental spray penetration data typically available. To get around this, researchers have augmented experimental spray results with complementary computational fluid dynamics (CFD) studies [3]. However, CFD occupies time and resources and risks distorting the original experimental data. There is the potential to remove CFD from the process and to train neural networks directly on experimental data [4]. This study proposes to encompass predictive uncertainty due to neural network under-training (due to limited training data) within confidence intervals around neural network predictions. The aim is to improve the practical usefulness of neural networks as predictive tools in engineering design, in cases where they are trained incompletely due to insufficient training data.

Confidence intervals for neural networks are not new. Chrissolouris et al. [5] derived confidence intervals for a neural network from fundamental statistics. To use this approach, the experimenter must assess the confidence intervals of each of the neural network's training inputs and the sensitivity of each neural network output to variations in each input. Confidence intervals are typically available for spray data, because once a new experimental condition is created, experiments are easily repeated. A matrix of  $dm/dn$  sensitivities sized  $m$  outputs by  $n$  inputs must be manipulated (transposed and multiplied) to calculate confidence intervals for the neural network. Trichakis et al. [6] reviewed numerical methods of estimating the confidence intervals on neural networks and applied the bootstrap method of Efron [7] to estimate confidence intervals on a neural network predicting the hydraulic head of aquifers. Although beyond the scope of Efron's original proposal, Trichakis et al. showed that the bootstrap method is a practical way to estimate confidence intervals for perceptron neural networks. Confidence intervals have been used with some success in other applications of neural networks, including applications related to solar power generation [8].

The present study applies the bootstrap method to calculate confidence intervals on spray penetration predictions. The novel contribution of the present study is to incorporate within the confidence intervals not only (1) uncertainty arising from sampling error on measured input values but also (2) residual random errors in the neural network due to initialisation and incomplete training. Because of the limited data available for training, the neural network training algorithm does not converge reliably. This means that neural network output contains random error due to residual randomness from the initialisation state. We allow this random error to

combine with variations that arise from resampling inputs (due to errors in experimental measurements). The confidence intervals produced by this method thus incorporate both sources of error. Thus, we prefer repeated, abortive attempts at neural network training, with suitable confidence intervals, over a single neural network that over-fits the data. We recognise that in general simpler neural networks (containing fewer nodes) can be trained on less abundant data, but there is typically a lower limit on neural network complexity whereby an over-simple neural network introduces model bias (a situation in which the neural network is insufficiently complex to represent adequately the output despite successful training). The methods suggested in this paper offer a means of training suitably complex neural networks from limited experimental data without relying on CFD or any data augmentation techniques. By providing confidence intervals, the methods suggested in this paper support the judicious application of neural networks to practical problems in engineering.

## 6.2 Methodology

This investigation uses liquid and vapour spray penetration data from Honecker et al. [9]. The authors began with a common rail injector having specific flow rate of 310 mL/30 s at 100 bar from 8 holes of 125  $\mu\text{m}$  diameter. They modified the injector to have only three holes, and they measured the injection plume from only the “downward facing” hole. Measurement was by means of three cameras with no filter, 308 nm filter and 520 nm filter, respectively. Images were processed in Matlab to identify contrast thresholds in each camera view representing the boundaries of the liquid and vapour phases.

The researchers ran diesel and polyoxymethylene dimethyl ethers (OME) fuel injection events across three different injection pressure conditions and captured images at 100 ns intervals. For this work we have used the OME data only. For each injection pressure condition, 20 injection events were measured, resulting in a total of 1260 images. For each group of 20 images having the same injection pressure condition and time stamp, the experimenters produced an average vapour penetration length with standard deviation and, where available, an average liquid penetration length with standard deviation. This resulted in 63 average penetration length data points for the vapour phase and 57 for the liquid phase. Wishing to use the raw, resampled data but having access only to the mean and standard deviation figures published by Honecker et al., the present study calculates a normally distributed population of 20 penetration lengths for every experimental condition using the *normdist* (normal distribution) function in Microsoft Excel [ver. 16.61.1 (2022)]. This resulted in  $63 \times 20$  data points for the vapour phase and  $57 \times 20$  for the liquid phase.

We build 100 separate training data sets of 57 data points each from the available liquid phase data, and again (100 training sets of 63 points each) from the vapour

phase data. The choice of 100 is arbitrary, but it is intentionally larger than the number of repeat samples of each experimental data point. We use the resulting  $2 \times 100$  data sets to train 100 neural networks on the liquid phase data and 100 neural networks on the vapour phase data. Each of the  $2 \times 100$  data sets contains one each of the permutations of injection pressure and time from the original experimental study (all 63 vapour phase permutations from the vapour phase or all 57 from the liquid phase). However, each of the data points in each of the  $2 \times 100$  sets is selected randomly from among the 20 available samples for that data point.

Each of the  $2 \times 100$  neural networks trained in this way involves just 8 nodes and 15 training epochs. Training is stopped at 15 epochs, with more typical convergence criteria suppressed. These hyperparameter values are informed by sensitivity studies (ranging from 2 to 16 nodes and 10 to 20 epochs). Because the neural networks produced within these ranges of hyperparameter values are undertrained, we observe variability in the results of the sensitivity study. The values were chosen subjectively after repeated runs, but more systematic approaches are suggested in the ‘Discussion’ section below.

We use Matlab’s Neural Network Toolbox [ver. R2022a (2022)]. We create feed-forward neural networks with one hidden layer of 8 nodes, represented in Fig. 6.1. We use the sigmoid activation function,  $\phi$ . Inputs are normalised ( $\hat{\varphi}$ ) and outputs are denormalised ( $\hat{\varphi}'$ ). We use the Levenberg–Marquardt training algorithm with a fixed learning rate of 0.001 to set weights  $w$ , which are initialised randomly with a mean value of 0.5 and a normal distribution. Training stops at 15 epochs, ensuring that the networks do not over-fit the limited available training data but also ensuring that every network is under-trained. The  $2 \times 100$  neural networks thus trained are expected to differ because they each retain some of the randomness introduced by the initialisation of weights. We do not consider alternative activation functions, because, in a single-layer network, saturated weights and vanishing gradients are not expected [10]. We do not consider alternative initialisation strategies.

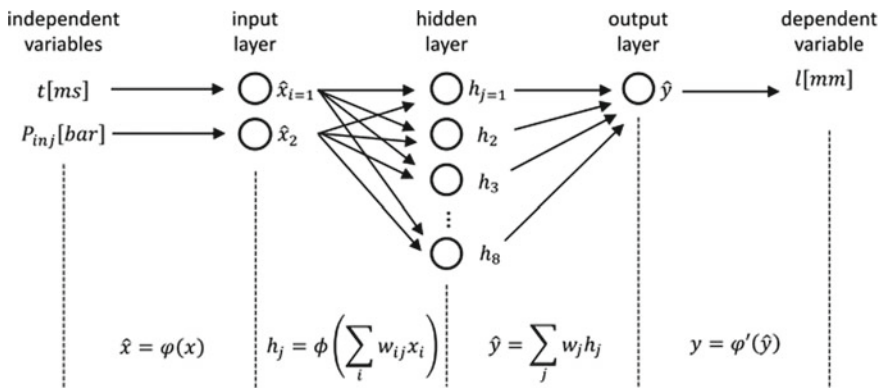


**Fig. 6.1** Layout of single-layer feed-forward neural networks used in this study, relating injection pressure  $P_{inj}$  and time  $t$  to liquid or vapour penetration length  $l$

To reiterate: the 20 repeat samples of each of the 63 + 57 data points are not aggregated to create a larger data set. Rather, each neural network is trained on a set of distinct data points (63 for the vapour phase or 57 for the liquid phase). The repeat sampling is reflected not in the training data for any one neural network but rather in the profusion of neural networks, each trained on a different data set wherein each point was selected randomly from among a population of 20 repeat samples of that data point.

After training a family of neural networks to predict spray penetration, the entire population of neural networks may be queried for any desired set of input values. The result of this query is a set of predictions having a mean and standard deviation. Thus, the family of neural networks collectively offers a prediction with confidence intervals corresponding to any input condition.

### 6.3 Results and Discussion

The mean outputs of the family of  $100 \times 2$  neural networks are shown in Fig. 6.1a, b with the experimental data (mean values) from Honecker et al. [9]. The same mean predictions are shown together with their upper and lower confidence intervals (single standard deviation) in Figs. 6.2, 6.3, and 6.4 for injection pressures of 700 bar, 1000 bar, and 1500 bar, respectively.

The figures show wider confidence intervals on neural network outputs in conditions where the experimental data of Honecker et al. [9] showed wider confidence intervals: in the vapour phase more than in the liquid phase, and in the spray breakup region of the liquid phase curves. Figure 6.6 reproduces graphs of experimental data from Honecker et al. [9].

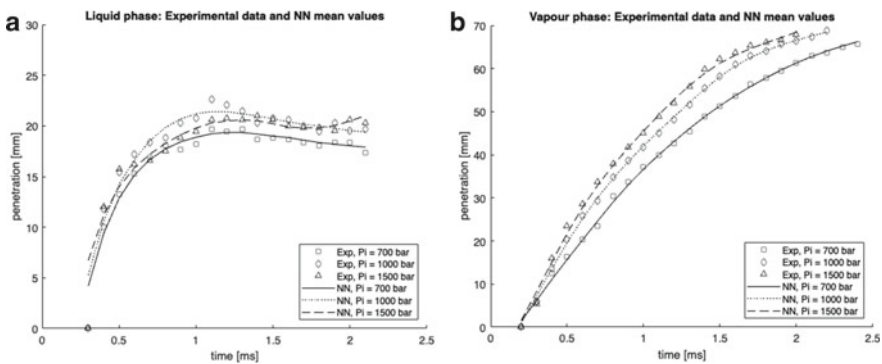


**Fig. 6.2** NN mean predictions (lines) with experimental data (points) **a** liquid phase, **b** vapour phase



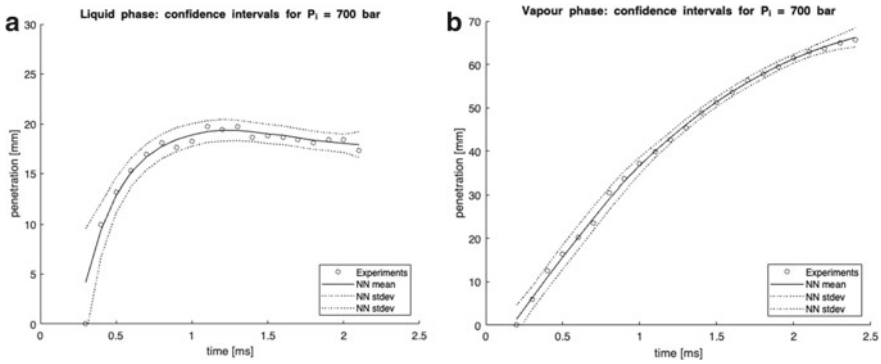


Fig. 6.3 NN mean predictions and confidence intervals at 700 bar **a** liquid phase, **b** vapour phase

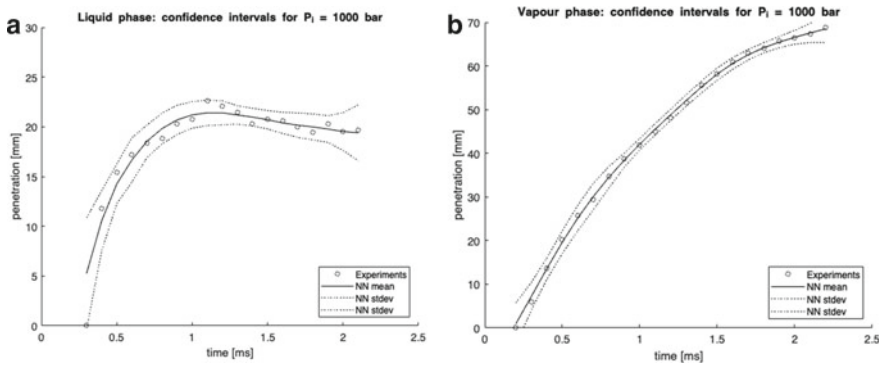


Fig. 6.4 NN mean predictions and confidence intervals at 1000 bar **a** liquid phase, **b** vapour phase)

Furthermore, the results show wider confidence intervals at the maximum penetration length of both liquid and vapour phases—conditions where the experimental data did not exhibit similarly wide confidence intervals. Thus, there is a source of uncertainty captured in this study that is not directly related to the uncertainty in the input data (Fig. 6.5).

This paper documents the application of bootstrap confidence intervals (following the method of Efron [7]) to neural networks, extending the work of Trichakis et al. [6] to deal with data sets that are limited in relation to the complexity of the neural network required to fit the data. The spray penetration data of Honecker et al. [9] are used to train a family of neural networks, each incorporating randomness from (1) random sampling of redundant input data per the bootstrap method and (2) residual randomness from initialisation of the neural networks (persisting in networks because of undertraining). With every set of predictions made by the family of neural networks, there is a mean and a confidence interval associated with that set.

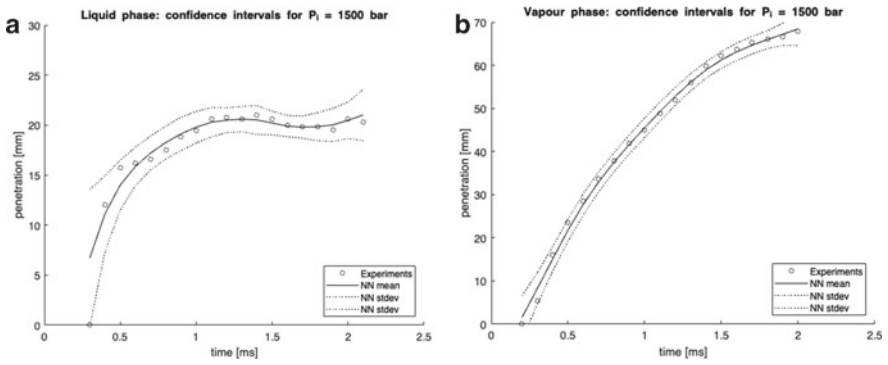


Fig. 6.5 NN mean predictions and confidence intervals at 1500 bar **a** liquid phase, **b** vapour phase)

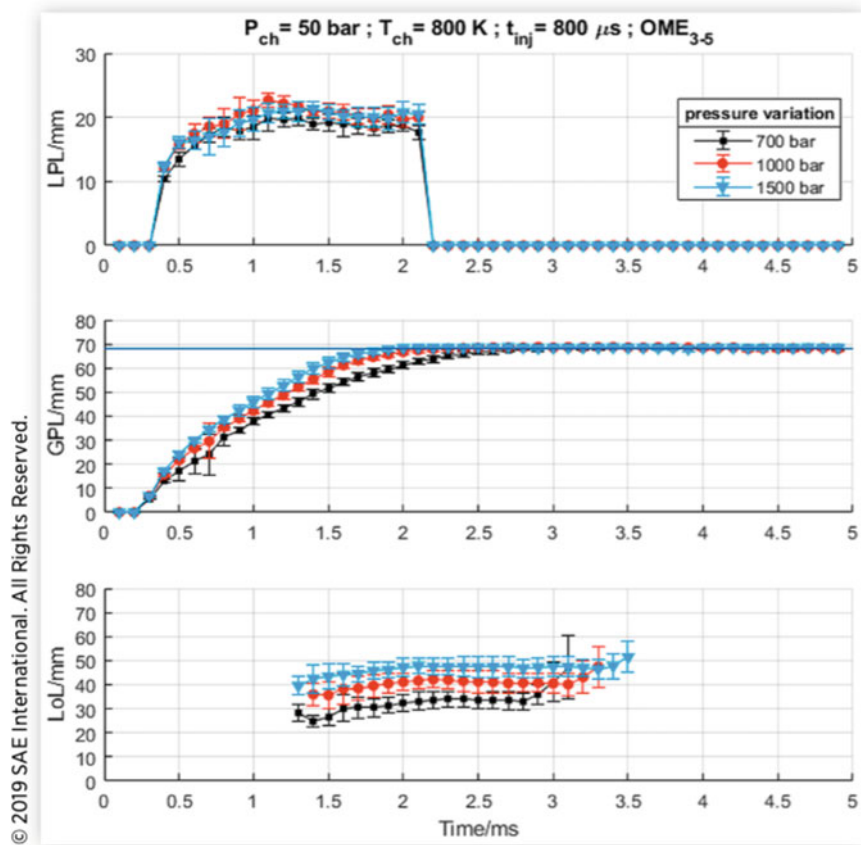


Fig. 6.6 Experimental data from Honecker et al. [9]

© 2019 SAE International. All Rights Reserved.

This study does not select the node number rigorously. Training stopped according to an epoch number limit, and again this was not assessed rigorously. Had this study sought to produce a rigorously optimised neural network, then a better approach would have been to produce a different family of neural networks representing bootstrapped confidence intervals for each permutation of hyperparameters. Rather than reserving precious data for the purpose of validating the selection of hyperparameters, the full population of families of neural networks may be examined to identify the set of hyperparameter values offering the narrowest confidence intervals. Rather than comparing the average size (across the predictive domain) of confidence intervals for each hyperparameter value, researchers may go a step further to compare weighted average standard deviations, where the weights are specified to give greater importance to the areas of interest within the curves, such as the droplet breakup region in the case of liquid spray penetration curves.

## 6.4 Conclusion

We have developed and applied a novel machine learning technique to predict synthetic fuel spray penetration from limited experimental data without computational fluid dynamics. When experimental data are scarce, confidence intervals on a neural network predictions are much more useful than confirming the neural network's performance with reference to a set of reserved test data. As the quantity of test data approaches infinity, the performance against test data approaches a confidence interval, but this is not an efficient use of data in the sense that it does not represent, for each data point, the greatest contribution of that data point toward improving the neural network's predictive accuracy. The bootstrap method applies every data point to the related (by statistical theory) tasks of minimising the error and quantifying the error. Thus, the bootstrap approach is preferable when data are limited.

The bootstrap confidence intervals produced in this study reflect both (1) the randomness associated with the input data, as measured by the confidence intervals on that data or the repeat sampling results of that data and (2) the residual randomness due to the random initialisation of the neural networks, surviving in the 'trained' neural networks because of under-training. It is not necessary that the training data incorporates repeat sampling or confidence intervals of its own; the method could be applied to show confidence intervals that arise entirely from under-training rather than from both sources of error. Likewise, the bootstrap method could be applied where randomness exists in the training data but under-training is not a factor, as in the study by Trichakis et al. [6].

We propose that, when data are limited, the best application of all the available data is toward the better training of neural networks and the narrowing of the confidence intervals around their predictions. When applied ad infinitum (with unlimited data), a validation study for a neural network approaches an accurate representation of a confidence interval on neural network predictions. Far better, we propose, when

data are limited, to apply all data to the narrowing of confidence intervals which are calculated from theory or from an a demonstrably sound numerical approximation of the relevant theory (such as the bootstrap method). These considerations are offered in the hope of improving the application of machine learning to limited data sets and the assessment of the uncertainty that arises from so doing.

## References

1. Y. Ikeda, D. Mazurkiewicz, Application of Neural Network Technique to Combustion Spray Dynamics Analysis, in *Progress in Discovery Science*. ed. by S. Arikawa, A. Shinohara (Springer, New York, 2002), pp.408–425
2. J. Tian et al., Experimental study on the spray characteristics of octanol diesel and prediction of spray tip penetration by ANN model. *Energy* **239**, 121920 (2022)
3. P. Koukouvinis, C. Rodriguez, J. Hwang, I. Karathanassis, M. Gavaises, L. Pickett, Machine learning and transcritical sprays: a demonstration study of their potential in ECN Spray-A. *Int. J. Engine Res.* (2021). 14680874211020292
4. J. Hwang, et al., A new pathway for prediction of gasoline sprays using machine-learning algorithms, SAE Technical Paper, (2022) 2022-01-0492
5. G. Chryssoulouris, M. Lee, A. Ramsay, Confidence interval prediction for neural network models. *IEEE Trans. Neural Netw.* **7**, 1 (1996)
6. I. Trichakis, I. Nikolos, G.P. Karatzas, Comparison of bootstrap confidence intervals for an ANN model of a karstic aquifer response. *Hydrol. Process* **25**, 2827–2836 (2011)
7. Efron (1979) Bootstrap methods: another look at the jackknife. *Annals of Statistics*, **7**(1), 1–26
8. H.Y. Lee, B.-T. Lee, Confidence-aware deep learning forecasting system for daily solar irradiance. *IET Renew. Power Gener.* **13**(10), 1681–1689 (2019)
9. C. Honecker, M. Neumann, S. Gluck, M. Schoenen, et al., Optical spray investigations on OME3–5 in a constant volume high pressure chamber. SAE Technical Paper, 2019-24-0234. (2019)
10. A. Géron, Hands-on machine learning with Scikit-Learn, Keras & TensorFlow, O'Reilly, Sebastopol, CA. (2019), pp. 331–373

**Open Access** This chapter is licensed under the terms of the Creative Commons Attribution 4.0 International License (<http://creativecommons.org/licenses/by/4.0/>), which permits use, sharing, adaptation, distribution and reproduction in any medium or format, as long as you give appropriate credit to the original author(s) and the source, provide a link to the Creative Commons license and indicate if changes were made.

The images or other third party material in this chapter are included in the chapter's Creative Commons license, unless indicated otherwise in a credit line to the material. If material is not included in the chapter's Creative Commons license and your intended use is not permitted by statutory regulation or exceeds the permitted use, you will need to obtain permission directly from the copyright holder.



# Chapter 7

## Computational Analysis of Hydro-powered Bunyip Pump



Scott Daniel Beard, Mansour Al Qubeissi, and Bidur Khanal

**Abstract** With the emerging energy demand, water shortage in rural areas, electric supply challenges, and urgent needs for net zero technologies, there has been a recent response with alternative Hydro-Powered Pumping (HPP) technology, known as the Bunyip. The recently developed system continues to build commercial success, designed to overcome several limitations associated with the previous technology of Hydraulic Ram Pump (HRP) system, such as capacity, height and water leakage issues. This paper is aimed at providing in-depth investigation into the HPP system and possible further hydraulic enhancement, using CFD parametric analysis. This could provide an insight into the fundamental flow mechanics, operational efficiency, standard capacity, and relative delivery. The investigation comprises an initial manufacture data appraisal of performance for three HPP devices. We paired our analysis with the meticulous application and numerical modelling to gather the parametric dataset, and validate against physical testing data. One key finding was that for a delivery head of 50 m, a 6 L/s supply at 4 m of head, resulted in an efficiency of 12% with respect to the water delivered relative to the volume ‘wasted’ through the discharge. Thus, in order to facilitate some of the distinguishing features for the Bunyip, the efficiency is sacrificed to a value lower than that comparable to an HRP.

**Keywords** Bunyip · Hydro-powered · Hydraulic pump · Modelling · Sustainable propulsion

---

S. D. Beard · B. Khanal

School of Mechanical, Aerospace and Automotive Engineering, Faculty of Engineering, Environment and Computing, Coventry University, Coventry, UK

M. Al Qubeissi (✉)

School of Mechanical Engineering, Coventry University, Coventry, United Kingdom  
e-mail: [ac1028@coventry.ac.uk](mailto:ac1028@coventry.ac.uk)

Department of Engineering, University of Doha for Science and Technology, Doha, Qatar

© The Author(s) 2023

J. D. Nixon et al. (eds.), *Energy and Sustainable Futures: Proceedings of the 3rd ICESF*, 2022, Springer Proceedings in Energy, [https://doi.org/10.1007/978-3-031-30960-1\\_7](https://doi.org/10.1007/978-3-031-30960-1_7)

## 7.1 Introduction

The conventional Hydraulic Ram Pump (HRP) depicted utilises two check valves that enable the system to generate cyclic changes in pressure [1]. The water hammer generated can be manipulated to pump water to a higher elevation than its initial source in the expense of a portion of expelled water. The cycle is described by three phases: The first phase, ‘acceleration’, supplies water through the body and discharges at the waste valve. Once the flow reaches a critical velocity, the drag forces acting upon the waste valve are sufficient to close the check-valve, trapping the high dynamic pressure flow to rapidly transfer into static pressure. This hammer surge in pressure breaches the delivery valve, injecting a small volume of high pressure water into the delivery line. This pumps water against the elevation pressure, known as the ‘delivery’ phase. To restart the cycle, the ‘recoil’ phase is a resultant of the drop in pressure within the device following delivery. This reopens the waste valve and enables the flow to accelerate out of the device once more. The air chamber is implemented to manage the peaks in pressure and results in a continuous stream of pumped water [2, 3].

In recent years, our understanding and approach towards the climate crisis has escalated, with ambitious commitments set across the globe [4]. Consequently, technologies powered by renewable sources have increased in demand and research has been reinvigorated into both the conventional system and alternative Hydro Powered Pump (HPP) mechanisms [5]. The following piece of research centres around an emerging alternative design, developed recently in Australia by Brett Porta and Ralph Glockemann called the Bunyip ‘pressure amplifier’ perpetual piston pump. Significant contributions were made by the author Young in [3] and [6]. This work continues to be frequently used today to support the numerical analyses undertaken, improving our understanding of the internal flow details and phenomena within HRP. The first piece of research to discuss, aimed to understand the influence of the waste valve entry region shape upon its performance [7]. The research identified that local diffuser enlargements performed best by reducing the head loss coefficient, drag coefficient and velocity uniformity across the component. The paper additionally highlighted that the abrupt changes in flow area and direction induce vortex regions, negatively influencing the performance. Consequently, conventional designs require precisely manufactured parts to achieve higher efficiency values, increasing their cost and complexity of manufacture. In what follows, the proposed system is designed with parametric analysis, using ANSYS-Fluent CFD software tool [8].

## 7.2 System Design

The initial stage of modelling was to extract the fluid body within the system and appropriately defeature the design in such a way that will simplify the modelling process, whilst being conscious not to introduce significant systematic error within

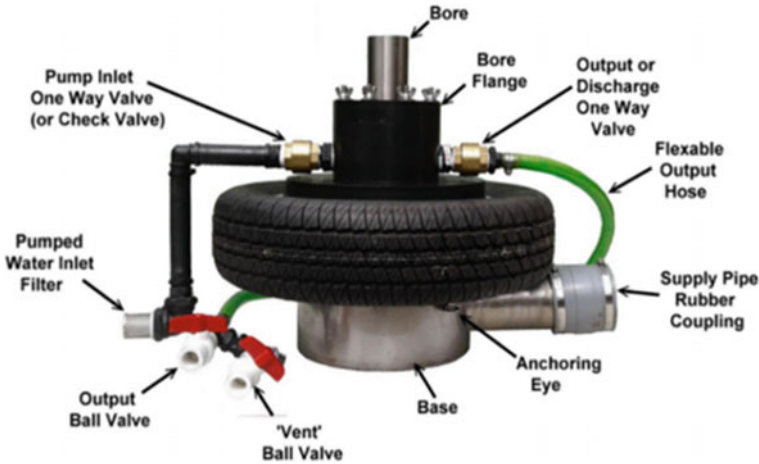


Fig. 7.1 Annotated Bunyip HPP [20]

the model. The system is powered solely by water, developed over the last decade through incremental invention [9, 10]. One of the founders had moved to the ‘Australian Bush’, opting to construct a HRP to supply water from a local creek [11]. However, with insufficient supply head and intermittent flow, failed to meet its requirements [12, 13]. Consequently, a series of concepts were developed, soon translating into commercial success, developing several models including the Oasis, Water Dragon and the Glockemann Pump, achieving a Gold Medal at the Geneva 2002 International Exhibition [14] and [15]. The system remained to be noisy and disruptive to the local area. Thus, in an attempt to reduce the undesired characteristics, the water hammer phenomena could be removed, leading to a series of redesigns and eventually the Bunyip PA-13 [8, 16–19], depicted in Fig. 7.1.

To attain a representative geometry, engagement with the pump manufacturers enabled a scaled cross section of the large Bunyip PA-13 model to be shared, depicted in Fig. 7.2. Initially, the known length could be taken from the 100mmØ supply pipe and used to determine the geometry throughout the system.

Following [21], when defeaturing the design, the following assumptions were made to reduce the modelling complexity, without introducing systematic errors from the real system. Initially within the lower region of the pump, the area below the inlet pipe can be assumed to be flat, without the requirement to model the fixings for the internal springs and fixed rod length, considered to have negligible influence upon the internal flow of the system [22, 23]. Additionally, the tyre mechanism deformation would add significant complexity to the wall definition and processing activities of the model, outlining the initial locations and profile of movement throughout the calculation. For this reason, the tyre has been constructed as a constant diameter cylinder that will simulate deformation and changes in volume through the extension of the cylinder height. Within the upper region, several defeatures could also be made. Firstly, the inlet and outlet check valves if modelled could introduce associated

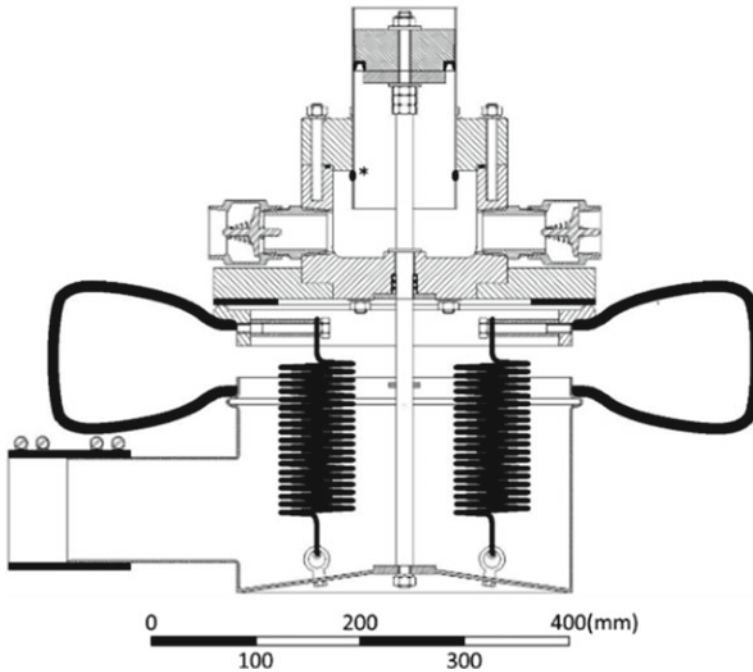


Fig. 7.2 Bunyip PA-13 scaled cross-section drawing

systematic error, without time to appropriately study their operation within the scope of research. Therefore, the valves will be manipulated as inlets and outlets, synchronised with the anticipated position of the valves throughout the cycle. Additionally, a series of discharge holes are located within the internal bore, highlighted within Fig. 7.2 using an asterisk, enabling the piston to discharge once it has descended beyond these points. The modelled geometry relocates the discharge point to the underside of the piston, eliminating the required interaction of the sliding piston and discharge locations, whilst ensuring the same access is available for water to freely exhaust from the volume.

### 7.3 Results

An execute commands have been defined and embedded within a Scheme file script of ANSYS-Fluent [8, 24]. This utilises a series of 'IF' logic statements and the flowtime within the calculation to manipulate TUI commands to define the boundary zone types and parameters [25]. The times for each phase could be determined, starting with a larger period than required and iteratively estimating the period using the previous result. At this stage, each of the inlets and outlets could be set, using



**Table 7.1** Boundary conditions for the associated system inlets and outlets

Zone	Named selection	Type	Defined value	Period [s]
Supply pipe	Inlet-lower	Velocity-inlet	0.764 [m/s]	0.00–1.50
Tyre discharge	Outlet-lower	Mass-flow-outlet	82.8 [kg/s]	1.01–1.35
Supply input	Inlet-upper	Pressure-inlet	100 [KPa]	1.01–1.50
Delivery output	Outlet-delivery-upper	Pressure-inlet Pressure-outlet	[490.5 kPa]	0.00–1.01
Piston discharge	Outlet-top-upper	Pressure-outlet	[0 Pa]	0.96–1.04

velocity, pressure, and mass-flow methods, suited for use with incompressible water. The zone details are provided in Table 7.1.

The post-processing of the CFD-Post module is conducted within ANSYS [26], enabling the efficient production of surface contours, vectors and streamlines for the velocity and pressure within the system [27]. The content will be discussed within Sect. 4. System Velocity Contours are shown in Fig. 7.3. The lower stream is shown in Fig. 7.4, the delivery streamlines are shown in Fig. 7.5, the upper piston operation is illustrated in Figs. 7.6 and 7.7.

In order to validate the model, two data sets will be used to contrast against the outputs attained through previous stages. Firstly, the publicly available Bunyip output chart enables direct reference for the supply rate, supply elevation and delivery head of 6 L/s, 4 m and 50 m as modelled. Additionally, having contacted the manufacturer, an advanced calculator tool was shared, used to quote customers, and advise the most suitable system for application [28]. The two data sets could be summarised for validation in Table 7.2.

## 7.4 Conclusions

The Bunyip dynamic motion was fully defined using the 6 degrees of freedom (DOF) solver, incorporating both the Bunyip mass and the internal spring stiffness, manipulating the mesh using the layering method to construct/destroy mesh layers. Once the model was processed the results were analysed and illustrated using the integrated CFD-post module to produce a series of figures and plots discussed. The model produced was successfully validated against two data sets, achieving agreement within the region of 10% for both the daily output and supply efficiency, recognised to consistently underestimate output parameters as a consequence of a slightly reduced piston diameter, deemed appropriate for the current research application. Despite the lack of information to validate the waste efficiency, the model emphasises that the larger diameter waste valve for pressure amplification will naturally exhaust larger volumes to provide some of the distinguishing features of the Bunyip. Consequently, it is expected that the Bunyip waste efficiency, determined at ~ 12%, is unlikely

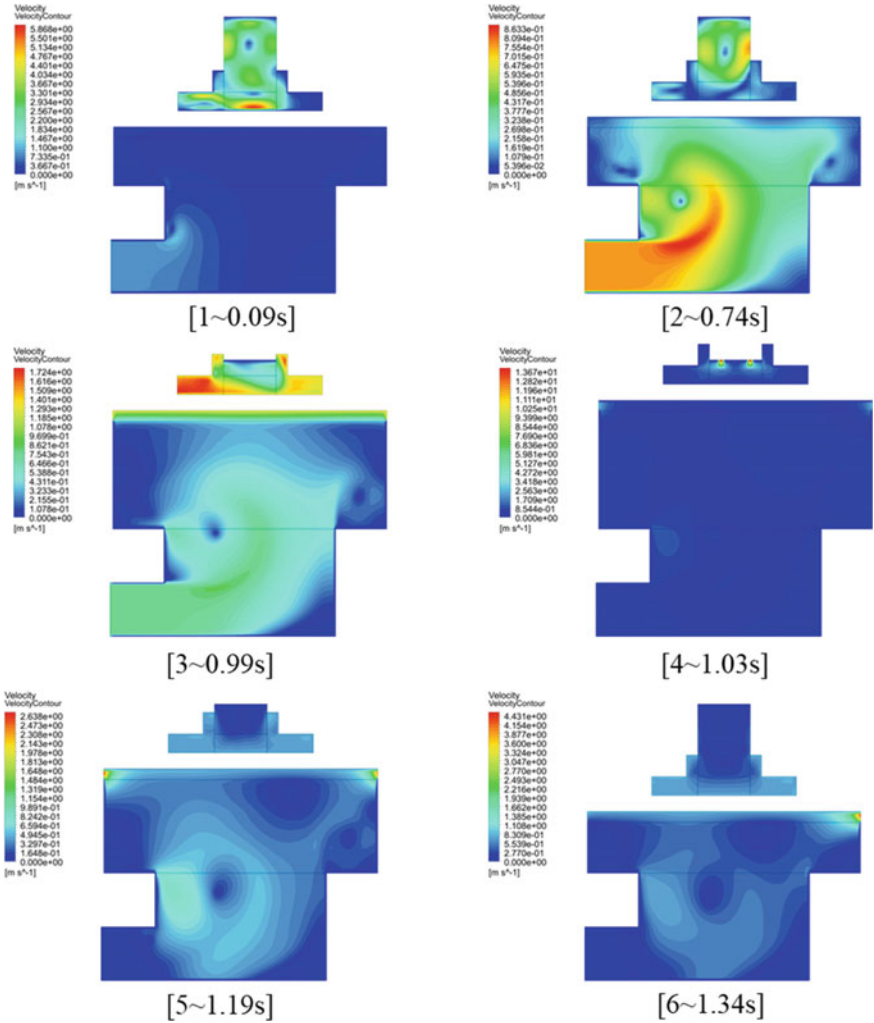


**Fig. 7.3** Bunyip cycle velocity contour illustrations with local axis, annotated [number ~ cycle time]

to achieve any greater than 30% waste efficiency. Thus, for water scarce applications, may not be as viable as precision made industry HRP alternatives achieving ~ 60% or more. Beyond quantitative data, the model enabled the flow mechanics and characteristics of the Bunyip to be visualised and discussed to elaborate upon operation, identifying potential ways to improve the function and share further research opportunities for the Bunyip system.

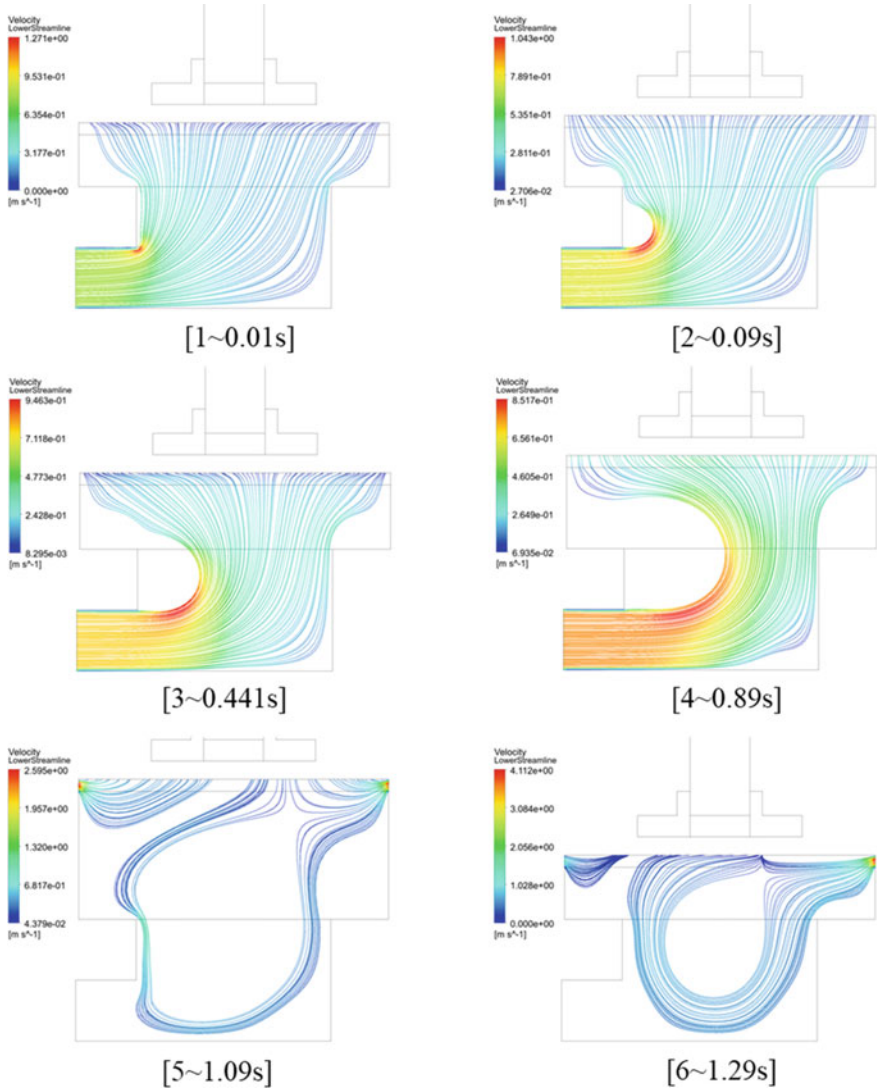


**Fig. 7.4** Bunyip cycle tyre expansion lower region streamline illustration, annotated [number ~ cycle time]

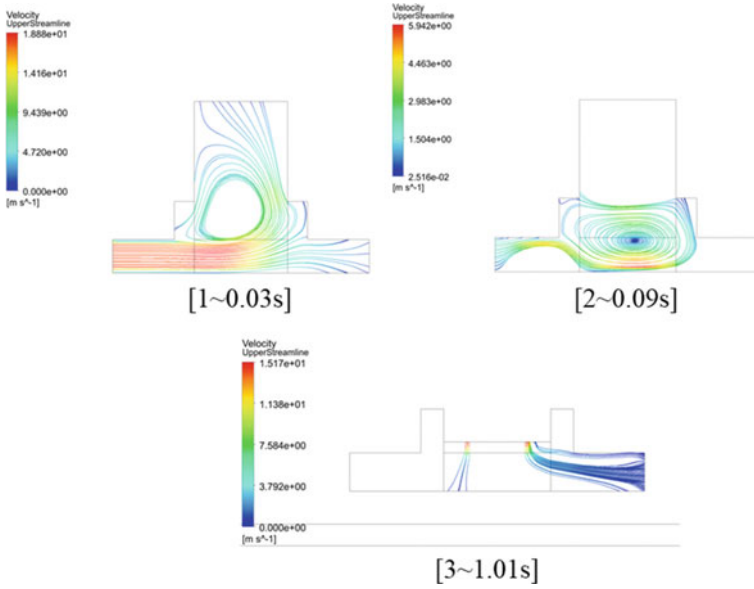


**Fig. 7.5** Bunyip cycle piston delivery, exhaust and inlet streamlines, annotated [number ~ cycle time]

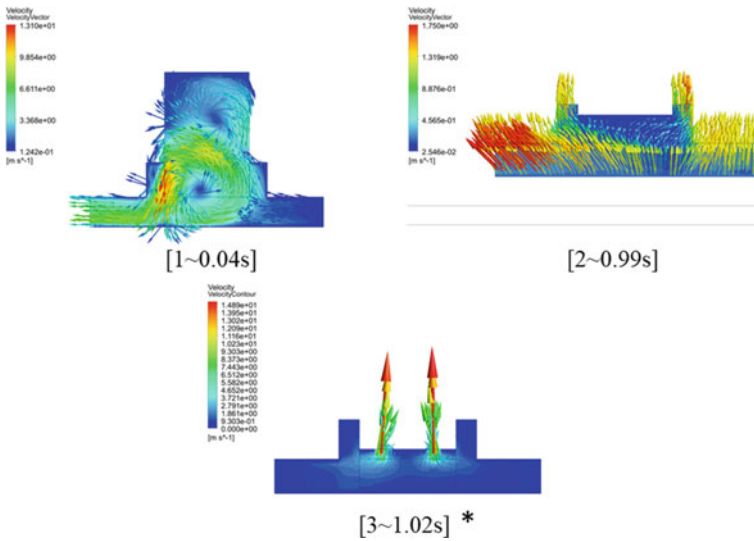


**Fig. 7.6** Normalised (\*non) velocity vectors and contours, to depict the flow mechanics within the upper region, annotated [number ~ cycle time]

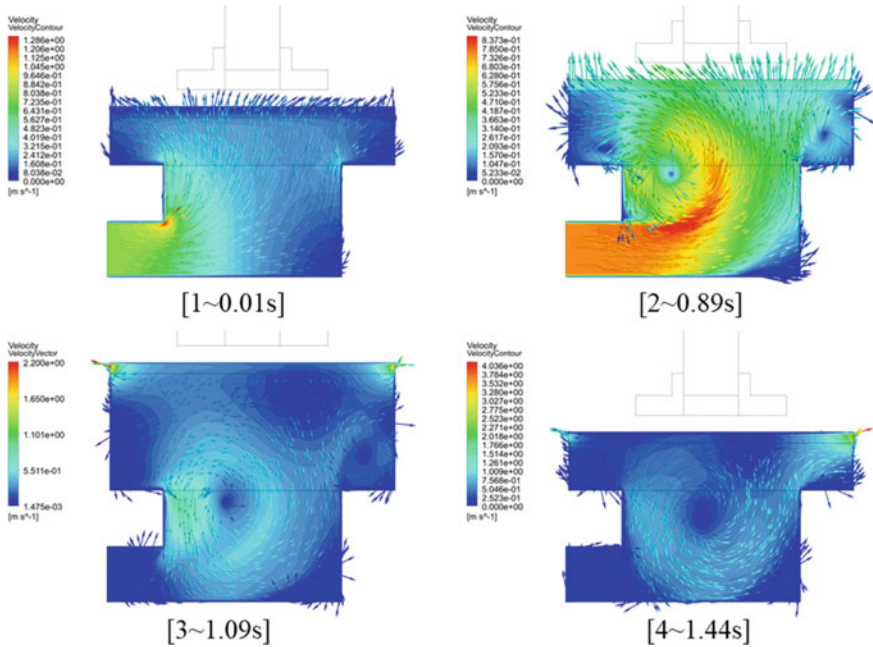


**Fig. 7.7** Normalised velocity vectors and contours to depict the flow mechanics within the lower region

**Table 7.2** Bunyip validation data

Parameter	Bunyip output chart	Bunyip advanced calculator (124 mm bore piston)
Daily capacity [L/day]	22,809 (+10.0%)	24,883 (+20.0%)
Cycle period [s]	–	~ 2
Supply efficiency [%]	–	~ 60%

**References**

1. The Pump Company, “History of the hydraulic ram,” n.d. [Online]. <http://www.theramcompany.com/history.html>. Accessed 20 Jan 2021
2. R. Balgude, S. Rupanavar, P. Bagul, M.R. Ramteke, Designing of hydraulic ram pump. Int. J. Eng. Comput. Sci. 4(5), 11966–11971 (2015)
3. B.W. Young- a, Design of hydraulic ram pump systems. Proc. IMechE Part A J. Power Energy 209(4), 313–322 (1995)
4. A. Kherde, A. Kadaskar, E. Dhoble, M. Gawal, T. Bawankar, T. Chavan, N. Singh, Research paper on hydraulic ram pump. IRE J. 3(10), 282–284 (2020)

5. D.F. Muriel, R.O. Tinoco, B.P. Filardo, E.A. Cowen, Development of a novel, robust, sustainable and low cost self-powered water pump for use in free-flowing liquid streams. *Renew. Energy* **91**, 466–476 (2016)
6. B.W. Young- b, The gravity pump: a new approach to a natural energy water pump. *J. Power Energy* **217**, 45–51 (2003)
7. X. Guo, J. Li, K. Yang, H. Fu, T. Wang, Y. Guo, Q. Xia, W. Huang, Optimal design and performance analysis of hydraulic ram pump system. *J. Power Energy: IMechE* **232**(7), 841–855 (2018)
8. ANSYS, “ANSYS free student software download,” [Online]. Available <https://www.ansys.com/academic/free-student-products>. Accessed 01 Oct 2020
9. M.N. Harith, R.A. Bakar, D. Ramasamy M. Quanjin, A significant effect on flow analysis and simulation study of improve design hydraulic pump. in *4th International Conference on Mechanical Engineering Research*, (2017)
10. W. Asvapoositkul, J. Juruta, N. Tabtimhin, Y. Limpongsa, Determination of hydraulic ram pump performance: *Hindawi: Adv. Civil Eng.* (2019), pp. 1–11
11. B. Porta, I. Trew, Introducing the Bunyip pump—no electricity or fuel needed (YouTube),” March 2019. [Online]. Available <https://www.youtube.com/watch?v=FHJmYeFKJU8>. Accessed 08 January 2021
12. J.C.I. Zambrano, J. Michavila, E.A. Pinilla, J.C. Diehl, M.W. Ertsen, Water lifting water: a comprehensive spatiotemporal review on the hydro-powered water pumping technologies. *Water* **1677**, 1–33 (2019)
13. J. Li, K. Yang, X. Guo, W. Huang, T. Wang, Y. Guo, H. Fu, Structural design and parameter optimization on a waste valve for hydraulic ram pumps. *J. Power Energy: IMechE*, pp. 1–19, (2020)
14. B. Porta, R. Glockemann- b, Bunyip vs. RAM comparison research [email] to S.Beard [01 February 2021], *Porta Affordable Pumps*, (2021)
15. B.P. Filardo, D.F. Muriel, R.O. Tinoco, E.A. Cowen, Development of a novel, robust, sustainable and low cost self-powered water pump for use in free-flowing liquid streams. *Renew. Energy* **91**, 466–476 (2016)
16. *Portas Affordable Pumps*, “Bunyip Output Chart,” n.d. [Online]. Available <http://portasaffordablepumps.com.au/assets/images/chart.pdf>. Accessed 20 Jan 2021
17. *Portas Affordable Pumps*, “PA Pump Output & Stroke Calculator,” n.d. [Online]. Available <http://portasaffordablepumps.com.au/about.html>. Accessed 20 Jan 2021
18. B. Porta, R. Glockemann- a, Bunyip, Install and user guide [email] to S. Beard [21 January 2021], *Portas Affordable Pumps*, (2021)
19. J. Tu, G.H. Yeoh, C. Liu, *Computational Fluid Dynamics: A Practical Approach*, 3rd edn. (Elsevier, Oxford, 2018)
20. M.N. Harith, R.A. Bakar, D. Ramasamy, K. Kardigama, M. Quanjin, A study of waste and delivery valve design modification to the pump performance. *Mater. Sci. Eng.* 1–12, (2018)
21. W. Sobieski, D. Gyro, Fluid flow in the impulse valve of a hydraulic ram. *Tech. Sci.* **22**(3), 205–220 (2019)
22. P.B. Shende, A.P. Ninawe, S.K. Choudhary, Analysis and enhancement of hydraulic ram pump using computational fluid dynamics (CFD). *IJRST–Int. J. Innov. Res. Sci. Technol.* **2**(3), 109–133 (2015)
23. ANSYS, “Module 09: Best Practice Guidelines,” ANSYS, Inc., (2016)
24. ANSYS, “Fluent User’s Guide—Fluent 2020 R2,” n.d. [Online]. Available [https://ansyshelp.ansys.com/account/secured?returnurl=/Views/Secured/corp/v202/en/flu\\_ug/flu\\_ug.html](https://ansyshelp.ansys.com/account/secured?returnurl=/Views/Secured/corp/v202/en/flu_ug/flu_ug.html). Accessed January–April 2021
25. J. Zhu, H. Zhu, J. Zhang, H. Zhang, A numerical study on flow patterns inside an electrical submersible pump. *J. Petrol. Sci. Eng.* **173**, 339–350 (2019)
26. *Portas Affordable Pumps- b*, “PA Pump Output & Stroke Calculator,” n.d. [Online]. Available <http://portasaffordablepumps.com.au/about.html>. Accessed 20 January 2021
27. M. Inthachot, S. Saehaeng, J.F. Max, J. Müller, W. Spreer, Hydraulic ram pumps for irrigation in Northern Thailand. *Agric. Agric. Sci. Procedia* **5**, 107–114 (2015)

28. Portas Affordable Pumps- a, “About Bunyip Pumps,” n.d. [Online]. Available <http://portasaffordablepumps.com.au/about.html>. Accessed 10 Jan 2021
29. P. Diwan, A. Patel, L. Sahu, Design and fabrication of hydraulic RAM with methods if improving efficiency. *Int. J. Current Eng. Sci. Res. (IJCESR)* 3(4), 5–13 (2016)

**Open Access** This chapter is licensed under the terms of the Creative Commons Attribution 4.0 International License (<http://creativecommons.org/licenses/by/4.0/>), which permits use, sharing, adaptation, distribution and reproduction in any medium or format, as long as you give appropriate credit to the original author(s) and the source, provide a link to the Creative Commons license and indicate if changes were made.

The images or other third party material in this chapter are included in the chapter’s Creative Commons license, unless indicated otherwise in a credit line to the material. If material is not included in the chapter’s Creative Commons license and your intended use is not permitted by statutory regulation or exceeds the permitted use, you will need to obtain permission directly from the copyright holder.



# Chapter 8

## Simulating the Effects of Inertia and Frequency Response Services on Transient Propagation in a Networked Grid



A. Christian Cooke and B. Benjamin Mestel

**Abstract** As part of climate change mitigation efforts, there has been acceleration in the deployment of distributed renewable generation replacing conventional thermal power plants in grids across the world. As a result, there has been a change in the aggregate and regional inertial capacity, with consequences for the stability of these networks and their ability to withstand large variations in frequency. Building on previous work that successfully simulated frequency events on the GB grid using a single bus model, this paper describes a networked grid model using an algebraic differential system of equations. This is used to simulate the effects of localized variation in inertia and frequency response services on the propagation of transients across a network. Using this model, the effects of varying responses to transients can be investigated, and grids of varying scales and topologies can be compared to determine differences in their response to outages. The propagation of disturbances across domains within the network that have different frequency response characteristics can be examined with a view to drawing conclusions about the optimal deployment of frequency response services, and their relative cost-effectiveness in delivering a stable supply as the proportion of renewable generation in the energy mix grows.

**Keywords** Transient analysis · Frequency response · Grid stability

### 8.1 Introduction

The reduction in cost of renewable energy and the advent of the energy crisis has accelerated the migration from conventional large-scale thermal electricity generation to distributed wind and solar resources. This has contributed to the reduction in aggregate and regional inertia of power grids, and consequently a reduced ability of these networks to withstand large variations in frequency. Sudden surges or dips in

---

A. C. Cooke (✉) · B. B. Mestel  
School of Mathematics and Statistics, The Open University, Milton Keynes MK7 6AA, UK  
e-mail: [christian.cooke@open.ac.uk](mailto:christian.cooke@open.ac.uk)



frequency are therefore more likely to result in cascading outages affecting the entire grid.

Renewable generation plants are generally smaller in scale and greater in number than conventional generators, and are more widely distributed across the network. As each of these are expected to contribute to the stability of supply in the event of outages, this adds complexity to the planning for the provision of adequate frequency response resources.

In addition, the possibility of regional variation in resources arises, where inadequate frequency response to a localised outage can lead to a variation in local frequency disproportionate to the grid average, causing regional instability and possible islanding. This local reduction in moderating the effects of outages can also serve to amplify their effects, with consequences for the reliability of the grid as a whole.

This greater complexity in planning for sufficient frequency response to mitigate reduced aggregate and regional inertia is a consequence of this trend towards smaller, more distributed renewable energy generation. It suggests the necessity of developing analyses that take these factors into account so that their effects, and the measures that can be taken to alleviate adverse outcomes that may result, can be investigated.

This paper outlines the results from a mathematical model that simulates sudden variations in frequency on a national grid with local variation in inertia and frequency response (FR) services. The model is adapted from that by Pagnier [1] which modelled the effects of inertia and damping on a grid network. The system is initialised to reflect the relevant conditions on standard network topologies of various scales and characteristics.

The simulation outputs show the effect these outages have on local and aggregate frequency, and the ability of each grid configuration to withstand large frequency deviations beyond stipulated operating bounds and its ability to recover and remain within stable limits in a reasonable timeframe.

After confirming the operation of a generically configured network, local variations in inertia and frequency response can be set up to analyse the behaviour of frequency in response to outages and surges both locally and overall. The effects of the anticipated reduction in inertia can thereby be projected, and possible remedial solutions tested that can minimise the risk of uncontrolled variations in a cost-effective manner.

## 8.2 Methodology

In previous work [2] it has been demonstrated that the principal factors counterbalancing a power imbalance on an electric grid are system inertia  $H_{SYS}$ , Primary Frequency Response (PFR), Secondary Frequency Response (SFR), damping effects and Demand Response (DR). Inertia is the conversion of the mechanical energy stored in rotating turbines coupled to the grid to and from electrical energy in opposition to a change in the power level of the system. PFR and SFR are services

provided by operators on the grid in agreement with the Transmission System Operator (National Grid ESO in the case of the GB grid) to make available resources that counter the deviation of frequency levels from safe operating levels. DR is the mechanical effect of the change in demand from load devices coupled to the grid in response to a change in frequency, where a drop in frequency will give rise to a proportional reduction in demand.

It was demonstrated [2] that it was sufficient to represent these effects in aggregate, without differentiating types of PFR, SFR or DR, in order to achieve a reasonable approximation of the frequency trace of an event. It was also shown that other network characteristics such as turbine response and deadbands have a limited additional influence on the trajectory of the frequency curve in the event of an outage or a surge. Whereas this work assumed that these effects were centralised, so that the disturbance and mitigation were acting on a single bus, in reality these services and network characteristics are distributed unevenly across a network, with consequent local variations in effects, and the incidents on the grid have a significant influence on its local and overall impact.

Using the example of [4] this single bus model is extended so as to examine the effects of this distribution in inertia, FR and disturbances. The one bus is separated into a number of buses with a single function, generation, transmission or load. Generation buses are responsible for FR, both PFR and SFR. They are also made the sources of system inertia, with each being assigned an inertia constant  $m_i$ . Demand inertia, from synchronous motors connected to the grid, is aggregated into the generator inertia profile. The distribution of grid load across the load buses is assumed to be on the basis of population density [1, 3] and load buses are the source of all DR on the network.

Disturbances are assumed to occur at one or more generator buses, so as to enable the simulation of cascading outages such as occurred on August 9, 2019 on the GB grid [4]. Whereas FR is expected to be active at these buses, there is assumed to be no inertia present. The frequency at each bus is assumed to change in response to the net imbalance in power at that bus. The propagation of the disturbance across the network is driven by the relative change in phase angles that are the result of this change in frequency, with greater phase angles between adjacent buses leading to a greater power flow between them, mediated by the susceptance of the line that connects them. These changes in frequency are resisted by FR at the generator buses and DR at the load buses. This flow of power across the network is responsible for the fluctuation in local frequency as well as the variation of aggregate frequency for the immediate area and the network as a whole.

By varying the conditions of the network at the time of a disturbance—the location of outages and surges, the distribution of inertia—as well as the magnitude of the mitigating measures—PFR, SFR, damping effects and DR—it is possible to compare the impact of similar incidents in a variety of configurations and the relative effectiveness of different counteracting network services in alternate configurations.

### 8.3 Models/Theory

The foundation of the model is the single-bus 3-dimensional system of differential equations set out in [2] (Table 8.1). The model was validated against frequency events on the GB grid during the period 2018–2019.

$$2H_{SYS}\dot{u} = p_{PFR} + p_{SFR} + p_{DR} - \Delta p \quad (8.1)$$

This model is adapted to the networked system described in [4] while preserving the FR characteristics of the single-bus system. The resulting model is an algebraic-differential system of equations representing an interconnected network of buses. In keeping with Pagnier the per-unit system is adapted to be in units of MW. Constants are modified accordingly and adopt a subscript, e.g.  $i$ , to indicate that these can be individual to the particular bus.

Central to the networked model is the flow of power between buses. Each bus has a relative voltage, and phase angle, and is connected to lossless transmission lines to adjacent buses. The power extracted at bus  $i$  at time  $t$ ,  $P_i^e$ , is determined by the aggregate difference in phase angle  $\theta_i$  at adjacent buses, for which the susceptance,  $B_{ij}$ , is non-zero. A larger variation in angle results in a greater flow of power between buses.

$$P_i^e = \sum_{j \in v} B_{ij} V_i V_j \sin(\theta_i - \theta_j) \quad \dot{\theta}_i = \omega_i \quad (8.2)$$

The propagation of these changes in power affects the calculation of the local frequency at each bus.

Generator buses have inertia and provide PFR and SFR. PFR at bus  $i$  is determined by the differential equation

$$\tau_p \dot{P}_{PFR,i} + P_{PFR,i} = P_i^e - P_i^{(0)} + \Delta P_i \quad (8.3)$$

where  $\Delta P_i$  is non-zero at buses where a disturbance occurs, while SFR is given by the equation

**Table 8.1** Single-bus 3-dimensional differential equation system for simulating frequency during an imbalance

$H_{SYS} = -\Delta p / (2\dot{u}(0))$	$u$ Frequency deviation	$H_{SYS}$ System inertia
$\tau_p \dot{P}_{PFR} = \Delta p - p_{PFR}$	$p_{PFR}$ Primary FR	$\Delta p$ Load imbalance
$\dot{p}_{SFR} = -K_i u$	$\tau_p$ Load reversal time	$p_{SFR}$ Secondary FR
$p_{DR} = \alpha_{DR} u$	$p_{DR}$ Demand FR	$K_i$ Secondary control gain
	$\alpha_{DR}$ DR coefficient	

$$\dot{P}_{SFR,i} = -K_{i,i}\omega_i \quad (8.4)$$

where  $K_{i,i}$  is a constant proportional to  $K_i$ .

The change in angular frequency at bus  $i$ ,  $\omega_i$ , is determined by the classic swing bus equation, depending on the amplitude of the imbalance between the initial power  $P_i^{(0)}$  and the current power  $P_i^e$ , and mitigated by inertia and the actions of the FR services.

$$m_i \dot{\omega}_i + d_i \omega_i = P_i^{(0)} - P_i^e + P_{PFR,i} + P_{SFR,i} \quad (8.5)$$

for  $m_i$  and  $d_i$  are the inertia and damping coefficients.

The bus (or buses) at which a disturbance occurs are assumed to be inertialess generator buses. The outage bus frequency is therefore determined by the imbalance resulting from net change in power at the bus, mitigated by Primary and Secondary Frequency Response

$$d_b \omega_b = P_b^{(0)} - \Delta P_b - P_b^e + P_{PFR,b} + P_{SFR,b} \quad (8.6)$$

The change in frequency at load buses is a result of the net power imbalance, moderated by DR.

$$\omega_i = P_i^{(0)} - P_i^e + P_{DR,i} \quad (8.7)$$

where DR is given by the equation

$$P_{DR,i} = -\alpha_i \omega_i \quad (8.8)$$

where  $\alpha_i$  is a constant proportional to  $\alpha$ .

The configuration of initial conditions and values is obtained for the relevant testcase from the OATS simulation tool [3] has a total number of buses  $v$ . A Runge-Kutta algorithm has been implemented to solve this algebraic differential system. It was found by experiment to converge to a solution with a precision of five decimal places using a step size of  $h = 0.0003$  s.

## 8.4 Results and Discussion

The model is demonstrated using the OATS 9 Bus testcase [3]. This consists of 3 generator buses and three load buses with three intermediate hub buses (Fig. 8.1). All generator buses are configured with the same coefficients for inertia, PFR and SFR. Load buses have the same coefficients for DR. A drop in power generation at bus Generator 2 with a magnitude of 100 MW is simulated at time  $t = 0$ . The resulting frequency simulation is shown in Fig. 8.2. The simulation shows a rapid drop in frequency at the loss bus, with more moderate drops at increasingly delayed

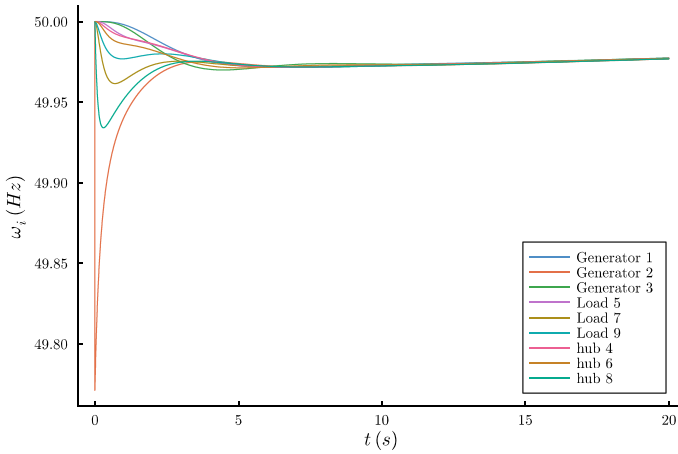


**Fig. 8.1** Frequency response of generator, hub and load buses in response to transient on Generator 2 at time  $t = 0$

intervals at the other buses. Focussing on the non-loss buses in Fig. 8.3 shows that the nearest adjacent bus to the loss bus, Hub 8, has the greatest fall in frequency, followed by the next nearest buses, Load 7 and Load 9. In addition to the magnitude of the drop in frequency, the trajectories of the frequency traces vary with distance from the loss bus, with the nadir of nearer buses occurring earlier than those further away. The overall system response, as demonstrated by the aggregate frequency trace, is moderated in its initial fall by the relative stability of buses more distant from the loss bus, which is situated at the edge of the network. The recovery of the aggregate frequency is limited by the propagation of the disturbance to these buses, resulting in a further fall after an initial recovery.

## 8.5 Conclusion

The model demonstrated shows an effective simulation for frequency change across a network of generator, hub and load buses in response to a transient that propagates across the grid. The system is configurable to simulate varied topologies and scales, with configurable inertia, frequency and demand response at each bus. The model could facilitate the investigation of these factors to ascertain optimal strategies to minimise the impact of network incidents on the system frequency. This will be the subject of further work [5].

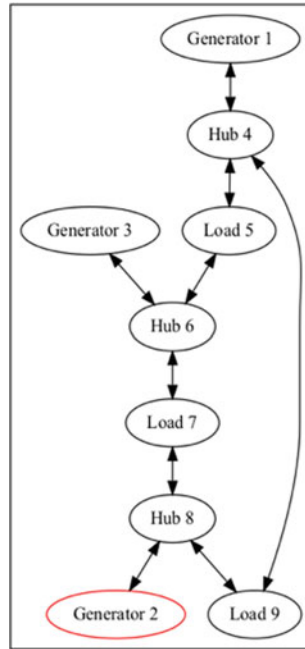


**Fig. 8.2** Layout for OATS 9 bus system

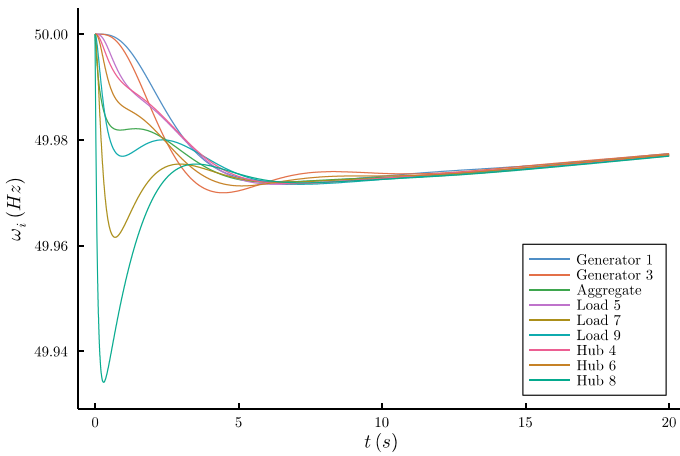


**Fig. 8.3** Non-loss generators, hub and load buses, and aggregate non-loss bus frequency response to transient

**Acknowledgements** This project has received funding from the European Union’s Horizon 2020 research and innovation programme under the Marie Skłodowska-Curie grant agreement No 801604. The contributions of Dr TC O’Neil and Prof. William Nuttall are also appreciated.

## References

1. L. Pagnier, P. Jacquod, Inertia location and slow network modes determine disturbance propagation in large-scale power grids. *PLoS ONE*, 14(3), (2019)
2. C. Cooke, Simulating the GB power system frequency during underfrequency events 2018–19. (2022) <https://doi.org/10.36227/techrxiv.19763122.v1>
3. W. Bukhsh, C. Edmunds, K. Bell, Oats: optimisation and analysis toolbox for power systems. *IEEE Trans. Power Syst.* **35**(5), 3552–3561 (2020)
4. National Grid ESO, Technical report on the events of 9 August 2019. Technical report, National Grid ESO, <https://www.nationalgrideso.com/document/152346/download>, (2020)
5. C. Cooke, Mathematical modelling of electrical power system stability—looking towards a zero carbon future, The Open University [in preparation] (2023)

**Open Access** This chapter is licensed under the terms of the Creative Commons Attribution 4.0 International License (<http://creativecommons.org/licenses/by/4.0/>), which permits use, sharing, adaptation, distribution and reproduction in any medium or format, as long as you give appropriate credit to the original author(s) and the source, provide a link to the Creative Commons license and indicate if changes were made.

The images or other third party material in this chapter are included in the chapter’s Creative Commons license, unless indicated otherwise in a credit line to the material. If material is not included in the chapter’s Creative Commons license and your intended use is not permitted by statutory regulation or exceeds the permitted use, you will need to obtain permission directly from the copyright holder.



# Chapter 9

## Multi-objective Energy Management Model for Stand-Alone Photovoltaic-Battery Systems: Application to Refugee Camps



Daniel Bammeke, Jonathan D. Nixon, James Brusey, and Elena Gaura

**Abstract** Despite the benefits of stand-alone solar photovoltaic (PV) systems in the context of refugee camps, these systems fail within the first few years of operations—typically the first three years. The leading causes of the failure of solar PV systems in refugee camps are lack of technical personnel and maintenance, lack of training and education, and demand modification leading to overconsumption of energy from lead-acid batteries. This paper proposes a multi-objective energy management model that aims to increase the longevity of lead-acid batteries while considering the Levelized Cost of Used Energy (LCUE) and user satisfaction. Scenarios incorporating different levels of demand modification are proposed to verify the effectiveness of the proposed model. A weighted sum approach was applied to solve the multi-objective optimization problem. A sensitivity analysis was performed to illustrate the effect of varying the battery objective weight, on the model’s performance. Results show that the proposed model can increase battery lifetime by up to 9 years with a 33% decrease in LCUE in some cases. The results indicate that the proposed model is likely to be useful for refugee camps that experience rapidly increasing energy demand.

**Keywords** Battery longevity · Levelised Cost of User Energy · Microgrids · Load-shedding · User satisfaction

### 9.1 Introduction

About 89% of displaced people in camps have either no or limited access to electricity [1]. Considering the vital role of electricity in camps in facilitating security, entrepreneurial activities, learning and social activities, it has become a necessary component of emergency response. Decentralized power systems, usually stand-alone diesel generator-based microgrids, have been used to power some refugee

---

D. Bammeke (✉) · J. D. Nixon · J. Brusey · E. Gaura  
Centre for Computational Science and Mathematical Modelling, Coventry University, Coventry, UK  
e-mail: [bammeked@uni.coventry.ac.uk](mailto:bammeked@uni.coventry.ac.uk)

© The Author(s) 2023  
J. D. Nixon et al. (eds.), *Energy and Sustainable Futures: Proceedings of the 3rd ICESF*, 2022, Springer Proceedings in Energy, [https://doi.org/10.1007/978-3-031-30960-1\\_9](https://doi.org/10.1007/978-3-031-30960-1_9)



camp. However, PV-based is encouraged due to its environmental and economic benefits and suitability—70% of camps are in areas with solar irradiance of over 2000 kWh/m<sup>2</sup>/year [2]. Despite the promise, stand-alone PV systems have not managed to thrive in refugee camps. No successful implementation of solar PV systems in refugee camps has been recorded. Studies have shown that failures are mostly due to battery degradation resulting from demand modification, typical of refugee camps, since they may be characterized by fluid populations [3, 4]. Demand modification, in most cases, leads to excessive energy consumption from the battery and, subsequently, lifetime reduction. Therefore, energy management and control needs to be implemented to ensure the resilience of PV-based microgrids in refugee camps, considering that the average lifespan of refugee camps is 18 years and finances for system/component replacement are usually unavailable [3].

Several methodologies and algorithms have been proposed in the energy systems management and control literature. Matallanas et al. [5] propose a neural network-based day-ahead controller for a residential grid-tied solar PV system to reduce electricity bills by shifting energy demands based on PV generation forecast and time-of-use tariffs. Shakeri et al. [6] present a real-time home Energy Management System (EMS) for a residential grid-connected PV-battery system to minimise electricity cost—battery health or lifetime was not considered. Ahmed et al. [7] propose a home EMS which minimises energy bills by limiting or shedding demand at specific times of the day—the optimisation problem was solved using a binary backtracking search algorithm.

It should be noted that every device is acquired to offer a particular amount of comfort to the user. For example, lights are installed to give visual comfort, especially at night; preventing the use of light at night may result in user dissatisfaction. Minimising the cost of energy and energy bills may involve limiting or shedding of demand, resulting in user dissatisfaction [8]. User satisfaction is defined as ‘the degree of desirability of the user to operate an appliance at a required time instant and for a particular time duration that results in a specific comfort’ [8]. Researchers have begun to consider user satisfaction in their energy management modelling. Lin et al. [9] proposed a home EMS for grid-connected houses. The energy management problem is considered a multi-objective optimization problem of ‘electricity bills versus customer satisfaction (waiting time)’ [9]. Ogunjigbe et al. [10] consider user satisfaction while controlling cost in a grid-connected system. Ogunjigbe et al. [10] propose a load shedding-based controller to maximise user-satisfaction for predetermined user electricity bill budgets. They employ Genetic Algorithm to solve the optimisation problem. Pamulapati et al. proposed a model that considers user satisfaction while reducing energy bills [8]. Like Ogunjigbe et al. [10], load shedding is applied to minimise the electricity bills, and loads were shed according to preference or user satisfaction indices assigned to devices. Cho et al. [11] propose a load shifting-based methodology for energy consumption scheduling in residential stand-alone PV-battery systems. The objectives of the proposed scheduling model were to maximise the utility of the PV system while maximizing user comfort, battery lifetime was not considered.

It is evident in the literature that most works have focused on grid-connected systems and therefore aim to minimise energy bills, cost of energy and maximizing user satisfaction; although essential, little or no relevance is given to battery longevity, which is vital to refugee camps. As a result, Narayan et al. [12] have suggested that battery lifetime should be considered in the design of EMS for off-grid solar photovoltaic systems in developing countries. To the best of the authors' knowledge, little or no work has combined energy cost, user satisfaction, and battery lifetime, all essential objectives for off-grid solar PV installations in refugee camps. By incorporating the battery lifetime objective, the effect of including battery lifetime on user satisfaction and energy cost can be investigated. Also, most works have not used real-life data, so verification may not necessarily be valid. EMS need to be verified with real data. This work proposes a multi-objective energy management model that considers the cost of user energy, user satisfaction and battery lifetime for off-grid solar PV systems in rural settings. The effectiveness of the proposed model is verified on real-life data from a refugee camp.

The rest of this paper is organised as follows: Sect. 9.2 presents the method used in this work. The proposed energy management model is formulated in Sect. 9.3, results are discussed in Sect. 9.4 followed by the conclusion in Sect. 9.5.

## 9.2 Method

A day-ahead energy management model was designed to achieve the aim and objectives of this work. The energy management model performs electrical load management (through load shedding) and controls the charge–discharge cycles of lead-acid batteries based on next-day PV forecast, load forecast and perceived user-satisfaction. Day-ahead PV forecast was obtained from Solcast—an online solar irradiance forecast service [13]. Load forecasting was achieved using the persistence forecast model and historical data [14]. Determination of user satisfaction was achieved with the user satisfaction model proposed by Pamulapati et al. [8].

A 2.04 kWp stand-alone PV system in Nyabiheke refugee camp in Rwanda (1°35'46" S, 30°15'40" E) (case study system) is selected to verify the proposed model. Possible demand modifications were modelled by adding loads to the case study system. These additional loads are actual loads connected to a diesel generator in the same refugee camp. Three scenarios were developed for consideration in this work, they are presented in Table 9.1.

The model's performance is assessed based on LCUE, battery life, user satisfaction and capacity shortage. Capacity shortage is defined in HOMER Pro as the total annual shortfall that occurs between required operating capacity and actual operating capacity.

**Table 9.1** The Nyabiheke hall case study system under 3 scenarios. Scenario 1 is the current baseline operation. Scenarios 2 and 3 (modified scenarios) considered extended connections for powering an office block, restaurants and sewing cooperatives

Scenario	Scenario description	Rationale
1	Nyabiheke hall solar PV system	This is a system that is greatly under utilised
2	Nyabiheke hall + UNHCR office + Restaurant	Other loads connected to a diesel generator in the camp were added to the benchmark system (Nyabiheke hall stand-alone solar PV system) to simulate informal modification which is characterised by an increase in the consumption of the system – this situation is a great challenge faced by solar systems in rural settings [3, 15, 16]
3	Nyabiheke hall + UNHCR office + 2 restaurants + sewing cooperative	

### 9.3 Model

In off-grid solar PV systems situated in refugee camps, it is essential to consider battery lifetime, user satisfaction and cost of energy. Due to the conflicting nature of these objectives, the problem is viewed as a multi-objective optimisation problem.

#### 9.3.1 Objective Function I

The first objective is to maximise battery lifetime. Lead-acid batteries' longevity is dependent on their State of Charge (SoC) throughout their lifetime. A battery is said to have exhausted its useful life when the cumulative throughput of the battery reaches the lifetime throughput provided by the manufacturer. SoC factor ( $f_{SoC}$ ), as proposed by Schiffer et al. [17], is a throughput multiplier representing a lead-acid battery's actual operating conditions. To reduce the cumulative throughput of lead-acid batteries,  $f_{SoC}$  must be minimized. Therefore, the first objective function is modelled as:

$$F_1 = \min \sum_{t=1}^T f_{SoC}(t) \quad (9.1)$$

$$f_{SoC}(t) = 1 + (c_{SoC,0} + c_{SoC,min}(1 - n_3(t)|_{t_0}^t)) \times \left(\frac{I_{10}}{I(t)}\right)^{1/2} \cdot \left(\exp\left(\frac{n_1(t)}{3.6}\right)\right)^{1/3} \times n_2(t) \quad (9.2)$$

$$n_1(t + \Delta t) = n_1(t) + \frac{0.0025 - (0.95 - SoC^{\max})^2}{0.0025} \quad (9.3)$$

where  $T$  is the total number of time slots in a day,  $n_1$  is the number of bad charges,  $n_2$  is the time since last full charge,  $n_3$  least SoC since last full charge.  $c_{SoC,0}$  and  $c_{SoC,min}$  are constants representing the increase in  $f_{SoC}$  when SoC = 0 and the impact of minimum SoC, respectively.

### 9.3.2 Objective Function II

The second objective,  $F_2$ , of the proposed energy management system is to maximise user satisfaction. This objective is formulated by:

$$F_2 = \max \sum_{t=1}^T \left( \frac{\sum_{n=1}^N \beta_{n,t} \times P_{n,t}}{\sum_{n=1}^N P_{n,t}} \right) \quad (9.4)$$

where  $\beta_{n,t}$  is a binary variable (equal to 1 if appliance is ON and 0 otherwise),  $P_{n,t}$  is the preference/priority index of electrical load  $n$  at time slot  $t$ .

### 9.3.3 Objective Function III

The third objective,  $F_3$ , of the proposed energy management system, is the maximisation of the performance ratio, and is formulated as:

$$F_3 = \max \frac{\left( \sum_{t=1}^T \sum_{n=1}^N E_{n,t} \times \beta_{n,t} \right)}{Y_R} \quad (9.5)$$

$$Y_R = \frac{A \times \eta_{STC} \times \int G_i}{P_o} \quad (9.6)$$

where  $E_{n,t}$  is the forecasted energy demand of electric load  $n$  in time slot  $t$  and  $Y_R$  is reference yield,  $\eta_{STC}$  is the efficiency of the PV array under standard test conditions,  $G_i$  is the solar irradiance incident on the tilted PV array (kW/m<sup>2</sup>) over a period,  $A$  is the area of the PV array,  $P_o$  is the peak power rating of the PV array (kWp).

### 9.3.4 Combined Objective Function

A weighted sum approach is applied to solve the multi-objective optimisation problem. By applying the weighted sum method, a single objective is developed from the weighted sum of the three objective functions of the optimisation problem, as seen in Eq. (9.7):

$$\text{OBJ} = \max \left( -w_{bl} \sum_{t=1}^T f_{SoC}(t) + w_{us} \sum_{t=1}^T \left( \frac{\sum_{n=1}^N \beta_{n,t} \times P_{n,t}}{\sum_{n=1}^N P_{n,t}} \right) + w_{pr} \frac{\left( \sum_{t=1}^T \sum_{n=1}^N \beta_{n,t} \times E_{n,t} \right)}{Y_R} \right) \quad (9.7)$$

where  $w_{bl}$ ,  $w_{us}$  and  $w_{pr}$  represent objective weights for battery lifetime, user satisfaction and performance ratio respectively.

### 9.3.5 Constraints

The maximisation of the objective or fitness function seen in equation is subject to a number of constraints.

To guarantee durability of battery, the SoC should always be between a minimum ( $SoC^{\min}$ ) and maximum ( $SoC^{\max}$ ) threshold SoC.

$$SoC^{\min} \leq SoC(t) \leq SoC^{\max} \quad (9.8)$$

Equation (9.9) ensures that charging and discharging of battery does not occur at the same time.

$$y_t^{ch} + y_t^{dch} \leq 1 \quad (9.9)$$

$$y_t^{ch}, y_t^{dch} \in \{0, 1\}, \forall t \quad (9.10)$$

where  $y_t^{ch}$  and  $y_t^{dch}$  are binary and indicate the charge and discharge state of the battery. The energy discharged from the battery ( $e_t^{usr\_bat}$ ) should not exceed the maximum discharge energy ( $R^{MDC}$ ) as specified on manufacturers' specification sheets.

$$e_t^{usr\_bat} \leq y_t^{dch} * R^{MDC} \quad (9.11)$$

Similarly, charge energy of battery ( $e_t^{chr}$ ) should not exceed maximum charge energy ( $R^{MCH}$ )

$$e_t^{chr} \leq y_t^{ch} * R^{MCH} \quad (9.12)$$

To ensure generation–demand balance and system stability, total energy consumption at time slot,  $t$ , ( $E_a^t$ ) should not exceed available energy.

$$\begin{cases} E_a^t \leq (SoC(t) * C_{bat}) + Y_t; & \text{if } y_t^{ch} = 0 \\ E_a^t \leq Y_t; & \text{if } y_t^{ch} = 1 \end{cases} \tag{9.13}$$

$$Y_t = A \times \eta_{STC} \times G_t \tag{9.14}$$

where  $C_{bat}$  is the nominal capacity of the battery and  $Y_t$  is the PV generation forecast at time slot  $t$ . Also, energy consumption ( $E_a^t$ ) cannot exceed the rated capacity of the inverter ( $P_{inv}$ ).

$$E_a^t \leq P_{inv} \tag{9.15}$$

### 9.4 Results and Discussion

The proposed energy management model was simulated against a whole month of data (November 2019) for the three scenarios presented in Table 9.1. Data used in this work can be found at <https://doi.org/10.5281/zenodo.4304799>. Genetic Algorithm was applied to solve the optimisation problem. A sensitivity analysis is performed to investigate the effect of objectives weight variation on the performance of the model. To achieve the variation, the weight of the battery longevity objective ( $w_{bl}$ ), is varied from 0.8 to 0.1 and  $w_{us} = w_{pr} = \frac{1-w_{bl}}{2}$ .

Without any form energy management, the performance for each scenario is presented in Table 9.2. It can be observed that possible demand modifications can significantly impact the longevity of batteries—battery life reduction of up to 12 years.

The effect of the proposed model and variation of its weight on the three scenarios are discussed in the following subsections. Determination of appropriate weights can also be achieved from the sensitivity analysis.

#### 9.4.1 Scenario 1

Scenario 1 can be classified as an oversized system since its average daily consumption is 1729 Wh, which is significantly less than the system’s generation and storage

**Table 9.2** Baseline performance of the stand-alone PV system without energy management

	Scenario 1	Scenario 2	Scenario 3
Battery life (years)	13.8	4.2	1.4
LCUE (\$/Wh)	0.022	0.015	0.038
Absolute satisfaction (%)	100	85.5	53.1

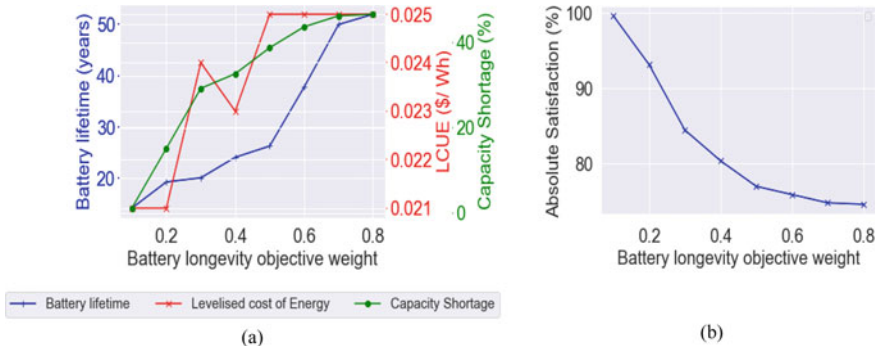


**Fig. 9.1** Plots for scenario 1—**a** effect of proposed EMS on battery lifetime and cost of energy **b** the effect of battery lifetime weight on absolute satisfaction

capacities—2.05 kWp and 10,560 Wh, respectively. The application of the model increases the battery life significantly for scenario 1. A corresponding decrease in LCUE is expected. However, the reverse is the case due to the dependence of LCUE on the trade-off between energy consumption and system lifetime. Since the system is originally oversized, an increase in  $w_{bl}$  which implies an increase in capacity shortage, will have a negative impact on the LCUE, as seen in Fig. 9.1a. For every increase in  $w_{bl}$  beyond  $w_{bl} = 0.1$ , user satisfaction decreases significantly. Increasing  $w_{bl}$  between 0.1 and 0.3 can decrease user satisfaction by up to 15%, as illustrated in Fig. 9.1b. Further increment of  $w_{bl}$  will lead to unnecessarily high user dissatisfaction.

For an oversized system such as scenario 1, the application of the proposed model may not be helpful since the battery life with energy management is satisfactory (13.8 years in the case of scenario 1), considering that the average lifetime of a refugee camp is about 17 years. Also, the energy management model has a significantly negative impact on user satisfaction and LCUE.

### 9.4.2 Scenario 2

The application of the proposed energy management model to scenario 2 can increase the battery life by up to 9 years as seen in Fig. 9.2a. The battery life increment is accompanied by increase in capacity shortage and an increase and subsequent decrease in LCUE. The initial unexpected increase for values of  $w_{bl}$  between 0.1 and 0.3 is due to a relatively small increase in battery life (from 4.5 to 4.99 years) accompanied by a relatively high increase in capacity shortage of approximately 85.9 kWh. Beyond  $w_{bl} = 0.3$ , there is a significant increase in battery life and a decrease in LCUE.

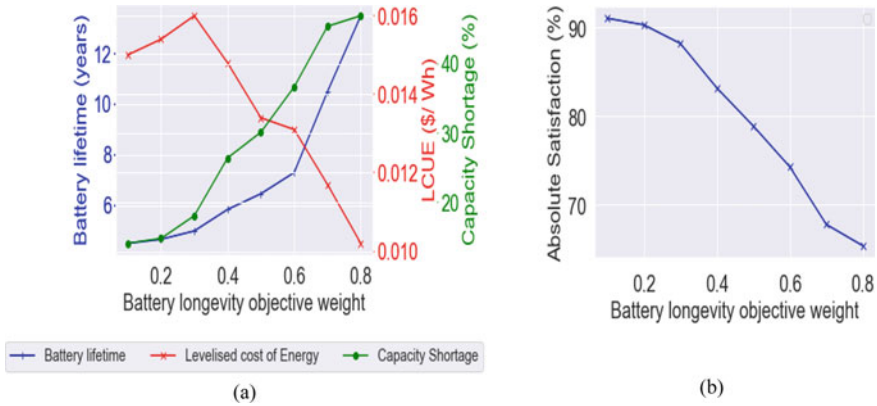


**Fig. 9.2** Plots for scenario 2—**a** effect of proposed EMS on battery lifetime and cost of energy **b** the effect of battery lifetime weight on absolute satisfaction

Selecting a value of  $w_{bl}$  equal to or greater than 0.6 may be a good point to operate. There needs to be a balance between battery lifetime and user satisfaction. LCUE may be ignored because it constantly decreases in this region ( $w_{bl} \geq 0.6$ ). Increasing the value of  $w_{bl}$  from 0.1 to 0.8 results in a decrement in user satisfaction from 91% to about 65%. The mid-point is approximately 77.5%, corresponding to  $w_{bl} = 0.5$  (battery life of 6.5). However, Fig. 9.2b depicts that sacrificing 10% more satisfaction corresponds to a  $w_{bl}$  of 0.8, which further increases the battery life by an additional 7 years.  $w_{bl} = 0.8$  may be considered the best option.

### 9.4.3 Scenario 3

Scenario 3 has the highest level of demand modification of all the scenarios considered. This demand modification can reduce the battery to 1.4 years. Due to high demand, there is a default capacity shortage of approximately 45%. Application of the energy management model can increase the battery life by up to 2.3 years with minimal impact on user satisfaction, as seen in Fig. 9.3a and b. The user satisfaction decreases by only 3%, varying the value of  $w_{bl}$  from 0.1 to 0.8. For this scenario, the proposed energy management model is beneficial since it can improve battery life by up to 2.3 years with an LCUE reduction of about 25% and minimal impact on user satisfaction.



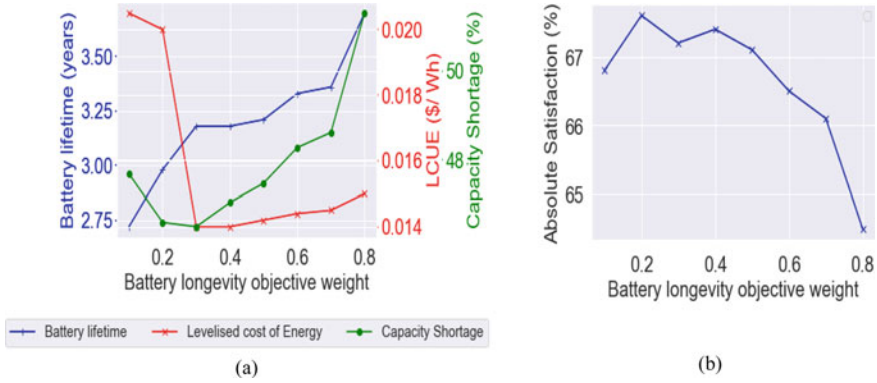


**Fig. 9.3** Plots for scenario 3—**a** effect of proposed EMS on battery lifetime and cost of energy **b** the effect of battery lifetime weight on absolute satisfaction

### 9.5 Conclusion

Our findings show that the proposed load-shedding-based energy management model is unsuitable for oversized systems, even though it can significantly increase the system’s lifetime. The significant increase in battery life is accompanied by an increase in LCUE and unnecessarily high user dissatisfaction. However, applying the proposed model to modified systems (as seen in scenarios 2 and 3) can increase the battery life and reduce LCUE with reasonable impact on user satisfaction. Therefore, the proposed model is suitable for refugee camps that experience a constant influx of refugees because it can protect standalone solar PV-Battery systems against informal demand modification typical of refugee camps.

### References

1. N. Verba, J.D. Nixon, E. Gaura, L.A. Dias, A. Halford, A community energy management system for smart microgrids. *Electr. Power Syst. Res.* **209**, 107959 (2022)
2. J. Ossenbrink, P. Pizzorni, T. Van Der Plas, Solar PV systems for refugee camps. *A Quant. Qual. Assess. Drivers Barriers*. ETH Zurich, Zurich (2018)
3. M. Fuentes, M. Vivar, H. Hosein, J. Aguilera, E. Muñoz-Cerón, Lessons learned from the field analysis of PV installations in the Saharawi refugee camps after 10 years of operation. *Renew. Sustain. Energy Rev.* **93**, 100–109 (2018)
4. L. Gollwitzer, D. Ockwell, B. Muok, A. Ely, H. Ahlborg, Rethinking the sustainability and institutional governance of electricity access and mini-grids: electricity as a common pool resource. *Energy Res. Soc. Sci.* **39**, 152–161 (2018)
5. E. Matallanas et al., Neural network controller for active demand-side management with PV energy in the residential sector. *Appl Energy* (2012)
6. M. Shakeri et al., An intelligent system architecture in home energy management systems (HEMS) for efficient demand response in smart grid. *Energy Build.* **138**, 154–164 (2017)

7. M.S. Ahmed, A. Mohamed, T. Khatib, H. Shareef, R.Z. Homod, J.A. Ali, Real time optimal schedule controller for home energy management system using new binary backtracking search algorithm. *Energy Build.* **138**, 215–227 (2017)
8. T. Pamulapati, R. Mallipeddi, M. Lee, Multi-objective home appliance scheduling with implicit and interactive user satisfaction modelling. *Appl. Energy* **267**(2), 114690 (2020)
9. Y.H. Lin, M.S. Tsai, An advanced home energy management system facilitated by nonintrusive load monitoring with automated multiobjective power scheduling. *IEEE Trans. Smart Grid* **6**(4), 1839–1851 (2015)
10. A.S.O. Ogunjuyigbe, T.R. Ayodele, O.A. Akinola, User satisfaction-induced demand side load management in residential buildings with user budget constraint. *Appl. Energy* **187**, 352–366 (2017)
11. D. Cho, J. Valenzuela, Scheduling energy consumption for residential stand-alone photovoltaic systems. *Sol. Energy* **187**, 393–403 (2019)
12. N. Narayan, J. Popovic, J. Diehl, S. Silvester, P. Bauer, M. Zeman, Developing for developing nations: Exploring an affordable solar home system design. *IEEE Global Humanitarian Technol. Conf. (GHTC)* **2016**, 474–480 (2016)
13. SOLCAST, Solar Forecasting & Solar Irradiance Data (2019)
14. S. Dutta et al., Load and renewable energy forecasting for a microgrid using persistence technique. *Energy Proc.* **143**, 617–622 (2017)
15. T. Berger, Practical constraints for photovoltaic appliances in rural areas of developing countries: lessons learnt from monitoring of stand-alone systems in remote health posts of North Gondar Zone, Ethiopia. *Energy Sustain. Dev.* **40**, 68–76 (2017)
16. J.D. Nixon, K. Bhargava, A. Halford, E. Gaura, Analysis of standalone solar streetlights for improved energy access in displaced settlements. *Renew. Energy* (2021)
17. J. Schiffer, D.U. Sauer, H. Bindner, T. Cronin, P. Lundsager, R. Kaiser, Model prediction for ranking lead-acid batteries according to expected lifetime in renewable energy systems and autonomous power-supply systems. *J. Power Sources* **168**(1), 66–78 (2007)

**Open Access** This chapter is licensed under the terms of the Creative Commons Attribution 4.0 International License (<http://creativecommons.org/licenses/by/4.0/>), which permits use, sharing, adaptation, distribution and reproduction in any medium or format, as long as you give appropriate credit to the original author(s) and the source, provide a link to the Creative Commons license and indicate if changes were made.

The images or other third party material in this chapter are included in the chapter's Creative Commons license, unless indicated otherwise in a credit line to the material. If material is not included in the chapter's Creative Commons license and your intended use is not permitted by statutory regulation or exceeds the permitted use, you will need to obtain permission directly from the copyright holder.



# Chapter 10

## Flow Simulation of a New Horizontal Axis Wind Turbine with Multiple Blades for Low Wind Speed



Essam Abo-Serie and Elif Oran

**Abstract** In this paper, a new design of a small horizontal-axis wind turbine is introduced. The design is based on the authors' patent, which uses permanent magnets impeded into a shroud that holds the rotor blades. The generator coils are installed on a fixed diffuser that houses the rotor and acts as a wind concentrator. Therefore, the new design has no hub and is based on direct coupling for electricity generation. The main features of the design have been explored to highlight the advantages with a focus on how the new design can be integrated with the recent development of green buildings. The effect of increasing the number of blades and blade chord distribution on turbine performance has been investigated for the new turbine. Initial design and analysis were carried out using the Blade Element Momentum method and CFD simulations to identify the turbine performance and examine the flow characteristics. The results showed that further energy can be extracted from the turbine if the blade chord size increases at the shroud location and reduces at the turbine hub for a low Tip Speed Ratio TSR within the range of 1.5–3. Furthermore, having more blades can significantly increase the power coefficient and extend the range of operation with a high power coefficient. The number of blades, however, has to be optimised to achieve maximum power relative to the cost. Adding a diffuser and flanges surrounding the turbine can further increase the energy extracted from the wind at low speed.

**Keywords** Wind energy · Wind power · Small wind turbines · Shrouded wind turbine · Magnetic levitated wind turbine blades

---

E. Abo-Serie (✉)  
School of Engineering, University of Leicester, Leicester, UK  
e-mail: [e.aboserie@leicester.ac.uk](mailto:e.aboserie@leicester.ac.uk)

E. Oran  
School of Mechanical Automotive and Aerospace Engineering, Coventry University, Coventry, UK

## 10.1 Introduction

There is a growing interest in using clean renewable energy resources due to recent energy demand and increasing energy prices. Moreover, a tendency toward clean renewable energy resources like wind, solar, and hydro has increased because of environmental pollution. Investment, thus, has considerably increased in wind energy over the last decade. In addition, nowadays smart buildings that produce their own power have also become very popular. Integrating renewable sources of green energy with new buildings is among the priority areas in the United States and Europe under the “Green Building” concept. Many small wind turbines are now available in the market and used in residential, agricultural, small commercial farm applications, remote communication stations, and industrial applications, either grid-connected or off-grid, using batteries for energy storage. To spread the use of small wind turbines, their drawbacks have to be limited or eliminated, particularly their limited power generation at low wind speed. The aerodynamic and mechanical noises are also major concern for small turbines to be used in residential areas [1]. More challenging; is the ability to operate efficiently micro wind turbines in urban environments and buildings [2].

Small wind turbines that operate in low-wind environments are prone to suffer performance degradation as they often fail to accelerate to a steady, power-producing condition. Flow separation at the leading-edge occurs at low Reynolds number and high attack angle, leading to sudden stall and, consequently, power loss. Previous studies showed that the design of aerofoil is critical to achieving a better start with a recommendation to use mixed-aerofoils. The improved starting capability effectively reduces the time that the turbine takes to reach its power-extraction period and, hence, an increase in overall energy, which can be as much as 40% of the generated energy [3]. Moreover, small turbines have low start-up torque because of their short rotor diameter and blade length. The power coefficient for this type of wind turbine can be about 0.25, much lower than their large counterparts with a power coefficient of 0.45 [4]. In urban areas, wind turbines typically operate at Reynolds numbers lower than  $5 \times 10^5$  due to their small rotor diameter, leading to reduced aerofoil's chord size [5]. The aerodynamics characteristic of the rotor aerofoil is a key factor that mostly affects the performance coefficient of turbines [6].

To overcome the drawback of small wind turbines, there has been continuing interest in concentrating wind flow into the turbine with the use of a smaller, lighter, and faster rotor to extract as much energy as that from a large rotor in open flow [7]. The typical way of concentrating the wind is by placing the rotor in a duct or diffuser, which allows extra mass to pass through the rotor compared to an open flow [8]. Concentrating the wind speed can reduce the ‘cut-in speed’, a wind speed below which the blades do not turn. According to Generalized Actuator Disc (GAD) method that considers a flow concentration device, the extracted energy from the wind can exceed the well-known Betz limit which is based on an open flow system. That increase is proportional to the flow augmentation achieved by the diffuser. With the GAD method, it is proved that the energy extracted by the rotor can reach as much

as 8/9 of the upstream wind energy [7, 9]. With some mathematical manipulation for the GAD method, and the Blade-Element Momentum method [10, 11], the blade twisting for the maximum lift-to-drag ratio can be identified. However, it is important to keep in mind that these methods are developed based on 2-D and inviscid flow and therefore, various correction factors have to be applied [12].

Further research work on using a shrouded turbine led to the use of a flange at the end of the diffuser [13–15]. The flange generates vortices downstream of the turbine blades causing a low-pressure zone that accelerates the flow through the turbine blades leading to a significant increase in the air mass flow rate. With the use of a large flange on a 500 W turbine, it was reported that the extracted power could be up to five times the power of an open wind turbine [16]. The use of a blade-shroud suppresses the vortices generated from the blade tips through the interference with the diffuser shroud boundary layer and therefore leads to a substantial reduction in the aerodynamic noise [17]. The shrouded structure is also providing safety toward possible damage to the blades upon hitting the tower [16]. In spite of the advantages the shrouded turbine can provide, there are challenges that need to be tackled for the shroud to be widely used and accepted. The main challenges are the extra cost and weight due to the material and manufacturing of the shroud surrounding the turbine blades. Moreover, the shrouded flanged turbine leads to higher blade speed which adds extra load on the wind turbine supporting the structure [18]. In order to limit the load and cost, the use of a short-flanged diffuser has been attempted by many researchers [19]. More recent research showed numerically that the use of a self-adaptive flange could reduce the wind load acting on the diffuser by 34.5% [20].

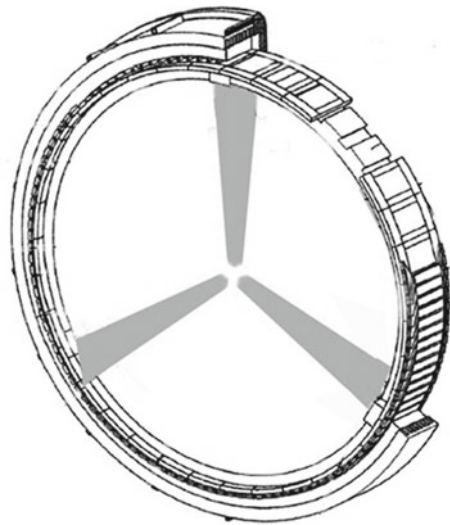
The effort to improve the performance of the wind turbine is not only limited to aerodynamics but also includes some changes in the architecture of the wind turbine system [21]. The wind generators are commonly coupled to a gearbox to transfer low-speed and high torque rotors to the generator. However, recent technology development removed the gearbox using a direct driver generator. The gearbox is not only costly but also needs regular maintenance and negatively affects the system efficiency. It is expected that further improvement will be carried out towards the direct coupling techniques with the further development in power electronics. In this work, a further improvement in the turbine design is proposed that can further increase the extracted power of the turbine, particularly for small size, and simplify the design with a more rigid structure. The proposed design uses a suspended shrouded rotor with permanent magnets impeded in the turbine shroud while the stator, which is part of the diffuser, carries the generator coils. The new design has a higher relative velocity between the rotor and stator and can have multiple coils; therefore, there is no need to have a gearbox. Moreover, the blades are no longer connected to a central hub but instead on the shroud of the rotor. The work shown here will provide a numerical analysis of how the new design can deliver more power than the conventional design.

## 10.2 New Design Approach

In the current design, the turbine blades are connected through a shroud; therefore, there is no need for a hub. Moreover, it can have more blades arranged in many different ways to achieve the best performance. Having more blades and no central hub can improve the efficiency of the turbine based on Betz's theory of wind machines [11]. The theory is based on assuming a turbine with an infinite number of rotor blades that do not result in any drag resistance to the wind flowing through them. The new turbine may have the rotor suspended by the magnetic field and therefore, there is no metal-to-metal contact or lubricant oil between the rotor and stator. This design, therefore, eliminates the mechanical noises. Furthermore, the blade can be made rigid enough without worrying about the turbine hub size. Moreover, it can easily be integrated into a diffuser to concentrate the wind that path through the blades. The turbine can be part of any building or civil construction work without a need for a special structure, as shown in Fig. 10.1. The blades are more secure as there is no way to have blades hitting the tower. The main advantages of the new design relative to the conventional turbine can be summarised as follow:

- Low wind noise as there is no clearance between the blade tip and diffuser.
- Mechanical noise due to friction is eliminated as the rotor is magnetically suspended.
- Lower stress is acting on the blade roots as the wind forces acting near the hub of the turbine are minimum.
- Rotor blades can be made more rigid and lighter.
- Rotor with multiple blades can be used.
- Efficiency is improved due to direct coupling and removal of the gearbox.

**Fig. 10.1** Proposed wind turbine design



- High torque can be generated at low wind speed. The pressure difference between the two sides of the aerofoil near the tip will produce high force and torque due to its relatively larger area and longer radius.
- There is more flexibility in blade shape design.
- The drawback of small size turbines in terms of noise can be eliminated using a suspended rotor.

Although these mentioned advantages can logically be explained, work is currently carried out to evaluate and maximise the benefits. It is also equally important to evaluate the drawbacks of the new design, particularly in terms of power density and cost.

### 10.3 Operating Parameters and Methodology

This work pays attention to two major parameters that can improve the turbine aerodynamic performance. The first parameter is chord distribution along the blade length and the second parameter is the number of blades. A small turbine of a diameter 4.3 m using NREL S822 aerofoil is used in this investigation. Detail of the operating conditions and main geometry is shown in Table 10.1 and Fig. 10.2. For BEM method, six different designs have been investigated. The first one has a chord length that is linearly increased from a minimum value  $C_{\min}$  at the hub to a maximum  $C_{\max}$  at the tip and has three blades. The second turbine also has three blades, but the chord length is inversely laid down where the large chord length is located at the tip and the smallest at the hub. The other three designs are similar to the second design but have 5, 8, 12 and 18 blades. The solidity of 3, 5, 8, 12 and 18 blades is 0.08, 0.13, 0.21, 0.32 and 0.49 respectively. The wind speed is varied from 2 to 16 m/s and tip speed ratios from 0.5 to 4. The different cases that have been analysed are shown in Fig. 10.3. The turbine shroud and concentrator have only been used in the CFD simulation to examine the effect of increasing the wind speed on the extracted power.

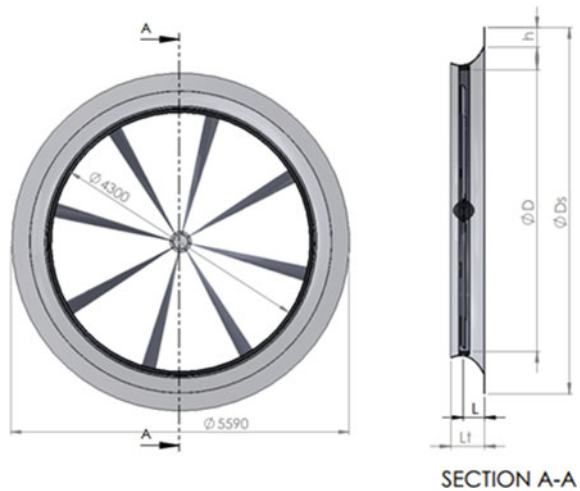
#### Blade Element Momentum Method

The design was carried out using BEM method which is the common method used in industry to provide the initial design of wind turbines. Although this method is developed for 2-D flow its results are reliable after the correction factors are applied [12]. Detail about the method and the derived equations can be found in many references [22]. The NREL S822 profile is used in Q-blade software [23] to carry out the BEM analysis. Based on the BEM method, the blade is divided radially into eight sections, and the values of axial induction factor ( $a$ ) and tangential induction factor ( $a'$ ) are calculated using an iterative method from the drag and lift coefficients of the blade at each section. The pitch angle of the blade can then be calculated at each section along the blade for a specific tip speed ratio [22]. The velocity triangle at the tip of the blade is shown in Fig. 10.4; similar triangles can be drawn at each of the eight sections of the turbine blade which has a different value of blade speed.

**Table 10.1** The main parameters used in the CFD simulation

Parameter	Unit	Symbol	
Wind velocity ( $V_o$ )	m/s	V	7
Rotational speed	Rpm	n	75
Diameter $D = 2R$	M	D	4.3
Tip blade speed	m/s	U	16.89
Tip speed ratio		TSR	2.41
Hub diameter	Cm	d	30
Min. chord length	Cm	$C_{min}$	5
Max. chord length	Cm	$C_{max}$	25
Blade number		Z	3,5,12,18
Blade length	M	$L_b$	2
Shroud diameter	M	$D_s$	1.3 D
The width of the brim	M	h	0.15 D
The diffuser length	M	Lt	1.47 D

**Fig. 10.2** Main dimensions of the diffuser and shroud used in the study



**Computational Fluid Dynamics**

This work also examines the 3-D flow pattern and the energy transmitted to the wind turbine blades using the commercial package STARCCM + version 10.04. Only the 8-blade turbine is investigated using CFD, considering a surrounded short diffuser and flange. The aim is to evaluate the percentage increase of power from the wind concentrator. The flow was assumed to be steady and incompressible since Mach number is approximately 0.03 which is much below to affect the density value. Reynolds Averaged Navier Stokes, RANS equations are employed together with the SST k-ε turbulence model equations to identify the flow pattern within the flow



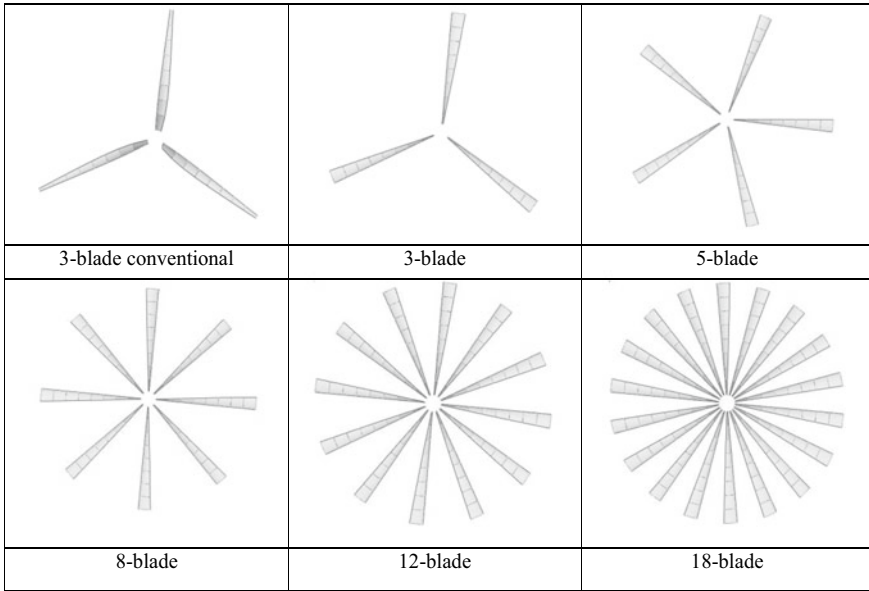


**Fig. 10.3** Turbine baseline and the new turbine with different blades number

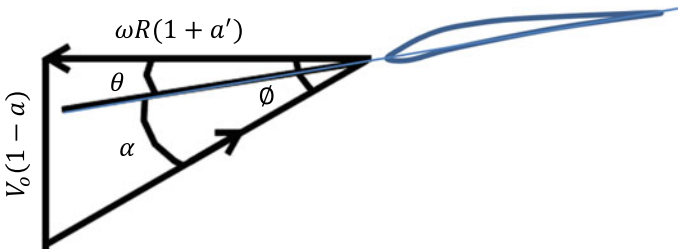


**Fig. 10.4** Sketch showing the velocity triangle at the tip of the blade

domain. The SST  $k-\epsilon$  model was selected based on previous studies, which showed the predicted results were close to the experimental data [24]. A rotating reference frame was employed to represent the rotation of the fluid region of the rotor.

The computation domain consists of a cylindrical segment that contains a single blade and part of the hub, shroud and the surrounded cylinder. The segment size for the 8-blade turbine has an angle of  $45^\circ$ . A periodic boundary condition is applied on the two sides of the segment. The domain is separated into two subdomains; the first is the rotating region which includes the rotating blades and a shroud, and the second subdomain contains the outer region, as shown in Fig. 10.5. The outer region has a length of five times the turbine radius downstream the turbine and a radius equal to 2.5 times the turbine radius. A uniform, steady velocity is assumed at the inlet of the computational domain with 5% turbulence intensity. The pressure outlet

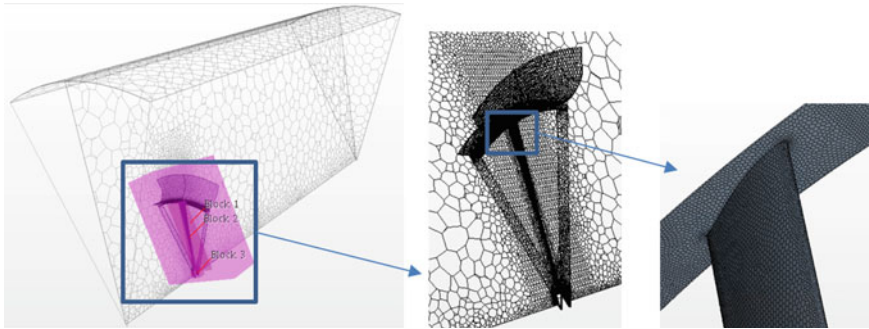


**Fig. 10.5** The polyhedral mesh with refining zones and blade surface refined mesh

boundary condition is applied at the outlet. A symmetrical wall boundary condition is applied across the curved cylinder segment surface of the outer domain. For all turbine surfaces, a no-slip boundary condition is specified.

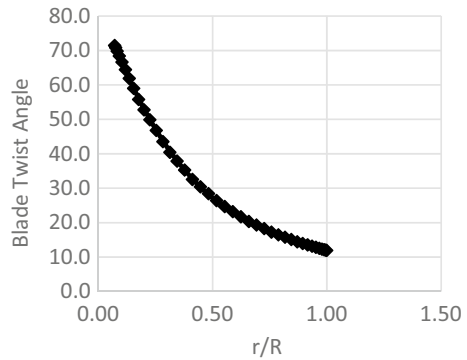
Figure 10.5 also shows the unstructured polyhedral mesh that is used in the computation domain with a refined mesh size in the rotating region and where a high-velocity gradient is expected. The effect of having different ways of refining the mesh can influence the simulation error [25]. In this study, different volumetric control zones have been selected and refined based on the expected velocity gradient while mesh size ratio expansion is set to slowly change the mesh size from the zone of large size mesh to the small size mesh. Special attention is paid to the mesh on the surface of the blades to keep the edges during the volume meshing. Prism layers are used around the surface of the turbine to accurately calculate the shear force and adjust  $y^+$  value to be within the recommended values of 30–100 in order to have the first cell adjacent to the wall located within the logarithmic region of the boundary layer.

## 10.4 Results and Discussions

### Blade Element Momentum Results

After the blade aerofoil is identified, the lift and drag coefficients have been estimated for various attack angles using XFOIL algorithm, which is implemented in QBlade software [26]. The evaluated drag and lift coefficients were found to be close to the values tabulated by NREL. The maximum lift-to-drag ratio was found to be at  $6^\circ$ . The optimum twist angle was calculated for each section for a tip speed ratio of 2.4. This value was chosen to allow the turbine to be used at low wind speed. The values of the twist angle along the blade radius are shown in Fig. 10.6. With the new blades, the twisting is not difficult since the high twist occurs near the hub, where the chord size is small.

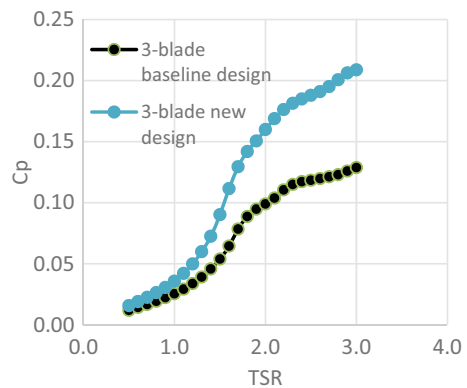
**Fig. 10.6** Blade twist angle along the blade radius



A comparison between the new chord distribution blade and the conventional blades is shown in Fig. 10.7. The power coefficient  $C_p$  for the new blade design is significantly more than the conventional blade with almost 36% at TSR of 2.4 for the 3-blade turbine. This value increases to 61% at TSR of 3. This is not a surprise since the interaction property between the fluid and the blades is the pressure, and having a large area toward the tip will increase the force which is multiplied by a long radius to produce the torque. The linear increase of the blade chord size is not the optimum profile, but it is selected here to simplify the model and to prove the concept.

In order to examine how the number of blades or solidity affects the turbine performance, the power coefficient has been evaluated for different blade numbers and TSR, as shown in Fig. 10.8. The figure shows significantly improved  $C_p$  values as the blade number increases. It also shows that the range of operation at high  $C_p$  values increases with the number of blades. In other words, the wind turbine can work with a high power factor over a broader range of wind speeds if the turbine speed remains constant. The figure also indicates that the turbine with more blades can work more efficiently at low wind speeds. It is also noticeable that the maximum

**Fig. 10.7** Blade power coefficient at different tip speed ratio for the new and conventional blades



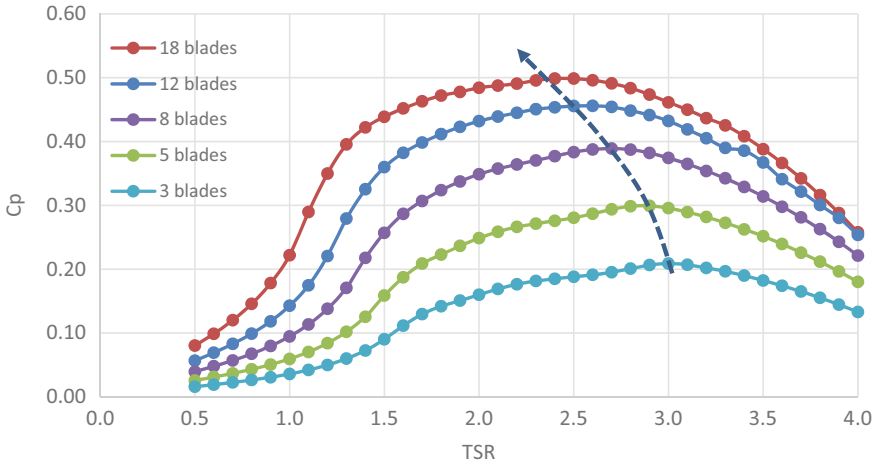


**Fig. 10.8** Effect of blade number on power coefficient for the new blades

value of  $C_p$  is shifted towards lower TSR as the blade number increases. For  $TSR = 1$ , the value of  $C_p$  for the 18-blade turbine is almost five times that of the 3-blade turbine. Almost the same ratio can be found at  $TSR = 1.5$ .

Since the speed of the small turbine can be varied based on the wind speed, it is possible to keep the TSR at its optimum value. Figure 10.9 shows how the wind power does not change considerably with the TSR compared to the change if TSR is kept at its optimum value.

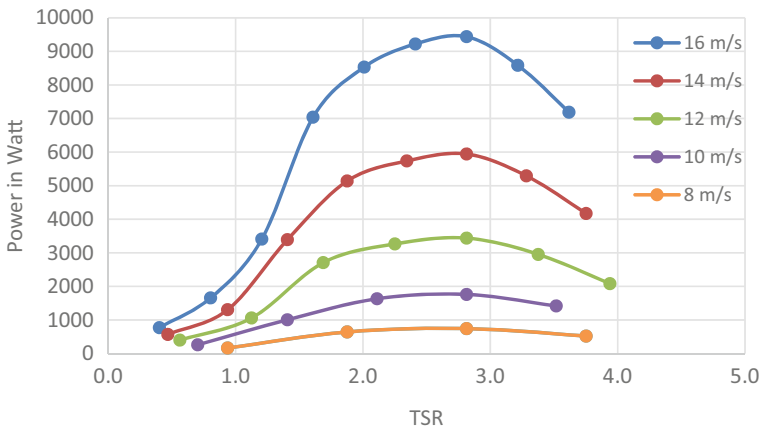


**Fig. 10.9** Effect of wind speed on the generated power for the 8-blade turbine

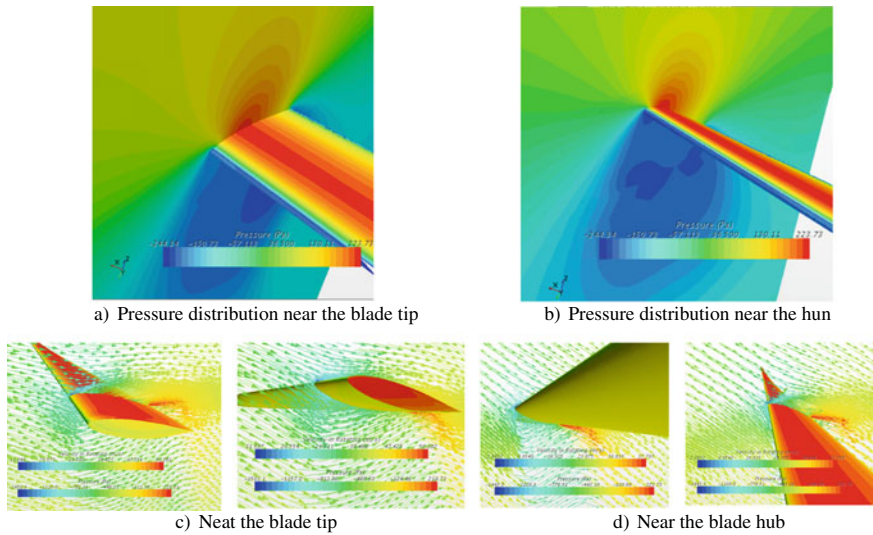


**Fig. 10.10** Flow velocity and blade pressure distribution near and tip and hub of the blade

### CFD Results

In order to demonstrate the effect of using a shroud and flange on the turbine to concentrate the wind and increase the spatial distribution of velocity and pressure were evaluated using the CFD simulation. The velocity vector around the blade was first investigated to examine the existence of flow separation around the blade. Figure 10.10 shows an attached flow near the tip of the blade and the pressure distribution at the back and front sides of the blades. From the figure, it can be seen that the values of the pressure near the hub and tip are almost the same. However, due to the larger surface area near the blade tip, a larger torque and consequently more power can be produced.

The effect of blade turbine shroud and flanges on flow pattern and pressure is shown in Fig. 10.11. A large vortex is formed behind the shroud flange generating a low-pressure region that extends downstream of the turbine by a distance almost equal to the blade radius. The location of the low-pressure region depends on the flange design. Nevertheless, the low-pressure region assists in driving more air to pass through the turbine blades and consequently increases the generated power. The turbine power is evaluated by integrating the torque over the turbine blade surface area, considering both the pressure and shear stress. The integrated torque was calculated for three wind speeds: 8, 12 and 16 m/s, while keeping the TSR at its optimum value of 2.41; therefore, the turbine rotational speed changes to 75, 130 and 172 rpm, respectively. The calculated torque is multiplied by the angular speed of the blades to evaluate the transmitted power. The power obtained using CFD for the flange and diffuser turbine is compared with the power calculated using the BEM method for the open turbine, as shown in Fig. 10.12. Adding the flange to the

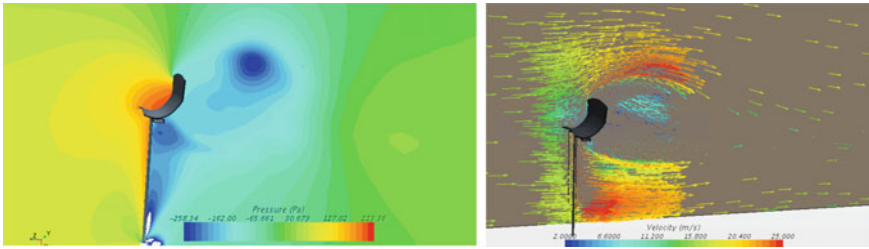


**Fig. 10.11** Flow pressure and velocity vector distribution along a plan showing the effect of the shroud and flange on flow distribution

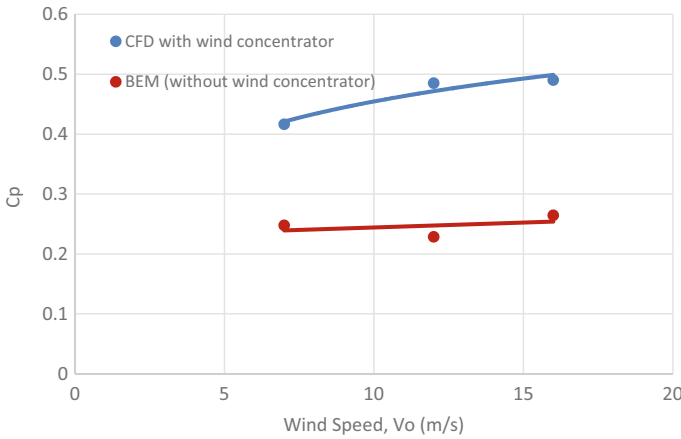


**Fig. 10.12** The effect of the concentrator on the power coefficient relative to the value calculated using BEM method for a bare turbine at  $TSR = 2.41$

shroud stator has a significant improvement in  $C_p$  value which may exceed the Bitz limit after optimising the flange geometry and the wind concentrator at low TSR. The increase of  $C_p$  value with wind speed may be attributed to the further drop in pressure in the wake region. Currently, experimental work is carried out to test a prototype.

### 10.5 Conclusions

A new innovative design for a small axial wind turbine that has a suspended rotor surrounded by a permanent magnet has been introduced. The performance has been explored considering inversely laid blades and having more blades. Using the BEM method and CFD simulation, it has conceptually proved that the newly designed turbine with a blade chord length increasing towards the tip can run at lower wind

speed and extract more power from the wind. Furthermore, increasing the number of blades can extend its range of operation to lower wind speeds and improve the power coefficient. Finally, the CFD results showed that adding a small size diffuser with a flange can concentrate the wind and therefore improve the aerodynamic performance of the wind turbine.

## References

1. N. Prabakaran, K.J. Krishnan, S. Dhamodharan, Design and analysis of horizontal axis wind turbine blade. *Int. J. Inf. Technol. Comput. Sci. Perspect.* **2**(1), 435–444 (2013)
2. Encraft Organization, ‘Warwick Microwind Trial project’ final Report, at <http://www.warwickkwindtrials.org.uk/resources/Warwick+Wind+Trials+Final+Report+.pdf>. Accessed on 13 June 2022
3. S. Worasinchal, Small Wind Turbine Starting Behaviour, Durham theses, Durham University, 2012. Available at Durham E-Theses Online: <http://etheses.dur.ac.uk/4436/>
4. R.K. Singh, M. Rafiuddin Ahmed, M. Asid Zullah et al., Design of a low Reynolds number airfoil for small horizontal axis wind turbines. Elsevier, *Renew. Energy* **42**, 66–76 (2012)
5. R.K. Singh, M. Rafiuddin Ahmed, Blade design and performance testing of a small wind turbine rotor for low wind speed applications. Elsevier, *Renew. Energy* **50**, 812–819 (2013)
6. J. Yao, W. Yuan, Wang et al., Numerical simulation of aerodynamic performance for two dimensional wind turbine airfoils. Elsevier, *Energy Proc.* **31**, 88–86 (2012)
7. P. Jamieson, *Innovation in Wind Turbine*, 1st edn. (John Wiley & Sons, 2011)
8. M.O.L. Hansen, N.N. Sørensen, R.G.J. Flay, Effect of placing a diffuser around a wind turbine. *Wind Energy Int. J. Progress Appl. Wind Power Conver. Technol.* **3**(4), 207–213 (2000)
9. B.L. Gilbert, K.M. Foreman, Experiments with a diffuser-augmented model wind turbine. *J. Energy Res. Technol.* **105**, 46–53 (1983)
10. R.E. Wilson, P.B.S. Lissaman, S.N. Walker, Applied aerodynamics of wind power machines (University of Oregon, 1976)
11. J. Tangler, J.D. Kocurek, Wind turbine post-stall airfoil performance characteristics guidelines for blade-element momentum methods. in *43rd AIAA Aerospace Sciences Meeting and Exhibit* (Reno, Nevada, 2005, January), pp 10–13
12. C. Anderson, *Wind turbines: Theory and practice* (Cambridge University Press, 2020)
13. K. Abe, M. Nishida, A. Sakurai, Y. Ohya, H. Kihara, E. Wada et al., Experimental and numerical investigations of flow fields behind a small wind turbine with a flanged diffuser. *J. Wind Eng. Ind. Aerodyn.* **93**(12), 951e70 (2005)
14. Y. Ohya, T. Karasudani, A. Sakurai, K.-I. Abe, M. Inoue Development of a shrouded wind turbine with a flanged diffuser. *J. Wind Eng. Ind. Aerodyn.* **96**(5), 524e39 (2008)
15. Y. Ohya, T. Karasudani A shrouded wind turbine generating high output power with wind-lens technology. *Energies* **131** (2010)
16. S. Rajakumar, D. Ravaindran, Computational fluid dynamics of wind turbine blade at various angles of attack and low Reynolds number. *Int. J. Eng. Sci. Technol.* **2**(11), 6474–6484 (2010)
17. K. Abe, H. Kihara, A. Sakurai, M. Nishida, Y. Ohya, E. Wada, K. Sato, An experimental study of tip-vortex structures behind a small wind turbine with a flanged diffuser. *Wind Struct.* **413–417** (2006)
18. W.X. Wang, T. Matsubara, J.F. Hu, S. Odahara, T. Nagai, T. Karasutani, Y. Ohya, Experimental investigation into the influence of the flanged diffuser on the dynamic behavior of CFRP blade of a shrouded wind turbine. *Renew. Energy* **78**, 386–397 (2015)
19. Y. Ohya, T. Karasudani, A shrouded wind turbine generating high output power with wind-lens technology. *Energies* **3**, 634–649 (2010)

20. J.-F. Hu, W.-X. Wang, Upgrading a shrouded wind turbine with a self-adaptive flanged diffuser. *Energies* **8**, 5319–5337 (2015). <https://doi.org/10.3390/en8065319>
21. M.M. Hossain, M.H. Ali, Future research directions for the wind turbine generator system. *Renew. Sustain. Energy Rev.* **49**, 481–489 (2015)
22. M.O.L. Hansen, *Aerodynamics of Wind Turbines*, 2nd edn. (Earthscan, London, UK)
23. D. Marten, J. Wendler, G. Pechlivanoglou, C.N. Nayeri, C.O. Paschereit, QBLADE: an open source tool for design and simulation of horizontal and vertical axis wind turbines. *Int. J. Emerg. Technol. Adv. Eng. ICERTSD* **3**(3), 264–269 (2013)
24. N. Sorensen, J. Michelsen, S. Schreck, Navier-stokes predictions of the NREL phase vi rotor in the NASA Ames 80 ft by 120 ft wind tunnel. *Wind Energy* **5**(2–3), 151–169 (2002)
25. A. Elyana, E. Abo-Serie, A. Gaylard, Mesh optimisation for ground vehicle aerodynamics. *CFD Lett.* **2**(1), 54–65 (2010)
26. D. Marten, J. Wendler, G. Pechlivanoglou, C.N. Nayeri, C.O. Paschereit, Qblade: an open source tool for design and simulation of horizontal and vertical axis wind turbines. *Int. J. Emerg. Technol. Adv. Eng. (IJETA)* **3**, 264–269 (2013)

**Open Access** This chapter is licensed under the terms of the Creative Commons Attribution 4.0 International License (<http://creativecommons.org/licenses/by/4.0/>), which permits use, sharing, adaptation, distribution and reproduction in any medium or format, as long as you give appropriate credit to the original author(s) and the source, provide a link to the Creative Commons license and indicate if changes were made.

The images or other third party material in this chapter are included in the chapter's Creative Commons license, unless indicated otherwise in a credit line to the material. If material is not included in the chapter's Creative Commons license and your intended use is not permitted by statutory regulation or exceeds the permitted use, you will need to obtain permission directly from the copyright holder.





# Chapter 11

## Indoor Thermal Comfort Controller Integrating Human Interaction in the Control-Loop as a Live Component



Edgar Segovia, Paul van Schaik, and Vladimir Vukovic

**Abstract** This research integrates the human component as a living part of the control loop, using preferences to optimise energy consumption. This paper presents an outline of a temperature controller, which is based on the theory of thermal comfort and uses fuzzy logic to optimise comfort and reduce energy consumption. The controller allows multiple-inputs, from more than one single user to set a temperature-setpoint. The control-logic was developed in MATLAB using the Simulink tool in the simulations, energy use is optimized, reducing energy consumption between 22 and 31%. The controller was tested in an office to improve the average thermal sensation of the participants between 14 and 17%. In future works increase the sample size and evaluate the non-energy impacts of the energy efficiency on thermal comfort.

**Keywords** Thermal comfort controller · Thermostat · Energy efficiency · Simulation · Predicted mean vote · Energy consumption · Built environment

### 11.1 Introduction

The human factor is the fundamental piece to understanding energy consumption, as people consume energy. Engineering systems often do not consider people as variables in time and less the differences that may exist between a group of people [1]. In this document, we integrate the people directly into a temperature controller that reduces energy consumption while using as the main indicator the thermal sensation of users.

---

E. Segovia (✉) · P. van Schaik  
School of Social Sciences, Humanities & Law, Teesside University, Middlesbrough, UK  
e-mail: [E.SegoviaLeon@tees.ac.uk](mailto:E.SegoviaLeon@tees.ac.uk)

E. Segovia · V. Vukovic  
School of Computing, Engineering and Digital Technologies, Teesside University,  
Middlesbrough, UK

**Table 11.1** Literature review

		Energy optimisation			Total
		Yes	No	NS	
User temperature input	Yes	[6–10]	[11, 12]	[–]	7
	No	[13–22]	[23, 24]	[–]	12
	NS	[–]	[25]	[–]	1
Total		15	5	0	

Thermal comfort is an essential concept in building design according to ASHRAE Standard 55 [2], thermal comfort occurs when the person feels contented with the surrounding environmental temperature. People's efficiency and productivity are associated with thermal comfort; at the same time, the thermal comfort level is estimated through the metabolic rate [3]. Having a good understanding of these relationships is important to improve the general conditions of a room and the quality of life of the occupants, and in some cases can save energy.

The predicted mean vote (PMV) methodology has the objective of predicting the thermal sensation in buildings [4]. The prediction is based on equations developed in 1960 which are described in the paper [5] The literature on PMV applied in fuzzy logic is extensive. Table 11.1 shows the studies in detail, classifying them according to the setpoint type (user temperature input, automatic setpoint, or not specified 'NS') and if taking in consideration the energy consumption on the control loop to do energy optimization, not in consideration or not specified.

Table 11.1 shows that most of the articles (15 out of 20) consider energy optimisation. Table 11.1 shows how fuzzy logic is almost always implemented to optimise energy consumption. In most of the identified research studies (12 out of 20 papers) users are not allowed to choose a setpoint-temperature. Rather, the researchers used fuzzy logic to automatically choose a temperature setpoint. Dovjak and Shukuya [11] apply fuzzy logic in thermal comfort control, such as temperature, and combine a level of thermal sensation, similar to how the PMV equation works. The PMV equation takes physical values and gives a thermal sensation value. However, in this study, they do not consider the thermal sensation and compared with the PMV model it.

According to [26] ASHRAE's [26] in the 1970s when the first steps were taken to develop a thermal comfort model, the concept of PMV was developed. The main concept in the PMV model is the body's thermal neutrality, The scale, 0 represents thermal neutrality, 1, 2 and 3 represent different levels of sensation of heat and – 1, – 2 and – 3 levels of sensation of cold.

Thermal comfort null (equal to 0), only when the heat generated minus heat transfer to the environment ( $L = Q_{\text{generate}} - Q_{\text{transfer}}$ ) is equal to 0. A body thermal load of 0 represents a heat transfer level to keep the temperature of the body stable, and a heat transfer at a comfortable value. Six factors directly affect thermal neutrality: Metabolic Rate ( $\text{W}/\text{m}^2$ ), Clothing insulation (dimensionless), Air temperature ( $^{\circ}\text{C}$ ), Radiant temperature ( $^{\circ}\text{C}$ ), Airspeed ( $\text{m}/\text{s}$ ), Humidity (dimensionless). The first two

factors, metabolic rate and clothing insulation depend on the users and correspond, respectively, to the activity they carry out and to the clothing they wear, the other 4 factors depend on the environment.

In the PMV model, it is necessary to calculate the predicted percentage of dissatisfaction (PPD). The equation that models PPD is an inverted Gaussian and is a function of the PMV, the equations are described in detail in the literature [5]. When PMV is 0 the PPD is equal to 5% (minimum); the PMV model keeps the PPD lower than 10%, which corresponds to 0.5 and  $-0.5$  PMV. In the literature, they suggest using the PPD as KPI for the building's thermostats [2].

## 11.2 Methodology

The chosen methodology combines the PMV model with fuzzy logic to set the temperature setpoint, with two objectives: to reduce energy consumption and improve thermal comfort. The control logic was tested in a simulated virtual environment and then tested in a real environment.

### 11.2.1 Simulation Components

Simulink provides access to control components in fuzzy logic, which is the type of control we have chosen for controller derived. The innovative approach is the input, a fuzzy variable ranging from cold to hot, which the controller can interpret. In the other studies, carried out in the literature review, the temperature setpoint is a numerical variable, while here we allow the input as a fuzzy-variable. The second innovation is to allow more than a single input of more than one user and give the system the tools to prioritise medium comfort.

Figure 11.1 shows the model designed in Simulink with the main components: (A) the user thermostat interface, (B) the thermostat (fuzzy temperature controller), (C) the boiler and (D) the house heat transfer system. The novel proposition of this project is the user interface, allowing the users to express their thermal sensation. The thermostat uses fuzzy logic and fuzzy-inputs to set a temperature setpoint.

### 11.2.2 Room

The model of the room in Fig. 11.2 is made with equivalent thermal components, thermal resistances, thermal inertias for the walls and ceiling and the thermal inertia of the air inside the room. To simulate the heat transfer the model uses material normally used in construction in the UK [27]. In this model, the only source of heat is a water heater that transmits heat to the room. The model takes the external

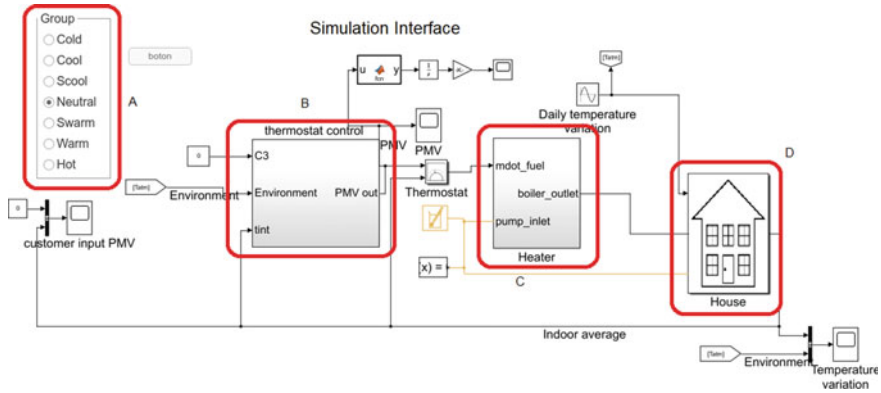


Fig. 11.1 Simulation interface is done in Simulink

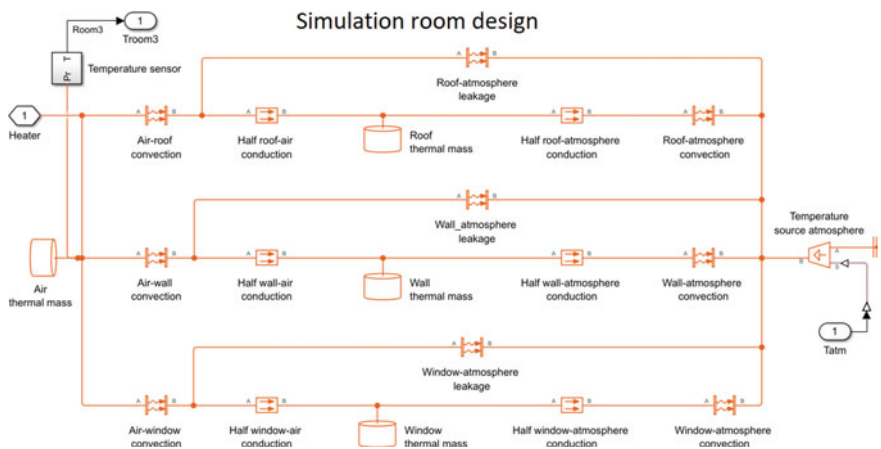
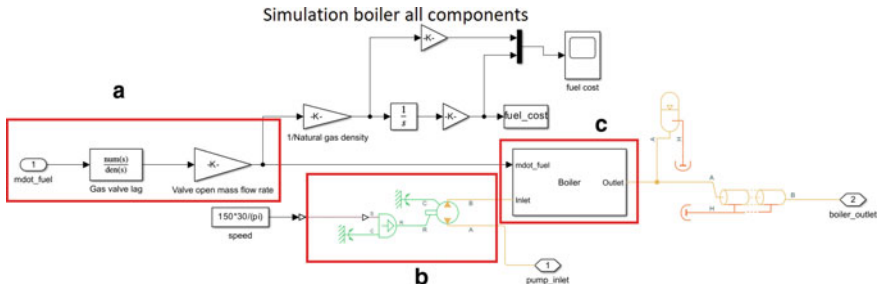


Fig. 11.2 Room design model, all the thermal components are part of the heat transfer circuit

temperature as input data, which transforms from digital to an analogue signal and then determines the internal temperature. The room temperature differential equation cannot be solved explicitly. Therefore, MATLAB uses numerical methods to provide a solution at each time step.

### 11.2.3 Boiler

The boiler system was built with the tools supplied by Simulink and with the parameters of the ASHRAE [27], such as the water temperature, the calorific value of the fuel, and the type of boiler, and the efficiency of combustion and the humidity of



**Fig. 11.3** Boiler system model: **a** the fuel pump, **b** the air compressor, and **c** the combustion chamber

the inlet air. Figure 11.3 shows the boiler components: (a) the fuel pump, (b) the air compressor, and (c) the combustion chamber.

### 11.2.4 Test Real Environment

A fundamental part of this project was to compare the PMV with the relative thermal comfort level and actual thermal sensation expressed by a user. For this, it would be advisable to implement a survey that allows users to provide relevant information for the study, such as the level of experienced thermal comfort, clothing factor, and metabolic activity level. The survey follows the standard structure [2].

The control system was tested in an office where users could express their thermal preferences on the ASHRAE scale. Figure 11.4 shows a diagram of how we proceeded in the experiment, in this case, we worked with a human operator who controlled the HVAC system. The test was done at Teesside University, lasted 2 weeks and 5 people participated.

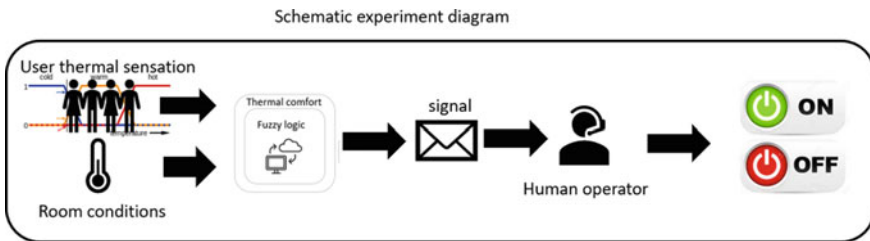


**Fig. 11.4** Schematic diagram from the data collection/experiment

During the first week of testing, the participants expressed their thermal sensation in the survey while the temperature of the office was not modified. During the second week the developed controller was tested, and the responses of the users were used to modify the temperature. In this case, a human operator entered the resulting setpoints from the developed controller and manually controlled the existing thermostat based on what the fuzzy temperature controller indicated.

### 11.3 Results and Discussion

The two results of this study are: (1) The results of the MATLAB simulation show that fuel consumption was reduced by 22% when implementing a controller with 5 multiple users and 31% with a single user (Fig. 11.5); (2) the results of the test in the offices show that the comfort of the participants was improved between 14 and 17% (Fig. 11.6).

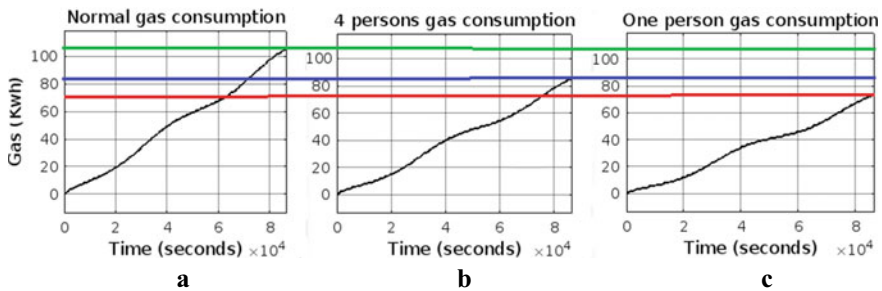


**Fig. 11.5** Gas consumption comparison, **a** normal gas consumption (106 kwh), **b** the new controller 4 users gas consumption (83 kwh) and **c** new controller one person gas consumption (73 kwh)

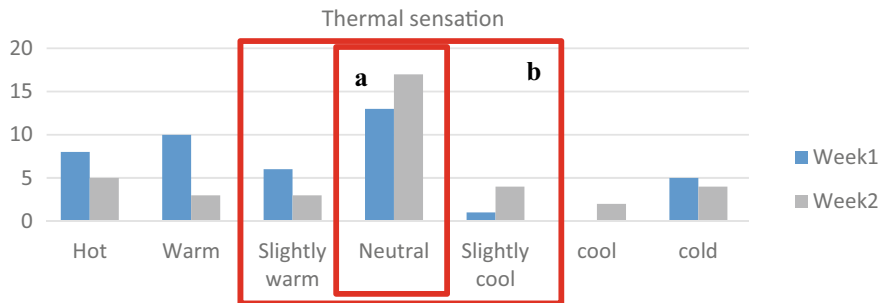


**Fig. 11.6** Thermal sensation survey answer comparison, thermal sensation neutral (**a**), and a slight degree of discomfort (**b**)

The improvement in thermal sensation was 14% if we compare only the ‘neutral’ responses but if we include the ‘Slightly warm’ or ‘Slightly cool’ responses, the improvement is 17%. ‘Slightly warm’ or ‘Slightly cool’ levels are points at which a person can adapt to that temperature because their level of discomfort is not very great, for example wearing or taking off a sweater. In the PMV model, the PPD is kept below 10%, that is, the PMV is between  $-0.5$  and  $0.5$ , for this reason taking box a would be more restrictive and on the other hand taking box b is more flexible than the PMV model.

## 11.4 Conclusion

The information shown in this document serves as a framework for the development of a fuzzy controller based on thermal comfort theory. The methodologies that allow the application of the theory of thermal comfort in practice were presented, as well as the tools that MATLAB offers to simulate laboratories.

On the subject of energy efficiency, there are many things that we still do not know. Integrating the human factor in the modelling of energy efficiency can yield good results. For example, in HVAC systems, the goal should be to keep people comfortable, rather than maintaining a fixed temperature. This way we can avoid unnecessary energy consumption and improve the thermal sensation of building users. The next step will be to test the controller in a larger and more complex environment to obtain conclusive results.

## References

1. J. Stermann, System dynamics: systems thinking and modeling for a complex world (2002)
2. ASHRAE, Thermal environmental conditions for human occupancy. Am. Soc. Heating, Refrigerating Air-Conditioning Eng. Atlanta (ANSI/ASHRAE Standard 55–2004) (2004)
3. S. Mohamed, K. Srinavin, Forecasting labor productivity changes in construction using the PMV index. *Int. J. Ind. Ergon.* **35**(4), 345–351 (2005)
4. J. Van Hoof, Forty years of Fanger’s model of thermal comfort: comfort for all? *Indoor Air* **18**(3), 182–201 (2008)
5. G. Ye, C. Yang, Y. Chen, Y. Li, A new approach for measuring predicted mean vote (PMV) and standard effective temperature (SET\*). *Build. Environ.* **38**(1), 33–44 (2003)
6. A. Keshtkar, S. Arzanpour, A fuzzy logic system for demand-side load management in residential buildings. in *2014 IEEE 27th Canadian Conference on Electrical and Computer Engineering (CCECE)* (IEEE, 2014, May), pp. 1–5
7. A. Keshtkar, S. Arzanpour, F. Keshtkar, An autonomous system via fuzzy logic for residential peak load management in smart grids. In *2015 North American Power Symposium (NAPS)* (IEEE, 2015 October), pp. 1–6
8. A. Keshtkar, S. Arzanpour, F. Keshtkar, P. Ahmadi, Smart residential load reduction via fuzzy logic, wireless sensors, and smart grid incentives. *Energy Buildings* **104**, 165–180 (2015)
9. P. Bermejo, L. Redondo, L. de la Ossa, D. Rodríguez, J. Flores, C. Urea, J.A. Gámez, J.M. Puerta, Design and simulation of a thermal comfort adaptive system based on fuzzy logic and on-line learning. *Energy Buildings* **49**, 367–379 (2012)

10. R. Alcalá, J. Alcalá-Fdez, F. Herrera, A proposal for the genetic lateral tuning of linguistic fuzzy systems and its interaction with rule selection. *IEEE Trans. Fuzzy Syst.* **15**(4), 616–635 (2007)
11. M. Dovjak, M. Shukuya, Integral control of hospital environment. in *2011 IEEE Power Engineering and Automation Conference*, vol 3 (IEEE, 2011, September), pp. 128–131
12. H. Yan, Y. Pan, Z. Li, S. Deng, Further development of a thermal comfort based fuzzy logic controller for a direct expansion air conditioning system. *Appl. Energy* **219**, 312–324 (2018)
13. Q.U. Ain, S. Iqbal, S.A. Khan, A.W. Malik, I. Ahmad, N. Javaid, IoT operating system based fuzzy inference system for home energy management system in smart buildings. *Sensors* **18**(9), 2802 (2018)
14. S. Merabti, B. Draoui, F. Bounaama, A review of control systems for energy and comfort management in buildings. in *2016 8th international conference on modelling, identification and control (ICMIC)* (IEEE, 2016, November), pp. 478–486
15. D. Makkar, P. Syal, Simulation of intelligent room lighting illuminance control. in *2017 IEEE International Conference on Computational Intelligence and Computing Research (ICIC)* (IEEE, 2017, December), pp. 1–4
16. F. Budiman, M. Rivai, I.G.B.P. Raditya, D. Krisrenanto, I.Z. Amiroh, Smart control of air conditioning system based on number and activity level of persons. in *2018 International Seminar on Intelligent Technology and Its Applications (ISITIA)* (IEEE, 2018 August), pp. 431–436
17. G. Palmieri, G. Fiengo, A hierarchical control strategy for energy optimization. *IFAC Proc. Vol.* **39**(19), 111–116 (2006)
18. A. Keshkar, S. Arzanpour, An adaptive fuzzy logic system for residential energy management in smart grid environments. *Appl. Energy* **186**, 68–81 (2017)
19. S. Javaid, N. Javaid, Comfort evaluation of seasonally and daily used residential load in smart buildings for hottest areas via predictive mean vote method. *Sustain. Comput. Inf. Syst.* **25**, 100369 (2020)
20. Y.Y. Ghadi, M.M.G. Rasul, M.K.K. Khan, Recent developments of advanced fuzzy logic controllers used in smart buildings in subtropical climate. *Energy Proc.* **61**, 1021–1024 (2014)
21. Y.Y. Ghadi, M.G. Rasul, M.M.K. Khan, Optimization of advanced fuzzy based control system of institutional building management system (BMS) in Australian subtropical climate (2016)
22. D. Kolokotsa, D. Tsiavos, G.S. Stavrakakis, K. Kalaitzakis, E. Antonidakis, Advanced fuzzy logic controllers design and evaluation for buildings' occupants thermal–visual comfort and indoor air quality satisfaction. *Energy Buildings* **33**(6), 531–543 (2001)
23. H. Khodadadi, A. Dehghani, Fuzzy logic self-tuning PID controller design based on smith predictor for heating system. in *2016 16th International Conference on Control, Automation and Systems (ICCAS)* (IEEE, 2016, October), pp. 161–166
24. M.I.M. Rawi, A. Al-Anbuky, Development of intelligent wireless sensor networks for human comfort index measurement. *Proc. Comput. Sci.* **5**, 232–239 (2011)
25. A. Dehghani, H. Khodadadi, Designing a neuro-fuzzy PID controller based on smith predictor for heating system. in *2017 17th International Conference on Control, Automation and Systems (ICCAS)* (IEEE, 2017, October), pp. 15–20
26. ASHRAE, Thermal environmental conditions for human occupancy. *Am. Soc. Heating, Refrigerating Air-Conditioning Eng. Atlanta (ANSI/ASHRAE Standard 55–2017)* (2017)
27. ASHRAE, High-performance sequences of operation for HVAC system, *Am. Soc. Heating, Refrigerating Air-Conditioning Eng. Atlanta (ANSI/ASHRAE Standard 36, No. 2018)* (2018)



**Open Access** This chapter is licensed under the terms of the Creative Commons Attribution 4.0 International License (<http://creativecommons.org/licenses/by/4.0/>), which permits use, sharing, adaptation, distribution and reproduction in any medium or format, as long as you give appropriate credit to the original author(s) and the source, provide a link to the Creative Commons license and indicate if changes were made.

The images or other third party material in this chapter are included in the chapter's Creative Commons license, unless indicated otherwise in a credit line to the material. If material is not included in the chapter's Creative Commons license and your intended use is not permitted by statutory regulation or exceeds the permitted use, you will need to obtain permission directly from the copyright holder.



# Chapter 12

## Investigating the Utilisation of Waste Sand from Sand Casting Processes for Concrete Products for Environmental Sustainability



Sirwan Faraj and Amin Al-Habaibeh

**Abstract** Concrete is one of the fundamental materials in the construction industry. Typically, concrete is composed of sand, cement, aggregate, and added water to the cement ratio. To enhance sustainability and reduce the negative effect on the environment from industrial waste, recycling waste material into the concrete mixture is becoming an area of research by substituting some of the concrete ingredients with some of the recycled waste material in order to reduce the amount of fine natural aggregate used in the construction industry, maximise the strength and minimise the overall weight of the concrete product. Waste foundry sand is a by-product of sand casting, a waste product of the metal casting industry. The improper disposal of this waste foundry sand (WFS) could cause environmental issues. Consequently, its possible use in building materials, product design, construction, and other fields is crucial for mitigating environmental limitations. To minimise negative environmental impacts, researchers have proposed reusing this waste foundry sand by replacing, fully or partially, some of the standard natural sand within the concrete mixture. This paper investigates the mechanical and physical properties of concrete cubes containing recycled sand-casting material by demonstrating the experimental work to determine the potential benefit or limitations of using this material within the concrete in the construction and product design industries. According to the experimental results, waste foundry sand, with a substitution ratio of up to 30%, had a compression strength of circa 23 N/mm<sup>2</sup> and reached up to 78% of the strength of a standard control sample within 7 days. The results hence suggest that waste foundry sand can be used in the production of concrete products when such reduction in strength is not critical. Such a range of products could include curbs, garden slabs, cycling pavements, gravel boards, etc. Additionally, utilising waste foundry sand will help

---

S. Faraj (✉) · A. Al-Habaibeh  
Product Innovation Centre, School of Architecture, Design and the Built Environment,  
Nottingham Trent University, Nottingham, UK  
e-mail: [sirwan.faraj2015@ntu.ac.uk](mailto:sirwan.faraj2015@ntu.ac.uk)

A. Al-Habaibeh  
e-mail: [Amin.Al-Habaibeh@ntu.ac.uk](mailto:Amin.Al-Habaibeh@ntu.ac.uk)

to reduce the use of natural sand and the need for landfill sites, which has several advantages, including cost savings and environmental protection by reducing CO<sub>2</sub> emissions during transportation.

**Keywords** Waste foundry sand · Sustainability · Concrete · Recycling · Eco-friendly

## 12.1 Introduction

Concrete is a composite material that generally consists of numerous ingredients. It usually includes cement, water, coarse aggregate, sand, and other additives or polymers to enhance workability. Concrete is one of the most often utilised construction materials in the current economy. It can be unutilised structural products, paving material, pipes, drains, etc. [1]. Concrete is an expensive material in terms of cost and carbon emission. Solving this issue is ideal by substituting fine aggregate (sand) with industrial waste materials such as waste foundry sand (WFS). In sand casting, moulds made of uniformly sized, clean, high-silica sand are used in such industries. After the casting process is completed, foundries usually recycle and reuse the sand multiple times. However, after a specific number of cycles, depending on the products and their required specifications, the sand is discarded as waste foundry sand [2]. The environmental impact of this sand and its disposal problem can be mitigated if it can be utilised in other engineering applications. For example, it has been reported that each year Indian foundries produce approximately 1.71 million tonnes of waste foundry sand [3, 4]. Globally, it has been estimated that the foundry industry generates approximately 100 million tonnes of waste foundry sands (WFS) annually on a global scale [5]. Reusing the sand from the foundry reduces the need for landfill space or the use of conventional sand in engineering applications. This is expected to enable the development of environmentally sustainable use of such waste sand [6]. Figure 12.1 presents the waste foundry sand used in this paper.



**Fig. 12.1** Waste foundry sand

The aim of this research is to explore the use and determine the potential strength of concrete products that contain waste foundry sand as a partial or complete replacement for normal sand.

## 12.2 The Methodology

In order to determine the potential strength of concrete products that include waste foundry sand as a partial or complete replacement for traditional sand, standard concrete cubes were made and tested under compressive stress. Concrete is usually tested in a laboratory environment. The primary objective of such tests is to ensure that the concrete meets the design specifications outlined in IS EN 206-1 or to compare the results relative to the benchmark. Because using different materials and ratios can cause varied effects, the standard helps to identify performance, production, and conformity. All applicable health and safety standards and regulations were followed during the laboratory work, and the appropriate personal protective equipment (PPE) was worn. Nine distinct concrete mixtures were created in one day for this test. Mould preparation starts by casting moulds (cubes) (100 × 100 × 100 mm) cast iron that must be rubbed with grease on the inner side to help the removal process. The specimen is properly compacted by vibration so that honeycombing formation does not occur. The cube test for compressive strength can be done in seven days. Having at least three specimens for testing from different batches is critical to calculating the average and any possible variation.

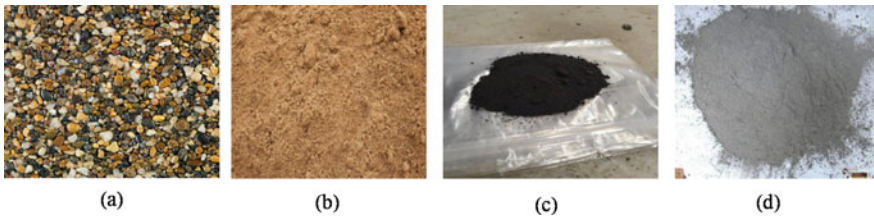
The concrete cubes are produced by placing the prepared concrete mix in the steel cube mould for casting. After it has been set for 24 h, the product (sample) is removed from the mould. The samples are then kept submerged underwater for seven days. The concrete samples must be dried and weighed prior to testing. The concrete cubes are placed on the compression machine for testing. The loading must be applied to the specimen axially without shock and increased at 140 kg/so cm/min until the specimen collapses.

## 12.3 The Selected Materials

This research study calculates and tests four designed mixes, each consisting of three cubes, making the total to be 12 samples. Table 12.1 contains the complete information about the proposed mixes. The ratio of 1:2:3 of Cement, Sand and Coarse Aggregate, respectively, was determined by the usual design process of the concrete type. The report's primary objective is to conduct compressive strength tests on the samples that have been cured under water. The results of the samples were analysed and compared. The models that include 100, 65 and 30% recycled waste sand were compared with the standard samples with 0% recycled sand (100% normal fine sand) as control samples, see Table 12.1.

**Table 12.1** The 12 samples used in this paper and their composition

Replacement WFS (%)	OPC (kg)	WSF (kg)	Natural fine sand (kg)	Natural coarse agg (kg)	Water (l)	Number of samples
WSF (100)	1.2	2.4	0	3.6	9.66	3
WSF (65)	1.2	1.56	0.84	3.6	7.32	3
WSF (30)	1.2	0.72	1.68	3.6	7.14	3
WSF (0) (Control)	1.2	0	2.4	3.6	6.6	3

**Fig. 12.2** The components of the mixture; **a** coarse aggregate, **b** fine aggregate, **c** waste sand and **d** Portland cement

The testing aggregate sample must comply with the BS EN 932-1:1997 standards as a benchmark. The rounded aggregate was used in this experiment with a size between 2 and 10 mm. Figure 12.2 shows the components sample used in this study for the concrete mix. Figure 12.2a presents the course aggregative, Fig. 12.2b presents the normal sand, Fig. 12.2c shows the recycled waste sand, and Fig. 12.2d gives the Portland cement used in this study.

To determine the samples' mechanical strength, the waste sand has been replaced with natural sand in proportions of 100, 65 and 30%. The water ratios used vary according to the mixing process. There are numerous types of cement on the market. This experiment used ordinary Portland cement with a compressive strength of 32 N/mm<sup>2</sup> according to the British standard (BS EN 1992-1-1). According to (EN 206-1-2000), the water/cement ratio is required to achieve the 30 MPa (M30). The water/cement ratio was determined to be 50% of the cement ratio. Plus, an additional 1% of added water because if the aggregate is dry, affecting the 'free water' needed. These values depend on the mixture of material proportions and conditions. The waste sand has high water absorption characteristics, increasing the water content by 15% to the sand ratio. At 28 days, concrete is expected to reach its maximum strength. Instead of checking the strength at 28 days, this research paper has tested the samples after 7 days, if concrete gains 65% of its target strength after seven days.

## 12.4 Experimental Results and Discussion

Table 12.2 presents the complete experimental data and results, including the compression tests. Figure 12.3 shows the average results of the samples at 7 days. It is clear from the data that the reduced sand reduced the compression strength of the samples. However, Fig. 12.3 will help design future products with specific strengths sufficient for the required applications from the product design perspective.

The three distinct concrete mixes were used, each with a different percentage of waste sand replaced with fine natural aggregates, such as 100, 65, and 30% in (kg). The results show that the average compressive strength of concrete cubes was reduced by roughly 64%, 46%, and 12%, respectively, compared to those made with fine natural sand. The maximum compressive strength cubes within seven days are shown in Fig. 12.3. The samples submitted to the compressive machine test for cubes made WFS, resulting in a satisfactory failure. The stress cracking that appears within the specimen is considered abnormal.

The specimens containing 30% WFS attained the desired compressive strength target. Figure 12.5 represents the compressive strength at 7 days and the calculated cube strength at 7 days (in %). However, according to the experimental results, the partial replacement of WFS should not exceed 30% in order to achieve the target strength. The samples were examined under the microscope following the testing process to reveal clear interfacial debonding between the aggregates and cement paste in some locations. The interfacial debonding (or separation) is clearly visible in Fig. 12.4 as the areas around the aggregates have micro-cracks caused by the direct axial force applied to the cubes. Except for sample (a) in Fig. 12.4, the crack propagation pattern is nearly the same throughout the remaining samples; binding difficulties cause this pattern. Figure 12.4a–d show no solid bond between coarse particles and cement paste. In this experiment, rounded form aggregates were used, which may have a negative effect on the total cube strength. Infiltration of water is another issue that might affect the strength of concrete. It was established during the cube testing procedure that the cubes made from recycled sand absorbed more water, causing the samples to collapse quicker under the compressive testing machine as stress was applied. The reason for these conclusions is unknown precisely. Therefore, additional study or testing is necessary to discover the cause.

## 12.5 Conclusion

This study aimed to evaluate the mechanical properties of recycled waste foundry sand and the impact of recycled material on the properties of concrete when used to replace the standard sand in the mixture. This study investigated introducing waste sand from sand casting processes to replace natural sand in concrete. In many sectors, recycling waste foundry sand instead of virgin materials can result in a slight decrease in the technical performances of the final products, which could still be acceptable

**Table 12.2** The Experimental design and results

Sample (%)	Date of casting	Description of sample	Building number	Target grade of concrete	Number of cubes	7 days testing date	Weight of cubes (kg)	The average weight of cubes (kg)	Load in (kN)	Comp strength N/mm <sup>2</sup>	Average comp. strength N/mm <sup>2</sup>	Cubes strength %
WS 100	13/10/2021	Cube	1	n/a	1	21/10/2021	2.22	2.25	91.3	9.13	7.90	26.34
					2	21/10/2021	2.19	75.6	7.56			
					3	21/10/2021	2.21	70.2	7.02			
WS 65	13/10/2021	Cube	2	n/a	1	21/10/2021	2.24	2.28	127.5	12.75	13.28	44.28
					2	21/10/2021	2.28	132	13.2			
					3	21/10/2021	2.26	139	13.9			
WS 30	13/10/2021	Cube	3	n/a	1	21/10/2021	2.26	2.31	244.3	24.43	23.58	78.60
					2	21/10/2021	2.28	248.6	24.86			
					3	21/10/2021	2.28	214.5	21.45			
Control	13/10/2021	Cube	4	M30	1	21/10/2021	2.37	2.37	270	27	27.07	90.22

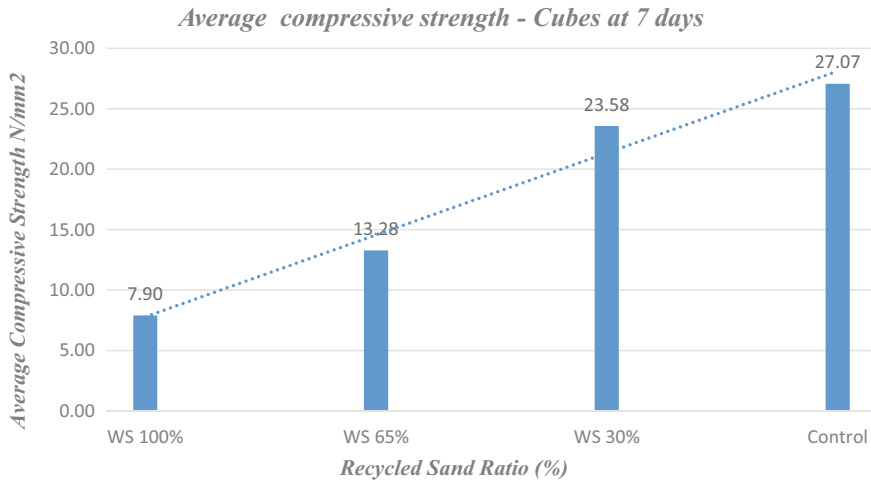


**Fig. 12.3** Average compressive strength of the tested samples in comparison to the control samples

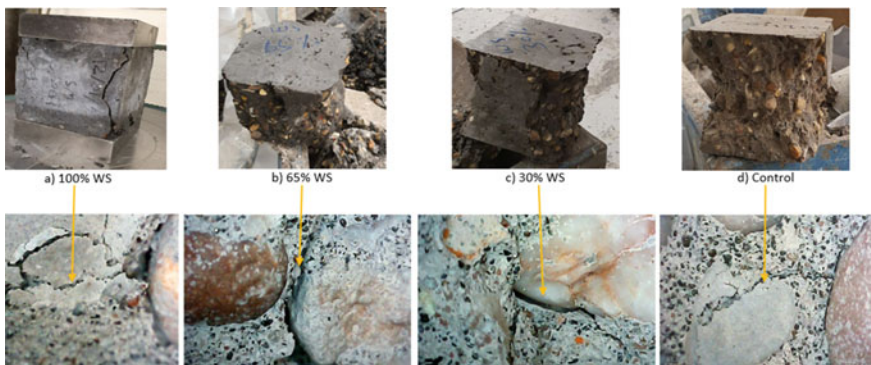


**Fig. 12.4** Crack propagation within the concrete cubes after testing

depending on the needed application. Recycled waste sand could be used effectively as a partial or complete replacement of standard sand in suitable quality mortars and concretes. This will depend on the required design characteristics and the intended applications. Further work is still needed to evaluate the long-term effect and strength of concrete, including a full life cycle assessment (LCA).



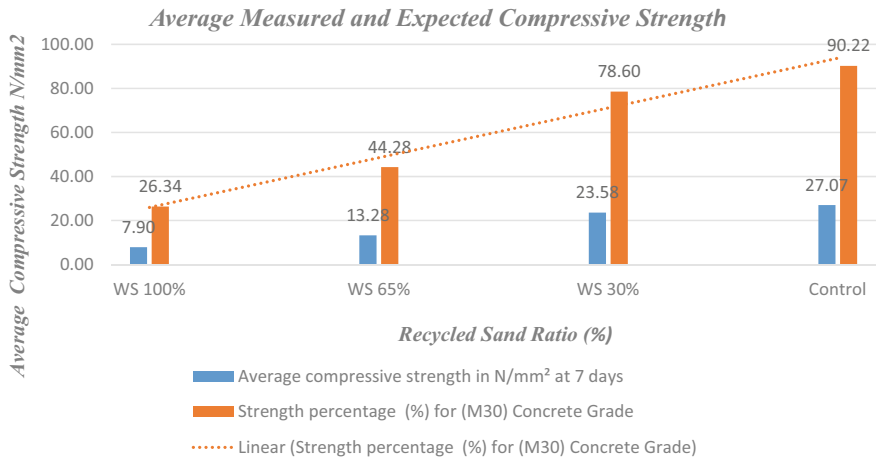


**Fig. 12.5** Average compressive strength versus recycled sand ratio

**Acknowledgements** The authors would like to thank our industrial partners and collaborators who have provided the waste sand for the experimental work.

## References

1. K.A. Gelim, Mechanical and physical properties of fly ash foamed concrete. *Fac. Civ. Environ. Eng. Univ. Tun Hussein Onn Malaysia* 10 (2011)
2. F. Tittarelli, *Waste foundry sand*. Elsevier Ltd., (2018)
3. C.D. Sahare, Experimental study on waste foundry sand and steel slag concrete *5*(2), 5–9 (2019)
4. F. Printing, Foundry sand facts for civil engineers. *Concr. Portable Handb.* (May), 299–372 (2012). <https://doi.org/10.1016/b978-0-12-382176-8.00024-7>
5. S. Seiter, D.M. Pittenger, State-of-the-practice literature scan for foundry sand quick search. (2) (2017)
6. G. Ganesh Prabhu, J.W. Bang, B.J. Lee, J.H. Hyun, Y.Y. Kim, Mechanical and durability properties of concrete made with used foundry sand as fine aggregate. *Adv. Mater. Sci. Eng.* **2015** (2015). <https://doi.org/10.1155/2015/161753>

**Open Access** This chapter is licensed under the terms of the Creative Commons Attribution 4.0 International License (<http://creativecommons.org/licenses/by/4.0/>), which permits use, sharing, adaptation, distribution and reproduction in any medium or format, as long as you give appropriate credit to the original author(s) and the source, provide a link to the Creative Commons license and indicate if changes were made.

The images or other third party material in this chapter are included in the chapter's Creative Commons license, unless indicated otherwise in a credit line to the material. If material is not included in the chapter's Creative Commons license and your intended use is not permitted by statutory regulation or exceeds the permitted use, you will need to obtain permission directly from the copyright holder.



# Chapter 13

## Application of Observational Weather Data in Evaluating Resilience of Power Systems and Adaptation to Extreme Wind Events



Francis Mujjuni, Tom Betts, and Richard E. Blanchard

**Abstract** In Great Britain, 70% of wind-related faults on the transmission power network are attributed to the top 1% gusts. These faults cause outages to millions of customers and have extensive cascading impacts. This study illustrated the application of historical ground measured wind data in a multi-phase resilience analysis process by: (i) projecting an extreme wind event, (ii) assessing components' vulnerabilities, (iii) analysing system's response, (iv) quantifying baseline resilience, and (v) evaluating the effectiveness of selected adaptation measures. The extreme event was modelled as a ubiquitous 100-year return gust event impacting upon the operations of the Reduced Great Britain transmission network test case. The results show an unmet demand of about 569 GWh/Week. Adaptation measures were necessary for 60% of transmission corridors with *responsiveness* improving resilience by 70%, *robustness* by 55%, and *redundancy* by 35%. The study implies that resilience enhancement can be prioritized within high potency corridors and organisational resilience could prove to be more effective than infrastructural and operational resilience.

**Keywords** Critical infrastructure · Outage · Blackout · High impact low probability · Windstorm

---

*Present Address:*

F. Mujjuni (✉) · T. Betts · R. E. Blanchard

Centre for Renewable Energy Systems Technology (CREST), Wolfson School of Mechanical, Electrical and Manufacturing Engineering, Loughborough University, Epinal Way, Loughborough LE11 3TU, UK

e-mail: [F.mujjuni@lboro.ac.uk](mailto:F.mujjuni@lboro.ac.uk); [francis.mujjuni@mak.ac.ug](mailto:francis.mujjuni@mak.ac.ug)

T. Betts

e-mail: [T.R.Betts@lboro.ac.uk](mailto:T.R.Betts@lboro.ac.uk)

R. E. Blanchard

e-mail: [R.E.Blanchard@lboro.ac.uk](mailto:R.E.Blanchard@lboro.ac.uk)

F. Mujjuni

Department of Mechanical Engineering, Makerere University, Kampala, Uganda

## 13.1 Introduction

Recent studies [1–3] have explored the conceptualisation and application of the resilience concept within power systems. The reasons vary but several studies [1, 2, 4] are motivated by the goal of developing power systems which are less vulnerable to extreme weather. This is because the resultant failure of power systems due to weather events have grave impacts on countries. For example, the ‘Great Ice Storm’ of 1998 that hit parts of Canada caused outages to 4 million people for over a month [5]. Up to 80% of power outages in USA are attributed to weather incidents affecting 22 million people annually [6].

In a study into Great Britain (GB) transmission system faults, it was reported that 50% of all faults were attributed to weather causes and that 30% of these were due to wind events [5]. Two-thirds of wind-related faults were caused by the top 1% of wind gusts [5]. Therefore, several studies [1, 3] have been conducted to assess GB transmission system resilience to extreme wind events but several gaps remain. Due to lack of long-term observations with wider coverage, previous studies [1, 7] used climate model, reanalysis, wind data to analyse and project extreme wind events. However, reanalysis data has been reported to be noisy, exhibits a wide range of biases and errors, and the assessment of its uncertainties is not well understood [8]. In addition, high intensity winds are rarely captured by climate models requiring several studies [1, 7] to arbitrarily scale up intensities for resilience analysis purposes. Moreover, several studies [1, 3] consider the effect of spatial variability of extreme weather events by dividing GB into large “weather regions” which are assigned homogeneous weather profiles. This is contrary to studies that have demonstrated that a met station’s record may not reliably represent weather of a location which is beyond 50 kms [5].

Therefore, this study’s aim was to assess the resilience of GB’s power transmission system and the effectiveness of selected adaptation measures against an extreme windstorm based on observed wind gusts. In particular, the study sought to model a ubiquitous 100-year wind gust event across GB, assess its impact on the network’s components, undertake a system response analysis, evaluate baseline resilience, and assess the effectiveness of *redundancy*, *responsiveness*, and *robustness*. Section 13.2 details the methods employed in determining and enhancing the system’s resilience. Section 13.3 presents and discusses the results whereas in Sect. 13.4, conclusions are drawn as well as implications and limitations of the study.

## 13.2 Methodology

This study builds upon a multi-phase approach implemented in several studies [1, 4]. As seen in Fig. 13.1, the process follows a five-phase modelling approach, namely: (i) weather threat characterization, (ii) components vulnerability analysis, (iii) systems

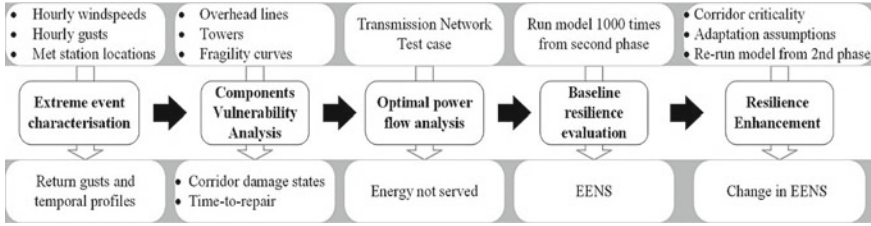


Fig. 13.1 Phased resilience assessment simulation flow chart

response analysis, (iv) baseline resilience quantification, and (v) resilience enhancement. Prior to modelling, historical observed wind data was obtained from the Met Office Integrated Data Archive System [9]. The dataset was comprised of 173 met stations with data spanning 1949–2021. Two data types were retrieved: the hourly wind mean speeds and gusts.

### 13.2.1 Extreme Windstorm Characterization

Similar to previous studies [1, 10] which projected a probable cataclysmic wind scenario, this study assumed a high-impact event in which gusts of 100-year return duration would occur simultaneously across GB. Great Britain was divided into cells corresponding to having no more than one met station per cell. A total of 173 weather regions were created based on met-stations locations. Cells without a station were assigned data of a station nearest to their centroid. The Generalized Extreme Value (GEV) theory was used to estimate return gusts in each weather region. In particular, the block maxima method was employed as detailed by [11]. Annual maxima gust values ( $x \in \mathbb{R}$ ) were retrieved for each station. These were then used to fit the GEV cumulative probability distribution function for each station as seen in (13.1).  $\mu \in \mathbb{R}$ ,  $\sigma > 0$ ,  $\xi \in \mathbb{R}$  are the location, scale, and shape parameters respectively. To fit the annual maxima data points to the GEV distribution, a numerical maximum log-likelihood function was used. The initial distribution parameters for each fitted curve of the station were considered as the mean ( $\mu$ ), standard deviation ( $\sigma$ ) and  $\xi = 0.1$ .

$$G(x; \mu, \sigma, \xi) = \begin{cases} \exp(-\exp[-((x - \mu)/\sigma)]) & , \xi = 0 \\ \exp\left(-[1 + \xi((x - \mu)/\sigma)]^{-\frac{1}{\xi}}\right) & , 1 + \frac{\xi(x - \mu)}{\sigma} > 0 \end{cases} \quad (13.1)$$

Given that there is no analytical solution for log likelihood function, the approximate solution was obtained from optimization by utilizing the Sequential Least Squares Programming method. To assess the goodness-of-fit of the optimized distribution parameters  $(\hat{\mu}, \hat{\sigma}, \hat{\xi})$ , a coefficient of determination ( $R^2$ ) was derived for ordered empirical and modelled data probabilities. The 100-year return gust ( $\hat{x}_{100}$ )

for each weather region was then estimated using (13.2). The time,  $t$ , of return level occurrence was denoted as zero (0) and beyond  $t = 0$ , the windstorm temporal profiles at each met station were determined by (13.3) in which  $\bar{x}_0$  is the station's maximum value for the average hourly wind mean speeds and  $\bar{x}_t$  are the subsequent mean wind speed values for a week  $t \in [0, 168]$ . This assumption is an inference from literature [12] in which significant reduction in intensity of windstorms were observed within one week. In the subsequent week of the model, the intensity was assumed to have a straight-line descent to 'normal' gusts.

$$\hat{x}_{100} = \hat{\mu} + \frac{\hat{\sigma}}{\hat{\xi}} \left[ \left( -\log(1 - 100^{-1}) \right)^{-\hat{\xi}} - 1 \right] \quad (13.2)$$

$$\hat{x}_{100t} = \frac{\hat{x}_{100} \times \bar{x}_t}{\bar{x}_0} \quad (13.3)$$

### 13.2.2 Vulnerability Analysis

The power system test case employed in this study is based on the Reduced Great Britain Network (RGBN) [13, 14]. RGBN comprises of 29 nodes, 24 of which have a total of 66 connected generators, 50 transmission corridors all with double circuit overhead lines (DC OHL) except one with a single circuit overhead line (SC OHL). Towers were assumed to be 350 m apart. The system has constant demand of 56.3 GW corresponding to peak winter consumption and available capacity of 75.3 GW. Only lines and towers were subjected to windstorms.

To determine the probability of failure,  $P_c(w_i)$ , of components with respect to the prevailing wind intensities, fragility curves employed in several studies [1, 7], were used. The highest intensity which an OHL would be subjected across all weather regions it spans, was considered to determine its probability of failure. Towers' failure states were determined by cells in which they are located. Given the randomness of failures, a uniformly distributed random number,  $r \sim U(0, 1)$ , was generated at every simulation step as proposed by [1] which was compared to the respective probability of failure of each component. If  $r < P_c(w_i)$ , the component was regarded permanently damaged. Failure of a single tower resulted in collapse of an entire corridor. Following a component's failure, the Time to Repair ( $TTR$ ) was estimated as proposed by others [1, 7].

### 13.2.3 System Response and Baseline Resilience Evaluation

An AC OPF was run for every timestep whilst recording the Energy not served (ENS) until all corridors were restored. To quantify uncertainties inherent in the damage determination and repair processes, the model was run 1000 times. The mean of ENS

values, expected energy not served (EENS), was used as an indicator for baseline resilience. The uncertainties were captured by a probability density function of ENS values.

### 13.2.4 Resilience Enhancement Modelling

This study adopted the Resilience Achievement Worth (RAW) index proposed by [3] to ascertain the criticality of corridors. The RAW index quantifies the increment in resilience by a corridor when it is assumed to be unaffected by a disturbance. The corridors were then ranked in descending order of their criticality. Three adaptation measures were modeled as proposed by [1, 3]; *robustness*, *responsiveness*, and *redundancy*. *Robustness* was modelled by moving the fragility curves 20% to the right. This implies that the threshold hazard was increased leading to a delay of components' outages. *Redundancy* was modeled by setting parallel corridors to existing ones. *Responsiveness* was modelled by assuming a constant TTR which is not contingent to the prevailing wind intensity. Each measure was then applied sequentially and cumulatively to groups of five corridors while recording the gains in resilience.

## 13.3 Results and Discussion

Figure 13.2b shows the expected 100-year gust returns for each weather region determined by the locations of met-stations in Fig. 13.2a. The proximity between each cell and the nearest met station is shown in Fig. 13.2c. 96% of cells are within 50 km of a met station. High altitude locations such as Cairngom Summit (85 m/s) have significantly higher return gusts than low altitudes sites such as Rochdale (27 m/s).

The modelled temporal profile for return gusts can be seen in Fig. 13.3a and the proportion of OHLs and towers in-service can be seen in Fig. 13.3b and c. Up to 79% lines were damaged and about 6% of towers. Line states were observed to be highly fluctuating with sudden spikes and drops given that they are relatively sensitive to wind intensities and have considerably short repair durations. Failures from towers could have significant impact on the system considering their longer restoration (i.e., 500 h compared to 312 h for OHLs) and the fact that most of them carry multiple circuits. For example, 6% of damaged towers caused 36% of corridors to go out of service as seen in Fig. 13.4a.

After evaluating 1000 instances of *ENS* for RGBN (Fig. 13.4b and c), the corresponding minimum and maximum values were 396 and 825 GWh/week as seen in Fig. 13.5a. Resilience, *EENS*, was evaluated as 569 GWh/week with a standard deviation of 63 GWh/week. This EENS is about 28% of the weekly domestic demand for 2019 which translates into consumption of about 8 million households [15]. In comparison, [1] evaluated *EENS* as 324 GWh/Week whereas [3] evaluated

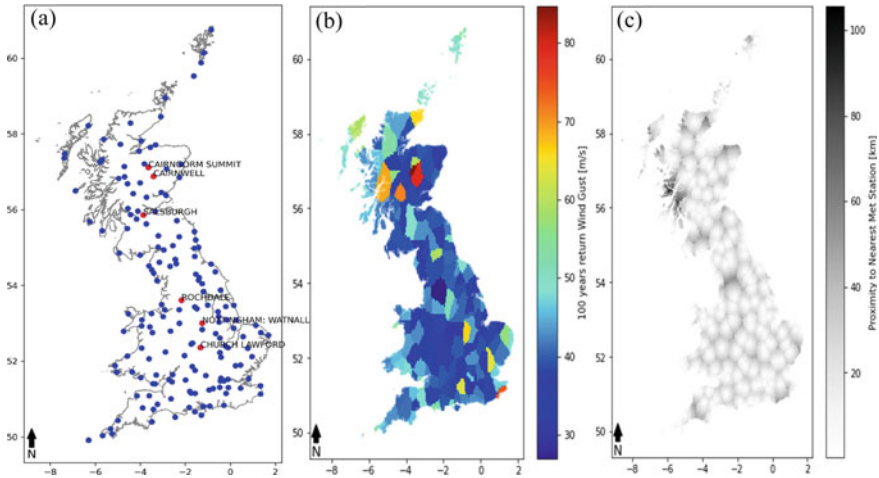


**Fig. 13.2** a Location of met-stations, b 100-year return gusts, and c proximity of cells to the nearest met-station

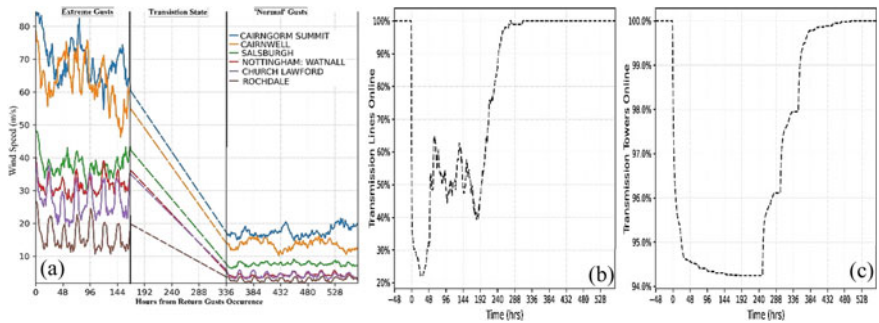
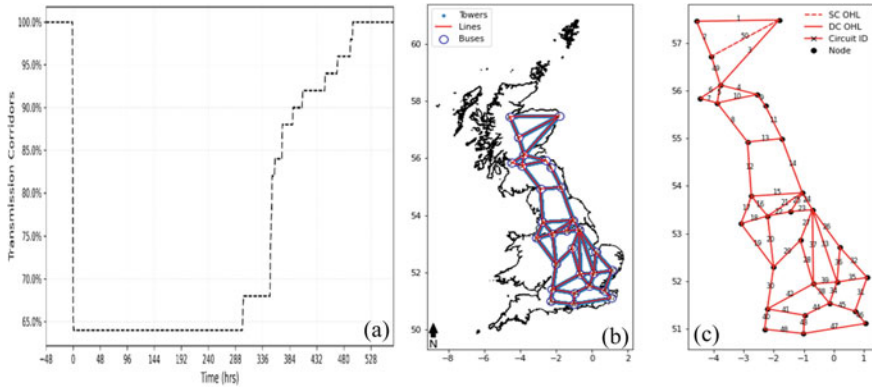


**Fig. 13.3** a Gust temporal profile, b impact on overhead lines, and c impact on towers

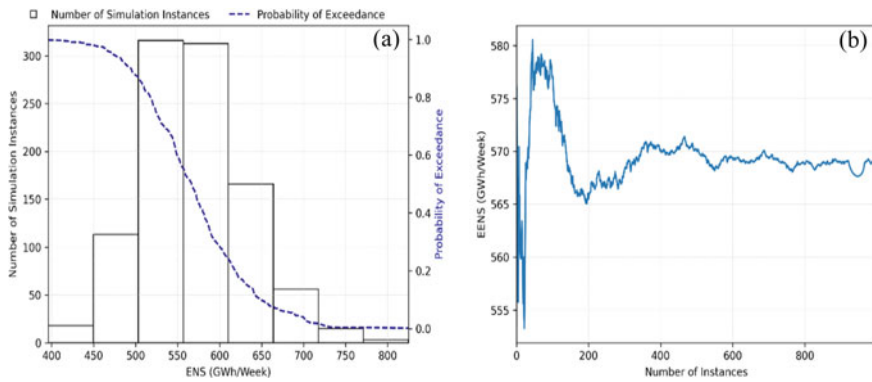
it as 690 GWh/Week. In both cases, climate model data were arbitrarily scaled to characterize windstorms and only 6 weather regions were considered for the entire GB.

Figure 13.5b shows that 1000 runs were sufficient in determining the EENS given that after 150 runs, the value deviates no more than  $\pm 1\%$ . Figure 13.6 shows the criticality of corridors based on the RAW index. The corridors on the (bottom) horizontal axis are arranged in descending order of RAW ranks, with corridor 41 being the most critical and 50, the least. The vertical segmented lines signify groups of five corridors which are considered simultaneously and cumulatively moving from left to right during the resilience enhancement process. It can be observed that 16 corridors have zero RAW, implying that adaptation measures may not improve system’s resilience to windstorms within these corridors. Of the three adaptation measures, *responsiveness* emerged to be the most effective compared to *robustness*





**Fig. 13.4** **a** Corridor failure conditional to tower failure, **b** RGBN components **c** transmission corridors IDs



**Fig. 13.5** **a** Frequency plot and probability of exceedance of evaluated ENS values, **b** moving average of ENS per additional model run

and *redundancy* as seen in Fig. 13.7. The increase in resilience peaked at 70%, 55% and 35% respectively. All scenarios peaked after applying measures to the top 60% critical corridors.

### 13.4 Conclusions

This paper presents a study of evaluating resilience of a power system against a projected extreme windstorm. Unlike previous studies that used reanalysis data and only had 6 weather regions, this study used historical ground observations from 173

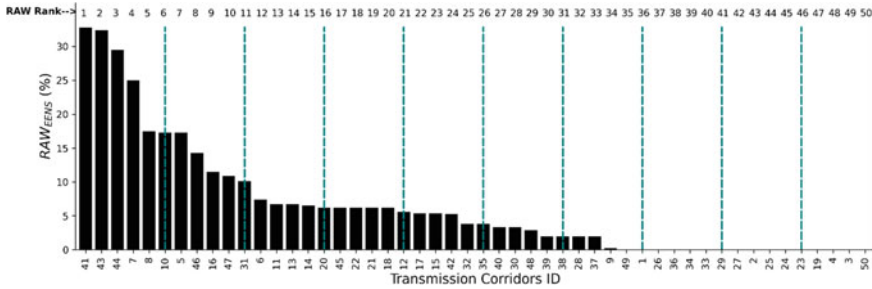


Fig. 13.6 Criticality of corridors based on 100-year return gusts

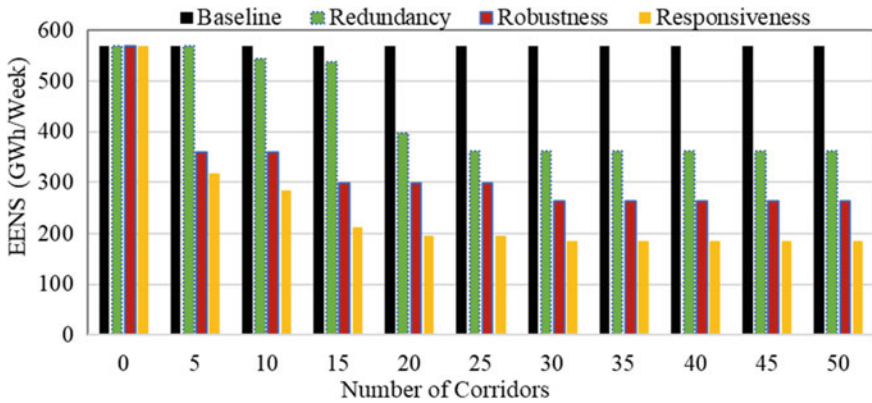


Fig. 13.7 Level of resilience of RGBN under selected adaptation measures when applied to a cluster of transmission corridors

met stations across the GB to characterize extreme wind threat with relatively high spatial resolution of weather regions.

The results show that a probable 100-year return gust event could have intensities ranging between 27 and 85 m/s. If such an event was to last a week, nearly 80% of OHL and 6% of towers could be damaged. This would result into load-shedding of 569 GWh/Week equivalent to consumption of about 8 million households. The study observed that *responsiveness* (70%) was a more effective adaptation measure than *redundancy* (55%) and *robustness* (35%). This is not conclusive considering that the study did not establish whether the assumptions made for the three measures were equally weighted. It was also observed that the level of criticality of corridors was dependent on the weather type and intensity, distribution of demand, network topology, and components’ vulnerabilities. The most vulnerable corridors are not necessarily the most critical in enhancing resilience. Moreover, organizational resilience could be more effective than infrastructural and operational resilience.

Future work will seek to explore resilience of the system under a dynamic load and evaluation of the individual capacities of resilience (*preparedness, absorptivity, and recovery*).

## References

1. S. Espinoza, M. Panteli, P. Mancarella, H. Rudnick, Multi-phase assessment and adaptation of power systems resilience to natural hazards. *Electric Power Syst. Res.* **136**, 352–361 (2016). <https://doi.org/10.1016/J.EPSR.2016.03.019>
2. G. Fu, S. Wilkinson, R.J. Dawson, H.J. Fowler, C. Kilsby, Integrated approach to assess the resilience of future electricity infrastructure networks to climate hazards. *IEEE Syst. J.* **12**(4), 3169–3180 (2018). <https://doi.org/10.1109/JSYST.2017.2700791>
3. M. Panteli, C. Pickering, S. Wilkinson, R. Dawson, P. Mancarella, Power system resilience to extreme weather: fragility modeling, probabilistic impact assessment, and adaptation measures. *IEEE Trans. Power Syst.* **32**(5), 3747–3757 (2017). <https://doi.org/10.1109/TPWRS.2016.2641463>
4. R. Moreno et al., From reliability to resilience: planning the grid against the extreme. *IEEE Power Energ. Mag.* **18**(4), 41–53 (2020). <https://doi.org/10.1109/MPE.2020.2985439>
5. K. Murray, K.R.W. Bell, Wind related faults on the GB transmission network. in *2014 International Conference on Probabilistic Methods Applied to Power Systems, PMAPS 2014—Conference Proceedings* (2014), pp. 1–6. <https://doi.org/10.1109/PMAPS.2014.6960641>
6. V. Sultan, B. Hilton, A spatial analytics framework to investigate electric power-failure events and their causes. *ISPRS Int. J. Geo-Inf.* **9**(1) (2020). <https://doi.org/10.3390/ijgi9010054>
7. M. Panteli, D.N. Trakas, P. Mancarella, N.D. Hatziaargyriou, Power systems resilience assessment: hardening and smart operational enhancement strategies. *Proc. IEEE* **105**(7), 1202–1213 (2017). <https://doi.org/10.1109/JPROC.2017.2691357>
8. M.R. Davidson, D. Millstein, C.R. Michael Davidson, Limitations of reanalysis data for wind power applications (2022). <https://doi.org/10.1002/we.2759>
9. NCAS British Atmospheric Data Centre, MIDAS: UK Mean Wind Data (2021). <https://catalogue.ceda.ac.uk/uuid/a1f65a362c26c9fa667d98c431a1ad38>. (Accessed 10 Jul 2021)
10. M. Panteli, P. Mancarella, S. Wilkinson, R. Dawson, C. Pickering, Assessment of the resilience of transmission networks to extreme wind events. In *2015 IEEE Eindhoven PowerTech, PowerTech 2015* (2015). <https://doi.org/10.1109/PTC.2015.7232484>
11. J. Beirlant, Y. Goegebeur, J. Teugels, J. Segers, D. De Waal, C. Ferro, Statistics of extremes: theory and applications (2005). <https://doi.org/10.1002/0470012382>
12. H. Liu, Y. Zhou, M. Panteli, Visualization of network vulnerability during extreme weather events for situation awareness enhancement. In *IEEE Power and Energy Society General Meeting*, vol. 2018-August (2018). <https://doi.org/10.1109/PESGM.2018.8586494>
13. M. Belivanis, K. Bell, Representative GB network model: notes. Online Source: <http://www.maths.ed.ac.uk/optenergy/NetworkData/reducedGB/> (2011)
14. L.P. Kunjumammed, B.C. Pal, N.F. Thornhill, A test system model for stability studies of UK power grid. in *2013 IEEE Grenoble Conference PowerTech, POWERTECH 2013* (June 2013), pp. 16–20. <https://doi.org/10.1109/PTC.2013.6652283>.
15. Department for Business Energy & Industrial Strategy, Digest of UK Energy Statistics 2020 (London, United Kingdom, 2020). [Online]. Available: [https://assets.publishing.service.gov.uk/government/uploads/system/uploads/attachment\\_data/file/1006701/DUKES\\_2021\\_Chapter\\_5\\_Electricity.pdf](https://assets.publishing.service.gov.uk/government/uploads/system/uploads/attachment_data/file/1006701/DUKES_2021_Chapter_5_Electricity.pdf)

**Open Access** This chapter is licensed under the terms of the Creative Commons Attribution 4.0 International License (<http://creativecommons.org/licenses/by/4.0/>), which permits use, sharing, adaptation, distribution and reproduction in any medium or format, as long as you give appropriate credit to the original author(s) and the source, provide a link to the Creative Commons license and indicate if changes were made.

The images or other third party material in this chapter are included in the chapter's Creative Commons license, unless indicated otherwise in a credit line to the material. If material is not included in the chapter's Creative Commons license and your intended use is not permitted by statutory regulation or exceeds the permitted use, you will need to obtain permission directly from the copyright holder.



# Chapter 14

## The ‘Mousetrap’: Challenges of the Fluctuating Demand on the Electricity Grid in the UK



George Milev and Amin Al-Habaibeh

**Abstract** Currently, in the UK the power demand fluctuates throughout the day, especially during wintertime. The shape of the demand curve resembles the profile of a ‘mouse’. Around the tail area the energy consumption increases gradually, and that represents the demand during early morning hours which eventually flattens until the early evening. The head of the ‘mouse’ represents the early evening hours and the load on the grid peaks sharply. These sudden surges in power demand could potentially damage the grid leading to possible blackouts. In addition, this makes it difficult to depend on renewable energy such as wind turbines and solar panels without the use of energy storage. To examine the link between people’s behaviour and the grid, Covid-19 lockdown patterns were explored as it was a time of change in behaviour. Even during COVID-19 restrictions, which had an impact on people’s lives, the shape of the power demand curve did not significantly change; it followed the same shape of a ‘mouse’ compared to pre and post Covid periods, but during the pandemic the energy demand levels were slightly lower. The results suggests that in order to improve the stability of the demand, and hence remove this ‘mousetrap’, alternatives such as using renewable energy combined with electric and thermal energy storage systems can be integrated into the grid, which eventually can lead to flatten the demand curve.

**Keywords** UK grid · Power consumption · Grid demand · Demand curve · Balancing the grid · Peak hours

---

G. Milev (✉) · A. Al-Habaibeh  
Product Innovation Centre, Nottingham Trent University, Nottingham, UK  
e-mail: [george.milev@ntu.ac.uk](mailto:george.milev@ntu.ac.uk)

A. Al-Habaibeh  
e-mail: [Amin.Al-Habaibeh@ntu.ac.uk](mailto:Amin.Al-Habaibeh@ntu.ac.uk)

## 14.1 Introduction

It is important for power stations to maintain capacity security, so the provided electricity is sufficient to satisfy the demand. In addition, a balance between the supply and the demand of electrical energy must be in place, as it affects the frequency of the grid. According to the GB Security and Supply Standard, the frequency fluctuations must be limited to  $\pm 0.2$  Hz for normal power station operation [1]. In wintertime, the load pattern of the grid fluctuates as seen in Fig. 14.1.

Figure 14.1 show cases the hourly power demand in the UK in cold seasons. The shape of the curve resembles a mouse. In particular, the back torso and the ears areas show when peaks on the grid appear. At around 5 a.m. the power demand gradually reaches approximately 42 GW over a period of 4 h. It remains relatively flat until around 4 p.m. where the load on the grid increases sharply by roughly 3 GW. With the demand curve's shape of a mouse, it would be challenging to use more renewable energy and provide stable electrical energy.

Currently, the UK is on the path to reduce fossil fuels from the energy generation mix. It is expected the country to reach net zero carbon emissions by 2050 [3]. Some of the strategies the government is planning to adopt in order to become carbon neutral is to increase the capacity of wind and solar sources of electricity, electrify the transportation by banning fossil fuel vehicles by 2050, and decrease dependence on fossil fuels for the heating sector by implementing heat pumps as part of the Heat and Building Strategy for meeting the net-zero 2050 targets [3]. In addition, lockdown restrictions led to 13% drop in carbon emissions in 2020 compared to 2019

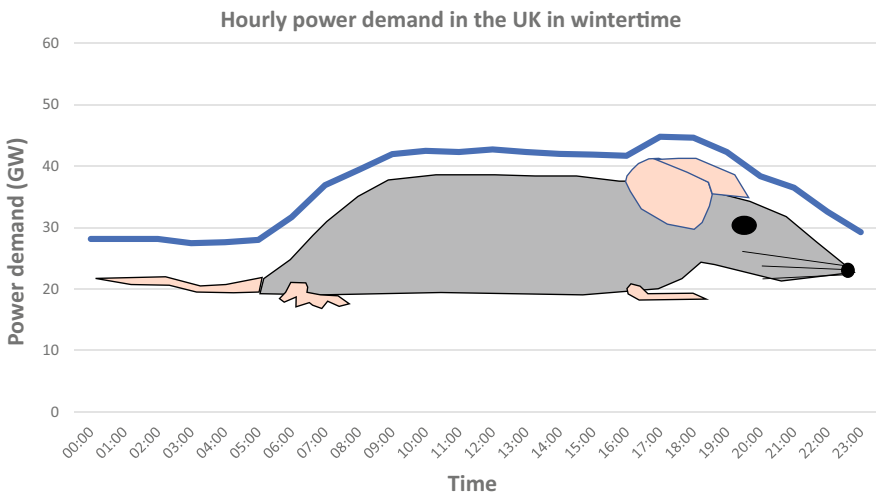
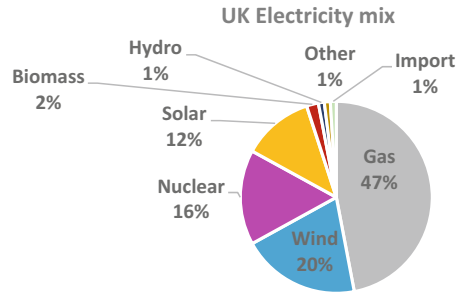


**Fig. 14.1** Hourly power demand in the UK in wintertime which resembles a mouse profile (based on data from [2])

**Fig. 14.2** UK electricity generation mix 2022 (based on data from [2])



[4]. On top of that the electricity price has increased sharply, approximately 43% as of 2022 compared to 2020 [5].

Figure 14.2 presents the current electricity generation mix in the UK. From the graph it is evident that the majority of the current electricity is generated by gas at around 47% [2]. The capacity of wind and solar have increased slightly in 2021 compared to 2020 [6]. Although, the wind and solar capacities have increased, the environmental conditions are still not favourable for these sources to provide and maintain steady electricity throughout the day [2]. This suggests that UK still have to rely on fossil fuels to provide electricity during peak hours or when wind and solar are not enough and therefore contribute to more carbon emissions [2].

The Covid-19 pandemic is considered as one of the most impactful global health emergencies in the century. It has not only affected the health of people, but also indirectly through lockdowns the economy of almost every country around the world as well as the energy demand and consumption.

With the confinement measures many people throughout the world were forced to work from home, which is expected to have some effect on the electricity consumption. For most countries the start of lockdown measures were implemented between February and March 2020. After that each country individually assessed the right time to open the businesses and the borders depending on the infection rates [7]. For Germany and most of the US, there was a considerable reduction in electricity demand [7]. In addition, Poland is a country that similar to the UK implemented more than one lockdown for 2020 [8]. Research investigating the impact on the energy demand in Poland due to Covid-19 concluded that the restrictions caused a drop of approximately 23% in energy consumption during the first lockdown in March–May period 2020 and around 11% during the second lockdown in October–November period of the same year [8]. A similar situation can be noticed in Turkey (Türkiye) where the first incident of Covid-19 was detected in March 2020 and restrictions followed soon after [9]. In April and May of the same year, the electricity production dropped by around 15% and 16.5% respectively compared to the same months in 2019 [9]. According to the same research, the electricity consumption of the industry and residential sectors increased slightly in 2020 compared to 2019, but there was a considerable reduction for the business sector in 2020, suggesting that the businesses have great influence on the energy consumption in Turkey [9].

In the UK the first lockdown measures were introduced on 26th March 2020. During this time people were advised to stay at home and work from home [10]. In June of the same year the restrictions were slowly removed until 5th November 2020, when a second lockdown came into force, which continued until 2nd December [10]. Particularly, in the UK the only increase that was noticed during 2020 was of gas consumption as the majority of people were forced to work from home [11]. Industry and business buildings tend to be more energy efficient when it comes to heating [11]. Overall, it was estimated that there was a drop in electricity consumption in the commercial and industrial sectors between March and June of 2020, which resulted in a significant reduction of carbon emissions. However, households with houses that were not properly insulated were affected by increased energy bills during the winter lockdown period [11].

## 14.2 Methodology

As shown in Fig. 14.1, the electricity demand in the UK resembles a mouse profile. What is the cause in the change in demand? To address this, the authors have investigated the grid patterns in the UK in winter before and during Covid-19 pandemic lockdown. Firstly, a graph using data from Gridwatch [2] has been developed to showcase the daily demand in wintertime along with each source of electricity in the UK. The reason for that was to see how the demand fluctuates throughout the day and when load peaks occur. After that we compared the annual electricity consumption in the UK from 2012 to 2021. This allowed us to monitor whether the overall consumption is increasing or decreasing. The Covid-19 restrictions took place in 2020 and 2021 in the UK. In particular, the strictest and longest measures happened between March 2020 and June 2020, as well as November 2020. That is why we looked into the daily electrical energy consumption on a November weekday and on a weekend for 2019, 2020, and 2021 as the ambient temperatures can drop as low as 1 °C during that month as shown in Fig. 14.3 [12]. This analysis allowed to determine not only how lockdown measures affected the energy consumption, but also if the demand curve followed the same fluctuations curve as pre and post pandemic period.

## 14.3 Results

Figure 14.4a and b represent the daily power demand in winter and the annual electricity consumption in the UK respectively.

From Fig. 14.4a it is evident that the majority of the demand is satisfied by gas. There are very sharp peaks on the grid at around 5 a.m. and again at 4 p.m. From Fig. 14.4b, it can be noticed that in 2020 the annual consumption was lower than the rest of the years. In 2020 there were 2 lockdowns that took place, one in spring and one in winter [10].



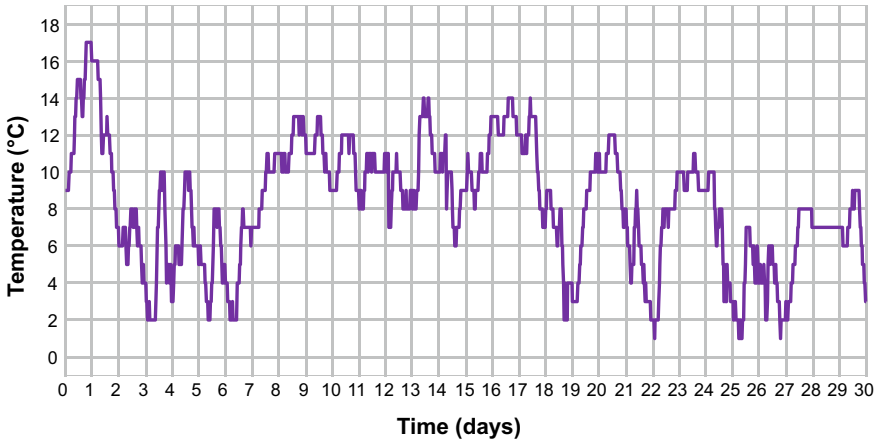


**Fig. 14.3** Ambient temperature in Nottingham, UK in November 2020 (based on data from [12])

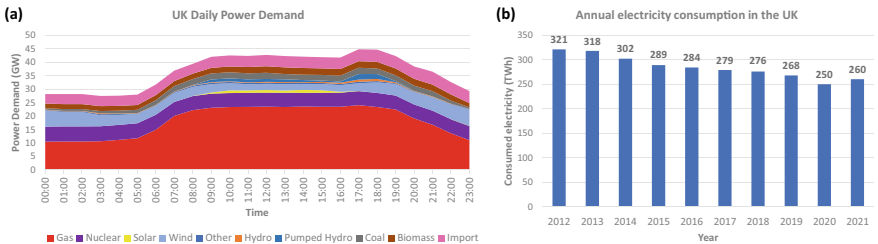


**Fig. 14.4** The daily power demand in the UK (a) and annual electricity consumption in the UK (b) (based on data from [2])

Figures 14.5a and b represent the hourly demand on weekdays and on weekends respectively in November. November was chosen specifically as the 2nd lockdown in the UK took place for the whole duration of that month in 2020. In both figures, the power demand followed a similar pattern, in the shape of a ‘mouse’. The main noticeable change is during the weekdays in 2020, the increased demand in the morning starts at around 7 a.m., and the evening one at around 5 p.m., compared to approximately 4 a.m. and 4 p.m. for 2018, 2019, and 2021. One of the reasons for the shift of the demand peaks is the daily habits and activities of people across the UK. Many were forced to work from home due to the Covid-19 restrictions [10]. In regard to Fig. 14.5b, there is no considerable change in the demand pattern during the weekends for all the analysed years.

Figures 14.6a and b present the shape of the power demand curves compared to previous years and with 2020 lockdown period. The shape of the 2020 curve resembles a mouse following the same trend as previous years. This shows that Covid-19 affected only the amount of consumed electricity, but it did not impact the shape of the demand curve.

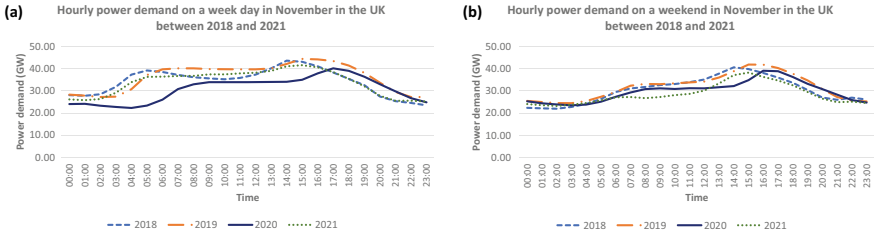


**Fig. 14.5** Hourly demand comparison on a weekday (a) and hourly demand comparison on a weekend (b)

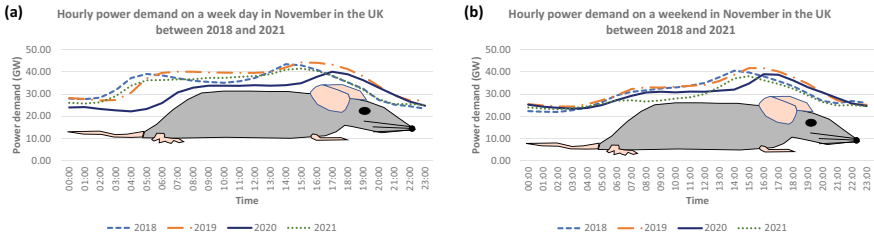


**Fig. 14.6** The shape of the hourly weekday demand (a) and the shape of the hourly weekend demand comparison (b)

### 14.4 Discussion and Conclusion

This paper has focused on the electricity consumption in the UK, and the electricity consumption patterns. It seems we are in the UK ‘trapped’ in user patterns by the ‘mouse’ shape, even during Covid-19 pandemic lockdown. This paper has considered the winter season before and after lockdown. We have examined in more details the month of November because the ambient temperature can drop below 2 °C and it was during the second lockdown in the UK. This suggests that households would use more heating, thus increasing the energy demand during that month. Whereas during the first lockdown between March and June, the weather is warmer. In our hourly demand comparison for the weekdays and weekends in November we analysed the data between 2018 and 2021. However, the pandemic did not affect the fluctuating power demand, as show in Fig. 14.6a and b as it followed similar trend as previous years. This current shape of a mouse creates a challenge ‘a trap’ in promoting more stable electricity. Especially when the UK electrifies the transport and heating sectors via electric vehicles and heat pumps. The strain on the grid could be severe if the same power demand is followed. For that reason, more battery storage systems combined with solar panels or wind turbines should be implemented along with thermal storage to reduce the peak load on the national grid and flatten the curve. More analysis will be performed in the future to analysis the reasons for such patterns and how to avoid them.

## References

1. F. Teng, Y. Mu, H. Jia, J. Wu, P. Zeng, G. Strbac, Challenges of primary frequency control and benefits of primary frequency response support from electric vehicles. *Energy Proc.* **88**, 985–990 (2016)
2. M. Stolworthy, *GB Fuel type power generation production* (2022) [online] Gridwatch.co.uk. Available at: <<https://gridwatch.co.uk/>> (Accessed 20 May 2022)
3. HM Government, *Net Zero Strategy: Build Back Greener*, 1st ed. (Crown copyright 2021), pp. 34–298
4. Climate Change Committee, *Reaching Net Zero in the UK—Climate Change Committee* (2022) [online] Climate Change Committee Available at: <<https://www.theccc.org.uk/uk-action-on-climate-change/reaching-net-zero-in-the-uk/#:~:text=The%20new%20Net%20Zero%20target,13%25%20from%20the%20previous%20year.>> (Accessed 20 May 2022)
5. E. Yurday, *Average Cost of Electricity per kWh in the UK 2022* (2022) [online] Nimblefins.co.uk. Available at: <<https://www.nimblefins.co.uk/average-cost-electricity-kwh-uk>> (Accessed 30 May 2022)
6. K. Harris, C. Michaels, S. Rose, D. Ying, V. Martin, W. Spry, *Energy Trends | UK, October to December 2021 and 2021*. Energy Trends. [online] Department for Business, Energy & Industrial Strategy | UK Government (2022) pp. 1–10. Available at: <[https://assets.publishing.service.gov.uk/government/uploads/system/uploads/attachment\\_data/file/1064782/Energy\\_Trends\\_March\\_2022.pdf](https://assets.publishing.service.gov.uk/government/uploads/system/uploads/attachment_data/file/1064782/Energy_Trends_March_2022.pdf)> (Accessed 20 May 2022)
7. Z. Li, H. Ye, N. Liao, R. Wang, Y. Qiu, Y. Wang, Impact of COVID-19 on electricity energy consumption: a quantitative analysis on electricity. *Int. J. Electr. Power Energy Syst.* **140**, 108084 (2022)
8. M. Malec, G. Kinelski, M. Czarnecka, The impact of COVID-19 on electricity demand profiles: a case study of selected business clients in Poland. *Energies* **14**(17), 5332 (2021)
9. M. Bulut, Analysis of the Covid-19 impact on electricity consumption and production. *Sakarya Univ. J. Comput. Inf. Sci.* (2020)
10. The Institute for Government, *Timeline of UK government coronavirus lockdowns and restrictions* (2022) [online] Available at: <<https://www.instituteforgovernment.org.uk/charts/uk-government-coronavirus-lockdowns>> (Accessed 10 May 2022)
11. A. Sen, A. Al-Habaibeh, The effect of Covid-19 pandemic on household budget, energy demand and carbon emission of households in England due to working from home. in *International Conference on Applied Energy 2020*. (Bangkok, ICAE, 2020), pp. 1–5. [online] Available at: <<https://www.energy-proceedings.org/wp-content/uploads/enerarxiv/1607143574.pdf>> (Accessed 10 May 2022)
12. Time and Date AS, *Weather in November 2020 in Nottingham* (England, United Kingdom, 2022) [online] Timeanddate.com. Available at: <<https://www.timeanddate.com/weather/uk/nottingham/historic?month=11&year=2020>> (Accessed 14 June 2022)

**Open Access** This chapter is licensed under the terms of the Creative Commons Attribution 4.0 International License (<http://creativecommons.org/licenses/by/4.0/>), which permits use, sharing, adaptation, distribution and reproduction in any medium or format, as long as you give appropriate credit to the original author(s) and the source, provide a link to the Creative Commons license and indicate if changes were made.

The images or other third party material in this chapter are included in the chapter's Creative Commons license, unless indicated otherwise in a credit line to the material. If material is not included in the chapter's Creative Commons license and your intended use is not permitted by statutory regulation or exceeds the permitted use, you will need to obtain permission directly from the copyright holder.



# Chapter 15

## Assessment of Effectiveness of Hollow Fins for Performance Enhancement of Solar Still Device Using Simulation Approach



Hafiz Khadim Ullah, Sikiru Oluwarotimi Ismail,  
and Kumar Shantanu Prasad

**Abstract** Unavailability of relatively clean water for several industrial, domestic and agricultural purposes is a serious concern to many regions of the world today. This challenge is growing worse with the increasing world global warming and human population. Therefore, there is need to research into an innovative, sustainable and/or improved technology for an efficient and effective solution, such as desalination. Desalination of freely available sea water is considered a promising source of fresh water. Solar radiation is abundant and can be used to desalinate water, using a solar still device. Also, it is important to increase the productivity of the solar still device through hollow fin modification. Therefore, the effectiveness of this improvement was investigated in this study, using an analysis system (ANSYS) Fluent computational fluid dynamic (CFD) simulation. Appropriate models were used to describe the physical processes, including condensation, evaporation, multiphase flow, surface tension and solar radiation. A close agreement between the simulation values of solar energy and the water temperature in the basin was observed when compared with the experimental data from the literature. Velocity of 0.259 m/s, pressure of 55.8 Pa, temperature of 57.85 °C and mass transfer rate of 1.41 kg/m<sup>3</sup>/s were obtained in the mid-plane of the improved double slope single basin (DSSB). The degree of improvement was 5–7% when compared with the existing models. Importantly, this process is economically efficient and can support the concepts of sustainability and healthy living, especially in rural areas.

**Keywords** Hollow fins · Solar still · Sustainability · Rural areas · Simulation approach

---

H. K. Ullah · S. O. Ismail (✉) · K. S. Prasad  
Centre for Climate Change Research (C3R), Centre for Future Societies Research (CFSR),  
University of Hertfordshire, Hatfield, Hertfordshire AL10 9AB, England, UK  
e-mail: [s.ismail3@herts.ac.uk](mailto:s.ismail3@herts.ac.uk)

## 15.1 Introduction

A solar still is a device or apparatus used for solar-powered thermal desalination. The efficiency of these devices is often low, and many changes are being proposed to increase it. Therefore, several studies are currently being conducted on the production of distilled water to address the scarcity of pure water sources. Solar stills [1–4] are one of the most common technologies for water distillation that use solar energy without causing environmental problems. The different construction designs of solar stills are shown in Fig. 15.1.

Moving forward, Abdelal and Taamneh [5] conducted research to improve water productivity in pyramid solar stills, using a carbon fiber/non-materials modified epoxy composite absorber. The output of the new modified pyramid was higher than the conventional one. According to Jordanian metrological data, Altarawneh et al. [6] studied the performance of pyramid solar stills both practically and theoretically throughout the year. The solar still performance and the availability of solar radiation are theoretically simulated. Kabeel et al. [7] investigated into a new design of pyramid solar still in an experimental setting. The still contained both V-corrugated and phase-change material (PCM). The results showed that the new design resulted to a higher productivity than the conventional counterpart. Manokar

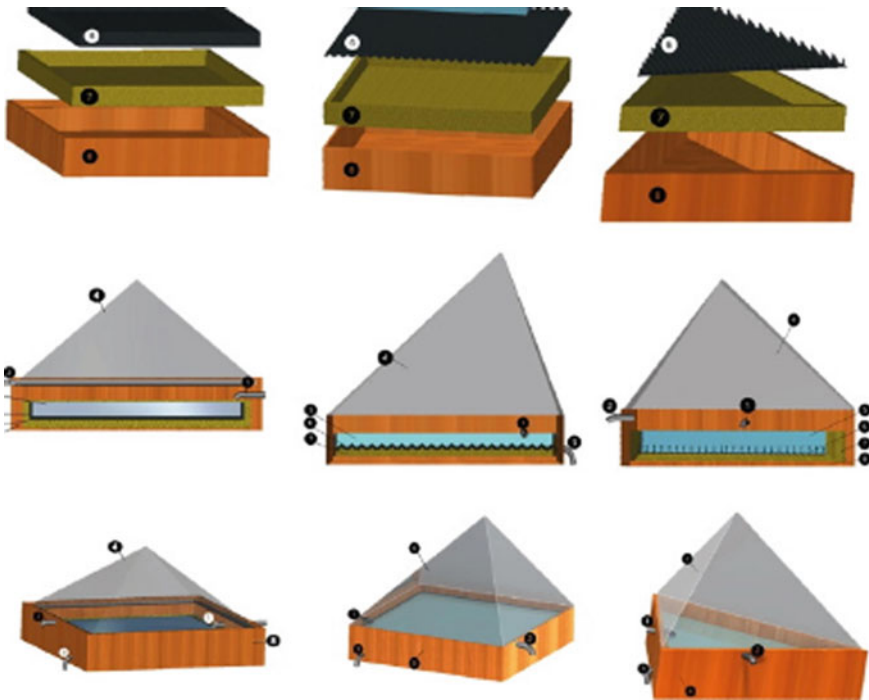


**Fig. 15.1** Different construction designs of solar stills

et al. [8] improved the performance of the pyramid solar still by using insulation to raise the basin water temperature. The water depth was increased from 1.0 to 3.5 cm, and the productivity of the solar still was calculated with and without insulation. In addition to the neural artificial network, Sharshir et al. [9] investigated into the thermal performance of pyramid solar stills, using an alternate prediction approach. The research was done in two ways: theoretically and experimentally, using neural artificial network and alternative prediction method, respectively. Kabeel et al. [10] used nanoparticles to the black absorber paint to improve the performance of the pyramidal basin type solar still.  $\text{TiO}_2$  nanoparticles were mixed with the black paint of the basin to test the performance under a wide variety of water depths. Velmurugan et al. [11] observed that attaching strip fins to the absorber plate boost the productivity of a single slope single basin (SSSB) solar still device by 45.5%. Pebbles, sand, black rubber and sponges were also added to improve the efficiency of the solar still device with fins. Omara et al. [12] studied the use of fins and corrugations on the absorber surface to boost freshwater production. 40% improvement was recorded with fins and a 21% improvement with the corrugations.

Besides, there are other varieties of solar still devices, but the double slope single basin (DSSB) was chosen for this research, because it is more efficient than the SSSB and produces fresh water at a faster rate. Because fins are passive and require little maintenance, there is need for a further research on relevant technology. Fins come in a variety of shapes and sizes, including solid fins with varied cross-sections and diameters, as well as pin-fins. These fins, on the other hand, have been investigated extensively using CFD. However, there are very few or no literature on CFD studies of hollow fins. Therefore, analysis system (ANSYS) simulation was used to determine the efficiency of hollow fins in this present study in an attempt to improve the performance of the solar still device. The objectives of the current study include: (i) application of ANSYS to create a model of a solar still device with hollow circular fins, as a productivity-enhancing change, (ii) selection of acceptable models for solar radiation, evaporation–condensation, multiphase flow and surface tension, as physical phenomena, (iii) simulation and its comparison with the experimental data from literature and (iv) assessment of the effectiveness of the fin adjustments by analysing the simulation results using appropriate contour plots.

## 15.2 Methodology

### 15.2.1 Model

The geometry of the DSSB with hollow circular fins was modelled, using ANSYS integrated computer-aided design (CAD) modeler, called space claim (Fig. 15.2). The absorber plate with hollow circular fins from the bottom, the galvanised iron box on the side and the glass cover on the top were used to simulate and contained the DSSB fluid domain. The geometry of real world DSSB is shown in Fig. 15.3.

**Fig. 15.2** Fluid domain of the DSSB with hollow circular fins and condensate water collecting channels

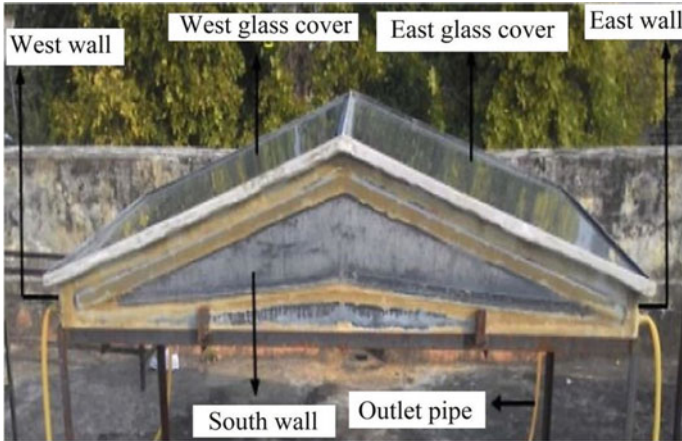
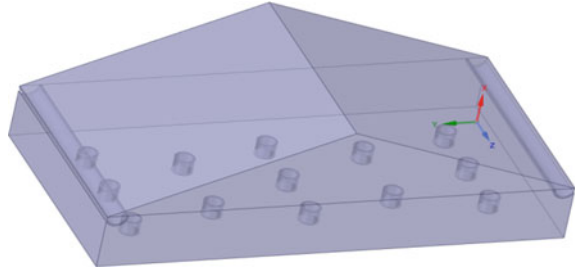


**Fig. 15.3** Real-world DSSB

The volume of fluid (VOF) model was chosen with the two Eulerian phases to model the multiphase behaviour of the fluids in the DSSB. The primary phase was water vapour and the secondary phase was water. Modelling of the solar load was performed using the Rosseland radiation model and the solar ray tracing technique. The ANSYS Fluent material database was used to incorporate the material properties of the fluid and solid materials. Two dimensional (2D) and 3D models were used for both steady state and transient simulations.

### 15.3 Results and Discussion

Figures 15.4 and 15.5 show the pressure contours in the mid-plane for steady-state and transient simulations, respectively. The maximum gauge pressure was initially around 27.2 Pa, but due to the evaporation of the water, it increased to 55.8 Pa. The pressure contour of the transient simulation showed increased pressure in the basin region above the water level. Comparatively, the pressure contour of the solar still device with hollow fins exhibited a better performance than other conventional solar still model with 22 Pa [13].



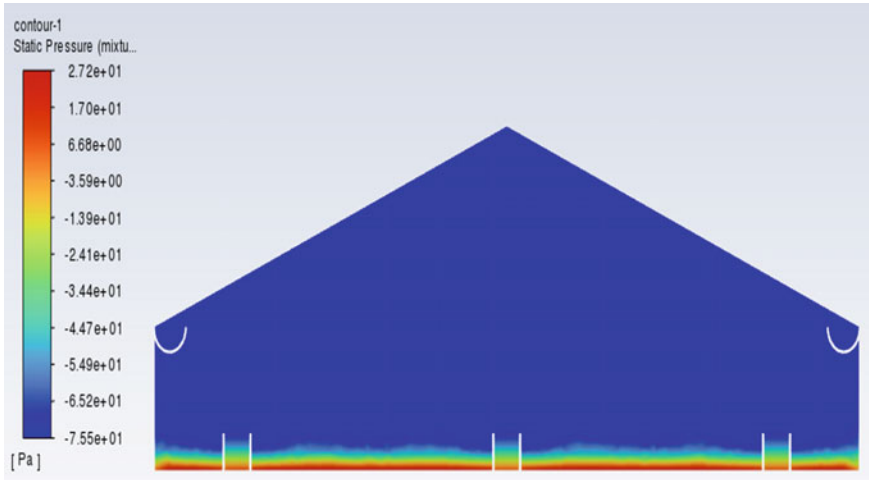


**Fig. 15.4** Pressure contour on the mid-plane for steady state 3D simulation

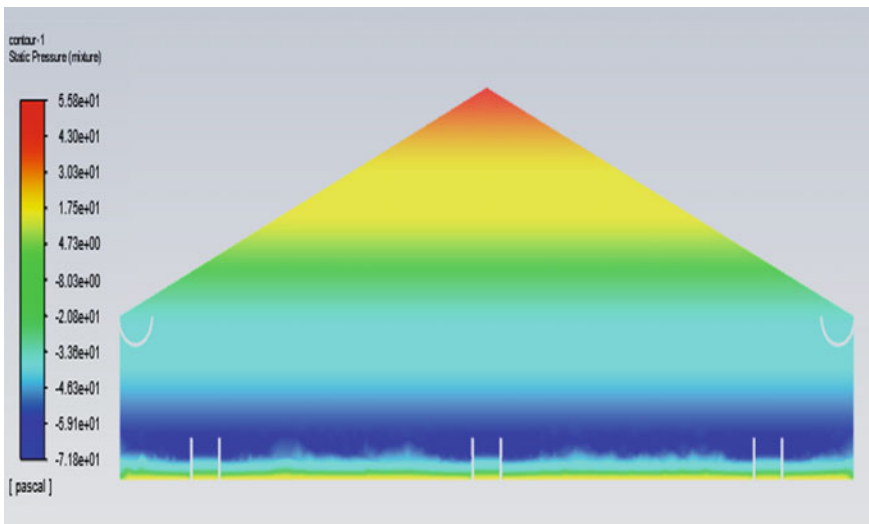


**Fig. 15.5** Pressure contour on the mid-plane for transient 3D simulation

The static temperature contour at the mid-plane for the steady state and transient 3D simulations of the improved DSSB are shown in Figs. 15.6 and 15.7, respectively. The initial maximum temperature was around 336 K (62.85 °C) and the water temperature was around 331 K (57.85 °C). The performance temperature of solar still device with hollow fins was lower than solar still device with single slope solar [14]. Therefore, solar still device with hollow fins recorded higher effectiveness than the single slope solar.

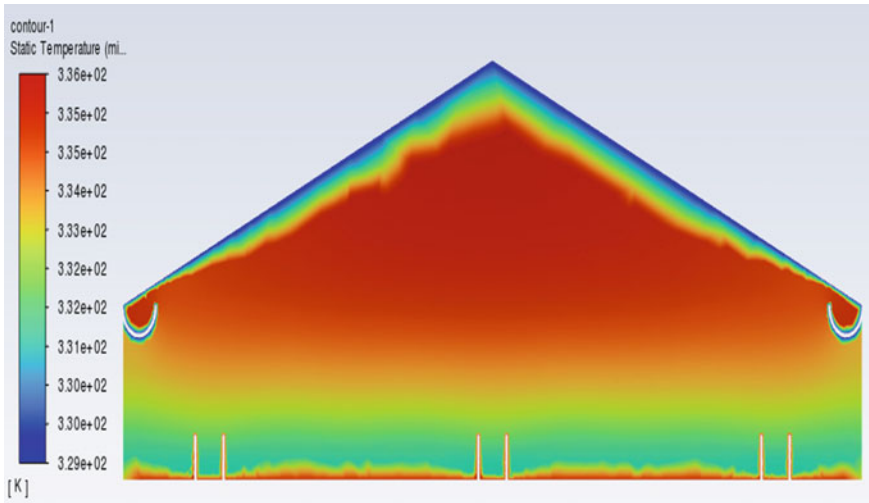


Fig. 15.6 Static temperature contour on the mid-plane for steady state 3D simulation

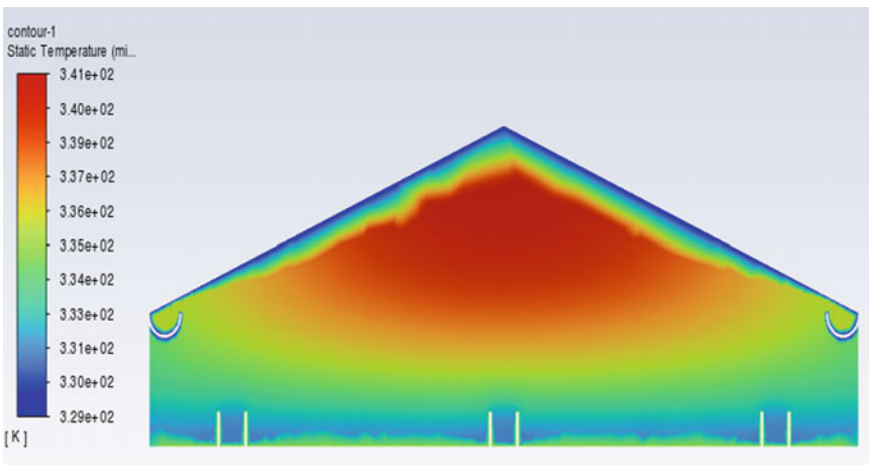


Fig. 15.7 Static temperature contour on the mid-plane for transient 3D simulation

The maximum temperature in the transient simulation contour was around 341 K (67.85 °C), and the water temperature near the collector increased to 335 K (61.85 °C). This value was very close to the water temperature obtained in the experiments shown in Fig. 15.8. Evidently, Fig. 15.8 shows the results obtained from the modified DSSB. Saline water recorded maximum temperature of 64.5 °C, which was close to the current study.

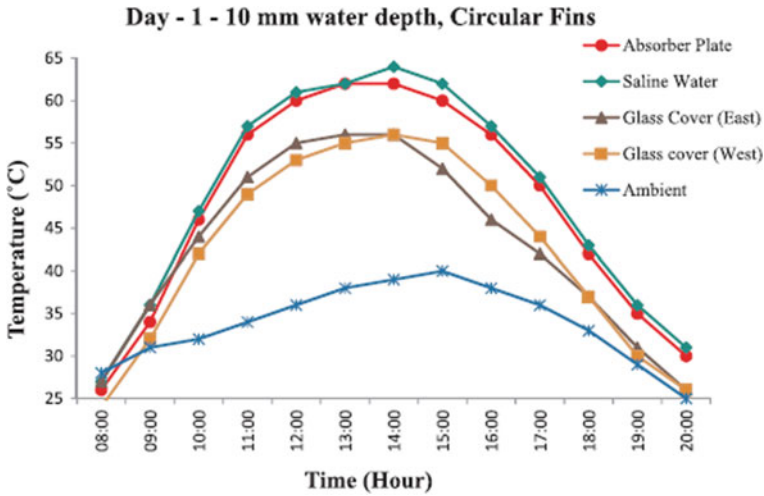


Fig. 15.8 Experimental results for temperature variation in the modified DSSB [15]

In addition, the mid-plane velocity magnitude contours for the steady state and transient 3D simulations are shown in Figs. 15.9 and 15.10, respectively. Due to the evaporation process caused as a result of the heating of water by solar radiation, higher velocity was recorded along the interface of the water and vapour phase. It was observed that the effectiveness of solar still device with hollow fins in term of velocity was more efficient than the traditional solar still desalination model. Moreover, velocity of solar still device with hollow fins was better than the velocity of tubular solar still operating under vacuum with velocity of 0.13 m/s [16].

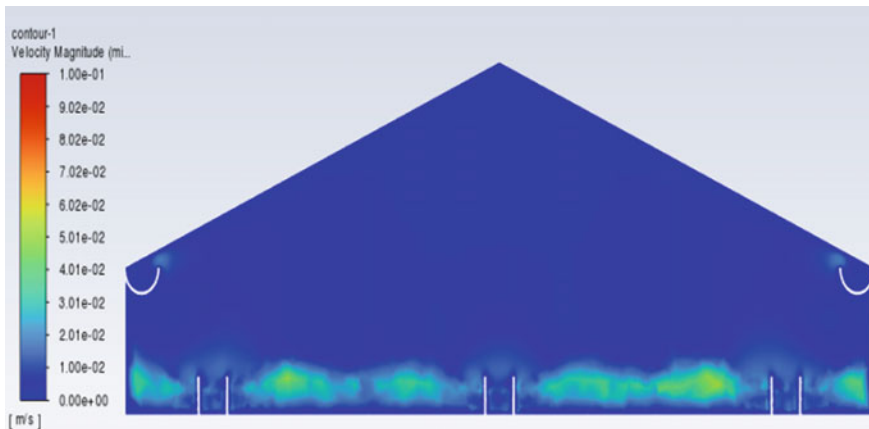
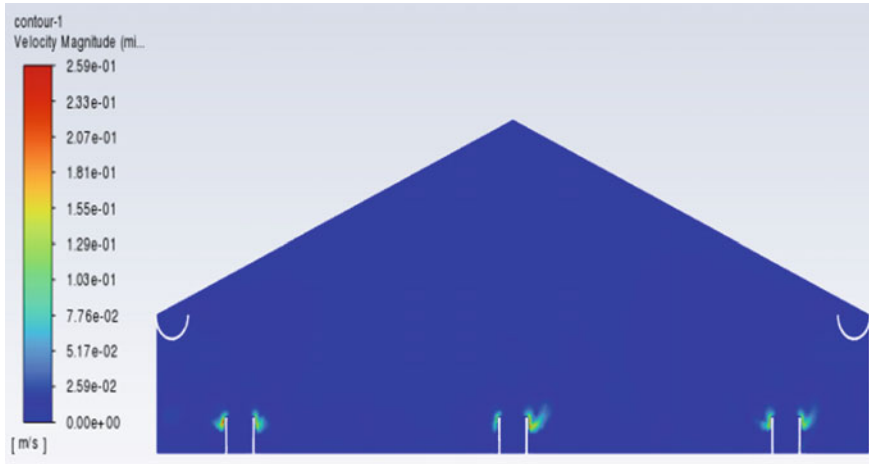


Fig. 15.9 Velocity magnitude contour on the mid-plane for the steady state 3D simulation



**Fig. 15.10** Velocity magnitude contour on the mid-plane for transient 3D simulation

In the transient simulation, as shown in Fig. 15.10, the velocity increased and reached a maximum value of 0.259 m/s. Due to the blockage of the fin flow and the increased heat transfer from the fins to the surrounding fluid, high velocity values were observed near the upper edge of the fins. Using the contour and the velocity vector plots, Fig. 15.11 depicts a detailed phenomenon at the velocity magnitude near the fins.

Figures 15.12 and 15.13 depict the mass transfer rate contours in the mixture, due to evaporation and condensation processes for steady state and transient simulations, respectively. The mass transfer rate in the water phase region was low, whereas the mass transfer rate in the vapour phase region was high. In the transitory case, the mass transfer rate increased, and the water inside the hollow fins evaporated to a greater extent than the surrounding water. The mass transfer rate of solar still device with hollow fins was greater than the solar still device without fins.

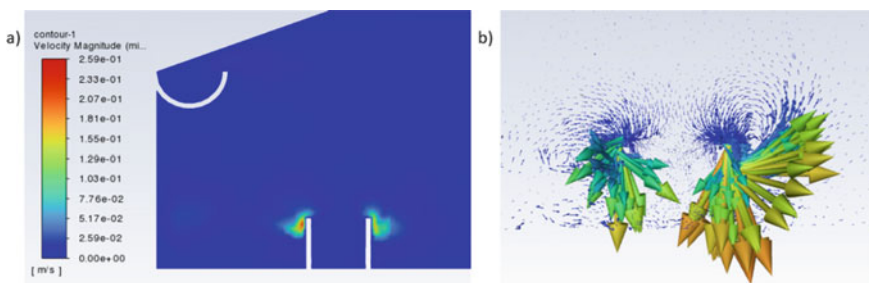


**Fig. 15.11** Closer visualisation of **a** velocity magnitude contour near the fin and **b** the velocity vectors near the fin

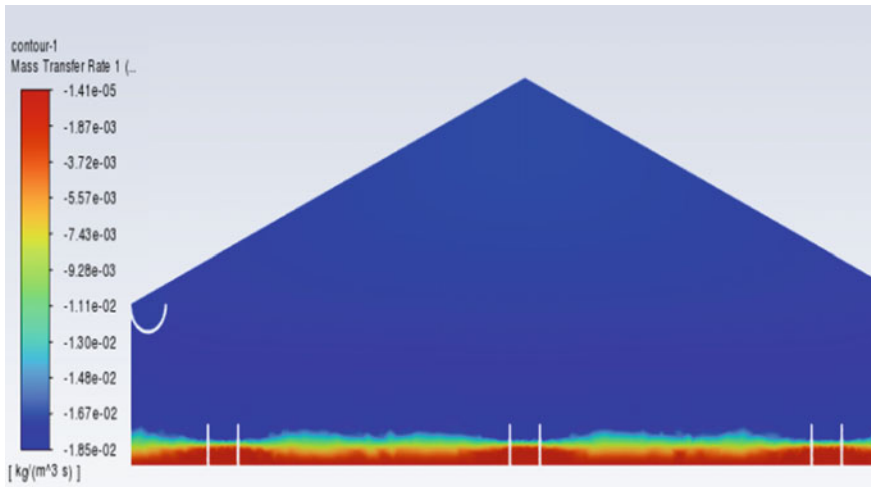


Fig. 15.12 Mass transfer rate contour on the mid-plane for steady state 3D simulation

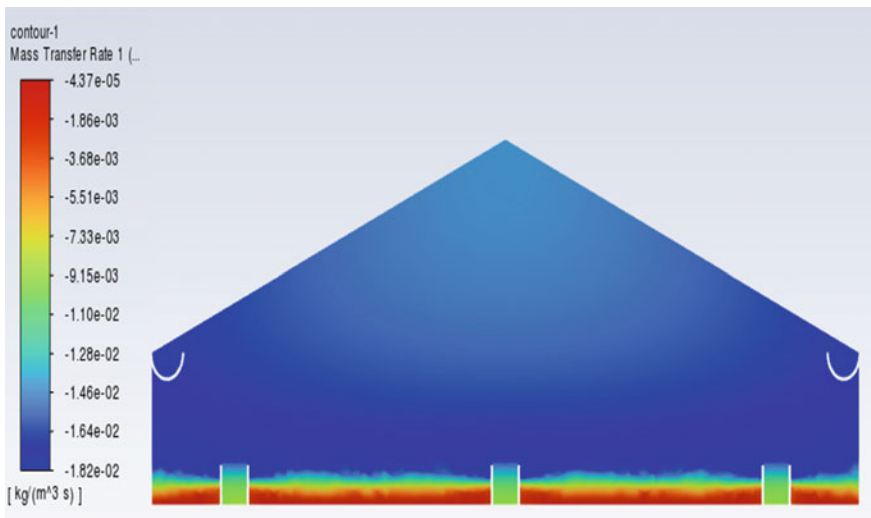


Fig. 15.13 Mass transfer rate contour on the mid-plane for transient 3D simulation

## 15.4 Conclusion

The current study has investigated into the effectiveness of hollow fins towards improving the effectiveness of DSSB. From this study, the following summarised remarks can be deduced:

- The values of solar radiation and water temperature observed in the simulation were close to the experimentally measured values, as the temperature of the water inside the basin was observed at the mid-plane.
- The variation in values from the initial condition to the transient simulation value was observed in pressure and velocity contours at mid-plane.
- The mass transfer rate near the hollow fins was examined, indicating the usefulness of fins towards improving heat transfer and more significantly, production of fresh water.

Lastly, the importance of this proposed sustainable and cost efficient model or design cannot be underestimated, considering its significance in conversion of dirty water to a clean water for domestic, agricultural and industrial applications, especially in rural areas.

## References

1. N. Ghaffour, I.M. Mujtaba, Desalination using renewable energy. *Desalination* **435**, 1–2 (2018)
2. V.G. Gude, Use of exergy tools in renewable energy driven desalination systems. *Thermal Sci. Eng. Progress* **8**, 154–170 (2018)
3. S.A. Kalogirou, Seawater desalination using renewable energy sources. *Prog. Energy Combust. Sci.* **31**, 242–281 (2005)
4. K.H. Nayi, K.V. Modi, Pyramid solar still: a comprehensive review. *Renew. Sustain. Energy Rev.* **81**, 136–148 (2018)
5. N. Abdelal, Y. Taamneh, Enhancement of pyramid solar still productivity using absorber plates made of carbon fiber/CNT-modified epoxy composites. *Desalination* **419**, 117–124 (2017)
6. I. Altarawneh et al., Experimental and numerical performance analysis and optimization of single slope, double slope and pyramidal shaped solar stills. *Desalination* **423**, 124–134 (2017)
7. A. Kabeel et al., Modified pyramid solar still with v-corrugated absorber plate and PCM as a thermal storage medium. *J. Clean. Prod.* **161**, 881–887 (2017)
8. A.M. Manokar et al., Effect of water depth and insulation on the productivity of an acrylic pyramid solar still—an experimental study. *Groundw. Sustain. Dev.* **10**, 100319 (2020)
9. S.W. Sharshir, M. Abd Elaziz, M. Elkadeem, Enhancing thermal performance and modeling prediction of developed pyramid solar still utilizing a modified random vector functional link. *Sol. Energy* **198**, 399–409 (2020)
10. A.E. Kabeel et al., Effect of water depth on a novel absorber plate of pyramid solar still coated with TiO<sub>2</sub> nano black paint. *J. Clean. Prod.* **213**, 185–191 (2019)
11. V. Velmurugan et al., Desalination of effluent using fin type solar still. *Energy* **33**, 1719–1727 (2008)
12. Z. Omara, M.H. Hamed, A. Kabeel, Performance of finned and corrugated absorbers solar stills under Egyptian conditions. *Desalination* **277**, 281–287 (2011)
13. M. Mostafa, H.M. Abdullah, M.A. Mohamed, Modeling and experimental investigation of solar stills for enhancing water desalination process. *IEEE Access* **8**, 219457–219472 (2020)
14. H. Panchal, P. Shah, Modelling and verification of single slope solar still using ANSYS-CFX. *Int. J. Energy Environ.* **2**, 985–998 (2011)
15. H.K. Jani, K.V. Modi, Experimental performance evaluation of single basin dual slope solar still with circular and square cross-sectional hollow fins. *Sol. Energy* **179**, 186–194 (2019)
16. T. Yan et al., CFD investigation of vapor transportation in a tubular solar still operating under vacuum. *Int. J. Heat Mass Transf.* **156**, 119917 (2020)

**Open Access** This chapter is licensed under the terms of the Creative Commons Attribution 4.0 International License (<http://creativecommons.org/licenses/by/4.0/>), which permits use, sharing, adaptation, distribution and reproduction in any medium or format, as long as you give appropriate credit to the original author(s) and the source, provide a link to the Creative Commons license and indicate if changes were made.

The images or other third party material in this chapter are included in the chapter's Creative Commons license, unless indicated otherwise in a credit line to the material. If material is not included in the chapter's Creative Commons license and your intended use is not permitted by statutory regulation or exceeds the permitted use, you will need to obtain permission directly from the copyright holder.



# Chapter 16

## Development of a CFD Model for the Estimation of Windage Losses Inside the Narrow Air Gap of an Enclosed High-Speed Flywheel



**Mahmoud Eltaweel, Christos Kalyvas, Yong Chen,  
and Mohammad Reza Herfatmanesh**

**Abstract** Concerns over global warming and the need to reduce carbon emissions have prompted the development of novel energy recovery systems. During urban driving, a significant amount of energy is lost due to continuous braking, which can be recovered and stored. The flywheel energy storage system can efficiently recover and store the vehicle's kinetic energy during deceleration. In this study, a Computational Fluid Dynamics (CFD) model was developed to assess the impact of air gap size, and rotor cavity pressure environment on the aerodynamic performance of an enclosed non-ventilated flywheel energy recovery system. Consequently, the flywheel rotor skin friction coefficients for various air gap sizes have been numerically determined to predict the windage losses over a wide operating range. The presented study aims to identify a correlation that accurately fits the rotor skin friction coefficients for a range of air gap sizes and operating conditions. Model validation was carried out to assess the validity of the CFD results, which showed good agreement between numerical and experimental data. The results demonstrated that the increase in the air gap size can lead to up to a 19% reduction in the windage loss depending on the operating speed of the flywheel, while the windage loss can be reduced by 33% when the operating pressure is reduced to 500 mbar. Windage losses can be reduced by 45% when the airgap size is greatest, and the operating pressure is lowest.

**Keywords** Energy recovery system · Mechanical storage · Taylor-Couette flow · Skin friction coefficient

---

M. Eltaweel (✉) · C. Kalyvas · Y. Chen · M. R. Herfatmanesh  
School of Physics, Engineering and Computer Science, University of Hertfordshire, Hatfield,  
Hertfordshire AL10 9AB, England  
e-mail: [m-eltaweel@outlook.com](mailto:m-eltaweel@outlook.com)



## 16.1 Introduction

Flywheel energy storage systems (FESS) are mechanical energy storage devices that use the moment of inertia of a rotating disc to store mechanical energy. By speeding or decelerating the flywheel rotor with an electric motor, generator, or Continuous Variable Transmission (CVT), energy can be provided to or withdrawn from the flywheel. FESS is designed for short-term energy storage, which is ideal for fault protection, peak shaving, frequency management, and vehicles. The optimal design for the flywheel rotor in FESS can improve energy storage performance while also lowering the cost of the system, making it a more commercially feasible energy storage solution [1].

The performance of a FESS can be influenced by rotor design parameters such as material, operating speed, overall size, topology, and shape. These affect the FESS's energy capacity by determining the moment of inertia and allowing for a uniform stress distribution. The total stored energy is influenced by the operating speed. The yield strength and density of the rotor material determine the maximum permitted stress and mass of the flywheel rotor, which in turn affect the maximum allowable stress of the flywheel rotor. To create an optimum flywheel for a given application, the rotor design and operating speed of the flywheel must be tuned [2]. The total standby losses, which contribute to self-discharge and might affect the FESS's overall efficiency, are influenced by the operating speed and rotor shape. Mechanical losses due to bearing friction and windage are the main causes of standby power losses. To assess standby losses, as well as run-time losses that occur while charging or discharging the FESS, literature studies have employed simulations based on analytical models [3] and empirical models based on experiments [4].

Gurumurthy et al. [5] used an experimental flywheel system at atmospheric pressure to measure the mechanical and electrical losses in the FESS. They increased the rotational speed of the FESS to 15,000 rpm and then allowed it to decelerate in various load and no-load scenarios. Mechanical losses, particularly drag losses, dominated power losses in their studies, accounting for 72% of total power losses at very high speeds. Skinner [4] investigated the mechanical and no-load electrical losses caused by the rotor's self-discharge during standby using a cylindrical composite rotor FESS accelerated to speeds of up to 5000 rpm. Mechanical losses were significantly affected by the running speed and vacuum pressure inside the FESS enclosure. Amiryar and Pullen [3] used analytical and empirical methods to calculate the windage and bearing friction losses in a cylindrical steel flywheel running at various low pressures and speeds ranging from 10,000 to 20,000 rpm. While windage losses increased nonlinearly with running speed, they could be significantly reduced by adjusting the vacuum pressure and the space between the rotor and the enclosure. In contrast, air pressure had little effect on bearing losses, which can be attributed to speed-dependent and load-dependent loss components. Furthermore, as operating speed increased, speed-dependent losses increased significantly more than load-dependent losses. As a result,

the operating speeds selected during FESS design may have a significant impact on these losses. The previous study discovered that FESS design parameters such as vacuum pressure, air gap, and operation speed had a significant impact on overall system standby power losses.

To create ideal FESS rotors with improved energy storage properties, it is critical to understand the relationship between critical rotor design parameters such as rotor length, airgap size, speed, and pressure level [2]. The goal of this paper is to first determine the effects of simultaneously changing multiple design parameters, such as operating speed and airgap size, on the rotor shape optimization problem, and to see if such an approach can offer a significant improvement in the FESS's energy storage characteristics. This will allow for the investigation of a much larger portion of the rotor design space, resulting in improved optimal rotor designs. A few studies have shown an interest in calculating windage losses inside FESS with small air gaps. Almost all empirical equations for estimating windage losses are derived from experimental apparatus with properties that differ significantly from those of FESS [6, 7]. As a result, the primary goal is to create some realistic tools that will enable designers to account for windage losses in their designs. Then, in this study, a numerical approach based on CFD calculations is used to quantify windage losses inside narrow air gaps of high-speed FESS. A parametric study was carried out to characterise the influence of rotation speed, air gap geometry, and pressure levels. A correlation based on CFD data is provided for the estimation of the rotor skin friction coefficient for a wide range of operations.

## 16.2 Numerical Models

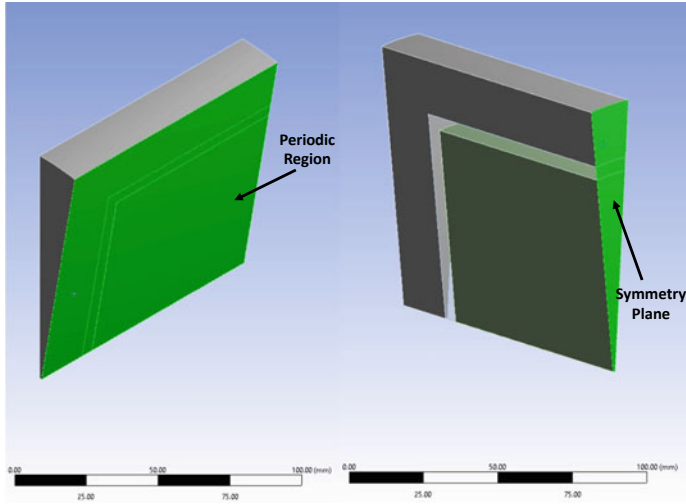
The current article suggests a numerical model of a smooth, narrow, and closed air gap. CFD methods are used to describe the air gap flow structure and predict the rotor skin friction coefficient. In order to estimate the skin friction coefficient, the air velocity distribution must be determined.

### 16.2.1 Mesh Generation and Boundary Conditions

The CFD programme used for this work is ANSYS Fluent 19.2 due to the improvement in the numerical analysis and its popularity in fluid and thermal analysis of complex designs. The parameter used in this study to define the airgap is a dimensionless parameter called the radius ratio which is  $\eta = R_i/R_o$  where  $R_i$  is the rotor radius and  $R_o$  is the internal housing radius. Another parameter is aspect ratio  $\Gamma = L/g$  where  $L$  is the rotor length and  $g$  is the airgap width ( $g = R_o - R_i$ ). The radius of the rotor was chosen to be 0.075 m. The values of the studied parameters are

**Table 16.1** Studied parameters values

Airgap $g$ (m)	0.0015	0.0048	0.0083
Radius ratio $\eta$	0.98	0.94	0.90
Rotor length $L$ (m)	0.1	0.15	0.2
Rotor cavity pressure (mbar)	1000	750	500

**Fig. 16.1** The simplified geometry of FESS with periodic region and symmetry plane

shown in Table 16.1. The allowable maximum rotational velocity for a solid cylinder rotor with a factor of safety of two was calculated to be 41,000 rpm when the rotor's material is steel 4340 [8].

The rotor and the housing walls are subjected to isothermal boundary conditions with an initial temperature of 24 °C. The FESS used in this investigation is shown in Fig. 16.1. To reduce the computational costs, the simulation was conducted on a 10°-slice from the FESS with a symmetry plane from the middle of it too.

### 16.2.2 Mesh Independence Analysis

Mesh independence analysis is essential before performing numerical analysis to select the appropriate mesh. A structured quadrilateral mesh is used in all of the airgap models in this study. The goal of this process is to find the best mesh that provides a solution independent of the mesh. To test the system, three different meshes were chosen. The airgap was 0.1–0.2 mm in size, and the rotor and housing were 1–2 mm in size. The average temperature of the air, rotor, and housing at a rotational speed of 40,000 rpm and atmospheric conditions were used for the independence

test. Figure 16.2 depicts the average temperature of the flywheel components for the three different meshes at different radius ratios. Mesh 2 was the most suitable mesh for this work for all radius ratios because the temperature of the airgap, rotor, and housing changed insignificantly between meshes 2 and 3. Further mesh refinement increases the computational time and costs of CFD modelling, making mesh 2 the best option. The inflation layers and the mesh used in the simulations are shown in Fig. 16.3.

CFD simulation was used to investigate the machine’s steady-state operation, as such steady-state models were used. Time-averaged steady-state solutions for the rotor’s relative motion are modelled using a moving reference frame (MRF). This method is appropriate for steady-state analysis and can resolve most flow characteristics such as mass flow rates and pressure rises and drops across the rotating components [9]. A turbulence model was required because the airgap had a Reynolds number in the turbulent region for all rotational velocities. Reynolds averaged Navier–Stokes (RANS) equations were solved using SST k-omega model. Based on a review of the existing literature for turbulence modelling of Taylor–Couette flow within concentric cylinders, the SST k-omega turbulence model is shown to be effective in estimating the fluid flow and heat transfer characteristics in concentric cylinders [10, 11]. The air was assumed to be an ideal gas and the viscosity was used under three equations sutherland and the effect of gravity was ignored. Thermal conductivity and specific heat were constant. The boundary conditions used in the solution are that the system

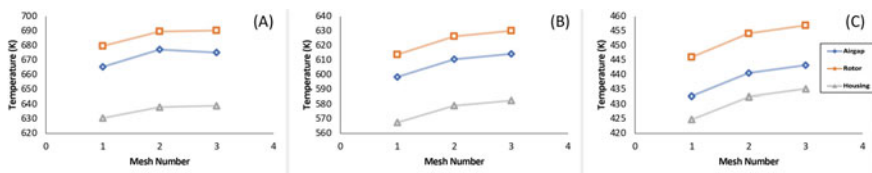


Fig. 16.2 Temperature values for the tested meshes for **a**  $\eta = 0.98$ , **b**  $\eta = 0.94$ , **c**  $\eta = 0.90$

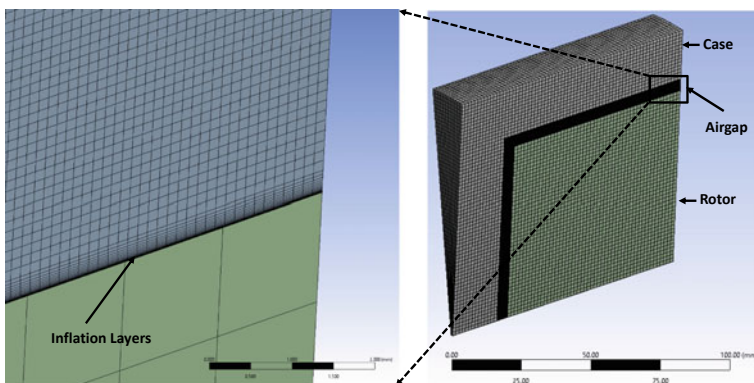


Fig. 16.3 The mesh used for the system

is closed with no inlet or outlet. The surfaces of the rotor and the housing are smooth with no-slip condition. Ambient temperatures of 24 °C and heat transfer coefficients of 30 W/m<sup>2</sup> K were used for the overall thermal boundary condition of the housing. The initial temperature for all the system components were selected to be 24 °C, room temperature. Wall treatment models were used to define the flow profiles in wall boundary layers because of the turbulence models' inability to accurately model the boundary layer regions affected by viscous effects. Near-wall flow velocities and distances are presented in the CFD section. The wall cell  $y_+ \leq 1$  was used to create a boundary layer mesh with a high resolution in order to resolve the viscous sublayer. Numerical discretization of the governing equations was carried out using a finite volume method to solve a linear algebraic equation system for each cell. The second-order upwind discretization scheme was used to simultaneously solve these problems based on mass, momentum, energy and turbulence parameter conservation. In order to ensure that the CFD solution is converged for each run, iterations were properly converged with respect to each other. The convergence criteria for all the residuals were set to be  $10^{-5}$  except for energy which was set at  $10^{-7}$ .

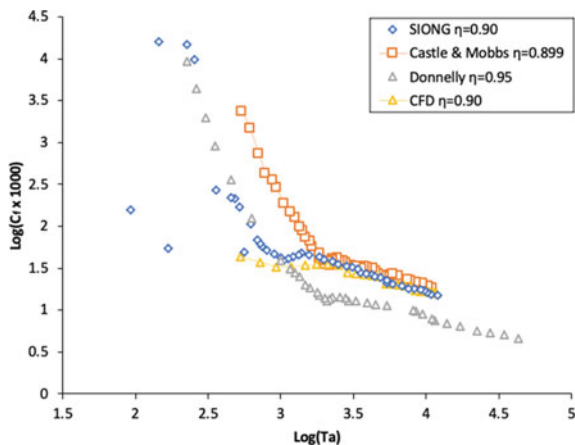
### 16.2.3 Validation

The skin friction coefficient variation as a function of Taylor number was compared to a number of experimental data points presented by Donnelly [12], Castle and Mobbs [13], and Siong [14], where the radius ratio was close enough to be compared with the experimental data. Figure 16.4 depicts the skin friction coefficient and Taylor number distributions. There are three distinct zones, the first of which is when the Taylor number is less than 1714 and the flow is laminar with no vortices, the second is a laminar flow with Taylor-Couette vortices, which can be referred to as non-linear theory due to the nonlinear aspect of the skin friction coefficient distribution, and the third zone is a turbulent flow in which the confined air is fully mixed. The numerically obtained critical Taylor numbers are in good agreement with the values proposed in the literature. Furthermore, when Taylor vortices form in the air gap, the skin friction coefficients estimated by CFD methods match well with Castle and Mobbs [13] and Siong [14], and the CFD calculations accurately reproduce the distribution of skin friction coefficients in the first zone. The predictions of the CFD model match the experimental data very well.

## 16.3 Results and Discussion

The effect of radius ratios on the skin friction coefficient for the rotor and disc sides of the flywheel at different rotational speeds is investigated. The outer cylinder (housing) is fixed. The inner cylinder (rotor) rotates at an angular velocity of 40,000 rpm, which is limited by the safety factor. The spike-shaped flow is caused by the creation of a

**Fig. 16.4** The variation between the skin friction coefficient of the rotor with respect to Taylor number



Taylor-Couette flow in the airgap. The air velocity closest to the housing is close to zero, while the velocity closest to the rotor is the greatest. A Taylor number critical value of 350 rpm can be obtained, indicating that the flow is not stable and Taylor vortices occur inside the airgap at all rotational speeds investigated. The intensity of the vortices increases as the rotational speed increases. Figure 16.5 represents the air velocity distribution plot for the Taylor vortices at the investigated rotational speeds. Within the air gap, Taylor vortices are symmetrical in the axial direction, where viscous forces are overcome by increasing rotational speed and inertial forces. The size of the Taylor vortex is affected by the speed of the rotor, where the vortices are reduced in terms of number at higher speeds. where the increase in rotational speed increases the distance between Taylor vortices.

Three rotor cavity pressure levels were investigated: 1000 mbar, 750 mbar, and 500 mbar. The rotor cavity pressure environment has little influence on the skin friction coefficient for both the rotor and disc surfaces; the only influencing parameter is the radius ratio with Taylor number, as shown in Fig. 16.6. While the effect is minor, lowering the pressure will result in a lower skin friction coefficient for both the rotor and the disc surfaces; however, the pressure will also lower the Taylor number under the same rotational velocity. Windage losses, on the other hand, are heavily influenced by rotor cavity pressure; lowering the pressure reduces windage losses, as illustrated in Fig. 16.7. For all radius ratios studied, the lowest pressure has the least windage losses, while the highest pressure has the most windage losses. Windage losses are significantly affected by pressure. The difference in total windage losses between 500 mbar for  $\eta = 0.98$  and 750 mbar for  $\eta = 0.90$  is less than 1%, making the choice of a larger airgap size with higher pressure a better solution in terms of complexity, because the lower the pressure, the more complex the vacuum system. Windage losses can be reduced by 16% and 33% for pressure environments of 750 mbar and 500 mbar, respectively, when compared to atmospheric pressure. Reducing the radius ratio from 0.99 to 0.94 and 0.90, on the other hand, can reduce total windage losses by 12% and 19%, respectively, under the three pressure environments studied.

When comparing  $\eta = 0.90$  and 500 mbar to  $\eta = 0.98$  and 1000 mbar, it is possible to achieve a 45% reduction in total windage losses, which could nearly double the standby time of a flywheel energy storage system.

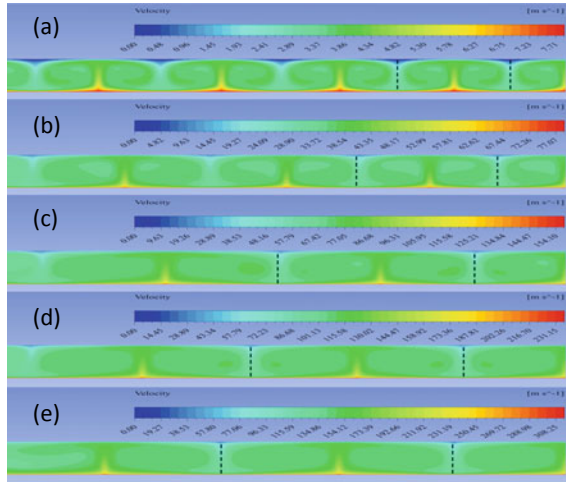


**Fig. 16.5** Air velocity distribution inside 0.90 radius ratio airgap for rotational speeds of (a) 1000 rpm, (b) 10,000 rpm, (c) 20,000 rpm, (d) 30,000 rpm, and (e) 40,000 rpm

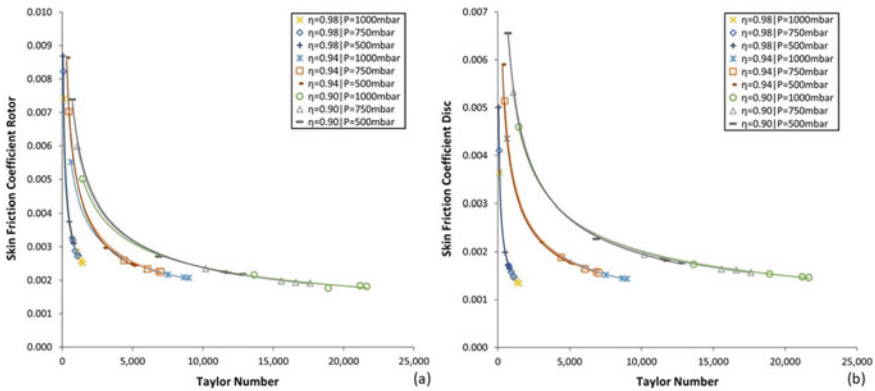
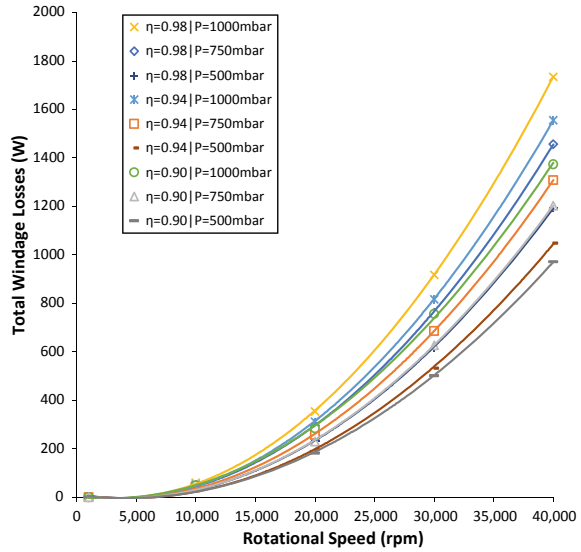


**Fig. 16.6** Taylor number for different radius ratios and pressure levels with skin friction coefficient for (a) rotor surface, and (b) disc surface

**Fig. 16.7** Variation of the total windage losses as a function of the rotational speed for three different pressure levels and radius ratios



### 16.3.1 Dimensionless Analysis

Based on the parametric study described above, a dimensionless analysis is performed to provide a piecewise expression of the rotor skin friction coefficient as a function of the studied parameters. The skin friction coefficient for the rotor and disc surfaces was expressed using two dimensionless parameters, the Reynolds number, and the radius ratio. This paper aims to establish new dimensionless parameter to better describe the skin friction coefficient for both the rotor and the disc surfaces for a pressure environment higher than 500 mbar. The proposed formulation is as follows:

$$C_{fr} = 0.3553 \times (1 - \eta)^{0.3} \times Re_r^{-0.4108} \tag{16.1}$$

$$C_{fd} = 0.4429 \times (1 - \eta)^{0.1} \times Re_d^{-0.4120} \tag{16.2}$$

where  $C_{fr}$  is the rotor skin friction coefficient,  $C_{fd}$  is the disc skin friction coefficient,  $Re_r$  is the Reynolds number between two concentric cylinders, and  $Re_d$  is the Reynolds number between a rotating disc and stationary wall.

### 16.4 Conclusion

Continuous braking causes a significant amount of energy to be lost while driving in cities, but this energy can be recovered and stored. The vehicle’s kinetic energy during deceleration can be effectively recovered and stored by the flywheel energy storage system. The aerodynamic performance of an enclosed non-ventilated flywheel energy



storage system was examined in this study using a computational fluid dynamics (CFD) model to determine the effect of air gap size, and rotor cavity pressure environment. In order to predict the windage losses over a broad operating range, the flywheel rotor skin friction coefficients for different scenarios have been numerically determined. Model validation was done to determine the validity of the CFD results, showing a good agreement between the numerical and experimental data. Based on the flywheel's operating speed, the results showed that increasing the air gap size can reduce windage loss by up to 19%, while lowering the operating pressure to 500 mbar can reduce windage loss by 33%. When the operating pressure is the lowest and the airgap size is the largest, windage losses can be reduced by 45%. A piecewise correlation was proposed for the estimation of the skin friction coefficient for the rotor and the disc surfaces for a variety of air gap sizes and operating circumstances.

**Acknowledgements** This work is supported by the European Union's Horizon 2020 research and innovation programme under the Marie Skłodowska-Curie grant agreement No 801604.

## References

1. A.K. Arani, H. Karami, G. Gharehpetian, M. Hejazi, Review of flywheel energy storage systems structures and applications in power systems and microgrids. *Renew. Sustain. Energy Rev.* **69**, 9–18 (2017)
2. V. Kale, M. Thomas, M. Secanell, On determining the optimal shape, speed, and size of metal flywheel rotors with maximum kinetic energy. *Struct. Multidiscip. Optim.* **64**(3), 1481–1499 (2021)
3. M.E. Amiryar, K.R. Pullen, Analysis of standby losses and charging cycles in flywheel energy storage systems. *Energies* **13**(17), 4441 (2020)
4. M.A. Skinner, Characterization of passive discharge losses in a flywheel energy storage system (2017)
5. S. Gurumurthy, A. Sharma, S. Sarkar, V. Agarwal, Apportioning and mitigation of losses in a flywheel energy storage system (2013), pp. 1–6
6. Y. Yamada, Torque resistance of a flow between rotating co-axial cylinders having axial flow. *Bull. JSME* **5**(20), 634–642 (1962)
7. E. Bilgen, R. Boulos, Functional dependence of torque coefficient of coaxial cylinders on gap width and Reynolds numbers (1973)
8. Y. Han, Z. Ren, Y. Tong, General design method of flywheel rotor for energy storage system, in *2012 International Conference on Future Energy, Environment, and Materials*, vol. 16 (2012), pp. 359–364. <http://doi.org/10.1016/j.egypro.2012.01.059>
9. J.D. Anderson, J. Wendt, *Computational Fluid Dynamics*, vol. 206 (Springer, Berlin, 1995)
10. A. Nachouane, A. Abdelli, G. Friedrich, S. Vivier, Estimation of windage losses inside very narrow air gaps of high speed electrical machines without an internal ventilation using CFD methods (2016), pp. 2704–2710
11. C. Jungreuthmayer et al., A detailed heat and fluid flow analysis of an internal permanent magnet synchronous machine by means of computational fluid dynamics. *IEEE Trans. Ind. Electron.* **59**(12), 4568–4578 (2011)

12. R. Donnelly, Experiments on the stability of viscous flow between rotating cylinders I. Torque measurements. Proc. R. Soc. Lond. Ser. Math. Phys. Sci. **246**(1246), 312–325 (1958)
13. P. Castle, F. Mobbs, Paper 6: hydrodynamic stability of the flow between eccentric rotating cylinders: visual observations and torque measurements, vol. 182, no. 14 (1967), pp. 41–52
14. L.S. Siong, An experimental investigation of Taylor Couette flow between eccentric cylinders (2007)

**Open Access** This chapter is licensed under the terms of the Creative Commons Attribution 4.0 International License (<http://creativecommons.org/licenses/by/4.0/>), which permits use, sharing, adaptation, distribution and reproduction in any medium or format, as long as you give appropriate credit to the original author(s) and the source, provide a link to the Creative Commons license and indicate if changes were made.

The images or other third party material in this chapter are included in the chapter's Creative Commons license, unless indicated otherwise in a credit line to the material. If material is not included in the chapter's Creative Commons license and your intended use is not permitted by statutory regulation or exceeds the permitted use, you will need to obtain permission directly from the copyright holder.



# Chapter 17

## The Analysis of Sensory Data from Smart Office Environment Towards the Development of an Intelligent System



Jack Hall, Bubaker Shakmak, Amin Al-Habaibeh, and Eiman Kanjo

**Abstract** With the increase in energy prices and the drive to reduce carbon emission, this paper presents an investigation of the use of smart office environments to monitor and evaluate the sustainability and behaviour of employees and the utilisation of space and resources. This paper presents analysis of data in an office environment in a company in Derby city to attempt to understand the behaviour of employees, pattern of work, power consumption and performance of heating and air-conditioning systems. Data from occupancy, room temperature, CO<sub>2</sub>, humidity, lighting, air temperature, windows status are all collected and analysed. The data also included external environmental conditions. The results indicate some correlation between CO<sub>2</sub> levels and the number of employees. They also show correlation between outside and inside environmental conditions. In addition, the utilisation of space was also monitored, and the results demonstrate low utilisation during most days, this was due to Covid-19 and to working from home and off-site patterns. However, the data is found useful to inform future decisions about the actual space needed for normal working conditions.

**Keywords** Smart buildings · Intelligent buildings · IoT · Smart office · AI · Sensor fusion · Netzero

### 17.1 Introduction

The main purpose of smart technologies is to collect data from the surrounding environment and assist users in day-to-day activities [1]. The application of smart

---

J. Hall

Scenariio Ltd, Derby, UK

B. Shakmak · A. Al-Habaibeh (✉)

Product Innovation Centre, Product Design, Nottingham Trent University, Nottingham, UK

e-mail: [Amin.Al-Habaibeh@ntu.ac.uk](mailto:Amin.Al-Habaibeh@ntu.ac.uk)

E. Kanjo

Smart Sensing Lab, Nottingham Trent University, Nottingham, UK

© The Author(s) 2023

J. D. Nixon et al. (eds.), *Energy and Sustainable Futures: Proceedings of the 3rd ICESF*, 2022, Springer Proceedings in Energy, [https://doi.org/10.1007/978-3-031-30960-1\\_17](https://doi.org/10.1007/978-3-031-30960-1_17)

technologies in manufacturing is discussed in terms of the automation of production and the benefit that this can bring due to the reduction of operational costs, human error and waste, which consequently increases productivity [2]. Current research lacks evidence on the outcomes of smart technologies in a workplace setting [3].

As times change and technology continues to advance—there is a need more than ever for people to be able to track and see what is going on in their working environments. There are a variety of reasons as to why there is now a need for this information to be gathered. Sustainability reasoning—not just an energy or emissions point of view, but staff well-being, and company health also fall under this category. This then also branches out to changes that are coming on the back of the pandemic. More people are working from home, leading to a condensing of the workplace size—hot desking, or people want to be more spread out in their working regions. Either way, space utilisation is a big issue for lots of businesses. When it comes to the office environment, research tends to discuss the utilisation and benefits to stand alone devices rather than considering the overall work environment embedded with smart technologies [4, 5]. In order for businesses to be able to make positive change, they need to identify what is it, that needs to be changed. They need to pinpoint strengths and weaknesses and continue to review and check them on a regular basis moving forward. Change/monitoring is in the best interest of everyone. Not only will it save money, cut emissions and increase productivity—it will also keep everyone in the know how as to what needs to be improved and how, especially with the cost-of-living crisis that is being faced.

By analysing the data that has been collected, it will be able to inform future decisions about space needed to satisfy for efficient working conditions; and carbon and energy savings.

As technology continues to advance, coming out of a pandemic, inflated energy prices—times are quite hard to predict. Things are very uncertain. This area is something that needs continuous further study as there is constant factors that change. However, the adoption of smart technologies in a work setting is an inevitable process [3], so it is important that the gaps start to be filled. The objective of this paper is to help addressing some of the current and on-going research and technology questions.

## 17.2 Methodology

In order to study the benefits of sensor data feed in office environment, a case study is presented in this paper. Figure 17.1 presents the first floor of the office environment. Details of the sensors are shown in Table 17.1. The rationale is based on a reasonable micro-SME office size to test the technology and data to address key findings that could be extrapolated in future installations of smart buildings.

This office is used as a case study of the technology development in terms of sensors, instrumentation, software platform; it also was used to reflect on small office culture during/post covid pandemic and energy use; but it is not meant to be for generalisation but as a case study to reflect upon future development.

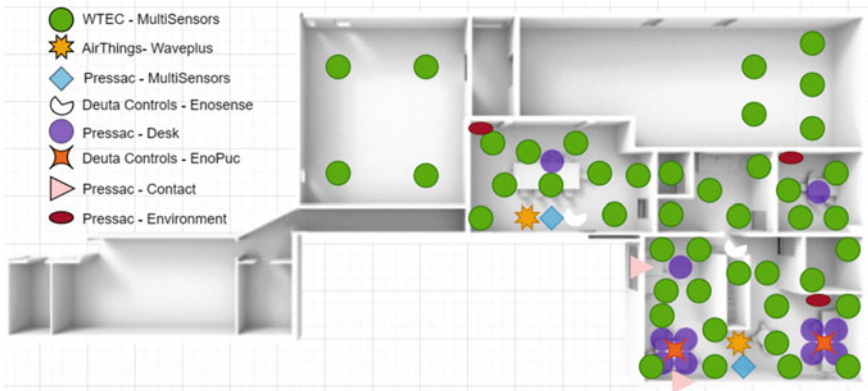


**Fig. 17.1** First floor office environment sensor location at the company

**Table 17.1** Details of the sensors implemented in the office environment

Provider	Sensor type	Data
WTEC	Multi-sensor	Temperature, Brightness, Motion, Power
Pressac	Desk	Occupancy
Pressac	Multi-sensor	Temperature, CO <sub>2</sub> , Humidity
Pressac	Current	Three channel (A)
Pressac	Environment	Temperature, Humidity
Pressac	Contact	Door, Window
Deuta Controls	EnoSense	Vibration, Temperature, Humidity, Brightness
Deuta Controls	EnoPuc	Sound pressure, CO <sub>2</sub> , Temperature, Humidity, Brightness, Motion
AirThings	Wave Plus	Radon, CO <sub>2</sub> , Temperature, Humidity, Air pressure, TVOC
Irisys	Vector 4D	IR/Time of flight people counter

The data was presented live to staff-office during the day via a monitor and it was anonymous and does not include any further information more than what the team could see in the office in-person in terms of attendance, etc. The purpose was for statistical analysis on the long term to link that with energy and other factors; and to test the smart technology.

Ethical concerns of monitoring will be addressed in a future paper; but in general, the data saved is anonymous and the main goal is to monitor energy use and space utilisation.

There was no staff with mobility issues in this study; however, this is an area of future work.

## 17.3 Data Analysis

Data processing has been carried out in the office environment, see Fig. 17.1. The data has been recorded for several months continuously for the day and the night from 17/11/2021 to 9/5/2022. The data was in an interval of five minutes each. The data shows the total number of people who have been occupying the office during this period. It also shows the amount of CO<sub>2</sub> in ppm, humidity, temperature, outside temperature, outside humidity, wind speed, electricity consumption by the radiators and the total office power consumption in amperes. It has been noted that some data such as the total office power has only been recorded from the 11th of January.

### 17.3.1 Total Number of People

Due to Covid-19 not many people were working from the office as most of the employees were working from home. However, despite that fact, even the maximum number of people was only six people at one time in the office, the outcome showed promised results for the research as will be explained in detail later.

Figure 17.2 presents the number of people during the whole research period which never exceeded six people. Table 17.2 shows that it is rare to find more than three people in the office at the same time. Number of people from four to six represents circa 5% of the monitored time. The office was mostly occupied by one person and sometimes two or three people only.

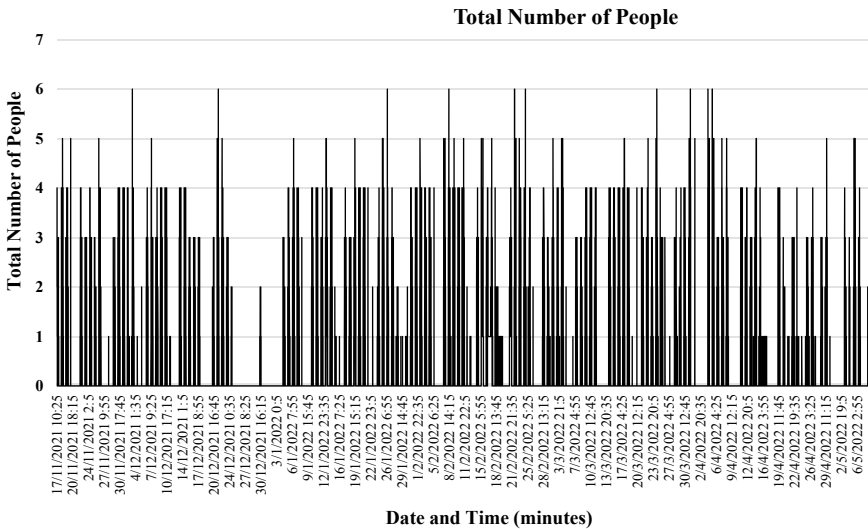


Fig. 17.2 Number of employees occupying the office every five minutes

**Table 17.2** Percentage of number of the people existed in the office at the same time

No. of people	Times	%
1	5645	50.37
2	3379	30.15
3	1622	14.47
4	475	4.24
5	71	0.63
6	14	0.12
Total	11,206	100

### 17.3.2 Correlation Coefficient of the Data

To initially determine if there is a relationship among all the aspects of the research that are being recorded, the correlation coefficient has been applied among all data. Table 17.3 shows the result of applying the correlation coefficient. Figure 17.4 shows the colour representation (colour map) of the results.

Figure 17.3 shows that number of people has a strong relation with the amount of CO<sub>2</sub> and temperature and reasonable correlation with the total office power and the RP Radiator while it has a weaker relation with the humidity, the outside temperature, the wind speed, the outside humidity, and the GP Radiator. This could mean that people existence in the office affects the amount of CO<sub>2</sub> and the temperature and increases the total power consumption. As it is well known that the temperature and the humidity are having inverse relation, Fig. 17.3 clarifies that as it did show a strong inverse relation between the two variables. Figure 17.3 also shows that the temperature has the most effective relation with other aspects. It has a strong relationship with CO<sub>2</sub>, Humidity, number of people, outside temperatures, outside temperature and total office power, and less important relationship with the radiator and the GP radiator and almost no relationship with wind speed.

### 17.3.3 Number of People Verses CO<sub>2</sub>

Figure 17.4 presents an example of a whole week; it clearly illustrates how the number of people is affecting the amount of CO<sub>2</sub> inside the office. Figure 17.4 also shows the day and the nights patterns, approximated as a square wave; the day has been categorized as 1 and the night as 2. When the number of people reached its peak on Thursday, the amount of CO<sub>2</sub> has significantly increased to its peak as well. It is obvious that the amount of CO<sub>2</sub> has dramatically decreased when there was no one in the office during the weekend. It must be mentioned that the level of CO<sub>2</sub> in this figure is scaled between 0 and 1 then multiplied by six to match the number of people in scale and to fit and appear clearly in the figure for comparison purposes.

**Table 17.3** Correlation coefficient of results

	CO <sub>2</sub>	Humidity	Temp.	No. of people	Outside temp.	Outside humidity	Wind speed	Desk RP radiator	Desk GP radiator	Total office power
CO <sub>2</sub>	<b>1.00</b>	-0.16	0.45	0.48	0.17	-0.18	-0.02	0.06	0.10	0.24
Humidity	-0.16	<b>1.00</b>	-0.55	-0.14	0.04	0.39	0.14	-0.27	-0.36	-0.43
Temp.	0.45	-0.55	<b>1.00</b>	0.34	0.57	-0.48	-0.03	0.26	0.14	0.47
No. of people	0.48	-0.14	0.34	<b>1.00</b>	0.12	-0.13	0.10	0.22	0.05	0.27
Outside temp.	0.17	0.04	0.57	0.12	<b>1.00</b>	-0.53	0.20	0.11	-0.01	0.35
Outside humidity	-0.18	0.39	-0.48	-0.13	-0.53	<b>1.00</b>	-0.11	-0.10	-0.12	-0.42
Wind speed	-0.02	0.14	-0.03	0.10	0.20	-0.11	<b>1.00</b>	-0.04	-0.09	-0.05
Desk RP radiator	0.06	-0.27	0.26	0.22	0.11	-0.10	-0.04	<b>1.00</b>	0.14	0.33
Desk GP radiator	0.10	-0.36	0.14	0.05	-0.01	-0.12	-0.09	0.14	<b>1.00</b>	0.33
Total office power	0.24	-0.43	0.47	0.27	0.35	-0.42	-0.05	0.33	0.33	<b>1.00</b>

The bold numbers are on the diagonal line that shows the correlation between the sensor and itself; which will always has a value of 1



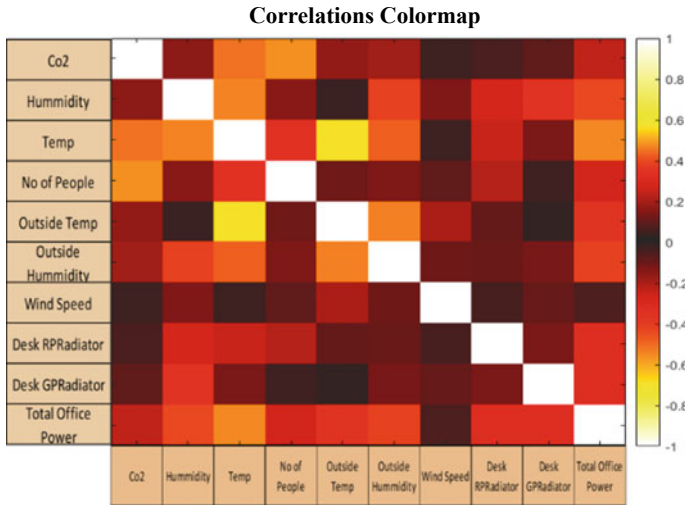


**Fig. 17.3** Correlation coefficient among all the aspects of the research work

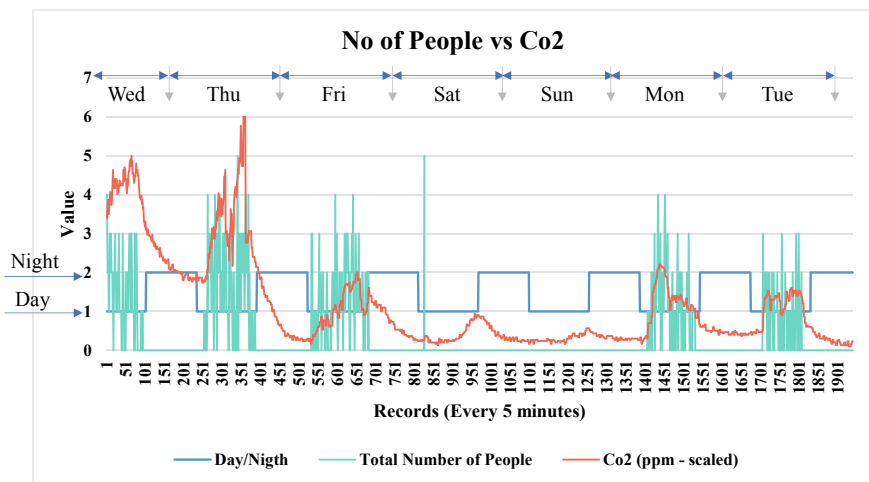


**Fig. 17.4** Example shows how the CO<sub>2</sub> is affected by the number of people during the day and the night

**17.3.4 Number of People Verses Temperature**

Similarly, Fig. 17.5 shows the strong relationship between the number of people and the temperature in the office. The temperature has gradually decreased to reach its lowest temperature during the weekend when the office was not occupied. Figure 17.5 shows clearly that the temperature increases in the daytime and decreases during the

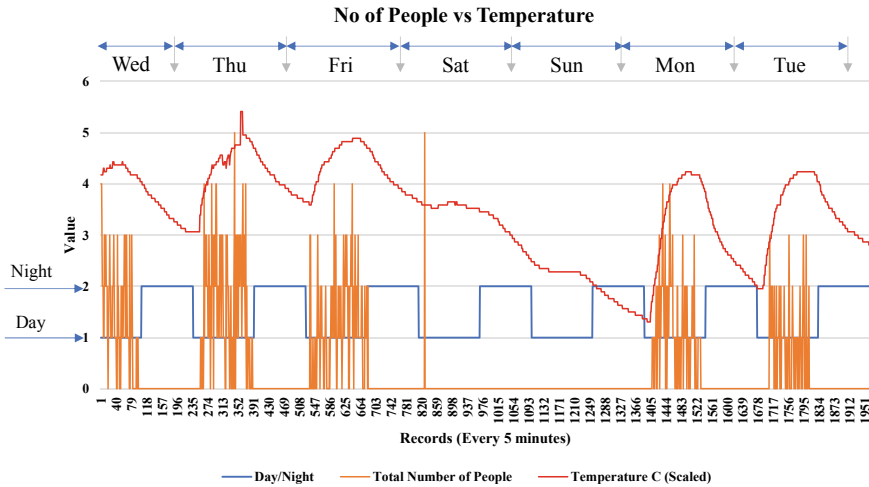


**Fig. 17.5** The relationship between the number of people and the temperature in the office

night. Again, it must be mentioned that the temperature values have been scaled to 0–1 and then multiplied by six to fit in the figure for comparison purposes.

### 17.3.5 Number of People Verses Total Office Power

As mentioned earlier, the total office power has been recorded much later than other records therefore, it demonstrated a fair correlation relationship with the number of people, but once the total office power plotted for one week within the recorded period it showed a strong relationship as indicated in Fig. 17.6. Figure 17.6 shows that the total office power is increasing significantly while the office is occupied and decreases dramatically when no people are in the office. The values of the total office power have been scaled to 0 and 1 and then multiplied by 6 to fit within the figure match with the number of people to enhance the comparison process.

## 17.4 Conclusion

From the results above, it can be concluded that current office facilities are not well utilised due to Covid pandemic or post-Covid culture of working from home. This indicates the need to utilise resources and facilities in a better way to enhance return on space investment. Also, the results show that with more people in the office, more energy consumption is presented. Temperature and CO<sub>2</sub> readings seem to be proportional to the number of people who are working in the office at any one time.

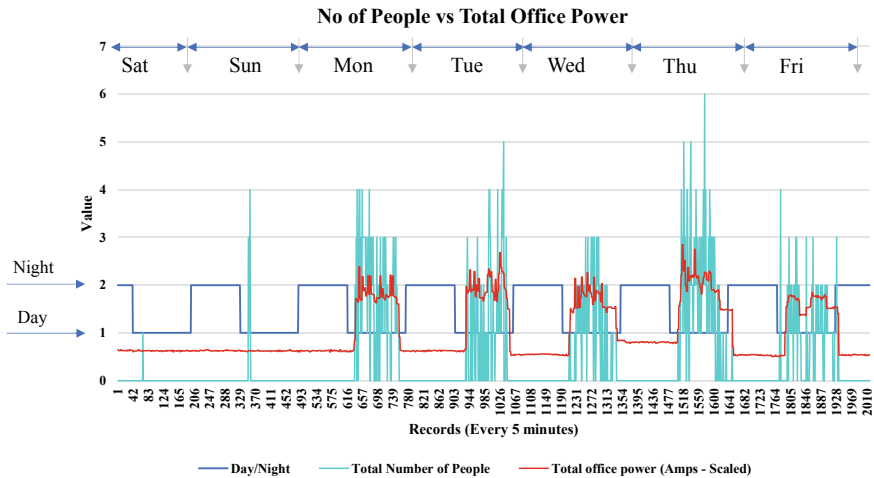


**Fig. 17.6** Full week of records show how the total office power is highly affected by the number of people

This also indicates the need in some cases for better ventilation which could lead to further energy consumption when windows are open in cold weather. Future work will include researching how the intelligent system can be developed to advise occupants on the best measure to be taken to save energy while at the same time maintaining air quality and environmental comfort. A wider scale of data will be collected over time, to see how different seasons impact the data, but to also see whether there does begin to be a more consistent, higher number of staff working in the building at a given time.

There will also be a comparison to another, larger site—where data can then be compared at both levels of space.

Further investment into greater number of sensors that will collect data for other elements—here further analysis can be undertaken to give even greater detail into the results.

**Acknowledgements** This paper is based on research work funded by Innovate UK, Knowledge Transfer Project (KTP), as a collaboration between Scenariio Ltd and Nottingham Trent University (KTP number 11968).

## References

1. M. Chan, D. Estève, C. Escriba, E. Campo, A review of smart homes—present state and future challenges. *Comput. Methods Programs Biomed.* **91**, 55–81 (2008)
2. H.S. Kang, J.Y. Lee, S. Choi, H. Kim, J.H. Park, J.Y. Son et al., Smart manufacturing: past research, present findings, and future directions. *Int. J. Precis. Eng. Manuf. Green Technol.*

- 111–128 (2016). P. Trebuna, M. Pekarciková, J. Kronová, Automation of the casting process by the use of simulation software. *Manag. Prod. Eng. Rev.* **9**(1), 82–89 (2018)
3. D. Marikyan, S. Papaginnidis, Smart offices: a productivity and well-being perspective (2020)
  4. R. Bootsman, P. Markopoulos, Q. Qi, W. Qi, A.A. Timmermans, Wearable technology for posture monitoring at the workplace. *Int. J. Human Comput. Stud.* **132**, 99–111 (2019)
  5. M. Chan, D. Estève, C. Escriba, E. Campo, A review of smart homes—present state and future challenges, in *Computer Methods and Programs in Biomedicine*, vol. 91, Issue 1 (2008), pp. 55–81. ISSN 0169-2607. <http://doi.org/10.1016/j.cmpb.2008.02.001>

**Open Access** This chapter is licensed under the terms of the Creative Commons Attribution 4.0 International License (<http://creativecommons.org/licenses/by/4.0/>), which permits use, sharing, adaptation, distribution and reproduction in any medium or format, as long as you give appropriate credit to the original author(s) and the source, provide a link to the Creative Commons license and indicate if changes were made.

The images or other third party material in this chapter are included in the chapter's Creative Commons license, unless indicated otherwise in a credit line to the material. If material is not included in the chapter's Creative Commons license and your intended use is not permitted by statutory regulation or exceeds the permitted use, you will need to obtain permission directly from the copyright holder.



# Chapter 18

## Investigation of Working Fluid Performance in a Refrigeration Cycle



J. Radulovic, J. Bull, and J. M. Buick

**Abstract** With global warming and climate change, the world is experiencing a steady temperature rise. Hence the need for effective and efficient air conditioning, cooling and refrigeration systems is higher than ever. One of the key elements influencing refrigeration system performance is the working fluid. From 2022, new refrigeration systems in the UK must not use refrigeration fluids with global warming potential (GWP) above 150. Widely used R134a, with GWP of 1430, is therefore being banned and the need for suitable replacement fluids, with equivalent or similar thermodynamic performance, is imminent. This paper looks into the potential of low GWP refrigerant fluids, and assesses their suitability to be utilised as replacement for historically used R134a. Operation of a refrigeration cycle based on R134a is comprehensively compared to selected low GWP fluids in different operating conditions. Low GWP fluids (R152a, R1234yf, R1234ze(E), R290, R600a) were carefully selected to include a broad range of thermophysical properties and cover several fluid categories. Compression work requirement, cooling capacity and the overall performance are evaluated in typical operating scenarios. We conclude that both R1234ze(E) and R1234yf are good alternatives. In particular, R1234yf outperformed R134a by requiring less compression work and achieving significantly higher COP based on the same cooling capacity.

**Keywords** Global warming potential · Coefficient of performance · Cooling capacity replacement fluids · Thermodynamic assessment

### *Nomenclature*

$h$	Specific enthalpy [kJ/kg]
$w$	Specific work [kJ/kg]
$q$	Specific heat energy [kJ/kg]

---

J. Radulovic (✉) · J. Bull · J. M. Buick  
School of Mechanical and Design Engineering, University of Portsmouth, Anglesea Building,  
Anglesea Road, Portsmouth PO1 3DJ, UK  
e-mail: [jovana.radulovic@port.ac.uk](mailto:jovana.radulovic@port.ac.uk)

## *Subscripts*

1–4	Point reference number within the refrigeration cycle
<i>comp</i>	Compressor
<i>e</i>	Evaporator

## 18.1 Introduction

For decades, and more so since the EU 517/2014 regulations [1], alternatives to working fluids with high Global Warming Potential (GWP) have been sought. Throughout the 20th century hundreds of refrigerant fluids have been synthesised and successfully employed in cooling and air-conditioning systems worldwide. The specific limit of GWP is dependent on the application. Nowadays high GWP refrigerant fluids are being phased out and over the years have investigations focused on identifying suitable replacements. From 2022 all refrigerants fluids with a GWP > 150 will be banned in the UK (there are some exceptions though, yet this is generally the norm). One of the most commonly used refrigerant fluids, R134a, has the GWP of 1430, which is significantly higher than currently acceptable threshold (an ideal refrigerant fluid would have a GWP  $\approx 0$ ). Hence, it is imperative to identify replacement refrigerant fluids which would yield similar, if not better, performance.

Zilio et al. [2] investigated the possibility of using R1234yf within an automotive air conditioning system designed for R134a. compared to R134a, a cycle based on R1234yf had lower cooling capacity and the coefficient of performance (COP). However, it was suggested that with some modifications to the cycle set up, R1234yf could reach higher COP at the same cooling capacity as R134a. Navarro-Esbri et al. [3] also concluded that cooling capacity of R1234yf was lower than that of R134a across the operational range examined. In addition to R1234yf, Sánchez et al. [4] considered other refrigerant fluids: R1234ze(E), R600a, R290, and R152a. R1234yf, as well as R1234ze(E) and R600a, showed a notable decrease in cooling capacity. In contrast, cooling capacity and COP with R290 increased, albeit significant increase in compressor power requirement. R152a had lower cooling capacity and power required; as a consequence, COP increased.

In the last decade there have been many other studies looking into suitability of these and other refrigerant fluids as suitable replacements in heat pumps and associated systems. In this paper we build upon the existing literature by examining the performance of refrigeration cycles utilising R600a, R152a, R1234yf, R1234ze(E) and R290. Comparison to R134a done on the basis of assessing compression work requirement for the equivalent cooling capacity of the refrigeration cycle.

## 18.2 Methodology

Refrigeration cycle was thermodynamically modelled as a steady-state system. Kinetic and potential energy losses, and heat transfer to the environment were neglected. Pressure drops in all cycle elements were ignored, with pressure changes occurring only during compression and expansion processes. Schematic of a simple refrigeration system is given in Fig. 18.1. Main processes can be outlined as: adiabatic compression, isobaric cooling in the condenser, expansion in the throttle, and isobaric heating in the evaporator. Evaporator pressure was kept constant as saturation pressure at 273 K in all cases. Compression inlet state, point 1, was slightly superheated refrigerant, 5 K above the saturation. Compression ratio ( $p_2/p_1$ ) was varied in 2–8 range, with fixed compressor efficiency at 70%. Saturated liquid state at the condenser outlet (point 3) was assumed. The expander operates isenthalpically ( $h_4 = h_3$ ). Fluid properties were retrieved from RefPROP. Safety classification and GWP of fluids considered in this study are given in Table 18.1. Heat and work exchanges were calculated as enthalpy gradients between relevant points of the cycle, as outlined below:

$$w_{comp} = h_2 - h_1 \quad (18.1)$$

$$q_e = h_4 - h_1 \quad (18.2)$$

with the coefficient of performance:

$$COP = q_e/w_{comp} \quad (18.3)$$

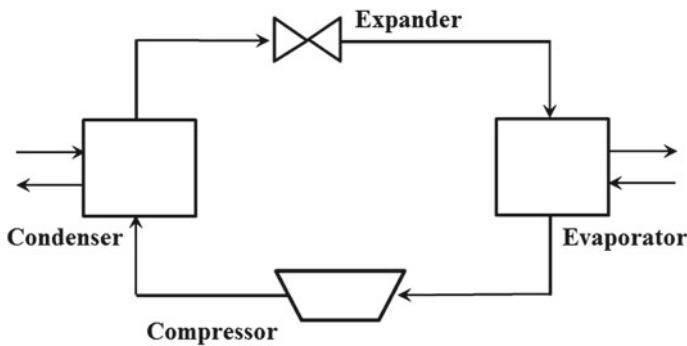


**Fig. 18.1** Schematic of a simple refrigeration cycle. Inlet points: 1—compressor; 2—condenser; 3—expander; 4—evaporator

**Table 18.1** Safety classification and GWP of selected refrigerant fluids

Fluid name	Safety classification	GWP
R134a	A1	1430
R600a	A3	0
R152a	A2	124
R1234yf	A2L	0
R1234ze(E)	A2L	6
R290	A3	3.3

### 18.3 Results and Discussion

In order to compare the performance of potential replacement refrigerant fluids to R134a, thermodynamic cycle across a range of compression ratios was modelled. Pressure ratios across the compressor stage considered in this study ( $p_2/p_1 = 2-8$ ) are typical for a standard refrigeration cycle. One of the main advantages of R134a is a relatively low compression work. Hence a suitable replacement fluid would have similar (ideally lower) compression work requirement. Evaluated compressor work requirement for replacement fluids considered in shown in Fig. 18.2.

All working fluids studied showed gradual increase in compression work requirement with increasing pressure ratio. R1234yf and R1234ze(E) required slightly less compression work than R134a. R290 has a significantly higher work requirement

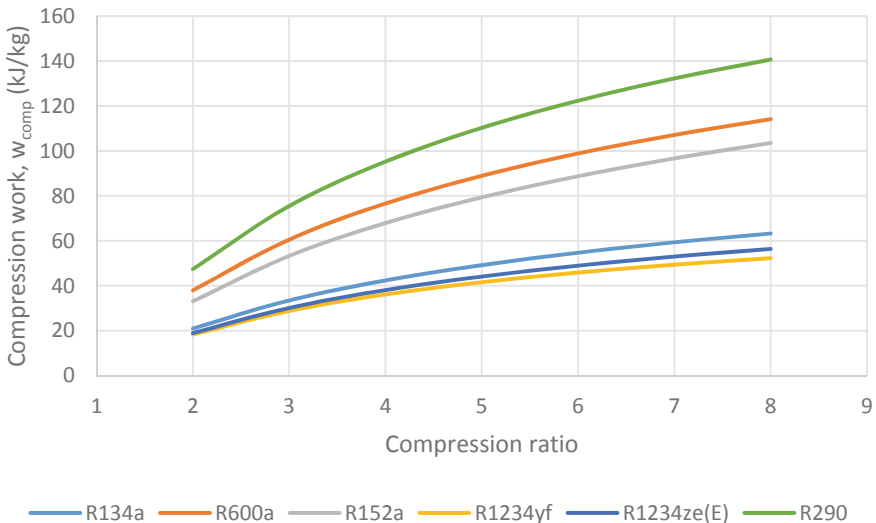


**Fig. 18.2** Compressor work ( $w_{comp}$ ) as a function of the compression ratio ( $p_2/p_1$ )



through the compressor, more than double compared to R134a across all compression ratios, which is in line with [3, 4]. R152a and R600a also required notably higher compression work.

Cooling capacity is a key measure of refrigeration system performance; an effective working fluid would therefore have the ability to remove a substantial amount of heat from refrigerated space. Evaluated cooling capacity for R134a replacement fluids is shown in Fig. 18.3. In agreement with previous findings [2, 3], R1234yf showed consistently lower value for cooling capacity compared to R134a, while that of R1234ze(E) was similar to R134a. However, cooling capacity of R152a and R600a were significantly higher, albeit decreasing more rapidly with increasing compression ratio. Interestingly, R290 showed almost linear trend of cooling capacity decrease with increasing pressure ratio, significantly higher than R134a at low compression ratios, and nearly the same at higher compression ratios.

In terms of COP (Fig. 18.4), performance of R1234ze(E) and R600a was virtually the same as that of R134a. R152a also had practically the same COP at lower compression ratios, and slightly higher COP at higher pressure ratios. Performance of R1234yf was poorer than that of R134a and R290 performed worse in terms of COP, which is contrary to the findings in [4]. Whilst COP and cooling capacity vary across R290, R152a and R600a, these fluids require higher compression work than R134a. Hereafter further analysis is based on R1234yf and R1234ze(E) only.

In Fig. 18.5, we compared cycle performance and cooling capacity in a scenario where compression work was fixed at 20 kJ/kg. Both R1234yf and R1234ze(E) had diminished performance compared to R134a, -24.95% and -9.91%, respectively. In an alternative scenario when cooling capacity was fixed at 125 kJ/kg, R1234yf had the

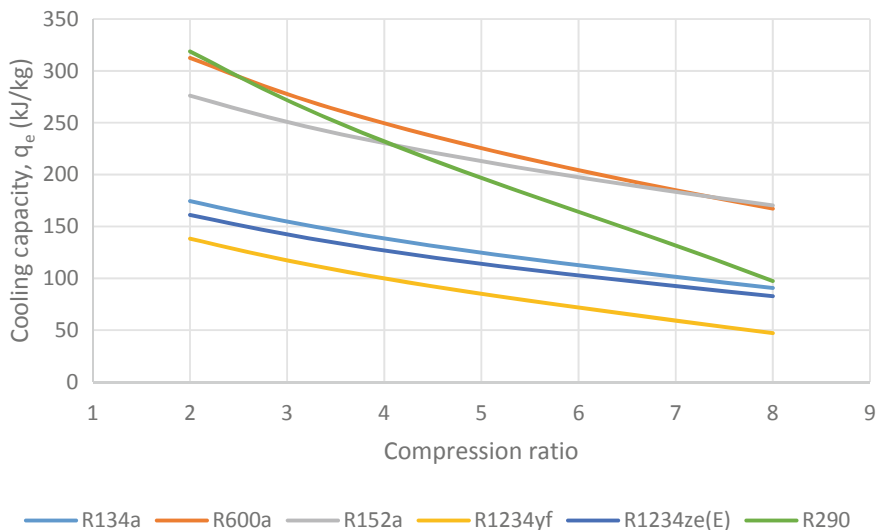
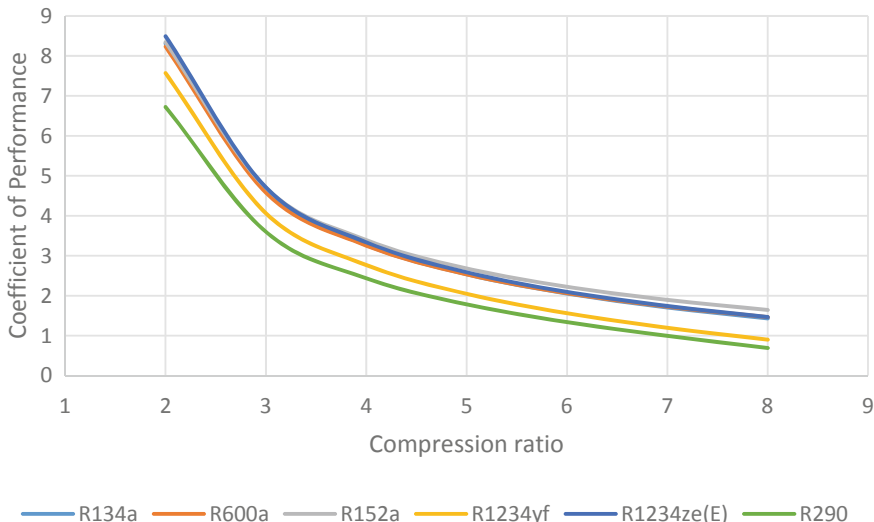


Fig. 18.3 Cooling capacity ( $q_e$ ) as a function of the compression ratio ( $p_2/p_1$ )



**Fig. 18.4** Coefficient of performance (COP) as a function of the compression ratio ( $p_2/p_1$ )

lowest compression work—53% less work than R134a. R1234yf also achieved the highest COP of 6.45 (114.77% higher compared to R134a) followed by R1234ze(E) with a value of 3.81 (26.91% higher). These two scenarios demonstrate that R1234yf and R1234ze(E) both outperform R134a at low cooling capacity loads. Alternatively, when compression work is low R134a achieves better performance. Hence, selection of suitable replacement refrigeration fluid should be based on carefully defined design criteria. In this study thermodynamic similarity was the basis of comparison. Future work may include consideration of broader set of properties as well as various losses in the system.

### 18.4 Conclusion

Compared to R134a, R290, R600a and R152a had higher cooling capacities, although the compression work was notably higher as well. Overall, these refrigerant fluids could act as replacements for R134a. Equally so, both R1234ze(E) and R1234yf are deemed to be good alternatives. In particular, R1234yf outperformed R134a by requiring less compression work and achieving significantly higher COP based on the same cooling capacity. However, performance of R1234yf and R1234ze(E) was not equivalently good based on the same compression work comparison.

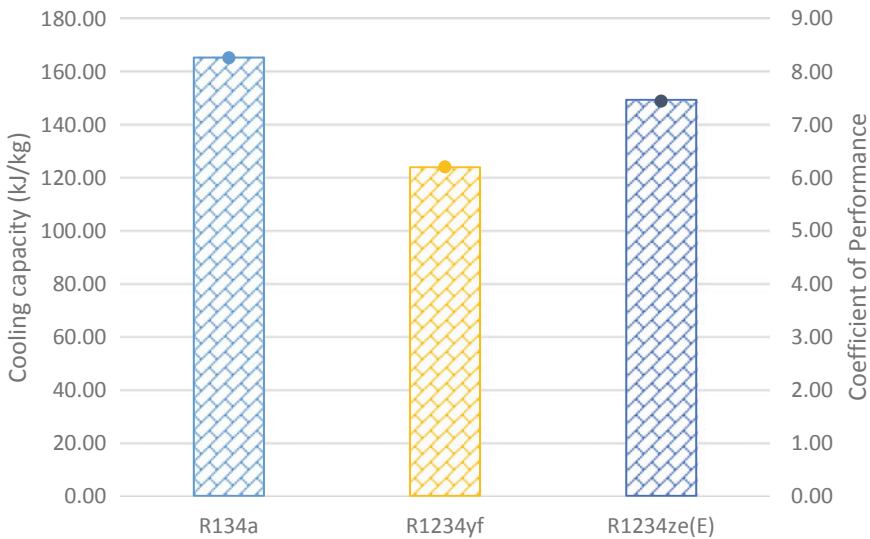


**Fig. 18.5** COP (solid circle) and cooling capacity (bar) for 20 kJ/kg compressor work

## References

1. Regulation (EU) No 517/2014, Regulation (EU) No 517/2014 of the European Parliament and the Council of 16 April 2014 on fluorinated greenhouse gases and repealing Regulation (EC) No 842/2006. *Official J. Eur. Union* **57** (2014)
2. C. Zilio, J. Brown, G. Schiochet, A. Cavallini, The refrigerant R1234yf in air conditioning systems. *Energy* **36**(10), 6110–6120 (2011)
3. J. Navarro-Esbrí, J. Mendoza-Miranda, A. Mota-Babiloni, A. Barragán-Cervera, J. Belman-Flores, Experimental analysis of R1234yf as a drop-in replacement for R134a in a vapor compression system. *Int. J. Refrig.* **36**(3), 870–880 (2013)
4. D. Sánchez, R. Cabello, R. Llopis, I. Arauzo, J. Catalán-Gil, E. Torrella, Energy performance evaluation of R1234yf, R1234ze(E), R600a, R290 and R152a as low-GWP R134a alternatives. *Int. J. Refrig.* **74**, 269–282 (2017)

**Open Access** This chapter is licensed under the terms of the Creative Commons Attribution 4.0 International License (<http://creativecommons.org/licenses/by/4.0/>), which permits use, sharing, adaptation, distribution and reproduction in any medium or format, as long as you give appropriate credit to the original author(s) and the source, provide a link to the Creative Commons license and indicate if changes were made.

The images or other third party material in this chapter are included in the chapter's Creative Commons license, unless indicated otherwise in a credit line to the material. If material is not included in the chapter's Creative Commons license and your intended use is not permitted by statutory regulation or exceeds the permitted use, you will need to obtain permission directly from the copyright holder.



# Chapter 19

## Energy Policy as a Tool for Promoting Power System Resilience: Malawi's Challenges and Potential Solutions



Joyce Nyuma Chivunga, Zhengyu Lin, and Richard Blanchard

**Abstract** A constant production and delivery of electricity is crucial to the functioning of the society. Power systems, however, suffer from either physical, institutional or community level challenges under climate change. Specifically, Malawi is exposed to both climatic and geologic hazards. One of the guiding principles of the needs assessment and recovery strategy is to move from response to long term resilience. The national energy policy (NEP) is considered as one of the drivers of long-term power system resilience (PSR). Understanding the status of NEP is critical in coming up with long term resilience solutions because the qualitative evaluation in this case considers information about risks, the perceived severity of risks and possible impacts of shocks. Although prior studies contributed significantly to the resilience of electricity systems, none of those studies explored the possibility of the NEP being a critical key in promoting the resilience of the electricity sector to extreme weather events. This novel study, therefore, assessed the capacity of the NEP to promote infrastructure and institutional PSR. It also identified challenges regarding the capability of the policy to support PSR. Finally, the study suggested key policy solutions to the identified challenges. Content and thematic analysis were used to analyse the status of energy policy. While the capacity of the policy to promote infrastructural resilience was assessed by evaluating the level of technical policy implementations and status of electricity supply, institutional resilience's capacity was determined through legal and capacity building policy implementations. Notably, the NEP fails to support PSR. Resilience policies, energy policy financing, energy

---

J. N. Chivunga (✉) · Z. Lin · R. Blanchard

Wolfson School of Mechanical, Electrical and Manufacturing Engineering, Centre for Renewable Energy Systems Technology (CREST), Loughborough University, Epinal Way, Loughborough LE11 3TU, UK

e-mail: [J.N.Chivunga@lboro.ac.uk](mailto:J.N.Chivunga@lboro.ac.uk); [jchivunga@must.ac.mw](mailto:jchivunga@must.ac.mw)

Z. Lin

e-mail: [zlin@ieee.org](mailto:zlin@ieee.org)

R. Blanchard

e-mail: [R.E.Blanchard@lboro.ac.uk](mailto:R.E.Blanchard@lboro.ac.uk)

J. N. Chivunga

Department of Energy Resources Management, NDATA School of Climate and Earth Sciences, Malawi University of Science and Technology, Post Office Box 5196, Limbe, Malawi

© The Author(s) 2023

J. D. Nixon et al. (eds.), *Energy and Sustainable Futures: Proceedings of the 3rd ICESF*, 2022, Springer Proceedings in Energy, [https://doi.org/10.1007/978-3-031-30960-1\\_19](https://doi.org/10.1007/978-3-031-30960-1_19)

187

policy management, coordination with key stakeholders, politics, energy data and capacity of the Ministry of energy are critical issues.

**Keywords** Infrastructure resilience · Institutional resilience · Policy financing · Resilience policies · Energy policy monitoring · Capacity · Energy data · Coordination

## 19.1 Introduction

A constant production and delivery of electricity is crucial to the functioning of the society. Energy plays a vital role in sustainable livelihoods and socioeconomic development [1]. Apart from servicing the other sectors, the energy sector is supposed to be among the sectors that contribute significantly to the country's GDP through exports of its products. However, surplus energy supply is one of the challenges that Malawi is facing, as its supplies are less than the projected demand [2–4]. Meeting sufficient energy needs for Malawians is becoming more challenging. The renewable energy (RE) role to the energy mix is also still low [5]. In addition to low energy access, Malawi is exposed to both climatic and geologic hazards [6–8] given its location along the great African Rift valley. Extreme weather events pose an enormous and increasing threat to the nation's electric power systems (PS) and the associated socio-economic systems that depend on the reliable delivery of electric power [9]. In January 2022, Malawi was severely hit by Tropical Cyclone Ana which caused national blackout due to lost power generation and transmission systems. One hundred thirty (130) MW of electricity generation were lost [10] and many transmission lines were brought down. This overwhelmed the mitigation measures that were put in place [11]. PS suffer from either physical, institutional or community level challenges under climate change (CC) hence, the need for appropriate adaptation strategies [12]. One of the guiding principles of the needs assessment and recovery strategy is to move from response to long term resilience [7].

Different authors [13–34] presented a range of power system resilience (PSR) definitions. Having reviewed the range of definitions, the grid resilience definition is proposed. It is the ability of an interconnected network of either components, institutions, grid operators or stakeholders to adequately plan for resilience, avoid adverse impacts of hazards, adapt to extreme disasters and transform into new stable zones. In doing so, the impact of threats and related disasters will be minimised, and systems will be restored quickly. Where appropriate, systems will be improved. Finally, disaster risk factors and vulnerability of the grid system to actual or expected impacts of hazards will be reduced in a cost-effective way. Resilient systems should have a maximum diversity of supply sources and should avoid reliance on a limited set of power supplies. In addition, systems should be sufficiently flexible to react rapidly to events and to alter working processes even in short times [35]. Further, priorities for supplying diverse loads ought to be well-known [36]. Erker et al. [37] argued that a resilient system should not be exposed to risks or potential risks, is efficient,

diverse and has redundant units or functions. The rise of power outages caused by extreme weather events and the frequency of extreme weather events has motivated the study of PSR [38]. The development of PSR assessment and enhancement tools, methods, approaches and/or guidelines is also another cause for PSR studies.

PSR can be evaluated either quantitatively or qualitatively [14, 18, 19, 39]. References [13, 14, 16, 20, 26, 27, 33, 36, 38, 40–47] evaluated PSR by quantifying the resilience of electricity networks to extreme events. Some suggested measures to enhance the resilience of the PS. While others [17, 27, 35, 48–51] looked at structural challenges and measures, [18, 29, 45, 52–59] considered operational strategies. Although all these studies contributed significantly to the resilience of electricity systems, none of the prior studies explored the possibility of the energy policy being a critical key in promoting the PSR. The national energy policy (NEP) is considered as one of the drivers of PSR [12]. According to [60], NEP is one of the dimensions in the testing of the *transformative resilience theory* where policy performance is considered one of the resilience indicators. This novel study, therefore, (1) assesses the capacity of the NEP to promote infrastructure and institutional PSR, (2) identifies implementation challenges regarding capability of the policy to support PSR and (3) suggests key policy solutions to PSR challenges of the NEP and thus the accomplishment of SDG 7 [61]. After the introduction, Sect. 19.2 is the methodology, followed by results and discussions in Sect. 19.3 under distinct sub-topics. Conclusions are drawn in Sect. 19.4.

## 19.2 Methodology

The study methodology was in two stages, one, data collection and extraction and two, data analysis. Data collection was through observations, review of documents and in-depth interviews. The population that qualified as subjects for this study included all individuals that have expert knowledge and hold key positions in the energy sector, grid operator, and power generating company. In this case, the study used purposive sampling where subjects are selected based on some characteristic poses that are predetermined before the study [84]. This was also to identify respondents who would provide relevant and critical information that would serve to answer the questions of this study. For in-depth interviews, semi-structured interview guide was used to collect data for the status of NEP. To analyse data, both content and thematic analyses were used. To evaluate the potential risks to infrastructural and institutional resilience, the approaches of [37, 62] were adopted. In view of this, the capacity of the Policy to promote PSR was evaluated by examining diversity, exposure, and efficiency. These are functions of preparation, anticipation, absorption, adaptation and transformation. While the capacity of the Policy to promote infrastructural resilience was assessed by evaluating the level of technical policy implementations and through status of energy supply, institutional resilience's capacity was determined through legal and capacity building policy implementations. This approach was adopted because effective address of preconditions that cause PS stresses is key to making the PS more

resilient [14]. Technical implementations that were considered are energy access, off grid and energy efficiency targets. These targets and the status of electricity supply together entail the level of infrastructure preparedness to mitigate impacts of CC. In addition, these also determine the potential to absorb, adapt or transform under extreme PS stresses. Anticipatory governance and long-term policy vision are critical in the adjustment of current behaviour to address future PS challenges [37]. It is important, therefore, to evaluate legal implementations to address regulatory uncertainties that compromise infrastructure improvement and modernisation. Capacity building enables institutions in moderating future disruptions. It is important to note that this study's scope was not to evaluate the provision of these variables in the Policy but their implementation to promote grid resilience. This is because preliminary policy review suggested that most of these are provided for. A key issue was to compare the provision against achieved targets (status of the NEP). If implementation is lagging, then the Policy is failing to promote one of the key functions of resilience. To identify the challenges of the Policy, themes were generated from interview responses following this study's investigations of the reasons for the implementation challenges. Solutions to the challenges were proposed by suggesting mitigation measures to the identified challenges, in addition to expert feedback. The major limitation of this approach was data scarcity. Some variables could not be extensively evaluated due to data availability challenges.

## 19.3 Results and Discussions

### 19.3.1 *The Structure of Electricity Supply*

Malawi's current electricity generation mix is divergent from the neighbouring countries and world trends where electricity generation from fossils is dominant (Table 19.1). Malawi has about 401.15 MW, 81.3 MW and 53.22 MW of installed hydro, commissioned solar PV and diesel generator capacities, respectively. A 21 MW Serengeti solar power plant is expected to be commissioned by June 2023. It is important to note that the available capacity is far much less than the installed capacity due to age of the infrastructure, sometimes due to low water levels and recently following a loss of generation due to effects of 2022 Cyclone Ana. Over dependence on hydro electricity generation is a threat to PSR in the wake of CC. Studies indicate that CC is responsible for the increase in frequency, duration, and intensity of extreme weather events [15, 43, 44, 63]. CC is also responsible for rising global temperatures, changes in rainfall patterns, elevated occurrence and strength of drought days, cloudiness, higher winds, and sea-level rise [15, 43, 63–69]. Cold waves, heavy snow and lightning strikes on or near overhead conductors [70] also result from CC. Each of these impacts of CC affects the PS in different ways, at different degrees either on their own or in combination as is usually the case. There is a risk that if Malawi does not receive enough rains or experience again a two-year drought that

**Table 19.1** Percentage of Malawi's electricity generation

Energy source	Percent of the total electricity generation in Malawi	Percent of the total electricity generation in Africa	Percent of the total electricity generation for the world
Fossil	9.94	82.44	70.04
Wind	0	2.23	8.25
Solar	15.17	0.99	4.35
Hydro	74.89	11.92	7.71
Nuclear	0	1.68	9.19
Geothermal	0	0.73	0.47

*Data source* [72]

was experienced in the year 1914, Shire River would stop flowing and there would be power crisis [71]. Emergency Power diesel generator sets (peaking generators) are a source of fossil generation. Due to the deficit in the electricity supply, Malawi government has provided for the interconnection to the Zambian, Mozambican and Tanzanian grids through Southern African Power Pool (SAPP) agreements. There are plans to import 30 MW, 50 MW and 150 MW from Zambia, Mozambique, and Tanzania, respectively, by December 2023 [5]. Further, plans to develop seven (7) new hydropower stations totalling 1073 MW by 2023 and coal fired power plants totalling 620 MW are outlined in [5, 61].

### **19.3.2 Policy Implementation**

Through the current implementation, there has been some improvement in the overall energy sector. This improvement is in line with the priority areas for Malawi's Action Agenda [61]. The following evidence demonstrates the effect of implementing the current NEP. The implementations are categorized into legal, capacity building and technical. Tables 19.2, 19.3 and 19.4 summarise the legal, capacity building and technical implementations, respectively, as of 2021. Table 19.2 presents policy targets that were to either be developed, adopted, reviewed, or enforced. Notably, there were more policy developmental activities than adoptions, reviews and enforcements. Similarly, Table 19.3 presents those that were to either be developed, conducted, or increased.

#### **19.3.2.1 Legal Implementations**

See Table 19.2.



### 19.3.2.2 Capacity Building Implementations

See Table 19.3.

### 19.3.2.3 Technical Implementations

These are categorized into energy access, off-grid, and energy efficiency targets. Table 19.4 summarises the Policy variable targets against percentage of implementation status for the selected targets that are related to electricity sector. Targets for 2020 (except where explicitly stated otherwise) and the current status are summarised. The dashes (–) mean that data is unavailable. This data depends on the availability of the Malawi energy survey reports whose activity is yet to be conducted. It should be noted that all new domestic connections are fitted with Energy Server Bulbs, LEDs.

## 19.3.3 Does the Malawi NEP Support PSR?

### 19.3.3.1 Infrastructure Resilience

This study revealed that energy access, off-grid, and energy efficiency targets were not adequately met. This has a bearing on infrastructure resilience because these targets

**Table 19.2** Legal implementations

Policy targets	Developments	Adoptions	Reviews	Enforcements
Activities undertaken	Mini grid framework Lifeline tariffs Policies facilitating expediting of customer connections Legislation banning illegal production of charcoal Guidelines for franchising of liquid fuels outlets Tax waivers on gas to support the initial stages of introducing and promoting LPG, biogas, and natural gas	Policies facilitating outsourcing of construction works by distribution licensees Global tracking framework	Grid code	Electricity act to unbundle electricity supply corporation of Malawi (ESCOM)

Data source [73]

**Table 19.3** Capacity building implementations

Policy targets	Developments	Awareness	Increment
Activities undertaken	RE capacity building plan Biomass Energy Technologies Training Strategy Nuclear Science and Materials Undergraduate Programs in some public universities DSM awareness materials	Safe use of Liquid Petroleum and Gas (LPG), biogas, and natural gas Household campaigns and distribution of LEDs Demand Side Management (DSM) campaigns	Number of training institutions implementing RETs

Data source [73]

are key to resilience enhancement. *Capacity expansion* is one of the long-term grid enhancement measures [75]. It allows for peak load transferring or shifting when there is generation loss in some parts to avoid overloading the substations. Notably, there is stagnation in the development of potential sites and other sources of electricity generation. Out of the proposed potential hydro sites, only less than 5% of the planned development was commissioned (Tedzani IV). By 2021, at least 50% of the target should have been developed to achieve the 2023 completion target. Three coal fired power plants were planned to be fully operational by 2023, adding 620 MW to the national grid. By 2021, only environmental impact studies for one were completed. Approximately 38% of the proposed solar power plants was commissioned. Although this is a good development, increase in intermittent generation needs adequate firm capacity to avoid frequency disturbances. There should be a corresponding increase in base generation like hydro, nuclear or thermal. Household biogas for cooking was piloted in 8 districts installing 80 systems, representing 14% of the 2020 projected target, and 4% of the 2030 target. Ideally, approximately 140 biogas plants were to be piloted per year if the 2030 target was to be met. Failure to achieve these targets decreases the *capacity mix* which was proposed by Handayani et al. [76] as one of the CC adaptation measures for PSR. Low percentage of RE to total energy in the country is another sign of un resilient systems [60]. The results further suggested a lack of *diversity* in electricity generation sources. Being a system that is almost wholly hydro-based, this exposes the PS to severe impacts of CC like droughts. *Off-grids* like micro grids are the mostly used *smart resilience enhancement measures* [27, 32, 77]. Microgrids take part in emergency response by supplying critical loads or essential. The T&D losses are approximately 19.5%—still off their targets. Efficient T&D structures limit the degree of impact during extreme events. An inefficient T&D system derates faster than an efficient one. Energy audits are expected to unmask system inefficiencies. Although regular audits were planned for public institutions especially in the health sector, only 28 were conducted in health, parliament and

**Table 19.4** Policy technical implementations

Area	Policy variable	Target	Implementation Status (%)
Energy access	Hydropower plants	1092 MW by 2023	< 5
	Solar PV plants	160 MW	38
	Coal fired power plants	620 MW by 2023	0
	No. of companies registered in LPG stoves distribution	20	>100
	LPG stoves	15,000	–
	No. of improved cookstoves distributed	2 million	> 100
	No. of household biogas piloted	560	14
	No. of solar water heaters	7500	–
	No. of electric cookers installed	94,000	–
	No. of homes/businesses connected to the grid	747,846	66
Off-grid	Mini grids	15 mini grids by 2021 in NEP and 30 mini grids by 2020 in AA	53
	Solar home systems and Pico solar systems	1.5 million	80 in 2018
Energy efficiency	Combined transmission and distribution (T&D) losses	17%	15%
	Installed prepaid/smart meters	564,000	83
	LEDs	2,750,000	–
	Energy efficient (EE) barns	2000	–
	Energy audits	Regular energy audits in institutions especially health facilities	–

*Data sources* [73, 74]

government offices. Inefficiencies reduce the current carrying capacity which consequently raise electricity demand [67]. Installation of smart meters is short by almost 17%. Data for the number of LEDs, EE barns, solar water heaters installed was not available. LEDs would relieve the grid from the demand pressure. In view of the above, failure of the Policy technical implementations predisposes the grid to severe impacts of climate change. Although NEP is effective, efficient, equitable and

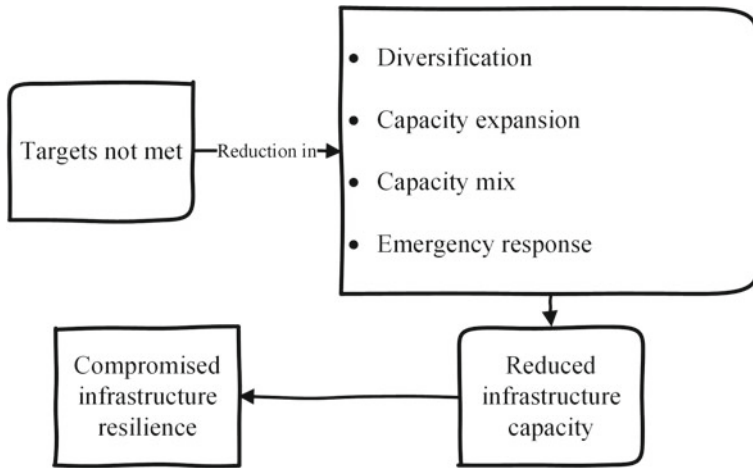


**Fig. 19.1** How NEP fails to support infrastructure resilience

institutionary feasible, it fails to support infrastructure resilience adequately. This is visualized in Fig. 19.1.

### 19.3.3.2 Institutional Resilience

Failure to review, promulgate, amend or develop different sets of standards, models, policies and guidelines in the energy and electricity sector is an institutional resilience setback. What was implemented is insignificant compared with the legal Policy targets. Panteli and Mancarella [43] classified the forms of climate adaptation strategies for PSR into (1) structural, (2) capacity building and (3) institutional. Institutional adaptation strategies are further categorised into economic tools, governance, laws and regulations. Similarly, failure to build capacity and/or recruit enforcement officers is another way of compromising institutional resilience. Failure to develop a bankable document for nuclear power generation investments was observed. Similar observations were noted for the regulations setting minimum standards for coal storage, transportation, importation, usage, marketing and pricing. The bankable document is ideal especially now when the NEP provides for coal fired power plants to increase electricity generation capacity. The document would among other things provide guidelines for optimal orientation of coal stockpiles which are vulnerable to precipitation, wind and temperature variations [78]. Amendment of legislation to include banning importation, distribution and use of incandescent bulbs is still pending. Similarly, the Liquid Fuels and Gas (LPG) Act reviews to facilitate institutional reforms for investments in and utilization of LPG, biogas and natural gas were not conducted. By 2019, the development of bio-fuel pricing model and of an Act to regulate fuel prices through use of transparent and verifiable fuel price adjustment system were supposed to have been completed. In addition, the Net Metering

Policy, appropriate RE regulations under the RE Act and the RE Act were not developed. Finally, the RE standards are yet to be reviewed, three (3) years after their deadline. Policy and regulatory instruments in RE were acknowledged by Fang and Wei [79] as adaptation measures in PS, which can be applied either at enterprise, regional, national, or international level. Further, rescheduling investments, investing more in carbon management technologies and the policy were also suggested in [80] as resilience enhancement measures. Similarly, RE plants to compensate for the uncertainty in hydropower generation are key PSR improvement strategies. Panteli and Mancarella [43] proposed capacity building, which was further classified into educational, informational, or behavioural adaptation as one of the PSR enhancement approaches. Sovacool [12] recommended, among others, training policy makers as a way of promoting institutional resilience. Education and awareness to achieve community resilience to impacts of CC were also recommended. Lack of provision for PSR awareness in the Policy and emergency response plans is another way of compromising institutional resilience. In addition, by 2020, Malawi government was supposed to have recruited district energy officers (DEOs) responsible for enforcement of efficient cookstoves. RETs like biogas, improved cookstoves, micro hydro and solar power were also recommended by Sapkota et al. [81] as a way of rural adaptation to CC. These do not only reduce traditional biomass use but also carbon dioxide emissions. Use of these also reduces pressure from the grid. The results suggested that NEP also fails to support institutional resilience adequately. This is summarized in Fig. 19.2.

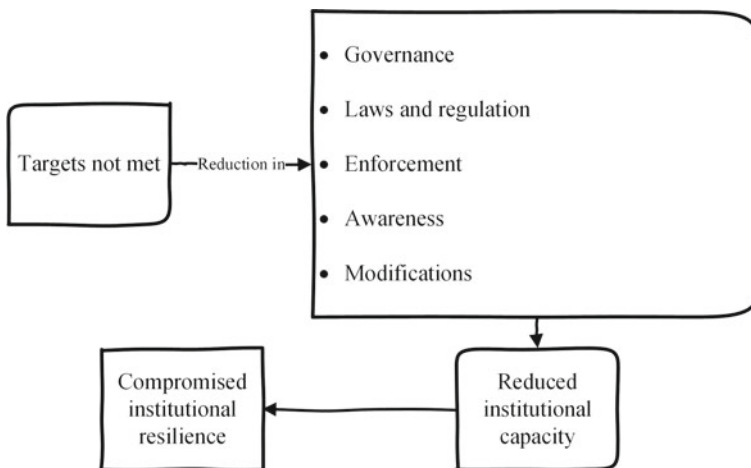


**Fig. 19.2** How NEP fails to support institutional resilience

### ***19.3.4 Challenges and Potential Solutions (Improvements) of Malawi's NEP***

Policy evaluation indicates that some measures to achieve SDG 7 have previously been implemented in Malawi. However, some unresolved concerns departing from the guiding principles and policy statements of Malawi's NEP and the international initiative for affordable, reliable, sustainable, and modern energy for all remain. These in turn compromise the resilience of the PS and electricity sector in general. Energy policy financing, energy policy management, resilience building policies, coordination of key stakeholders, politics, energy data and capacity of the Ministry of energy (MoE) are critical issues in Malawi. Addressing these preconditions is key in making the grid more resilient [14]. In this section, we summarise the unresolved issues which were identified, and formulate key policy solutions for the problems as follows.

#### **19.3.4.1 Energy Policy Financing**

Much as some of the commendable progress is noted, a significant portion of measures are behind their scheduled time frames. The stagnation in development of potential sites and other sources of electricity generation is worrisome because poor infrastructure development compromises infrastructure resilience [60]. For the proposed power plants, the developers are still seeking finances for the development activities [73]. Implementation of Malawi's NEP 2018 needs sufficient human, financial, material and technical resources. Most of the activities that have not been completed according to their planned time frames lack financing [73]. Some capacity building exercises also lack funding. The follow-up on targets is also not done due to financial constraints. Desirable resources were indicated in the Policy but what the Government provides through the Ministry of Finance (MoF) is not adequate. There is a need for deliberate actions by the government to finance the activities of the energy policy—*Energy Policy Financing*. Government, through MoF should have the core responsibility of committing adequate financial resources for the implementation of the Policy [82]. The MoF should consider putting aside a budget to support the energy sector. The funding would also help with follow-up of activities of the NEP. This is in line with [85] where lack of financial resources implies that laws will not be enforced, services will not be provided, and reasonable regulations will not be developed. Financial resources also help with the acquisition of land, equipment, and buildings. The government may benefit from reaching out to different foreign investors through MoF. Another thing to be considered is for the government to increase budgetary allocation for the energy sector. The energy sector currently relies on donor funding. An adequate budget would facilitate the development of the entire energy sector.

#### **19.3.4.2 Resilience Policies**

It was observed that existing policies and regulations were inadequate to respond to the complex challenges presented by extreme events. The NEP has eight main priority areas: electricity, biomass, petroleum fuels, bioethanol and other biofuels, liquid petroleum, gas, biogas and natural gas, coal, nuclear energy and DSM. Although these areas indirectly support PSR, resilience is not prioritized in the Policy. Prioritization of resilience in energy policies or existence of resilience policies provide the preventive and anticipative capacities which enable institutions to prepare for and to commit resources as well as to formulate legal and contractual frameworks within which they would operate during an unusual event [83]. These capacities, ensure that the impacts resulting from such occurrences are greatly reduced by reducing both the vulnerability and exposure of the PS to extreme events and by creating a proactive system in which present development actions inherently address future risks. The next Policy review should emphasize the inclusion of resilience of PS.

#### **19.3.4.3 Energy Policy Monitoring/Management**

It is appreciated that some of the planned activities are not achieved within their proposed time frames due to financial constraints. However, some have just lagged for no reason. Some 2019 Policy targets were still unattained by 2021, two years down the line. Most of activities in the NEP are supposed to be completed by 2023 and others by 2035 in the long term. Most of the 2023 targeted activities are yet to be commenced. It is unlikely that targeted time frames will be achieved. Although the Malawi's NEP is scheduled to be reviewed every five years, this study revealed that it takes longer than that, with the main reason being financial constraints. However, other views consider that this is attributable to lack of seriousness from responsible personnel. Often, the personnel are just good at setting targets which leads to over-ambitious targets that are often not implementable. [85] identified some other obstacles that affect policy implementation in developing countries. Among them were insufficient definition of goals, over-ambitious policy goals, and choice of unsuitable organizational structure in implementation. Regarding over-ambition in policy making, in developing countries, several policies tend to be over-ambitious, broad, and basic in nature. This is because of some of those developing countries are being inspired by special conditions, usually defined by developed countries that affect how programmes and policy goals are decided, in exchange for government funding. Further to the above issues, the lack of a framework to help with checking or tracking NEP is another critical issue. The absence of a policy tracking framework has also contributed to unachieved monitoring and evaluation. The Policy has an implementation and evaluation plan, but this is embedded in the Annexes of the Policy. Implementation tracking framework may offer competitive benefits if it is a standalone document under some legal custodians. One of the many reasons for Policy implementation failure is the model of functionality within the MoE. Although decentralization is considered one of the ideal approaches to management functions,

the MoE, who is the custodian of the NEP, works centrally. This puts pressure on the personnel. To curb these challenges highlighted above, different solutions are suggested. First, regular monitoring and evaluation are needed to inform custodians of the next steps. The civil society organisations can also play a part in monitoring implementation and promoting unique approaches to enhance implementation, working as watchdogs to ensure that funding is allocated, and appropriate activities are carried out [86]. The interim reviews should look at what was supposed to be achieved in a particular year. This also works well with mindset change. Mindset change can be advocated through different approaches. Learning from other nations that have successfully implemented their energy policies is one way in addition to mindset change programmes that can be introduced by the government through the ministry of information and civic education. The feeling of not owning the Policy leaves a lot of things unattended to. Also, the setting of realistic goals heavily depends on meaningful engagement with different key stakeholders. For example, legal targets are supposed to be set with serious consultations with the Ministry of Justice. Finally, decentralization of the MoE may offer Policy managerial/administrative benefits. The MoE may also benefit from employing more energy officers in different Policy areas.

#### **19.3.4.4 Coordination with key stakeholders**

Policy implementation cannot be achieved by the MoE alone. There is a need for collaborative efforts among different stakeholders for the implementation of the NEP to take place. Communication is an important component for successful implementation of Policy [85]. Through communication, instructions to implement policies are anticipated to be conveyed to the suitable personnel in a transparent manner while such instructions must be precise and coherent. Insufficient information can result in a misunderstanding on the part of the implementors who may be confused as to what exactly is required of them. In effect, implementation directives that are not communicated, that are twisted in communication, that are ambiguous, or that are conflicting may cause serious barriers to policy implementation [85, 86]. On the other hand, orders that are too specific may impede implementation by suppressing innovation and flexibility [85]. In Malawi, stakeholders within the sector do not specifically own policy statements. This has led to some activities not to be achieved. Most stakeholders assume that every statement is the responsibility of the MoE. In addition to this, there is no 100% linkage between key sectors such as the Ministries of Treasury and Justice. There are Policy statements that directly require the involvement of these key sectors. Further, policy plans (targets) depend on other stakeholders. For example, investors are not coming to invest in coal fired power plants. Only memorandums of understanding have so far been signed. The government is on its own because foreign investors consider coal damaging to the environment. This has caused implementation failure due to lack of donor funds. A lack of coordination with key stakeholders has also led to unavailability of energy data. Some of the data to determine implementation of NEP was not available at the MoE. The data was



with responsible stakeholders such as ESCOM, Malawi energy regulatory authority (MERA) and the National Statistical Office (NSO). This data was supposed to be publicly available. However, the MoE does not have a database of the activities of the energy policy. This is a drawback in policy implementation because the current energy data informs next decisions. Accurate energy data is also a basis for research and development activities. Engaging key policy stakeholders during policy target setting phase may encourage policy statements ownership. In addition, collaboration with other ministries or departments such as mining may benefit the MoE to solve energy data challenges. One of the collaborative agreements would be to have a common database, under the MoE but whose input can be done from different sectors or ministries. Another agreement would be for responsible stakeholders to commit to providing their services, for example the MoF committing to providing financial resources.

#### **19.3.4.5 Politics**

The study reveals that lack of political will is one of the contributing factors for the policy implementation failure. This owes to the fact that in the implementation process, political resources are needed [86]. This is in line with [85], where disposition or attitude is an additional significant factor that affects policy implementation. In Malawi's context, energy investment timelines are different from political timelines. Energy investments take long unlike the political timelines which are 5-year terms. Because political leaders are focusing on projects or activities that will lead to some tangible outputs in 5 years, Policy activities tend not to be prioritized. This is why some energy investment directions are not politically supported i.e., shot down by parliamentarians. A policy that operates opposite to the manifesto of the government in power may suffer at the implementation phase because it may lack support, both financial and organisational [85]. As national political environment changes, some policy perspectives also change, in turn affecting which players are involved, which policy decisions are made, and what processes take place at various levels, including the operational and service delivery levels [86]. The other political problem is that energy is not regarded as a critical infrastructure, hence not prioritised. This is why there is some significant political interference in the energy sector, especially in rural electrification. It is high time that political leaders supported the Policy by taking part in political deliberations that encourage energy investments. The political leaders should be willing to develop the energy sector by advocating for the implementation of the Policy activities. Also, there is need to advocate for energy as a critical infrastructure. State political officials may benefit from policy learning related to the re-construction of policy challenges and goals. In some cases, learning means assessment of political viability with respect to policy activity and the political price to be paid for implementation [86].

#### **19.3.4.6 Energy data**

The study suggests that energy statistics or data is important not only for research and development but for informing policy formulation, policy reviews and decision making [87, 88]. This calls for high level understanding of energy data. The availability of energy data relies on energy surveys. In Malawi, surveys rely on the NSO. This results in limited survey questions because NSO surveys are generic in nature. There is a need for energy-dedicated surveys. These energy dedicated surveys may be conducted by the MoE in collaboration with academia. These energy-dedicated surveys will help in managing unrealistic or ambiguity of Policy targets. As stated in 19.3.4.4, the MoE does not have a database. The Ministry may need to compile annual energy statistics. These energy statistics may come from dedicated energy surveys and databases from energy companies. These statistics provide an energy balance which is a major tool in the implementation of the energy policy.

#### **19.3.4.7 Capacity of the MoE**

This study revealed that the MoE lacks some capacity to champion the Policy. There was insufficient human capacity in terms of numbers, evidenced by lots of vacant positions. The capacity to enforce was also not there. This all goes down to vacant positions since the 28 District Energy Officers who were to be recruited by 2019 to enforce the Policy are yet to be employed. Capacity development programs on how the Ministry can undertake various activities of the Policy may be beneficial. Capacity building on how to interpret NEP may also help with the implementation challenge. Recruitment of additional energy officers is long overdue. Human resources such as adequate number of staff who are well equipped to carry out the implementation, relevant and adequate information on implementation process, the authority to ensure that policies are carried out as they are intended, may be deemed necessary for the successful implementation of the policy [85]. Without sufficient human resources it means that laws will not be enforced, services will not be provided, and reasonable regulations will not be developed. Since the capacity of the MoE also depends on various key stakeholders, sensitizing these stakeholders on their expected roles and criticality of the energy sector is another positive approach to dealing with implementation challenges. Some Policy targets may need an increase in various capacities, especially in numbers. The challenges and potential solutions discussed above are summarized in Table 19.5.

### **19.4 Conclusion and Future Research Direction**

Energy plays a vital role in sustainable livelihoods and socioeconomic development. The PS, however, suffers from different challenges under CC hence, the need for appropriate adaptation strategies. This study was conducted to examine the policy

**Table 19.5** Summary of Policy implementation challenges and potential solution

Challenges	Potential solutions
Lack of funding	Energy policy financing [82, 85]
Inadequacy of existing Policy to respond to complex challenges presented by the extreme events	Resilience policies [83]
Lack of policy administration, monitoring and clear policy targets	Energy policy management [85, 86]
Lack of coordination with key stakeholders	Meaningful stakeholder involvement [85, 86]
Lack of political will and political interference	Policy learning [86]
Lack of statistical energy data	Compilation of annual energy statistics [87, 88]
Incapacitation of MoE to champion the Policy	Capacity building [85]

challenges that could compromise the resilience of the PS and to suggest potential solutions. In addition, the capacity of the NEP to promote PSR was examined. Study revealed that Malawi's current electricity generation mix is divergent from the neighbouring and world trends where electricity generation from fossils is dominant. Almost 75% of Malawi's electricity generation is from hydro whose 99% of generating plants are cascaded on one river. This exposes the PS to severe impacts of CC like drought. Through current implementation, there has been some improvement in the overall energy sector. This improvement is in line with the priority areas for Malawi's Action Agenda. *The development of some regulatory frameworks, increase in electricity generation capacity, increased utilization of improved biomass technologies, provision of incentives to promote adoption of alternative energy sources, increased uptake, or adoption of alternative means of cooking energy sources to biomass, increased production of biofuels, and increase in number of institutions conducting energy efficiency interventions* and many more contribute to the fair progress. The results suggested that although NEP is effective, efficient, equitable and institutionally feasible, it fails to support both institutional and infrastructure resilience adequately. Most of the activities that have not been completed according to their planned time frames lack financing. It was also observed that existing policies and regulations were inadequate to respond to the complex challenges presented by extreme events. Lack of policy monitoring largely contributes to non-implementation. Other implementation challenges are incapacitation of the MoE in different areas, lack of energy data, political interference and lack of coordination with key stakeholders. To improve the infrastructure and institutional resilience, policy enhancement measures were proposed. Energy policy financing, resilience policies, guidelines and/or frameworks enhancing energy policy tracking, capacity building, compilation of annual energy statistics, policy learning and meaningful stakeholder engagement are possible improvement approaches. In summary, a supportive policy environment can be regarded as one of the cornerstones of improved and effective policy implementation for PSR. In further studies, the resilience of an

entire energy sector with respect to policy's capacity will be investigated. In addition, comparison of Malawi's NEP to other sub-Saharan policies will also be conducted.

**Acknowledgements** The author would like to acknowledge Commonwealth Scholarship Commission and Schlumberger Foundation Faculty for The Future for the Fellowship for the Ph.D. research support. Sincere appreciations are also extended to the Electricity Supply Corporation of Malawi and the Department of Energy Affairs for granting this research with useful data.

## References

1. M. Jeuland et al., Is energy the golden thread? A systematic review of the impacts of modern and traditional energy use in low- and middle-income countries. *Renew. Sustain. Energy Rev.* **135** (2021). <https://doi.org/10.1016/J.RSER.2020.110406>
2. Electricity Generation Company (Malawi) Limited—Generating Power for Generations. <https://www.egenco.mw/>. Accessed 28 Jul 2021
3. Electricity Supply Corporation of Malawi Limited (ESCOM). <http://www.escom.mw/>. Accessed 28 Jul 2021
4. C. Zalengera, R.E. Blanchard, P.C. Eames, A.M. Juma, M.L. Chitawo, K.T. Gondwe, Overview of the Malawi energy situation and a PESTLE analysis for sustainable development of renewable energy. *Renew. Sustain. Energy Rev.* **38**, 335–347 (2014). <https://doi.org/10.1016/J.RSER.2014.05.050>
5. Government of Malawi, in *Malawi National Energy Policy* (2018)
6. Government of Malawi, in *Malawi Drought 2015–2016: Post-Disaster Needs Assessment* (2016). <https://openknowledge.worldbank.org/handle/10986/25781>. Accessed 10 Jul 2021
7. Government of Malawi, in *Malawi 2015 Floods Post Disaster Needs Assessment Report* (2015)
8. Government of Malawi, in *Malawi 2019 Floods Post Disaster Needs Assessment Report* (2019)
9. Grid Resilience and Intelligence Platform (GRIP)|Grid Modernization Lab Consortium. <https://gmlc.doe.gov/projects/1.5.01>. Accessed 28 Jul 2021
10. Over K18bln needed to restore 32% of power lost from Kapichira due to Cyclone Ana—Maravi Express—Your Kind of News. Clear and accurate. <https://www.maraviexpress.com/over-k18bln-needed-to-restore-32-of-power-lost-from-kapichira-due-to-cyclone-ana/>. Accessed 08 Feb 2022
11. A dark, disastrous night after storm Ana—The Nation Online. <https://www.mwnation.com/a-dark-disastrous-night-after-storm-ana/>. Accessed 08 Feb 2022
12. B.K. Sovacool, Expert views of climate change adaptation in the Maldives. *Clim. Change* **114**(2), 295–300 (2012). <https://doi.org/10.1007/s10584-011-0392-2>
13. Y. Yang, W. Tang, Y. Liu, Y. Xin, Q. Wu, Quantitative resilience assessment for power transmission systems under typhoon weather. *IEEE Access* **6**, 40747–40756 (2018). <https://doi.org/10.1109/ACCESS.2018.2858860>
14. B. Chiu et al., *Resilience Framework, Methods, and Metrics for the Electricity Sector* (2020)
15. E.L. Ratnam, K.G.H. Baldwin, P. Mancarella, M. Howden, L. Seebeck, Electricity system resilience in a world of increased climate change and cybersecurity risk. *Electr. J.* **33**(9) (2020). <https://doi.org/10.1016/j.tej.2020.106833>
16. F. Mujjuni, R. Blanchard, T. Betts, A case for a new approach in theorizing and operationalisation of resilience for electrical systems in developing countries, in *Bhattacharyya, SC, 2021, Proceedings of the Virtual International Conference on Aligning Local Interventions with the UN Sustainable Development Goals* (2021)
17. P. Cicilio et al., Electrical grid resilience framework with uncertainty. *Electr. Power Syst. Res.* **189** (2020). <https://doi.org/10.1016/j.epsr.2020.106801>

18. Z. Bie, Y. Lin, G. Li, F. Li, Battling the extreme: a study on the power system resilience. *Proc. IEEE* **105**(7), 1253–1266 (2017). <https://doi.org/10.1109/JPROC.2017.2679040>
19. Y. Lin, Z. Bie, A. Qiu, A review of key strategies in realizing power system resilience. *Glob. Energy Interconnect.* **1**(1), 70–78 (2018). <https://doi.org/10.14171/j.2096-5117.gei.2018.01.009>
20. H. Zhang, H. Yuan, G. Li, Y. Lin, Quantitative resilience assessment under a tri-stage framework for power systems. *Energies (Basel)* **11**(6) (2018). <https://doi.org/10.3390/en11061427>
21. B. Li, D. Ofori-Boateng, Y.R. Gel, J. Zhang, A hybrid approach for transmission grid resilience assessment using reliability metrics and power system local network topology. *Sustain. Resilient Infrastruct.* **6**(1–2), 26–41 (2021). <https://doi.org/10.1080/23789689.2019.1708182>
22. N. Bhusal, M. Abdelmalak, M. Kamruzzaman, M. Benidris, Power system resilience: current practices, challenges, and future directions. *IEEE Access* **8**, 18064–18086 (2020). <https://doi.org/10.1109/ACCESS.2020.2968586>
23. M. Panteli, P. Mancarella, Modeling and evaluating the resilience of critical electrical power infrastructure to extreme weather events. *IEEE Syst. J.* **11**(3), 1733–1742 (2017). <https://doi.org/10.1109/JSYST.2015.2389272>
24. M. Panteli, D.N. Trakas, P. Mancarella, N.D. Hatziargyriou, Power systems resilience assessment: hardening and smart operational enhancement strategies. *Proc. IEEE* **105**(7), 1202–1213 (2017). <https://doi.org/10.1109/JPROC.2017.2691357>
25. M. Panteli, P. Mancarella, D.N. Trakas, E. Kyriakides, N.D. Hatziargyriou, Metrics and quantification of operational and infrastructure resilience in power systems. *IEEE Trans. Power Syst.* **32**(6), 4732–4742 (2017). <https://doi.org/10.1109/TPWRS.2017.2664141>
26. A. Gholami, T. Shekari, M.H. Amiroun, F. Aminifar, M.H. Amini, A. Sargolzaei, Toward a consensus on the definition and taxonomy of power system resilience. *IEEE Access* **6**, 32035–32053 (2018). <https://doi.org/10.1109/ACCESS.2018.2845378>
27. S. Biswas, M.K. Singh, V.A. Centeno, Chance-constrained optimal distribution network partitioning to enhance power grid resilience. *IEEE Access* **9**, 42169–42181 (2021). <https://doi.org/10.1109/ACCESS.2021.3065577>
28. E.B. Watson, A.H. Etemadi, Modeling electrical grid resilience under hurricane wind conditions with increased solar and wind power generation. *IEEE Trans. Power Syst.* **35**(2), 929–937 (2020). <https://doi.org/10.1109/TPWRS.2019.2942279>
29. J. Wang, W. Zuo, L. Rhode-Barbarigos, X. Lu, J. Wang, Y. Lin, Literature review on modeling and simulation of energy infrastructures from a resilience perspective. *Reliab. Eng. Syst. Saf.* **183**, 360–373 (2019). <https://doi.org/10.1016/j.res.2018.11.029>
30. D.T. Ton, W.-T.P. Wang, A more resilient grid: the U.S. Department of Energy Joins with Stakeholders in an R&D Plan. *IEEE Power Energy Mag.* (2015). <https://doi.org/10.1109/MPE.2015.2397337>
31. E. Ciapessoni, D. Cirio, A. Pitto, M. Panteli, M. van Harte, C. Mak, *CIGRE WG C4.47 Defining Power System Resilience* (2019) [Online]. Available: <https://e-cigre.org>. Accessed: 02 Nov 2021
32. S. Poudel, A. Dubey, Critical load restoration using distributed energy resources for resilient power distribution system. *IEEE Trans. Power Syst.* **34**(1), 52–63 (2019). <https://doi.org/10.1109/TPWRS.2018.2860256>
33. H. Raoufi, V. Vahidinasab, K. Mehran, Power systems resilience metrics: a comprehensive review of challenges and outlook. *Sustainability (Switz.)* **12**(22), 1–24 (2020). <https://doi.org/10.3390/su12229698>
34. R. Rocchetta, E. Patelli, Assessment of power grid vulnerabilities accounting for stochastic loads and model imprecision. *Int. J. Electr. Power Energy Syst.* **98**, 219–232 (2018). <https://doi.org/10.1016/j.ijepes.2017.11.047>
35. M. Ghiasi et al., Resiliency/cost-based optimal design of distribution network to maintain power system stability against physical attacks: a practical study case. *IEEE Access* **9**, 43862–43875 (2021). <https://doi.org/10.1109/ACCESS.2021.3066419>
36. H. Gao, Y. Chen, Y. Xu, C.C. Liu, Resilience-oriented critical load restoration using microgrids in distribution systems. *IEEE Trans. Smart Grid* **7**(6), 2837–2848 (2016). <https://doi.org/10.1109/TSG.2016.2550625>

37. S. Erker, R. Stangl, G. Stoeglehner, Resilience in the light of energy crises—part I: a framework to conceptualise regional energy resilience. *J. Clean. Prod.* **164**, 420–433 (2017). <https://doi.org/10.1016/J.JCLEPRO.2017.06.163>
38. F.H. Jufri, V. Widiputra, J. Jung, State-of-the-art review on power grid resilience to extreme weather events: definitions, frameworks, quantitative assessment methodologies, and enhancement strategies. *Appl. Energy* **239**, 1049–1065 (2019). <https://doi.org/10.1016/j.apenergy.2019.02.017>
39. Resilience Measurement Technical Working Group, *Qualitative Data and Subjective Indicators for Resilience Measurement* (2015) [Online]. Available: [http://www.fsincop.net/fileadmin/user\\_upload/fsin/](http://www.fsincop.net/fileadmin/user_upload/fsin/)
40. A.M. Amani, M. Jalili, Power grids as complex networks: resilience and reliability analysis. *IEEE Access* **9**, 119010–119031 (2021). <https://doi.org/10.1109/ACCESS.2021.3107492>
41. M. Panteli, P. Mancarella, The grid: stronger, bigger, smarter?: Presenting a conceptual framework of power system resilience. *IEEE Power Energ. Mag.* **13**(3), 58–66 (2015). <https://doi.org/10.1109/MPE.2015.2397334>
42. X. Liu et al., A planning-oriented resilience assessment framework for transmission systems under typhoon disasters. *IEEE Trans. Smart Grid* **11**(6), 5431–5441 (2020). <https://doi.org/10.1109/TSG.2020.3008228>
43. M. Panteli, P. Mancarella, Influence of extreme weather and climate change on the resilience of power systems: impacts and possible mitigation strategies. *Electr. Power Syst. Res.* **127**, 259–270 (2015). <https://doi.org/10.1016/j.epr.2015.06.012>
44. L. Shen, Y. Tang, L.C. Tang, Understanding key factors affecting power systems resilience. *Reliab. Eng. Syst. Saf.* **212** (2021). <https://doi.org/10.1016/j.res.2021.107621>
45. Z. Li, M. Shahidehpour, F. Aminifar, A. Alabdulwahab, Y. Al-Turki, Networked microgrids for enhancing the power system resilience. *Proc. IEEE* **105**(7), 1289–1310 (2017). <https://doi.org/10.1109/JPROC.2017.2685558>
46. X. Liu et al., A resilience assessment approach for power system from perspectives of system and component levels. *Int. J. Electr. Power Energy Syst.* **118** (2020). <https://doi.org/10.1016/j.ijepes.2020.105837>
47. S. Espinoza, M. Panteli, P. Mancarella, H. Rudnick, Multi-phase assessment and adaptation of power systems resilience to natural hazards. *Electr. Power Syst. Res.* **136**, 352–361 (2016). <https://doi.org/10.1016/j.epr.2016.03.019>
48. D.J. Thompson, W.C.H. Schoonenberg, A.M. Farid, *A Hetero-functional Graph Resilience Analysis of the Future American Electric Power System* (2020). <https://doi.org/10.1109/ACC ESS.2021.3077856>
49. L. Souto et al., Power system resilience to floods: modeling, impact assessment, and mid-term mitigation strategies. *Int. J. Electr. Power Energy Syst.* **135** (2022). <https://doi.org/10.1016/j.ijepes.2021.107545>
50. Y. Li, K. Xie, L. Wang, Y. Xiang, Exploiting network topology optimization and demand side management to improve bulk power system resilience under windstorms. *Electr. Power Syst. Res.* **171**, 127–140 (2019). <https://doi.org/10.1016/j.epr.2019.02.014>
51. M. Nazemi, M. Moeini-Aghaie, M. Fotuhi-Firuzabad, P. Dehghanian, Energy storage planning for enhanced resilience of power distribution networks against earthquakes. *IEEE Trans. Sustain. Energy* **11**(2), 795–806 (2020). <https://doi.org/10.1109/TSSTE.2019.2907613>
52. K. Lai, Y. Wang, D. Shi, M.S. Illindala, X. Zhang, Z. Wang, A resilient power system operation strategy considering transmission line attacks. *IEEE Access* **6**, 70633–70643 (2018). <https://doi.org/10.1109/ACCESS.2018.2875854>
53. G. Huang, J. Wang, C. Chen, J. Qi, C. Guo, Integration of preventive and emergency responses for power grid resilience enhancement. *IEEE Trans. Power Syst.* **32**(6), 4451–4463 (2017). <https://doi.org/10.1109/TPWRS.2017.2685640>
54. C. Wang, Y. Hou, F. Qiu, S. Lei, K. Liu, Resilience enhancement with sequentially proactive operation strategies. *IEEE Trans. Power Syst.* **32**(4), 2847–2857 (2017). <https://doi.org/10.1109/TPWRS.2016.2622858>

55. Y. Wang, L. Huang, M. Shahidehpour, L.L. Lai, H. Yuan, F.Y. Xu, Resilience-constrained hourly unit commitment in electricity grids. *IEEE Trans. Power Syst.* **33**(5), 5604–5614 (2018). <https://doi.org/10.1109/TPWRS.2018.2817929>
56. A.S. Musleh, H.M. Khalid, S.M. Muyeen, A. Al-Durra, A prediction algorithm to enhance grid resilience toward cyber attacks in WAMCS applications. *IEEE Syst. J.* **13**(1), 710–719 (2019). <https://doi.org/10.1109/JSYST.2017.2741483>
57. M. Yan et al., Enhancing the transmission grid resilience in ice storms by optimal coordination of power system schedule with pre-positioning and routing of mobile DC de-icing devices. *IEEE Trans. Power Syst.* **34**(4), 2663–2674 (2019). <https://doi.org/10.1109/TPWRS.2019.2899496>
58. B. Taheri, A. Safdarian, M. Moeini-Aghtaie, M. Lehtonen, Enhancing resilience level of power distribution systems using proactive operational actions. *IEEE Access* **7**, 137378–137389 (2019). <https://doi.org/10.1109/ACCESS.2019.2941593>
59. M. Kamruzzaman, J. Duan, D. Shi, M. Benidris, A deep reinforcement learning-based multi-agent framework to enhance power system resilience using shunt resources. *IEEE Trans. Power Syst.* (2021). <https://doi.org/10.1109/TPWRS.2021.3078446>
60. B. Manyena, F. Machingura, P. O’Keefe, Disaster resilience integrated framework for transformation (DRIFT): a new approach to theorising and operationalising resilience. *World Dev.* **123** (2019). <https://doi.org/10.1016/J.WORLDDEV.2019.06.011>
61. Government of Malawi, in *SE4ALL Malawi Action Agenda* (2017)
62. R. Wyss, S. Mühlemeier, C.R. Binder, *An Indicator-Based Approach for Analysing the Resilience of Transitions for Energy Regions. Part II: Empirical Application to the Case of Weiz-Gleisdorf, Austria.* <https://doi.org/10.3390/en11092263>
63. D. Chattopadhyay, E. Spyrou, N. Mukhi, M. Bazilian, A. Vogt-Schilb, Building climate resilience into power systems plans: Reflections on potential ways forward for Bangladesh. *Electr. J.* **29**(7), 32–41 (2016). <https://doi.org/10.1016/j.tej.2016.08.007>
64. G. Harrison, *Climate Adaptation and Resilience in Climate Adaptation and Resilience in Energy Systems* gy
65. V.M. Nik, A.T.D. Perera, D. Chen, Towards climate resilient urban energy systems: a review. *Natl. Sci. Rev.* **8**(3) (2021). <https://doi.org/10.1093/nsr/nwaa134>
66. M.V. Martello, A.J. Whittle, J.M. Keenan, F.P. Salvucci, Evaluation of climate change resilience for Boston’s rail rapid transit network. *Transp. Res. Part D Transp. Environ.* **97** (2021). <https://doi.org/10.1016/j.trd.2021.102908>
67. M. Panteli et al., *Impact of Climate Change on the Resilience of the UK Power System* (2015)
68. L.M. Shakou, J.L. Wybo, G. Reniers, G. Boustras, Developing an innovative framework for enhancing the resilience of critical infrastructure to climate change. *Saf. Sci.* **118**, 364–378 (2019). <https://doi.org/10.1016/j.ssci.2019.05.019>
69. N. Kumar, V. Poonia, B.B. Gupta, M.K. Goyal, A novel framework for risk assessment and resilience of critical infrastructure towards climate change. *Technol. Forecast. Soc. Change* **165** (2021). <https://doi.org/10.1016/j.techfore.2020.120532>
70. J. Jasiūnas, P.D. Lund, J. Mikkola, Energy system resilience—a review. *Renew. Sustain. Energy Rev.* **150** (2021). <https://doi.org/10.1016/j.rser.2021.111476>
71. ESCOM, *Electricity Supply Corporation of Malawi: Presentation on Executive Exchange on Developing an Ancillary Service Market for SAPP*
72. Malawi: energy mix for electricity generation|GlobalPetrolPrices.com. [https://www.globalpetrolprices.com/energy\\_mix.php?countryId=81](https://www.globalpetrolprices.com/energy_mix.php?countryId=81). Accessed 12 Jul 2022
73. The Ministry of Energy, *The Status of Energy Policy* (2021)
74. The Electricity Supply Corporation of Malawi (ESCOM), in *The Status of Energy Policy* (2022)
75. D. Burillo, M.V. Chester, S. Pincetl, E.D. Fournier, J. Reyna, Forecasting peak electricity demand for Los Angeles considering higher air temperatures due to climate change. *Appl. Energy* **236**, 1–9 (2019). <https://doi.org/10.1016/j.apenergy.2018.11.039>
76. K. Handayani, T. Filatova, Y. Krozer, P. Anugrah, Seeking for a climate change mitigation and adaptation nexus: analysis of a long-term power system expansion. *Appl. Energy* **262**, 114485 (2020). <https://doi.org/10.1016/j.apenergy.2019.114485>

77. A. Arab, A. Khodaei, R. Eskandarpour, M.P. Thompson, Y. Wei, three lines of defense for wildfire risk management in electric power grids: a review. *IEEE Access* **9**, 61577–61593 (2021). <https://doi.org/10.1109/ACCESS.2021.3074477>
78. J. Sieber, Impacts of, and adaptation options to, extreme weather events and climate change concerning thermal power plants. *Clim. Change* **121**(1), 55–66 (2013). <https://doi.org/10.1007/s10584-013-0915-0>
79. Y. Fang, Y. Wei, Climate change adaptation on the Qinghai-Tibetan Plateau: the importance of solar energy utilization for rural household. *Renew. Sustain. Energy Rev.* **18**, 508–518 (2013). <https://doi.org/10.1016/j.rser.2012.10.037>
80. O.J. Guerra, D.A. Tejada, G.V. Reklaitis, Climate change impacts and adaptation strategies for a hydro-dominated power system via stochastic optimization. *Appl. Energy* **233–234**, 584–598 (2019). <https://doi.org/10.1016/j.apenergy.2018.10.045>
81. A. Sapkota, Z. Lu, H. Yang, J. Wang, Role of renewable energy technologies in rural communities' adaptation to climate change in Nepal. *Renew. Energy* **68**, 793–800 (2014). <https://doi.org/10.1016/j.renene.2014.03.003>
82. Republic of Zambia, *National Energy Policy*, (2019).
83. S. Mcmanus, E. Seville, D. Brunsdon, J. Vargo, in *Resilience Management: A Framework for Assessing and Improving the Resilience of Organisations* (2007), p. 79 [Online]. Available: <http://ir.canterbury.ac.nz/handle/10092/2808>
84. D. Stockemer, *Quantitative Methods for the Social Sciences*. (2019). <https://doi.org/10.1007/978-3-319-99118-4>
85. T. Makinde, “Problems of Policy Implementation in Developing Nations: The Nigerian Experience,” *Kamla Raj Enterprises*, **11**(1), 63–69 (2017). <https://doi.org/10.1080/09718923.2005.11892495>
86. Policy implementation. <https://journals.co.za/doi/epdf/10.10520/ejc-adminpub-v17-n4-a2> (accessed Jan. 22, 2023).
87. D. Millard, “The Role and Importance of Energy Statistics,” 2015.
88. T. D. Lujanskaya, “Energy Statistics: Importance, Challenges, Needs,” 2013. Accessed: Jan. 22, 2023. [Online]. Available: [http://www.inogate.org/documents/Session%206.1\\_Moldovan%20experience\\_AEER%20Energy%20Statistics\\_ENG.pdf](http://www.inogate.org/documents/Session%206.1_Moldovan%20experience_AEER%20Energy%20Statistics_ENG.pdf)

**Open Access** This chapter is licensed under the terms of the Creative Commons Attribution 4.0 International License (<http://creativecommons.org/licenses/by/4.0/>), which permits use, sharing, adaptation, distribution and reproduction in any medium or format, as long as you give appropriate credit to the original author(s) and the source, provide a link to the Creative Commons license and indicate if changes were made.

The images or other third party material in this chapter are included in the chapter's Creative Commons license, unless indicated otherwise in a credit line to the material. If material is not included in the chapter's Creative Commons license and your intended use is not permitted by statutory regulation or exceeds the permitted use, you will need to obtain permission directly from the copyright holder.





# Chapter 20

## Quantitative Assessment of Damage in Composites by Implementing Acousto-ultrasonics Technique



Kumar Shantanu Prasad, Gbanaibolou Jombo, Sikiru O. Ismail, Yong K. Chen, and Hom N. Dhakal

**Abstract** This study focused on quantitative damage severity assessment in composite materials using Acousto-Ultrasonics (AU), an in-service and active non-destructive inspection technique in which Lamb waves are communicated through a damaged zone. This was done by activating a signal onto the composite material surface and acquiring the received waves after their interactions with the damage. It relied on early research that presented a series of stress wave factors (SWFs) derived from the frequency-domain of the AU data, as quantitative identifiers of the received signal. Although, the SWFs have previously been proven to determine the understanding of the spatial arrangements of the impact damage, the degree or severity of the damage inside the impact damage area has not been assessed. Therefore, the current research was a step in the right way toward that aim. AU waves were generated via a laminate with increasing concentrations of ply faults, across longitudinal length. The stress wave factors were first examined for an undamaged composite, and the SWFs were then connected with the fault concentration. The significance of the found linkages and the possible futures of quantitative assessment of the degree of damage by such relationships were examined. The stress wave factors showed clear and consistent patterns, as the fault concentration increased. With a rise in fault density, an element measuring the energy content of the waves significantly changed with  $R\text{-sq}(\text{adj}) = 91.33\%$  and almost linearly, and provided a robust measurable trend, while other parameter exhibited lesser shifts with  $R\text{-sq}(\text{adj}) = 51.86\%$ . The result obtained from the presented work provided a base to cost-effective and in-service measure to early detection of catastrophic failures in composite structures, including the wind turbine blades for renewable and sustainable energy generation.

**Keywords** Acousto-ultrasonics · Non-destructive evaluation · Wave propagation · Wave dispersion · Stress wave factor

---

K. S. Prasad (✉) · G. Jombo · S. O. Ismail · Y. K. Chen  
Centre for Engineering Research, School of Physics, Engineering and Computer Science,  
University of Hertfordshire, Hatfield AL10 9AB, UK  
e-mail: [k.prasad@herts.ac.uk](mailto:k.prasad@herts.ac.uk)

H. N. Dhakal  
Advanced Polymers and Composites (APC) Research Group, School of Mechanical and Design  
Engineering, University of Portsmouth, Portsmouth PO1 3DJ, UK

## 20.1 Introduction

In spite of the fact that polymer composites are finding increasing uses in a diverse selection of constructions, there is always the possibility that its overall safe functionality might be compromised in specific circumstances. If somehow the boundaries for the commencement of damage or flaws are surpassed, this is the primary cause of unanticipated damage occurring in confined places, including such after an impact or in the stress concentration locations. These conditions include either of above cases. If the localised damage cannot be identified and proceeds to uncontrolled development of successive damage, ultimately malfunctions are probable to occur. These failures might be caused by a variety of factors. In order to give resistance to the accumulation of damage, steps are taken while the structural engineering phase. Nevertheless, in several circumstances, cost-effective design requires the implementation of structural health monitoring (SHM) procedures, while the structure is in operation. Although, appreciated works have been achieved in the area of SHM, a study [1] drew a conclusion that one of the most significant obstacles is making the shift from research to practice. Linking in-service monitoring of laminated composites to the status of a material in the localised damage zones is one of the obstacles that must be overcome. In order to overcome this challenge, this work proposed a damage severity assessment that was based on stress wave factors obtained by an AU approach.

## 20.2 Theory of Structural Health Monitoring Based on Acousto-ultrasonics

Many investigations of guided waves in damaged composite materials [2, 3] have been reported, but very few have focused on in-service damage detection and quantification. The quantitative approach should work for same-side assessment of a damaged composite material. With this in mind, the acousto-ultrasonics (AU) approach with pitch-catch setup was investigated. Figure 20.1 shows this localised damage inspection arrangement. Preliminary research on the AU approach [4, 5] used a stress wave factor to experimentally connect a performance measure assumed to represent the damage zone material condition with the acquired signal by introducing the stress wave factor (SWF). Such parameter, originally described in [4, 6] primarily and updated subsequently [7], counted maxima in the received signal employing some pre-specified constraints.

Time and frequency domain relationships are quite well known for steady Gaussian random transmissions. For the fairness of explaining the new SWFs, a quick description of relevant theory is as follows [8].

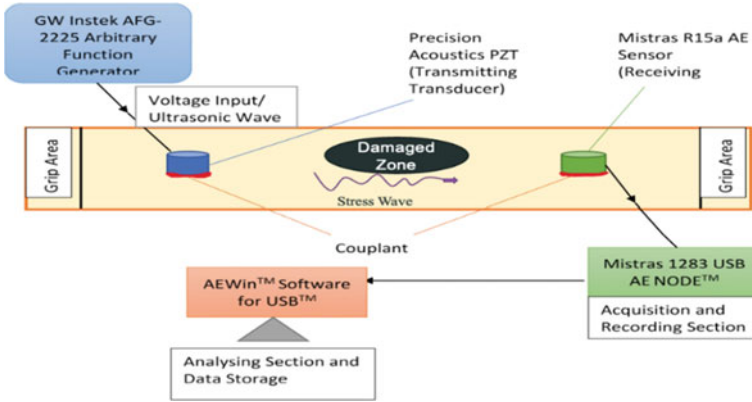


**Fig. 20.1** Acousto-ultrasonics approach with pitch-catch setup for detecting a faulty zone

Let  $(V_{avg})$  be an average voltage/signal and can be expressed as:

$$x(t) = V_{avg} = \sum_{i=1}^n \frac{V_i}{n} \tag{20.1}$$

and

$$V_i^u = V_i - V_a \tag{20.2}$$

where,  $(V_i)$  is the original voltage,  $(V_{avg})$  is the average voltage and  $(V_i^u)$  is the unbiased voltage values.

The FFT of  $x(t)$  or  $V_{avg}$  is needed to get the frequency domain descriptions [8] as shown:

$$W(f) = \int_{t_a}^{t_b} x(t)e^{-i\omega t} \tag{20.3}$$

where,  $(f)$  is the frequency and  $(t)$  is the time of the signal;  $\omega = 2\pi f$ .

The inverse conversion done at  $t = 0$  provides:

$$x(0) = \int_{f_a}^{f_b} W(f)df \tag{20.4}$$

### 20.2.1 Acousto-ultrasonics Components (SWFs)

Moment analysis was introduced to quantify AU components to get quantitative information from the Fourier transform [8]:

Generally, these can be calculated from the following:

$$M_s = \int_{f_a}^{f_b} W(f) f^s df \quad (20.5)$$

At  $s = 0$ :

$$M_0 = \int_{f_a}^{f_b} W(f) df \quad (20.6)$$

This graphically relates to the area under the power spectral density plot. Theoretically, it is the average square voltage and is the energy of the received signal. This value is stated as (A1):

$$A1 = M_0 \quad (20.7)$$

Next SWF is defined as:

$$A2 = \frac{M_1}{M_0} \quad (20.8)$$

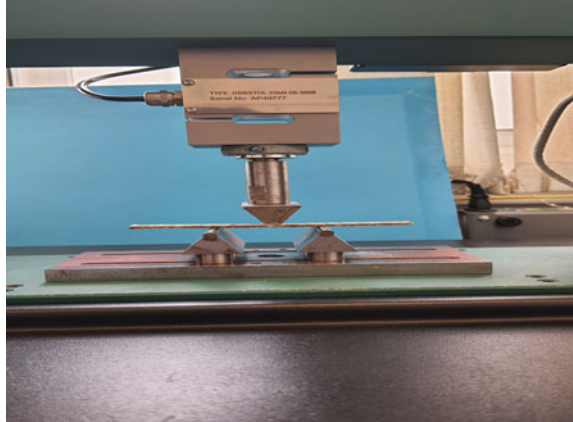
Graphically,  $A2 =$  Central Frequency.

Other SWFs are as follows:

$$\begin{aligned} A3 &= \left( \frac{M_2}{M_0} \right)^{0.5} \\ A4 &= \left( \frac{M_4}{M_2} \right)^{0.5} \\ A5 &= \frac{A4}{A3} \end{aligned} \quad (20.9)$$

The first two stress wave factors (Eqs. 20.7 and 20.8) are the shape and location of the power spectrum and are the most important SWFs. Hence, in this study only these two were considered.

**Fig. 20.2** Three-point bending test



## 20.3 Experimental Methodology

### 20.3.1 *Material and Mechanical Testing*

A carbon fibre reinforced polymer specimen of  $[90_8]_s$  was fabricated using epoxy/resin system with hand-layup. The flexural test was performed according to the ASTM D790 standard. The test samples were tested on a 3-point bending equipment with a span to thickness ratio of 16. The test sample has length, width and height of 125, 25 and 2 mm, respectively. The Tinius and Olsen universal testing machine was used with a feed rate of 2.5 mm/min, as shown in Fig. 20.2. The sample was subjected to ten progressively higher fractions of load, using the ultimate flexural strength as a maximum baseline and was ultrasonic C-scanned at every step for the fault concentration measurement.

The sample was examined using AU technique at each of the higher stresses. The method for measuring and analysing AU was subsequently elucidated.

### 20.3.2 *Acousto-ultrasonics Testing*

AU technique is premised on the idea that stress waves which have passed through a damage region and reacted with fractures emit acoustic energy. The American Society for Testing and Materials (ASTM) recognised the procedure by publishing “Acousto-Ultrasonic Assessment of Composites, Laminates and Bonded Joints” in 1992 and amended it in 2012 [7]. The Document describes pitch-catch, through-transmission and their variations as a sensor configuration.

### 20.3.2.1 Study for Undamaged Material

As a transmitter and a receiver, respectively, an ultrasonic piezo-electronic transducer with a frequency of 1 MHz and a resonant-type AE transducer with a resonance frequency of 150 MHz were used and placed at a distance of 80 mm from each other. Wax was used to connect sensors to the plate. Throughout the experiment, a sensor-to-testing-plate contact pressure of 0.060 MPa was employed. An arbitrary function generator was used to transmit a 3-cycle sine wave tone burst manual signal to the ultrasonic transducer. This signal was sent to a 50-dB RF power amplifier to increase the transmission wave to 5 V. Figure 20.3 shows the oscilloscope readings before and after the power amplifier.

Using AU Lamb wave theory, it was established that only the  $A_0$  and  $S_0$  modes transmitted in thin sheets under 1 MHz frequency [8]. Also, Because  $S_0$  has a larger phase velocity at these frequencies, the front component of the output signal was  $S_0$  wave phase. Thus, Fig. 20.4 depicts two pulse modes in a standard output signal and also the FFT/frequency domain of the output signal.

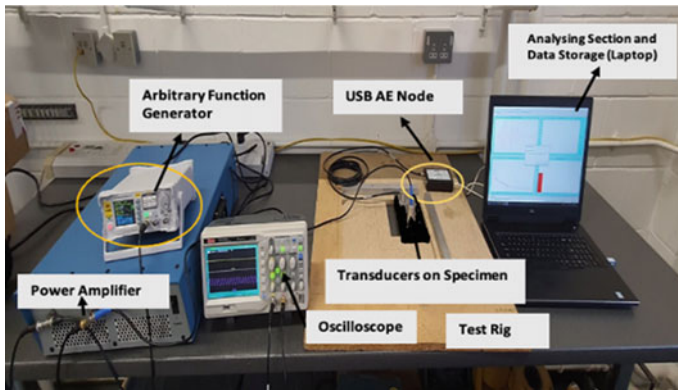


Fig. 20.3 Acousto ultrasonics experimental set-up

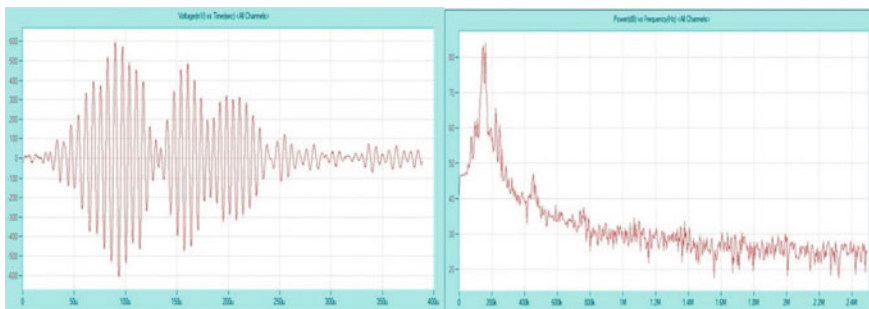
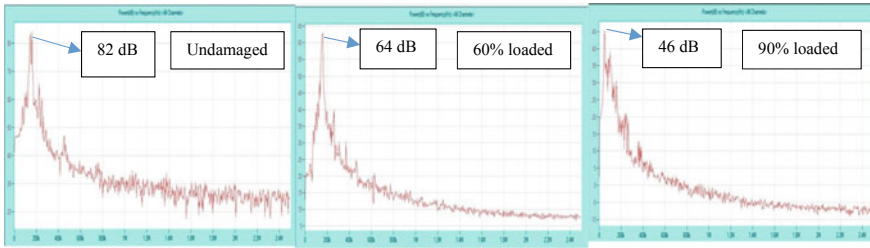


Fig. 20.4 Output signal in a time-domain b frequency-domain (FFT)



**Fig. 20.5** Frequency-domain plots of the initial (undamaged) sample compared with the loaded samples

### 20.3.2.2 Study for Damaged Material

Section 3.1 describes how to induce different-concentration fractures in the laminate. The sample was transferred from the testing equipment and AU signals were received as similar with the unbroken laminate. Frequency-domain graphs for each faulted specimen evaluated the signals. Figure 20.5 shows how these plots altered at two stress levels relative to zero load (undamaged sample).

## 20.4 Results and Discussion

Figures 20.6a, b depict that the suggested technique yielded significant trends in associations of SWFs and fault concentration. According to the in-service assessments, the existing non-destructive examination (NDE) can reveal damage existence and geometric extent, but not severity. SWF correlated with composite tensile strength [9]. This association was factual and not significant. Breakdown was tensile, compressive or shear strength. Before this final state, many failures happen from pre-existing degradation. The link across SWFs and fault concentration reflects material condition and external impulse response. Obviously, upon impact on a multi-layer composite, matrix cracking, fibre breakings, delamination and different crack densities across layer occurred. However, fault concentration was an integrative indicator of the flaws in the impacted zone, and similar to the SWF. It was related to the AU waves, which were associated with the faults across the same volume.

Due to the noticeable trend in the energy content, variations in the (A1) were predicted to measure the severity of damage (in this case, the fault concentration). In Fig. 20.6, the value of this component, derived using the signal's energy and normalised by its undamaged stage estimate, was displayed against the fault concentration. As shown in Fig. 20.6a, there was a definite association.

In actuality, the straight line in the illustration represents a linear connection that gives an indication of the damage severity (fault concentration). A2 is a representation of the received wave centre frequency. A decrease in this frequency indicated that a few of the high frequency component of the wave was dispersed, due to contact

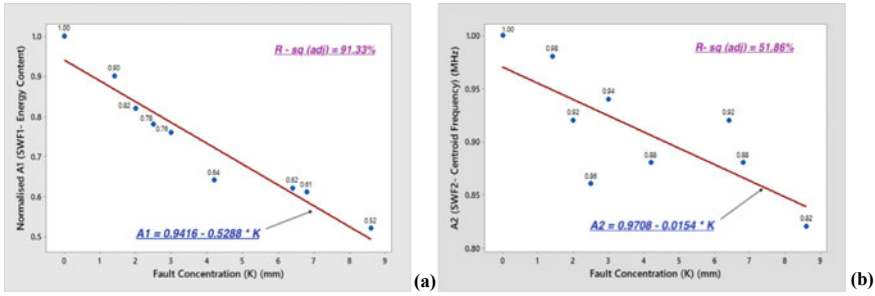


**Fig. 20.6** Variation in **a** A1 and **b** A2, SWF associated with energy content and central frequency with fault concentration (K), respectively

with faults. Figure 20.6b depicts the fluctuation of the (A2), as a function of fault concentration.

However, the entire decrease in central frequency (A2) from healthy to maximum fault concentration was a lower with  $R\text{-sq}(\text{adj}) = 51.86\%$  when compared with the (A1) change with  $R\text{-sq}(\text{adj}) = 91.33\%$ . Therefore, (A1) is a decent initial assessment of damage severity as per the  $R\text{-sq}(\text{adj})$  analysis, whereas (A2) provides further information.

### 20.5 Conclusion

This research quantified damage severity in laminated composites, using AU technique. Frequency-domain analysis was performed on the intact composite material. When the composite had varying fault concentrations, the same power spectrum (frequency-domain) exhibited differential modifications that might be characterised by previously suggested stress wave parameters based on spectral moments. Both stress wave factors increased with fault concentration. An element describing the energy content (A1) of the waves exhibited a substantial and obviously quantifiable trend with the rise in fault, whereas the other factor (A2) showed a lower change and seemed to indicate secondary alterations in the received waves that had engaged with the flaws. This current study offers a cost-effective and in-service technique, using AU to identify severe breakdowns in composite structures, as applicable to the wind turbine blades. Further investigations with other SWFs may provide more and detailed insights on the damage severity, in the future work.

**Acknowledgements** This research was funded by DTA3/H2020 as a part of COFUND programme with University of Hertfordshire through University Alliance Scheme.



## References

1. C. Farrar, K. Worden, An introduction to structural health monitoring. *Phil. Trans. R. Soc. A* **365**, 303–315 (2007)
2. Z. Su, L. Ye, Y. Lu, Guided Lamb waves for identification of damage in composite structures: a review. *J. Sound Vib.* **295**, 753–780 (2006)
3. Z. Su, L. Ye, *Identification of Damage Using Lamb Waves* (Springer, London, 2009)
4. A. Vary, K. Bowles, An ultrasonic-acoustic technique for nondestructive evaluation of fiber composite quality. *Polym. Eng. Sci.* **19**, 373–376 (1979)
5. H. Kautz, *Ray Propagation Path Analysis of Acousto-Ultrasonic Signals in Composites* (NASA Technical Memorandum, 2013), pp. 1–19
6. A. Vary, *The Acousto-Ultrasonic Approach* (Springer, Boston, 1988)
7. ASTM E1495/E1495M : Standard Guide for Acousto-Ultrasonic Assessment of Composites, Laminates, and Bonded Joints (n.d.). [https://global.ihs.com/doc\\_detail.cfm?document\\_name=ASTME1495%2FE1495M&item\\_s\\_key=00592876](https://global.ihs.com/doc_detail.cfm?document_name=ASTME1495%2FE1495M&item_s_key=00592876). Accessed 20 July 2022
8. M. Kiernan, J. Duke, PC analysis of an acousto-ultrasonic signal. *Mater. Eval.* **46**, 1344–1352 (1996)
9. P. Bajpai, I. Singh, *Reinforced Polymer Composites: Processing, Characterization and Post Life Cycle Assessment* (Wiley, London, 2020)

**Open Access** This chapter is licensed under the terms of the Creative Commons Attribution 4.0 International License (<http://creativecommons.org/licenses/by/4.0/>), which permits use, sharing, adaptation, distribution and reproduction in any medium or format, as long as you give appropriate credit to the original author(s) and the source, provide a link to the Creative Commons license and indicate if changes were made.

The images or other third party material in this chapter are included in the chapter's Creative Commons license, unless indicated otherwise in a credit line to the material. If material is not included in the chapter's Creative Commons license and your intended use is not permitted by statutory regulation or exceeds the permitted use, you will need to obtain permission directly from the copyright holder.



# Chapter 21

## Multiple-Criteria Optimization of Residential Buildings Envelope Toward nZEBs: Simplified Approach for Damascus Post-war



Lina A. Khaddour and Siegfried K. Yeboah

**Abstract** Syria faces significant challenges in optimizing residential building energy consumption to subsequently reduce CO<sub>2</sub> emissions due to its conventional construction methods and systems, exacerbated by the recent conflict. Post-war re-construction provides new opportunities for improvement in building standards through the 2009 BIC insulation code towards nearly Zero Energy Buildings (nZEBs). However, the decline in economy growth poses significant challenges. In this study, we formulate a simplified building envelope selection approach using multi-criterion optimization methodology based on simulated thermal loads using IESVE and cost-energy trade-off. IESVE was used to evaluate the thermal performances of five cases representing 5 different building envelope structures on existing buildings in Damascus, Syria. Four out of the five cases were BIC compliant, and their thermal performances and cost energy trade-offs were evaluated against that of a conventional building representing the construction-as-usual case. Payback on the investment in insulation improvement of the envelope structures were also calculated. The results overall shows that the envelope structures incorporating insulation layer reduced annual heating, cooling, and combined energy loads of those buildings. Comparatively, these improvements were slightly better under winter conditions than in summer. Based on payback period analysis, none of the improvements provided acceptable economical payback within five years, as energy consumption tariffs were extremely low and insulation material costs were extremely high. A Multi-Criteria Decision Making (MCDM) framework was developed and applied to the cases investigated. Based on the limitations of the BIC, no optimal solution was obtained. However, the framework provides a good basis for stakeholders to make sound decisions in transitioning buildings especially under post war context towards nZEBs.

---

L. A. Khaddour (✉)

School of Computing, Engineering and the Built Environment, Edinburgh Napier University, Edinburgh, UK

e-mail: [L.Khaddour@napier.ac.uk](mailto:L.Khaddour@napier.ac.uk)

S. K. Yeboah

School of the Built Environment and Architecture, London South Bank University, London, UK

© The Author(s) 2023

J. D. Nixon et al. (eds.), *Energy and Sustainable Futures: Proceedings of the 3rd ICESF*, 2022, Springer Proceedings in Energy, [https://doi.org/10.1007/978-3-031-30960-1\\_21](https://doi.org/10.1007/978-3-031-30960-1_21)

219

**Keywords** Insulation · Housing · Energy · Simulation · Thermal loads

### *Nomenclature*

$A$	Total envelope area ( $m^2$ )
$A_s$	Annual savings in running energy consumption considered for 50 years lifetime
$C_{\text{enr}}$	Energy cost actual value over $n = 50$ years housing life-cycle
$C_t$	Total cost per wall surface square meter which includes $C_{\text{enr}}$ (the running energy cost present value)
$C_i$	(The insulation purchase and installation costs)
$d$	Time value of money during $n = 50$ years housing life-cycle
$d_i$	Layer thickness (m) where $i$ is the number of layers
$i$	Inflation rate effects on energy cost
$PWF$	Present Worth Factor
$R_i$	Thermal resistance ( $K.m$ )/W
$R_T$	Thermal resistance ( $K.m^2$ )/W
$R_{Se}$	Heat transfer resistance (externally) ( $K.m^2$ )/W (Table 21.1)
$R_{Si}$	Heat transfer resistance (internally) ( $K.m^2$ )/W (Table 21.1)
$\Delta T$	Temperature difference [k]
$U$	Heat transmission $W/(K.m^2)$

### *Greek Letters*

$\lambda_i$	Thermal conductivity $W/(K.m)$
$\Phi$	Is measured in units of Power [W] (i.e. energy units per second)

## **21.1 Introduction**

Between 1990 and 2019, global CO<sub>2</sub> emissions from buildings increased by 50%, while global final energy demand from buildings grew by 38%. Over the same period global final electricity demand increased by 161% out of which residential buildings accounted for 70% (90 EJ) [1]. By 2020, buildings accounted for 36% of global energy demand and 37% of energy-related CO<sub>2</sub> emissions [1]. To place the building sector on-track to net zero emissions by 2050, IEA [2] proposes a move towards nearly Zero Energy Buildings (nZEBs) improvement pathway, increasing the share of building stock that is zero carbon ready, increasing the stock of solar thermal

systems, growing solar PV generation and ensuring all new buildings are zero-carbon-ready by 2030. Decarbonizing the building sector requires cutting down on energy consumption and increasing nZEBs investments [1]. However, significant challenges exist for developing countries in terms of investment R&D in nZEBs, viable building techniques, building standards and regulations [3].

Post war Syria faces significant challenges including a slow economy, difficulties in accessing affordable and reliable energy supplies, decline in construction sector activities amongst many others. The war created chaos in the country's energy sector dramatically diminishing oil and natural gas production [3]. This severely affected economic activities between 2011 and 2020 as the state electricity supply reduced to 15% of 2010 capacity [3]. Current available energy hardly supports half the housing energy demand resulting in long hours of power cuts, decreased families heating fuel allocations and increasing energy prices [1]. The country's post-war reconstruction has experienced significant growth in demand for energy efficient affordable housing, mainly due to the wartime disruption, infrastructural damage, scarcity, and sanctions [4]. This move potentially can help reduce energy consumption and CO<sub>2</sub> emissions as Syria's residential buildings contribute to 49% of the country's energy consumption and up to 40% of the energy-related carbon emissions [3].

Successful, orderly, and broad-based transitions to nZEBs where Syria benefits from global investment will depend on adapting new energy efficient codes and building regulations. Syria's post-war energy sector involves varied and often complex interactions between electricity, fuels, and storage markets, creating fresh challenges for regulation and buildings design [3]. Its construction sector traditionally has challenges in its methods and systems that negatively impacts the environment and consume significant natural resources [4]. Customarily, there is the widespread use of unsustainable construction materials that does not fit with the climate, occupants' wellbeing, and environmental requirements [4].

Increasing the heat transfer resistance of the building envelope is one of the key approaches towards reducing building energy consumption towards achieving nZEBs ([5, 6]). Many countries around the globe have developed building insulation codes to enhance housing energy-saving towards minimizing negative environmental impacts. Syria has initiated similar steps through the Building Insulation Code (BIC), Energy Efficiency for Homes Labels in addition to the Energy Conservation Law enacted in 2009 by the National Centre for Energy Research (NCER). The BIC sets an objective of 20% reduction of energy demand, 20% reduction of CO<sub>2</sub> emission, and 20% increase of renewable energy introduction by 2020. It contains five Chapters and seven Appendices covering the general requirements, building envelope scope and thermal compliance, building insulation material selection and implementation, humidity in buildings and operational energy efficiency. It also sets standards for envelop components compliance parameters such as the ratio of openable window to floor area, windows thermal transmittance (U-window), roof thermal performance (U-roof) and external walls thermal transmittance (U-wall), based on the climate zone [6]. There are many barriers for implementing BIC towards nZEBs. For instance, Khaddour [7] identified the main barriers including economic (e.g. low financial

horizons, investment risk, sanction, and limited income), institutional (e.g. insufficient regulatory processes, lack of essential enforced regulations, poor knowledge and professional expertise) and behavioural customs (e.g. routines, and important behavioural characteristics, lack of knowledge about potential for conserving, undervaluing and lacking interest in Energy Efficiency) that threatens the implementation of such measures towards nZEBs [7].

Reviewing the BIC insulation code, it is apparent that selecting building envelope construction technique that complies with thermal comfort, energy efficiency, low building thermal loads and cost-saving towards nZEBs will be a new challenge for Syria's post-war re-construction. Hence, the aim of this study is to develop a simplified building envelope selection approach using multi-criterion optimization methodology, simulated thermal loads (IESVE heating and cooling) and cost-energy trade-off, to assist engineers in the early-design phases of new residential projects to achieve expense-efficient energy performance solutions. The selection criteria were used to examine efficient envelop structures suitable for the climate in Damascus.

## 21.2 Methodology

The research was on a case study of building performance in Damascus, Syria. Five cases representing 5 different building envelope structures on existing buildings in Damascus were investigated. The research focused on the analysis of data from a conventional building and an energy-efficient pilot building project in Damascus. The thermal performances of the 5 cases representing the different building envelope structures were evaluated via simulation using IESVE. After the thermal performance analysis, cost-energy efficiency trade-off and payback period were calculated for the five cases. A simplified multiple-criteria decision approach was then developed to assess the appropriate building envelop technique suitable for the climate in Damascus.

### 21.2.1 *The Case Study*

The case study area is Damascus (36° 13' N, 33° 29' E). It is in the southern part of Syria, about 80km from the western side of the Mediterranean Sea and separated by mountains bordering Lebanon. In summer, cooling is typically required for approximately 120 days from 1st June to 31st September. In winter, heating is typically required for roughly 150 days from 15th November to 15th April. At the peak of summer, Damascus records maximum temperatures of around 40°C whereas in winter the lowest temperature is about - 2 °C. All the five cases have same building design and total external wall surface area of 398 m<sup>2</sup> each. Figure 21.1 shows the case study building with external insulation layer.

**Fig. 21.1** Case 1 the pilot project compliant building



The building envelope structures and components U-values for the 5 cases calculated based on Eq. (21.1) from the BIC document- Appendix 4 [6] are presented in Table 21.1.

The envelope material specifications including thermal resistance properties and thickness obtained from the building contract specifications were used to calculate the U-values in Table 21.1 by applying Eq. (21.1).

$$U = \frac{1}{R_T} = \frac{1}{R_{Se} + \frac{d_1}{\lambda_1} + \frac{d_2}{\lambda_2} + \dots + R_{Si}} \quad (21.1)$$

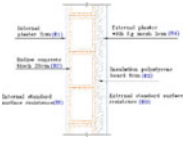
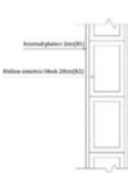
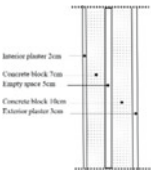
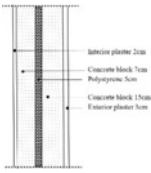
The building envelope structures and components surface resistances for upward and horizontal flow directions are presented in Table 21.2.

### 21.2.2 Simulation Methodology

The thermal loads for the 5 cases were simulated in IESVE to evaluate the BIC compliance of the buildings' envelope structures. The key requirements here were the building models with the respective 5 envelope structures, thermal properties data for the materials and weather data for Damascus. The cases were modelled following typical Syrian residential design parameters of 7.8 W/m<sup>2</sup> lighting power density, 8.0 W/m<sup>2</sup> equipment power density and 25.5 m<sup>2</sup>/person average occupancy density. For this reason, there were variations in annual heating and cooling load estimations due to the variation in parameters and envelope construction materials.

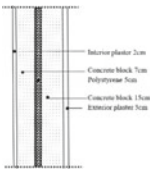
It was assumed that envelope inside and outside surfaces had the same surrounding air temperature, thermal conductivity coefficients, convection, and radiation properties. Yearly thermal loads were calculated for each day of the summer cooling season (June to September) and for winter heating season (November to April). The fixed indoor comfort design temperature was 22 °C in summer and 19 °C in winter. The

**Table 21.1** Building envelope structures and components U-values

Cases	Wall cross section	External wall construction technique	Overall wall thickness (cm)	Wall U-value (W/m <sup>2</sup> /k)	Glazing U-value (W/m <sup>2</sup> /k) (material specification)	Roof U-value (W/m <sup>2</sup> /k)
Case-1		20 cm Concrete block, 5 cm polystyrene & 2 cm internal mortar, and 3 cm external cement mortar	30	0.44	1.9	0.4
Case-2		20 cm concrete block & 2 cm internal mortar and 3 cm external cement mortar (Base line)	25	2.045		2.69
Case-3		(7 cm and 10 cm) Double Concrete block, 5 cm empty space, 2 cm internal mortar and 3 cm external cement mortar	27	1.4	1.9	2.69
Case-4		(7 cm and 15 cm) Double Concrete block, 5 cm polystyrene and 2 cm internal mortar and 3 cm external cement mortar	32	0.15	1.9	2.69

(continued)

**Table 21.1** (continued)

Cases	Wall cross section	External wall construction technique	Overall wall thickness (cm)	Wall U-value (W/m <sup>2</sup> /k)	Glazing U-value (W/m <sup>2</sup> /k) (material specification)	Roof U-value (W/m <sup>2</sup> /k)
Case-5		(7 cm and 10 cm) Double Concrete block, 5 cm styropor, 2 cm internal mortar and 3 cm external cement mortar	27	0.2	1.9	2.69

**Table 21.2** BIC Building Envelope and Surface resistance

Surface resistance (K·m <sup>2</sup> /W)	Heat flow direction	
	Upward	Horizontal
$R_{s,i}$	0.1	0.13
$R_{s,e}$	0.04	0.04

selected design Window to Floor Ratio (WFR) was determined to be 16.66% for all cases. Daily thermal loads were then added up for each season to obtain annual cooling and heating loads. The estimated wind speed was assumed to be 5.5m/s. The heat loss through the building was calculated using Eq. (21.2).

$$\Phi = (\sigma A_i \times U_i) \times \Delta T \tag{21.2}$$

( $\sigma A_i \times U_i$ ) is the sum of all heat transfer areas (walls, roof, windows, etc.)

The BIC [6] specifies the maximum (allowable) U-values hence those values were considered in the simulation. Each building wall had (n) layers of different materials and thicknesses. The building envelope design temperature  $T_i$  was specified as fixed on the inside surface, whereas the outside surface was exposed to the periodic temperature variation per the weather data. The cooling load and heating load were evaluated for each case. The five cases used the same building design as shown in Fig. 21.1 but with different envelope structures as specified for the cases in Table 21.1. The percentage improvement for annual total, annual heating or annual cooling load was determined using Eq. (21.3).

$$\% \text{ Improvement} = \frac{[\Phi_{Baseline(Total \text{ or Heating or Cooling})} - \Phi_{Total \text{ or Heating or Cooling}}]}{\Phi_{Baseline(Total \text{ or Heating or Cooling})}} \tag{21.3}$$



### 21.3 Results and Discussion

The simulation results cover the annual cooling and heating transmission loads per square meter for both cooling and heating seasons for the different envelope structures. The results presented in Table 21.3 show significant impact of envelope structure on building thermal performance. Case-2, the baseline building with no insulation (conventional building), had the highest heating and cooling loads with a total of 345.1 MWh. Out of the four BIC compliant cases (1, 3, 4 and 5), the best improvement was achieved with case-4 with total heating and cooling annual load of (72.5153 MWh). The polystyrene insulation in case-4 achieved slightly better results than the styropor insulation layer in case-5. The worst envelope performance among the selected BIC compliant cases was case-3 with higher values of annual transmission loads of 185.5054 MWh due to the empty cavity space in the walls resulting in a high u-value of 1.4 W/m<sup>2</sup>/k. The results overall shows that having the envelope structure incorporating insulation layer reduced the annual heating, cooling, and combined energy loads. For cases 1, 3, 4 and 5 respectively, the % improvement in annual cooling loads achieved from the simulation ranged between 62 and 79% depending on the envelope structure improvement type. For heating, the % improvement ranged between 61 and 89%, also depending on the envelope structure utilized. The combined % improvement for the annual total energy utilized for cases 1, 3, 4 and 5 respectively were 78.89%, 61.53%, 84.96% and 84.23%. It is evident from the results that the envelope structure improvement resulted in a slightly better winter building thermal performance than summer.

### 21.4 Payback Period Analysis

Equations (21.4, 21.5 and 21.6), payback calculation method developed by Sullivan et al. [8] were used to calculate the payback on investment in the envelope structure. This approach was used to calculate the payback in years for all cases to allow comparison between the BIC compliant cases (1, 3, 4, 5) and case 2, the baseline. Here considerations were made in terms of the initial cost of materials and construction and the running costs once the envelope structure was installed and functioning.

$$PWF = \sum_{u=1}^n \left( \frac{1+i}{1+d} \right)^u = \begin{cases} \frac{1+i}{d-i} \left[ 1 - \left( \frac{1+i}{1+d} \right)^n \right] & i \neq d \\ \frac{n}{1+i} & i = d \end{cases} \quad (21.4)$$

$$C_{enr} = PWF \left( \frac{Q_c}{COP} \frac{C_{el}}{(3.6 \times 10^6)} + \frac{Q_h}{H_u \eta_s} C_g \right) \quad (21.5)$$

$$C_t = C_{enr} + C_i = PWF \left( \frac{Q_c}{COP} \frac{C_{el}}{(3.6 \times 10^6)} + \frac{Q_h}{H_u \eta_s} C_g \right) + C_{ins} L_{ins} \quad (21.6)$$

**Table 21.3** Annual loads including heating and cooling (calculated with IESVE) for the five cases

Cases	Annual cooling load (MWh)	Annual heating load (MWh)	Total annual energy load (MWh)	% Improvement—annual cooling loads (%)	% Improvement—annual heating loads (%)	% Improvement—total annual energy loads (%)
Case1	59,4931	40,4489	99,942	72.77	88.66	78.89
Case2	218,4933	263,6767	482.17	Baseline		
Case3	83,383	102,1224	185,5054	61.84	61.27	61.53
Case4	44,2974	28,2179	72,5153	79.73	89.30	84.96
Case5	45,294	30,7593	76,0533	79.27	88.33	84.23

The inflation rate effect on energy cost was determined by Eq. (21.7)

$$PWF = \frac{C_i}{A_s} \quad (21.7)$$

From the calculated results, the payback periods for cases 1, 3, 4 and 5 were 10.5, 7.8, 15.7 and 13.1 years respectively. Sullivan et al. [8] considered the payback period to be acceptable economically if it is within five years. Therefore, neither of the selected cases evaluated were profitable or economically viable as all payback periods were longer than five (5) years. The main reasons for the long payback periods are that the Syrian tariff for household energy consumption is extremely low while the cost of the imported insulation materials is very high [5]. This does not translate into affordable housing as developers aim to sell at a market price regardless of construction cost savings.

## 21.5 Multiple-Criteria Optimization Analysis

Determining the best building envelope solution towards nZEBs requires consideration of many design variables and factors, such as building thermal performance, CO<sub>2</sub> emissions, construction and running costs etc. This is challenging as these variables affect each other and their individual optimisation goals can change significantly. Figure 21.2 shows a phased approach towards decision making in the transition to nZEBs. The simplified criteria shown are targeted to guide decision making towards nZEBs in Syria. This phased approach can be applied to the concept of nZEBs and assigned with values and weights to assess the post-war reconstruction. It can incorporate a synthesized list of energy efficient indicators associated with post-war housing to enable decision makers to undergo a Multi-Criteria Decision Making (MCDM) process that considers their objectives and priorities. The MCDM in Fig. 21.2 consists of the following phases: (a) objective identification; (b) criteria development; (c) alternative generation, evaluation, and selection; (d) implementation and monitoring [8]. It can enhance the handling of the energy sector uncertainty, the demand for housing, deal with multiple project requirements and address conflicts amongst stakeholders [9]. The framework in Figure (2) considers nZEBs' key decision makers such as regulators/policy makers, project managers, contractors (private, public, PPP), consultants, designers, and property developers/owners. Other major industry stakeholders, out of this study's scope, include building material manufacturers, suppliers, international partners, and new buyers. Their opinions could be integrated into a more comprehensive approach in future research.

nZEBs should be scheduled in a precise order based on each country priorities, assessing the possibility of any knock-on effects. Seminara et al. [9] suggests a cost-effective method, with an approach that aims to improve building envelop first

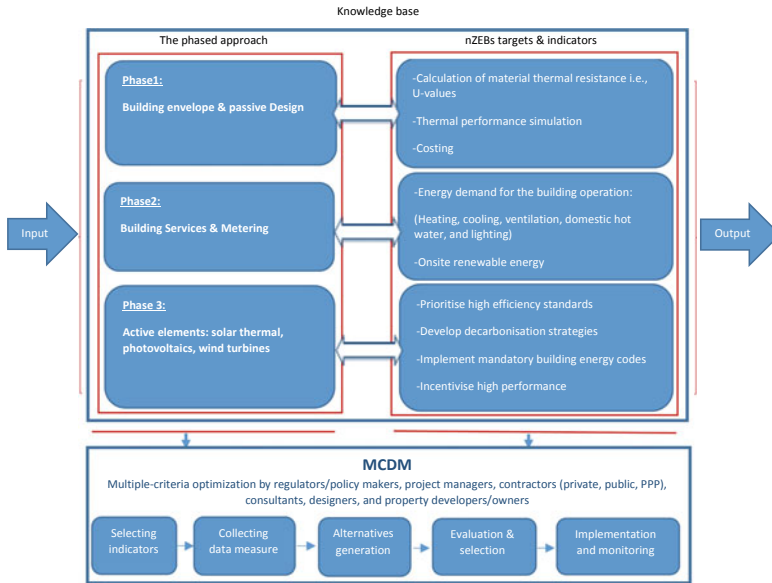


Fig. 21.2 Simplified multiple-criteria optimization analysis of residential buildings envelope

followed by building services then more active elements. In this sense our framework in Figure (2) has three levels (Phases) with the following roles: **Phase 1**—Building envelope and passive design. This could start form the Pre-design phase to assist the owner, planner and others involved at the planning (pre-design) stage of the project. This phase’s main indicators are calculation of material thermal resistance i.e., U-values, using thermal performance simulation and costing analysis). **Phase 2**—Building services and metering offers a self-assessment check system that allows architects and engineers to raise nZEBs under consideration during its design process. Assessments here is based on the design specification and the anticipated performance of building operations (heating, cooling, ventilation, domestic hot water, and lighting and potentially onsite renewable energy). **Phase 3**—Active elements. This has the highest cost implications as it involves the inclusion of solar thermal, photovoltaics, and wind turbines etc. The main indicators at this phase are prioritising high efficiency standards, developing decarbonisation strategies, implementing mandatory building energy code for high nZEBs performance.

The key inputs are climate zones data and design specifications. The knowledge base in Figure (2) is to assist in grasping measurable nZEBs indicators such as the thermal performance, cost estimate, payback period at the Pre-design stage. The framework output indicators help to evaluate/rate the level of impact of nZEBs targets for decision making. The MCDM follows each phase developed criteria and indicators to evaluate the alternatives based on collecting data, cost calculations, and thermal performance simulation. The monitoring stage allows decision making by

Client/Owner via monitoring of the overall construction status (by contractor) and building risk register updates (by project team).

Considering the economic and technical challenges associated with the post-war reconstruction of Damascus, improving building envelope insulation appears to be an effective approach towards nZEBs. To apply the simplified multiple-criteria optimization framework in Figure (2) to the five cases studies, output indicators were outlined as shown in Table 21.4. The incorporation of the insulation material in the envelope structure resulted in a reduction in heat losses. Each envelope (material and construction) costs were calculated, according to 2020 market prices in Syrian pounds per square meter (SP/m<sup>2</sup>). This resulted in cost increases ranging between 27.3 and 54.5% above baseline levels. Case 4 was found to have the best thermal performance improvement but the highest increase in material and construction cost whereas the cheapest compliant solution, case 3, had the lowest thermal performance. The payback calculated showed that none of the four compliant cases met the 5-year payback threshold hence all were considered unacceptable economically for affordable housing as developers aim to sell at a market price regardless of energy cost savings. Despite it's the cases being BIC compliance, none of them proved the cases to be optimal solution.

To reach an optimal envelope solution a couple of considerations need to be made. Firstly, it may be necessary to generate alternative envelope solutions based on the locally available materials that can be cheaply accessed in significant quantities. This is because, the availability and installation capacity for insulation material, is a dominant factor in the selection of appropriate building envelope under post-war reconstruction condition. Despite compliant buildings higher initial cost, the simplified analysis shows that there is the need to minimize the total cost over building lifetime which includes the insulation (purchase and installation) and the energy (consumption and maintenance) costs. Secondly, the BIC will benefit from a rating scale to drive building envelope selection. Various internationally recognized building rating and certification systems value the improvements in building envelope performance in relation to thermal performance and reductions in energy/emission

**Table 21.4** Simplified multiple-criteria optimization analysis applied for the five cases

Building Envelop Output Indicators						
Cases	Annual cooling load (MWh)	Annual heating load (MWh)	Total annual energy load (MWh)	Envelope cost (Syrian pounds SP/m <sup>2</sup> )	Payback period (Years)	BIC compliant
Case 1	59.4931	40.4489	99.942	30,000	10.5	Yes
Case 2	59.4931	40.4489	99.942	22,000	–	No (baseline case)
Case 3	218.4933	263.6767	482.17	28,000	7.8	Yes
Case 4	83.383	102.1224	185.5054	34,000	15.7	Yes
Case 5	44.2974	28.2179	72.5153	32,000	13.1	Yes

consumption. The USA's LEED, for example, offers one credit point for buildings that offer good level of thermal comfort system control by personal occupant [10]. The UK's BREEAM offers two credits for thermal comfort system control by personal occupant [11]. Japan's CASBEE rating identifies five levels of control [11] and Australia's Green Star offers two points for buildings that facilitate individual control of thermal comfort [12]. These credits and ratings are non-existent in the BIC hence a compliant building may still consume significant amounts of energy and emit significant CO<sub>2</sub> yet will pass compliance. This obviously will not help with the transition of post-war reconstruction buildings to nZEBs in Syria as cost challenges may unlikely encourage investors to spend toward nZEBs when they are BIC compliant [13–15]. In comparison to previous research on multi-approach decision making toward energy-efficient buildings [16–18], the results obtained by this research can be replicable for multi-target decision-making-objectives and optimisation goals so that different actors can decide between optimal solutions for different objectives. In this sense, BIC no doubt can be considered as the first steps towards a low carbon future for Syria however it will need to be reviewed and improved with low carbon targets to push newly constructed buildings towards nZEBs.

## 21.6 Conclusion

A simplified building envelope selection approach using multi-criterion optimization methodology, simulated thermal loads (IESVE heating and cooling) and cost-energy trade-off, for a pilot project in Damascus, Syria has been investigated.

- The results obtained from the IESVE simulation shows that for BIC compliant cases 1, 3, 4 and 5 respectively, the % improvement in annual cooling loads ranged between 62 and 79% depending on the envelope structure. For the same cases in winter, the % improvement ranged between 61 and 89%. Overall, combined % improvement of annual total energy utilized for the cases (1, 3, 4 and 5) were 78.89%, 61.53%, 84.96% and 84.23% respectively.
- The payback analysis for the investment in the envelope structures represented by the BIC compliant cases, 1, 3, 4 and 5 returned 10.5, 7.8, 15.7 and 13.1 years respectively. These long payback periods were deemed unacceptable economically as they exceeded the typical 5 years threshold of acceptable economic payback period.
- The results obtained were also applied to multiple objectives and optimisation goals for a multi-target decision-making framework so that different actors can decide between optimal solutions for different objectives. The findings yielded no singular optimal solution from all the cases investigated. However, the Multi-Criteria Decision Making (MCDM) framework developed offers opportunities for regulators/policy makers, project managers, contractors (private, public, PPP), consultants, designers, and property developers/owners to address conflicts and consider their objectives and priorities in a structured manner.

Occupant behaviour can influence the performance of nZEBs especially when they embark on modification to have control on buildings. Hence, we recommend that future studies consider the influence of occupants' behaviour in developing effective nZEBs indicators in post war reconstruction.

## References

1. IPCC, Climate Change 2022: mitigation of climate change, in *Working Group III contribution to the Sixth Assessment Report of the Intergovernmental Panel on Climate Change. IPCC AR6 WG III* (2022). Available at [https://report.ipcc.ch/ar6wg3/pdf/IPCC\\_AR6\\_WGIII\\_FinalDraft\\_Chapter09.pdf](https://report.ipcc.ch/ar6wg3/pdf/IPCC_AR6_WGIII_FinalDraft_Chapter09.pdf)
2. I. Hamilton, O. Rapf, D.J. Kockat, D.S. Zuhaib, T. Abergel, M. Oppermann, M. Otto, S. Loran, N. Nass, 2021 Global status report for buildings and construction. United Nations Environmental Programme (2020)
3. B. Hassan, M. Beshara, Using renewable energy criteria for construction method selection in Syrian buildings. *Jordan J. Mech. Indust. Eng.* **13**(2), 125–130 (2019)
4. M. Abogheda, M.F. Altan, Recommendations for constructing green buildings in Syria. *MAS J. Appl. Sci.* **6**(1), 175–185 (2021)
5. H. Li, Y. Li, Z. Wang, S. Shao, G. Deng, H. Xue, Z. Xu, Y. Yang, Integrated building envelope performance evaluation method towards nearly zero energy buildings based on operation data. *Energy Build.* **268**, 112219 (2022), ISSN 0378-7788. <https://doi.org/10.1016/j.enbuild.2022.112219>
6. BIC, The Syrian building insulation code the national centre for energy research (NCER) (2009). Available in Arabic online: <https://civteam.files.wordpress.com/2012/02/d8a7d984d985d984d8add9824-d8a7d984d8b9d8b2d984-d8a7d984d8add8b1d8a7d8b1d98a.pdf>
7. L.A. Khaddour, Comparative analysis of residential building envelopes newly implementing the building insulation code in Damascus. *Int. J. Environ. Sci. Technol. (IJEST)* (2023). Accepted, ref: JEST-D-20-01595R2
8. W.G. Sullivan, E.M. Wicks, C.P. Koelling, *Engineering Economy*. 16th edn. Pearson (2015). J. Vivian, U. Chioldarelli, G. Emmi, A. Zarrella, A sensitivity analysis on the heating and cooling energy flexibility of residential buildings. *Sustain Cities Soc.* **52**, 101815 (2020). <https://doi.org/10.1016/j.scs.2019.101815>
9. P. Seminara, B. Vand, S.M. Sajjadian, L. Tupenaite, Assessing and monitoring of building performance by diverse methods. *Sustainability* **14**(3), 1242 (2022)
10. USGBC, Green building design and construction: LEED reference guide for green building design and construction, Washington, DC, US Green building council (2009). [https://www.usgbc.org/sites/default/files/LEED%202009%20RG%20BD%2BC\\_Supplement\\_GLOBAL\\_10\\_2014\\_Update.pdf](https://www.usgbc.org/sites/default/files/LEED%202009%20RG%20BD%2BC_Supplement_GLOBAL_10_2014_Update.pdf)
11. R.J. de Dear, T. Akimoto, E.A. Arens, G. Brager, C. Candido, K.W.D. Cheong, B. Li, N. Nishihara, S.C. Sekhar, S. Tanabe, Y. Zhu, Progress in thermal comfort research over the last twenty years. *Indoor air*, **23**(6), 442–461 (2013). <https://doi.org/10.1111/ina.12046>
12. GBCA, Technical manual: green star office design and office as built v3, Sydney, Australia, green building council of Australia (2010). <https://new.gbca.org.au/green-star/rating-system/>
13. L.A. Khaddour, W. Deng, Multi-criteria sustainability risk management for post-war residential re-construction projects: the case of Damascus. *J. Housing Built Environ.* (2023). <https://doi.org/10.1007/s10901-023-10024-2>, <https://rdcu.be/c7JX7>
14. L.A. Khaddour, Strategic framework of operational energy performance improvement potential for Damascus post-war social housing. *Intell. Build. Int.* 1–15 (2021). <https://doi.org/10.1080/17508975.2021.1874859>

15. L.A. Khaddour, Life-cycle sustainability risk management a multi-stakeholder approach: the case of Damascus post-war residential projects. *J. Environ. Dev. Sustain.* 1–31 (2022). <https://doi.org/10.1007/s10668-021-01963-3>
16. M.A. William, M.J. Suárez-López, S. Soutullo, A.A. Hanafy, Building envelopes toward energy-efficient buildings: a balanced multi-approach decision making. *Int. J. Energy Res.* **45**(15), 21096–21113 (2021)
17. J. Si, L. Marjanovic-Halburd, F. Nasiri, S. Bell, Assessment of building-integrated green technologies: a review and case study on applications of multi-criteria decision making (MCDM) method. *Sustain. Cities Soc.* **27**, 106–115 (2016)
18. L.A. Khaddour, S.K. Yeboah, J.K. Dodoo, Ecological and carbon footprints of cities. In *Encyclopedia of Sustainable Technologies*, 2nd edn. (Elsevier, 2023). <https://doi.org/10.1016/B978-0-323-90386-8.00044-9>

**Open Access** This chapter is licensed under the terms of the Creative Commons Attribution 4.0 International License (<http://creativecommons.org/licenses/by/4.0/>), which permits use, sharing, adaptation, distribution and reproduction in any medium or format, as long as you give appropriate credit to the original author(s) and the source, provide a link to the Creative Commons license and indicate if changes were made.

The images or other third party material in this chapter are included in the chapter's Creative Commons license, unless indicated otherwise in a credit line to the material. If material is not included in the chapter's Creative Commons license and your intended use is not permitted by statutory regulation or exceeds the permitted use, you will need to obtain permission directly from the copyright holder.





# Chapter 22

## Design and Prototype an Educational Proton-Exchange Membrane Fuel Cell Model



M. R. Rahman, F. S. Hosseini, P. Taleghani, M. Ghassemi, and M. Chizari

**Abstract** Proton-exchange membrane (PEM) cells fuel cells are being used as highly efficient and zero-emission power units to produce electricity from a renewable source. The purpose of the current study is to present the design of a simple PEM type fuel cell model that can be used in an educational environment. The study has illustrated possibility of the design through a product design specification (PDS) process. Three different designs were studied and ranked based on design parameters such as cost, environmental safety, size and weight, educational application etc. Then the highest score design was selected. The selected design then improved by utilizing a 3D computer modelling to come up with the final design. The developed design was then manufactured in house and assembled to form a full functional prototype. The model then was tested, and outcome was compared against existing fuel cell models. Test results show that the prototype can produce reasonable amount of electricity. However, the efficiency of the higher heating value and lower heating value of hydrogen was about 15% less compared to the existing fuel cell model. Furthermore, there are some concerns about the controlling combustible and flammable gas which need to be consumed immediately inside the system instead of storing the gas. The project is under development to be safe enough for any educational environment.

**Keywords** Electrolyser · Fuel cell · Proton exchange membrane · Educational model · Membrane electrode · Gas diffusion layer

---

M. R. Rahman · M. Chizari  
Department of Engineering, SPECS, University of Hertfordshire, Hatfield AL10 9AB, UK

F. S. Hosseini (✉) · P. Taleghani · M. Ghassemi  
Department of Mechanical Engineering, K.N. Toosi University of Technology, Tehran, Iran  
e-mail: [fatemehsadat.hosseini@email.kntu.ac.ir](mailto:fatemehsadat.hosseini@email.kntu.ac.ir)

P. Taleghani  
e-mail: [Parastoo.Taleghani@email.kntu.ac.ir](mailto:Parastoo.Taleghani@email.kntu.ac.ir)

## 22.1 Introduction

Today increasing the global warming and air pollution due to the combustion of fossil fuels are an environmental issue. On the other hand, the fossil fuels and non-renewable energy sources are limited so the renewable energies and renewable energy sources become more important than before [1]. Fuel cells are one of the great renewable energy systems which can directly convert the chemical energy of Hydrogen into electricity without combustion process. They do not emit greenhouse gases and their only products are water and heat [2]. Between all fuel cell types, proton-exchange membrane (PEM) fuel cells have the highest power density and lowest operating temperature [3]. For a wide range of applications like portable electronic telecommunications, transportation applications and educational purposes.

Electrode has an important role in the PEM fuel cells and improving its performance and durability affects the PEM fuel cell efficiency and performance. In the PEM fuel cells, platinum is used as the catalyst and despite its high price, it is still used due to its high chemical stability and other advantages. There are attempts to use metals like Cobalt as the catalyst in PEM fuel cells which are non-noble metal and cheaper than Platinum [4].

Several research have been done to investigate the effects of various parameters such as water management on the PEM fuel cells performance and durability so far. Goßling et al. studied a 2D and 1D model of a PEM fuel cell stack considering the water management and water balance in the fuel cell [5]. Wang et al. studied the effect of liquid water in porous electrodes and developed a 3-D and two-phase model of the PEM fuel cell [6]. Rahimi-Esbo et al. manufactured a transparent PEM fuel cell according to a numerical design and introduced this transparent PEM fuel cell as the cheapest and simplest method for investigation of water management [7]. Ferreira et al. have studied the effect of gas diffusion layer (GDL) with a microporous layer (MPL) on improving water management and the effect of membrane thickness changes on the operation of PEM fuel cells [8]. Robert et al. studied the effects of chemical and mechanical degradation on the morphology and physicochemical properties of Nafion® membranes. Chemical structure, water transport and sorption using tailor-made devices that can mimic the chemical and mechanical conditions typical of fuel cell operation. Membrane degradation was induced by simultaneously exposing the membrane to a free radical environment and cyclic compression. On the other hand, repetition of the 0.1 Hz compression sequence was implemented to induce mechanical fatigue close to that caused by membrane expansion/contraction during transient fuel cell operation [9].

Kahveci et al. coated the flow channels of the bipolar plates of the PEM fuel cell with different materials and studied water management in each case experimentally. They also found out the PEM fuel cell stack with the hydrophobic Polytetrafluoroethylene (PTFE) coated plates supply the maximum power density and current density compared to others [10]. Smith et al. Introduced a team-based design fuel cell modules which Includes the latest PEMFC science. This module is intended to

focus on fuel cells Revitalize the Pinewood Derby R New generation PFSA performance improvements of the new generation of PFSA's over conventional Nafion, Increased efficiency and power density as a function of improved proton conductivity. This educational module also A compromise between conductivity and mechanical durability in the PEMs [11].

There is numerous research in the field of PEM fuel cells experimentally but there are a few research about the PEM fuel cells for using in the educational environments such as schools, colleges and universities for educating the students about renewable energy sources and fuel cells. Therefore, this study has aimed to build a fuel cell that is portable, easy to assemble and disassemble, safe and visible to show the functions are taking place in that. The study has designed and manufactured a fuel cell prototype based on PEM fuel cell technique which is suitable to be used in the educational environment. The model must be safe and have adjustable parameters, such as voltage, have a sturdy base as well as visible for students to observe what is happening in the model.

### 22.2 Methodology

**Initial design:** The initial design kept simple to make sure it is feasible at student level. The schematic of design illustrated in Fig. 22.1. The design was included with platinum mesh electrodes as a catalyst with a Proton Exchange Membrane as its electrolyte along with distilled water to hydrate the membrane. The electrolyser container consists of two clear acrylic plates with a square cut-out in each to house the electrodes, gas diffusion layer and distilled water with both plates being secured together with bolts at each corner. The membrane will be sandwiched in-between both plates and act as a gasket to prevent gas escaping. The diagram of this fuel cell and the table of its components and the used materials is shown in Fig. 22.2 and Table 22.1.

The initial concept is a reasonable choice for educational purpose because it is portable and safe as the liquid electrolyte is used in that, is distilled water which

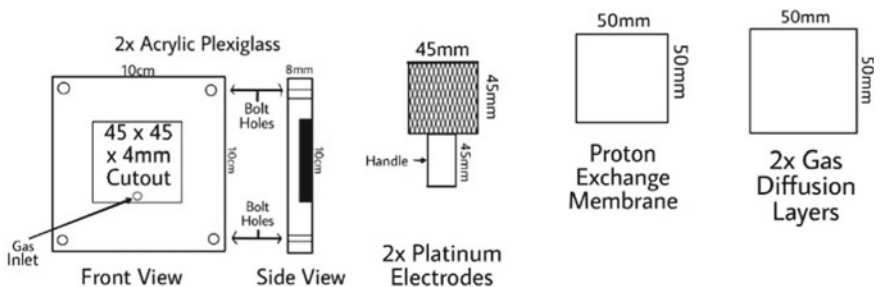
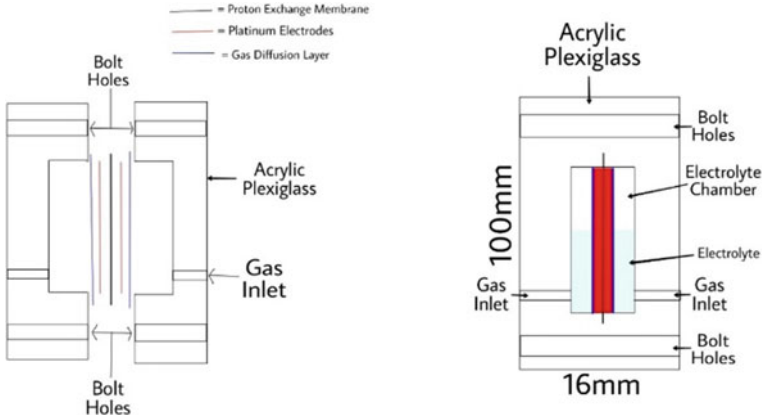


Fig. 22.1 Diagram of used components and materials for PEM fuel cell



**Fig. 22.2** Side view (by part and assembled) of the general design’s schematic

**Table 22.1** Components and materials used in initial design

Component	Material
Anode	Platinum mesh
Cathode	Platinum mesh
Electrolyte	PEM membrane and distilled water
Power source	2 × 1.5 V AA Batteries
Power output	LED

won’t cause any harm. This concept also clearly shows what is happening inside the fuel cell and where each gas is going. Another key characteristic is that it is secured using bolts and can easily be taken apart to show each component. The concept can also be reversed to be used as an electrolyser too, which can be done by attaching a power source to the electrodes instead of a load. However, a notable disadvantage of this concept is that the materials were used in this concept, may be expensive and cannot be created at home by students.

**Final design:** The study was considering 20 different parameters of the proposed concepts such as weight, size, environmental safety, cost, educational application and etc. and based on the importance of each parameter. A weighting score of 1 to 5 for each parameter was given and then the parameters rated between 1 and 5 for each feature. The rating of 5 implies that the design is excellent in that characteristic, whereas a rating of 1 show that the design is very poor in that characteristic. The overall score was calculated by multiplying the weight and the rating of that parameter and all the overall scores was added together to give the total score of that initial concept. The higher the total score, the better the design concept. Among few initial concepts, the concept with highest score was candidate for further study and prototyping.

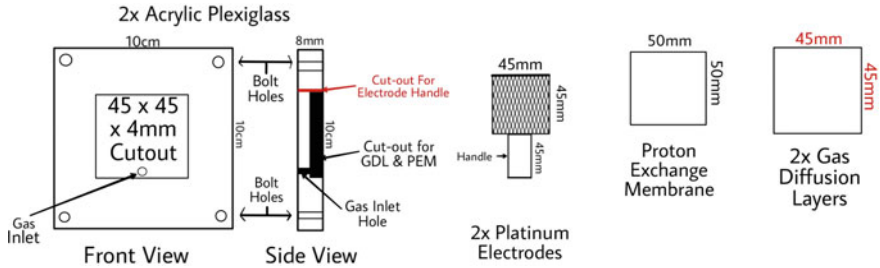


Fig. 22.3 Components of initial design

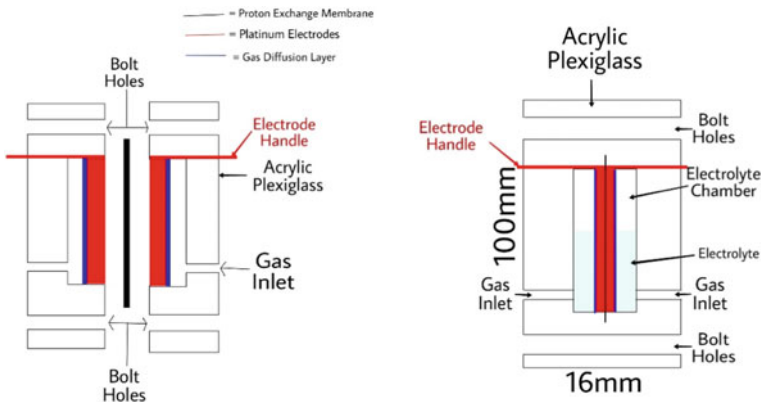


Fig. 22.4 Modified fuel cell halves and assembled side view

Amendments made on the initial design are displayed in red in Fig. 22.3. The base will be a 200 × 200 × 2 mm sheet of acrylic which will hold the fuel cell and any other parts sturdy (Fig. 22.4).

## 22.3 Models

### Fuel Cell Manufacture

Figure 22.5 shows the different parts which were used in the assembly of the fuel cell. These parts are also listed with its materials and dimensions in Tables 22.2 and 22.3. The electrodes were cut from its original length to 45 × 45 mm to allow it to fit in the prototype and the gas diffusion layer was also cut to fit. We see the assembled fuel cell in Fig. 22.6 that showing the side and front profiles with all parts inside, such as the membrane, electrodes and GDL. Some amendments such as drilling a new hole under the electrode handle, a sealant, a washer and etc. were applied to the prototype.



**Fig. 22.5** All parts required for the assembly of the prototype

**Table 22.2** Tabulated list of components, materials and measurements

Component	Material	Measurements (mm)(H × W × ID)	
Casing	Acrylic plexiglass	100 × 100 × 8	
Electrodes	Platinum coated Titanium	Coating thickness	0.5 um
		Dimensions	45 × 45 × 13
Gas diffusion layer	Carbon paper	45 × 45 × 10.19	
Electrolyte	Perfluorosulfonic acid membrane (Nafion N117) [9]	50 × 50 × 10.183	
Bolts	Stainless steel	4 × 20 (Dia. × Length)	

**Table 22.3** Technical specification of prototype fuel cell

Parameter	Specification
Fuel cell type	Proton exchange membrane (PEM)
Output voltage	< 1 V
Working temperature	0–95 °C
Weight	~ 290 g
Dimensions (Fuel Cell) (mm)	100 × 100 × 116
Dimensions (Kit) (mm)	200 × 1200 × 1200
Features	Clear, electrolyser function, easy to assemble/disassemble, easy set-up
Estimated electrical efficiency	40–60%
Maintenance	Clean plates and dry out PEM after use
Hydrogen Inlet Volume	20 ml/min
Oxygen Inlet Volume	10 ml/min
Emissions	Water and heat
Cooling	Air cooled

Figure 22.7 shows the full assembly of the prototype on the base with the gas collecting cylinders. The side with the red-wire is the oxygen side and the side with the black wire is the hydrogen side. The prototype is without gas diffusion layer. The electrode handles had also been cut to fit a spade terminal to make ease of connecting loads, as well as a multi-meter to test different parameters of the prototype.

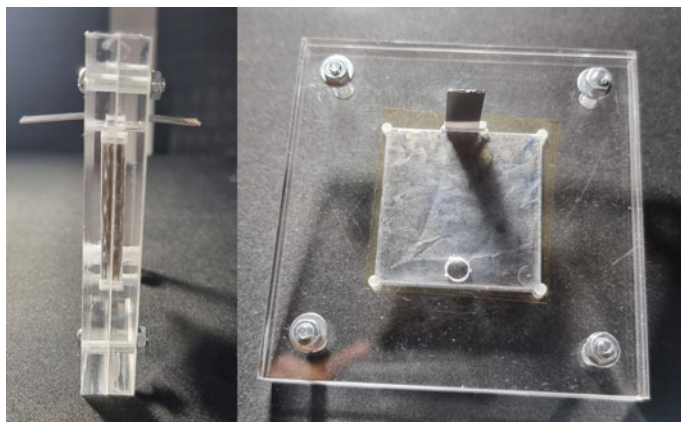


**Fig. 22.6** Assembled fuel cell prototype

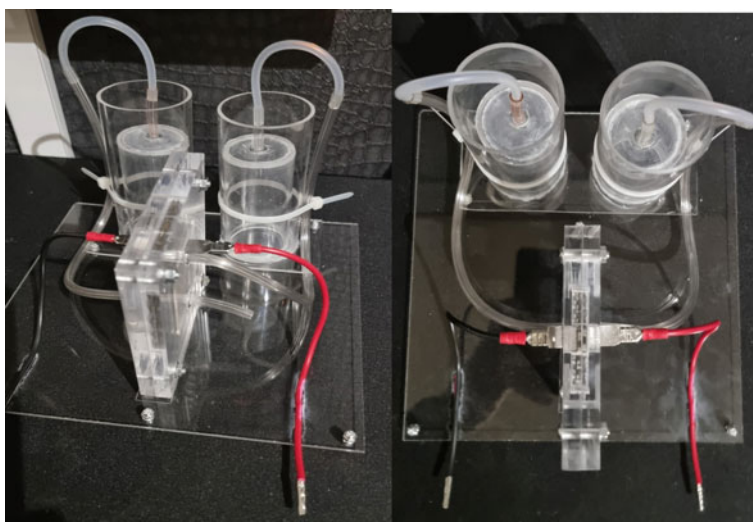


**Fig. 22.7** Assembled fuel cell prototype on base with gas collecting cylinders

**Testing:** We tested both educational fuel cell kit and prototype fuel cell in terms of their efficiency and the hydrogen and oxygen they consume. We tested the prototype fuel cell in two steps. In first step, the hydrogen was inputted to the prototype via the educational kit working as an electrolyser. In second step, the fuel cell was used as an electrolyser to make hydrogen and then was used as a fuel cell to use the hydrogen. The multi-meter showed the output voltage of the prototype as well as the hydrogen and oxygen it consumed in both steps. The efficiencies based on higher heating value and lower heating value was also calculated by Eqs. 22.1 and 22.2, respectively.

**Fig. 22.8** PEM Membrane after attempting electrolysis



$$\eta = \frac{V}{1.482} \quad (22.1)$$

$$\eta_{LHV} = \frac{V}{1.254} \quad (22.2)$$

During the 2nd attempt at testing the fuel cell, gas tubes were connected from the fuel cell to the gas containing cylinders and a power supply of 2 V at 0.7A were attached to the anode and cathode of the prototype. This resulted in oxygen bubbles being created at the cathode, however after a few minutes, no gas had entered the cylinders and the distilled water had started leaking from the membrane. After this occurrence, the prototype was again taken apart to diagnose any issues (Fig. 22.8).

The above picture shows the membrane once it was removed from the prototype after attempting electrolysis. The membrane had a few spots that looked as if it had been burnt and there was a yellow looking liquid coming off the membrane which could be the perfluoro sulfonic acid (liquid form of the membrane) mixing with the water. The possible reasons for this could be due to the electrodes tearing the membrane during assembly, causing a short and sparking which could explain the burn-looking marks [9]. Another reason could be due to the electrode handle not being platinum, causing an adverse reaction between the titanium and the membrane. From the comparison of the experimental results with the Horizon model [12], it was found that the current prototype is not work well enough and need to improve the design which is in progress in an ongoing project.

## 22.4 Results and Discussion

Results show that the educational fuel cell kit produces a voltage of 0.918v at the electric current of 0.13A, while it consumes 2.39 ml/min of hydrogen and 1.2 ml/min of



oxygen. The efficiencies of the educational fuel cell kit based on higher heating value and lower heating value are 61.9% and 73.2%, respectively. The normal efficiency of a PEM fuel cell is in the 40% to 60% range. So, the educational kit efficiency is higher than the PEM fuel cell efficiency. As we discussed previously, the hydrogen that the prototype fuel cell consumes is supplied either by the educational fuel cell kit as an electrolyser or the prototype itself works as an electrolyser. When the educational kit works as an electrolyser, the prototype fuel cell produces a voltage about 0.778 v and consumes 7.94 ml/min of hydrogen and 3.97 ml/min of oxygen and its higher heating value and lower heating value efficiencies are 52.5% and 62%, respectively which is the middle of the normal efficiency of a PEM fuel cell (40%–60%). Results show that the prototype would not serve as a good educational model as it couldn't function as an electrolyser to provide hydrogen and oxygen to be used when functioning as a fuel cell. If the prototype is put in an educational environment, the prototype cannot work as an electrolyser and as a fuel cell at the same time. Therefore, in this case, we need a hydrogen and oxygen tank would be required as well as flow meters and flow regulators to prevent damage to the prototype itself. To save the hydrogen and oxygen that the prototype produced use them when the prototype functions as a fuel cell. But having a tank that contains flammable gas like hydrogen is not safe for use in an educational environment.

## 22.5 Conclusion

In the present investigation, a PEM fuel cell prototype for educational purposes based on the best-evaluated parameters had designed and manufactured. Considering the high score parameters at play in this model are evaluated to efficiency of the model and compared to an existing fuel cell model. Fuel cell kit also can supply Self-consumed hydrogen as an electrolyser.

Test results show that the efficiency of the educational kit is relatively high between 50 and 60% compared to existing fuel cell models based on higher heating value and lower heating value. A prototype can produce hydrogen. However, there is a concern that flammable gas and control of flammable gas require immediate consumption in the system rather than storing the gas.

Considering that the storage of hydrogen fuel for the fuel cell in the tank for educational purposes is risky and does not have enough security, so we can use an electrolyser instead of fuel storage. Therefore, hydrogen produced by the electrolyser can be consumed directly and there is no risk. Thus, this method is safe and can be easily used in educational environments. It should be noted that to reduce the risk as much as possible, the time between production and consumption of hydrogen should be minimized. In the next steps, we will aim to be able to minimize the possible risks of storing hydrogen fuel and the time of its production and consumption with a more optimal design and the use of a suitable electrolyser to produce the required fuel, and a fuel cell with high security which is suitable for use in educational environments.

## References

1. A.A. Ebrahimzadeh, I. Khazaei, A. Fasihfar, Experimental and numerical investigation of obstacle effect on the performance of PEM fuel cell. *Int. J. Heat Mass. Transf.* **141**, 891–904 (2019)
2. L. Giorgi, F. Leccese, Fuel cells: technologies and applications. *Open Fuel Cells J.* **6** (2013)
3. J. Kurtz, C. Ainscough, L. Simpson, Caton M. Hydrogen storage needs for early motive fuel cell markets. National Renewable Energy Lab.(NREL), Golden, CO (United States); 2012.
4. E.H. Majlan, D. Rohendi, W.R.W. Daud, T. Husaini, M.A. Haque, Electrode for proton exchange membrane fuel cells: a review. *Renew Sustain. Energy Rev* **89**, 117–134 (2018)
5. S. Göbbling, N. Nickig, M. Bahr, 2-D+ 1-D PEM fuel cell model for fuel cell system simulations. *Int J Hydrogen Energy* **46**, 34874–34882 (2021)
6. Y. Wang, S. Wang, S. Liu, H. Li, K. Zhu, Three-dimensional simulation of a PEM fuel cell with experimentally measured through-plane gas effective diffusivity considering Knudsen diffusion and the liquid water effect in porous electrodes. *Electrochim Acta* **318**, 770–782 (2019)
7. M. Rahimi-Esbo, A. Ramiar, A.A. Ranjbar, E. Alizadeh, Design, manufacturing, assembling and testing of a transparent PEM fuel cell for investigation of water management and contact resistance at dead-end mode. *Int J Hydrogen Energy* **42**, 11673–11688 (2017)
8. R.B. Ferreira, D.S. Falcão, V.B. Oliveira, A. Pinto, Experimental study on the membrane electrode assembly of a proton exchange membrane fuel cell: effects of microporous layer, membrane thickness and gas diffusion layer hydrophobic treatment. *Electrochim Acta* **224**, 337–345 (2017)
9. M. Robert, A. El Kaddouri, J.-C. Perrin, K. Mozet, M. Daoudi, J. Dillet et al., Effects of conjoint mechanical and chemical stress on perfluorosulfonic-acid membranes for fuel cells. *J Power Sources* **476**, 228662 (2020)
10. E.E. Kahveci, I. Taymaz, Experimental study on performance evaluation of PEM fuel cell by coating bipolar plate with materials having different contact angle. *Fuel* **253**, 1274–1281 (2019)
11. J.D. Smith, M. Novy, Design of a modern proton-exchange membrane fuel cell module for engineering education, in *2018 IEEE Conference on Technologies Sustainability* (IEEE, 2018), pp. 1–6
12. Horizon Educational, Solar Hydrogen Science Kit, Horizon Fuel Cell Europe. Available from: <https://www.horizoneducational.com/solar-hydrogen-science-kit/p1224>. Last seen 28 Nov 2021

**Open Access** This chapter is licensed under the terms of the Creative Commons Attribution 4.0 International License (<http://creativecommons.org/licenses/by/4.0/>), which permits use, sharing, adaptation, distribution and reproduction in any medium or format, as long as you give appropriate credit to the original author(s) and the source, provide a link to the Creative Commons license and indicate if changes were made.

The images or other third party material in this chapter are included in the chapter's Creative Commons license, unless indicated otherwise in a credit line to the material. If material is not included in the chapter's Creative Commons license and your intended use is not permitted by statutory regulation or exceeds the permitted use, you will need to obtain permission directly from the copyright holder.



# Chapter 23

## The Impact of Strategic Environmental Management Capabilities on the Competitiveness of an Oil and Gas Industry's Supply Chain: An Empirical Evaluation of the Natural Resource-Based View of Firms



Olatunde Olajide, Muhammad Mustafa Kamal, Dong-Wook Kwak, Qile He, and Ming Lim

**Abstract** The Oil and Gas (O&G) industry has been subjected to stringent environmental regulations and increasing stakeholders' criticisms because of its devastating negative environmental impacts. Consequently, firms operating in the industry's supply chain are increasingly facing intense pressures to develop the strategic capabilities for implementing green practices to reduce the environmental impacts of operations. From a theoretical perspective, the Natural Resource-Based View (NRBV) suggests that the strategic environmental capabilities of pollution prevention (PPC), product stewardship (PSC) and clean technology (CTC) can generate sustained competitive advantage for firms. However, the extant empirical research investigating the impact of the three NRBV strategic environmental capabilities (PPC, PWC and CTC) on firms' competitive performance has yielded inconsistent results. Therefore, this paper adopts the theoretical lens of NRBV to develop and empirically assess an integrated framework of strategic environmental management capabilities (SEMC) and competitiveness in the context of the Nigerian O&G industry. Using a multiple regression technique to analyse the responses of 214 managers across the supply

---

O. Olajide (✉)

Sustainable Energy Supply Chain Management, Centre for Business in Society (CBiS), Coventry University, Conentry, UK

e-mail: [olajide3@uni.coventry.ac.uk](mailto:olajide3@uni.coventry.ac.uk)

M. M. Kamal

Supply Chain Management, Faculty of Business and Law, Coventry University, Conentry, UK

D.-W. Kwak

International Logistics, Kyungpook National University, Daegu, South Korea

Q. He

Strategy and Performance Management, University of Derby, Derby, UK

M. Lim

Supply Chain and Operations Management, Faculty of Business and Law, Coventry University, Conentry, UK

chain of the Nigerian O&G industry, this study examines the impact of the three NRBV-based SEMC (PPC, PWC and CTC) on the economic and environmental competitiveness of the firms operating in the supply chain of the Nigerian O&G industry. First, the results indicate that the three SEMCs have positive impacts on the environmental competitiveness of the O&G firms. However, while PPC and PSC are positively related to the economic competitiveness of firms, CTC has no statistically significant impact on economic competitiveness. These findings suggest that O&G firms in developing nations need to channel efforts to build their SEMCs for implementing green practices to enhance their economic and environmental competitiveness. The results further highlight the need for policymakers in petroleum-producing nations to promote policies that foster the adoption of green practices by O&G firms.

**Keywords** NRBV · Pollution prevention · Product stewardship · Clean technology · Sustainable supply chain management

## 23.1 Introduction

The O&G industry continually experiences stakeholders' pressures to rethink operations towards sustainability due to the devastating negative impacts of the O&G operations and products on the environment [1]. Recently, various countries such as the Republic of Ireland and New Zealand have announced their commitment to divestment from fossil fuels (including O&G) [2]. Also, more stringent regulations are increasingly targeted at the O&G industry globally to manage climate change issues linked with the GHG emissions traceable to the industry [3, 4]. O&G firms can minimise operation and product environmental impact and improve economic performance by activating their strategic environmental management capabilities (SEMCs) [5].

The Natural Resource Based-View (NRBV) proposes pollution prevention (PPC), product stewardship (PSC) and clean technology (CTC) as SEMCs that may help firms attain sustained competitive advantage [6, 7]. Recently, O&G practitioners are showcasing their sustainability strategies to earn legitimacy against stakeholder pressures. For instance, Royal Dutch Shell has continually popularised its environmental management capabilities through its drive toward huge investment in cleaner energy [8]. While these strategies mostly align with the NRBV-SEMC of PPC, PSC and CTC, there is no empirical evidence that these SEMCs positively impact the competitiveness of O&G firms in line with NRBV's postulations. Considering that such evidence may justify petroleum managers' investment in green practices while influencing the O&G policy framework toward sustainability; the current paper sets out to answer the following research question (RQ):

Do strategic environmental capabilities (SEMCs) enhance the competitiveness of firms in the oil and gas supply chain?

For this purpose, this paper proposed an integrated SEMC-competitiveness model that links the three NRBV-based SEMCs (PPC, PSC and CTC) with firms' environmental and economic competitiveness. The proposed model was assessed with data from selected managers in the Nigerian O&G supply chain. The remainder of this paper covers various sections, which include: Theoretical Background and Hypothesis development (Sect. 23.2), Methodology (Sect. 23.3), Results and Discussion (Sect. 23.4) and Conclusion and Recommendations (Sect. 23.5).

## 23.2 Theoretical Background and Hypotheses Development

### 23.2.1 *Natural Resource-Based View (NRBV)*

NRBV integrates the '*voice of the environment*' into the Resource-Based View theory and argues that the future competitive advantage would be attained by firms' ability to manage their natural environment effectively [6]. Accordingly, firms must channel their valuable, rare, inimitable and non-substitutable resources to activate the SEMCs of pollution prevention, product stewardship, clean technology and *Base of the pyramid* to attain sustained competitive advantage [7]. Empirical studies have validated the existence of PPC, PST and CTC in a supply chain context [7, 9]. However, the presence of the Base of the Pyramid strategies was not empirically validated in the UK Agrofood industry's supply chain [9]. Few studies examining NRBV in the O&G industries have also sparingly focused on PPC and PSC [5, 10]. Therefore, the current research conceptualises PPC, PSC and CTC as the SEMCs that may enhance the competitiveness of O&G firms.

Pollution prevention is a process-based approach to eliminating unnecessary pollution within internal operations. One of its key objectives is proactively and effectively minimising emissions, effluents and waste from operations. In contrast, product stewardship capabilities enable firms to adopt a lifecycle approach to tackling social and environmental concerns at every stage of a product and production process to improve an organisation's product sustainability [7]. A firm's product stewardship capabilities transcend internal frameworks but depend mainly on stakeholder integration [6, 11]. Finally, Clean technology capabilities result in firms adopting a radical approach to pollution prevention and environmental management practices [12]. Generally, acquiring clean technology capabilities usually requires considerable investment [13]. Nevertheless, clean technology capabilities can enhance a company's environmental reputation. The relationships among the constructs of this research are hereafter discussed.

### 23.2.2 *Strategic Environmental Management Capabilities (SEMC) and Competitiveness*

According to [6], the ability of firms to adopt pollution prevention strategies instead of end-of-the-pipe pollution control can help firms attain a higher level of economic performance. This is because pollution control methods such as waste disposal result in substantial financial costs and waste of managerial time, which could be saved through a proactive pollution prevention strategy. According to [5], O&G firms that integrate pollution prevention strategies into their operations achieve higher performance levels. Furthermore, firms may attain a higher level of competitive performance by applying a product stewardship strategy [6]. This is because firms pursuing product stewardship strategies can integrate environmental management strategies into a product lifecycle in collaboration with stakeholders [6, 7]. This improves firms' ability to minimise the environmental impacts of products, leading to a good reputation among stakeholders and consumers.

Many leading O&G companies are gradually investing in clean technology to foster the energy transition in response to stakeholder pressures against climate change. For example, Shell increased its original annual clean energy budget in 2016 from \$200 million to \$1.2 billion in 2017 [14]. Although a clean technology strategy requires substantial financial capital, available subsidies and tax credits can ameliorate attributable financial requirements. Companies pursuing a clean technology strategy can also benefit from green financing. Based on the above, this research hypothesises that:

*H1a: Pollution prevention capabilities positively impact firms' environmental competitiveness in the O&G industry.*

*H1b: Pollution prevention capabilities positively impact firms' economic competitiveness in the O&G industry.*

*H2a: Product stewardship capabilities positively impact firms' environmental competitiveness in the O&G industry.*

*H2b: Product stewardship capabilities positively impact firms' economic competitiveness in the O&G industry.*

*H3a: Clean Technology capabilities positively impact the environmental competitiveness of firms in the O&G industry.*

*H3b: Clean Technology capabilities positively impact firms' economic competitiveness in the O&G industry.*

Following the hypotheses stipulated in this paper, the theoretical model of this research is presented in Fig. 23.1.

Our model consists of five constructs made up of three SEMC constructs (PPC, PSC and CTC) and two competitiveness constructs (EcoCom and EnvCom). The model specifies a causal impact of each of the SEMC constructs on the competitiveness constructs. The definition of each construct is provided in Table 23.1.

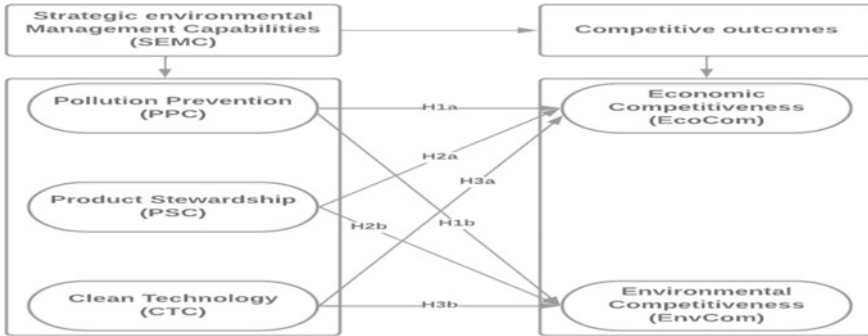


Fig. 23.1 SEMC-Competitiveness conceptual model of the O&G industry

Table 23.1 Definition of constructs

Construct	Definition
Pollution Prevention Capabilities (PPC)	Innovative capacity for reducing operational emissions, wastes and effluents
Product Stewardship Capabilities (PSC)	Ability to implement measures that minimise the ecological impacts of products throughout the lifecycle
Clean Technology Capabilities (CTC)	Ability to implement disruptive change by adopting green technologies causing changes or diversification in products or operations
Economic Competitiveness (EcoCom)	Economic benefits derived from taking proactive environmental measures ahead of the competition
Environmental Competitiveness (EnvCom)	Reputational benefits resulting from managing environmental issues better than the competition

### 23.3 Methodology

#### 23.3.1 Survey Development

Latent constructs are operationalised either by developing measurement scales or adapting existing indicators from the literature [15]. The five latent constructs in this research are measured with items adapted from the extant literature. PPC is measured with five items adapted from [16], initially tested in the Canadian O&G industry. PSC is operationalised with five indicators adapted from [17]. These items were also verified in the O&G industry. Measuring CTC is attained with the adaptability of combined items from [16, 18]. Finally, the competitiveness constructs (EcoCom and EnvCom) are operationalised with combined items modified from [19, 20]. To forestall the risk of measurement errors, the definitions of constructs and the measurement items were given to five academicians and five managers across the

supply chain of the Nigerian O&G industry, who provided feedback that eventually refined the questionnaire items. The details of the questionnaire items are presented in Appendix 1.

### **23.3.2 Samples**

The respondents in this research are top and middle-level managers across the supply chain of the Nigerian O&G industry. The Nigerian O&G industry is considered a relevant case study in this research because of its history of unsustainable operations across the supply chain, as documented in the literature. Also, strategic management staff across the Nigerian O&G industry are targeted in this research because they are considered knowledgeable in organisational strategies, including sustainability. A list of 2750 firms operating in the upstream and downstream sectors of the Nigerian O&G industry was obtained from the Department of Petroleum Resources (DPR), the regulator of the Nigerian O&G industry. The list contains the address and contact information of the relevant officers of the companies. Using a stratified random sampling technique, the list was classified into two groups: upstream (1100) and downstream (1650). Based on the sample size, 728 and 1092 questionnaires were respectively sent to the upstream and downstream firms using Qualtrics online survey platform. Between May and June 2019, 214 responses were received from various managers across the Nigerian O&G supply chain. The details of the respondents are provided in Table 23.2.

As per the view of [21] that sample sizes between 100 to 400 are sufficient for path analysis methodology based on regression analysis, the sample size of 214 is considered suitable for this research. Whereas this research records a low response rate of 12%, previous studies in operations management have also identified low response rates as a challenge in operations management research.

To ensure a higher ethical standard in this research, respondents were assured of anonymity to protect their identities. Also, informed consent was sought before completing the questionnaire, evidencing that respondents willfully volunteered the information analysed in this research. Furthermore, the informed consent emphasised the respondents' right to withdraw their responses anytime before publication, without any reason.

## **23.4 Results and Discussion**

### **23.4.1 Measurement Model Assessment**

The measurement items were first assessed for reliability using Cronbach's alpha. As shown in Table 23.2, all results are sufficiently above the recommended value of 0.70 [15], indicating that the reliability of the questionnaire items is satisfactory.



**Table 23.2** Demography of the respondents

Criteria	Frequency	Percentage
<i>Oil and Gas industry sector</i>		
Upstream	88	41
Downstream	126	59
Total	214	100
<i>Respondents' job designation</i>		
CEO/Directors	23	11
Operations managers	64	30
Supply chain managers	37	17
Procurement managers	38	18
Logistics managers	35	16
Compliance managers	17	8
Total	214	100
<i>Respondents' years of experience</i>		
1–10	8	4
11–20	74	35
21–30	122	57
31 and above	10	5
Total	214	100

Further reliability and validity assessments were carried out within the context of Confirmatory factor Analysis (CFA) using AMOS software. Items were assessed in a complete measurement model using CFA. As the modification indices in AMOS suggested, three measurement items (PPC5, CTC 4 and CTC5) were deleted from the respective constructs due to poor loadings [22]. The final results of the measurement model assessment are presented in Table 23.2.

The relative Chi-square of 1.336 is less than the recommended maximum value of 3.00 [21]. Also, other model fit indices (RMSEA, 0.40, TLI = 0.966, CFI = 0.970, IFI = 0.971, NFI = 0.903) are higher than the 0.90 recommended minimum value [22], providing evidence of good fit of the research model. Furthermore, all the t-values are above the recommended value of 2.575 and are significant at 0.01. level, indicating satisfactory convergent validity.

### 23.4.2 Hypotheses Testing and Results

Upon validating the measurement model, the constructs were classified into independent and dependent variables with causal relationships specified in line with

the research model hypotheses. For this purpose, PPC, PSC and CTC are independent variables that impact EcoCom and EnvCom as dependent variables. The results of the individual hypotheses based on AMOS output are presented in (Table 23.4).

**Table 23.3** The results of measurement model assessment

Constructs	Alpha	Standardised coefficient	t-values
Pollution Prevention Capabilities (PPC)	0.841		
PPC1		0.516	6.92
PPC2		0.928	5.14
PPC3		0.967	7.02
PPC4		0.519	6.18
Product Stewardship Capabilities (PSC)	0.945		
PSC1		0.757	4.51
PSC2		0.878	3.92
PSC3		0.934	6.31
PSC4		0.940	6.12
PSC5		0.832	3.01
Clean Technology Capabilities (CTC)	0.739		
CTC1		0.659	4.19
CTC2		0.793	6.21
CTC3		0.660	3.46
Economic Competitiveness (EcoCom)	0.845		
EcoCom1		0.905	6.41
EcoCom2		0.873	5.12
EcoCom3		0.804	5.14
EcoCom4		0.865	4.76
EcoCom5		0.700	5.41
Environmental Competitiveness (EnvCom)	0.911		
EnvCom1		0.905	6.02
EnvCom2		0.873	3.13
EnvCom3		0.804	4.22
EnvCom4		0.865	6.05
EnvCom5		0.700	3.70

Fit Indices: Relative Chi-square = 1.336, RMSEA, 0.40, TLI = 0.966, CFI = 0.970, IFI = 0.971, NFI = 0.903

**Table 23.4** The results of hypotheses testing

Constructs relationships	Standardised coefficient	P-Value	Position
<b>Pollution Prevention Capabilities (PPC)</b>			
Economic Competitiveness (EcoCOM)	0.21	*	H1a: supported
Environmental Competitiveness (EnvCom)	0.15	*	H1b: supported
<b>Product Stewardship Capabilities (PSC)</b>			
Economic Competitiveness (EcoCOM)	0.05	***	H2a: supported
Environmental Competitiveness (EnvCom)	0.39	**	H2b: supported
<b>Clean Technology Capabilities (CTC)</b>			
Economic Competitiveness (EcoCOM)	0.21	0.33	H3a: not supported
Environmental Competitiveness (EnvCom)	0.27	*	H1b: supported

*Note* \*\*\* significant at 0.001 level \*\* significant at 0.01 level; \* significant at 0.05 level; ns: not significant; Chi-square = 1.48; RMSEA = 0.047, TLI, 0.920, CFI = 0.950, IFI = 0.949, NFI = 0.872.

All hypotheses are positive and statistically significant except for H3a (CTC → EcoCom), which is not significant, thus mostly confirming the proposed research model. Therefore oil and gas firms that develop the strategic environmental management capabilities (SEMC) of pollution prevention and product stewardship are likely to derive the benefits of a higher level of economic and environmental competitiveness, in line with the NRBV logic [6, 7]. In contrast, while O&G firm’s capabilities for clean technology may enhance environmental competitiveness, it may not necessarily result in higher economic competitiveness. With these results, the current research has answered the proposed research question.

### 23.5 Conclusion

This research examined whether O&G firms that channel efforts into activating their strategic environmental capabilities of pollution prevention, product stewardship and clean technology can derive a higher level of competitiveness as proposed in the NRBV [6, 7]. While there is a positive association between the three SEMCs and environmental competitiveness, clean technology has no statistically significant effect on economic competitiveness, unlike pollution prevention and product stewardship strategies that positively and significantly impact economic competitiveness. The findings of our study have important implications for theory and managerial practice. From an academic perspective, our study has attempted to bring

empiricism to the NRBV, which has hitherto been considered a mere theoretical lens in GSCM literature. The research has also deepened the application of theory in O&G-focused GSCM research. From the managerial perspective, the findings of this research justify O&G firms' investment in the examined green practices as they all yielded positive impacts on environmental and economic competitiveness (except for CTC, which has no significant effect on economic competitiveness). Policymakers may also promote sustainability policies for the O&G industry because of the validated environmental benefits. Incentives such as subsidies can motivate O&G firms' investment in clean technology to lessen the financial burden. Future studies may address this research's limitations which include non-inclusion of participants from other O&G countries, expungement of other SEMCs from the research model and deemphasising the antecedents of SEMCs.

**Acknowledgements** The researchers hereby acknowledge the Federal Republic of Nigeria for funding this research through the Petroleum Technology Development Fund (PTDF).

## References

1. T.F. Cojoianu, F. Ascui, G.L. Clark, A.G. Hoepner, D. Wójcik, Does the fossil fuel divestment movement impact new oil and gas fundraising? *Journal of Economic Geography* **21**(1), 141–164 (2021)
2. J. McKenzie, A.V. Carter, Stepping stones to keep fossil fuels in the ground: Insights for a global wind down from Ireland. *The Extractive Industries and Society* **8**(4), 101002 (2021)
3. N.K.W. Ahmad, M.P. de Brito, J. Rezaei, L.A. Tavasszy, An integrative framework for sustainable supply chain management practices in the oil and gas industry. *J. Environ. Planning Manage.* **60**(4), 577–601 (2017)
4. Y.Y. Yusuf, A. Gunasekaran, A. Musa, N.M. El-Berishy, T. Abubakar, H.M. Ambursa, The UK oil and gas supply chains: an empirical analysis of the adoption of sustainable measures and performance outcomes. *Int. J. Prod. Econ.* **146**(2), 501–514 (2013)
5. M. Hastings, A new operational paradigm for oil operations in sensitive environments: an analysis of social pressure, corporate capabilities and competitive advantage. *Bus. Strateg. Environ.* **8**(5), 267–280 (1999)
6. S.L. Hart, A natural-resource-based view of the firm. *Acad. Manag. Rev.* **20**(4), 986–1014 (1995)
7. S.L. Hart, G. Dowell, Invited editorial: a natural-resource-based view of the firm: fifteen years after. *J. Manag.* **37**(5), 1464–1479 (2011)
8. Sheppard, D. (2018). Oil producers face their 'life or death' question.
9. N. McDougall, B. Wagner, J. MacBryde, An empirical explanation of the natural-resource-based view of the firm. *Production Planning & Control* **30**(16), 1366–1382 (2019)
10. M. Michalisin, B. Stinchfield, Climate change strategies and firm performance: an empirical investigation of the natural resource-based view of the firm. *Journal of Business Strategies* **27**(2), 123–149 (2010)
11. Y.S. Chen, C.H. Chang, Enhance environmental commitments and green intangible assets toward green competitive advantages: an analysis of structural equation modelling (SEM). *Qual. Quant.* **47**(1), 529–543 (2013)
12. P. del Río González, Analysing the factors influencing clean technology adoption: a study of the Spanish pulp and paper industry. *Bus. Strateg. Environ.* **14**(1), 20–37 (2005)

13. X. Shi, C. Dong, C. Zhang, X. Zhang, Who should invest in clean technologies in a supply chain with competition? *J. Clean. Prod.* **215**, 689–700 (2019)
14. IPIECA, Mapping oil and gas industry to sustainable development goals: an atlas, in *International Petroleum Industry Environmental Conservation Association* (2017). Available: <http://www.ipieca.org/resources/awareness-briefing/mapping-the-oil-and-gas-industry-to-the-sustainable-development-goals-an-atlas/>
15. J.F. Hair, W.C. Black, B.J. Babin, R.E. Anderson, *Multivariate Data Analysis*, 7th edn. (Pearson Prentice Hall, 2009)
16. S. Sharma, H. Vredenburg, Proactive corporate environmental strategy and the development of competitively valuable organisational capabilities. *Strateg. Manag. J.* **19**(8), 729–753 (1998)
17. W.N.K.W. Ahmad, M.P. de Brito, L.A. Tavasszy, Sustainable supply chain management in the oil and gas industry: a review of corporate sustainability reporting practices. *Benchmarking Int J.* (2016)
18. K.V. Bhupendra, S. Sangle, What drives the successful implementation of the product stewardship strategy? The role of absorptive capability. *Corp. Soc. Responsib. Environ. Manag.* **24**(3), 186–198 (2017)
19. Q. Zhu, J. Sarkis, K.H. Lai, Institutional-based antecedents and performance outcomes of internal and external green supply chain management practices. *J. Purch. Supply Manag.* **19**(2), 106–117 (2013)
20. C.E. Moreno, J.F. Reyes, The value of proactive environmental strategy: an empirical evaluation of the contingent approach to dynamic capabilities. *Cuadernos de Administración* **26**(47), 87–118 (2013)
21. R.B. Kline, in *Principles and practice of structural equation modelling*. Guilford publications (2015)
22. B.M. Byrne, *Structural equation modelling with Mplus: basic concepts, applications, and programming* (Routledge, 2013)

**Open Access** This chapter is licensed under the terms of the Creative Commons Attribution 4.0 International License (<http://creativecommons.org/licenses/by/4.0/>), which permits use, sharing, adaptation, distribution and reproduction in any medium or format, as long as you give appropriate credit to the original author(s) and the source, provide a link to the Creative Commons license and indicate if changes were made.

The images or other third party material in this chapter are included in the chapter's Creative Commons license, unless indicated otherwise in a credit line to the material. If material is not included in the chapter's Creative Commons license and your intended use is not permitted by statutory regulation or exceeds the permitted use, you will need to obtain permission directly from the copyright holder.



# Chapter 24

## Towards the Tees Valley Energy Transition—Residential Decarbonisation and Skills Analysis



**Paul van Schaik, Matthew Cotton, Huda Dawood, Nashwan Dawood, Elena Imani, Michael Knowles, Charlotte Leighton, Susan Lorrimer, Andrea Mountain, Edgar Segovia, Rosemary Stubbs, and Natasha Vall**

**Abstract** Guided by the theory of planned behaviour, we conducted an interview study to identify beliefs that potentially influence social-housing residents' future behaviour with domestic low-carbon technology in retrofit housing. The study included (group interview  $n = 6$ , individual interviews  $n = 14$ ). Behavioural beliefs, normative beliefs and control beliefs were identified from participants' answers using the theory of planned behaviour and thematic analysis. For successful implementation, it will be important to ensure that the predominant benefits (positive beliefs) emerging from this study are implemented (e.g., lower heating bills) and the barriers (negative beliefs) are avoided or alleviated (e.g., upfront costs). The results will be quantified in a follow-up, survey study.

**Keywords** Low-carbon technology · Theory of planned behaviour · Heat pump · Solar panels · Battery energy storage system

---

P. van Schaik (✉) · M. Cotton · C. Leighton · S. Lorrimer · A. Mountain · E. Segovia · R. Stubbs · N. Vall

School of Social Sciences, Humanities and Law, Teesside University, Middlesbrough, UK  
e-mail: [p.van-schaik@tees.ac.uk](mailto:p.van-schaik@tees.ac.uk)

H. Dawood · N. Dawood · E. Imani · M. Knowles · E. Segovia  
School of Computing, Engineering and Digital Technologies, Teesside University,  
Middlesbrough, UK

N. Dawood  
Net Zero Industry Innovation Centre, Teesside University, Middlesbrough, UK

## 24.1 Introduction

One of the measures to alleviate the effects of global warming currently under consideration is residential decarbonisation. Technical solutions (heat pump, solar panel, battery energy storage systems) are available, but initiatives that do not consider residents' acceptance will not be successful. Psychological theories and models such as the theory of planned behaviour and the technology acceptance model [1] provide tools that allow us to qualitatively identify beliefs that guide human behaviour with technology [2] and quantitatively predict behaviour [3]. The aim of the current study is therefore to identify beliefs that potentially guide social-housing residents' future behaviour with domestic low-carbon technology. The objectives are to identify behavioural beliefs (a person's subjective probability that performing a behaviour of interest will lead to a certain outcome or provide a certain experience), normative beliefs (injunctive normative belief: the expectation or subjective probability that a given referent individual or group approves or disapproves of performing the behaviour under consideration; descriptive normative belief, belief as to whether important others themselves perform the behaviour) and control beliefs (about the presence of factors that can facilitate or impede performance of the behaviour) that may underly residents' behaviour with domestic low-carbon technology according to the theory of planned behaviour [1], as well as any other beliefs.

## 24.2 Methodology and Theory

*Participants.* Twenty participants were recruited via two methods: email and social media. Potential participants could either respond to a dedicated email address or complete an online form, both of which were monitored for responses collected; participants were subsequently contacted by email or phone. All were offered either an online interview via VoIP or a face-to-face interview in their own home. The twenty participants (6 in a group interview and 14 in individual interviews) consisted of tenants, a mixture of men (10) and women (9), with an age range from 26–75. All residents lived in the Tees Valley in the north-east of England.

*Group interview.* Before the questions (see Table 24.1), the participants listened to a short presentation on global warming and UK climate change targets. It was explained how low-carbon homes, a critical part of the UK's efforts, are to meet climate change. At the start of the interview, participants were further presented with still images and a short video of a model retrofit home with explanatory live commentary, that demonstrated how a low-carbon technology home would look. The walkthrough video was created by Teesside University's School of Computing, Engineering and Digital Technologies using Autodesk REVIT, 3D modelling software.

**Table 24.1** Interview questions guided by theory of planned behaviour (TPB)

TPB belief		Questions
Behavioural beliefs	Advantages Disadvantages	<ul style="list-style-type: none"> <li>• What do you see as the advantages of you living in and using a low-carbon technology home?</li> <li>• What positive feelings do you associate with you living in and using a low-carbon technology home?</li> <li>• What do you see as the disadvantages of you living in and using a low-carbon technology home?</li> <li>• What negative feelings do you associate with you living in and using a low-carbon technology home?</li> </ul>
Normative beliefs	Approval Adopters Disapproval Non-adopters	<ul style="list-style-type: none"> <li>• Please tell me about the individuals or groups who would approve or think you should live in and use a low-carbon technology home</li> <li>• Please tell me about the individuals or groups who are most likely to live in and use a low-carbon technology home</li> <li>• Please tell me about the individuals or groups who would disapprove or think you should not live in and use a low-carbon technology home</li> <li>• Please tell me about the individuals or groups who are least likely to live in and use a low-carbon technology home</li> </ul>
Control beliefs	Drivers Barriers	<ul style="list-style-type: none"> <li>• Please tell me about any factors or circumstances that would make it easy or enable you to live in and use a low-carbon technology home</li> <li>• Please tell me about any factors or circumstances that would make it difficult or prevent you from living in and using a low-carbon technology home</li> </ul>

Semi-structured questions with open answers (see Table 24.1), based on the theory of planned behaviour, were used to encourage discussion of ideas. The theory of planned behaviour is appropriate to use in this research, as the theory accounts for beliefs that guide human behaviour (behavioural beliefs, normative beliefs and control beliefs) [1] and has been used to qualitatively understand [2] and quantitatively predict [3] people’s use of technology. In this study, the benefits of conducting a group interview were to ensure the questions were understood and the other tools used, i.e., video, were effective for purpose [4]. As the Interview guide or questions are the main tool for providing consistency in the generation of qualitative data and, consequently, the conclusion of the research [5], this group interview was carried out as a pre-cursor to individual interviews.

*Individual interviews.* The procedure was adapted from the group interview. The participants were shown the pre-recorded presentation, including the content of both group interview presentations; then followed a short testimonial, from a tenant with low-carbon technology already installed. (The decision to include this testimonial was made following the results from the group interview where ‘lived experience’ of tenants currently using low-carbon technology was a high priority for potential acceptance). The interview questions (Table 24.1) were then asked.



The interviews were conducted and transcribed verbatim by five researchers. In order to avoid preconceptions and bias, three researchers analysed the data from the interviews, checking results against one another to come to a final agreement; this increased the credibility and trustworthiness of the results.

### 24.2.1 Data Analysis

Thematic analysis [6] was applied to the data sets and deductive coding began with the theory of planned behaviour belief questions on low-carbon homes to identify the broad, overarching emergent themes. Iterative coding included searching the data for relationships, similarities and differences and beginning to organise these into themes. Within the coding and themes, comparisons, frequency and elaborations were considered for determinants of behaviour and specific emerging themes [6]. The three researchers compared and reached a consensus on the codes and themes included in the results, and another researcher checked these for clarity.

## 24.3 Results and Discussion

*Group interview.* Four themes identified were unique to the group interview: participants expressed the desire to experience how the heat pump system would look and work inside their own home when installed. As lived experience of residents currently using the technology was a high priority for them, a testimonial was suggested. This feedback was incorporated into the individual face-to-face interviews and proved effective as these specific themes did not arise in this cohort. Participants expressed their wish to have choice in which place, if any, low-carbon technologies they would like installed—this may be due tenants fearing increased rent as a result. The questions of noise from the system and possible vandalism were also raised. The participants discussed the issue of skills gaps within the energy sector and suggested upskilling of current staff—this was seen as an opportunity to create new opportunities and jobs (Table 24.2).

*Individual interviews.* Control beliefs, behavioural beliefs, normative beliefs and other themes were identified (Table 24.3). *Control Beliefs:* environmental and climate change benefits were cited by almost all participants as the main motivator along with the benefits of lower running costs. Upfront costs were viewed as a barrier by five participants, but this was mostly likely from the point of view of self-funding the system. Retrofitting was viewed as a motivator, providing insulation was sufficient for effectiveness of the system. Further information regarding fitting the systems into multi-occupancy building or flats would improve motivation. *Behavioural Beliefs:* lower running costs were cited by almost all participants as a huge benefit; only two participants expressed concern around cost; environmental benefits were viewed,

**Table 24.2** Group interview results

Belief categories	Belief topics
Control beliefs	Energy/running costs Retrofit versus new build installation Ability to control the system
Normative beliefs	Realism of representation (of a low-carbon home) Evidence of system effectiveness from current users Who should live in a low-carbon home—variety of answers but lack of information on the system prevented further hypothesising
Behavioural beliefs	Environmental benefits Resistance to low carbon home Tenants' choice for installation
Other themes	Noise, tamperproof system Skills gap

alongside this, as a major advantage. Solar energy was regarded positively and as a free energy source. Temperature regulation was seen as an advantage, especially if it could be controlled and included the ability to provide zoned heating. Loss of storage space in the home was mentioned, along with the issue of maintenance. A few participants were concerned with technology flaws—these fears could be reduced by providing further information and engaging with tenants. *Normative Beliefs*: most participants believed that nobody would disapprove of or refuse the opportunity to live in a low-carbon home. *Other themes*: political—the issues surrounding renewables and the environment were viewed as complex, with confusing and conflicting information given to the public, but regardless of this most people were willing to engage in environmentally friendly initiatives. It was felt that a national plan is required, which includes low-carbon housing. Some participants felt that they did not have enough information to decide on whether low-carbon technology would function correctly or be suitable within their home.

## 24.4 Conclusion

Based on our findings, housing association tenants may benefit from clear, transparent information (e.g. from others who have experience of living in a low-carbon home) and support throughout the whole process, before, during and after fitting of low-carbon technologies. Specifically, they may profit from information about the benefits (e.g. improved health) and facilitators (e.g. potential savings on running costs) of changing to a low-carbon home. They may also benefit from information about the potential disadvantages (e.g. any flaws in the technology) and barriers (e.g. pre-requisites such as good home insulation), and explanation of how these can be overcome and refutation of any that are not true. Successful interaction between the new energy technology and the individual [7] could be encouraged by including

**Table 24.3** Individual-interview results

Control beliefs (barriers and motivators)	Behavioural beliefs (advantages and disadvantages)	Normative beliefs (important referents)	Other themes (beyond TPB)
<p><b>Environmentally friendly/save the planet (13)</b>                      “Well, it’ll benefit climate change. You know, because I’m not burning fossil fuels.” [P2]  <b>Running costs—see behavioural beliefs</b> Motivator: “So there’s the basic cost list and that it would cost less definitely.” [P6]                      Barrier: Cost Concerns (3)  <b>Multi-occupancy building/flats (3)</b>                      Barrier: “I don’t know how it would work with the set up in my ground floor flat.” [P8]  <b>Initial up-front costs (5)</b>                      Barrier: “So, not discounting things like climate change and things like that, from an economic point of view, and being a lease owner, it’s not a financially viable project for me.” [P2]                      Motivator: “Would cost you £10,000 to buy it, you save £50,000 in a lifetime, that’s worth it.” [P14]  <b>Retrofitting versus new build (3)</b>                      Barrier: I can’t help thinking that as a retrofit to this property it wouldn’t work without other things being done. [P1]                      Motivator: “Maybe upgrading the properties and as they’re doing that, installing it.” [P12]  <b>Disruption (2)</b>                      “[M]y main concern is the upheaval” [P3]  <b>Insulation (5)</b>                      “There would have to be a lot of insulation to the home before the low carbon side of it would work.” [P1]</p>	<p><b>Running costs (13)</b>                      Advantage: “Well it’s going to be cheaper fuel, that’s a big factors isn’t it?” [P9]                      Disadvantage (3): “My concerns are cost” [P2]  <b>Environmentally friendly/save the planet—see control beliefs</b>                      “I think I can help me to warm more ecological and reduce my carbon emission and all that.” [P7]  <b>Using solar energy (6)</b>                      “The easy one would be solar panels, because it’s a long building and it’s an East West building, and we’ve got ample room on the roof for solar panels.” [P5]  <b>Temperature regulation (7)</b>                      Advantage: “Well, they’d be warmer. They’d just run constantly. Don’t have to mess about with the thermostat or anything like that. They’d be set with the weather.” [P12]                      Disadvantage: “I just don’t want to have my bedroom heated or anything. Can it be switched off from there?” [P9]  <b>Technology flaws (4)</b>                      “I suppose the problem would be with any batteries wouldn’t it, cause all the all the rest is nice and sufficient.” [P11]  <b>Loss of storage space (1)</b>                      “you’d lose a bit of wall space, perhaps with the size of the radiators, but I would say none [disadvantages] that you couldn’t overcome very readily.” [P1]  <b>Maintenance (2)</b>                      “So when it comes to maintenance of systems like this it might be nice to be a bit long and costly but that’s it really.” [P4]</p>	<p>Who would approve of/live in a low-carbon home                      Younger people (4)                      People on low income (3)                      Environmentally conscious (4)                      Big families (4)                      Those who see other people with it (3)                      Councils, social housing provider and the government (3)                      Who would disapprove of/not live in a low-carbon home                      No-one would disapprove (9)                      Older people (4)</p>	<p><b>Politics (5)</b>                      “We all can help the planet and help our pockets by doing something or speaking about it. The more we yell at the government the more they will think they’ve got to do this.” [P14]  <b>Further information on low-carbon technology and instructions on use (7)</b>                      “I think they would be really interested, it would be positive impact on them and possibly they didn’t know anything about it, because I didn’t know anything about it until I went to [organisation’s] open day. These retrofits, I’ve never heard of it before, so yeah, I think that would be a positive note.” [P3]  <b>Social housing/income inequalities (4)</b>                      “Others do not have the same luxury. The only negative feeling is that I’ve I wish everybody else was having this system so they wouldn’t have to, you know, families with kids, wouldn’t have to worry about their cost of keeping themselves warm when it comes to winter.” [P4]  <b>Current rise in energy prices (3)</b>                      “We run entirely on electric, so we’re all feeling the pinch, but even more so if you’re just running on electric for your heating.” [P2]</p>

different audiences and social groups and to consider individuals, while making efforts to adapt to their reality.

**Acknowledgements** The authors are grateful to Thirteen Housing Group Limited for access to their residents for the recruitment of participants. The authors are also thankful to UK Community Renewal Fund for financially supporting this research.

## References

1. I. Ajzen, The theory of planned behavior: frequently asked questions. *Hum. Behav. Emerg. Technol.* **2**(4), 314–324 (2020). <https://doi.org/10.1002/hbe2.195>
2. K.M. White et al., Identifying safety beliefs among Australian electrical workers. *Saf. Sci.* **82**, 164–173 (2016). <https://doi.org/10.1016/j.ssci.2015.09.008>
3. Q. Deng, Y. Zheng, J. Lu, Z. Zeng, W. Liu, What factors predict physicians' utilization behavior of contrast-enhanced ultrasound? Evidence from the integration of the theory of planned behavior and technology acceptance model using a structural equation modeling approach. *BMC Med. Inform. Decis. Mak.* **21**(1) (2021). <https://doi.org/10.1186/s12911-021-01540-8>
4. L. Harvey, Social research glossary social research glossary. *Soc. Res.* 2022 [Online]. Available: <http://www.qualityresearchinternational.com/socialresearch/knowledge.htm>
5. N.I.A. Gani, M. Rathakrishnan, H.N. Krishnasamy, A pilot test for establishing validity and reliability of qualitative interview in the blended learning English proficiency course. *J. Crit. Rev.* **7**(5), 140–143 (2020). <https://doi.org/10.31838/jcr.07.05.23>
6. V. Braun, V. Clarke, Using thematic analysis in psychology. *Qual. Res. Psychol.* **3**(2), 77–101 (2006). <https://doi.org/10.1191/1478088706qp063oa>
7. N. DellaValle, A. Bisello, J. Balest, In search of behavioural and social levers for effective social housing retrofit programs. *Energy Build.* **172**, 517–524 (2018). <https://doi.org/10.1016/j.enbuild.2018.05.002>

**Open Access** This chapter is licensed under the terms of the Creative Commons Attribution 4.0 International License (<http://creativecommons.org/licenses/by/4.0/>), which permits use, sharing, adaptation, distribution and reproduction in any medium or format, as long as you give appropriate credit to the original author(s) and the source, provide a link to the Creative Commons license and indicate if changes were made.

The images or other third party material in this chapter are included in the chapter's Creative Commons license, unless indicated otherwise in a credit line to the material. If material is not included in the chapter's Creative Commons license and your intended use is not permitted by statutory regulation or exceeds the permitted use, you will need to obtain permission directly from the copyright holder.



# Chapter 25

## Multi-objective Optimisation of a Wastewater Anaerobic Digestion System



R. J. Ashraf, Jonathan D. Nixon, and J. Brusey

**Abstract** This paper looks at multi-objective optimisation of a wastewater AD system where the model is demonstrated for a case study plant. Anaerobic Digestion Model No. 1 (ADM1) was used to predict biogas yields from the digester. Interviews, with plant owners, and plant data were used to identify the objective functions and decision variables. The decision variables were defined to be the substrate feeding rate for each of the digesters and the ratio of biogas sent between a combined heat and power (CHP) plant and a biogas upgrading unit (BUU). The objectives set were to maximise the overall substrate feeding rate through the AD plant, maximise the overall energy output and minimise the running cost of the plant. Results from the optimisation study showed that the amount of sludge processed through the AD plant increased by 17.7% and the running cost of the plant reduced by 6.2%. These results demonstrate how performance of AD plants can be significantly improved by multi-objective optimisation techniques.

**Keywords** ADM1 · Cost · Biomethane · CHP · Plant data

### 25.1 Introduction

Anaerobic digestion (AD) is a process in which biodegradable organic wastes are broken down in the absence of oxygen by microbes to produce biogas and digestate which can be used for energy and fertilizer, respectively [3]. AD systems are considered as an environmental friendly technology for dealing with various organic waste including wastewater.

In global terms, with increasing populations, the amount of sludge is expected to increase and wastewater AD plants are constantly faced with the challenge of increasing the throughput through their systems [10]. Hence, optimal values of digester operating parameters are usually found for AD systems so that the quality

---

R. J. Ashraf (✉) · J. D. Nixon · J. Brusey  
Centre for Computational Science and Mathematical Modelling, Coventry University, Priory  
Street, Coventry CV1 5FB, West Midlands, UK  
e-mail: [ashrafr7@uni.coventry.ac.uk](mailto:ashrafr7@uni.coventry.ac.uk)

and quantity of biogas and effluent produced can be improved [2, 7, 11]. However, optimising just the digester might not result in the most efficient design and components in the system, other than the digester, also need to be taken into account. Furthermore, in addition to the technical performance of the system, the financial and environmental performances also need to be optimised.

Some researchers did perform multi-objective optimisation of a system where they aimed to simultaneously improve the technical, financial and environmental performance however, their work was not limited to just the AD process and included other technologies such as composting, gasification and pyrolysis [14]. Where research was focused on just AD, it predominantly looked at finding optimal combination of technologies and pathways that improved the performance of the system and these studies did not consider optimisation of AD system design parameters [5]. Yan et al. [17] and Li et al.'s [13] work were the only two studies that optimised both system parameters and the combination of technologies in an AD system. Nonetheless, a limitation of their work was that they used correlations between temperature and biogas yields, found in literature, to predict biogas yields values and not a comprehensive model such as the state of the art Anaerobic Digestion Model No. 1 (ADM1). Hence, there is a need for a multi-objective optimisation of an AD system, which integrates an extensive digester model with an optimisation algorithm, to improve the performance of an AD system.

This paper aims to outline an optimisation problem that couples ADM1 with multi-objective optimisation, to improve the technical and financial performance of an AD system. The model is demonstrated for a wastewater anaerobic digestion system where optimal values of different system design parameters are found.

In the following section, the methodology is outlined and a rationale for the chosen objectives functions and decision variables is given. An overview of the case study system is outlined in Sect. 25.3 and a detailed model is described in Sect. 25.4. The results and discussion are provided in Sect. 25.5 and the paper concludes with the key findings from the study and recommendations for future work.

## 25.2 Methodology

The multi-objective optimisation model developed in this study uses ADM1 to predict biogas yields from a digester and optimises values of different design parameters for a wastewater AD system. The model was demonstrated for a case study AD plant and predicted biogas yield values were validated with measured data. Objective functions and decision variables were representative of the current challenges faced by the case study's plant owners. Semi-structured interviews and plant performance data were used to identify these challenges. Analysis of the data and the interview results showed that at present, sludge often has to be strategically moved through the wastewater treatment plant because the AD side is at full capacity. Furthermore, the plant owners would also like to determine the optimal ratio of biogas that should be sent between the CHP and Biogas Upgrading Units (BUU) so that overall energy

output from the plant is maximised and the energy costs are kept low. Based on these findings, the decision variables were defined to be the substrate feeding rates for each of the digester and the ratio of biogas sent between the CHP and BUU. The objectives set were to maximise the sludge throughput through the AD plant, maximise the overall energy output and minimise the running costs. Objective functions were normalised and a single utility function was created and minimised using genetic algorithm (GA) in Python.

### 25.3 Case Study Plant

Thickened sewage sludge is blended with water and divided between eight digesters. Biogas produced goes either into a CHP where it is converted into electricity, or a BUU where it is converted to biomethane and sent to the grid. Data recorded from the plant consists of the substrate feeding rate ( $m^3/day$ ) for each of the digesters and the total energy generated, in megawatt hours (MWh), from the CHP and biomethane sent over the grid.

Figure 25.1 shows a schematic of the plant layout and the plant components and Table 25.1 shows values of the parameters associated with the case study system.

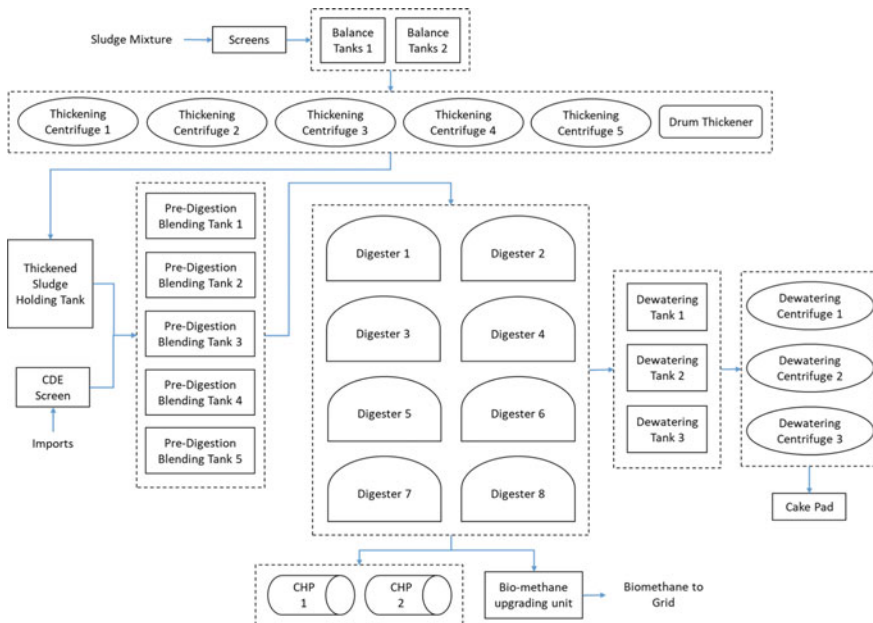


Fig. 25.1 Layout of the waste water anaerobic digestion plant

**Table 25.1** Values of the different parameters associated with the case study system

Parameter	Definition	Units	Value	Reference
V <sub>dig</sub> (1–4)	Total volume of digester	m <sup>3</sup>	2050	Case study data
V <sub>dig</sub> (5–8)	Total volume of digester	m <sup>3</sup>	2500	Case study data
V <sub>liq</sub>	Working volume of digester	m <sup>3</sup>	0.9V <sub>dig</sub>	Case study data
r	Radius of all digesters	m	8	Case study data
T <sub>D</sub>	Digestion temperature	°C	37.8	Case study data
B <sub>ch4</sub>	Percentage of methane in biogas	%	60	Case study data
B <sub>energy</sub>	Energy content of biogas	m <sup>3</sup> /MWh	400	Case study data

## 25.4 Models/Theory

### 25.4.1 Using ADM1 to Determine Biogas Yield

To predict biogas yield values, a modified ADM1 model by [15] was used and the ADM1 coefficients and substrate initial conditions for sewage sludge were taken from Rosen and Jeppsson's [16] work. The assumption made was that the sewage sludge modelled by Rosen and Jeppsson [16] would be representative of the sludge processed at the case study plant.

Before predicted biogas yields were validated with measured data, ADM1 was calibrated for ten days to allow the model to adjust to the system. During this time, the flowrate of sludge was gradually increased from 0 to 90 m<sup>3</sup>, in increments of 10 m<sup>3</sup>. Since the case study plant consisted of eight digesters, with different flowrates and digester volumes, ADM1 was run individually for each digester and then the total predicted biogas yield was determined by adding the biogas yields from each of the individual digesters. The overall measured biogas yield values were determined using the plant data. Equations (25.2) and (25.3) were used to back calculate the biogas entering the CHP and BUU, using the energy values given in the plant data. The predicted and measured biogas yield values were compared for the months of October 2020 and September 2021.

### 25.4.2 Optimisation Problem

Once the objective functions and decision variables were defined the optimisation problem was formulated. Equation 25.1 shows how the objective functions were normalised and added together to form a utility function.

$$\min_{x \in R} f(x) = \sum -\frac{F(x)}{|F(x_{\text{raw}})|} - \frac{E(x)}{|E(x_{\text{raw}})|} + \frac{C(x)}{|C(x_{\text{raw}})|} \quad (25.1)$$



$$\begin{aligned}
0 < x_1 < 109, x \in R & \quad 0 < x_2 < 140, x \in R & \quad 0 < x_3 < 109, x \in R \\
0 < x_4 < 140, x \in R & \quad 0 < x_5 < 133, x \in R & \quad 0 < x_6 < 133, x \in R \\
0 < x_7 < 133, x \in R & \quad 0 < x_8 < 133, x \in R & \quad 0 < x_9 < 1, x \in R
\end{aligned}$$

where,  $F(x)$  is the total sludge added through the AD plant ( $\text{m}^3/\text{day}$ ),  $E(x)$  is the total energy produced by the system (MWh) and  $C(x)$  is the total running cost of the plant (\$),  $x_1$  to  $x_8$  are the substrate feeding rates for each of the digesters ( $\text{m}^3/\text{day}$ ) and  $x_9$  is the ratio of biogas sent between the BUU and the CHP.

The electricity produced from the CHP was determined using the energy content of biogas and the CHP efficiency.

$$E_{\text{CHP}} = \frac{B_{\text{CHP}}\eta_{\text{CHP}}}{B_{\text{energy}}} \quad (25.2)$$

where,  $E_{\text{CHP}}$  is the electricity from the CHP (MWh),  $B_{\text{CHP}}$  is the biogas sent to the CHP ( $\text{m}^3/\text{day}$ ),  $\eta_{\text{CHP}}$  is the electrical efficiency of the CHP unit (%) and  $B_{\text{energy}}$  is the energy content of biogas ( $\text{m}^3/\text{MWh}$ ).

The energy produced from the BUU was calculated using the amount of methane in biogas and the methane recovery ratio of the BUU.

$$E_{\text{G2G}} = \frac{B_{\text{G2G}}\eta}{B_{\text{energy}}B_{\text{ch4}}} \quad (25.3)$$

where,  $E_{\text{G2G}}$  is the energy from the biomethane sent to the grid (MWh),  $B_{\text{G2G}}$  is the biogas sent to the BUU ( $\text{m}^3/\text{day}$ ),  $\eta$  is the methane recovery percentage of the BUU (%) and  $B_{\text{ch4}}$  is the concentration of methane in biogas (%).

The total energy was determined by adding the amount of electricity produced by the CHP unit and the biomethane sent to the grid.

The total running cost of the system was determined by calculating the energy needed to heat the digesters and heat loss through the digesters walls using the input parameters shown in Table 25.1 and equations in [4]. The running costs of the CHP and BUUs were determined by multiplying the energy produced from those systems with the cost values shown in Table 25.2.

## 25.5 Results and Discussion

### 25.5.1 Validating ADMI with Measured Data

Figure 25.2 shows a comparison between the predicted and measured biogas yields for October 2020 and September 2021.

**Table 25.2** Values of the input parameters used in the model

Parameter	Definition	Units	Value	References
<i>CHP (Jenbacher 320 series)</i>				
$\eta_{elec}$	Electrical efficiency	%	41.2	GE Power and Water [8]
$\eta_{thermal}$	Thermal efficiency	%	41	GE Power and Water [8]
Cost_chp	Cost to maintain CHP unit	\$/MWh	10	Burgis [6]
<i>Airliquide biogas upgrading unit (BUU) and grid connection</i>				
$\eta$	Methane recovery efficiency	%	98.5	Air Liquide [1]
$\dot{m}$	Maximum throughput	m <sup>3</sup> /h	1800	Case study data
Cost_bmt	Cost to upgrade biogas	\$/MWh	6.9	Iea [12]
<i>Overall plant</i>				
C_elc	Electricity cost	\$/kWh	0.21	Gov.uk [9]

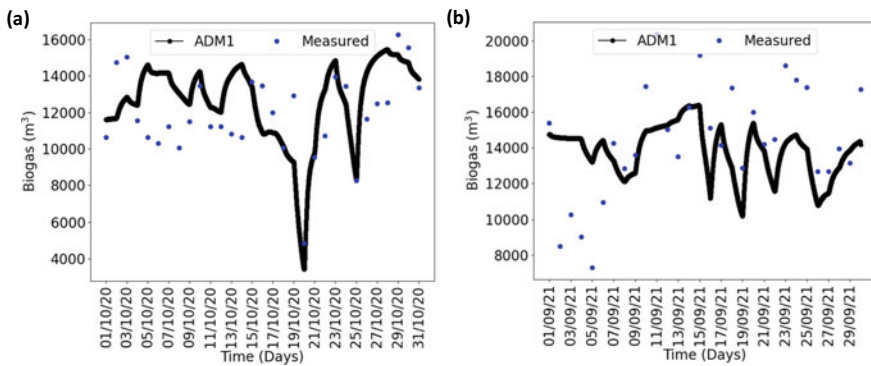


**Fig. 25.2** Predicted biogas yield versus measured for the months of October 2020 and September 2021

It can be seen that a good agreement exists between predicted and measured biogas yields for both months hence, this model can be used in the optimisation study to predict biogas yields. The small discrepancy between the results can be improved by characterising the feedstock used in this case study plant instead of using generic sludge ADM1 coefficients found in literature.

### 25.5.2 Current Versus Optimised System

Figure 25.3 shows the substrate feeding rates for each of the digesters 1–8 in the current and optimised system.

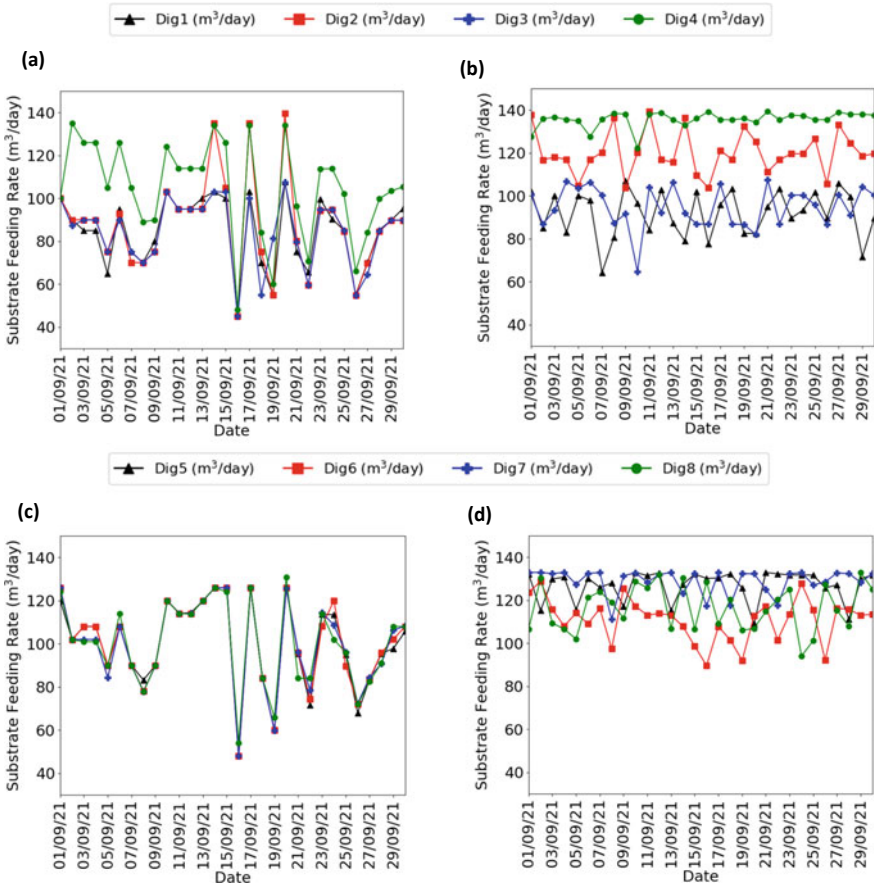


**Fig. 25.3** Substrate feeding rate for each of the digesters 1–4 and 5–8 in the current (a, c) and optimised system (b, d), respectively

At present, the substrate feeding rate for each of the digesters 1–3 and 5–8 are approximately similar to each other. However, the optimiser suggests different feeding rates for each of the digesters based on their maximum allowable capacity. This results in higher and more consistent daily sludge volumes through the plant and allows for more stable operation (Fig. 25.4a, b). Furthermore, optimising sludge volumes for each of the digesters based on their capacity allows them to perform at their optimal capacity, increases their lifetime and reduces their operation and maintenance costs.

Figure 25.4 shows the overall substrate feeding rate and biogas produced from the system and the amount of electricity and biomethane produced along with the running costs of the plant, for the current and optimised system.

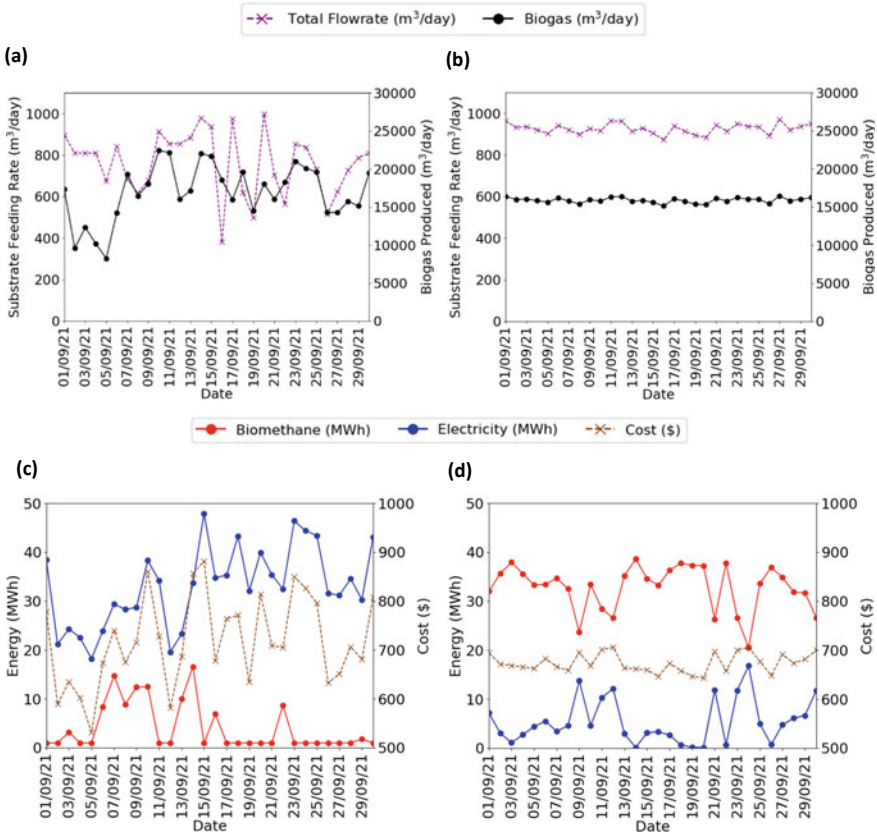


**Fig. 25.4** Electricity and biomethane produced and the running cost of current (a) and optimised (b) AD system

Electricity from the CHP is the predominant downstream pathway for biogas in the current system however, this causes the running cost of the plant to be inconsistent and higher throughout the month. The optimiser suggests to produce more biomethane as that results in an overall higher energy from the plant and lower running costs. More consistent and higher sludge volumes are now also processed through the plant and this allows the system performance to be more consistent and predictable. Table 25.3 shows the percentage change in the value of the objective functions, for September 2021, after implementing the multi-objective optimisation approach. The amount of sludge processed through the plant and overall energy output have increased by 17.7% and 3.0%, respectively. The running cost of the plant has reduced by 6.2%. These are significant improvements in system performance achieved by making minor modifications to the plant such as optimising the sludge feeding rates for each of the digesters and the ratio of biogas sent between the CHP and BUU.

**Table 25.3** Change in the values of the objective functions after applying the multi-objective optimisation approach

Scenario (September 2021)	Objective function		
	Max. total flowrate (m <sup>3</sup> )	Max. total energy (MWh)	Min. cost (\$)
Original	22,869.3	1113.3	21,567.6
Optimised	27,779.3	1147.0	20,232.3
% Change	↑ 17.7%	↑ 3.0%	↓ 6.2%

## 25.6 Conclusion and Further Work

Results from this optimisation study show that higher and more consistent sludge volumes can now be processed through the case study AD plant. This will meet the current challenge of having to process large volumes of sludge through the wastewater AD plant, while keeping the running costs low. By implementing the multi-objective optimisation approach, the total sludge volumes processed through the plant increased by 17.7% and the energy costs reduced by 6.2%. The ratio of biogas converted to electricity and biomethane was also optimised so that higher overall energy can be achieved from the plant.

The optimiser can be extended to determine whether sending biomethane to the grid is the most optimal choice or would another end use of biomethane be more suitable. The environmental performance of the plant can also be added as an objective function in the optimisation study so that any biogas flaring and greenhouse gas (GHG) emissions from the plant can be taken into account. Results from the optimisation study can be communicated back to case study partners so that their suggestions and feedback can be incorporated into the model to further optimise the system's performance.

**Acknowledgements** This project has received funding from the European Union's Horizon 2020 research and innovation programme under the Marie Skłodowska-Curie grant agreement No 801604.

## References

1. Air Liquide, Biogas upgrading (2021)
2. H. Akbaş, B. Bilgen, A. Melih Turhan, An integrated prediction and optimization model of biogas production system at a wastewater treatment facility. *Bioresour. Technol.* **196**, 566–576 (2015). <https://doi.org/10.1016/j.biortech.2015.08.017>
3. J.G. Akinbomi, R.J. Patinvo, M.J. Taherzadeh, Current challenges of high-solid anaerobic digestion and possible measures for its effective applications: a review. *Biotechnol. Biofuels Bioproducts* **15**(1), 1–13 (2022). <https://doi.org/10.1186/s13068-022-02151-9>
4. Ashraf, R.J., J.D. Nixon, and J. Brusey, Using multi-objective optimisation with ADM1 and measured data to improve the performance of an existing anaerobic digestion system. *Chemosphere* **301**, 134523 (2021). <https://doi.org/10.1016/j.chemosphere.2022.134523>

5. Ş.Y. Balaman, H. Selim, A network design model for biomass to energy supply chains with anaerobic digestion systems. *Appl. Energy* **130**, 289–304 (2014). <https://doi.org/10.1016/j.apenergy.2014.05.043>
6. E. Burgis, Understanding CHP and the cost of installation (2018). <https://understandingchp.com/blog/understanding-chp-and-the-cost-of-installation/#:~:text=Reciprocatingengine> CHP systems are,smallercommercialbuildings(%24%2FkW)
7. A.M. Enitan, J. Adeyemo, O. Oluwatosin Olofintoye, F. Bux, F.M. Swalaha. *Multi-objective Optimization of Methane Producing UASB Reactor Using a Combined Pareto Multi-objective Differential Evolution Algorithm (CPMDE)*. *EVOLVE—A Bridge between Probability, Set Oriented Numerics, and Evolutionary Computation V. Advances in Intelligent Systems and Computing*, vol. 288 (Springer, Cham, 2014). <https://doi.org/10.1007/978-3-319-07494-8>
8. GE Power and Water, Jenbacher Type 3 (2013)
9. Gov.uk, Quarterly energy prices (2022). [https://assets.publishing.service.gov.uk/government/uploads/system/uploads/attachment\\_data/file/1086569/quarterly\\_energy\\_prices\\_uk\\_june\\_2022.pdf](https://assets.publishing.service.gov.uk/government/uploads/system/uploads/attachment_data/file/1086569/quarterly_energy_prices_uk_june_2022.pdf).
10. F. Hanum, L.C. Yuan, H. Kamahara, H.A. Aziz, Y. Atsuta, T. Yamada, H. Daimon, Treatment of sewage sludge using anaerobic digestion in Malaysia: current state and challenges. *Front. Energy Res.* **7**, 1–7 (2019). <https://doi.org/10.3389/fenrg.2019.00019>
11. M. Huang, W. Han, J. Wan, Y. Ma, X. Chen, Multi-objective optimisation for design and operation of anaerobic digestion using GA-ANN and NSGA-II. *J. Chem. Technol. Biotechnol.* **91**(1), 226–233 (2014). <https://doi.org/10.1002/jctb.4568>
12. Iea, Sustainable supply potential and costs (2020). [https://iea.blob.core.windows.net/assets/03aeb10c-c38c-4d10-bccc-de92e9ab815f/Outlook\\_for\\_biogas\\_and\\_biomethane.pdf](https://iea.blob.core.windows.net/assets/03aeb10c-c38c-4d10-bccc-de92e9ab815f/Outlook_for_biogas_and_biomethane.pdf)
13. W. Li, J.K. Huusom, Z. Zhou, Y. Nie, Y. Xu, X. Zhang, Multi-objective optimization of methane production system from biomass through anaerobic digestion. *Chin. J. Chem. Eng.* **26**(10), 2084–2092 (2018). <https://doi.org/10.1016/j.cjche.2018.01.001>
14. G. Mavrotas, N. Gakis, S. Skoulaxinou, V. Katsouras, E. Georgopoulou, Municipal solid waste management and energy production: consideration of external cost through multi-objective optimization and its effect on waste-to-energy solutions. *Renew. Sustain. Energy Rev.* **51**, 1205–1222 (2015). <https://doi.org/10.1016/j.rser.2015.07.029>
15. H.H. Nguyen, Modelling of food waste digestion using ADM1 integrated with Aspen Plus. Doctor thesis (2014)
16. C. Rosen, U. Jeppsson, *Aspects on ADM1 Implementation within the BSM2 Framework* (Lund, Sweden, 2006)
17. N. Yan, B. Ren, B. Wu, D. Bao, X. Zhang, J. Wang, Multi-objective optimization of biomass to biomethane system. *Green Energy Environ.* **1**(2), 156–165 (2016). <https://doi.org/10.1016/j.gee.2016.05.001>

**Open Access** This chapter is licensed under the terms of the Creative Commons Attribution 4.0 International License (<http://creativecommons.org/licenses/by/4.0/>), which permits use, sharing, adaptation, distribution and reproduction in any medium or format, as long as you give appropriate credit to the original author(s) and the source, provide a link to the Creative Commons license and indicate if changes were made.

The images or other third party material in this chapter are included in the chapter's Creative Commons license, unless indicated otherwise in a credit line to the material. If material is not included in the chapter's Creative Commons license and your intended use is not permitted by statutory regulation or exceeds the permitted use, you will need to obtain permission directly from the copyright holder.



# Chapter 26

## Energy Demand Reduction in Data Centres Using Computational Fluid Dynamics



**R. Sethuramalingam, Abhishek Asthana, S. Xygkaki, K. Liu, J. Eduardo, S. Wilson, and C. Bater**

**Abstract** A data centre is a facility where it hosts the server systems, computer systems, and its associated components such as cooling units, redundancy power supplies and power storage systems. Data centres are a very energy-demanding sector. Data Centre Dynamics magazine forecasts that by 2025, Data Centres will consume more than 2% of the global electricity supply. Due to this forecast, it is become vital to reduce the energy consumption in the data centre industry. On average, data centres use 30–50% of their total energy supply on mechanical cooling to cool their IT equipment. However, many of them still have difficulties with high-temperature regions such as hot spots in the server data hall which contributes to server downtime. Along with this, the power densities of the data centres are on the rise as the telecommunication industry at exponential growth over the years. This inefficiency in the temperature distribution can be resolved through advanced computational fluid dynamics software. It also becomes essential to expand the use of CFD (computational fluid dynamics) into key sections of Data Centre design, to reduce thermal inefficiencies. It is necessary to identify the potential issues at the initial stages to deliver efficient solutions which will work at a low Power Usage Effectiveness (PUE), to future-proof data centre facilities. This paper outlines the importance of a computational fluid dynamics (CFD) analysis in the data centre design. The mock-up data centre internal and external models are analysed in 6Sigma Software. The various parameters were investigated to optimise the energy performance of the infrastructure. The results also provided the analysis of the data hall with detailed rack inlet and 3D modelling of the data hall, external simulations with chillers and generators inlet temperatures highlighting trouble areas. Additional to this, Water cooled, and Air-cooled chiller performance comparison also studied and concluded that Water cooled chiller performance well than Air cooled chiller. Having the data hall air

---

R. Sethuramalingam (✉) · A. Asthana  
Sheffield Hallam University, Howard Street, Sheffield City Centre, Sheffield S1 1WB, UK  
e-mail: [rs1653@hallam.shu.ac.uk](mailto:rs1653@hallam.shu.ac.uk); [rsethuramalingam@bw-engineering.com](mailto:rsethuramalingam@bw-engineering.com)

S. Xygkaki · K. Liu · J. Eduardo · S. Wilson · C. Bater  
Black and White Engineering Ltd, Generator Studios, Newcastle Upon Tyne NE1 2LA, UK

supply temperature 27 °C than 24 °C, has improved the energy efficiency in the data centre. The model developed in this study can be used as a benchmark study for the present and future thermal optimization of data centres.

**Keywords** Computational fluid dynamics · Data centre cooling · 6Sigma · k-epsilon RANS model · Internal modelling · External modelling

## 26.1 Introduction

The rapid increase in the number of internet users in recent years has demanded very high heat density servers. Data centres are a very energy-intensive sector with rapid developments in the 5G and AI (Artificial Intelligence). The number of internet users will increase from 3.6 million to 5 billion between 2018 to 2025 respectively [1]. In 2018, data centres' electricity consumption has reached 1% of global electricity demand [2]. During pandemic conditions, the data centres industry has seen rapid growth in its IT loads due to digitalization. Energy consumption in data centres is expected to rise by 15–20% each year [3]. Cooling of the IT equipment demands substantial power as 40% of the total power consumption in the data centres is from the cooling equipment. Also, the high demand for cloud-based data centres and High-Power Computers (HPSs) is leading to an increase in the cooling demand.

Traditionally all data centres are air cooled where they use the hot/cold containment systems to decrease the air circulation, reducing hot–cold air mixing and removing thermal inefficiencies. However, these energy-efficient design solutions are not alone enough to make the data centre very efficient. An in-depth analysis of thermal distribution is needed to avoid any downtime and to make the design flawless. CFD analysis method could be used to identify any flaws in the design in the early development stage. Therefore, this study will investigate reducing the cooling energy demand in the data centre by using external and internal CFD Simulations.

Simulation of internal and external thermal conditions in a data centre by using the CFD has become a very thriving research area in recent years. Swift development in the computational power and accuracy in the numerical models in the last decade made CFD a more viable and reliable option to understand the flow behaviour in the data centre. 6Sigma CFD models are important in the data centre industry because of their flexibility due to their specific features that are specifically designed for data centre sectors [4]. Commercial CFD solver software is proven to be accurate in data centre thermal modelling. Cho et al. [5] studied a series of simulations for various design options using commercial software to investigate thermal performance in data centres. Similarly, Nada and Said [6] analysed the importance of the CRAC (Computer Room Airconditioned Unit) layout for the high heat density data centre and found that placing the CRACs perpendicular to the data hall containment improved the thermal performance of the data hall.



So, the aim of this study is to develop a design of an external and internal layout of the data centre with a focus on enhancing their thermal performance that changes the dynamics of data centre cooling to energy savings. Therefore, the main objective is to accurately model the data centre and enhance the thermal distribution. Finally, evaluate the energy performance in the data centre.

## 26.2 Models

Internal computational fluid dynamics (CFD) studies have been conducted for the server data hall room. These studies are intended to determine the flow direction of air and assess the intake air temperature at the electrical equipment and the average temperature of the IT cabinet data hall room. The capability of the cooling system to deliver the required cooling capacity within the temperature tolerance under both normal operation and failure scenarios has also been assessed. The CFD simulations have been conducted using 6SigmaRoom R15 software to build the 3D geometry of the IT data hall room. All structural obstructions such as columns and beams have been included in the 3D CFD model. Figure 26.1 illustrates the 3D model of the data hall.

Along with this, A computational fluid dynamics (CFD) external study was conducted for the data centre, to investigate the potential uplift in supply air temperature for the chillers on the roof. The principal concern is the risk of cooling unit's derating due to warm air entering from the neighbouring cooling units (normal operation) exhaust vents and generator exhaust flues (emergency operation). Figure 26.2 illustrates the 3D model layout for the roof of the data centre which includes the generators and chillers. The local microclimate was evaluated based on historical meteorological data from the NOAA (National Oceanic and Atmospheric Administration) weather website [7]. The meteorological data, which was associated with

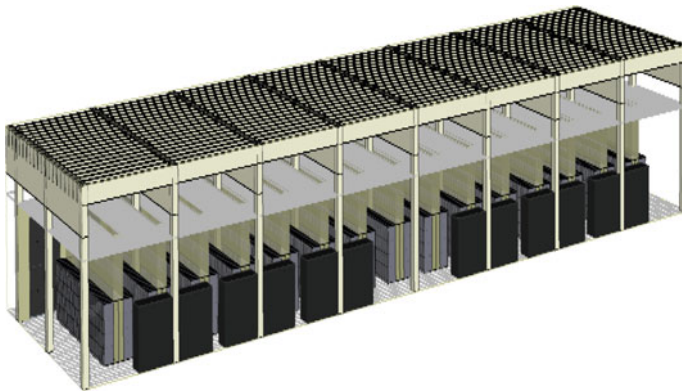


**Fig. 26.1** Internal design of data hall

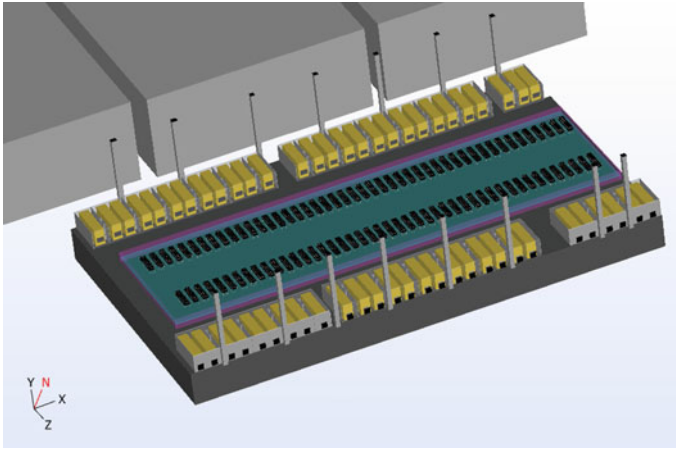


**Fig. 26.2** External design of data centre roof with chillers and generators

the hourly wind speeds recorded over a 20-year period between 2001 and 2020, were analysed., the maximum recorded dry-bulb temperature in the area is 39.1 °C in a 20-year period. Following the wind analysis, a temperature analysis was conducted for the 20-year period (2001–2020). As per the analysis, the dominant wind of 7 m/s from the SW direction was chosen for this study. Additional to this, the key properties that need to be considered in the energy-efficient data centre design are the cooling load and total facility load. For this application, the total IT load (Each rack 8.33 kW heat load) and cooling load are assumed as 96 MW IT data centre and chiller load 112.32 MW for this study.

### 26.3 Theory

The airflow, temperature and pressure differences were governed by the following continuity, momentum and energy conservation equations including buoyancy effects. The solver breaks down the Navier stokes equation as Reynolds averaged Navier stoked equations to solve simulations within the realistic time scale and with less computational power [8]. A comprehensive description of the RANS model equations is expressed in Eqs. (26.1–26.4). 6Sigma uses the K-epsilon RANS Turbulence model to simulate the flow characteristics.

Continuity equations:

$$\text{div}\underline{U} = 0 \quad (26.1)$$

Momentum equation for the RANS model:

$$\frac{\partial}{\partial t}(\underline{U}) + div(\underline{U}\underline{U}) = \frac{1}{\rho}div(\underline{\sigma} - \rho\underline{u}'\underline{u}') + \frac{1}{\rho}\underline{S} \tag{26.2}$$

where

$$\underline{\sigma} = -PI + \mu(grad(\underline{U}) + grad(\underline{U}^T)) \tag{26.3}$$

$\underline{U}$ —Average velocity vector,  $\underline{\sigma}$ —Average stress tensor,  $\underline{u}'$ —Velocity fluctuational vector,  $\underline{S}$ —additional momentum source and energy term for the RANS can be expressed as below:

$$\frac{\partial T}{\partial t} + div(\underline{U}T) = div\left(\left(\frac{v}{Pr} + \frac{v_r}{Pr_r}\right)gradT\right) + \frac{1}{\rho C_p}S_Q \tag{26.4}$$

$T$ —Temperature,  $V$ —Dynamic Viscosity,  $Pr$ —Prandtl Number,  $S_Q$ —energy source.

Table 26.1 illustrates the boundary conditions and assumptions made in the 6Sigma Solver.

The simulations are not conducted on transient simulation and along with this simulation has not considered the solar gain on the roof of the building.

**Table 26.1** Boundary conditions and assumptions

Boundary conditions	Value/units	Boundary conditions	Value/units
External wind conditions	7 NE/37.5 °C	RANS model	K-epsilon
Data hall air supply	Ranges between 24 and 27 °C	Mesh count internal	6 million
CRAC redundancy	N + 2	Mesh count external	24 million
Max chiller cooling load	2745 kW	Algorithm	SIMPLE
Building orientation	N 33°	Computational time/internal simulations	7 h/HPC Solver
GE heat rejection loads	2442 kW/through exhaust 3034 kW	Computational time/internal simulations	16 h/HPC solver
CRAC cooling max capacity	450 kW	Cabinet heat capacity	8.33 kW

## 26.4 Energy Metric

The most popular method to calculate energy effectiveness is PUE (power usage effectiveness). This method was initially proposed and promoted by Green Grid (a non-profit IT organization) [9]. PUE is described as the ratio between the total facility power divided by the power required by the IT to operate. Along with PUE, the green grid also developed and promoted the DCiE (Data Centre Infrastructure Efficiency) which is inverse of the PUE. Equation 26.5 states the description of the PUE.

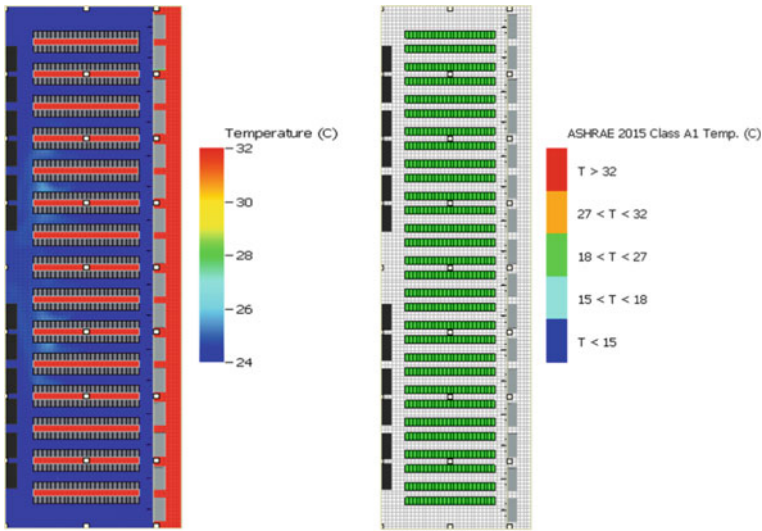
$$\text{PUE} = \frac{\text{Total Data Centre Facility Energy Consumption}}{\text{IT Equipment Energy Consumption}} \quad (26.5)$$

## 26.5 Results and Discussion

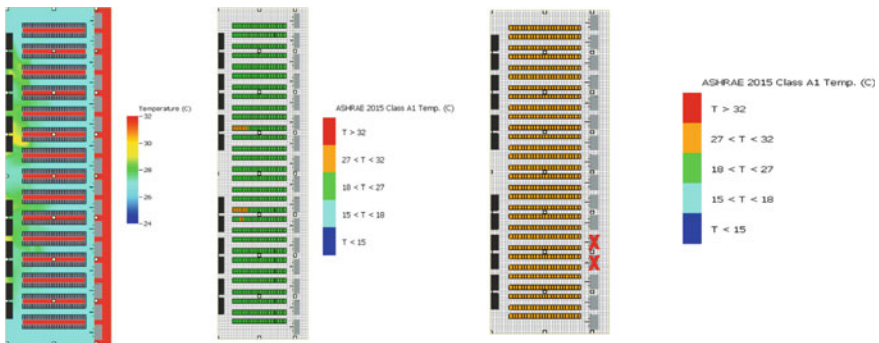
In this section of the article, several results of the internal and external simulations are presented along with two various options for the chiller. The proposed sample data centre internal and external simulation illustrated vital role of the CFD to enhance the thermal performance of the data centre and increase its efficiency.

Figure 26.3a illustrate results as follows, data hall normal operation at 24.0 °C room temperature results showed that average room temperature distribution at 1.0 m from the floor level at 25.0 °C, highest data hall cold aisle temperature is—26.0 °C, highest averaged IT cabinet inlet temperature is 25.3 °C, maximum IT cabinet inlet temperature—26.2 °C, highest return temperature is 35.3 °C and average air velocity within cold aisle—1.2 m/s.

To push the data centres further to their thermal limits, the inlet temperature has been set to increase, to achieve the most efficient solutions possible. Figure 26.4a illustrate results as, data hall normal operation at 27.0 °C showed that average room temperature distribution at 1.0 m from floor level at 27.5 °C, highest cold aisle temperature is—31.0 °C, highest averaged IT cabinet inlet temperature is—28.9 °C, maximum IT cabinet inlet temperature—29.4 °C, highest return temperature is 38.2 °C, Average air velocity within cold aisle—0.9 m/s with the highest velocity as 3 m/s. Figure 26.4b illustrates ASHRAE standards for the rack inlet temperature in a failure scenario, failure scenario simulation results have illustrated that the rack inlet temperature has slightly in comparison with CRAC 24.0 °C increased but not exceeded the ASHRAE standards. The uplift (27.0 °C) in the inlet rack temperature made the data centre more efficient in comparison with the rack inlet temperature of 24.0 °C.



**Fig. 26.3** a Temperature contour of data hall at 24.0 °C, b ASHRAE temperature limit for data hall cabinets at 24.0 °C



**Fig. 26.4** a Temperature contour of data hall at 27.0 °C, b ASHRAE temperature limit for data hall cabinets at 27.0 °C, c ASHRAE temperature limit for data hall cabinets at 27.0 °C (failure scenario—where are 2-cooling units failed)

Figure 26.5 illustrates the external CFD simulation temperature contour at roof level. Following boundary conditions are simplified to analyse the thermal performance of the roof design. Velocity: 7 m/s; Wind Direction: NE; Power failure so Generator’s Engine so all generators ON; All chillers status: On; the results showed that given roof layout design could work under the peak thermal and dominant wind conditions along with power failure mode where generator will be running. This has given very high confidence on the design work which will work flawlessly under any given worst-case conditions. Chart 26.1 presents the analytical calculation of cost

saving on various inlet conditions along with the Water-Cooled Chiller (WCC) versus Air Water Cooled Chiller (ACC) option. Inlet water Temperature under options at 20.0 °C and 24.0 °C respectively. These results indicated that WCC chillers could potentially save money by around €100,000 per annum than ACC chillers. Along with this, Table 26.2 illustrates that better PUE also can be also achieved by using the WCC chiller as increasing the supply water temperature to the data halls.

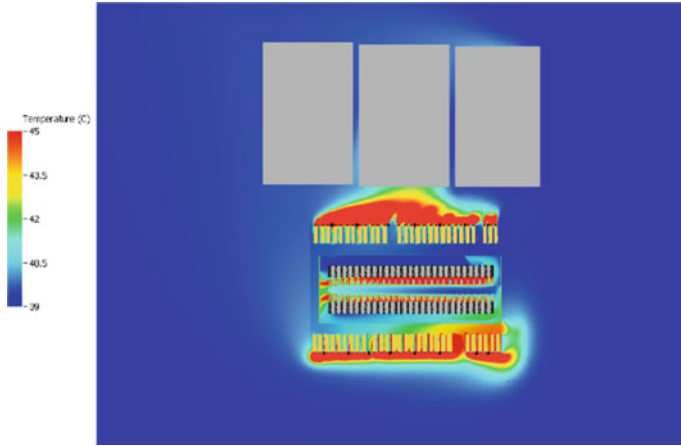


Fig. 26.5 External temperature contour on the roof of the data centre building

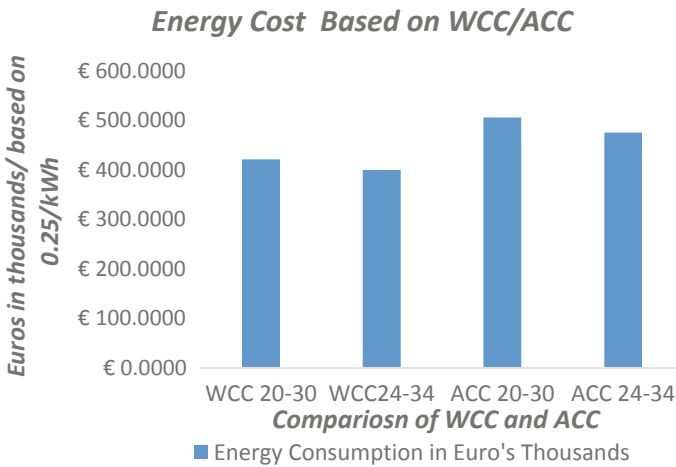


Chart 26.1 Energy cost in comparison of WCC and ACC

**Table 26.2** PUE comparison

Chiller types	Water supply temperature ( C )	Annual PUE
Water cooled chiller	20	1.32
	24	1.28
Air cooled chiller	20	1.42
	24	1.38

## 26.6 Conclusion

The following conclusions are drawn from this article and future work is to improve the CFD analysis strategies to further improve the energy efficiency of the data centre.

- High inlet temperature to data hall within the ASHRAE limit potentially improves the efficiency.
- External simulation of the CFD concluded that the design of the data centre roof will work flawlessly under peak thermal and wind conditions.
- 6sigma CFD solver proven to be extremely useful and reliable in simulating the data centre CFD scenarios both internally and externally.
- Finally, this study also found that a water-cooled chiller solution is more efficient than air-cooled chillers.
- As the solver only capable of using K-epsilon model to solve the simulations, more RANS model cannot be investigated. Addition to this, solver also not accounted the solar gain on the roof. This could be investigated further to model the roof behaviour very accurate.
- As future work of this study, more realistic experimental data will be recorded in comparison with the CFD results to evaluate the accuracy of the solver in detail.

**Acknowledgements** This work is supported by Black and White Engineering Ltd.

## References

1. J. Koomey, Growth in data centres electricity use 2005 to 2010. A report by Analytical Press, completed at the request of The New York Times (2011)
2. E.R. Masanet, *Global Data Centre Energy Use: Distribution, Composition, and Near-Term Outlook* (Evanston, IL, 2018)
3. K. Ebrahimi., G.F. Jones., A.S. Fleischer, A review of data centre cooling technology, operating conditions, and the corresponding low-grade waste heat recovery opportunities. *Renew. Sustain. Energy Rev.* **31**, 622–638 (2014)
4. Future Facilities White Paper—David King, The benefits of supply air temperature control in the data centre (2010). <https://www.futurefacilities.com/resources/whitepapers/electronics-cooling-cfd-trends/>
5. J. Cho, J. Yang, W. Park, Evaluation of air distribution system’s airflow performance for cooling energy savings in high-density data centres. *Energy Build* **68** (Part A), 270–279 (2014)

6. S.A. Nada, M.A. Said, Effect of CRAC units' layout on thermal management of data centre. *Appl. Therm. Eng.* **118**, 339–344 (2017)
7. NOAA (National Oceanic and Atmospheric Administration), *Weather Website*. <https://www.noaa.gov/weather>
8. H.K. Versteeg, W. Malalasekera, *An Introduction to Computational Fluid Dynamics: The Finite Volume Method*, 2nd edn. (Pearson Education Limited, 2007). ISBN 978-0-13-127498-3b
9. M. Mitch, K. Mukesh, G. Mark, High-density heat Containment. *ASHRAE J.*, pp. 35–42 (2008–2009)

**Open Access** This chapter is licensed under the terms of the Creative Commons Attribution 4.0 International License (<http://creativecommons.org/licenses/by/4.0/>), which permits use, sharing, adaptation, distribution and reproduction in any medium or format, as long as you give appropriate credit to the original author(s) and the source, provide a link to the Creative Commons license and indicate if changes were made.

The images or other third party material in this chapter are included in the chapter's Creative Commons license, unless indicated otherwise in a credit line to the material. If material is not included in the chapter's Creative Commons license and your intended use is not permitted by statutory regulation or exceeds the permitted use, you will need to obtain permission directly from the copyright holder.





# Chapter 27

## Short Review of Biodiesel Production by the Esterification/Transesterification of Wastewater Containing Fats Oils and Grease (FOGs)



**Rawaz A. Ahmed and Katherine Huddersman**

**Abstract** Nowadays, the transformation of biomass into valuable chemicals and fuels through thermochemical, biochemical or even mixed technologies, is becoming increasingly popular and challenging. A promising solution for the near future is the substitution of non-renewable fossil fuels with a sustainable liquid feedstock for biofuel (biodiesel) production. The cost of conventional biodiesel production is higher than that of petroleum-based diesel production since it is produced mostly from expensive high-quality virgin oil. Conventionally, commercial biodiesel is produced via liquid base-catalyzed transesterification of triglycerides components of oil/fat with short-chain alcohols. It is that about 70–80% of the overall biodiesel production cost is associated with the cost of raw materials. Brown grease (with free fatty acid levels > 15%) is created from rendered trap waste and is known as Fats, Oils, and Greases (FOGs), it is a potential source of biodiesel feedstocks and is available at no cost. Many researchers are interested in using low-cost high Free Fatty Acid (FFA) oils as the feedstock for biodiesel production. This paper reviews the effect of feedstock pre-treatment and process parameters on the conversion of FOGs-wastewater to biodiesel by esterification-transesterification process.

**Keywords** Triglyceride (TGs) · Esterification/transesterification reaction · Methyl ester · Heterogeneous base or acid solid catalyst

### 27.1 Introduction

Sustainable renewable energy production is being intensely disputed worldwide and has many alternative energy resources that exist in varied forms and could be used to substitute the conventional fossil fuels (Fig. 27.1), because gradually fossil fuel

---

R. A. Ahmed (✉) · K. Huddersman  
Faculty of Health and Life Science, De Montfort University, Leicester, England  
e-mail: [rawaz.ahmed2@dmu.ac.uk](mailto:rawaz.ahmed2@dmu.ac.uk); [rawaz.ahmed@ntu.ac.uk](mailto:rawaz.ahmed@ntu.ac.uk)

K. Huddersman  
e-mail: [huddzeo1@dmu.ac.uk](mailto:huddzeo1@dmu.ac.uk)

resources are declining [1]. One of the promising solutions for the replacement of fossil fuels is substitution with a sustainable biomass feedstock for biofuel (especially biodiesel) production [2]. Biodiesel is a fuel derived from edible and non-edible biomass oils made by chemically reacting lipids such as animal fat (tallow), soybean oil, or some other vegetable oil with an alcohol producing a methyl, ethyl, or propyl ester [3, 4]. It is a well-known process involving the transesterification of oil via homogeneous base catalysis and commercially it is an established method for biodiesel production [5–7]. However, homogeneous base catalysts are very sensitive to free fatty acids present in low-quality oil feedstocks, requiring additional acid pre-treatment and neutralization steps which not only cause environmental pollution but also increase the overall cost of biodiesel production. Encouragingly, solid catalysts can provide a green, efficient, and economical pathway for biodiesel production using low-cost oil feedstocks such as waste cooking oil, fats, oils and grease (FOGs) in wastewater [8, 9]. Heterogeneous base or acid solid catalysts have been developed and successfully applied in esterification and transesterification processes of FFAs and triglyceride (TGs) by many researchers [10, 11].

This paper focuses on heterogeneous catalysis in the esterification of high free fatty acid lipid feedstock from wastewater containing fats, oils and greases (FOGs) and their transformation via esterification/transesterification to biodiesel as a promising solution to achieve renewable energy in near future. Esterification/transesterification of FFAs and TGs to alkyl esters in the presence of an acidic or basic catalyst is a route

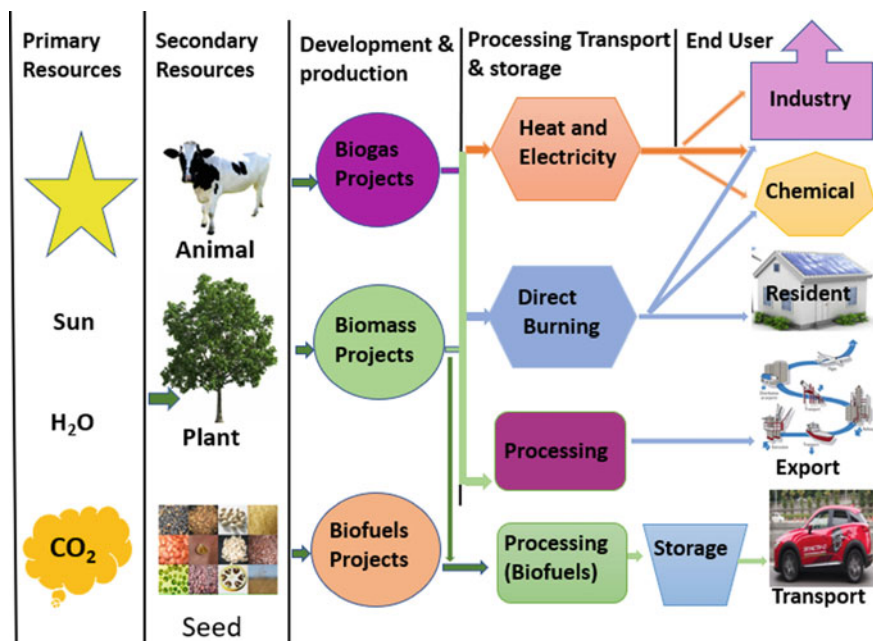


Fig. 27.1 Biofuel supply chain from primary resources to end user

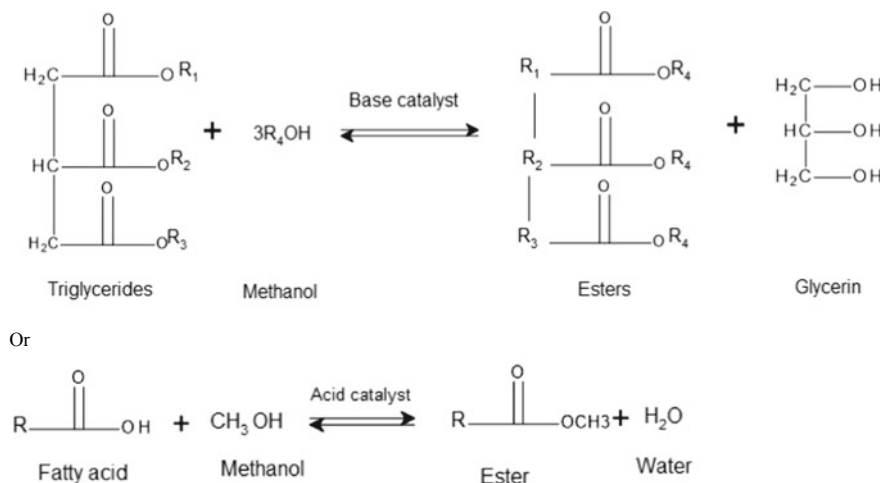
to improving the use of high FFA-TGs oils (e.g., some animal and vegetable oils) in biodiesel production. This work aims to review and understand the parameters that affect the conversion of fatty acids reacted with short chain alcohols to achieve better biodiesel yields.

## 27.2 Esterification-Transesterification Reaction of FOGs

Biodiesel can be produced by three technologies: 1. Alkaline catalyzed transesterification (suitable for feedstock with low free fatty acid content); 2. Acid catalyzed transesterification/esterification (good for feedstock with high FFA content); and 3. Transesterification two-step process (good for feedstock with high FFA content) [12, 13]. In general, alkaline metal hydroxides or methoxides are very effective catalysts for transesterification. The rate of alkaline catalyzed transesterification is about 4000 times faster than acid catalyzed transesterification, but its drawback is that FFA cannot be converted to ester. The FFAs are only neutralized to fatty soap, which further complicates the separation causing an additional loss of biodiesel in the separation step. Acid is a good catalyst for both esterification and transesterification, however the rate of transesterification over acid catalyst is very much slower than that of esterification [5]. This is the reason why some researchers choose the two-step process for high FFA feedstock (esterification of FFA with acid catalyst followed by alkaline catalyzed transesterification). Total reaction times are still shorter than those experienced in the one step acid catalysis.

Fat/vegetable oil is primarily a triglyceride (glycerol ester of fatty acids), whereas biodiesel is the mono-methyl ester of fatty acids. For this reason, biodiesel production process is a transesterification (see Scheme 1) process which is carried out by substituting glycerol groups by methyl groups in the presence of sodium methoxide as catalyst with the glycerol obtained as a side product. It is this trans-esterification process which is used often in technology today, but, instead of this single step process, sometimes the vegetable oil is hydrolyzed in a first step by, for example, enzymatic hydrolysis or water vapor hydrolysis at high temperature and high pressure to free the fatty acids which are then converted to biodiesel by the esterification (see Scheme 1) reaction with methyl alcohol. However, this method is not generally preferred by industry.

One of the holistic effective ways for FOG management is biodiesel production by esterification/transesterification of fats. Since FOGs is rich in lipids, it is suggested as a cost-effective feedstock for biodiesel, which overcomes many economic disadvantages associated with the utilization of other feedstocks. FOG possesses various ranges of lipids and FFAs, with different biodiesel conversion technologies showing specificity towards the type of raw material for effective conversion. Thus, not all FOG constituents can be effectively converted into biodiesel using a single technology. For instance, only TGs are highly preferred raw material for conventional transesterification to attain the maximum biodiesel yield. However, some sources of



**Scheme 1** Esterification and transesterification reaction for biodiesel synthesis [12, 13]

FOG may contain up to 90% of FFAs which hinders the transesterification reaction [14–17].

### 27.3 Literature Review of Esterification-Transesterification Reaction of FOGs

In this review we mostly focused on conversion of FFAs in fats, oils and grease (FOG) of wastewater, very little was known about FOG discharged at household level. To address this shortcoming, following a year-long monthly collection of household waste, FOG production was calculated at 2.3 kg/year per household, equivalent to 0.8 kg/year per capita in the United Kingdom, these numbers translate to an annual estimated household FOG production of 62,380 tonnes. Physico-chemical characterization of household FOG showed promising results for biodiesel production [14]. It can be summarized that the use of FOGs for biodiesel production also resolves the problems related to their discharge and complex contamination to the environment. Unfortunately, as discussed above FOGs normally contain large amounts of free fatty acids (FFA), which readily react with alkaline catalysts via saponification, thus lowering the biodiesel yield. Usually, a pre-esterification step is carried out to firstly convert FFAs to FAME with a homogeneous acid catalyst, and then transesterification is performed with alkaline catalyst. However, direct in situ transesterification refers to simultaneous conversion of FOG into biodiesel that was recently discussed as an alternative route to overcome the two-step conversion (See Fig. 27.2). The simultaneous conversion involves the reagents, catalyst and oil mixed directly without prior extraction [18, 19].

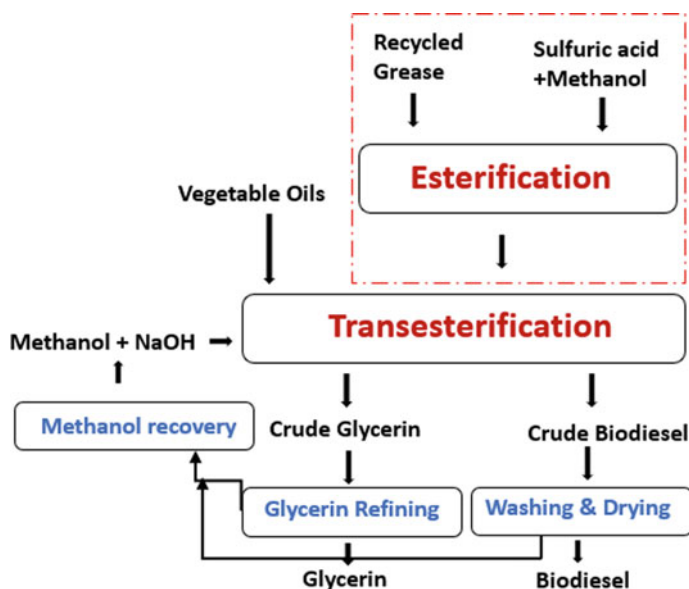
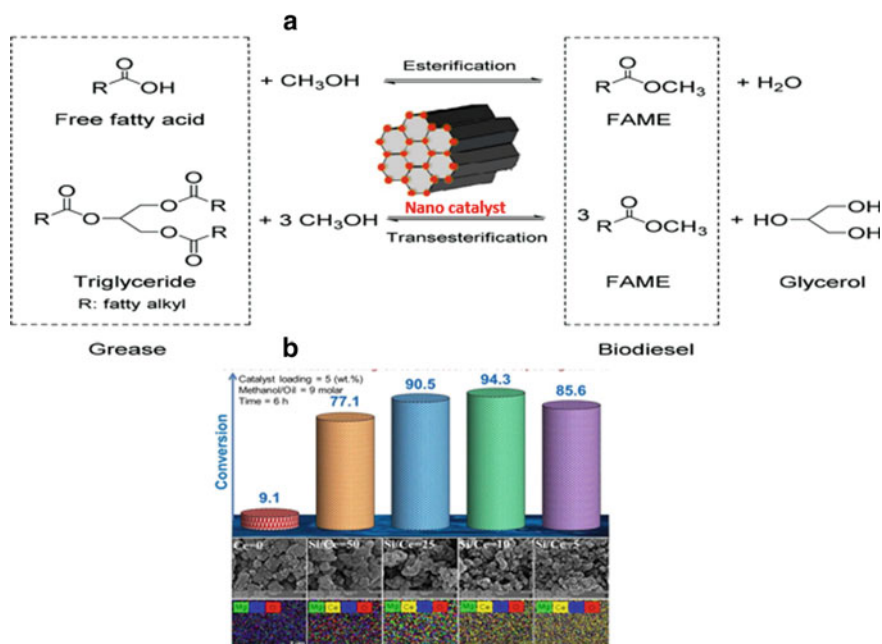


Fig. 27.2 In situ esterification and transesterification reaction via acid/base catalyst

The skipping of the extraction step results in significant reduction in the energy consumption and total cost, as well as reduction of physical footprint [20]. Few studies have been performed to explore the feasibility of biodiesel production by the application of in situ transesterification [21, 22]. For example, the work done by Dehghani and Haghighi is shown in Fig. 27.3a, which summarizes the esterification and transesterification reaction of FOGs constituents for FAMES formation. Si/Ce was used as a nano-catalyst and enhanced the conversion rate of the waste cooking oil into biodiesel significantly (Fig. 27.3b) [15] to about 94.3%, at the end of the seventh cycle the biodiesel conversion dropped to 88.7% conversion suggesting that the nano-catalyst could be re-used [15]. While, Fig. 27.3b illustrated that biodiesel conversion rate is increased extraordinarily as a consequence of Ce introduction into support structure. By increasing the Ce amount (decreasing Si/Ce ratio) to Si/Ce ratio of 10, the conversion increases steadily but for smaller Si/Ce ratios the conversion rate decreases significantly. So, among the synthesized catalysts, the best catalyst for biodiesel production is Mg/CeMCM-41 (Si/Ce = 10), with conversion percentage of 94.3%. According to an early investigation conducted by Tu et al. [22], the optimum operating conditions for in situ transesterification of FOG were 20% H<sub>2</sub>SO<sub>4</sub> and 10:1 methanol: FOG at 65 °C for 7 h, whereby 85.43% of FOG in the raw sewer grease was converted to biodiesel.

In addition, Abbaszaadeh et al. [16] estimated the effectiveness of the thermally induced simultaneous esterification/transesterification of FOG samples to FAMES through typical homogeneous acid (e.g., H<sub>2</sub>SO<sub>4</sub>) catalyzed reactions. Conventional H<sub>2</sub>SO<sub>4</sub> catalyzed reaction produced FAMES with 27.7% (from FOG-high) and 9.2%



**Fig. 27.3** The esterification and transesterification reaction for fat, oil, and grease (FOG) conversion into biodiesel (a) and conversion efficiency of yellow grease into biodiesel using different molar ratios of Si/Ce (0, 5, 10, 25, and 50) (b) [15]

(from FOG-low) yields. These results indicated that it was difficult to convert the FOG to FAMES by the conventional catalyzed methods [16]. Lee et al. also reported the thermally induced esterification/transesterification reaction at  $340^\circ\text{C}$  for samples derived from FOG-high and FOG-low sources by conventional synthesis of FAMES over an acidic homogeneous  $\text{H}_2\text{SO}_4$  catalyst. The highest total FAME yield for FOG-high reached 83.4% at  $380^\circ\text{C}$  at a methanol/feedstock ratio of 20 and  $\text{H}_2\text{SO}_4$  to feedstock molar ratio was 1.3. A further increase in temperature from 380 to  $390^\circ\text{C}$  led to a decrease in the yield from 83.4 to 78.7%. In contrast the highest FAME yield for FOG-low was 74.1% at  $350^\circ\text{C}$  at the same methanol/feedstock ratio of 20. Again, an increase in temperature from 350 to  $390^\circ\text{C}$  led to a decrease in the yield from 74.1 to 59.3%. They suggested that only 83.4% of the initial masses of FOG-high and 74.1% of FOG-low could be converted into FAMES. FOG-high contains lipids (85.2 wt.%), FFAs (11.6 wt.%), and impurities (3.2 wt.%), and FOG-low contains lipids (76 wt.%), FFAs (9.9 wt.%), and impurities (14.1 wt.%). Impurities are not converted into FAMES, meaning that they remain after the thermally induced simultaneous esterification/transesterification process. Taking into account the number of impurities in the feedstock, the total FAME yield from FOG-high and FOG-low would be 86.2% and 86.3%, respectively. Their observation suggested that thermally induced FAME production can be achieved via a single step by combining esterification and transesterification without removing impurities in FOGs [18].

The high lipid content contained in waste spent coffee grounds (SCG) was converted to biodiesel through an in-situ transesterification method by Tarigan et al. [3]. A new approach reactive extraction soxhlet (RES) method of simultaneously extracting and converting lipid from wet SCG biomass to biodiesel in a single-step process at a mild reaction temperature and short reaction time was proposed. Homogeneous sulphuric acid or sodium hydroxide with a concentration of 0.75 M were used as catalysts. The FA to FAME conversion efficiency was more than 90% using sodium hydroxide in methanol with hexane as co-solvent and a ratio of 1:2, and 30-min reaction time. The FA extraction efficiencies averaged 58.1 mol% ranging from 48.6 to 78.1 mol% [3]. The new approach of situ transesterification of wet SCG using RES method resulted in lower energy consumption and reaction time compared to the two-step method which requires a separate extraction and transesterification process [3]. In addition, Suryani et al. [23] developed an in-situ biodiesel transesterification production process using the residual oil from spent bleaching earth (SBE). The stirring speeds applied were 650 rpm and 730 rpm, and the reaction time varied from 60, 90 and 120 min. The combination of 730 rpm stirring speed for 90 min transesterification resulted in the best biodiesel characteristics with the yield of 85%, a specific energy of 6738 kJ/kg and a heater efficiency of 48% [23]. Endalew et al. [24] investigated mixtures of solid base (CaO and Li-CaO) and acid ( $(\text{Fe}_2(\text{SO}_4)_3)$ ) heterogeneous catalyst for single-step simultaneous esterification and transesterification of high content free fatty acid (FFA) containing *Jatropha curcas* oil (JCO).

The reaction conditions used were: 60 °C reaction temperature, 3 h of reaction time, 6:1 molar-based alcohol to oil ratio, 5 wt.% catalyst (based on the amount of oil) and an agitation speed of 300 revolutions per min (rpm). Adjusting the CaO: $\text{Fe}_2(\text{SO}_4)_3$  weight ratio to 3:1, the FAME yield was 93.37%, while for the Li-CaO catalyst gave a FAME yield of 96% with the same ratio [24]. Mixture of solid base catalysts (CaO and Li-CaO) and solid acid catalyst ( $\text{Fe}_2(\text{SO}_4)_3$ ) were found to give complete conversion to biodiesel in a single-step simultaneous esterification and transesterification process. Later, a new method for waste grease extraction (WGE) was developed, where yellow grease was mixed with raw sewer grease (3.15:1, w/w) at 70 °C for 240 min [25]. During the process, 100% of the FOG in the sewer grease was dissolved/extracted into the liquid yellow grease phase, which separated into two phases with the upper layer containing the FOG (see Fig. 27.4). This extraction method resulted in FFAs content increasing from 2.68 wt.% in the yellow grease to 8.48 wt.% in the extracted FOG, which can be converted directly into biodiesel by in situ transesterification. Using WGE for in situ conversion of FOG into biodiesel has several advantages comparing to the conventional methods. WGE avoids the drying of raw sewer grease that is necessary for many other conversion techniques including in situ transesterification. In addition, using yellow grease for WGE is cost-effective when compared with other techniques used for FOG separation from sewer grease, such as centrifugation. In situ transesterification contains fewer steps compared to other conversion methods and can achieve satisfactory results with FFAs-rich feedstocks. Therefore, it might reduce the complexity and capital investment of FOG conversion. However, methanol and  $\text{H}_2\text{SO}_4$  inputs are significantly

higher for in situ transesterification due to mass transfer limits, even though most of the methanol is recovered after conversion. Therefore, future research is needed in order to improve WGE and in situ transesterification through enhancement of extraction and conversion rates, respectively [25].

Moreover, Harvianto and Ulfasha [26] firstly performed the esterification (pre-treatment) using a volume ratio of methanol:FOG ratio of 0.09, at 70 °C for 180 min with 1.2 ml of 98% H<sub>2</sub>SO<sub>4</sub> (10 wt.% of FFA). The amount of conversion in the esterification reaction was shown by the acid value at the end of the reaction. The lower the acid value the greater the conversion with the authors achieving a low value of 0.68 mg KOH/g acid. This was then followed by the transesterification reaction which was carried out with a methanol: FOG ratio of 0.26(v/v) at 70 °C for 30 min with 2.55 g of KOH catalyst [26]. The current study proposed a new approach for biodiesel synthesis from wet spent coffee grounds (SCGs) using 1,8-diazabicyclo [5.4.0] undec-7-ene (DBU) as both a green solvent and catalyst. The maximum biodiesel yield was 97.18%, with reaction condition a methanol amount of 6.25 mL/g of wet SCGs, DBU amount of 14.46 mL/g of wet SCGs, temperature of 60.2 °C, and reaction time of 28.65 min through response surface methodology

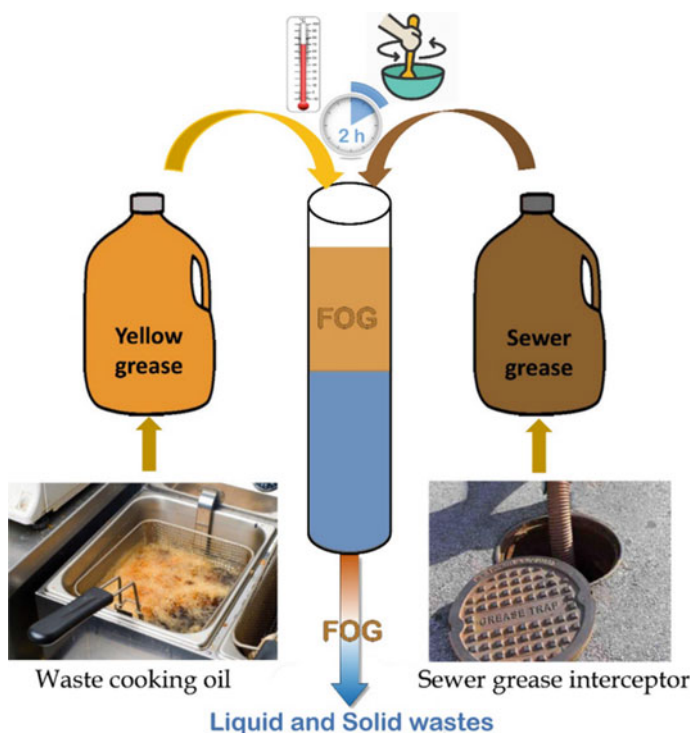


**Fig. 27.4** Solvent-free extraction of waste grease for separation of fat, oil, and grease (FOG) from sewer system



(RSM) [27]. Author reported that DBU-catalyzed direct transesterification could be an economically feasible method for biodiesel synthesis from SCGs. This is due to reusability of DBU for 10 cycles at a lower temperature (60.2 °C) than does the conventional process (95 °C) [28].

Furthermore, this process is eco-friendly because it eliminates the use of harmful solvents and catalyst. Furthermore, an extensive literature review has been carried out in order to assess the advantages and disadvantages of the different methodologies in biodiesel production via catalytic esterification and transesterification (see Table 27.1). A summary of work performed so far shows that catalyst structure, morphology, texture, optimization and reaction parameters such as temperature, catalyst concentration, reaction time, alcohol to substrate molar ratio, type of alcohol have a significant influence on catalytic activity in biodiesel production. Despite a large number of studies carried out on the heterogeneous solid acid or base catalytic esterification/transesterification, there are still a number of drawbacks that hinder industrial application. Therefore, there is a need to develop cheaper more efficient solid base catalysts that are less energy demanding in terms of their process conditions and that have optimal lifetime stability.

## 27.4 Conclusions

This review has shown that the esterification/transesterification of high FFAs-lipid feedstocks from wastewater containing FOGs is a possible alternative route to biodiesel production as a renewable energy. Based on this literature review, a number of studies have been done on the esterification/transesterifications of FFAs and their transformation into fatty acid methyl esters (FAMES) which is the main constituent of biodiesel. The yield of biodiesel depends on a number of parameters; such as catalyst concentration, catalyst type, and molar ratio of reactants, reaction temperature, and reaction time and optimization of these reaction conditions. The optimal temperature ranged between 60 and 70 °C, depending on the amount of free fatty acids that the oil contains and the molar ratio of alcohol to feedstock should be increased to between 6:1 up to 20:1 with the use of an acidic catalyst with concentration about 6 wt.% up to 10 wt.% for heterogeneous solid acidic catalysts and between 3 to 5%v/v for H<sub>2</sub>SO<sub>4</sub>, which is the most commonly used catalyst. Therefore, all reaction parameters are co-related to each other and all of them have significant influence on the reaction, therefore all parameters have to be optimized.

If heterogeneous acid catalysts could be as efficient in the esterification/transesterification of FOGs as it is with fresh oil such as vegetable oil, this would motivate its use in industry, even if catalyst production increases some costs but, at the same time, decreases the associated costs of catalyst separation and purification after the reaction and indeed can enable catalyst re-use. Future steps should include an analysis of heterogeneous catalyst usage in the transformation of FOGs into a biofuel.

**Table 27.1** Summarise esterification and transesterification of biodiesel production parameters

Catalyst	Feedstocks	Transesterification/esterification reaction conditions	Biodiesel yield (%)	Cycles	Refs.
H <sub>2</sub> SO <sub>4</sub>	Fats, oils, and grease (FOGs) without treatment	<ul style="list-style-type: none"> <li>Methanol to feedstock molar ratio of 30, and (H<sub>2</sub>SO<sub>4</sub> to FOGs feedstock molar ratio of 1.3)</li> <li>Thermal esterification/transesterification at 240–350 °C and 10 s reaction time., 10 mL of FOGs, 200 mL of methanol, and 100 mg of silica were used</li> </ul>	> 86		[18]
Acid cat. using coconut meal residue (CMR)-CMR-DS-SO <sub>3</sub> H	Grease trap wastewater (GTW)	Methanol: oil (molar ratio) (6:1–16:1), reaction time (6–16 h), and (5%wt.) catalyst loading at 65–70° C. CMR-DS-SO <sub>3</sub> H catalyst had high acid density (3.8 mmol/g)	> 80	4	[29]
Acidic homogeneous catalyst HCl	Wastewater treatment plant (WWTP) municipal sludge	Novel direct liquid-liquid lipid extraction used as pre-treatment of feedstock. Compared to standard drying method, direct liquid-liquid lipid extraction resulted with 53% higher lipid and 56% higher biodiesel production	56		[30]
H <sub>2</sub> SO <sub>4</sub>	Two types of WWTP sewage sludge obtained from the anaerobic–anoxic–oxic (A <sup>2</sup> /O) and membrane bioreactor (MBR) processes as lipid	<ul style="list-style-type: none"> <li>Methanol-to sludge mass ratio of 10:1, a temperature of 60 °C, and a H<sub>2</sub>SO<sub>4</sub> concentration of 5% (v/v), (from A<sup>2</sup>/O reactor)</li> <li>Methanol-to-sludge mass ratio of 8:1, a temperature of 50 °C, and a H<sub>2</sub>SO<sub>4</sub> concentration of 5% (v/v), (from MBRreactor)</li> </ul>	96.7 92.7		[31]

(continued)

Table 27.1 (continued)

Catalyst	Feedstocks	Transesterification/esterification reaction conditions	Biodiesel yield (%)	Cycles	Refs.
H <sub>2</sub> SO <sub>4</sub>	Wastewater treatment plant (WWTP) municipal sludge	The lipid sample (up to 50 mg), dissolved in 1 mL of hexane. After that, 2 mL of 1% sulfuric acid in methanol was added, heated overnight at 50 °C. 5 mL of 5% sodium chloride in water was added and the FAMES were extracted 2 times with 5 mL of hexane	87	2	[32]
H <sub>2</sub> SO <sub>4</sub>	WWTO-Municipal wastewater sludges	75 °C, 5% (v/v) H <sub>2</sub> SO <sub>4</sub> , and 12:1 methanol to sludge mass ratio	75	/	[33]
H <sub>2</sub> SO <sub>4</sub>	<ul style="list-style-type: none"> <li>• WWTP: dried sludge</li> <li>• WWTP: dewatered primary sludge</li> </ul>	<ul style="list-style-type: none"> <li>• 10 g of dried sludge were suspended in 100 mL methanol with 0.25 mL of H<sub>2</sub>SO<sub>4</sub> (96%), kept at 65 °C for 7 h</li> <li>• 150 g of dewatered primary sludge mixed with methanol (300 or 750 mL) and 1.5 mL of sulphuric acid (96%). Kept at 65 °C for 7 h</li> </ul>	60.7 85	4	[34]
A homogeneous base, KOH and acid, H <sub>2</sub> SO <sub>4</sub> catalyst	Waste spent coffee grounds (SCG)	Combines simultaneous soxhlet extraction-esterification/transesterification in a single step to produce biodiesel directly from wet SCG, molar ratio of co-solvent methanol to hexane of 1:2 and reaction time 30 min, 10 g of wet SCG biomass, 0.75 M of KOH or H <sub>2</sub> SO <sub>4</sub> was used as catalyst. Base catalyst showed superior catalytic activity	97	5	[3]

(continued)

Table 27.1 (continued)

Catalyst	Feedstocks	Transesterification/esterification reaction conditions	Biodiesel yield (%)	Cycles	Refs.
H <sub>2</sub> SO <sub>4</sub>	Fats, oil, and grease (FOG), the main composition of dewatered grease trap waste (GTW)	After Hexane extraction of FOGs, the FOG-ethanol molar ratio was 1:3, 3 wt.% H <sub>2</sub> SO <sub>4</sub> based on the amount of FOG, the reaction temperature was set at 65 °C and the stirring speed was kept at 300 rpm	96		[35]

**Acknowledgements** This work is supported by funding from the co-sponsors Daphne Jackson Trust, Society of Chemists in Industry (SCI) and Royal Society of Chemistry (RSC), and hosted at De Montfort University, Leicester.

## References

1. W. Nabgan, A.A. Jalil, B. Nabgan, A.H. Jadhav, M. Ikram, A. Ul-Hamid, M.W. Ail, N.S. Hassan RSC, Sustainable biodiesel generation through catalytic transesterification of waste sources: a literature review and bibliometric survey RSC Adv. **12**, 1604 (2022)
2. S.R. Medipally, F.M. Yusoff, S. Banerjee, M. Shariff, Microalgae as sustainable renewable energy feedstock for biofuel production. Biomed. Res. Int. **3**, 519513 (2015)
3. J.B. Tarigan, M. Ginting, S.N. Mubarakah, F. Sebayang, J. Karo-karo, T.T. Nguyen, J. Ginting, E.K. Sitepu, Direct biodiesel production from wet spent coffee grounds. RSC Adv. **9**, 35109 (2019)
4. S. Semwal, A.K. Arora, R.P. Badoni, D.K. Tuli, Review Biodiesel production using heterogeneous catalysts. Bioresour. Technol. **102**, 2151–2161 (2011)
5. M.K. Lam, K.T. Lee, A.R. Mohamed, Homogeneous, heterogeneous and enzymatic catalysis for transesterification of high free fatty acid oil (waste cooking oil) to biodiesel: A review. Biotechnol. Adv. **28**, 500–518 (2010)
6. D. Samios, F. Pedrotti, A. Nicolau, Q.B. Reiznautt, D.D. Martini, F.M. Dalcin, A transesterification double step process-TDSP for biodiesel preparation from fatty acids triglycerides. Fuel Process. Technol. **90**, 599–605 (2009)
7. C. Urrutia, N. Sangaletti-Gerhard, M. Cea, A. Suazo, A. Aliberti, R. Navia, Short communication: two-step esterification–transesterification process of wet greasy sewage sludge for biodiesel production. Bioresour. Technol. **200**, 1044–1049 (2016)
8. A. Munitywali, H. Li, Q. Qihua Yang, Review of advances in bifunctional solid acid/base catalysts for sustainable biodiesel production. Appl. Catal. A Gen. **633**, 118525 (2022)
9. I. Istadi, S.A. Prasetyo, T.S. Nugroho, Characterization of K<sub>2</sub>O/CaO-ZnO Catalyst for Transesterification of Soybean Oil to Biodiesel. Procedia Environ. Sci. **23**, 394–399 (2015)
10. M. Prabu, M. Manikandan, P. Kandasamy, P.R. Kalaivani, N. Rajendiran, T. Raja, Synthesis of biodiesel using the Mg/Al/Zn hydrotalcite/SBA-15 nanocomposite catalyst. ACS Omega **4**, 3500–3507 (2019)
11. G. Lawer-Yolar, B. Dawson-Andoh, E. Atta-Obeng, Synthesis of biodiesel from tall oil fatty acids by homogeneous and heterogeneous catalysis. Sustain. Chem. **2**(1), 206–221 (2021)
12. J.M. Marchetti, A.F. Errazu, Short communication esterification of free fatty acids using sulfuric acid as catalyst in the presence of triglycerides, Biomass Bioenergy **32**, 892–895 (2008)
13. Z. Khan, F. Javed, Z. Shamair, A. Hafeez, T. Fazal, A. Aslam, W.B. Zimmerman, F. Rehman, Current developments in esterification reaction: a review on process and parameters, J. Ind. Eng. Chem. **103**, 80–101 (2021)
14. T. Collin, R. Cunningham, M. Deb, R. Villa, J. MacAdam, B. Jefferson, Energy potential of household fats, oils and grease waste, Water Environ. J. , **36**, 1–8 (2022). Retrieved from <https://doi.org/10.1111/wej.12744>
15. S. Dehghani, M. Haghighi, Sono-dispersed MgO over cerium-doped MCM-41 nanocatalyst for biodiesel production from acidic sunflower oil: Surface evolution by altering Si/Ce molar ratios. Waste Manag. **95**, 584–592 (2019)
16. A. Abbaszaaseh, B. Ghobadian, M.E. Omidkhah, G. Najafi, Current biodiesel production technologies: a comparative review, Energy Convers. Manag. **63**, 138–148 (2012)
17. R.A. Ahmed, S. Rashid, K. Huddersman, Esterification of stearic acid using novel protonated and crosslinked amidoximated polyacrylonitrile ion exchange fibres. J. Ind. Eng. Chem. **119**, 550–573 (2023)



**Open Access** This chapter is licensed under the terms of the Creative Commons Attribution 4.0 International License (<http://creativecommons.org/licenses/by/4.0/>), which permits use, sharing, adaptation, distribution and reproduction in any medium or format, as long as you give appropriate credit to the original author(s) and the source, provide a link to the Creative Commons license and indicate if changes were made.

The images or other third party material in this chapter are included in the chapter's Creative Commons license, unless indicated otherwise in a credit line to the material. If material is not included in the chapter's Creative Commons license and your intended use is not permitted by statutory regulation or exceeds the permitted use, you will need to obtain permission directly from the copyright holder.



# Chapter 28

## The Use of Photovoltaic Solar Panels to Reduce Temperature-Induced Bridge Deformations



Sushmita Borah and Amin Al-Habaibeh

**Abstract** Civil infrastructure such as bridges undergo deformations such as displacement and strain due to environmental temperature variations. Temperature causes deformations equal to or larger than that due to traffic load on bridges. This research evaluates whether the deformations due to temperature load on bridges can be minimised by incorporating photovoltaic solar panels on the bridge surface. The panels can be attached to the bridge truss, piers, and the periphery of the deck excluding the pavement, i.e., excluding bridge superstructure elements under direct traffic load to avoid wear and tear of the solar panels. The hypothesis is that solar panels will generate electricity from solar radiation and the bridge elements underneath the panels will experience less temperature load. The truss will experience smaller deformations and thereby increasing its lifespan. This hypothesis is tested with a laboratory experiment on a bridge truss. A combination of solar panels is attached to the surface of an Aluminium truss. The truss is subjected to 1-h heating and cooling cycles created using infrared lamps. The truss is monitored with linear variable differential transformers and thermocouples. Displacements and surface temperature of the truss are recorded. Results have shown a 34.0% reduction in displacement due to the installation of solar panels. The temperature of the truss has been also reduced by 15–25.6%. This research shows the benefit of integrating renewable energy means in infrastructure such as bridges to reduce temperature-induced structural deformations. Such integration can enhance the bridge lifespan along with generating green energy to electrify the bridge or the local area.

**Keywords** Bridge · Displacement · LVDT · Solar panels · Temperature load

---

S. Borah (✉) · A. Al-Habaibeh  
Product Innovation Centre, Nottingham Trent University, Nottingham, UK  
e-mail: [sushmita.borah@ntu.ac.uk](mailto:sushmita.borah@ntu.ac.uk)

A. Al-Habaibeh  
e-mail: [Amin.Al-Habaibeh@ntu.ac.uk](mailto:Amin.Al-Habaibeh@ntu.ac.uk)

S. Borah  
Civil Engineering Department, Nottingham Trent University, Nottingham, UK



## 28.1 Introduction

Temperature plays an important role in the structural performance of bridges. Bridges undergo deformations such as displacement, strain, tilt, crack etc. because of their operational loads such as traffic and temperature. Such deformations should be minimised to ensure public safety, bridge serviceability, and lower life-cycle maintenance cost. Several case studies in real-life bridges demonstrated the impact of temperature load on bridges [1]. For example, temperature load caused strains of magnitude equal to or larger than static and traffic load on the Yangtze River Bridge in Jiangsu, China [2], it induced a 4–8% change in natural frequency in Dowling Hall Footbridge in the USA [3]. Besides the normal ambient temperature, extreme temperature events pose threats to bridge safety as well. For instance, the Hammer-smith Bridge in London was closed to traffic in August 2020 due to tiny cracks in cast-iron pedestals caused by hot temperatures [4]. The same bridge, which was opened to pedestrians and cyclists after the 2020 event, was wrapped in silver insulation foil in July 2022 heatwave to prevent it from overheating [5]. While wrapping a bridge in insulation foil is a temporary solution to extreme events, there is a need for a long-term sustainable solution to minimise temperature-induced deformations in bridges.

This research investigates if incorporating small-scale photovoltaic (PV) solar panels on the bridge surface can reduce temperature-induced deformations. Solar cells have been incorporated into road infrastructure for a long time. For example, the *SolaRoad* pilot, a bike lane in Krommenie, Netherlands [6] and the *Wattway* project, a 1-km vehicular road in Normandy village, France [7] integrated solar cells in the road pavement. However, these innovative projects did not succeed due to excessive wear and tear and unfavourable inclination angle of solar panels [8, 9]. The South Korean *Bike Highway* eliminates these issues by integrating solar panels on the elevated shade of a 20-km bike lane running parallel to the highway [10]. The elevated panels provide a flexible inclination angle and reduce wear and tear due to traffic load. Solar panels have been successfully integrated to power several bridges such as Blackfriars Bridge, UK and Kennedy Bridge, Germany.

Higher public acceptance of solar panels compared to other renewable alternatives such as wind turbines, due to reduced human hazards, also encourages the implementation of solar panels in bridges. This paper evaluates the structural health benefit of integrating solar panels on bridges in addition to generating renewable energy. The solar panels attached to the bridge surface are expected to utilise solar radiation to generate electricity and reduce temperature load on the bridge elements underneath the panels. The bridge will undergo smaller deformations and thereby increasing its lifespan. The panels are proposed to be installed on exposed bridge surfaces such as truss, deck periphery, roof etc. excluding pavement to avoid direct traffic load. This hypothesis is tested in the laboratory on a bridge truss. An Aluminium truss is equipped with small solar panels and is exposed to 1-h heating and cooling cycles of two infrared heaters. The deformation of the truss before and after the installation of solar panels is monitored with Linear Variable Differential Transformer (LVDT)

and strain gauges. Variation of deformations such as displacement and strain before and after solar panel installation reflects the effect of the panels. A reduced deformation will indicate that solar panel installation in strategic locations can improve the structural performance of bridges. The next sections describe the methodology and results of the laboratory experiments.

## 28.2 Methodology

The solar panels attached to the bridge surface will utilise solar energy to generate electricity, creating a shading effect for the bridge underneath. The bridge will undergo less deformation due to reduced temperature load, thereby enhancing the serviceability and life of the bridge. This hypothesis is tested using experimental methods. Figure 28.1 demonstrates the conceptual framework of the experiments. Bridges deform due to ambient temperature load throughout their lifetime. These bridges are monitored using suitable structural health monitoring (SHM) system under two operational conditions: (i) before installation of solar panels and (ii) after installation of solar panels. The SHM system measures responses such as displacement, strain, surface temperature, etc. The SHM measurements can be analysed to create two outputs: (A) bridge deformation without solar panel installation and (B) bridge deformation with solar panel installation. The magnitude of A being greater than B will indicate that bridge deformation is reduced after solar panel installation.

## 28.3 Case Study

The proposed concept is examined in the laboratory with a series of experiments. A test rig is designed to test the effect of solar panels on bridge deformations due to temperature load. This section briefs the experimental setup and enumerates the results.

### 28.3.1 Description of the Test

Figure 28.2 shows an Aluminium truss equipped with an SHM system and solar panels. The SHM system consists of Linear Variable Differential Transformers (LVDT) and thermocouples to measure displacement and temperature. The truss is painted black. Details of the both end pinned truss are provided elsewhere [11]. The truss is exposed to cyclic heating and cooling cycles using two infrared heaters. Figure 28.3 shows the location of the solar panels and sensors (L: LVDT and T: Thermocouple) on the truss.

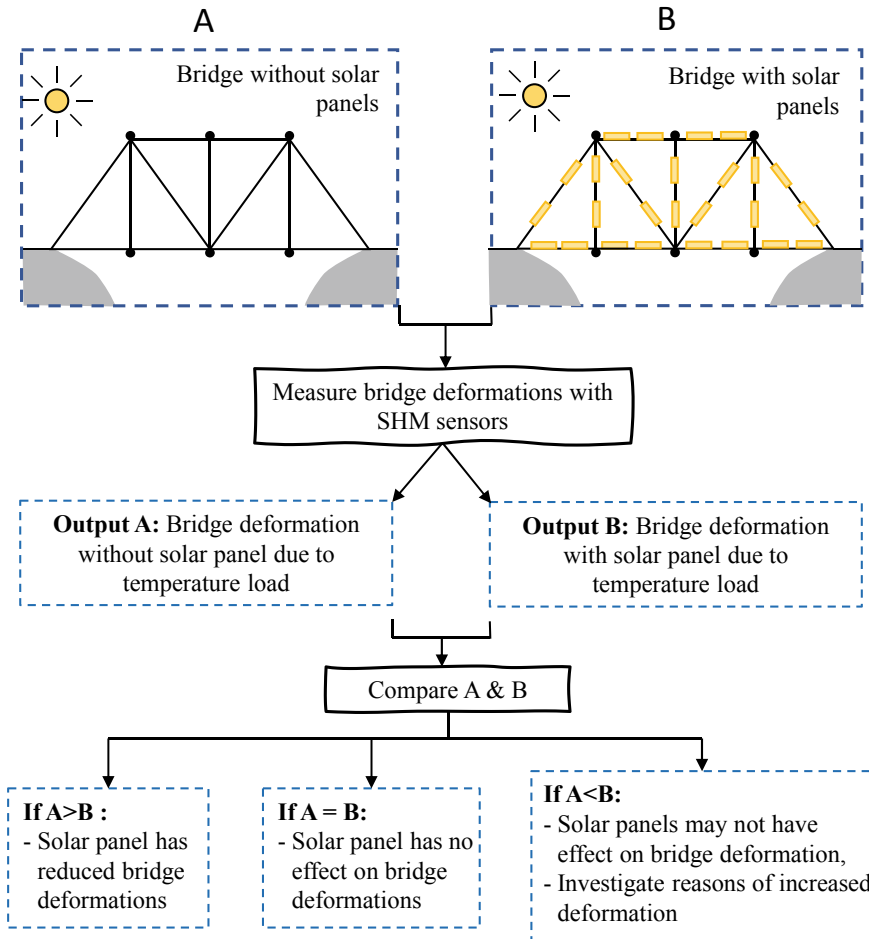


Fig. 28.1 Conceptual framework of the experiment

The solar panels are 55 mm × 70 mm in size and have a typical power output of 0.5W. Experiments are carried out in three stages: E1: truss is not equipped with solar panels, E2: truss is equipped with a limited number of solar panels (Fig. 28.3a) and E3: truss is equipped with more solar panels (Fig. 28.3b). The number of panels is increased in stages (E2 and E3) to see the effect of increased panelling on bridge deformations. E1, E2 and E3 were carried out on three different days with heaters placed approximately 1 m away from the truss.

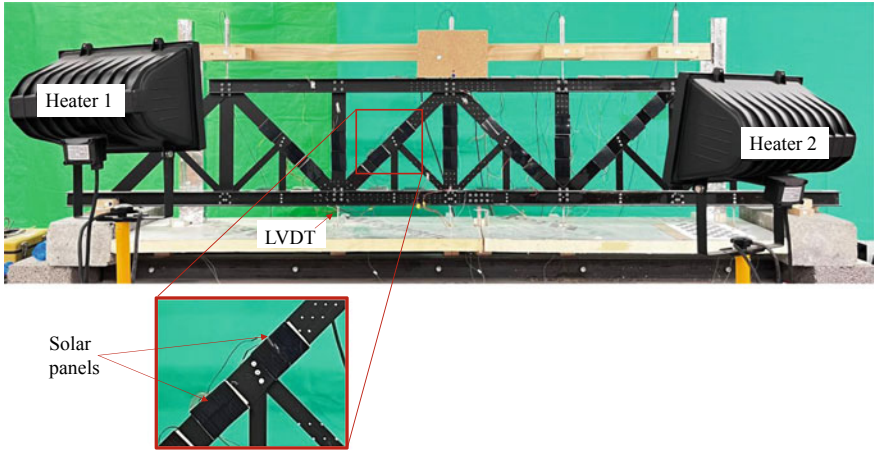


Fig. 28.2 Test rig set-up

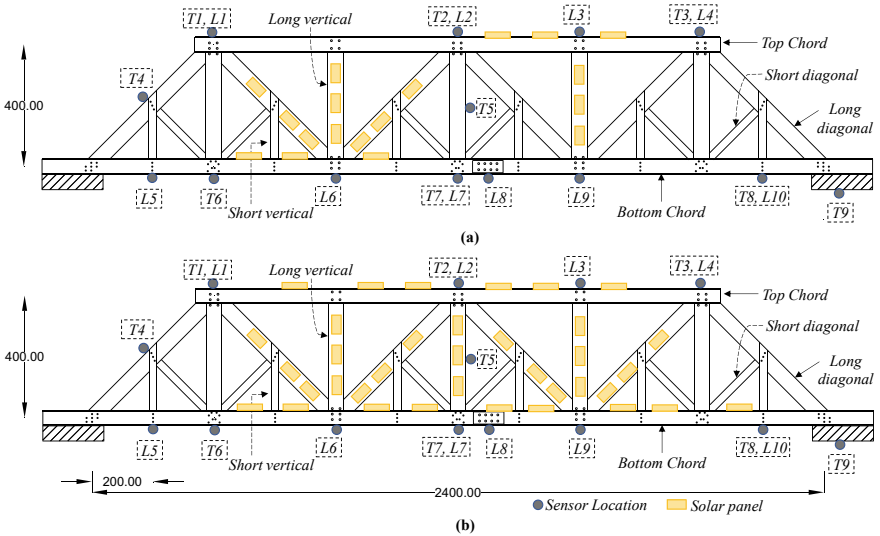


Fig. 28.3 Layout of the SHM sensors and solar panels, (a) in E2, limited solar panels and (b) in E3, all solar panels. (Symbol T# thermocouple number and L# LVDT number)

### 28.3.2 Results and Discussion

The three events, i.e., E1, E2 and E3 are carried out with 1 h of heating and an average 1 h of cooling cycle, except in E3 where the intermediate cooling cycle was 2 h long. Constant supervision is needed when heaters are turned ON to ensure health and safety requirements. The cooling cycles are performed without constant

supervision as the heaters are turned OFF. The longer cooling cycle in E3 is caused by the unavailability of the supervisor to monitor the heating cycle after 1 h. Such irregular durations are also seen in the real-world where daily daylight and night durations are not identical. The LVDTs and thermocouples measured displacement and temperature without much noise (see Fig. 28.4). A summary of the temperature and displacement range due to the temperature cycles is listed in Table 28.1. The peaks reported here are the difference between the maximum temperature or displacement and the minimum temperature or displacement during the entire experiment duration.

Figure 28.4 shows the displacement time history of L6 and the temperature history of T7 (refer to Fig. 28.3 for sensor location). L6 is towards the left of the bottom chord while T7 is at the centre of the bottom chord. The PV panels are concentrated around L6 in both E2 and E3. However, the T7 location has a denser network of PV panels in E3 than in E2. The base temperature of each location is its mean temperature during the hour before the heating is first turned ON. The temperatures reported in Fig. 28.4 are normalized by deducting the base temperature from the thermocouple

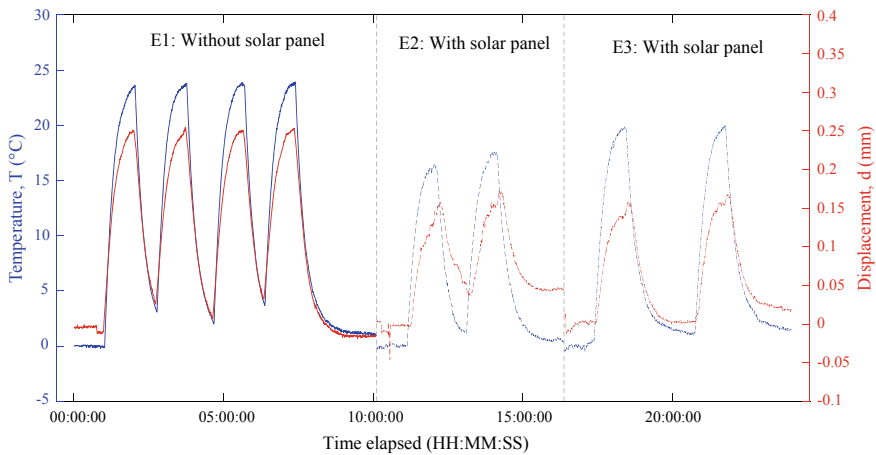


**Fig. 28.4** Temperature (in blue) and displacement (in red) time history before and after installation of solar panels

**Table 28.1** Summary of temperature and displacement change due to solar panel installation

Event	Scenario	Number of heating cycles	Peak temperature range (°C)	Peak displacement range (mm)	Percentage reduction (%)
E1	No solar panels	4	24.142	0.274	–
E2	Limited solar panels	2	17.968	0.181	T: 25.6 d: 33.9
E3	More solar panels	2	20.523	0.180	T: 15.0 d: 34.3

readings. A clear reduction in surface temperature and displacement of the truss is evident because of the shading effect of solar panels. Displacement was reduced by 33.9% for a 25.6% reduction in temperature in E2. While displacement was reduced by 34.3% for a 15.0% reduction in temperature in E3.

It is interesting to note a similar reduction in displacement in E3 although temperature reduction due to PV panel mounting is less by 10.6% compared to E2. The higher temperature gradient in E3 (by 2.56 °C) can be attributed to the combined effect of (i) human error in the placement of heaters in the exact location and at a constant angle in every event, (ii) a slightly longer first heating cycle in E3 (by 3 min) than E2, (iii) a longer cooling period before the second heating cycle in E3 than E2, and (iv) due to the reflective surfaces of the solar panels. Nevertheless, the displacement range of E2 and E3 are similar despite the higher temperature gradient in E3. Structural deformations are caused by the combined effect of all loads in a structure rather than a local load at a particular location. Thus, the combined shading effect of the extra solar panels in E3 may have caused a similar displacement range in E2 and E3. Further, the peak temperature load above the base temperature in E2 and E3 are comparable (17.66 °C and 20.01 °C respectively).

The thermal response of real bridges with mounted PV is expected to be similar although not as straightforward as the simplified experiment on the aluminium truss. Steel and concrete bridges will have lower temperature gradients than the aluminium truss due to the lower coefficient of thermal expansion. Further, the temperature rise will be slow in the longer heating and cooling cycles in a day. Yet, the shading of the mounted PV panels will reduce the temperature of the surface underneath it and thereby reduce the deformation.

## 28.4 Conclusion

This research has investigated the effect of solar panel installation to reduce temperature-induced deformations in bridges. Small size solar panels are suggested to install as tiling on bridge surfaces excluding the pavement. The shading of panels is expected to reduce the bridge surface temperature and thereby reduce temperature-induced deformations such as displacement. The hypothesis was tested in a laboratory aluminium truss equipped with solar panels, LVDT and thermocouples. The truss was subjected to artificial heating and cooling cycles. The following conclusions can be drawn from the results:

- The temperature of the truss was reduced by 15–25.6% near midspan after the installation of the solar panels.
- The displacement of the truss was reduced by around 34.0% in experimental events E2 and E3 after solar panels installation.
- Variation in displacement was found to be similar when the number of solar panels is increased on the surface of the truss. Whereas the temperature gradient increased by 2.56 °C when the number of panels are increased. This oddness could

be related to experimental error, non-identical setup of the experiment events or caused by the reflective surfaces of the solar panels. This will be investigated further in future work.

The results show the promising potential of solar panel installation to improve the structural health of bridges. This is encouraging to promote more solar panel integration in civil infrastructures. Installing solar panels will enhance the lifespan of bridges and infrastructures due to the reduction in thermal stresses due to solar heating and at the same time provide renewable energy to be utilised in the urban environment.

**Acknowledgements** The authors would like to acknowledge Dr Rolands Kromanis, Assistant Professor, University of Twente, Netherlands, for his contribution to the design of the truss and SHM system. The authors also acknowledge the support of the technical team at the School of Architecture, Design and the Built Environment at Nottingham Trent University for their support. Special thanks to Mr Mathew Garlic, Senior Technician, for his contribution to the test-rig technical support of this paper.

## References

1. S. Borah, A. Al-habaibeh, R. Kromanis, The effect of temperature variation on bridges—a literature review, in *2nd International Conference on Energy and Sustainable Futures (ICESF 2020)*, pp. 1–5
2. Q. Xia, L. Zhou, J. Zhang, Thermal performance analysis of a long-span suspension bridge with long-term monitoring data. *J. Civ. Struct. Health Monit.* **8**(4), 543–553 (2018). <https://doi.org/10.1007/s13349-018-0299-y>
3. P. Moser, B. Moaveni, Environmental effects on the identified natural frequencies of the Dowling Hall Footbridge. *Mech. Syst. Signal Process.* **25**(7), 2336–2357 (2011). <https://doi.org/10.1016/j.ymssp.2011.03.005>
4. S. Baker, *UK Heat Wave: London Victorian Bridge Wrapped in Foil to Stop Cracking*. Insider Inc. (2022). <https://www.insider.com/uk-heat-wave-london-victorian-bridge-wrapped-foil-stop-cracking-2022-7>
5. BBC, *Hammersmith Bridge wrapped in foil during heatwave—BBC News*. Bbc.Com (2022). <https://www.bbc.com/news/uk-england-london-62162687>
6. SolaRoad, *Press release SolaRoad opens The first road in the world that converts sunlight into electricity is ready for use*. Solaroad.Nl (2014). [https://www.solaroad.nl/wp-content/uploads/2013/06/PressReleaseSolaRoadOpened\\_21Oct.pdf](https://www.solaroad.nl/wp-content/uploads/2013/06/PressReleaseSolaRoadOpened_21Oct.pdf)
7. K. Willsher, *World's first solar panel road opens in Normandy village*. The Guardian (2016). <https://www.theguardian.com/environment/2016/dec/22/solar-panel-road-tourouvre-au-perche-normandy>
8. D. Grossman, *French Solar Road Wattway Fails | Do Solar-Powered Roads Work?* Popular Mechanics (2019). <https://www.popularmechanics.com/technology/infrastructure/a28720252/french-solar-road-failure/>
9. A. Thomson, *Solar freakin' roadways? Why the future of this technology may not be so bright*. The Conversation (2015). <https://theconversation.com/solar-freakin-roadways-why-the-future-of-this-technology-may-not-be-so-bright-51304>
10. D. Ozdemir, *South Korean 20-Mile Solar Bike Highway Generates Electricity*. Interesting Engineering, Inc. (2021). <https://interestingengineering.com/south-korean-20-mile-solar-bike-highway-generates-electricity>

11. S. Borah, A. Al-Habaibeh, R. Kromanis, Measuring thermal response of bridges using vision-based technologies and LVDTs, in *Lecture Notes in Civil Engineering (LNCE)*, vol. 254, ed. by P. Rizzo, A. Milazzo (Springer Science and Business Media Deutschland GmbH, 2023), pp. 496–505. [https://doi.org/10.1007/978-3-031-07258-1\\_51](https://doi.org/10.1007/978-3-031-07258-1_51)

**Open Access** This chapter is licensed under the terms of the Creative Commons Attribution 4.0 International License (<http://creativecommons.org/licenses/by/4.0/>), which permits use, sharing, adaptation, distribution and reproduction in any medium or format, as long as you give appropriate credit to the original author(s) and the source, provide a link to the Creative Commons license and indicate if changes were made.

The images or other third party material in this chapter are included in the chapter's Creative Commons license, unless indicated otherwise in a credit line to the material. If material is not included in the chapter's Creative Commons license and your intended use is not permitted by statutory regulation or exceeds the permitted use, you will need to obtain permission directly from the copyright holder.





# Chapter 29

## Exploring Windows Opening Behaviour of Occupants of Residential Buildings Using Artificial Intelligence



**Sherna Salim and Amin Al-Habaibeh**

**Abstract** The residential sector contributes significantly to the overall energy consumption in the UK. Occupant's behaviour is a major factor that sometimes could be overlooked when considering energy efficiency of buildings. Although building simulations play a major role in the design of energy efficient buildings, significant discrepancies have been seen between the actual and predicted energy values in simulation models. This is because simulation does not consider occupant behaviour in many cases or finds it difficult to present such behaviour. This study attempts to investigate the reason behind occupant's behaviour of windows opening; to analyse the collected data, to understand the occurrences that lead to an occupant opening window in a residential building. In this paper, data were collected from a selected house in Nottingham. Data were experimentally collected in peak winter of 2020, from end of Nov/20 to March/21 during Covid-19 pandemic. Sensors were fitted to measure radiator temperature, room temperature, room humidity and near-window temperature both upstairs and downstairs. Outdoor ambient temperature for the same period was also collected. Stochastic models were implemented with datasets with window opening behaviour as response. The input parameters to the model were the radiator temperature, room temperature, outside ambient temperature, and time. The predicated output was the window status (open/close). The prognostic precision of the suggested model was verified by testing the models with the rest of the collected data. The predicted values were compared with the actual measured values. The results show a strong prediction with success rate of 76.2%. The findings from this investigation have been found to be able to identify the factors that contribute to the 'performance gap' in energy efficiency of a building.

**Keywords** Energy efficiency · Net zero · Thermal comfort · Air quality · Energy consumption · Carbon reduction · Sustainability

---

S. Salim (✉) · A. Al-Habaibeh  
Department of Product Design, School of Architecture, Design and the Built Environment,  
Product Innovation Centre, Nottingham Trent University, Nottingham, UK  
e-mail: [sherna.salim2017@my.ntu.ac.uk](mailto:sherna.salim2017@my.ntu.ac.uk)

A. Al-Habaibeh  
e-mail: [Amin.Al-Habaibeh@ntu.ac.uk](mailto:Amin.Al-Habaibeh@ntu.ac.uk)

## 29.1 Introduction

Under the Paris Agreement, the UK government has committed to net-zero carbon emissions by 2050. But steps need to be taken in order to reach this target [1, 2]. The Committee on climate Change (CCC), an advisory board to the government of the UK suggests that although UK is progressing well, further steps will need to be taken at the earliest for this target to be met. According to CCC, of the UK's greenhouse-gas emissions, the residential housing accounts for about 14% [3]. The net zero strategy updated in October 2021 mentions insulation only once [4]. The government also scrapped its Green Homes Grant scheme [5]. One reason for this might be because of the data from the latest English Housing Survey; according to which in 2019, 7% of residents dwelling in residential homes reported that at least one part of their home got uncomfortably hot. Of these, 11% lived in homes built in 2003 or later [6]. This overheating invariably leads to window opening behaviour which in turn contributes to the stochastic nature of energy usage in buildings.

The International Energy Agency (IEA) is an organisation of 26 countries around the world, that came together to shape energy policies for a secure and sustainable future. The IEA project Energy in Buildings and Communities (EBC) is a collaborative research and development project among the member countries. Annex 53 of EBC, employed an interdisciplinary approach, integrating building science, architectural engineering, computer modelling and simulation, and social and behavioural science to develop and apply methods to analyse and evaluate the real energy use in buildings considering the six influencing factors namely climate, building envelope, building services and energy systems, building operation and maintenance, occupants' activities and behaviour, and indoor environmental quality and found that better prediction of building and energy- related behaviour may result in benefits for energy savings, cost saving and better thermal comfort of occupants [7]. Pilkington et al. [8] examined how occupant behaviour affected the energy efficiency of six passive solar homes with sunrooms and discovered that space heating demand varied by a factor of 14 between homes, with evidence suggesting that it may vary by a factor of up to 45. The energy demand varied with different locations, ranging from 96 to 171 kWh/m<sup>2</sup>/year, according to Jang and Kang's study of individual apartments in a high-rise building. They created a model integrating and implementing the unit specific consumption variation [9]. When Van den Brom et al. [10] compared the average energy consumption of 1.4 million Dutch households living in social housing with theoretical values, one of their conclusions was that rehabilitated buildings did not perform as well in practise as predicted. The study by Yan et al. [11] suggests that occupant behaviour significantly affects the energy performance of buildings and emphasises the need to include OB representation in building simulation models for more accurate findings. Delzendeh et al. [12] studied the literature to find gaps in the evaluation of energy demand and its utilisation in buildings and observed an alarming EPG, with a variance of up to 300%. In their analysis of the existence and size of the

energy gap in residential buildings in Switzerland, Cozza et al. [13] found that while buildings with high energy ratings (A and B) consumed more energy than expected, those with low energy ratings (Energy ratings C to G) consumed less energy than expected.

Accurate evaluation of energy-related occupant's behaviour is a key factor for bridging the gap between predicted and actual energy performance of buildings [14]. One of the key energy-related human behaviours is window control behaviour that has been modelled by different probabilistic modelling approaches. Identifying the factors that impact residential energy consumption is a key factor to be considered when designing of models and in the implementation of policies for energy efficiency. To analyse this, both the contextual and behavioural factors should be considered. Contextual factors include the local climate, building characteristics; and the behavioural factors include the user demography, their behavioural differences and energy usage pattern. Esmailimoakher et al. [15] conducted a survey which collected information about several building and occupant related factors, including floor area, household size, household income in Perth, West Australia. Perth is warm throughout the year with temperatures ranging in between 15 and 30 °C during most of the year. The survey showed that floor area, household size, and income were significant factors affecting energy consumption, rather than window opening behaviour. This might be because the survey did not include any temperature data or windows opening behavioural data, and because it is a warm country where heating was not a factor contributing to high energy consumption. Since the last decade, building energy performance simulation models have been seen to consider occupant behaviour by including stochastic models of occupant behaviour in relation to energy efficiency of buildings [16–19]. However, validation of these models has been sporadic. Developed models must be validated with similar but not the same data, and the results analysed to understand the usability of a model. Haldi et al. [16] compared simulated model values to actual values to get an estimate of the forecast realism. They proposed a new procedure called 'validation by simulating' wherein the combined predictive accuracy of two existing behavioural models of window opening and thermostat adjustments were estimated and compared to actual values taken in sensors fitted in apartments in Copenhagen, Denmark. Data were collected for two months and compared with data from a simulated model of the same building. Building energy performance simulations (BEPS) IDA ICE tool was used for simulation. It was found that although the predicted and actual values were in the same range, the model was unable to predict the actual indoor environmental conditions, which meant the model needed to be improved. For the above discussion, further research is still needed in relation to windows opening behaviour and the effect on energy consumption and the behavioural prediction using artificial intelligence.

## 29.2 Methodology

To monitor windows opening behaviour of occupants and to understand its relation to house heating and thereby energy efficiency, data were collected in peak winter of 2020, from end of Nov/20 to March/21 in social housing in Nottingham. This report analyses data collected in one of the three considered houses. Data in this house was collected between Nov 27 and Dec 17, 2020.

Sensors are fitted near windows in the dining room, the radiator in the dining room and in the hall to monitor the downstairs window temperature and humidity, downstairs radiator temperature and downstairs room temperature and humidity respectively. In total, six sensors were fitted, and data samples were collected every minute, see Fig. 29.1. The sensors used were temperature and humidity data loggers Omega OM-CP-RATemp101A. Temperature is measured in degree Celsius. For this study, the humidity measurement is not considered.

House A is an end-of-terrace house, floor plan shown in Fig. 29.1. It has two floors, downstairs consisting of the kitchen, a w/c and an open dining/sitting room layout, and the upstairs consists of a landing, three bedrooms and a bathroom. The external wall was insulated 8 years ago and since then the residents feel considerable improvement in the heat retention property of the house. However, they tend to open the windows more often, for air circulation, even though they have vents, which are kept open all the time.

This paper focuses on the analysis of data from the selected house, which is used to develop a model which will help to predict the windows opening status and hence the factors influencing such decisions. As shown in Fig. 29.2, a block diagram presents the developed Artificial Intelligence models to predict the windows status from inputs based on outside ambient temperature, time of the day, radiator temperature and room temperature.

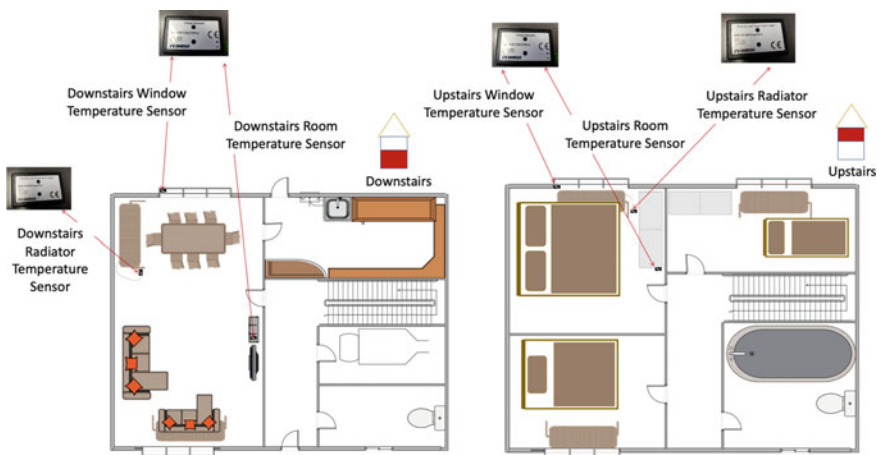
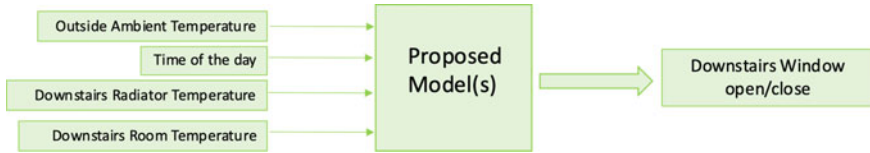


Fig. 29.1 House 1 layout with location of sensors



**Fig. 29.2** The proposed model to predict windows status from other variables

Selecting a model involves considering all factors to be considered, and a trade-off between specific characteristics of the algorithm like speed, memory usage, transparency etc. The basic structure of a decision tree consists of three basic parts called root node containing data, internal nodes (branches), and end nodes (leaves). The fundamental idea behind creating a decision tree structure may be summed up as asking a series of questions about the data and acting on the results as quickly as possible by using the attribute information of the training data. In this manner, the decision tree gathers the responses to the inquiries and develops the guidelines for making decisions. To classify the data and create the tree structure, questions are first asked of the root node, the tree's initial node. A coarse tree is where the classification is broad, and the branching is minimum. A fine tree is one where the main node or root branches to form several nodes, based on the classification criteria for the problem in hand [20, 21].

The study aims to understand the window opening behaviour of occupants; to find the conditions under which window is opened. Measurements of window opening and room temperature, radiator temperature, time of day and outside ambient temperature are taken. In the proposed mode, window status of the downstairs room is the 'response' and the outside ambient temperature, time of the day, downstairs radiator temperature and downstairs room temperature are the 'predictors'. Based on 1 day of data (selected randomly) taken for training and testing, 'Fine decision tree' was found to provide the best solution with 99% accuracy. Hence the fine tree is chosen to test the rest of the days data. Support Vector Machine, Logistic Regression, Gaussian Naive Bayes are some of the other models tested on the Matlab classification Learner app.

The percentage error of the model is calculated. The total error is the number of times the window status (open or closed) is wrongly predicted (see Eq. 29.1). Therefore, the error is the sum of inequality between the two logical arrays, as shown in equation. The percentage error is the total error over the total number of observations (Eq. 29.1). In this study, data is collected every minute giving observations of 1440 per day.

$$Error = (predicted\ window\ status \sim = measured\ window\ status) \quad (29.1)$$

$$Percentage\ error = \frac{\sum_{i=0}^n Error}{n} \times 100 \quad (29.2)$$

where  $n = 1440$ .

The average error for the Model A1 to Model A15 is calculated as shown in Eq. (29.3)

$$Average\ error\ Model\ A_i = \frac{Model\ A_i\ day_{i+1}\ error + \dots + Model\ A_i\ day_n\ error}{n - i} \quad (29.3)$$

where I is the number of days taken for training and n is the total number of days (n = 1440 in this case).

### 29.3 Results and Discussion

Figure 29.3 presents the data of outside ambient temperature, downstairs radiator temperature and room ambient temperature, upstairs radiator and room ambient temperature, window temperature, (measured using the sensor placed as shown in Fig. 29.4) between 1st December and 8th December 2020, as an example of the data captured. The other factor considered in this study is the outside ambient temperature. A daily average value of the nearest met weather station nearest to the location is obtained [22].

It should be noted that this study focuses on the temperature values and window status and does not include other factors that might influence window opening behaviour like ventilation type, noise level, security issues etc. Window temperature is the raw sensor data obtained to indicate the window status. The window temperature from the sensor is converted into binary values 0 indicating closed window and 1 indicating open window (the degree of opening is not considered in this study).

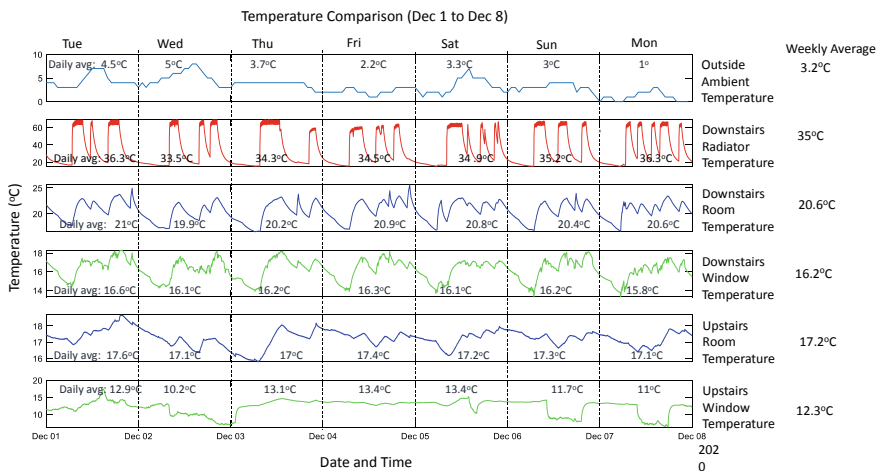


Fig. 29.3 House 1 sensor values recorded from December 1 to December 8

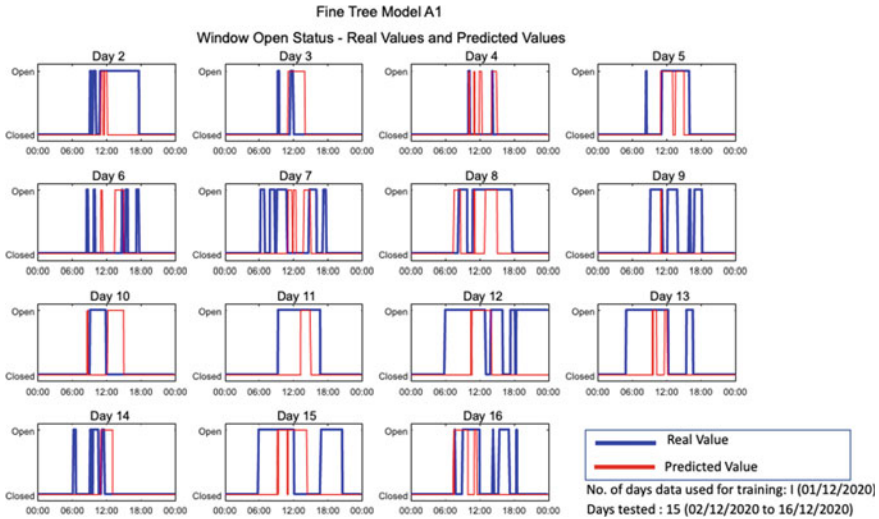


Fig. 29.4 Model A1 testing—actual values and predicted values from day 2 to day 16

This is done taking into consideration, the window temperature, outside ambient temperature, room temperature and radiator temperature. The degree of opening of window is not considered in this study.

Based on the Block diagram of the proposed machine learning model shown in Fig. 29.2, Fine Tree algorithm is used to develop different training and testing models.

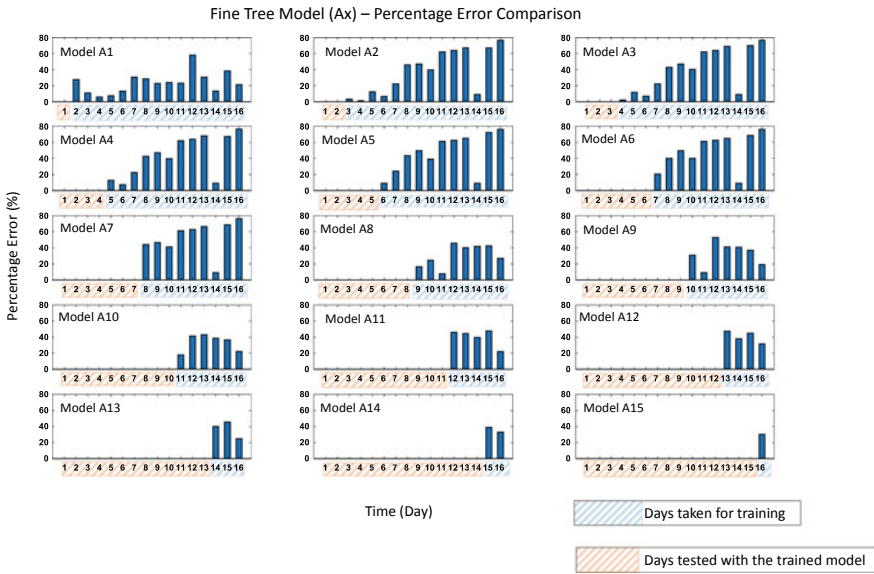
Models A1 to A15 are developed based on the training process presented in Table 29.1. In Model A1 the available data of House 1 (16 days data) is split as one day data set for training and the other 15 days data for testing the model. Hence Model Ax, is the Fine Tree algorithm training, where x is the number of training days, and the number of testing days will be (16 – x). In this study, weekends and weekdays were not considered separately, since the occupants of the house were not working and did not have a different pattern of living for weekends/weekdays.

Figure 29.4 shows the graph of actual values and predicted values from day 2 to day 16 for Fine Tree Model A1 (training using day 1 and testing using days 2 to 16). In Model A1, one day data is taken for training and the remaining 15 days data are used for testing the model. In the same way the process is repeated by taking two days data for training and 14 days data for testing the model (Model A2); 3 days data for training and 13 days data for testing (Model A3) and so on. The percentage error between the predicted and actual window opening status is calculated using (1) and (2).

The predicted window status is calculated using the machine learning models. Model A1 uses one day data to train and day 2 to day 16 data is used to test the performance of the developed model. The results and the difference between the actual and predicted data is shown in Fig. 29.5.

**Table 29.1** Models trained and tested as part of iteration process

Number of days used		Fine Tree Model Model Ax
Training	Testing	
1 day	15 days	Model A1
2 days	14 days	Model A2
3 days	13 days	Model A3
4 days	12 days	Model A4
5 days	11 days	Model A5
6 days	10 days	Model A6
7 days	9 days	Model A7
8 days	8 days	Model A8
9 days	7 days	Model A9
10 days	6 days	Model A10
11 days	5 days	Model A11
12 days	4 days	Model A12
13 days	3 days	Model A13
14 days	2 days	Model A14
15 days	1 day	Model A15



**Fig. 29.5** Percentage error for Model A1 to Model A15



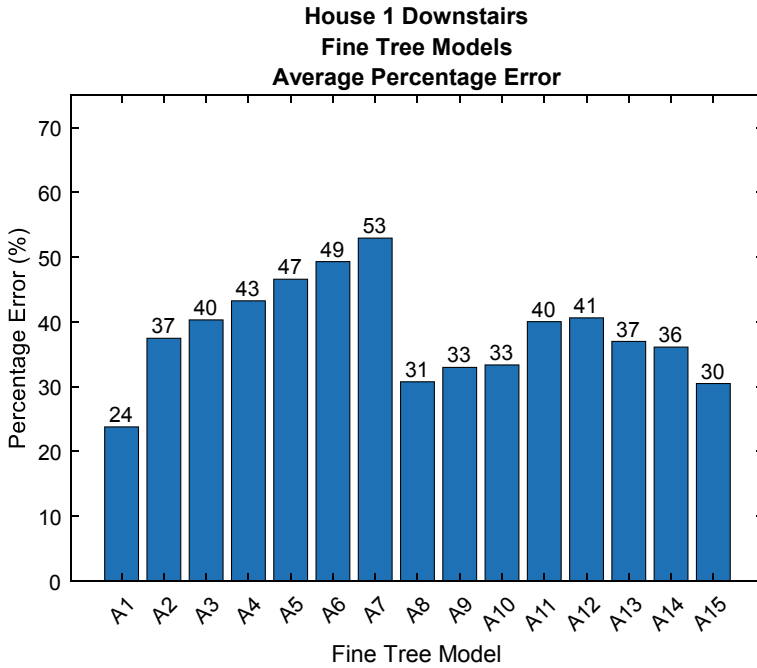


**Fig. 29.6** Average percentage error for Model A1 to Model A15 (rounded to the nearest integer)

The testing data is used to validate the developed model. This is done by testing the data with the developed model and comparing the result with the actual measured value. Model A2 uses 2 days of data to train the model and the developed model is tested with the rest of the days (day 3 to day 16), and so on. Figure 29.6 presents the training data and the error levels for the test models, Models A1 to A15.

Model A1 is found to have the lowest percentage prediction error of 23.8%. In this case, the proposed model of using temperature of room, radiator, external temperature, and time is found useful in predicting the reason for opening or closing of windows with 76.2% accuracy.

## 29.4 Conclusion

Temperature data were collected from one house in Nottingham. Data were collected in peak winter of 2020, from end of Nov 2020 to March 2021. Sensors were fitted to measure radiator temperature, room temperature, room humidity and window temperature for both upstairs and downstairs. Outdoor ambient temperature for the same period was also collected. Stochastic models were implemented, using machine learning of Fine Tree model, with datasets of window opening behaviour as response.

The inputs to the model were the radiator temperature, room temperature, outside ambient temperature, and time. Results have shown a reasonable prediction capability of windows opening behaviour, as the output of the model. Results have shown that Fine Tree model with 1 day data taken for training had the smallest percentage error of 23.8%. Further investigation needs to be undertaken to explore whether the presence of humidity plays a role in the window opening behaviour of occupants. This is a pilot study to investigate the potential applicability of classification models to find the relationship between energy efficiency of a building and windows opening behaviour of house occupants. Findings from this investigation can be used to identify the factors that contribute to 'performance gap' in energy efficiency of a building.

## References

1. BBC News, Climate Change: Is the UK on Track to Meet Its Targets?—BBC News. *BBC News*, 10 Nov 2021, <https://www.bbc.co.uk/news/58160547>
2. United Nations, PARIS AGREEMENT, Paris, 2015, [https://unfccc.int/sites/default/files/english\\_paris\\_agreement.pdf](https://unfccc.int/sites/default/files/english_paris_agreement.pdf)
3. EPSRC, *Carbon, Control and Comfort: User-Centred Control Systems for Comfort, Carbon Saving and Energy Management* (2010)
4. HM Government, Net Zero Strategy: Build Back Greener. Gov.Uk (2021), <https://www.gov.uk/government/publications/net-zero-strategy>
5. The Department for Business, Energy & Industrial Strategy, Green Homes Grant Voucher Scheme—National Audit Office (NAO) Report (2021), <https://www.nao.org.uk/report/green-homes-grant/>
6. Ministry of Housing Communities & Local Government, *English Housing Survey 2019 to 2020* (2020), pp. 1–73, [https://assets.publishing.service.gov.uk/government/uploads/system/uploads/attachment\\_data/file/945013/2019-20\\_EHS\\_Headline\\_Report.pdf](https://assets.publishing.service.gov.uk/government/uploads/system/uploads/attachment_data/file/945013/2019-20_EHS_Headline_Report.pdf)
7. H. Yoshino, T. Hong, N. Nord, IEA EBC annex 53: total energy use in buildings—analysis and evaluation methods. *Energy Build.* **152**, 124–136 (2017)
8. B. Pilkington, R. Roach, J. Perkins, Relative benefits of technology and occupant behaviour in moving towards a more energy efficient, sustainable housing paradigm. *Energy Policy* **39**(9), 4962–4970 (2011)
9. H. Jang, J. Kang, An energy model of high-rise apartment buildings integrating variation in energy consumption between individual units. *Energy Build.* **158**, 656–667 (2018)
10. P. Van den Brom, A. Meijer, H. Visscher, Performance gaps in energy consumption: household groups and building characteristics. *Build. Res. Inf.* **46**(1) (2018)
11. D. Yan, W. O'Brien, T. Hong, X. Fenga, H.B. Gunayb, F. Tahmasebid, A. Mahdavid, Occupant behavior modeling for building performance simulation: current state and future challenges. *Energy Build.* **107**, 264–278 (2015)
12. E. Delzende, S. Wu, A. Lee, Y. Zhou, The impact of occupants' behaviours on building energy analysis: a research review. *Renew. Sustain. Energy Rev.* **80**, 1061–1071 (2017)
13. S. Cozza, J. Chambers, M.K. Patel, Measuring the thermal energy performance gap of labelled residential buildings in Switzerland. *Energy Policy* **137**, 111085 (2020)
14. V.M. Barthelmes, B. Cristina, V. Fabi, S.P. Corgnati, Occupant behaviour lifestyles and effects on building energy use: investigation on high and low performing building features. *Energy Procedia* **140**, 93–101 (2017). <https://doi.org/10.1016/j.egypro.2017.11.126>
15. P. Esmaeilmoakher, T. Urmee, T. Pryor, G. Baverstock, Identifying the determinants of residential electricity consumption for social housing in Perth, Western Australia. *Energy Build.* **133**, 403–413 (2016). <https://doi.org/10.1016/j.enbuild.2016.09.063>

16. F. Haldi, D. Calì, R.K. Andersen, M. Wesseling, D. Müller, Modelling diversity in building occupant behaviour: a novel statistical approach. *J. Build. Perform. Simul.* **10**(5–6), 527–544 (2016). <https://doi.org/10.1080/19401493.2016.1269245>
17. J. Rouleau, L. Gosselin, Probabilistic window opening model considering occupant behavior diversity: a data-driven case study of Canadian residential buildings. *Energy* **195** (2020). <https://doi.org/10.1016/J.ENERGY.2020.116981>
18. F. Haldi, D. Robinson, On the behaviour and adaptation of office occupants. *Build. Environ.* **43**(12), 2163–2177 (2008). <https://doi.org/10.1016/j.buildenv.2008.01.003>
19. C.M. Clevenger, J.R. Haymaker, M. Maral Jalili, Demonstrating the impact of the occupant on building performance. *J. Comput. Civ. Eng.* **28**(1), 99–102 (2014). [https://doi.org/10.1061/\(asce\)cp.1943-5487.0000323](https://doi.org/10.1061/(asce)cp.1943-5487.0000323)
20. L. Rokach, O. Maimon, *Data Mining with Decision Trees, Theory and Applications*, ed. by H. Bunke, P.S.P. Wang. Series in Machine Perception and Artificial Intelligence, 2nd edn., vol. 81 (World Scientific, 2015)
21. T.Ç. Akinci, H.S. Noğay, Application of decision tree methods for wind speed estimation. *Eur. J. Tech.* **9**(1), 74–83 (2019). <https://doi.org/10.36222/ejt.558914>
22. MET Office UK, NCIC Monthly Summary, 6 Jan 2021, [https://www.metoffice.gov.uk/binaries/content/assets/metofficegovuk/pdf/weather/learn-about/uk-past-events/summaries/uk\\_monthly\\_climate\\_summary\\_202012.pdf](https://www.metoffice.gov.uk/binaries/content/assets/metofficegovuk/pdf/weather/learn-about/uk-past-events/summaries/uk_monthly_climate_summary_202012.pdf)

**Open Access** This chapter is licensed under the terms of the Creative Commons Attribution 4.0 International License (<http://creativecommons.org/licenses/by/4.0/>), which permits use, sharing, adaptation, distribution and reproduction in any medium or format, as long as you give appropriate credit to the original author(s) and the source, provide a link to the Creative Commons license and indicate if changes were made.

The images or other third party material in this chapter are included in the chapter's Creative Commons license, unless indicated otherwise in a credit line to the material. If material is not included in the chapter's Creative Commons license and your intended use is not permitted by statutory regulation or exceeds the permitted use, you will need to obtain permission directly from the copyright holder.



# Chapter 30

## Performance of Different Optimization Solvers for Designing Solar Linear Fresnel Reflector Power Generation Systems



M. P. G. Sirimanna, Jonathan D. Nixon, and M. S. Innocente

**Abstract** Linear Fresnel Reflector (LFR) is an emerging solar thermal power generation technology that benefits from a simple and low-cost construction in comparison to more conventional Concentrating Solar thermal Power (CSP) generation technologies such as parabolic trough and power tower. Although LFR technology presents the drawbacks of lower energy conversion efficiency and higher energy cost, these can be offset by optimizing its design. This has not been sufficiently addressed due to the complex interactions between solar rays, heat transfer modes, and design variables. This work presents a systematic approach to select suitable optimization methods for the design of LFR systems. Thus, a mathematical model is developed to carry out simultaneous raytracing and thermal simulations aiming to provide an estimation of the system's total conversion efficiency to be maximized. In order to compare the performance at solving this problem of a range of optimization algorithms with different characteristics, three derivative-based, two derivative-free, one population-based, and the simulated annealing methods are used in the numerical experiments. Only one design variable and a simple LFR system with a trapezoidal receiver are considered in the first instance. Only those algorithms which are successful at solving this simple problem are then tested on the optimal design with multiple variables. An exhaustive search is also conducted to check accuracy. Results show that pattern search, simulated annealing, and genetic algorithms perform best at solving the simulation-based LFR optimal design problem.

**Keywords** Concentrating solar thermal power (CSP) · Pattern search · Genetic algorithm · Simulated annealing · Ray-tracing

---

M. P. G. Sirimanna (✉) · J. D. Nixon  
Centre for Fluid and Complex Systems (FCS), Coventry University, Priory Street, Coventry CV1 5FB, UK  
e-mail: [ae0094@coventry.ac.uk](mailto:ae0094@coventry.ac.uk); [gayanmrt@gmail.com](mailto:gayanmrt@gmail.com)

M. S. Innocente  
Autonomous Vehicles and Artificial Intelligence Laboratory (AVAILAB), Centre for Future Transport and Cities (CFTC), Coventry University, Priory Street, Coventry CV1 5FB, UK

## 30.1 Introduction

With appropriate support, Concentrating Solar thermal Power (CSP) could contribute to 9.6% of global electricity from solar power alone by 2050 [1]. CSP has been developed under four technology categories: Power Tower, Parabolic Trough Collectors, Linear Fresnel Reflector (LFR), and Solar Parabolic Dish. Although LFR has shown potential low energy costs due to its simple design, its annual conversation efficiency is still low (8–10%) compared to the other technologies [2]. Mathematical optimization can be used to improve the efficiency of LFR systems and reduce energy costs, thus making this technology more attractive. In line with this, efficiency improvements to an existing prototype were achieved in 2015 using an analytical design approach [3], although the authors only carried out an optical analysis without optimizing the mirror field design variables. In [4], the geometry of a trapezoidal cavity receiver of an LFR plant was designed to minimise heat loss using ray tracing to simulate heat flux patterns on the receiver tube. However, they did not conduct a detailed analysis of the effect of the mirror field on the receiver. Another optical optimization of the arrangement of LFR mirrors was conducted in [5] considering mirror width, spacing, and focal length. The authors assumed a flat horizontal receiver and suggested including a thermal analysis with a more detailed receiver in future work. Barbón et al. [6] studied the lateral variation of solar energy received on an absorber of small-scale LFR plants. Their main focus was end loss and reflected light loss, which is typically disregarded as they are often negligible in large-scale plants. In 2017, Abbas et al. [7] addressed the optical design of an LFR considering different numbers of mirrors, filling factors, and collector widths. However, the authors made use of a set of pre-designs for a solar field without incorporating ray tracing models to reduce the required computational resources facilitating the optimization process. The optimal design of LFR systems making use of coupled optical ray-tracing and thermal models and considering both mirror field and receiver design parameters simultaneously has not been sufficiently investigated. The aim of this study is to identify a suitable optimization method which can solve this challenging problem.

## 30.2 Methodology

A mathematical model is developed by combining energy balance, ray tracing, and thermal modelling. The objective function for the LFR optimal design is given by the total theoretical efficiency ( $\eta_{total,th}$ ) assuming a coupled Carnot cycle [8, 9]. The design variables are the number of mirrors ( $n_m$ ), mirror width ( $w_m$ ), mirror spacing ( $s_m$ ), receiver height ( $h_r$ ), and receiver width ( $w_r$ ).

Seven optimization methods with different characteristics are tested to investigate their efficiency, as well as their different trade-offs between accuracy and required computational effort. Namely, interior-point (IP), sequential quadratic programming

(SQP) and active-set (AS) methods are derivative-based; pattern search (PS), Nelder-Mead simplex (NMS) and simulated annealing (SA) methods are derivative-free; whilst genetic algorithm (GA) is both a derivative-free and population-based method. This particular choice of methods is based on the literature and on their availability within Matlab's optimization toolbox.

The optimization problem is initially reduced to a single design variable, namely the receiver height. The problem is then solved using the PS, NMS, SA and GA methods. The worst-performing algorithm is eliminated (NMS, referred to as fminsearch in Matlab), and the other three are tested on the original five-dimensional optimization problem discussed before. It is fair to note that the number of mirrors ( $n_m$ ) is a discrete variable. In order to avoid a mixed-discrete problem, a four-dimensional continuous problem is solved instead for each of a few selected values of  $n_m$ .

### 30.3 Models

Based on the conservation of energy principle, the energy output of the LFR system ( $Q_o$ ) can be found from the difference between the heat input ( $Q_{in}$ ) to the receiver and the heat loss to ambient air ( $Q_{loss}$ ) [10].

$$Q_o = Q_{in} - Q_{loss} \quad (30.1)$$

After reflection on the mirrors, the solar energy incident over the receiver area,  $A_r$ , is absorbed by the working fluid as heat, increasing the receiver temperature ( $T_r$ ). The absorbed solar energy becomes the heat input to the system ( $Q_{in}$ ). A portion of absorbed energy is lost to the surrounding, which is at temperature  $T_a$ . The heat output of an LFR system can therefore be described by [11, 12]

$$Q_o = I_{r,abs} A_r - A_r U_L (T_r - T_a) \quad (30.2)$$

where  $I_{r,abs}$  and  $U_L$  are absorbed solar radiation and heat loss coefficient of the receiver.

There are analytical methods and numerical approaches to calculate  $I_{r,abs}$  for different LFR systems. SolTrace tool has been used in this study considering its ability to model complex geometries with good accuracy [13].  $U_L$  is calculated using analytical and empirical correlations considering conduction, convection and radiation losses of the receiver [11, 14].

If solar energy received on the effective aperture of all mirror elements is  $E_m$ , the total theoretical efficiency ( $\eta_{total,th}$ ) can be obtained as in Eq. (30.3), assuming coupled Carnot cycle [8, 9].

$$\eta_{total,th} = \frac{Q_o \left(1 - \frac{T_a}{T_r}\right)}{E_m} \quad (30.3)$$

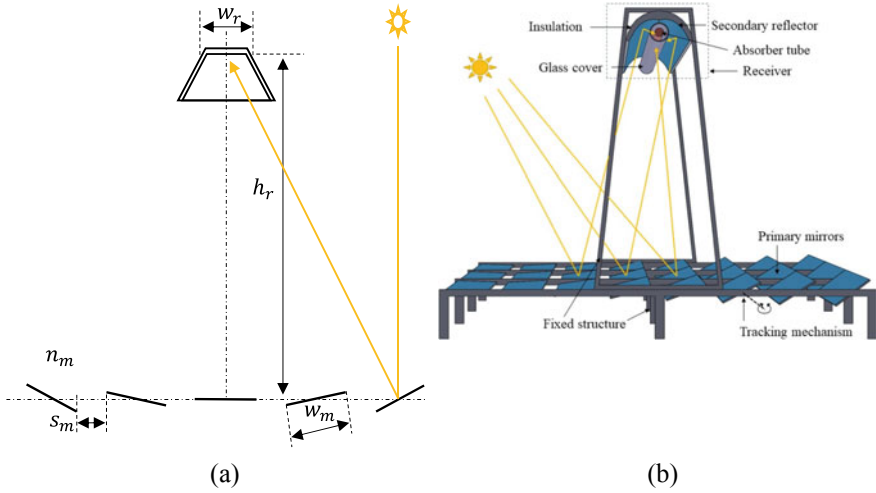


**Fig. 30.1** **a** Schematic of a 2D view of an LFR system with a trapezoidal cavity receiver, **b** a schematic diagram of a typical LFR system

The objective function to be optimized is  $\eta_{total,th}$  and the design variables are the number of mirrors ( $n_m$ ), mirror width ( $w_m$ ), mirror spacing ( $s_m$ ), receiver height ( $h_r$ ) and receiver width ( $w_r$ ), as shown in Fig. 30.1.

## 30.4 Results and Discussion

### 30.4.1 Candidate Derivative-Free and Population-Based Methods

Two derivative-free methods, pattern search and fminsearch solver in Matlab, were selected and eight simulations were carried out for each method. Figure 30.2a shows that all eight optimization results are gathered around the neighbourhood of the global optimum. These results show a very good agreement with the exhaustive search. Two global optimization methods, Simulated Annealing and GA, were also used to check their behaviour for the objective function. Five simulations were run for Simulated Annealing and three simulations were run for GA. As seen in Fig. 30.2b, all these results lay between 22 and 23 and were very close to the global optimum,  $h_r = 23$ . All simulations were run using default settings except the function tolerance, which was reduced to  $10^{-3}$  to minimise the effect of numerical disturbance of the model. It is seen that simulated annealing and GA have shown the best results in consecutive runs showing close solutions to each other.

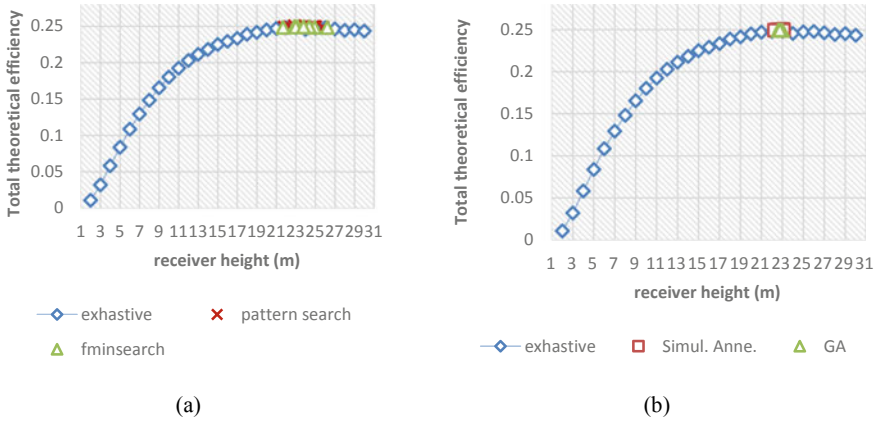


**Fig. 30.2** **a** Comparison of exhaustive search results against two derivative-free methods **b** against a population-based method (GA) and simulated annealing

### 30.4.2 A Candidate Optimization Method for a Multidimensional Problem

Optimization was expanded to four continuous variables ( $w_m, s_m, h_r, w_r$ ) while keeping the fifth one ( $n_m$ ) at a few selected discrete values. Thus a four-dimensional continuous optimization problem is solved for each value of  $n_m$ . Only the PS, SA and GA algorithms are tested here, which are the ones which performed best in the one-dimensional problem. In order to assess the accuracy of the optimizers, an exhaustive search was performed discretizing all four continuous variables (see Table 30.1).

The ten best simulation results from the exhaustive search for  $n_m = 10$  are shown in Table 30.2. It can be observed that the differences between the efficiency of the global optimum and that of neighbouring designs are very small. In fact, the first two solutions may be deemed global maxima if rounding efficiency to three decimals. Then, the global maxima would be found at  $h_r = 9$  m,  $w_r = 0.9$  m,  $w_m = 0.9$

**Table 30.1** Design variables and their discretization for exhaustive search

Variable	Range	Discretization for exhaustive search	
		Step size	Sample values
Receiver height ( $h_r$ )	$1 \leq h_r \leq 30$	4 m	1, 5, 9, ..., 21, 25, 29
Mirror width ( $w_m$ )	$0.1 \leq w_m \leq 1.2$	0.2 m	0.1, 0.3, 0.5, ..., 0.9, 1.1
Mirror spacing ( $s_m$ )	$0.05 \leq s_m \leq 0.3$	0.05 m	0.05, 0.1, 0.15, ..., 0.25, 0.3
Receiver width ( $w_r$ )	$0.1 \leq w_r \leq 1.2$	0.2 m	0.1, 0.3, 0.5, ..., 0.9, 1.1
Number of mirrors ( $n_m$ )	$2 \leq n_m \leq 78$	4	2, 6, 10, ..., 74, 78



m, whilst  $s_m$  could take either 0.09 m or 0.13 m. However, the design variables are discretised. For the continuous case, the actual global optimum may lie nearby. Therefore, it is possible that a global search algorithm is able to find even better solutions than this so-called exhaustive search.

The optimal designs returned by PS, SA and GA are shown in Table 30.3. It is seen that all solvers achieve a maximum  $\eta_{total,th}$  between 0.170 and 0.172 (i.e. 17–17.2%). Figure 30.3 shows a comparison of these results in terms of the maximised solution.

**Table 30.2** Results of the exhaustive search for  $n_m = 10$

$h_r$ (m)	$w_r$ (m)	$w_m$ (m)	$s_m$ (m)	Max $\eta_{total,th}$	Max $\eta_{total,th}$ rounded
9	0.9	0.9	0.09	0.169046	0.169
9	0.9	0.9	0.13	0.168863	0.169
13	0.9	0.9	0.29	0.168355	0.168
13	0.9	0.9	0.17	0.168300	0.168
13	0.9	0.9	0.25	0.167729	0.168
9	0.9	0.9	0.05	0.167573	0.168
13	0.9	0.9	0.21	0.167472	0.167
9	0.9	0.9	0.17	0.167419	0.167
13	0.9	0.9	0.09	0.167098	0.167
13	0.9	0.9	0.05	0.166906	0.167

**Table 30.3** Optimization results of three optimization algorithms for  $n_m = 10$

Number of mirrors ( $n_m$ ) = 10		Pattern search		Simulated annealing		Genetic algorithm	
		Optimal design (m)	Max $\eta_{total,th}$	Optimal design (m)	Max $\eta_{total,th}$	Optimal design (m)	Max $\eta_{total,th}$
1st run	$h_r$	10.5	0.1713	9.92	0.1715	8.92	0.1711
	$w_r$	0.878		0.852		0.799	
	$w_m$	0.89		0.861		0.833	
	$s_m$	0.247		0.103		0.115	
2nd run	$h_r$	11	0.1701	9.9	0.1703	10.276	0.1715
	$w_r$	0.8		0.867		0.867	
	$w_m$	0.89		0.889		0.885	
	$s_m$	0.285		0.076		0.157	
3rd run	$h_r$	10	0.1717	8.738	0.1697	9.86	0.1719
	$w_r$	0.878		0.81		0.873	
	$w_m$	0.89		0.788		0.902	
	$s_m$	0.193		0.166		0.177	

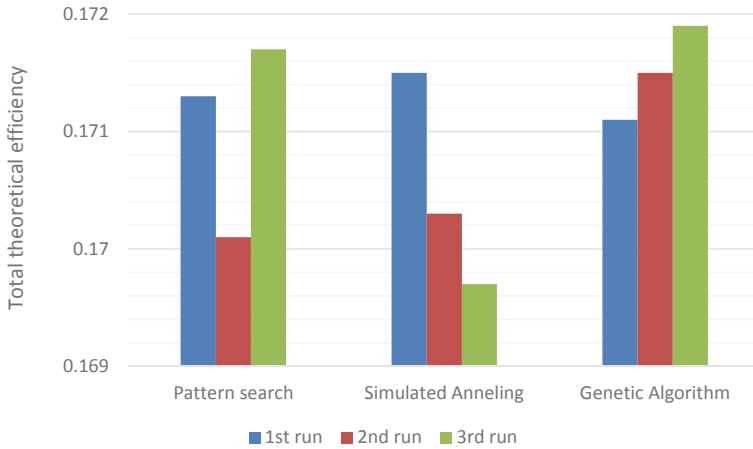


**Fig. 30.3** Comparison of maximised  $\eta_{total,th}$  using three optimization algorithms ( $n_m = 10$ )

The same process of comparing the exhaustive search and optimal solutions was repeated for  $n_m = 30$  and  $n_m = 54$ . Results show a similar behaviour to  $n_m = 10$ , where an optimal solution was found within the same region of the search-space as the exhaustive search. Although the three optimization algorithms found better solutions, it should be noted that the discretization of continuous search space has greatly affected these results. A comparison of the results of these two different simulations is shown in Fig. 30.4. The average simulation times for the three algorithms are shown in Fig. 30.5.

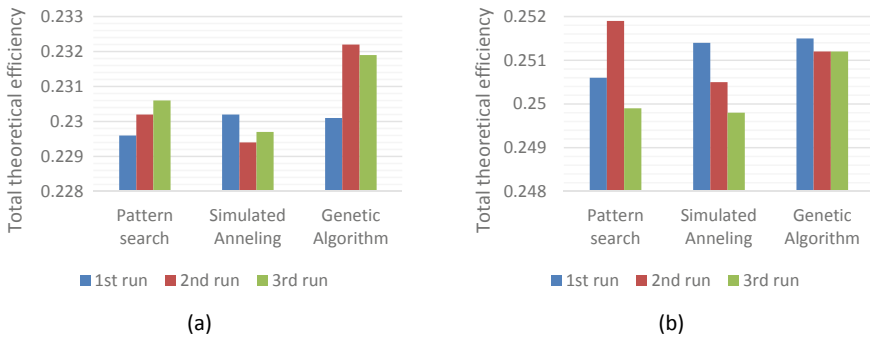


**Fig. 30.4** A comparison of three optimization algorithms: **a**  $n_m = 30$ ; **b**  $n_m = 54$

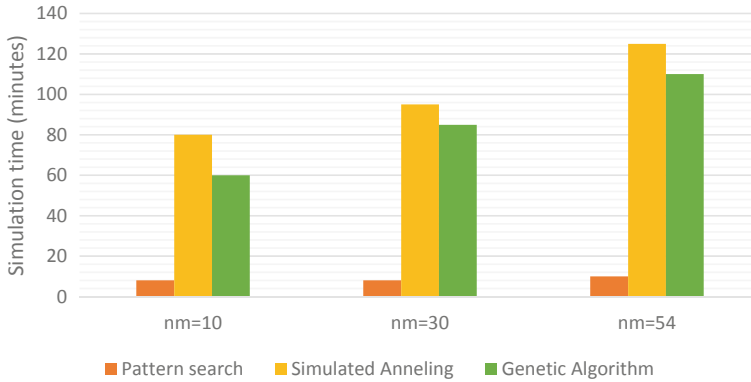


**Fig. 30.5** Average simulation time for all three optimization algorithms

### 30.5 Conclusion

After considering all the simulation results, it is seen that pattern search, simulated annealing and genetic algorithm provided acceptable solutions. The differences between the best and the worst solutions using pattern search, simulated annealing and GA were 0.0012–0.0020, 0.0008–0.0018 and 0.0003–0.0020 respectively. The largest difference found was 0.002, equal to 0.2% of the total theoretical efficiency, which is more than enough for many practical applications. Since all algorithms provided acceptable results, the selection of an algorithm for further work can be decided based on the simulation time and the ease of handling the discrete design variable, number of mirrors, within the optimization codes.

It is clearly seen that the pattern search is 8–10 times faster than the other two algorithms in terms of computational time. Increasing the simulation time for larger mirror numbers is also significantly lower in comparison. The genetic algorithm seems to be slightly better than simulated annealing taking 10–20 min less simulation time. However, it is important to note that for population-based methods like GA, the initial setup is usually time consuming and adding extra variables is relatively easy.

### References

1. IRENA, *Technology Roadmap, Concentrating Solar Power* (International Energy Agency, 2010)
2. M.T. Islam et al., A comprehensive review of state-of-the-art concentrating solar power (CSP) technologies: current status and research trends. *Renew. Sustain. Energy Rev.* **91**, 987–1018 (2018), Available at: <http://www.sciencedirect.com/science/article/pii/S1364032118303113>. <https://doi.org/10.1016/j.rser.2018.04.097>
3. R. Abbas, J.M. Martínez-Val, Analytic optical design of linear Fresnel collectors with

- variable widths and shifts of mirrors. *Renew. Energy* **75**, 81–92 (2015), Available at: <http://www.sciencedirect.com/science/article/pii/S0960148114005941>. <https://doi.org/10.1016/j.renene.2014.09.029>
4. M.A. Moghimi, K.J. Craig, J.P. Meyer, Optimization of a trapezoidal cavity absorber for the Linear Fresnel Reflector. *Solar Energy* **119**, 343–361 (2015), Available at: <http://www.sciencedirect.com/science/article/pii/S0038092X15003771>. <https://doi.org/10.1016/j.solener.2015.07.009>
  5. P. Boito, R. Grena, Optimization of the geometry of Fresnel linear collectors. *Solar Energy* **135**, 479–486 (2016), Available at: <http://www.sciencedirect.com/science/article/pii/S0038092X16301785>. <https://doi.org/10.1016/j.solener.2016.05.060>
  6. A. Barbón et al., Optimization of the length and position of the absorber tube in small-scale Linear Fresnel Concentrators. *Renew. Energy* **99**, 986–995 (2016), Available at: <http://www.sciencedirect.com/science/article/pii/S0960148116306851>. <https://doi.org/10.1016/j.renene.2016.07.070>
  7. R. Abbas et al., Design of an innovative linear Fresnel collector by means of optical performance optimization: a comparison with parabolic trough collectors for different latitudes. *Solar Energy* **153**, 459–470 (2017), Available at: <http://www.sciencedirect.com/science/article/pii/S0038092X17304255>. <https://doi.org/10.1016/j.solener.2017.05.047>
  8. M. Romero, J. Gonzalez-Aguilar, E. Zarza, Concentrating solar thermal power, in *Energy Efficiency and Renewable Energy Handbook*, 2nd edn., ed. by D.Y. Goswami, F. Kreith (CRC Press, Boca Raton, 2015), pp.1237–1246
  9. J.D. Nixon, P.A. Davies, Cost-exergy optimisation of linear Fresnel reflectors. *Solar Energy* **86**(1), 147–156 (2012), Available at: <http://www.sciencedirect.com/science/article/pii/S0038092X11003501>. <https://doi.org/10.1016/j.solener.2011.09.024>
  10. G. Morin et al., Comparison of linear Fresnel and parabolic trough collector power plants. *Solar Energy* **86**(1), 1–12 (2012), Available at: <https://www.sciencedirect.com/science/article/pii/S0038092X11002325>. <https://doi.org/10.1016/j.solener.2011.06.020>
  11. J.A. Duffie, W.A. Beckman, *Solar Engineering of Thermal Processes*, 4th edn. (Wiley, New Jersey, 2013)
  12. H. Zheng, Chapter 2—solar energy utilization and its collection devices, in *Solar Energy Desalination Technology*, ed. by H. Zheng (2017), Available at: <https://www.sciencedirect.com/science/article/pii/B9780128054116000026>. <https://doi.org/10.1016/B978-0-12-805411-6.00002-6>
  13. T. Wendelin, A. Dobos, A. Lewandowski, *SolTrace: A Ray-Tracing Code for Complex Solar Optical Systems* (United States, 2013)
  14. R. Forristall, *Heat Transfer Analysis and Modeling of a Parabolic Trough Solar Receiver Implemented in Engineering Equation Solver* (US Department of Energy (US), United States, 2003), Available at: <http://www.osti.gov/scitech/biblio/15004820>. <https://doi.org/10.2172/1504820>

**Open Access** This chapter is licensed under the terms of the Creative Commons Attribution 4.0 International License (<http://creativecommons.org/licenses/by/4.0/>), which permits use, sharing, adaptation, distribution and reproduction in any medium or format, as long as you give appropriate credit to the original author(s) and the source, provide a link to the Creative Commons license and indicate if changes were made.

The images or other third party material in this chapter are included in the chapter's Creative Commons license, unless indicated otherwise in a credit line to the material. If material is not included in the chapter's Creative Commons license and your intended use is not permitted by statutory regulation or exceeds the permitted use, you will need to obtain permission directly from the copyright holder.



# Chapter 31

## Thermal Optimisation Model for Cooling Channel Design Using the Adjoint Method in 3D Printed Aluminium Die-Casting Tools



Tongyan Zeng, Essam F. Abo-Serie, Manus Henry, and James Jewkes

**Abstract** In the present study, the adjoint method is introduced to the optimisation of the corner cooling element in two baseline cooling designs for a mould cavity, as examples of the Aluminium metal die-casting process. First, a steady thermal model simulating the Aluminium die-casting process is introduced for the two-corner cooling design scenario. This steady model serves as the first iteration of the optimised model using the adjoint method. A dual-parameter objective function targets the interfacial temperature standard deviation and pressure drop across the internal cooling region. For both design cases, multi-iterative deformation cycles of the corner cooling configurations result in optimised designs with non-uniform cross-section geometries and smooth surface finishing. Numerical simulations of the resulting designs show improvements in uniform cooling across the mould/cast interfacial contact surface by 66.13% and 92.65%, while the optimised pressure drop increases coolant fluid flow by 25.81% and 20.35% respectively. This technique has been applied to optimise the complex cooling system for an industrial high-pressure aluminium die-casting (HPADC) tool (Zeng et al. in SAE Technical Paper 2022-01-0246, 2022, [1]). Production line experience demonstrates that the optimised designs have three times the operational life compared to conventional mould designs, providing a significant reduction in manufacturing and operation costs.

**Keywords** Additive manufacturing · Adjoint optimisation · Conformal cooling optimisation

---

T. Zeng (✉) · E. F. Abo-Serie · M. Henry  
Centre of Fluid and Complex Systems, Coventry University, Coventry CV1 2NL, UK  
e-mail: [zengt5@uni.coventry.ac.uk](mailto:zengt5@uni.coventry.ac.uk)

J. Jewkes  
Department of Engineering, University of Leicester, Leicester LE1 7RH, UK

## 31.1 Introduction

The additive manufacturing (AM) approach known as three-dimensional (3D) printing technology has reshaped the traditional design concept and enabled significant design freedom across numerous industry fields. One application is the manufacture of Aluminium metal die-casting tools via selective laser sintering (SLS). The lifecycle of mould cavities is required to exceed 100,000 casting cycles to be economically viable [2]. Working under extreme operating conditions, the Aluminium die-casting tool's lifespan is determined by thermal fatigue induced by temperature gradients. Cooling channels, embedded within the mould to dissipate heat, are responsible for maintaining thermal stability during the casting period. AM techniques can now overcome a significant constraint imposed by conventional computer numerical control (CNC) machining methods, which can only generate straight cooling channels. More complex and efficient cooling systems can now be designed and implemented, resulting in prolonged tooling life and improved cast quality [3]. Accordingly, the development of optimal cooling layouts for rapid-prototyped (RP) mould inserts is of considerable interest for sustainable manufacturing.

The application of AM to casting tools is focused on introducing advanced rapid tooling (RT) techniques such as direct metal laser sintering (DMLS), SLS, stereolithography (SLA) and others [4]. In addition, the introduction of high thermal conductive material or alloys [5, 6], adding an intermediate lubrication layer or an additional spraying process [7, 8], provide improvements in thermal efficiency and mechanical performance. While external optimisation is still limited by the manufacturing process and material type, optimisation of the internal cooling passage design remains the most favoured and effective research approach to improving injection moulding [9]. Researchers explore the possibilities of modifying different basic elements of the cooling channel design such as pipe numbers, diameter, depth, etc. or adding internal baffles, lattices and secondary layers [10]. Adopting non-circular cross-section profiles such as the grooved square also demonstrated thermal and fatigue enhancements [9]. Although the use of a non-circular cooling channel profile has been proposed, typically the cross-sectional shape remains constant at all locations [11]. Prior investigations into the potential application of non-uniform cross-sectional profiles for conformal cooling channels are very limited.

The idea of creating a non-uniform cross-section profile for designing internal cooling channels can be linked to the study of surface sensitivity response. The adjoint method initially proposed by Lions and Pironneau [12, 13] is a powerful numerical approach used to calculate a pre-defined mesh sensitivity based on a defined objective function. Two types of optimisation approaches using the adjoint method currently exist. Firstly, topology optimisation generates the surface mesh based on pre-defined satisfactory criteria within the domain space [14]. Secondly, surface deformation optimisation morphs the existing mesh surface based on the defined objective conditions; this second approach has yet to be investigated for

aluminium die-casting applications. Accordingly, this paper investigates the use of adjoint surface deformation optimisation for the design of the cooling element for aluminium die-casting.

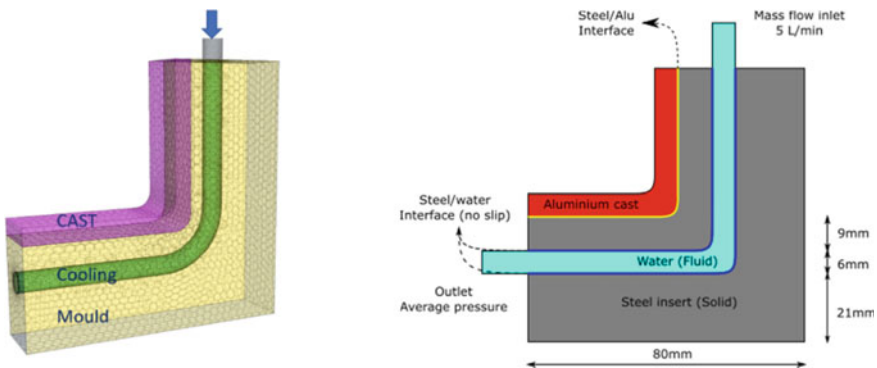
### 31.2 Methodology

A steady-state model of the two corner cooling designs provides initial solutions. The adjoint model is then applied to conduct multi-iterative optimisation, which includes a dual-parameter objective function and a user-specified surface point displacement function to achieve optimal cooling designs. The resulting optimisation models are discussed and demonstrated below.

#### 31.2.1 Preliminary Steady Model

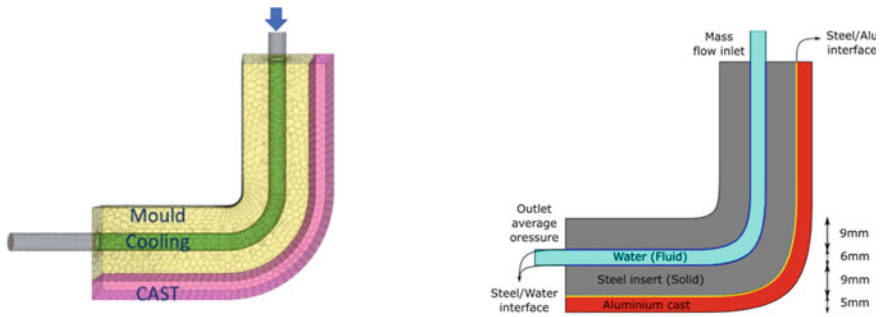
The initial steady simulation for the aluminium die-casting model is established for three defined regions, the Aluminium A380.0-F alloy cast, the H13 steel mould and the water coolant channel. Figure 31.1 shows the general layout and schematic of the first corner cooling scenario, where the cast is located at the internal side of the corner as the single cooling channel passes through the mould cavity. The mould block has dimensions of  $80 \times 18 \times 80$  mm. The baseline cooling channel diameter is set to 6 mm, entering the block from above. The pitch distance between the top pipe surface to the mould/cast interface is kept constant at 9 mm.

Figure 31.2 shows the corresponding schematic model layout for the second corner cooling scenario where the casting layer is located on the mould’s external side. Modifications are made to the mould external surfaces to maintain the same 9 mm



**Fig. 31.1** General layout of the three regions and schematic diagram for the internal casting layer corner cooling scenario





**Fig. 31.2** General layout of the three regions and schematic diagram for the external casting layer corner cooling scenario

pipe-to-interface pitch distance so that the embedded cooling channel design remains unchanged. The entrance and exit of both corner cooling channel designs are extended by 30 mm, i.e.  $5 \times$  the channel diameter, to ensure a fully developed flow within the body of the cast. The casting layer follows the surface shape of the mould with a 5 mm thickness and acts as a solid region providing a constant volumetric heat generation at  $4.5E7 \text{ W/m}^3$ , simulating the constant heat transfer from the cast aluminium to the mould body for this steady condition.

Both baseline models are discretised into polyhedral mesh cells by adopting the commercial CFD software package STARCCM + ®. A total cell count of 108,489 and 86,100 for internal and external designs are generated which give an overall mesh quality of 98.71 and 98.25% based on the evaluation of mesh validity and skewness angle. Two sets of in-place close-contact interfaces between the aluminium and steel, and steel and cooling channels are established for each corner case. A zero thermal resistance assumption is made between the mould/cast interface to enhance the thermal heat transfer effect. Each top/front and left-right surface of the mould and cast is defined as a periodic topological interface relationship, with the remaining boundary surfaces defined as impermeable boundary walls and adiabatic thermal conditions. A conventional conjugate heat transfer (CHT) model is implemented for solving the conductive and convective heat transfer between the three bodies. The initial temperature of the cast and mould is set to  $650 \text{ }^\circ\text{C}$  and  $200 \text{ }^\circ\text{C}$  respectively, coolant water inlet/outlet is defined as a 5 L/min mass flow inlet at a constant temperature of  $68.4 \text{ }^\circ\text{C}$  and boundary-normal pressure outlet. Given the Reynolds number of approximately 43,000, the fluid flow is solved using a Reynolds-Averaged Navier-Stokes (RANS) turbulence model together with a shear-stress transport (Menter) K-Omega turbulence model.

### 31.2.2 *Adjoint Optimisation Model*

A well-converged solution with continuity residual below  $1E-5$  indicates a sufficiently accurate solution for the initial steady simulation, as the basis for the subsequent optimisation. The adjoint model is now enabled to solve the sensitivity objectives for the two input parameters, mould/cast interface temperature standard deviation and pressure drop across the cooling channel. A vector function links the cumulative morph distance and the adjoint results of the two parameters using a weighted sum approach with a 50/50 ratio, including a user-defined steepest descent constant (SDC) that controls the amount of surface morph distance per iteration. A combined multi-objective displacement function is assigned to an evenly distributed point-set around the deformation cooling region. These supporting point-sets are 0.005 mm in relative target spacing and 0.004 mm offset distance from pipe surface; these values maintain geometry and mesh validity. The new position of points is determined based on a radial basis function (RBF) interpolation and the adjoint sensitivity results. The iterative surface deformation can be looped until the stopping criteria or loop count has been reached. A re-solve for the adjoint sensitivity and surface mesh is also necessary after each optimisation cycle to ensure the accuracy of results.

## 31.3 Results and Discussion

Figure 31.3 compares the spatial distribution of temperature for the initial steady simulation of the internal corner cooling case with that of the optimised cooling design. In the baseline case, the high-temperature regions located around the cast inlet and outlet reach a maximum of 428 °C. The optimised cooling surface has non-uniform morphed sections in the high-temperature regions by shifting closer to the aluminium cast, increasing the global cooling channel diameter. As a result, the peak temperature drops to 378 °C. A total of 28 optimisation cycles were run for the internal corner cooling case. Table 31.1 lists three key parameter values for the baseline and optimal designs. The mould interface temperature standard deviation and pressure drop show significant improvements, reduced by 66.13% and 25.81% respectively for the final optimal mould design, while there is a 37 °C drop in interface average temperature.

Results for the second external cooling case are shown in Fig. 31.4. The peak temperature is 530 °C for the baseline design. The optimised design showed an increase in global pipe diameter and small shifting in position, which reduced the maximum temperature to 444 °C. 11 optimisation cycles were conducted to obtain the final design for this external corner cooling case. Parameter results in Table 31.1 show 92.65% improvement in mould interface thermal uniformity and 20.35% refinement in pressure drop.

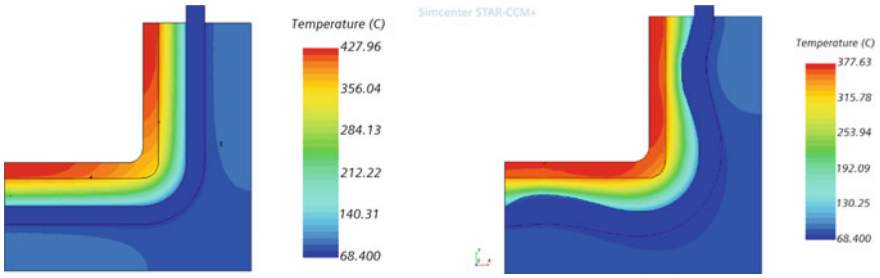


**Fig. 31.3** Section thermal distribution results for the baseline and optimised internal corner cooling design

**Table 31.1** Numerical solutions between two baseline and optimised corner cooling scenarios

Internal corner cooling mould case				
	Baseline design	Optimal design	Difference in value	Difference in %
Surface temp SD	18.87	6.39	12.48	66.13
Pressure-drop (Pa)	5729.68	4250.84	1478.84	25.81
Surface average temp (°C)	395.65	358.32	37.33	N/A
<i>External corner cooling mould case</i>				
	Baseline design	Optimal design	Difference in value	Difference in %
Surface temp SD	26.52	1.95	24.57	92.65
Pressure-drop (Pa)	6196.99	4935.96	1261.03	20.35
Surface average temp (°C)	470.979	424.749	46.23	N/A

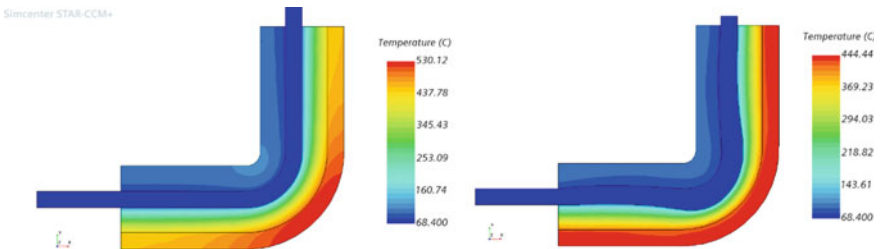


**Fig. 31.4** Section thermal distribution for the baseline and optimised external corner cooling design

## 31.4 Conclusion

A thermal optimisation model using the adjoint method has been applied to two baseline mould configurations for the aluminium die-casting process. The resulting designs have shown significant improvements in interfacial temperature uniformity and pressure drop refinement. This innovative approach has been adopted in a large-scale industrial design with complex cooling systems and has achieved prominent results in material and cost savings of more than 200%.

**Acknowledgements** The author would like to acknowledge CastAlum Team for their contribution and technical support. The authors would like also to acknowledge Innovate UK project no. P16874 for the funding.

## References

1. T. Zeng, E.F. Abo-Serie, J. Jewkes, P. Dodd et al., Adjoint Method for the optimisation of conformal cooling channels of 3-d printed high-pressure tools for aluminium casting. SAE Technical Paper 2022-01-0246 (2022). <https://doi.org/10.4271/2022-01-0246>
2. C. Mitterer, F. Holler, F. Ustel, D. Heim, Application of hard coatings in aluminium die casting—soldering, erosion and thermal fatigue behaviour. *Surf. Coat. Technol.* **125**, 233–239 (2000)
3. G.S. Phull, S. Kumar, R.S. Walia, Conformal cooling for moulds produced by additive manufacturing: a review. *Int. J. Mech. Eng. Technol.* **9**(1), 1162–1172 (2018)
4. W. Tong et al., Design optimisation of plastic injection tooling for additive manufacturing. *Procedia Manuf.* **10**, 923–934 (2017)
5. D.G. Ahn, H.W. Kim, Study on the manufacture of thermal management mould with three different materials using a direct metal tooling process. *Proc. Inst. Mech. Eng. Part B: J. Eng. Manuf.* **224**(3)
6. A.B.M. Saifullah et al., Thermal-structural analysis of bi-metallic conformal cooling for injection moulds. *Int. J. Manuf. Technol.* **62**, 123–133 (2012)
7. K. Altaf et al., Determining the effects of thermal conductivity on epoxy moulds using profiled cooling channels with metal inserts. *J. Mech. Sci. Technol.* **30**(11), 4901–4907 (2016)
8. S. Asthana, Innovative die lubricant trends for evolving productivity and process requirements (NADCA Die casting Cong, Holbrook, 2013)
9. K. Altaf et al., Prototype production and experimental analysis for circular and profiled conformal cooling channels in aluminium filled epoxy injection mould tools. *Rapid Prototyping J.* **19**(4), 220–229 (2013)
10. F. Shehata, M. Abd-Elhamid, Computer-aided foundry die-design. *Mater. Des.* **24**, 577–583 (2003)
11. K. Altaf, V.R. Raghavan, A.M.A. Rani, Comparative thermal analysis of circular and profiled cooling channels for injection mould tools. *J. Appl. Sci.* **11**(11), 2068–2071 (2011)
12. J.L. Lions, *Optimal control of systems governed by partial differential equations (Grundlehren der Mathematischen Wissenschaften)*, vol. 170 (Springer, Berlin, 1971)
13. O. Pironneau, On optimum design in fluid mechanics. *J. Fluid Mech.* **64**(1), 97–110 (1974)
14. Z. Li et al., Topology optimisation for the design of conformal cooling systems in thin-wall injection molding based on BEM. *Int. J. Adv. Manuf. Technol.* **94**, 1041–1059 (2018)

**Open Access** This chapter is licensed under the terms of the Creative Commons Attribution 4.0 International License (<http://creativecommons.org/licenses/by/4.0/>), which permits use, sharing, adaptation, distribution and reproduction in any medium or format, as long as you give appropriate credit to the original author(s) and the source, provide a link to the Creative Commons license and indicate if changes were made.

The images or other third party material in this chapter are included in the chapter's Creative Commons license, unless indicated otherwise in a credit line to the material. If material is not included in the chapter's Creative Commons license and your intended use is not permitted by statutory regulation or exceeds the permitted use, you will need to obtain permission directly from the copyright holder.



# Chapter 32

## The Effect of Vane Number in Casing Treatment of an Axial-Flow Compressor



Sara Soodani, SeyedVahid Hosseini, Mohammad Hakimi,  
and Mohammad Akhlaghi

**Abstract** Improvement of the operating range of compressors will help the power and energy plant to work more flexibly to integrate with other energy generation systems. The stall, rotating stall, and resulting surge are the most dominant limiting phenomenon in axial compressor operating envelop. Several active and passive methods have been employed to eliminate occurring of these phenomena and to extend compressors' stable range. Among these, casing treatment is one of the most useful methods. This study aims to investigate the effect of the number of stationary blades on the performance and stall margin of an axial compressor through numerical simulation. Casing treatments in two different configurations of 33.3 and 53.5% of rotor blade tip exposure and with six different numbers of vanes, 30, 40, 60, 80, 90, and 120, are simulated with computational fluid dynamics in ANSYS software. The numerical simulation is validated with available experimental data. The results reveal that in a high rotor exposure configuration, the highest number of vanes provides the best performance for the compressor. However, in a low exposure configuration, the optimum number of the vanes, 90 for the 33.3% exposure, can be found with the proposed numerical procedure based on stall margin improvement.

**Keywords** Stall margin · Efficiency · Compressor · Casing treatment · Wall improving

---

S. Soodani · M. Akhlaghi  
School of Mechanical Engineering, Iran University of Science and Technology, Tehran, Iran

S. Hosseini (✉)  
University of Hertfordshire, Hatfield, UK  
e-mail: [v.hosseini@herts.ac.uk](mailto:v.hosseini@herts.ac.uk)

M. Hakimi  
School of Aerospace Engineering, Amirkabir University of Technology, Tehran, Iran

## 32.1 Introduction

The sustainable supply of energy and electricity is still challenging and the development of efficient, flexible, and low-cost energy systems can contribute significantly to several social, industrial, and economical aspects in certain areas of the world [1]. The gas turbine is considered one of the main solutions to generate reliable power on land, sea and air. High flexibility and availability of the GTs regarding fuel type and short start-up time, respectively, have made them capable to combine with other energy sources to compensate for inherent intermittencies of renewable energy sources [2]. The stable operation range of axial flow compressors is limited by the onset of stall and surge instabilities. These phenomena occur due to the disturbances such as variation in rotor speed, change in upcoming flow angle and airfoil flow separation due to geometry anomaly. The challenge that compressor designers often deal with is finding solutions in order to prevent the occurrence of stall and surge phenomena. A variety of active and passive methods have been applied to extend the stable operating range. Using bleed valves, air injection systems and variable inlet guide vanes are the most common examples of active methods. Passive methods include using different types of casing treatments. One of the interesting approaches in the design of improving walls is the use of the concept of recirculation flow. In this approach, the mass flow resulting from the vortices of the tip leakage flow as well as the low-pressure region resulting from the flow separation on the rotor blade is directed into the empty space in the improving wall and injected into the flow upstream of a preceding rotor blade row. Gourdain and Leboeuf [3] performed a numerical investigation of a casing treatment with non-axisymmetric slots. The method showed a good ability to control the tip leakage flow but failed to reduce the boundary layer separation on the suction side. An increase in the operability range was observed but with a penalty in efficiency. Yang et al. [4] performed an unsteady numerical simulation to study the effect of multiple cylindrical holes casing treatment (MHCT) with pre-swirl blowing. Parametric studies of the total extraction holes area and their axial locations show that the compressor performance deteriorates as the area ratio increases but the stall margin is extended. He also concluded that there is an optimum extraction hole axial location for stall margin extending. Guinet et al. [5] carried out a numerical parametric study using the URANS method on a recirculating tip blowing casing treatment configuration (TBCT) to drive design rules. The wall treatment geometry consists of a recirculating channel with an air off-take above the rotor and an injection nozzle in front of the rotor. A variation of the geometry of the tip blowing, more specifically the nozzle aspect ratio, the axial position, or the tangential orientation of the injection port, was investigated. Kendall-Torry and Gümmer [6] presented the aerodynamic design of 3.5 stage axial compressor. The application and development of axial slot casing treatments (CT) into the smooth casing is performed, aimed at improving the local stage and overall stall margin with particular emphasis on avoiding efficiency penalties within stages. Ahmad et al. [7] designed two models of single groove casing treatment and tested them numerically to improve the performance and stable range of NASA rotor 37.

Both models consisted of a single rectangular groove which was located from 10 to 90% of the axial chord. Their work showed that the single rectangular groove structure can enhance the stall margin but reduce the adiabatic efficiency. Chen et al. [8] proposed a coupled casing treatment (CCT), which was built with an injector, a bridge, a plenum chamber, and several slots for a recirculating loop. They carried out a parametric study on the slot axial location, skewed and lean angle and also number of slots and optimized the geometry parameters to enhance the stability of the compressor. The optimized CCT improves the compressor stability and efficiency under the design condition by 75.8% and 0.71%, respectively. Akhlaghi [9] investigated the effect geometric parameters in a casing treatment consists of a cavity with and 120 vanes skewed vanes which directed the recirculated flow toward the main flow. They studied the influences of rotor blade tip exposure and cavity path curve. Other geometric parameters such as vane profile and the number of vanes have not investigated in the introduced casing treatment so far. The objective of this work is to numerically investigate the effect of the vane numbers in the casing treatment wall with semi-circular flow path and recessed vanes in two values of rotor—casing treatment exposure. In the first step, he computational model of the research compressor has been developed and validated against experimental data from Akhlaghi [9]. In the second step, the casing treatment configuration for the vane numbers of 30, 40, 60, 80, 90 and 120 were modelled and applied on the compressor to find the optimum geometry in the rotor blade tip exposure of 33.3 and 53.3%.

## 32.2 Numerical Methodology

The first stage of a low-speed research compressor rig was used to study casing treatment geometric parameters. The flow path consists of a bellmouth entrance region, inlet guide vanes row, rotary blades row, stator vanes row, the outlet region and the casing treatment which is described in detail in Ref. [3]. The compressor characteristics are presented in Table 32.1. The computational domain has been constructed using a single passage of each blade row and the corresponding inlet and outlet region using rotational periodic boundary conditions as shown in Fig. 32.1.

**Table 32.1** Characteristics of the compressor test rig

Number of inlet guide vanes	38
Number of rotary blades	37
Number of stationary vanes	34
Profile type	$C_4$
Tip leakage distance (mm)	0.6
Shaft speed (rpm)	3000
Corrected mass flow rate	2.295
Total to total pressure ratio	1.0113



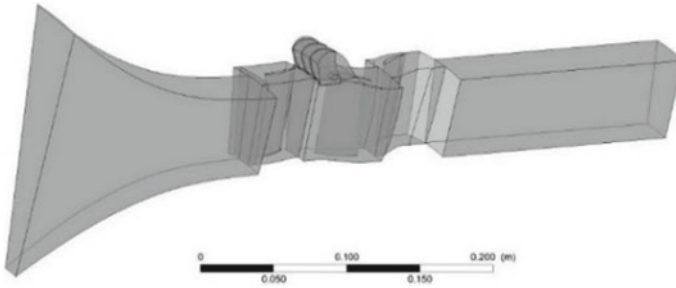


**Fig. 32.1** Geometry modelling of compressor first stage with casing treatment

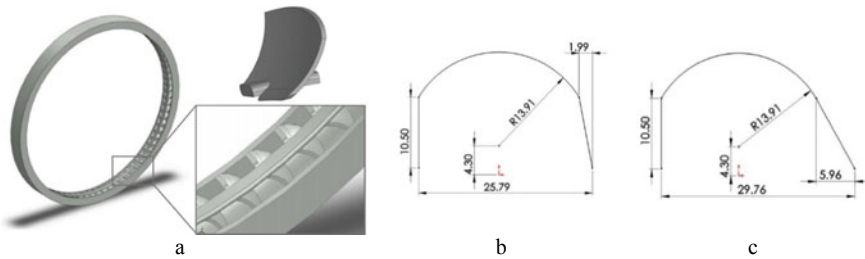


**Fig. 32.2** **a** Configuration of casing treatment with 80 vanes and 33.3% rotor exposure, **b** dimension of casing treatment tubular passage for 33.3% rotor exposure and **c** 53.5% rotor exposure

The CAD modelling of the inlet guide vane and stator vane has been performed using ANSYS BladeGen. The casing treatment is made up of an outer cover ring, a tubular passage inside and a set of curved vanes which are fixed on an inner ring. The configuration of the casing treatment and the dimensions of the tubular passage for two rotor tip exposure values is shown in Fig. 32.2.

ANSYS TurboGrid is used to generate the mesh of inlet guide vane and rotor blade components. The computational grid for the rotor blade, bellmouth and outlet grid section are generated using the structured mesh method and for the casing treatment, the unstructured mesh method of ANSYS ICEM is applied. As shown in Fig. 32.3a casing treatment recessed vanes direct the recirculated flow toward the upstream main flow to preserve appropriate mixing conditions. In order to model the interference region, a part of the computational domain of the rotor passage is removed and this volume is added to the casing treatment computational domain (Fig. 32.3b). The blocking strategy and the mesh created for the rotor are presented in Fig. 32.3c.

Mesh independence study has been performed for the integrated CFD domain. The result which is presented in Table 32.2 shows that for the 2.5 million elements or more, the solution is dependent on the number of meshes.

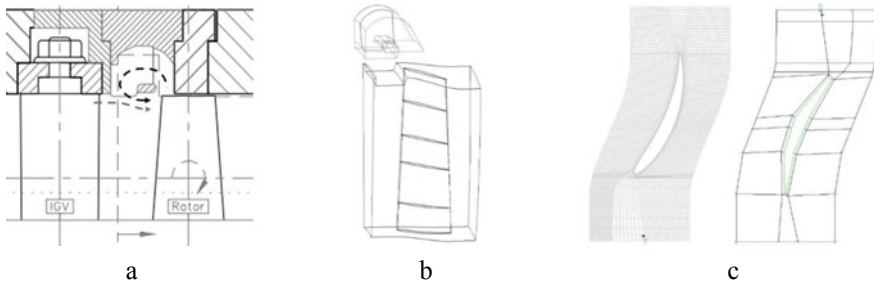


**Fig. 32.3** a Rotor and casing treatment positioning, b CAD modelling of rotor and casing treatment, c rotor blocking and meshing strategy

**Table 32.2** Result of mesh independency study

Number of mesh elements	Total pressure @ outlet
1,727,292	102,750
2,583,419	102,849
3,866,981	102,853

The numerical solution of the flow has been done using the Reynolds-Averaged Navier–Stokes equations via *SST*  $k - \omega$  turbulence model. In order to serve the requirements of the selected turbulence model, the setting of the boundary layer mesh has been tuned to reach the  $y^+ < 1$  which results in the value of  $3 \times 10^{-6}$  for the first node height from the wall. To consider the effects of compressibility and temperature changes along the compressor, the energy equation is also solved along with the RANS equations.

Since the inlet flow of the compressor is at subsonic speed, the total pressure and total temperature profiles are considered as the inlet boundary conditions. The turbulence intensity of the flow at the inlet of the current model, which is considered a low-pressure compressor, is 2% and the turbulence viscosity coefficient is 10. The boundary condition at the compressor outlet at lower pressure ratios is considered to be the static pressure, but as the compressor pressure ratio increases and the compressor approaches the stall starting point, the mass flow rate is used as the outlet boundary condition. The adiabatic temperature and no-slip condition are used for all rotary and stationary walls. As mentioned earlier, the rotational periodic boundary condition for a single passage has been used to simulate a full annular blade row. The frozen rotor model is used in the interfaces of IGV to the rotor, rotor to the stator and casing treatment to the rotor to simulate the changes in the coordinate system, the connection of two areas with non-homogeneous grids and the change in the flow scale between the two areas. The general connection interface model is used for the inlet to IGV and stator to outlet interfaces. The characteristics maps of the compressor are presented in the form of the total to total pressure ratio and isentropic efficiency against corrected mass flow rate which are defined in Eqs. (32.1), (32.2) and (32.3), respectively.

$$PR_{stage} = P_{03}/P_{01} \quad (32.1)$$

$$\eta_{t-(isentropic)} = (h_{03ss} - h_{01})/(h_{03} - h_{01}) \quad (32.2)$$

$$\dot{m}_{corrected} = \left( \dot{m} \sqrt{\frac{T_{amb}}{T_{std}}} \right) / \left( \frac{P_{amb}}{P_{std}} \right) \quad (32.3)$$

The performance Enhancement due to applying different casing treatment configurations is compared using Stall Margin Improvement parameters (SMI) for pressure ratio and corrected mass flow rate which quantifies the amount of increment in the operating range (Eqs. 32.4 and 32.5) and the penalty in efficiency (Eq. 32.6).

$$SMI_{\dot{m}_{corrected}} = \frac{(\dot{m}_{corrected})_{SC} - (\dot{m}_{corrected})_{TC}}{(\dot{m}_{corrected})_{SC}} \quad (32.4)$$

$$SMI_{PR} = \frac{(PR)_{SC} - (PR)_{TC}}{(PR)_{SC}} \quad (32.5)$$

$$\Delta\eta = \eta_{peak-CT} - \eta_{peak-NC} \quad (32.6)$$

### 32.3 CFD Validation

Compressor characteristics for the 33.3% rotor blade tip exposure and 120 CT vanes have been compared against experimental data of the same model from [9] (Fig. 32.4a, b). The conducted simulations predict the corrected mass flow rate at the point corresponding to the beginning of stall phenomena and at the maximum opening of the discharge valve with an error of 5.17% and 4.95% respectively. The error of total to total pressure ratio at these operating points is predicted 6.6% and 7.8% respectively. The trend of the pressure ratio graphs obtained from the numerical solution is completely consistent with the experimental results and both the total to total and total to statics show a lower value than the experimental data. Figure 32.4b shows the experimental data for the total to total and total to static efficiency and the corresponding numerical simulation. The behaviour of the graphs obtained from the numerical solution is in good agreement with experimental data. The total to total efficiency predicted by numerical simulation, in arbitrarily modified mass flow, shows a higher value and the total to static efficiency shows a lower value than the experimental data. The comparison with experimental results demonstrates the validity of the simulation in the prediction of trends and less than 10% error in stall initiation mass flow rate.

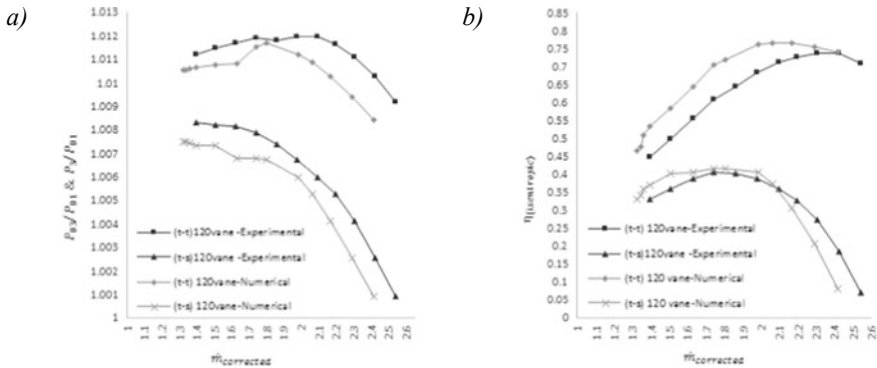


**Fig. 32.4** Comparison of numerical simulation with experimental data for casing treatment with 120 vanes and 33.3% rotor exposure **a**  $P_{03}/P_{01}$ , **b**  $\eta_{iso}$  versus  $\dot{m}_c$

### 32.4 Results and Discussion

The streamlines through the compressor model are shown in Fig. 32.5. The low energy fluid flow of the blade tip has been sucked into the casing treatment cavity and replaced by the high energy fluid of the lower span which results in an improvement in the rotor performance.

The results obtained from the numerical simulation of the casing treatment with the rotor blade tip exposure of 33.3% are presented in Table 32.3. The results show that there is no clear upward or downward trend between the number of blades and the compressor performance improvement. The best performance is for the casing treatment with 120 blades.

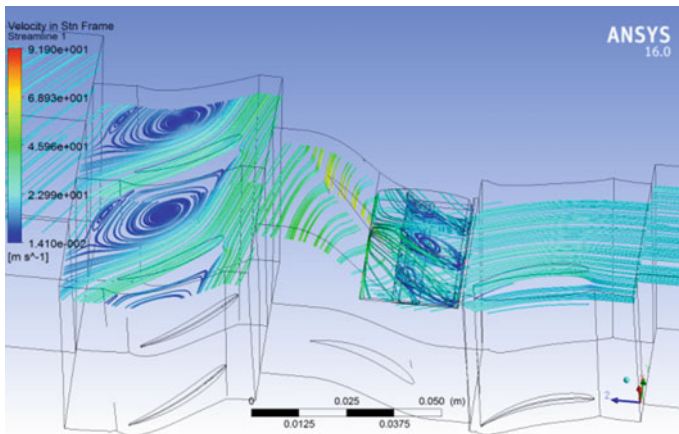


**Fig. 32.5** Streamlines of the compressor model with casing treatment—33.3% rotor exposure

**Table 32.3** Characteristics of 33.3% rotor exposure casing treatment

Number of vanes	$SMIPR$ (%)	$SMI_{\dot{m}_{corrected}}$ (%)	$\Delta\eta$ (%)
120	- 0.07122	30.0774	0.148
90	- 0.03695	29.0017	0.004
80	- 0.04147	24.6987	- 3.514
60	0.00812	23.6230	0.212
40	0.41853	25.7745	- 3.544
30	- 0.02164	22.4705	- 3.623

Figure 32.6 shows the graphs of the total to total efficiency and total-to-total pressure ratio for 33.3% rotor blade tip exposure and the number of 120, 90, 80, 60, 40 and 30 CT vanes, respectively. For higher mass flow rates, close to the maximum opening of the discharge valve, both graphs have similar behaviours and values with insignificant differences, while with the decrease of the mass flow rate and approaching the conditions of the stall initiation point, the effect of the casing treatment on the compressor performance is increased and the number of different blades shows different behaviours. Despite no casing treatment case, in the compressor with casing treatment, graphs of pressure ratio in Fig. 32.6a have an extremum which means the maximum pressure ratio occurs in the mass flow rates greater than the mass flow rate of the stall initiation point.

The results obtained from the numerical solution of the casing treatment with 53.5% rotor blade tip exposure are presented in Table 32.4. As with the casing treatment with 33.3% rotor blade tip exposure, there is no clear upward or downward trend between the number of blades and improvement in compressor performance. The best performance is for the casing treatment with 90 blades.

Figure 32.7 shows the graphs of the total to total pressure ratio and total to total efficiency for the number of 120, 90, 80, 60, 40 and 30 casing treatment vanes. As the rotor blade tip exposure increases, the effect of change in the number of casing

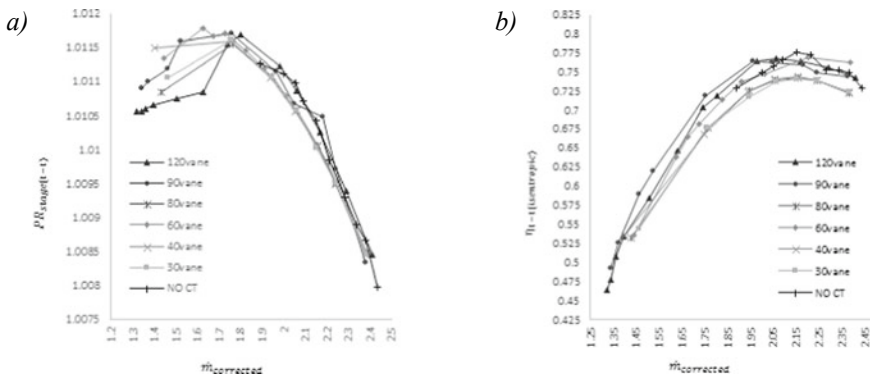


**Fig. 32.6** Comparison of **a**  $P_{03}/P_{01}$ , **b**  $\eta_{t-iso}$  for casing treatment with 120, 90, 80, 60, 40, 30 vanes and 33.3% rotor exposure

**Table 32.4** Values of stall margin improvement for casing treatment with 53.5% rotor exposure

Number of vanes	$SMI_{PR}$ (%)	$SMI_{\dot{m}_{corrected}}$ (%)	$\Delta\eta$ (%)
120	0.04566	28.5665	- 6.1
90	0.14684	31.8410	- 8.8
80	0.11376	25.4012	- 6.8
60	0.09722	29.2195	- 9.9
40	0.16824	21.3551	- 9.9
30	0.15559	26.5980	- 8.55

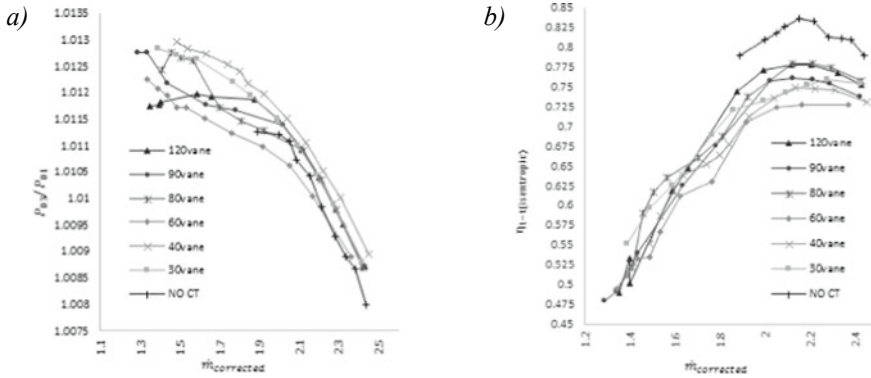


**Fig. 32.7** Comparison of **a**  $P_{03}/P_{01}$ , **b**  $\eta_{t-iso}$  for casing treatment with 120, 90, 80, 60, 40, 30 vanes and 53.5% rotor exposure

treatments vanes on the stall margin improvement becomes more distinct. Unlike the pressure ratio graphs for the casing treatment with 33.3% rotor blade tip exposure, for the value of 53.3% exposure, the maximum pressure ratio occurred at the stall beginning point. The diagram of the total to total efficiency, as in the previous case, has an extremum in the mass flow rates close to the maximum opening of the discharge valve (Fig. 32.7b).

### 32.5 Conclusion

A numerical model has been developed to simulate the performance of a low-speed axial compressor stage with different casing treatment configurations. CFD model using RANS equation and  $SST k - \omega$  turbulence model has been validated using existing experimental data of the same compressor for the casing treatment with 120 vanes and 33.3% rotor blade tip exposure. The effect of the number of vanes in two values of rotor blade tip exposure has been investigated. Numerical results of casing treatment with vane numbers of 30, 40, 60, 80, 90, 120 and 33.3% rotor blade tip exposure show that there is no clear relation between vane numbers and improvement

in performance characteristics and casing treatment with 120 number of vanes has the best performance. For the casing treatment with 53.3% rotor blade tip exposure, and 30, 40, 60, 80, 90 and 120 number of vanes, the variations in compressor map due to applying casing treatment are more distinct and the casing configuration with 90 number of vanes has the best results in stall margin improvement. This simulation procedure and treatment technique make it possible to design an optimum geometry for a more stable compressor that can work in a wider operating range.

## References

1. Y. Liu et al., Multi-fidelity combustor design and experimental test for a micro gas turbine system. *Energies* (2022)
2. S. Hosseini et al., Design procedure of a hybrid renewable power generation system, in *Energy and Sustainable Futures*. Springer Proceedings in Energy (Springer, Cham, 2021)
3. N. Gourdain, F. Leboeuf, Unsteady simulation of an axial compressor stage with casing and blade passive treatments (2009)
4. C. Yang et al., Investigation on multiple cylindrical holes casing treatment for transonic axial compressor stability enhancement. *J. Therm. Sci.* **23**(4), 346–353 (2014)
5. C. Guinet, A. Inzenhofer, V. Gümmer, Influencing parameters of tip blowing interacting with rotor tip flow. *J. Turbomach.* **139**(2), 021010 (2017)
6. C. Kendall-Torry, V. Gümmer, Design of a rear-stage subsonic axial compressor with casing treatments. *CEAS Aeronaut. J.* **11**(4), 1083–1096 (2020)
7. N. Ahmad et al., CFD investigation of an axial compressor with casing treatment for the enhancement of the stall margin. *Sci. Iran.* **28**(6), 3156–3167 (2021)
8. Y. Chen et al., Method of improving stability of a highly-loaded axial compressor stage by coupling different casing treatments. *J. Appl. Fluid Mech.* **15**(3), 645–657 (2022)
9. M. Akhlaghi, *Application of a Vane-Recessed Tubular-Passage Casing Treatment to a Multistage Axial-Flow Compressor* (Cranfield University, 2001)

**Open Access** This chapter is licensed under the terms of the Creative Commons Attribution 4.0 International License (<http://creativecommons.org/licenses/by/4.0/>), which permits use, sharing, adaptation, distribution and reproduction in any medium or format, as long as you give appropriate credit to the original author(s) and the source, provide a link to the Creative Commons license and indicate if changes were made.

The images or other third party material in this chapter are included in the chapter's Creative Commons license, unless indicated otherwise in a credit line to the material. If material is not included in the chapter's Creative Commons license and your intended use is not permitted by statutory regulation or exceeds the permitted use, you will need to obtain permission directly from the copyright holder.



# Chapter 33

## Development of an Affordable MGT-CHP for Domestic Applications



Seyedvahid Hosseini, Seyed Hossein Madani, Sara Hatami, Ali Izadi, Mohamad Ali Sarkandi, Ali Norouzi, and Mahmoud Chizari

**Abstract** The micro gas turbine (MGT) is considered one of the main solutions for the future power generation system to provide secure and stable energy. Thanks to its multi-fuel capability and high values of power-to-weight ratio, it is a suitable candidate for many applications such as Combined Heat and Power (CHP) systems, range extenders, and auxiliary power units. Among these applications, the micro-CHP system benefits from both the electricity and exhaust heat of the MGT for household or industrial process applications. The MGT could be integrated with a heat exchanger to introduce a CHP boiler to the domestic boiler market. To reduce the cost and size of the package and to compete with a traditional boiler the simple Brayton cycle without the recuperator is considered and all of the useful energy in the exhaust gas is transferred to the heat exchanger to provide hot water. To further reduce the cost of the system to compete in the market, off-the-shelf components were adopted in this project. In this article, the development process of this product is presented including conceptual design based on the type and size of the market. It follows with an evaluation of off-the-shelf compressor and turbine modulus from the automotive turbochargers to match the operating conditions. Here, the MGT is designed in a way that can be adapted to the boilers with minimum components change. A high-speed alternator was powered with a tie grid drive/inverter to enable a bi-directional connection of the power unit to the network. A comparison between the product definition and experimental results of a demonstrator prototype is presented which reveals gaps between design and prototype outcomes. Analysis shows that 23% of the power degradation can be recovered by enhancing the cooling. Potential development and improvement scenarios are addressed for future development.

**Keywords** Micro gas turbine · CHP · Simple cycle · Boiler · Performance · Experiment

---

S. Hosseini (✉) · M. Chizari  
University of Hertfordshire, Hatfield AL10 9AB, UK  
e-mail: [v.hosseini@herts.ac.uk](mailto:v.hosseini@herts.ac.uk)

S. H. Madani · S. Hatami · A. Izadi · M. A. Sarkandi · A. Norouzi  
Samad Power Ltd., Milton Keynes MK11 3JB, UK



### 33.1 Introduction

Micro gas turbine technology has been under development for past decades. Gas turbines brought several advantages such as high power-to-weight ratio, low emission, and fuel flexibility in the automotive industry in the late 80s to substitute the internal combustion engine technology. Employing a high-speed generator, MGT was converted to be used in hybrid vehicles in the 1990s. Although the hybrid electric drive was not mature enough in that period [1], the turbomachinery side has advanced in superchargers. Besides, the MGT has been adapted in the hybrid power generation system on the decentralized power generation market to cover the intermittencies of renewable resources [2, 3] and to adjust the frequency of the distributed power generators.

The MGT has already been proved to be utilized satisfactorily in many engineering fields and specialized applications [1], however, the combined heat and power generation system is one of the most widespread general applications.

There are some challenges in transferring the technology from industrial gas turbine to micro-scale. Visser et al. [4] reported the high viscous losses of low Reynolds flow in the turbomachinery passages, high tip clearances to blade height ratio, high heat losses and relatively high auxiliary system losses as the major technical issues besides the cost.

The micro gas turbine, specifically in the lower power rate, provides lower electrical efficiency in comparison to internal combustion engines, however, it could provide higher overall efficiency in CHP mode as well as lower maintenance and operating cost due to lower moving parts and lower oil consumption.

Samad Power Ltd. (SP) was founded in 2011 to develop micro gas turbines for several applications including a small-size CHP system for a domestic application. This paper reviews the development process and the challenges in one of the early generations of SP's products. Based on the market study and thermodynamic cycle analysis, the appropriate size for the domestic CHP, related cycle parameters and the required specifications of each subsystem are designed. The MGT components are mostly sourced from the off-the-shelf automotive turbocharger parts to reduce the production cost, however, the combustion chamber is designed based on cycle parameters to match the system requirements. The overall system is arranged in the format of a domestic boiler. Test results showed some gaps between the prediction values and actual performance output from the experimental prototype which is discussed in this paper.

### 33.2 Market Study

Approximately, there are 26 million household boilers, in the range of up to 30 kW heat output, exist in the UK. On top of this, a further 1.4 million boilers installation per year is required to keep the demand stable [5]. The figures can be much higher if

**Table 33.1** Product requirement definition

Performance		Operating life	
Power output	2.5–3.0 kW	Service intervals	~ 5000 h
Heat output	20–30 kW	Overhaul	~ 20,000 h
Total efficiency	90%	Design life	~ 40,000 h

Europe or global demand be added. Also, for a CHP to be eligible for Feed-in-Tariff (FiT) incentive in the UK market, the output of the appliance was limited to up to 2 kW of electricity [6]. Hence a product in the range of 2 kW electrical output and 30 kW heat output was considered to be appropriate for this application to get the best share of the market. Considering the power electronic losses including generator, rectifier and inverter, 2.5–3 kW shaft power is considered for the MGT. A summary of the required micro-CHP system is presented in Table 33.1.

### 33.3 Concept Development

Although the clean-sheet design of turbomachinery for new application requirements sounds like the most optimized solution, it is not the optimum method due to the required R&D cost and effort. Therefore, the selection of the off-the-shelf turbomachinery elements of the automotive industry is chosen as a design strategy in this phase to reduce the cost of development. Thermodynamic cycle analysis reveals that the MGT pressure ratio, turbine entry temperature and shaft rotational speed are about 2.0, 1200 K, and 120,000–180,000 RPM, respectively.

### 33.4 Preliminary and Detailed Design

#### Turbomachinery

To achieve the design scopes based on the chosen strategy, the matching of several turbomachinery components is investigated. There are various manufacturers in this field, among which, the products of Garrett Motion Inc are considered for component matching analysis. An in-house component matching tool was developed in the course of this study. The matching procedure which is based on mass flow balance and pressure consistency in the components is shown in Fig. 33.1. Based on this procedure, using the steady-state energy equations and the compressor and turbine characteristic map, one can estimate the necessary power requirement during the compression process and extra shaft power.

The output of integration scenarios that resulted from the above-mentioned procedure is plotted in Fig. 33.2. Each turbomachinery combination is indicated in XX-YY-ZZ name format in which XX, YY and ZZ are turbine family, compressor size and



Fig. 33.1 Turbomachinery matching procedure

turbine trim, respectively. Considering the detailed characteristics of the components, the scenario with the turbine family of 20 and compressor size of 44 is selected. In this stage, design point calculation is carried out by GasTurb to indicate the characteristics of the cycle as well as the boundary condition of each component.

Figure 33.3 shows the model of the proposed concept in GasTurb [7] and the cycle parameters at defined stations. This model has been used to provide the required data for the detailed design of the combustion chamber and test analysis.

### Combustion Chamber

A can-type combustor to provide a diffusion flame combustion is designed to accommodate the required air mass flow and turbine entry temperature. The reverse flow concept that originated from the aero gas turbine is employed to not only provide

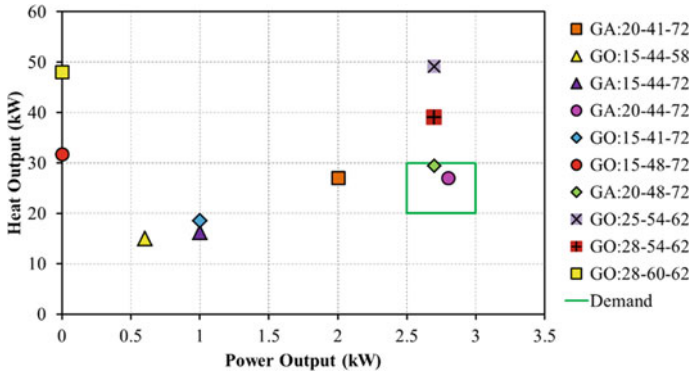


Fig. 33.2 Estimated output opportunity of turbomachinery combination scenarios

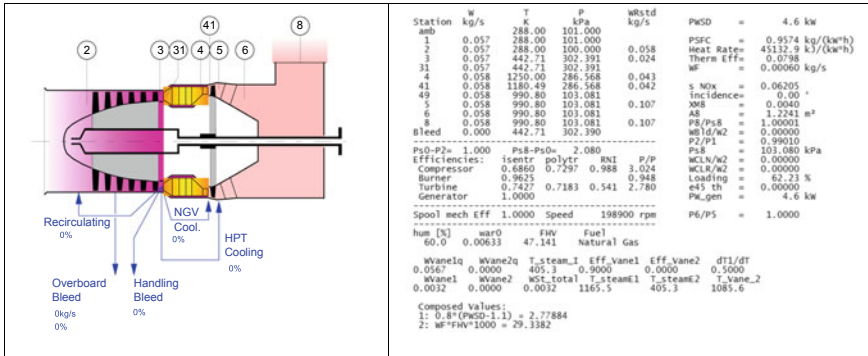


Fig. 33.3 GasTurb simulation model and sample results

sufficient cooling all around the chamber but to reduce the heat radiation to the ambient. The well-known zero-dimensional method of [8] (Sect. 33.4) is utilized the design the overall dimensions of the combustion chamber as well as the number, size and position of cooling holes. Cold flow simulation with specific fuel–air ratios [9] is carried out in ANSYS CFX for the detailed design of swirlers and holes to deliver the desired air/fuel mixing. Figure 33.4 shows the CFD result of cold and hot analysis in the designed combustion chamber.

### 33.5 Experimental Evaluation

A CHP test rig was developed to measure the performance parameters of the develop micro gas turbine. The test rig is equipped with appropriate sensors and techniques to provide the following measurements of cycle parameters:

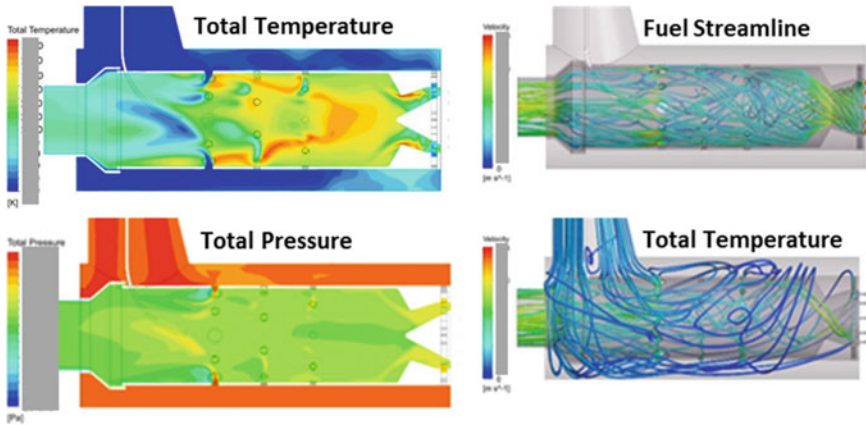


Fig. 33.4 CFD result of the combustion chamber

- Ambient temperature and pressure
- Compressor outlet temperature and pressure
- Turbine inlet temperature and pressure
- Turbine outlet temperature
- Compressor inlet mass flow
- Fuel mass flow
- Shaft output power.

A high-speed alternator was powered with a tie grid drive/inverter to enable a bi-directional connection of CHP to the network. Moreover, the temperature of the oil and cooling water in both inlet and outlet are measured to calculate the heat loss through these two systems. The micro-CHP test rig, equipped with mentioned measurements, is shown in Fig. 33.5.

### 33.6 Results and Discussion

Several tests were conducted to experimentally investigate the performance of the engine in different scenarios. In Fig. 33.6 three different results are compared. It shows the result of a performance of a fresh engine (test after assembly) at 170 kRPM, the performance of the degraded engine (after 20 h of operation) at 170 kRPM, and the performance of the engine at 200 kRPM. It could be seen that the power output is considerably less than the estimated power of the simulation which could be the result of neglected losses mainly the mechanical loss of the bearing, heat loss of the hot sections and the power loss of the generator. The other issue that can be seen in these results is that the output power of the system degrades after a couple of hours of operation. This power degradation is obvious in comparing the results of the fresh

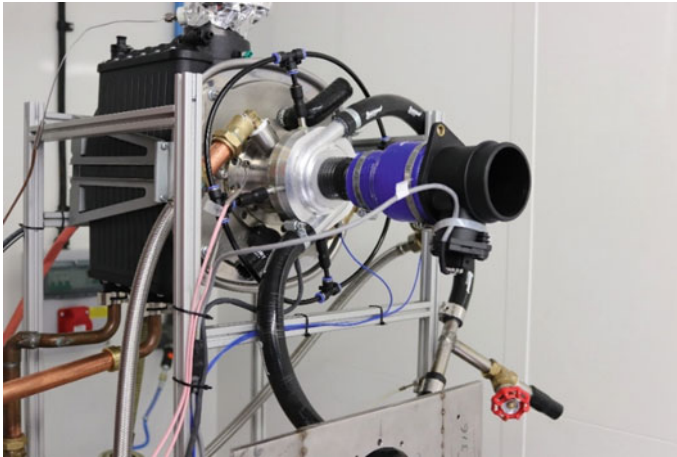


**Fig. 33.5** Micro-CHP experimental test rig

engine with the one after 10 h of operation at the rotational speed of 170 kRPM. Moreover, it could be seen that at the rotational speed of 200 kRPM, the power does not increase with higher turbine inlet temperatures.

The effect of several parameters including mass flow rate, oil feed temperature, shaft speed, and oil feed pressure have been investigated to find a possible correlation between these parameters and the observed power reduction. In Fig. 33.7, it could be seen that mechanical losses do not have a meaningful correlation with the first three mentioned parameters but do have a correlation with oil feed pressure.

This mechanical loss has a constant value in pressures higher than 19 PSIG but increases linearly at pressures lower than this value. It was also found that the oil feed pressure can be correlated with the oil feed temperature (Fig. 33.8).

Having these correlations, it is estimated that by providing better cooling for the oil system, it would be possible to keep the oil pressure higher than 20 PSIG. The micro gas turbine power, consequently, would reach 2000 W at 1275 K, 200 kRPM.

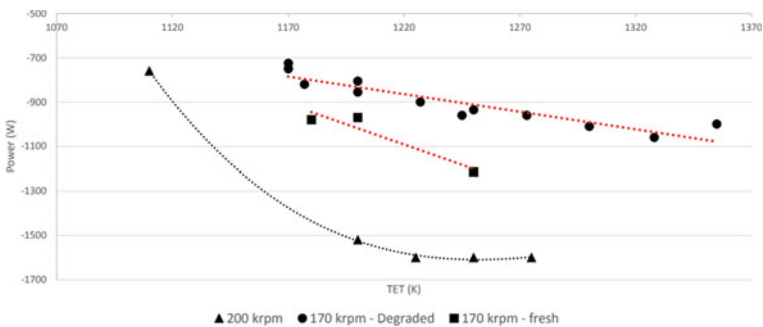


**Fig. 33.6** Sample test results in different conditions (negative value for generation)

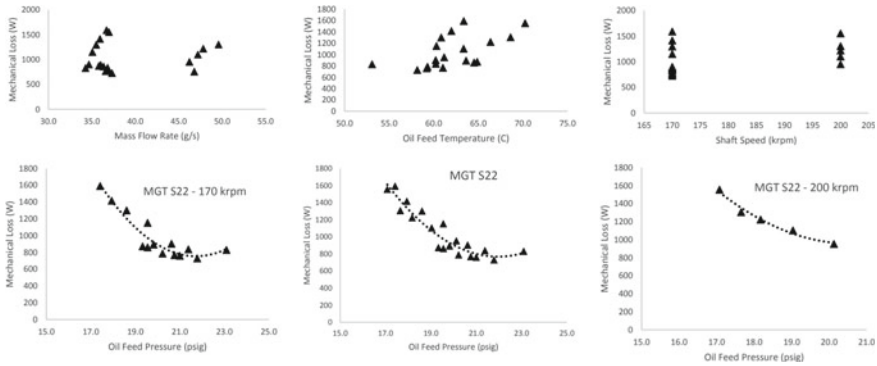
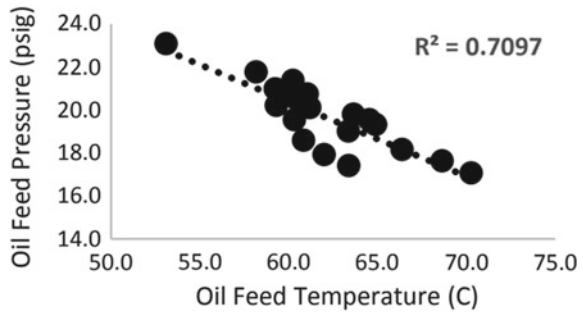


Fig. 33.7 Effect of different parameters on the MGT power loss

Fig. 33.8 Correlation between oil feed pressure and temperature



The predicted trend is shown in Fig. 33.9 which needs further development and testing to be verified.

### 33.7 Conclusion

This paper reviewed the development process of the micro gas turbine for a micro-CHP system based on available off-the-shelf turbocharger technology. An in-house code was developed to match the turbomachinery performances to define the product concept regarding the overall power and heat output. The concept was modelled into GasTurb for detailed test analysis and to provide the boundary condition for combustion chamber design. OD equations and 3D CFD simulation were employed in the conceptual and preliminary design of the combustion system. A prototype was integrated and experimental tests were conducted to validate the design. Experimental results show significant deviation from predicted values. Although the available turbocharger technology shows a great potential to integrate an MGT in small sizes within the proposed procedure, there are technical gaps that need to be addressed to

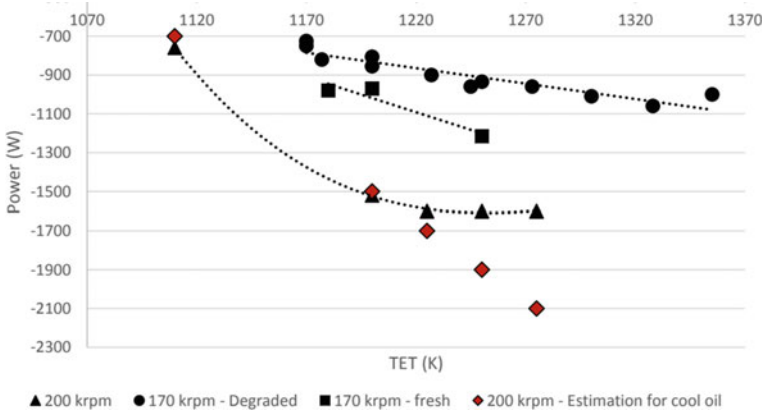


**Fig. 33.9** Estimation of the performance with enhanced oil cooling (negative value for generation)

achieve the target power and efficiency targets. The authors believe that this would be established by enhancing the efficiency of components and reducing the consumption of auxiliary systems.

**Acknowledgements** This project was supported by the UK Department of Business, Energy, and Industrial Strategy (BEIS) under the scheme of Energy Entrepreneurs Fund phase 3 and patented under application numbers GB1409412.2 and GB1313176.8.

## References

1. E. Global, *Micro Gas Turbine Technology Summary; Research and Development for European Collaboration* (ETN Global, Brussels, 2018)
2. S. Hosseini, A. Izadi, S.H. Madani, Y. Chen, M. Chizari, Design procedure of a hybrid renewable power generation system, in *Energy and Sustainable Futures* (Cham, 2021)
3. S. Hosseini, A. Izadi, A.S. Bolorchi, S.H. Madani, Y. Chen, M. Chizari, Optimal design of environmental-friendly hybrid power generation system, in *Energy and Sustainable Futures* (Cham, 2021)
4. W.P.J. Visser, S.A. Shakariyants, M. Oostveen, Development of a 3 kW microturbine for CHP applications. *J. Eng. Gas Turb. Power* **133**(4) (2010)
5. H. Singh, A. Muetze, P.C. Eames, Factors influencing the uptake of heat pump technology by the UK domestic sector. *Renew. Energy* **35**(4), 873–878 (2010)
6. S. Pellegrino, A. Lanzini, P. Leone, Techno-economic and policy requirements for the market-entry of the fuel cell micro-CHP system in the residential sector. *Appl. Energy* **143**, 370–382 (2015)
7. GasTurb. [Online]. Available: <https://www.gasturb.de/software/gasturb.html>
8. A.H. Lefebvre, *Gas Turbine Combustion* (Hemisphere Pub. Corp, Washington, 1983)
9. Y. Liu, T. Nikolaidis, S.H. Madani, M. Sarkandi, A. Gamil, M.F. Sainal, S.V. Hosseini, Multifidelity combustor design and experimental test for a micro gas turbine system. *Energies* **15**(7) (2022)



**Open Access** This chapter is licensed under the terms of the Creative Commons Attribution 4.0 International License (<http://creativecommons.org/licenses/by/4.0/>), which permits use, sharing, adaptation, distribution and reproduction in any medium or format, as long as you give appropriate credit to the original author(s) and the source, provide a link to the Creative Commons license and indicate if changes were made.

The images or other third party material in this chapter are included in the chapter's Creative Commons license, unless indicated otherwise in a credit line to the material. If material is not included in the chapter's Creative Commons license and your intended use is not permitted by statutory regulation or exceeds the permitted use, you will need to obtain permission directly from the copyright holder.

